Universitat de Girona

BIOINSPIRED COPPER AND NONHEME IRON MODELS FOR OXYGEN ACTIVATION: UNPRECEDENTED REACTIVITIES

Joan Serrano Plana

Per citar o enllaçar aquest document:
Para citar o enlazar este documento:
Use this url to cite or link to this publication:
http://hdl.handle.net/10803/398418

ADVERTIMENT. L'accés als continguts d'aquesta tesi doctoral i la seva utilització ha de respectar els drets de la persona autora. Pot ser utilitzada per a consulta o estudi personal, així com en activitats o materials d'investigació i docència en els termes establerts a l'art. 32 del Text Refós de la Llei de Propietat Intel·lectual (RDL 1/1996). Per altres utilitzacions es requereix l'autorització prèvia i expressa de la persona autora. En qualsevol cas, en la utilització dels seus continguts caldrà indicar de forma clara el nom i cognoms de la persona autora i el títol de la tesi doctoral. No s'autoritza la seva reproducció o altres formes d'explotació efectuades amb finalitats de lucre ni la seva comunicació pública des d'un lloc aliè al servei TDX. Tampoc s'autoritza la presentació del seu contingut en una finestra o marc aliè a TDX (framing). Aquesta reserva de drets afecta tant als continguts de la tesi com als seus resums i índexs.

ADVERTENCIA. El acceso a los contenidos de esta tesis doctoral y su utilización debe respetar los derechos de la persona autora. Puede ser utilizada para consulta o estudio personal, así como en actividades o materiales de investigación y docencia en los términos establecidos en el art. 32 del Texto Refundido de la Ley de Propiedad Intelectual (RDL 1/1996). Para otros usos se requiere la autorización previa y expresa de la persona autora. En cualquier caso, en la utilización de sus contenidos se deberá indicar de forma clara el nombre y apellidos de la persona autora y el título de la tesis doctoral. No se autoriza su reproducción u otras formas de explotación efectuadas con fines lucrativos ni su comunicación pública desde un sitio ajeno al servicio TDR. Tampoco se autoriza la presentación de su contenido en una ventana o marco ajeno a TDR (framing). Esta reserva de derechos afecta tanto al contenido de la tesis como a sus resúmenes e índices.

WARNING. Access to the contents of this doctoral thesis and its use must respect the rights of the author. It can be used for reference or private study, as well as research and learning activities or materials in the terms established by the 32nd article of the Spanish Consolidated Copyright Act (RDL 1/1996). Express and previous authorization of the author is required for any other uses. In any case, when using its content, full name of the author and title of the thesis must be clearly indicated. Reproduction or other forms of for profit use or public communication from outside TDX service is not allowed. Presentation of its content in a window or frame external to TDX (framing) is not authorized either. These rights affect both the content of the thesis and its abstracts and indexes.

Universitat de Girona

DOCTORAL THESIS

BIOINSPIRED COPPER AND NONHEME IRON MODELS FOR OXYGEN ACTIVATION: UNPRECEDENTED REACTIVITIES

Joan Serrano Plana

2016

Doctoral programme in Chemistry

Supervised by: Dr. Anna Company Casadevall and Dr. Miquel Costas Salgueiro

Tutor: Dr. Miquel Costas Salgueiro

Presented in partial fulfilment of the requirements for a doctoral degree from the University of Girona

Universitat de Girona

Dr. Anna Company Casadevall and Dr. Miquel Costas Salgueiro, from Universitat de Girona,

WE DECLARE:

That the thesis entitled “Bioinspired copper and nonheme iron models for oxygen activation: unprecedented reactivities”, presented by Joan Serrano Plana to obtain a doctoral degree, has been completed under our supervision and meets the requirements to opt for an International Doctorate.

For all intents and purposes, we hereby sign this document.

Dr. Anna Company Casadevall

Dr. Miquel Costas Salgueiro

Girona, May 1, 2016

Si penses que ets massa petit com per marcar la diferència,
és que no has dormit mai amb un mosquit a l'habitació

Proverbi africà

If you're not failing every now and again,
it's a sign you're not doing anything very innovative

Woody Allen

Als meus pares i a la meva germana

a l'Alicia

FULL LIST OF PUBLICATIONS

This thesis is based on a compendium of the following publications:

Chapter III

Building Complexity in O_2-Binding Copper Complexes. Site-Selective Metalation and Intermolecular O_2-binding at Dicopper and Heterometallic Complexes Derived from an Unsymmetric Ligand. Joan Serrano-Plana, Miquel Costas, and Anna Company in *Inorg. Chem.*, **2014**, *53*, 12929-12938. (Impact factor: 4.762, position 4/45 in Chemistry, Inorganic & Nuclear, 1st quartile)

Chapter IV

Selective O*rtho*-Hydroxylation-Defluorination of 2-Fluorophenolates with a Bis(μ-oxo)dicopper(III) Species. Joan Serrano-Plana, Isaac Garcia-Bosch, Ryosuke Miyake, Miquel Costas, and Anna Company in *Angew. Chem. Int. Ed.* **2014**, *53*, 9608-9612. (Impact factor: 11.261, position 13/157 in Chemistry, Multidisciplinary, 1st quartile)

Chapter V

Trapping a Highly Reactive Nonheme Iron Intermediate That Oxygenates Strong C-H Bonds with Stereoretention. Joan Serrano-Plana, Williamson N. Oloo, Laura Acosta-Rueda, Katlyn K. Meier, Begoña Verdejo, Enrique Garcia-España, Manuel G. Basallote, Eckard Münck, Lawrence Que, Jr., Anna Company, and Miquel Costas in *J. Am. Chem. Soc.* **2015**, *137*, 15833-15842. (Impact factor: 12.113, position 10/157 in Chemistry, Multidisciplinary, 1st quartile)

Chapter VI

Exceedingly fast oxygen atom transfer to olefins via a catalytically competent nonheme iron species. Joan Serrano-Plana, Almudena Aguinaco, Raquel Belda, Enrique García-España, Manuel G. Basallote, Anna Company, and Miquel Costas in *Angew. Chem. Int. Ed.* **2016**, *55*, 6310-6314. (Impact factor: 11.261, position 13/157 in Chemistry, Multidisciplinary, 1st quartile)

Chapter VII

Evidence for acid-triggered heterolytic O-O cleavage in a nonheme Fe^{III}-OOH species. Joan Serrano-Plana, Williamson N. Oloo, Vlad Martin-Diaconsescu, Lawrence Que, Jr., Anna Company, Miquel Costas. (*in preparation*)

All these papers have been published in journals that belong to the first quartile according to JCR.

Publications not included in this thesis

Structural and Reactivity Models for Copper Oxygenases: Cooperative Effects and Novel Reactivities. Joan Serrano-Plana, Isaac Garcia-Bosch, Anna Company, and Miquel Costas in *Acc Chem. Res.* **2015**, *48*, 2397-2406

Design, Preparation, and Characterization of Zn and Cu Metallopeptides Based on Tetradentate Aminopyridine Ligands Showing Enhanced DNA Cleavage Activity. Marta Soler, Eduard Figueras, Joan Serrano-Plana, Marta González Bártulos, Anna Massaguer, Anna Company, Ma Ángeles Martínez, Jaroslav Malina, Viktor Brabec, Lidia Feliu, Marta Planas, Xavi Ribas, and Miquel Costas in *Inorg. Chem.* **2015**, *54*, 10542-10558.

LIST OF ABBREVIATIONS

Å	Angstrom
Abs	Absorbance
Acac	Acetylacetonate
ACC	1-aminocyclopropane-1-carboxylic acid
CSI-MS	Cryospray mass spectrometry
^{C}P	*cis*-μ-1,2-peroxodicopper(III)
cpd	Compound
DFP	Difluorophenolate
DFT	Density functional theory
ee	Enantiomeric excess
EPR	Electron Paramagnetic Resonance
equiv	Equivalents
ESI-MS	ElectroSpray Ionization Mass Spectrometry
Et	Ethyl
EtCN	Propionitrile
GC	Gas chromatography
HAT	Hydrogen Atom Transfer
HRMS	High Resolution Mass Spectrometry
His	Histidine Residue
HRP	Horseradish peroxidase
Kcal	Kilocalorie
KIE	Kinetic isotope effect
Kcal	Kilocalorie
L	Ligand
LMCT	Ligand to Metal Charge Transfer
M	Metal
Me	Methyl
MeCN	Acetonitrile
min	Minutes
mL	Millilitre
mM	millimolar
MW	Molecular weight
MS	Mass Spectrometry
n.d.	Not-detected
NMR	Nuclear Magnetic Ressonance
O	bis(μ-oxo)dicopper(III)
OAT	Oxygen Atom Transfer

Oxone	potassium peroxysulfate
OTf	CF_3SO_3 anion
p.	Page
Ph	Phenyl
Porph	Porphyrin
ppm	Part per million
Py	Pyridine
Ref.	Reference
rR	Resonance Raman
r.t.	Room temperature
SOD	Superoxide Dismutase
^{S}P	μ-η^2:η^2-peroxodicopper(II)
T	Temperature
TAML	Tetra-amido macrocylclic ligand
THF	Tetrahydrofurane
TON	Turn Over Number
^{T}P	*trans*-μ-1,2-peroxodicopper(III)
UV-Vis	Ultraviolet-Visible spectroscopy
X-ray	X-ray diffraction data

LIST OF FIGURES

LIST OF TABLES

LIST OF SCHEMES

AGRAÏMENTS / ACKNOWLEDGEMENTS

El temps passa volant. Un dia en Miquel t'escriu amb una proposta totalment inesperada... vols venir a fer el doctorat? I de cop i volta passen cinc anys i et trobes escrivint els agraïments per una tesi, molt i molt satisfet d'aquesta experiència al mirar enrere. No m'agradaria tancar aquest cercle sense fer una mica de memòria i donar les gràcies a tothom qui hi ha contribuït.

En primer lloc i per motius obvis, als meus supervisors de tesi. En Miquel, no tan sols per haver-me donat aquesta oportunitat sinó per haver-me recolzat i sabut motivar personalment en tot moment. El teu esperit científic s'encomana! I òbviament per igual a l'Anna, amb qui he compartit moltíssimes hores durant aquests anys i hem acabat tenint un vincle especial. Des del primer dia em vas ensenyar com anava això de tenir llargues llistes de coses a fer, però també que el secret és anar-les fent pas a pas. Al final ens ha sortit prou bé no? Em costa expressar amb paraules la gratitud que sento cap a vosaltres, però de debò que és molt molt gran. I a en Xavi, el tercer *jefe*, gràcies per ser-hi sempre que convingui i ajudar-me en tots els *marrons* de burocràcia. I per deixar-me la pantalla per escriure la tesi!

El grup QBIS és molt gran i hi ha anat passant molta gent, a veure si aconsegueixo no deixar-me a ningú. Començant per la gent dels laboratoris del Qbis4, m'agradaria agrair a la Cristina totes les bones estones que hem passat durant tots aquests anys (10 ja??), i els seus cursets *express* de combinar roba (els quals compliquen el tema vestir-se ràpid al matí). A l'Uri per ser així de ben parit i tocar-li la moral al personal per animar les tardes monòtones, i a la Mireia perquè sempre té alguna cosa per explicar i el seu bon dia rialler et treu la son de les orelles. A en Carles, que espero que no perdem el contacte per si mai em roben la bicicleta i necessito recuperar-la... quin crack, molta sort pel doctorat! I a en Jordi, *danke* per aguantar les meves invasions a la poiata i al despatx. En Cédric per avisar-me als matins de l'hora del cafè i a l'Elise. Màrius, sort a la nova etapa aquí a Girona. I als ex-membres, *professor* Chris Whiteoak, en Marc Font (merci per deixar-nos aquell minicalendari a la paret!). A la Marta Soler i l'Imma, perquè els partidets de pàdel van de conya per refrescar les idees. I als nous estudiants Lorena, Cristian, Alba i Pau, molta sort.

Als tallers també hi ha bona gent. En primer lloc, algú a qui ara ja fa uns quants anys que aguanto. Sóc un dèbil per escriure't això enlloc d'un parell d'insults ben posats, però... gràcies per tot Olaf! I a la *bambina* Michela, tu sí que vales... gràcies per les bones estones. A en Diego, *el guardià dels tallers* sempre disposat a ajudar, i en Giorgio que sempre té un somriure o una anècdota per explicar. A la Carlota i la Teresa (ànims per escriure la tesi!), a en Ferran, >*Opt*_gràcies, i en Vlad per les mesures de XAS. I també als qui ja han deixat el grup: l'Isaac (el *cowboy* del QBIS, sort amb el Garcia-Bosch group!), l'Irene i la Mercè. I en Zoel, un crack, gràcies per no haver-me arruïnat cobrant-me la llicència del *quadreitor* de l'UV, m'has estalviat incomptables hores de feina! Molta sort als nous: Carla (benvinguda al club del $PyNMe_3$), la Margarida (que sempre ho diu tot tal com raja), Laia, Sara, Giulia, Marco i Valeria. També gràcies al clan del taller 13, que és el territori d'en Gerard (pots estar tranquil, mai explicaré el que vaig veure al refugi d'ulldeter aquella nit...). I a la Mònica, que en absència d'en Gerard és la *jefa* del 13, la Ilaria que sempre té alguna riallada per regalar i a la Raquel, per tenir tanta paciència amb tots nosaltres i els nostres *capritxos* de reactius. I en David Font, que durant un temps els va poder mantenir tots a ratlla.

A la part qbis-STR, gràcies Laura, per les estones amb el cryospray, colar-me alguna mostra de tant en tant i escoltar les meves *xapes* quan ja estava avorrit de xerrar sol amb l'UV. Hi ha una part del QBIS que es va exiliar a Tarragona. En primer lloc a en Julio, un autèntic crack que malauradament no he pogut disfrutar aquests últims anys, sort amb el nou grup! A l'Arnau (amb la tonteria al final he estat 4 anys pujant les TLC's rectes amb el pot de Nutella que em vas regalar...) i a la Carla Casadevall, alguns dies de cop se la sent riure de Tarragona a Girona!

Durant el doctorat he tingut col·laboracions externes, i m'agradaria agrair les més rellevants:

I would like to kindly acknowledge Prof. Dr. Lawrence Que, Jr. for taking care of me during my stay in University of Minnesota. It was a great pleasure having the chance to work in your labs, and also spending some spare time together, I keep really good memories from Minneapolis. Obvioulsy I would also like to thank Dr. Williamson N. Oloo for making my time in Minnesota much more pleasant, and also for being patient enough to teach me all sort of things. A true *high class* doctor. Also to all the other group members of Que's group, especially to Dr. Mayank Puri for helping me any time that I had a question in the lab.

Me gustaria agradecer al Dr. Manuel G. Basallote su excelente colaboración con las medidas de *stopped*-flow, así como la oportunidad de haber podido estar unos días en sus laboratorios. Y a las doctoras Laura y Almudena, por saber lo que es pelearse con el acylperóxido, por tener tanta paciencia con las cinéticas y por su buena acogida en mi breve estancia en Cádiz.

Fora de l'àmbit del laboratori, hi ha molta gent que ha contribuït a que aquests anys hagin passat literalment volant. Als meus companys de pis, gràcies per haver compartit tantes bones estones. Especialment a en Txus (*diablo*!), les teves teories i històries múltiples tenen més fonament al cap d'un parell de vins. I òbviament gràcies als meus amics de sempre, la colla de castelló, per els incomptables bons moments junts. Gràcies Vice i en Guille *per pagar-me el sou amb el vostre IRPF* (si no fos per vosaltres…), en Jofre (molta sort a la teva recta final cap a Dr. Güell... serem imparables hehe), l'Albert (recorda't de nosaltres quan ompliu el Sant Jordi), en Miquel per encomanar sempre entusiasme i també a la Lídia (el sisè element!). Finalment, el mèrit de la portada és per els *Diaggo*, Ramon Casas i la Silvia Casitas, moltíssimes gràcies per haver-me ajudat en aquesta part, ha quedat genial.

Per acabar, aquesta tesi va dedicada a la meva família, tan els que hi són i com els que ja no. Però sobretot als tres de casa: als meus pares, per haver-me fet veure sempre que les coses eren més fàcils quan jo les veia tant complicades. Moltes gràcies per ser el model a seguir. I a la meva germana Roser, que sempre hi és pel que calgui. Persegueix els teus somnis perquè amb les ganes i l'empenta que tens arribaràs on tu vulguis. Ja ho veuràs! Us ho dec tot.

A l'apartat d'ex-*qbisencs* hi ha una persona que no he mencionat. Algú que va marxar del grup quan feia poquet que havia entrat de ple a la meva vida, fins al punt de passar a ser-ne una part imprescindible. A l'Alicia, la meva *backup*, gràcies per la paciència i per recolzar-me sempre, i per tants bons moments al meu costat. Aquesta tesi també va dedicada a tu.

A tots, moltes gràcies, de debò.

Joan

ACKNOWLEDGEMENTS

This work would have not been possible without the following collaborations:

- Serveis Tècnics de Recerca from Universitat de Girona for technical support, with especial remark to Dr. Laura Gómez and her dedication in setting up the cryospray mass spectrometer.
- Prof. Dr. Lawrence Que, Jr. (University of Minnesota) for hosting a scientific visit and the collaborative research in the highly reactive nonheme iron species.
- Dr. Williamson N. Oloo (University of Minnesota) for all the collaborative research in the highly reactive nonheme iron species project and his supervision during my scientific visit.
- Prof. Dr. Manuel G. Basallote (Universidad de Cádiz) for all the collaborative work in the highly reactive nonheme iron species and for hosting a short scientific visit.
- Dr. Laura Acosta-Rueda and Dr. Almudena Aguinaco (Universidad de Cádiz) for the collaborative work in the measurement of reaction rates by *cryo*-stopped-flow.
- Prof. Dr. Eckard Münck and Dr. Katlyn K. Meier (Carnegie Mellon University) for spectroscopic analysis (EPR, Mössbauer) of the highly reactive nonheme iron species.
- Dr. Isaac Garcia-Bosch (SMU Texas) and Dr. Ryosuke Miyake (Ochanomizu University) for collaboration in the copper-mediated *ortho*-hydroxylation-defluorination work.
- Prof. Dr. Enrique Garcia-España (Universitat de València) for initial design of $PyNMe_3$ ligand.
- Financial support from the Spanish Ministry of Science through project CSD-2010-00065 to Dr. Miquel Costas.

GRAPHICAL ABSTRACT

Chapter V. Trapping a Highly Reactive Non-heme Iron Intermediate That Oxygenates Strong C-H Bonds with Stereoretention (p. 87)

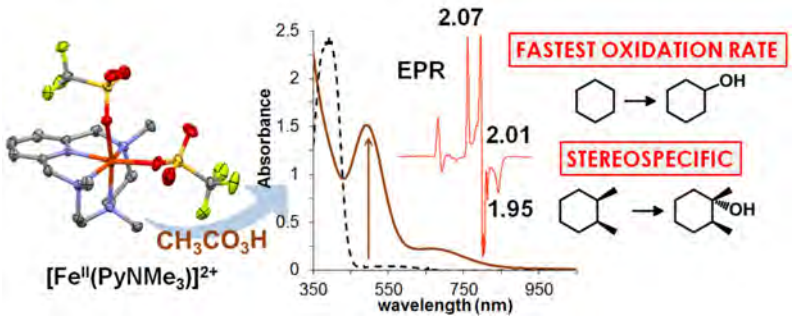

Chapter VI. Exceedingly fast oxygen atom transfer to olefins via a catalytically competent nonheme iron species (p. 99)

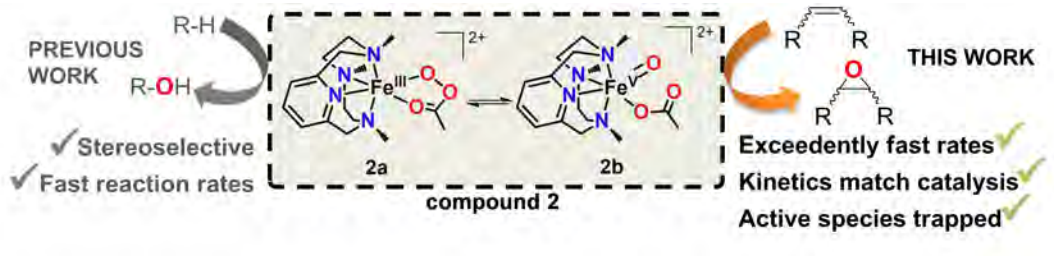

Chapter VII. Evidence for acid-triggered heterolytic O-O cleavage in a nonheme Fe^{III}(OOH) species (p. 107)

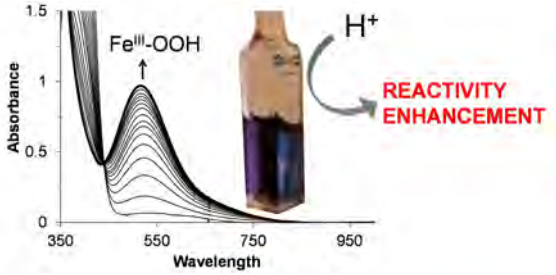

Chapter VIII. Results and Discussion (p. 121).

Chapter IX. General Conclusions (p. 163).

ANNEX (p. 167).

TABLE OF CONTENTS

SUMMARY

The oxidation of hydrocarbons is one of the most important processes in the chemical industry, and it is often related to highly toxic reagents that generate a big amount of undesired residues. In sharp contrast, oxygenase enzymes found in natural systems catalyze the oxidation of hydrocarbons in a regio- and stereoselective manner using O_2 as sacrificial oxidant. These enzymes, that often contain iron and/or copper in their active site, are the source of inspiration for the development of novel methodologies to perform oxidative transformations in a more environmentally friendly way, using benign oxidants such as O_2 or H_2O_2. In this line, bioinorganic chemistry constitutes a discipline in which chemistry, biology and even physics join with the aim of studying both the structure and reactivity of enzymes. One of the key issues to further develop more effective *bioinspired* catalysts is learning the basis of their performance. This doctoral dissertation is focused in the development of copper and iron-based synthetic model systems for oxygen activation.

On the first place, we have developed a novel unsymmetric ligand inspired in the unsymmetric active site of some copper-based enzymes. This ligand allows the synthesis of various heterodimetallic complexes using copper(I) and a complementary metal that react with oxygen at low temperatures giving raise to the formation of different copper-dioxygen adducts. Also in the topic of copper-based synthetic models, we have developed novel reactivity for a high valent copper(III) compound generated after reaction of the corresponding copper(I) complex and O_2 at cryogenic temperatures. We have discovered that this compound is capable of *ortho*-hydroxylating-defluorinating aromatic carbon-fluorine bonds, which is a very challenging reaction owing to the strong bond dissociation energy associated with this bond.

In the second half of the thesis we have turned our interest towards the development of an iron-based synthetic model. Interestingly, when the ferrous complex reacts with peracids at low temperatures it generates a metastable species that is competent for the oxidation of alkanes and olefins. The spectroscopic characterization of this compound points towards a high valent oxoiron compound that has been postulated along the catalytic cycle of the oxidations mediated by nonheme iron systems even though direct detection of such species remained elusive. Thus, the results obtained during this thesis are of great relevance, because for the first time the compound responsible for the oxidation event has been trapped and kinetically interrogated. Finally, the same ferrous precursor reacts with hydrogen peroxide to form a metastable iron(III) species that is an sluggish oxidant but that it is biologically relevant in the catalytic cycle of iron oxygenases. Interestingly, the addition of acid to this compound promotes the formation of a strong oxidizing species that shows great selectivity in hydrocarbon oxidation. This reactivity pattern is reminiscent to the heterolytic O-O lysis in heme systems to form high valent oxoiron compounds.

RESUM

L'oxidació d'hidrocarburs és un dels processos més importants de la indústria química, i sovint està relacionada amb reactius oxidants altament tòxics i que generen grans quantitats de residus. En els sistemes naturals, en canvi, els enzims oxigenases catalitzen l'oxidació d'hidrocarburs de manera regio- i estereoselectiva utilitzant O_2 com a oxidant. Aquests enzims, que sovint contenen ferro i/o coure al seu centre actiu, són la font d'inspiració per desenvolupar noves metodologies que permetin realitzar processos oxidatius de manera respectuosa amb el medi ambient utilitzant oxidants benignes com O_2 o H_2O_2. Així doncs, la química bioninorgànica neix de la confluència entre diferents camps de la ciència, des de la biologia a la química, passant per la física, amb l'objectiu d'estudiar l'estructura i la reactivitat de determinats enzims. Sens dubte, un dels punts clau per avançar en el desenvolupament de catalitzadors *bioinspirats* que siguin més eficaços és aprendre les bases de funcionament dels enzims. Aquesta tesi està centrada en el desenvolupament de sistemes model per l'activació d'oxigen basats en coure i ferro.

En primer lloc, hem desenvolupat un nou sistema inspirat en el centre actiu asimètric d'alguns enzims basats en coure. Aquest lligand permet la síntesi de diferents complexos heterodinuclears mitjançant coure(I) i un metall complementari que reaccionen amb O_2 a baixa temperatura donant lloc a la formació de diferents adductes coure-oxigen. A continuació, també en el camp de models de coure, hem desenvolupat nova reactivitat per un intermedi en alt estat d'oxidació format després de la reacció d'un complex dinculear de coure(I) amb O_2 a -90ºC. Aquest intermedi és capaç d'hidroxilar enllaços fluor-carboni aromàtic, un procés que representa tot un repte ja que aquest és l'enllaç senzill més fort amb carboni.

La segona meitat de la tesi està centrada en el desenvolupament d'un sistema basat en ferro. Quan reacciona amb peràcids a baixa temperatura, aquest complex dóna lloc a una espècie meta-estable que és cinèticament competent per l'oxidació d'alcans i alquens. La seva caracterització espectroscòpica apunta cap a una espècie en alt estat d'oxidació que prèviament s'havia postulat en el cicle catalític de les oxidacions mediades per sistemes no hemo però que no s'havia pogut atrapar fins ara. Així doncs, aquest treball és de gran rellevància perquè per primer cop s'ha pogut estudiar amb detall l'espècie responsable de l'oxidació. Finalment, el mateix complex de ferro també reacciona amb peròxid d'hidrogen per donar lloc a la formació d'un hidroperòxid de ferro(III), típicament poc reactius però molt rellevants en el cicle catalític de les oxigenases de ferro. L'addició d'un àcid genera una espècie que no hem pogut detectar però que mostra un gran poder oxidant i una selectivitat remarcable en l'oxidació d'hidrocarburs. Aquest patró de reactivitat concorda amb el trencament heterolític de l'enllaç O-O en sistemes hemo per donar lloc a una espècie d'alta valència de tipus ferro-oxo.

RESUMEN

La oxidación de hidrocarburos es uno de los procesos más importantes de la industria química, y frecuentemente está relacionada con el uso de reactivos oxidantes altamente tóxicos y que generan grandes cantidades de residuos. En los sistemas naturales, en cambio, las enzimas de tipo oxigenasa catalizan la oxidación de hidrocarburos regio- y esteroselectivamente usando O_2 como oxidante. Estas enzimas, que suelen contener hierro y/o cobre en su centro activo, son la fuente de inspiración para desarrollar nuevas metodologías que permitan realizar procesos oxidativos de modo respetuoso con el medio ambiente utilizando oxidantes benignos como O_2 o H_2O_2. Así pues, la química bioinorgánica nace de la confluencia entre distintos campos de la ciencia, desde la biología a la química, pasando por la física, con el objetivo de estudiar la estructura y reactividad de enzimas. Sin duda, uno de los puntos clave para avanzar en la síntesis de catalizadores *bioinspirados* es aprender las bases del funcionamiento de las enzimas. Esta tesis doctoral está centrada en el desarrollo de sistemas modelo basados en cobre y hierro para la activación de O_2.

En primer lugar hemos creado un nuevo sistema inspirado en el centro activo asimétrico de algunas enzimas basadas en cobre. Este ligando permite la síntesis de distintos complejos heterodinucleares mediante el uso de cobre(I) y un metal complementario que reaccionan con O_2 a baja temperatura dando lugar a la formación de distintos aductos cobre-oxígeno. A continuación, también en el campo de modelos de cobre, hemos descubierto nueva reactividad para un intermedio en alto estado de oxidación generado después de la reacción de un complejo dinuclear de cobre(I) con O_2 a -90ºC. Dicho intermedio es capaz de hidroxilar enlaces fluor-carbono aromático, un proceso muy interesante ya que éste es el enlace simple más fuerte con el carbono.

La segunda mitad de la tesis está centrada en el desarrollo de un sistema basado en hierro. Cuando éste reacciona con perácidos a baja temperatura, se observa la formación de una especie meta-estable que es cinéticamente competente para la oxidación de alcanos y alquenos. Su caracterización espectroscópica apunta a una especie en alto estado de oxidación que previamente se ha postulado en el ciclo catalítico de las oxidaciones mediadas por sistemas no hemo pero que nunca hasta ahora se había podido atrapar. Así pues, este trabajo es de gran relevancia puesto que por primera vez se ha podido estudiar con detalle la especie responsable de la oxidación. Finalmente, el mismo complejo de hierro también reacciona con peróxido de hidrógeno dando lugar a la formación de un hidroperóxido de hierro(III), típicamente poco reactivos pero relevantes en el ciclo catalítico de las oxigenasas de hierro. La adición de un ácido fuerte da lugar a la generación de un intermedio que no hemos podido detectar pero que muestra un gran poder oxidante y una selectividad remarcable en la oxidación de hidrocarburos. Este patrón de reactividad concuerda con la rotura heterolítica del enlace O-O en sistemas hemo para dar lugar a una especie de alta valencia de tipo hierro-oxo.

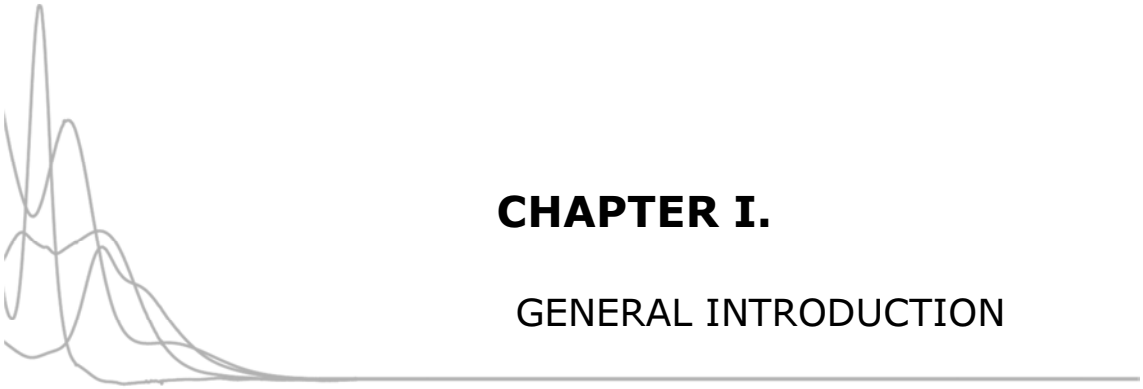

CHAPTER I.

GENERAL INTRODUCTION

I. INTRODUCTION

(Note: For ligand nomenclature of this section, see Annex p.169)

I.1 O_2 activation: the green alternative

Selective oxidations of organic molecules, especially those related to hydrocarbons, are of huge importance in industry.[1-3] Millions of tons of alcohols, carbonyl compounds and epoxides are produced every year in large amounts and used as reaction precursors in all areas of chemical industries. Because of environmental reasons, attention has been focused on the development of catalytic methodologies (rather than stoichiometric) in order to minimize the cost of waste disposal and avoid the use of harmful oxidants such as dichromate, permanganate or osmium tetraoxide. Thus, the development of new procedures that allow the performance of oxidation reactions under mild conditions using green oxidants such as O_2 or H_2O_2 is one of the biggest challenges that chemists have been facing during the last decades.[5]

In this regard, nature has served as a source of inspiration, giving rise to the so-called bioinspired methodologies.[6] Metalloenzymes use O_2 to perform a wide range of functions and chemical transformations with exquisite selectivity. These transformations often involve multielectron redox processes coupled with proton transfers, via reaction pathways that are difficult to model. Still, finding strategies to mimic metalloenzymes is highly desirable. Especially attractive from an environmental point of view is the selective oxidation of organic precursors in late stage synthetic routes using small molecules under mild conditions. This would result in greener and less expensive industrial procedures for the synthesis of value-added products.

- **Taking a closer look at nature: O_2 activation in metalloenzymes**

The reaction of O_2 with closed shell organic molecules, a process that involves the O-O bond cleavage and the formation of C-O and O-H bonds, is favorable from the thermodynamic point of view. However, under ambient conditions such oxidation reactions are very slow. This lack of reactivity results from unfavorable kinetics: O_2 has two unpaired electrons in its π antibonding orbitals (S = 1, triplet ground state) and this makes the reaction towards organic substrates (generally S = 0) spin forbidden. However, O_2 can interact with molecules containing unpaired electrons such as radicals (S = 1/2) or paramagnetic transition metal centers ($S \geq 1/2$). Indeed, aerobic organisms have evolved to take advantage of metal-oxygen interactions with the final aim of using their oxidizing power. Interestingly, such reactions take place in a controlled fashion in the active site of various enzymes (mainly oxidases and oxygenases).

Copper- and iron-based (heme and nonheme) proteins are commonly found in processes related to O_2-activation, either O_2 storage and transport or oxidation of organic substrates. Specially relevant for the purpose of this thesis is their activity as mono- or dioxygenases, incorporating one or two oxygen atoms from O_2 into an organic substrate. Upon O_2 binding to the metallic center, reduced species that are more prone to react with organic substrates such

as superoxide ($O_2^{\bullet-}$, S = 1/2) or peroxide (O_2^{2-}, S = 0) (Scheme I.1) are formed. In some cases, these species can evolve to form high valent species bearing metal-oxo moieties after cleavage of the O-O bond (Figure I.1).[1] Overall, unravelling the structure and learning the intimate details of the reactivity of such molecules constitutes a more than exciting challenge for chemists, and at the same time it represents the first step towards the development of more sustainable oxidation processes accomplishing the final goal of boosting potential uses in catalysis.

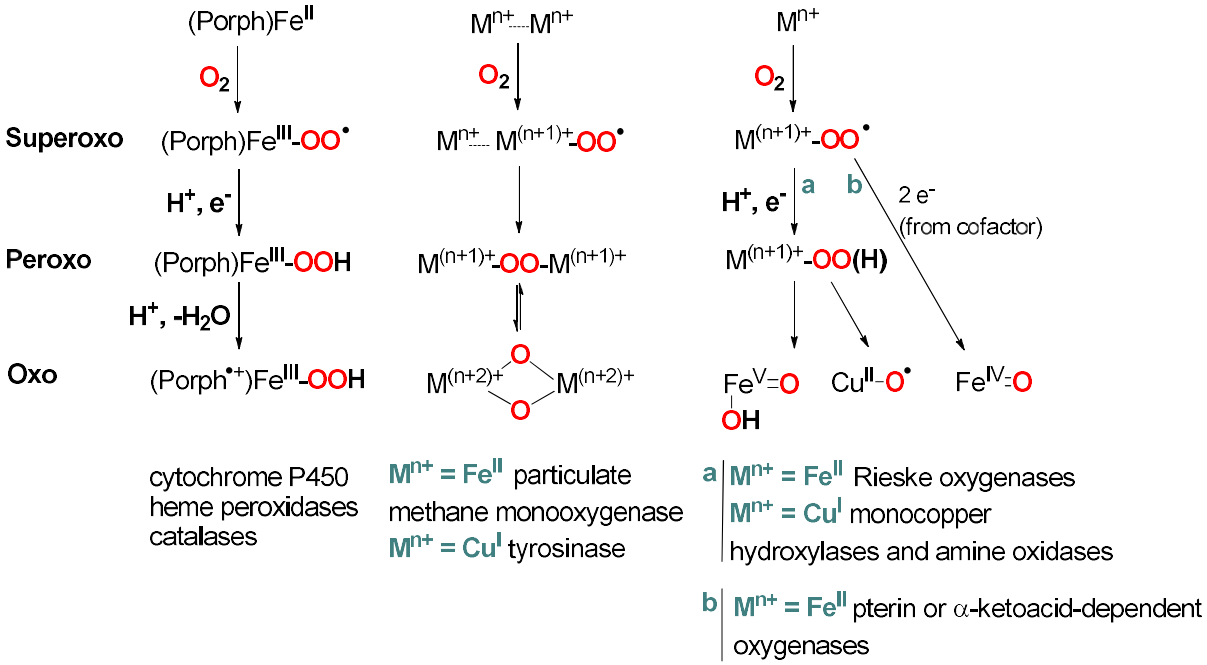

Scheme I.1. Mechanisms of O_2 activation by heme, nonheme, and copper-based metalloenzymes.[1]

I.2 Bioinspired model systems

I.2.1 Bioinspired model systems as a common strategy to study enzymes

By definition, *biomimetics* is the study and development of synthetic systems that imitate the formation, function, or structure of biologically produced substances and materials and biological mechanisms and processes. Thus, the purpose of synthetic model chemistry is two-fold. The first objective consists in mimicking the function of an enzyme involved in a relevant chemical transformation. Equally important is the second one, namely gaining insight into the biological system by providing mechanistic, structural, and spectroscopic data. The development of *bioinspired* synthetic model systems has been specially effective to help accomplishing these two objectives.

The direct study of metalloproteins is often a challenge due to their very high molecular weight and their difficult isolation and purification. In order to overcome these issues, the synthesis of model systems of much lower molecular weight has been commonly applied. These model systems are composed by an organic ligand (synthesized through conventional organic chemistry) able to bind metals, thus resembling the chemical architecture of the enzyme's active site (Figure I.1). Comparison of the spectroscopic features of the enzyme with those of the synthetic model may be a useful tool to unravel the nature of the former. Much progress has been made in developing bioinspired synthetic model systems that mimic enzymes structurally, and in the best cases, also functionally. By tuning the nature of the ligand (donor atom type, redox potential of the metals, coordination geometry), a wide variety of compounds can be obtained to be spectroscopically examined and subjected to reactivity studies. In this line, O_2-binding and activation in model systems containing transition metals has been extensively explored, not only for the biological relevance of this reaction, but also for the potential industrial interest regarding selective oxidation catalysis. Overall, the preparation of novel compounds that reproduce enzyme functions could provide new reagents or catalysts for practical applications. The development of model systems can also lead to explore reactivity beyond the scope of the inspiring system, which is perhaps an even more motivating objective.

Thus, biomimetic inorganic chemistry is an important discipline within biological inorganic chemistry where physical, chemical and biological sciences converge. The sum of the advances in crystallographic techniques, new spectroscopic techniques, computational design, inorganic coordination chemistry among others has greatly allowed the progress in this topic.

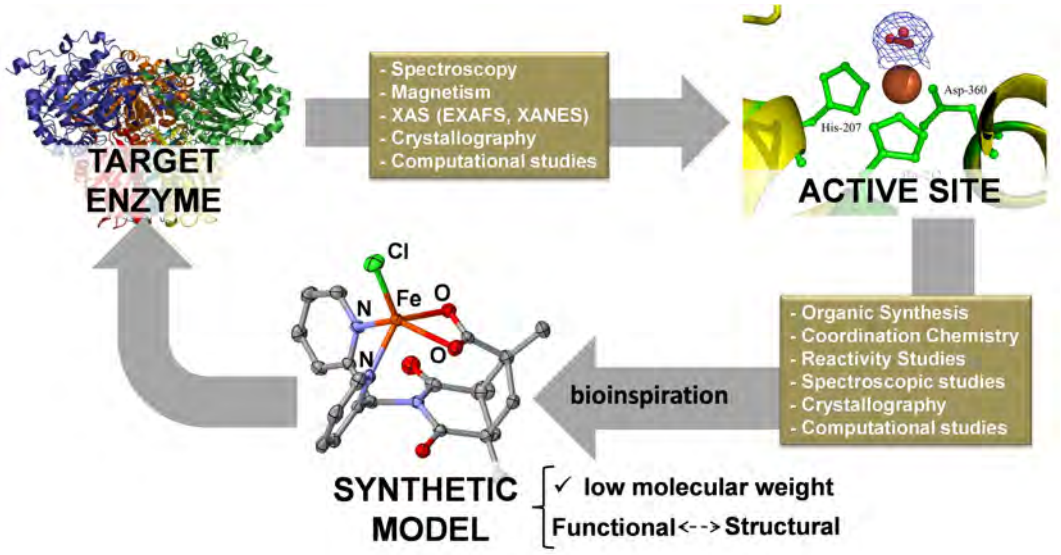

Figure I.1. Development of synthetic models to reproduce the structure and reactivity of enzymes.[7,8]

I.2.2 Ligand design for O_2 activation: General approach

Nature is far beyond our knowledge in many aspects, and the activation of O_2 is not an exception. Every metal in the active site of O_2-processing metalloenzymes is bound in a specific way so that it is prepared for accommodating changes of oxidation state in the metal. The active site environment is robust to prevent side reactions but flexible enough to allow conformational changes. The central cavity around the active site is also shape-optimized, so that the substrates interact with the metallic centers in a specific way. Moreover, the active site is often buried in the protein rather than in its surface, and thus substrates have to access through channels before reaching the cavity. For these reasons, the design of a synthetic model fulfilling all the requirements to successfully activate small molecules is a challenge by itself. Last but not least, the surrounding of the active site, that is the secondary coordination sphere, plays a key role in ensuring the optimal substrate positioning through non-covalent interactions to favor the activity.[9] While strong efforts have been devoted to control the first coordination sphere, mimicking the second coordination sphere in model systems is even more difficult, because it requires the design of particularly complex ligand architectures without dramatically affecting reactivity. Moreover, the manipulation of such non-covalent secondary sphere interactions is very challenging due to their weak and non-directional character.

The structure of copper and iron enzymes involved in O_2 activation is diverse. In some cases the active site contains only one metallic center. Thus, all metal-oxygen and substrate interactions exclusively occur on that center. However, active sites containing two (or more) metallic centers are also very common. In these cases, if the metallic centers are close enough, the metal atoms can interact and cooperate to reductively activate O_2. The presence of multiple metallic centers opens a wide dimension of structural possibilities. For example, the two centers

can be totally equivalent, containing the same metal ion in the same coordination environment, leading to a symmetric active site. However, the active site may also be unsymmetric, meaning that the two metals are not equivalent. This unsymmetry can originate from the presence of two different metals (heterodimetallic systems) but also from different coordination environments of the same metal ion type.[10]

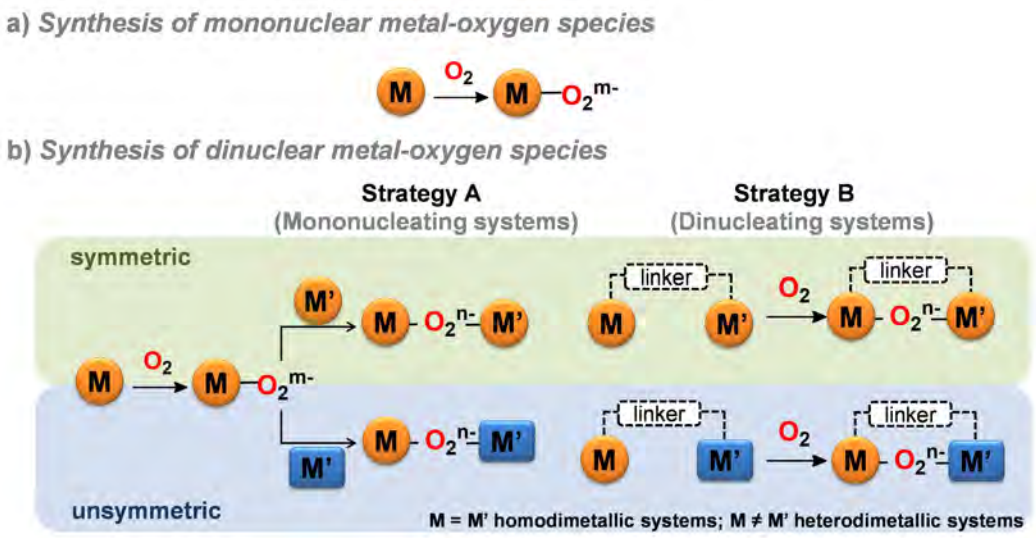

Scheme I.2. Different strategies used for the preparation of mono- and dinuclear metal-oxygen species.

The general strategy for the preparation of mononuclear models for O_2 activation (Scheme I.2.a) consists in the synthesis of a mononuclear transition metal complex bearing a predesigned ligand, which then reacts with oxygen (or its activated forms, such as H_2O_2 or peracids) forming a metal-oxygen adduct that will be trapped and characterized.[11] Usually, these reactions are studied at low temperatures because the resulting metal-oxygen adducts tend to be thermally unstable.

Due to its biological relevance, many efforts have also been directed towards the investigation of dinucleating systems capable of binding and activating O_2 (Scheme I.2.b). In order to accomplish the preparation of bioinspired models for both symmetric and unsymmetric centers, mainly two strategies can be differentiated. The first one consists in the self-assembly of a mononuclear metal-dioxygen adduct, formed by reaction of a mononuclear transition-metal complex and O_2 (LM-O_2), with a second mononuclear complex (L'M'). If the two metal fragments are the same (LM = L'M'), a homodimetallic complex is formed. Indeed, this strategy has been widely applied for the synthesis of homodimetallic symmetric copper-dioxygen species. The use of different metal centers (M ≠ M') can give rise to heterodimetallic systems. The main difficulty in this case is preventing the formation of homodimetallic complexes after the generation of the first mononuclear metal-dioxygen species (LM-O_2) by reaction with an identical LM unit. This limitation has been overcome in selected cases by using bulky ligands. The second methodology for synthesizing dinuclear systems consists in the preparation of a dinucleating ligand, which contains two binding sites in its structure. Since the unsymmetry is already

inferred from the synthetic pathway, this approach is a blueprint for succeeding in the preparation of unsymmetric or heterodimetallic species upon reaction with small molecules. In this case, the difficulty resides in the design and synthesis of the desired ligand that, in the case of the heterodimetallic systems, has to allow a site-selective metal binding avoiding the formation of mixtures. Since this requirement is hard to be fulfilled, the reported examples of unsymmetric systems for O_2 activation are much more scarce compared to symmetrical compounds.[10,12]

I.3 Structural and functional models for copper oxygenases

I.3.1 Biological role of copper

Archaeological evidence demonstrates that copper was one of the first metals used by humans, around 10,000 years ago. The word "Copper" derives from the Latin *aes cyprium* (later corrupted to *cuprum*, hence the English word), that means "metal from the island of Cyprus", place where the Phoenician, Greek and Roman empires fulfilled their needs for this metal.[13]

Apart from the extensive material use of copper by humans, copper (Cu) is an essential element for life from the biological point of view.[14] This metal can be found in trace amounts in most living organisms. A wide range of metalloenzymes contain copper in their active site, either alone or coupled to other centers, thus sharing the active site with other metals such as iron, zinc or additional copper ions. The catalytic cycle of these metalloenzymes normally involves the binding and activation of small molecules such as CO_2, CO, NO_x or O_2, often coupled to an electron transfer reaction. Copper proteins play multiple roles in biological systems: superoxide disproportionation, four electron water reduction, reactions of the NO_X metabolism, electron transfer, O_2 activation (for subsequent substrate oxidation) and O_2 transport to name some of the most remarkable.[6] Many efforts have been directed towards the understanding of the reaction mechanisms for O_2 binding by copper proteins. In nature, Cu can be found in the +1 and +2 oxidation states, resulting in a convenient redox pair Cu^{I}/Cu^{II} that makes it suitable to participate in a broad range of biological reactions serving as a 1 electron shuttle. The oxidation state +3 has also been proposed in some biological reactions. However, direct evidence of the presence of copper in this oxidation state in natural systems has not been obtained so far.

I.3.2 Copper metalloenzymes for O_2 activation

Copper-containing proteins are one of the most relevant subgroups of O_2-activating enzymes, and multiple active site structures have been characterized. A large variety of structural configurations containing different number of copper centers in the active site exist. The simplest configuration is shown by mononuclear copper proteins (amine oxidase, galactose oxidase), but dinuclear copper proteins (such as dopamine-β-monooxygenase, catechol oxidase, hemocyanin and tyrosinase) or trinuclear copper proteins (laccase, ascorbate oxidase,

or ceruloplasmin) have also been characterized. Moreover, the structure of a few heterometallic copper-containing enzymes such as cytochrome *c* oxidase, CuZn superoxide dismutase or peptidylglycine-α-hydroxylating monooxygenase is also known (see I.3.2.2).

Among the reported copper enzymes, one that deserves special attention due to the transformation it catalyzes is particulate methane monooxygenase (pMMO). This enzyme catalyzes the hydroxylation of strong C-H bonds of methane to form methanol but its mechanism of action remains unclear,[15-17] in part because the difficulty in handling the purified pMMO has prevented an accurate structural characterization. Accumulated spectroscopic and recent crystallographic studies point towards the presence of a trimer in which different subunits can be differentiated. The first one contains a dicopper center, the second a mononuclear copper and a third is based on zinc ions.[18-20] The responsible site for the enzyme activity is still under debate but some mechanistic analogies have been established between pMMO and other dinuclear copper-containing oxygen-activating enzymes such as catechol oxidase or tyrosinase.[5,21,22]

For the purpose of this thesis, in the following pages special focus will be put on both tyrosinase and unsymmetric copper-containing enzymes for O_2 activation.

I.3.2.1 Tyrosinase: structure and reactivity

Tyrosinase is a copper-containing enzyme found in many living organisms, involved in wound healing processes, immune response or browning processes of skin, hair and fruit.[23] More specifically, tyrosinase catalyzes the aromatic *ortho*-hydroxylation and subsequent two-electron oxidation of tyrosine (which contains a phenol moiety) to dopaquinone, which constitutes the first step of melanin biosynthesis. Apart from the biological relevance of this reaction, it also interesting from a chemical point of view: the reaction is highly *ortho*-regioselective, a challenging achievement with nonenzymatic synthetic methodologies. Moreover, this reaction is also unique as a full catalytic cycle involves a $4e^-$ oxidation of the substrate, thus fully reducing the O_2 molecule.

Many efforts have been directed during the last decades towards unraveling the structure of the active site of tyrosinase and the oxidation state of the metallic centers. Even though insight had been achieved through spectroscopic studies and by comparison with related type 3 copper proteins, it was not until 2006 that conclusive X-ray characterization was provided by Sugiyama and co-workers.[22] The solid state structure confirmed that tyrosinase contains two copper centers, each one coordinated by three histidine residues.[24] In the absence of oxygen (reduced or *deoxy* form), both metallic centers are Cu^I in a distorted trigonal planar coordination geometry and they are separated by 4.6 Å. Reaction with O_2 affords the formation of the *oxy* form, which consists of a μ–η^2:η^2-$Cu^{II}_2O_2$ species (side-on peroxo, $^{\mathbf{S}}\mathbf{P}$) in which each copper center is oxidized to Cu^{II} and the oxygen is two-electron reduced to its peroxide form and it is bound as a bridging ligand between the two copper centers. The X-ray structure of tyrosinase shows that at this point the structure is more contracted, with the two Cu^{II} centers disposed at 3.6 Å, each one

five coordinated in a distorted square-pyramidal geometry (Scheme I.3a). In the subsequent step, a phenolic substrate coordinates to the Cu_2O_2 core. This interaction promotes the rotation of the Cu_2O_2 moiety and orientates one of the oxygens towards the arene ring. At this point the O-O bond is cleaved and the close proximity of the substrate facilitates an electrophilic attack of the peroxo moiety on the aromatic ring, so that *ortho*-hydroxylation occurs. In the last step, the *deoxy* form is regenerated after release of the *ortho*-quinone product and a water molecule (Scheme I.3b).[25,26]

Hemocyanin is a copper-based enzyme that can be found in many mollusks and arthropods acting as an oxygen carrier, analogously to hemoglobin in vertebrates. The structure of its active site[27] is very closely related to tyrosinase and, in fact, the active site of both enzymes is nearly superimposable. However, after the reductive activation of O_2 (forming the ^{s}**P** species in both cases) the reactivity of these two enzymes follow completely different reaction pathways. Hemocyanin reversibly binds O_2 (so that it is an oxygen carrier) and it is not able to perform the monooxygenase oxidase activity observed for tyrosinase. This difference in the reactivity is not due to the active site itself, but to external factors: in tyrosinase the substrate is properly oriented towards the Cu_2O_2 moiety so that it is prone to oxidation. On the other hand, the access to the active site in hemocyanin is sterically impeded, so that the phenolic substrate cannot reach the Cu_2O_2 core.[27,28] The comparison between tyrosinase and hemocyanin is a clear example to illustrate to which extent the interactions of the second coordination sphere can affect the activity of a given enzyme. Because of the biological relevance of the reaction, modelling tyrosinase has been a topic of major interest in synthetic bioinorganic chemistry during the last decades (see section I.3.4)

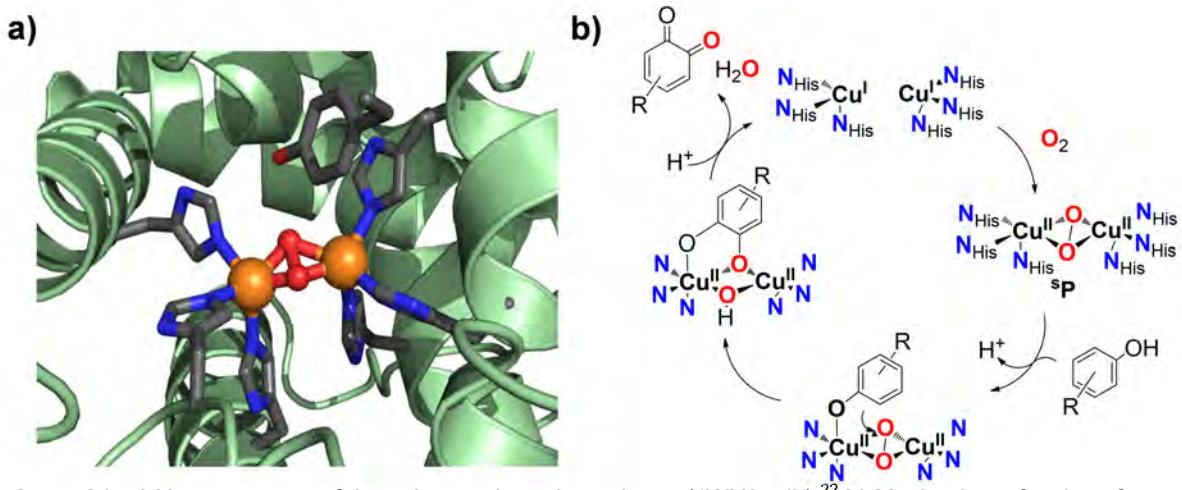

Scheme I.3. a) X-ray structure of the substrate-bound tyrosinase (1WX2.pdb).[22] **b)** Mechanism of action of tyrosinase toward the hydroxylation of a monophenolic substrate.

I.3.2.2 Coper-containing unsymmetric enzymes for O_2 activation

There are several examples of copper-based enzymes containing an unsymmetric active site. As introduced in I.3.2., in heterodimetallic systems, the copper shares the active site with another metal (Figure I.2). Cytochrome c oxidase is the paradigmatic example of this class of enzymes, which contains a heme site that cooperates with a tricoordinated copper center to activate a single O_2 molecule.[29] This enzyme has an important role in the cellular respiration, and during the reaction a peroxo moiety is formed between the heme and the Cu center. Another example of this class of enzymes are CuZn superoxide dismutases, which mediate superoxide (O_2^-) disproportionation to O_2 and H_2O_2.[30] Unsymmetric systems can also originate from the presence of two different coordination environments for the same metal ion. This is the case of peptidylglycine-α-hydroxylating monooxygenase (PHM), which catalyzes the first step of the amidation reaction in peptides.[31,32] In its active site two tridentate copper centers are present, but one of them is bound to three histidine residues and the other coordinates to two histidines and one methionine (Figure I.2c).[10]

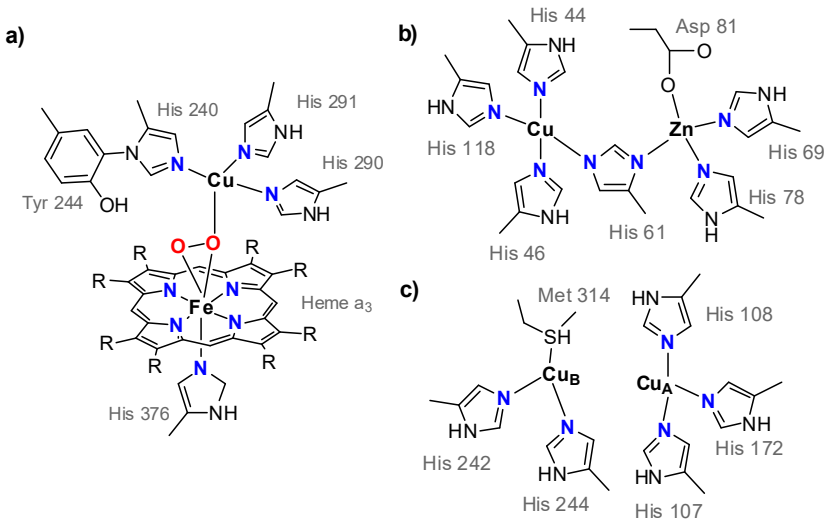

Figure I.2. Active site of **a)** cytochrome *c* oxidase in the O_2-bound form (CcO), **b)** CuZn superoxide dismutase (CuZnSOD), and **c)** peptidylglycine-α-hydroxylating monooxygenase (PHM).

I.3.3 Bioinspired copper-containing complexes for O_2 binding and activation

Over the last decades an extensive library of copper-dioxygen adducts showing a great variety of structural features and chemical properties have been reported.[12,33-36] From these studies it has been made evident that the ligand architecture is one of the most important aspects to consider when designing the system, as it highly affects the formation and reactivity of the resulting metal-dioxygen species. In general, copper-dioxygen adducts are highly unstable and it is necessary to generate them under very particular reaction conditions, e.g. very low temperatures, anhydrous conditions. In this line, the improvement in the instruments and the development of new spectroscopic techniques has been crucial. Different copper-dioxygen

species have been successfully trapped at cryogenic temperatures, studied and fully characterized through an array of spectroscopic techniques, and the reactivity of some of them has also been studied. Thus, several copper-dioxygen adducts have been well characterized (Figure I.3), revealing a variety of Cu:O_2 stoichiometries and different oxidation states at the metal center.[12]

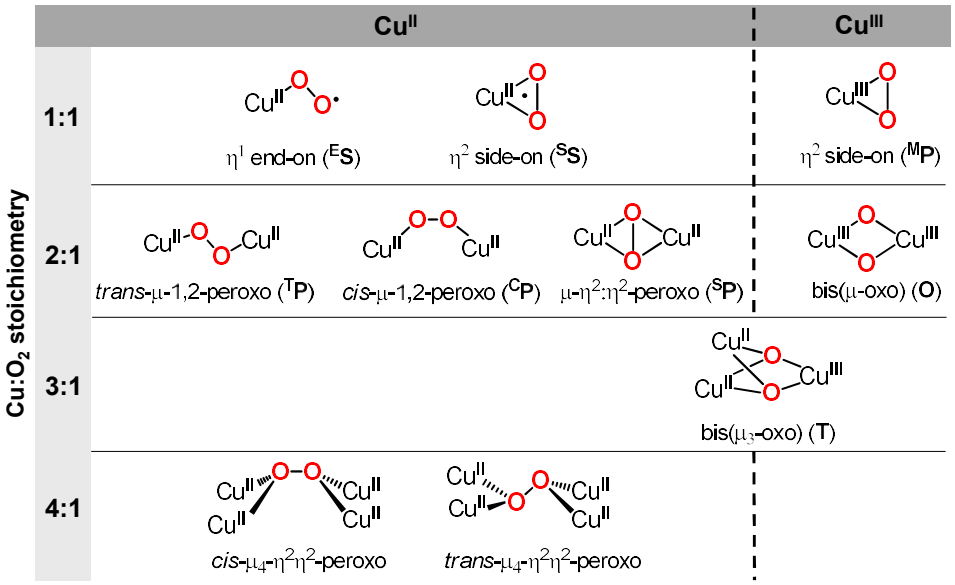

Figure I.3. Main $Cu_n:O_2$ (n = 1-4) species trapped and characterized through model systems.

In most cases, reaction of a copper(I) center with O_2 is proposed to occur through the formation of a short lived end-on superoxo-like intermediate species (^{E}**S**, Figure I.4a). Indeed, Amzel and co-workers were able to trap such species in the reaction of the enzyme PHM with oxygen (Figure I.4b).[37] These compounds tend to be very unstable and they rapidly react with another copper(I) center to form Cu_2O_2 moieties. Thus, the scarce examples of isolated Cu:O_2 superoxo species rely on the use of sterically hindered ligands with the aim of preventing the interaction with another metal center.[14,36,38] So far, the only crystallographically characterized example of a ^{E}**S** species in model systems was provided by Sundermeyer and Schindler in 2006 by using a bulky tripodal tetradentate ligand TMG_3tren (**1**) that has a strong electron-donating character (Figure I.4c).[39]

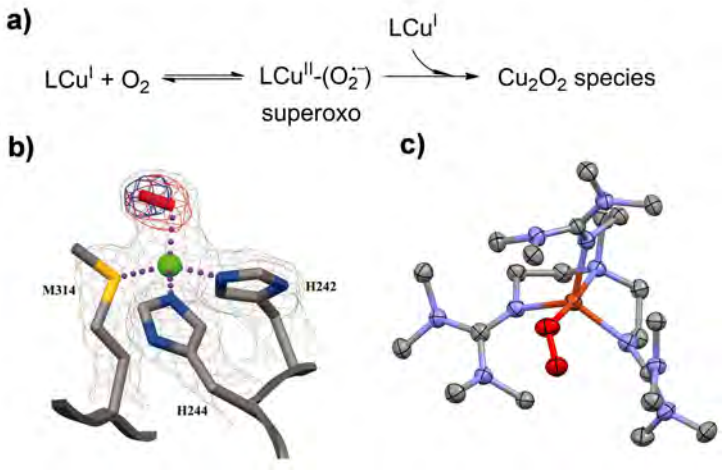

Figure I.4. a) Formation of short-lived superoxo species after reaction of Cu^{I} and O_2, and its rapid reaction with another Cu^{I} center to form Cu_2O_2 species. **b)** X-ray characterization of an end-on copper(II)-superoxo intermediate species in PHM reported by Amzel.[37] **c)** Molecular structure of $[Cu^{II}(O_2)(\mathbf{1})]^{+}$ reported by Schindler after reacting the Cu^{I} precursor and O_2.[39] Hydrogen atoms have been omitted for clarity.

Dimeric Cu_2O_2 species resulting from the self-assembly of Cu^{I} complexes after oxygenation have been commonly characterized in bioinspired model systems (Figure I.3). Configurations containing three or four copper center per O_2 have also been reported in a few cases with very particular ligands that impose some steric constraints.[40,41] Such configurations are reminiscent to those found in multicopper oxidases (laccases[42] and ascorbate oxidase,[43] for example).[14,44]

Dimeric Cu_2O_2 species can be classified in four structural types: *trans*-μ-1,2-peroxodicopper(II) ($^{T}\mathbf{P}$), *cis*-μ-1,2-peroxodicopper(II) ($^{C}\mathbf{P}$), μ–η^2:η^2–peroxodicopper(II) ($^{S}\mathbf{P}$) and bis(μ-oxo) dicopper(III) (**O**). All four are isoelectronic isomers with distinct spectroscopic features and show different reactivities.[33] For the purposes of this thesis, in the following sections different examples of dimetallic copper-dioxygen species will be further discussed.

I.3.3.1 Symmetric dimetallic Cu_2O_2 species

- ***trans*-μ-1,2-peroxodicopper(II) (^{T}P)**

Zubieta and co-workers reported in the late 80's the first crystallographically characterized copper-dioxygen species by reaction of the tpa-based complex $[Cu^{I}(EtCN)(\mathbf{2})]^{+}$ with O_2 at -90ºC that resulted in the formation of a purple species (Scheme I.4).[45,46] The structure of this transient species was confirmed by spectroscopic techniques such as UV-Vis (LMCT at λ_{max} = 530, ε = 10000 $M^{-1}cm^{-1}$) and rRaman (presence of two sensitive bands, O-O stretching at 830 cm^{-1} and Cu-O at 555 cm^{-1}). X-ray diffraction of a dark purple crystal obtained at -85ºC revealed the presence of a peroxo moiety bound between two copper(II) centers in an end-on fashion (^{T}**P**).

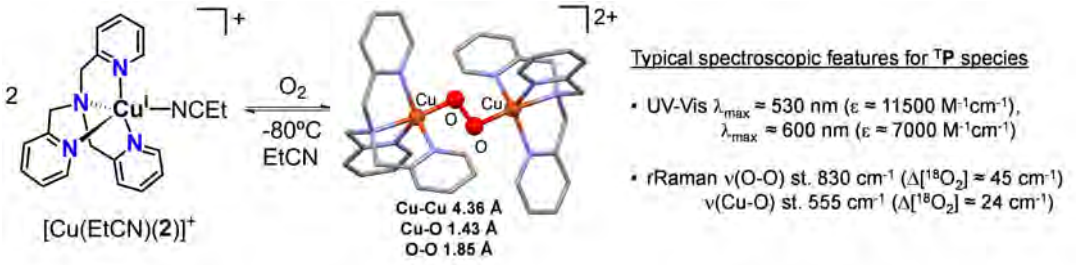

Scheme I.4. Reaction of $[Cu^{I}(EtCN)(\mathbf{2})]^{+}$ with O_2 at -80ºC to form the first crystallographically characterized ^{T}**P** species. Hydrogen atoms in the molecular structure of $[Cu^{II}_2(O_2)(\mathbf{2})_2]^{+}$ have been omitted for clarity.

Ever since, an array of synthetic dicopper(II) ^{T}**P** species that present similar spectroscopic UV-Vis and rRaman features have been reported. In some cases, the X-ray structure has also been obtained.[47,48] In general, these species act as nucleophiles, for example they react with acids releasing H_2O_2 or with aldehydes to form the corresponding carboxylic acid, even though they tend to be sluggish. From a biological point of view, ^{T}**P** species are not considered relevant so far.

- **μ–η^2:η^2–peroxodicopper(II) (^{S}P)**

A great contribution to the field of copper-dioxygen adducts was provided by Kitajima and co-workers in the early 90's by preparing and fully characterizing by spectroscopic means, as well as by X-ray analysis, the first example of a peroxodicopper(II) species bound in a side-on fashion.[49] Reaction of the copper(I) complex bearing a hydrotris(pyrazolyl)borate ligand (**3**) with O_2 at cryogenic temperatures led to the formation of a bridged μ-η^2:η^2-peroxodicopper(II) (^{S}**P**) where each copper is found in a distorted square-pyramidal geometry and the two copper centers are separated by 3.56 Å (Scheme I.5).

Beyond solving for the first time the crystal structure of a new Cu_2O_2 species, the work performed by Kitajima's was a global achievement for bioinorganic chemists. The spectroscopic features obtained for this ^{S}**P** species matched those obtained for the *oxy*-form of tyrosinase (of unknown nature at that time). X-ray resolution of the structure of tyrosinase 14 years later confirmed this assignment.[22] This is probably one of the most evident examples of how building

model complexes can help unravelling the nature of the enzyme active sites and intermediate species. Moreover, the development of other synthetic **^{S}P** species has allowed to mimicking tyrosinase activity, that is phenol *ortho*-hydroxylation. This will be further discussed in section I.3.4.

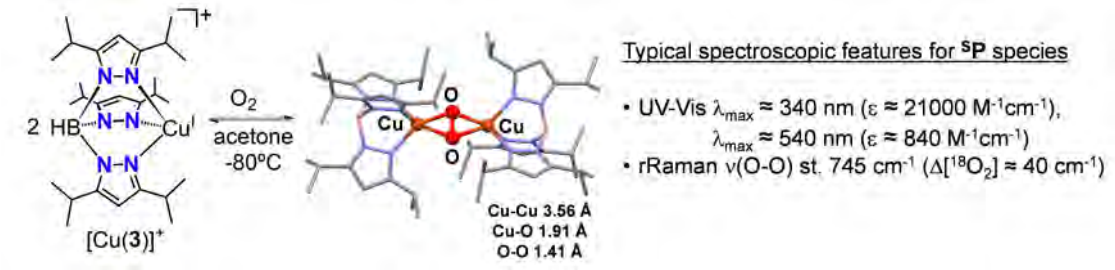

Scheme I.5. Formation of **^{S}P** species after reaction of [Cu(**3**)]$^{+}$ and O_2 at -80ºC. Hydrogen atoms in the molecular structure of [Cu$^{II}_2$(O_2)(**3**)$_2$]$^{+}$ have been omitted for clarity.

- ***cis*-μ-1,2-peroxodicopper(II) (**^{C}P**)**

Cis-μ-1,2-peroxo (**^{C}P**) is the most recent copper-dioxygen binding mode that has been crystallographically established, and it remains much less explored than the others. In contrast to **^{T}P**, the **^{C}P** configuration is thought to have more biological relevance. DFT calculations performed by Solomon and co-workers suggested that at the very early stages of O_2 binding in hemocyanin the **^{C}P** coordination mode precedes the formation of the final **^{S}P** species.[50]

Meyer and co-workers presented in 2014 the first example of a well-defined **^{C}P** compound [Cu$^{II}_2$(O_2)(**4**)]$^{2+}$ by exposing to O_2 a dicopper complex of a dinuclear sterically crowded pyrazole-triazacyclononane hybrid ligand scaffold (**4**) (Scheme I.6.). Similar UV-Vis and rRaman to **^{T}P** species were observed. However, X-ray analysis provided unequivocal evidence about the binding mode of the peroxo moiety in a *cis* conformation. This compound reacted with dihydroanthracene upon warming up to produce anthracene in 25% yield, but reactivity studies are limited.

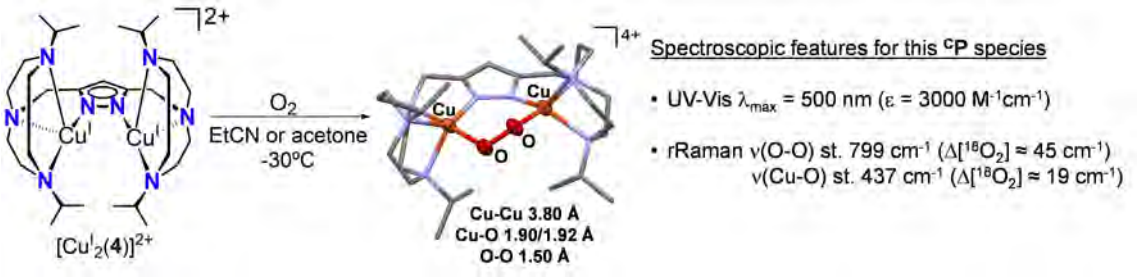

Scheme I.6. Reaction of [Cu$^{I}_2$(**4**)]$^{2+}$ with oxygen at -30ºC leading to the formation of the a **^{C}P** species crystallographically characterized. Hydrogen atoms and X-ray dimeric species have been omitted for clarity.

- **bis(μ-oxo)dicopper(III) (O)**

The first well-characterized bis(μ-oxo)dicopper(III) core (**O**) was reported in 1996 by Tolman and co-workers by using the facial tridentate ligand **5** (Scheme I.7). Similarly to ^{S}**P**, the X-ray structure (obtained at -80ºC using the perdeuteraded ligand) revealed the formation of a Cu_2O_2 core where each copper is in a distorted square-pyramidal geometry. More importantly, as a result of the O-O cleavage, shorter Cu-Cu (2.79 Å) and larger O-O (2.29 Å) distances were found in comparison to ^{S}**P** species.

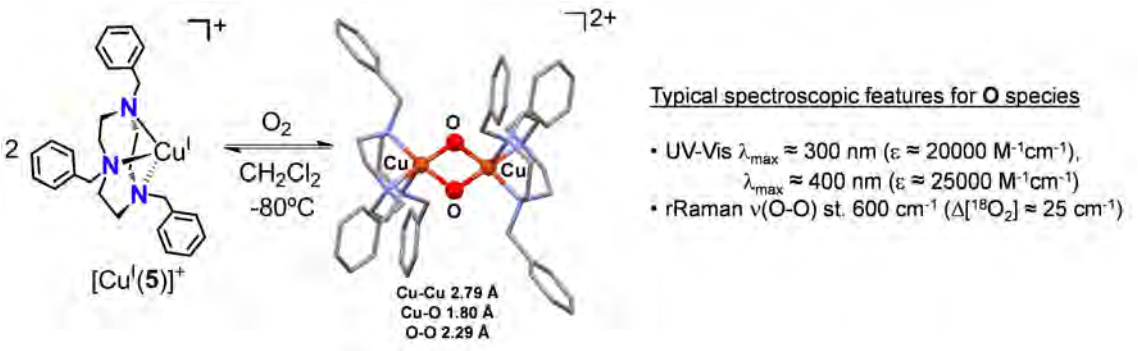

Scheme I.7. Formation of bis(μ-oxo)dicopper(III) species after reaction of [Cu^{I}(**5**)]$^{+}$ and O_2 at -80ºC. Hydrogen atoms in the molecular structure of [Cu$^{III}_2$(μ-O)$_2$(**5**)$_2$]$^{+}$ have been omitted for clarity.

Even though many **O** species with similar spectroscopic features have been characterized since then, such high valent species has not been identified in any catalytic cycle of enzymes so far. Through the use of model systems it has been reported that **O** species behave as electrophilic species able to perform hydrogen atom abstraction (HAT) of various C-H, O-H, N-H and S-H bonds or oxygen atom transfer (OAT) to PPh_3 or thioanisole.

Another benchmark work was reported by Tolman group in 1997 when it was demonstrated that in fact, ^{S}**P** and **O** compounds are in equilibrium through the reversible formation/cleavage of the O-O bond. This observation was exceptional because formation of the O-O bond constitutes one of the key reactions taking place during photosynthesis, and this study constituted the first case where formation and cleavage of the O-O bond was experimentally linked. Furthermore, this report opened the debate about whether the real active species in tyrosinase responsible for the *ortho*-hydroxylation of phenols was ^{S}**P** or **O**. Through the use of model systems it has been demonstrated that **O** is also capable of performing *ortho*-hydroxylation of phenols to catechols. Interestingly, the ^{S}**P**/**O** equilibrium is highly dependent on steric factors induced by the ligand, but it is also influenced by other factors such as solvent, electronic effects on the ligand or counterions. As a general trend, non-bulky ligands favor the formation of **O** species (shorter Cu-Cu distance).

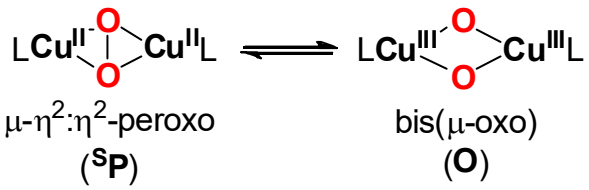

Scheme I.8. Equilibrium between ^{S}**P** and **O** species.

I.3.3.2 Copper-containing unsymmetric dinuclear Cu-O_2-M' species (M' = Cu, Fe, Zn, Pt, Pd, Ge).

As introduced in section I.2.2, the synthesis and characterization of biomimetic dinuclear unsymmetric complexes containing metal ions in distinct coordination geometries remains very little explored compared to the symmetric systems. Preparing model compounds that give raise to the formation of unsymmetric M_2O_2 species is interesting because it can help unravelling aspects of the enzymatic O_2-binding/activation reactions, often occurring in unsymmetric environments. Also, the reactivity of unsymmetric M_2O_2 species may differ from the symmetric ones, thus potentially giving rise to novel reactivities and unprecedented selectivities.

Van Koten and co-workers[51] and a few years later Carpenter and co-workers[52] reported during the 90's the first examples of dimetallic unsymmetric complexes by reacting two different monomeric palladium-, molybdenum-, platinum- or germanium-based complexes and O_2 (strategy A, Scheme I.2). Following the same approach, Tolman and co-workers reported an array of unsymmetric copper-based $LM(O)_2M'L'$ complexes (L ≠ L', M = Cu, M' = Cu, Ni, Ge). Anionic bulky β-diketiminate-type ligands (NacNac, **6**^{Me} and **6**^{iPr}) were used to prevent dimerization and to isolate the mononuclear copper(III)-O_2 building block (Scheme I.9). Reaction of [Cu^{III}(O_2)(**6**^{R})] (R = Me or iPr) with a L'Cu^{I} monomer (L' = **5**^{Me}, **6**^{R}, **7**) allowed the preparation of various unsymmetric homodimetallic **O** species.[53] The same [Cu^{III}(O_2)(**6**^{R})] building block was also suitable for synthesizing heterodimetallic copper-nickel[54] and copper-germanium[55] **O** species by reacting it with the corresponding monomers bearing ligands **8** and **9**. Ray, Limberg and co-workers also prepared an heterometallic copper-nickel **O** species by reaction of a side-on superoxidonickel(II) [Ni(O_2)(**6**^{iPr})] with [Cu^{I}(**10**)]$^{+}$ (Scheme I.9).[56]

O heterodimetallic compounds could also be obtained from the isolation of the building block [M^{II}(η^2-O_2)(**11**)$_2$] (M = Pt or Pd) and its reaction towards different L'Cu^{I} complexes (L' = **5**^{iPr}, **6**^{Me}, **11**) (Scheme I.9).[57] Finally, in a more recent example by Tolman and co-workers, an unsymmetric ^{T}**P** species was formed after reaction of an isolated superoxocopper(II) with a sterically hindered ligand [Cu^{II}(O_2)(**13**)] and a copper(I) complex supported by ligand **2**.[58]

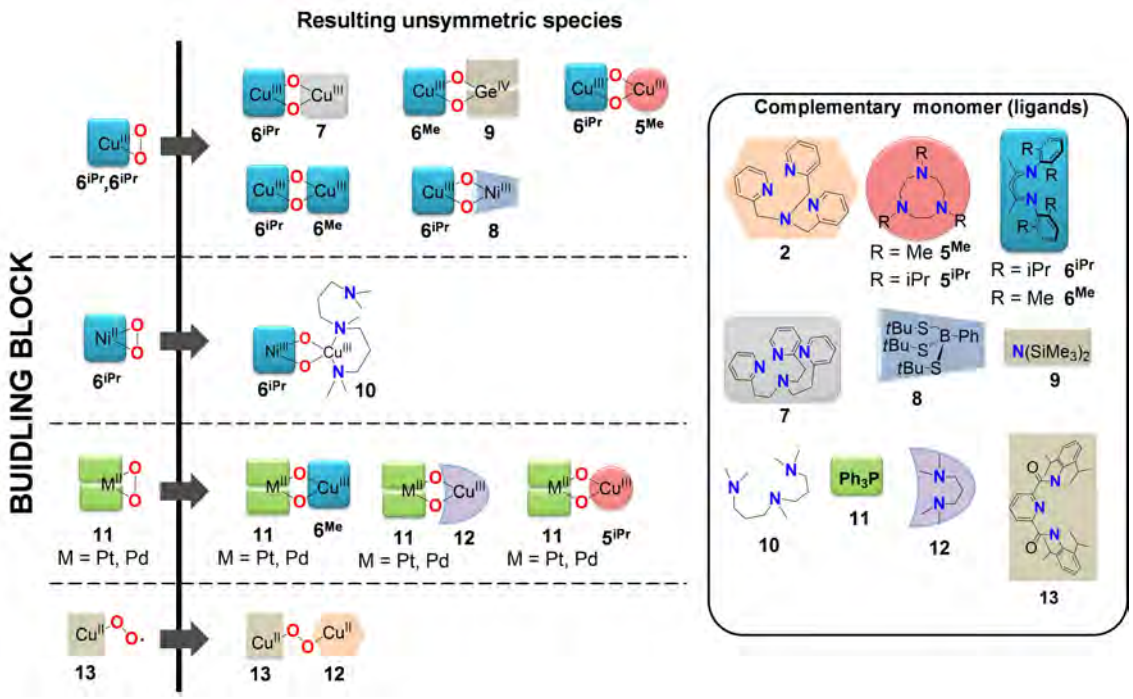

Scheme I.9. Heterodimetallic CuO_2M species obtained by self-assembling of two mononuclear units.

Interestingly, these unsymmetric dinuclear synthetic models show a markedly different reactivity compared to their homodimetallic analogs. For example, Tolman and co-workers observed that while [(**11**)$_2$Pt^{II}(μ-O)$_2$Cu^{III}(**6^{Me}**)] behaved as a nucleophile and it reacted with weak acids or CO_2, the symmetric [Cu$^{III}_2$(μ-O)$_2$(**6^{Me}**)$_2$] analog showed no reaction. More interestingly, the C-C biphenol coupling product was observed upon addition of 2,3-di-*tert*-butylphenol via hydrogen atom abstraction, while the symmetric counterpart again did not show reactivity. It was proposed that the higher basicity of the unsymmetric species facilitated substrate deprotonation at the initial stages of the reaction. Ray, Limberg and co-workers also observed reactivity differences when comparing the reactivity of [(**6^{iPr}**)Ni^{II}(μ-O)$_2$Cu^{III}(**10**)] with its symmetric analogs. While [M$^{III}_2$(μ-O)$_2$(**10**)$_2$]$^{2+}$ (M = Cu, Ni) did not show reactivity towards electrophiles, [(**6^{iPr}**)Ni^{II}(μ-O)$_2$Cu^{III}(**10**)] reacted immediately with aldehydes, forming deformylated products in good yields. A positive slope obtained in the Hammett plot for *para*-substituted benzoyl chloride further supported the nucleophilicity of the intermediate species.

Unsymmetric copper-oxygen species have also been obtained through the use of unsymmetric dinucleating ligands (Figure I.5a). Karlin and co-workers reported the synthesis of several dinuclear copper(I) complexes using unsymmetric xylyl-type ligands for O_2 activation. For example, [Cu^{I}(**13**)][59] reacted with O_2 forming a **^{S}P** species that then underwent oxidation on the aryl ring upon warming up. Also, a mixed valence dicopper complex bearing Cu^{I}-Cu^{II} connected through a phenoxo group in the ligand (**14**)[60] underwent reversible formation of a superoxo intermediate species. Itoh and co-workers designed the unsymmetric pentapyridine ligand **15** which consisted in the 2- and 5- substitution of a pyridine ring with tridentate arms, thus

obtaining a tri- and a tetracoordinating binding sites.[61] Indeed, in the dicopper(I) precursor one copper was tricoordinated in a T-shaped trigonal planar geometry to one nitrogen atom and two pyridines, while the other was tetracoordinated in a distorted trigonal pyramidal geometry. For comparison, the monomeric complex bearing only the tetradentate arm gave a ^{T}**P** species, and ^{S}**P** is typically obtained after exposing tridentate copper(I) complexes to O_2.[33] Thus, by using ligand **15**, which combined both environments, a hybrid binding mode between a ^{T}**P** and a ^{S}**P** was observed. This intermediate species showed both typical electrophilic character (reaction with Ph_3P or PhSMe afforded the oxigenated product, and phenols gave the C-C coupling product, thus resembling ^{S}**P** reactivity) but also showed nucleophilic character (with acids to give H_2O_2, similarly to ^{T}**P** species).[61] Fukuzumi and co-workers prepared an heterodimetallic imidazolate-bridged complex $[Cu^{II}Zn^{II}(\mathbf{16})]^{4+}$ with the aim of reproducing the Cu,Zn-SOD activity. An enhancement of the SOD activity was found compared to the homodimetallic Cu^{II}-Cu^{II} analog.[62] The unsymmetric model also allowed the preparation of a metastable $Cu^{II}(OOH)Zn^{II}$, which was proposed to form during the catalytic cycle of the enzyme. In contrast to the natural system that produces the –OOH moiety by binding and reducing O_2 to superoxide and subsequent protonation, in this model system the oxygen source was hydrogen peroxide in the presence of triethylamine.[63]

Naruta and co-workers achieved in 2003 a great success in the heme-Cu/O_2 chemistry by providing complete characterization of an heterodimetallic model of cytochrome c oxidase (Figure I.5b). The model consisted of an iron in a porphyrinic environment linked to a non porphyrinic tetradentate site (ligand **17**) where a copper was bound. Upon reaction with dioxygen at -30ºC the formation of a copper-iron(heme)-peroxide intermediate species was detected and characterized by X-ray crystallography (Figure I.5b).[64]

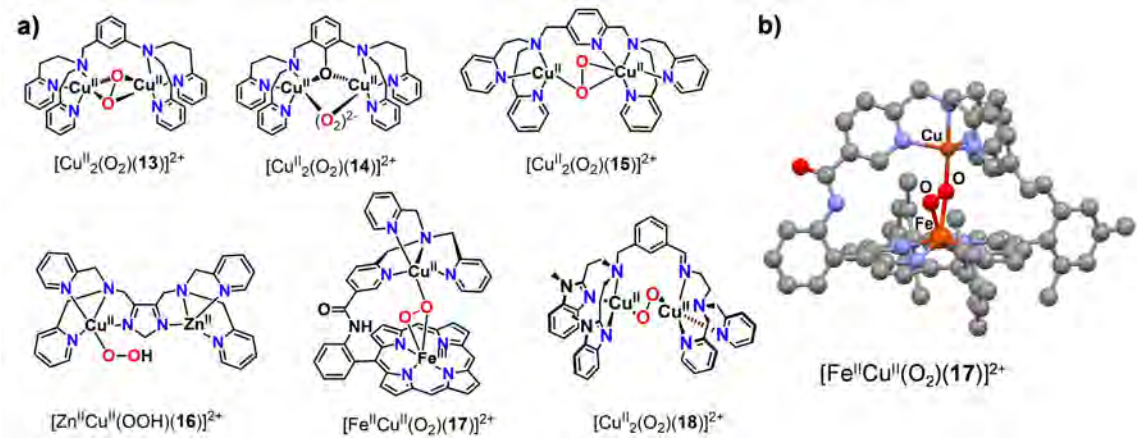

Figure I.5. a) Unsymmetric complexes for oxygen activation. **b)** Molecular structure of $[Fe^{II}Cu^{II}(O_2)(\mathbf{17})]^{2+}$ reported by Naruta and co-workers.[64]

In 2010 our group reported the synthesis of an unsymmetric dinucleating ligand **18** for the synthesis of an unsymmetric copper complex (Figure I.6).[65] This ligand offered a tridentate environment (provided by two benzimidazole rings and an aliphatic nitrogen), and a tetradentate site (composed by two pyridines and two aliphatic nitrogens) linked through a *meta*-xylyl moiety. $[Cu^{I}_2(\mathbf{18})]^{2+}$ reacted with O_2 in acetone at -90ºC to form a $^{T}\mathbf{P}$ species between the two copper centers. Strikingly, this Cu_2O_2 species showed completely different reactivity patterns compared to the symmetric $^{T}\mathbf{P}$ analogue $[Cu^{II}_2(O_2)(\mathbf{19})]^{2+}$, generated after reaction of the Cu^{I} complex of ligand **19** bearing two tetradentate sites (Figure I.6).[65,66] Both the symmetric and the unsymmetric $^{T}\mathbf{P}$ reacted with strong acids releasing H_2O_2, and they were unable to oxidize thioanisole. Moreover, only the symmetric reacted with benzaldehyde to quantitatively afford benzoic acid. Very remarkably, only the unsymmetric $^{T}\mathbf{P}$ compound was able to perform *ortho*-hydroxylation of external phenolates to form the catechol product, a reaction not observed before for any $^{T}\mathbf{P}$ species. Mechanistic studies revealed that the unsymmetric $^{T}\mathbf{P}$ was acting as an electrophilic oxidant, contrary to the typical nucleophilicity shown by $^{T}\mathbf{P}$ species. Recently, Solomon, Karlin and co-workers performed new DFT calculations and proposed that in this system $^{T}\mathbf{P}$ is not the actual executor of the reaction, but instead it is in equilibrium with a **O** species that performs the hydroxylation.[67] The same authors provided experimental evidence of an equilibrium between $^{T}\mathbf{P}$ and **O** species in a related system.[67] However, Solomon and Karlin proposal of a rapid $^{T}\mathbf{P}$ and **O** equilibrium failed to explain the lack of electrophilic reactivity in typical substrates for **O** type of species such as phosphines and sulfides, suggesting that isomerization, if taking place, occurs only after phenolate binding.

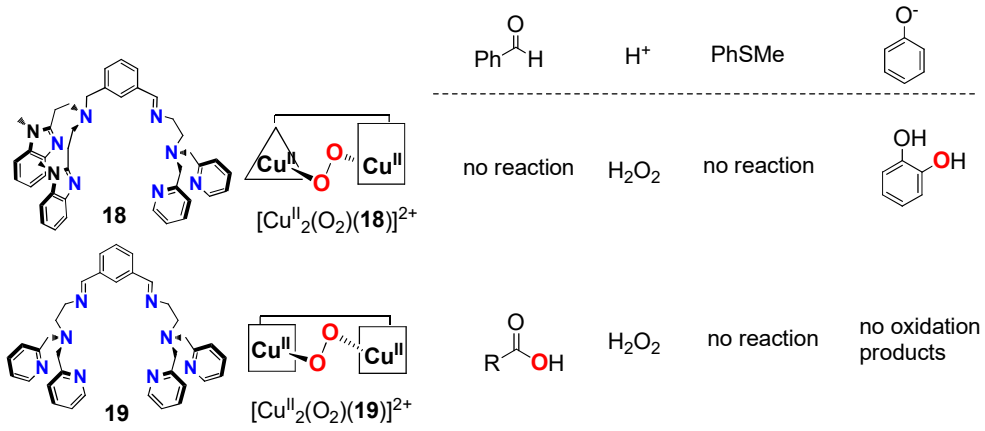

Figure I.6. Different reactivity of $[Cu^{II}_2(O_2)(\mathbf{18})]^{2+}$ compared to the symmetric $[Cu^{II}_2(O_2)(\mathbf{19})]^{2+}$.

I.3.4 Models for tyrosinase-like activity: hydroxylation of phenols

Karlin and co-workers reported in 1984 the first example of a ^{S}**P** species that was capable of hydroxylating an aromatic C-H bond.[68] They used a dicopper(I) complex in which the two copper centers are bound in tridentate sites connected through a *meta*-xylyl moiety ([Cu^{I}_2(**20**)]$^{2+}$, Scheme I.10). Upon reaction with O_2 at low temperatures, the formation of an intramolecular ^{S}**P** species was observed. By warming the sample up to room temperature, intramolecular hydroxylation of the *meta*-xylyl linker occurred. Mechanistic insight was gained by introducing electron-withdrawing groups in the aromatic ring. The decrease of the hydroxylation rate indicated that the reaction occurred through and electrophilic aromatic substitution mechanism, and permitted accumulation and spectroscopic characterization of the peroxide intermediate.[69]

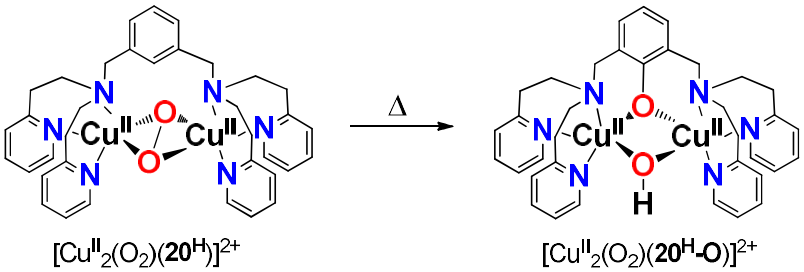

Scheme I.10. First reported aromatic hydroxylation by a Cu_2O_2 species.

As it has been mentioned before, structural changes in the ligand architecture can dramatically affect the reactivity of the resulting Cu_2O_2 species (or even hamper its formation).[33] Thus, replacement of the pyridines in Karlin's **20**^{H} ligand[68] by 1-methylimidazoles (**21**), Casella and co-workers made important progress in the field. Exposure of the dicopper(I) complex to O_2 at cryogenic temperatures afforded the formation of ^{S}**P** species (Figure I.7). Interestingly, no aromatic hydroxylation of the ligand was observed in this case. However, very remarkably this intermediate species reacted with 4-methoxyphenol affording the corresponding catechol product.[70,71] Labeling studies showed full incorporation of ^{18}O from $^{18}O_2$ into the final product. Thus, this represented the first example where a stable copper-dioxygen adduct was able to *ortho*-hydroxylate external phenolates, reproducing the activity of tyrosinase.

Inspired by these precedents, several examples of Cu_2O_2 systems that are able to perform *ortho*-hydroxylation of phenolates have been reported, including different Cu_2O_2 binding modes (Figure I.7).[26] Itoh and co-workers provided more insight about the capability of ^{S}**P** species to exhibit tyrosinase-like activity towards phenolates. [Cu^{II}_2(O)$_2$(**22**)$_2$]$^{2+}$, generated from reaction of two [Cu^{I}(**22**)]$^{+}$ monomers with O_2 in acetone at -94ºC, reacted with different phenolates to afford good yields of the catechol derivatives.[72] In a more recent example, Stack and co-workers reported the formation of a ^{S}**P** species by the strikingly simple self-assembling of imidazole rings, copper(I) and oxygen at -125ºC to form [Cu^{II}_2(O$_2$)(**23**)$_6$]$^{2+}$.[73] The structure of this model compound closely reproduced the first coordination environment in tyrosinase, and it could carry out the *ortho*-hydroxylation of various phenolates obtaining the catechol as major product.

A ^{S}**P** compound was also trapped by Stack and co-workers upon reaction of O_2 and a bidentate mononuclear copper complex $[Cu^{I}(\mathbf{24})]^{+}$ at -120ºC.[74] Very remarkably, upon addition of 2,4-di-*tert*-butylphenolate the authors spectroscopically detected a change in the nature of the Cu_2O_2 core from ^{S}**P** to **O** species (hence O-O cleavage occurred). These new **O** features subsequently decayed following a first-order process. Upon analysis of the oxidation products 30% of 3,5-di-*tert*-butylcatechol was found along with another 30% of the corresponding quinone. Thus, this example revived the dilemma whether the real executor of the hydroxylation reaction is a ^{S}**P** species or if this compound is in a left-lying equilibrium with the **O** species, which would be the true reactive compound.[74]

More evidence about the capability of **O** species to hydroxylate phenolates was reported by our group in 2008.[75] A dicopper complex was synthesized using a dinucleating ligand scaffold (**25**) that consisted in a *meta*-xylyl moiety connecting two tridentate sites. Upon reaction with O_2 at -90ºC the **O** species $[Cu^{III}_2(\mu\text{-}O)_2(\mathbf{25})]^{2+}$ was formed and fully characterized by several spectroscopic techniques. This intermediate was proved to be kinetically competent for the oxidation of phenolates to catechols. Interestingly, upon addition of the phenolate a new purple intermediate species was formed. Trapping and further characterization revealed that it corresponded to the phenolate bound to the Cu_2O_2 core prior to oxidation. In the same reactivity line, Stack and co-workers reported in 2009 the full characterization of another **O** species $[Cu^{III}_2(\mu\text{-}O)_2(\mathbf{26})_2]^{2+}$ that was able to *ortho*-hydroxylate 2,6-di-*tert*-butylphenolate in good yields.[76]

Finally, as detailed in section I.3.3. the *ortho*-hydroxylation of phenols to catechols can be also performed by an unsymmetric ^{T}**P** species reported by our group, $[Cu^{II}_2(O_2)(\mathbf{18})]^{2+}$. Thus, this Cu-dioxygen binding mode can also serve as a tyrosinase reactivity model.[65]

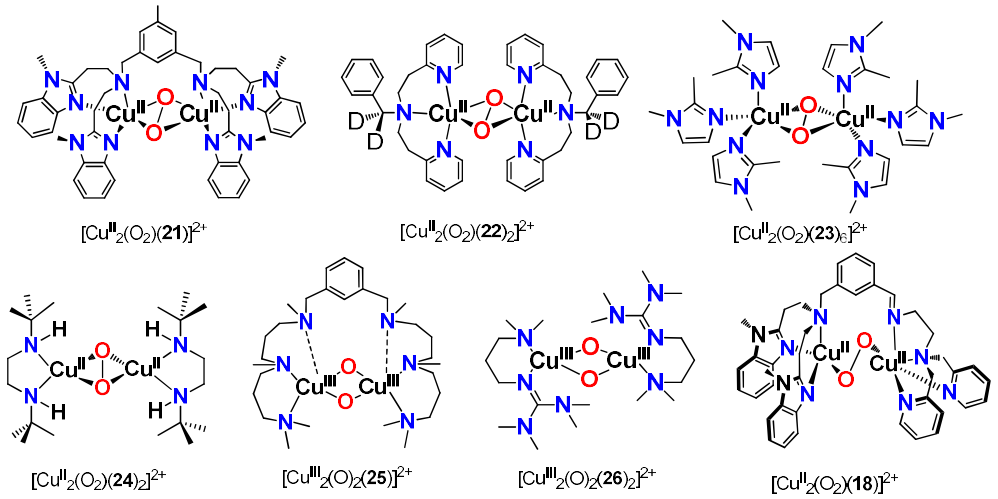

Figure I.7. Reported Cu_2O_2 systems that act as functional tyrosinase models.

To conclude, it is worth highlighting that a few examples of synthetic model compounds of tyrosinase have been proved to achieve significant catalytic phenol hydroxylation using oxygen (Figure I.8). Réglier and co-workers[77] reported the first example of catalytic phenol *ortho*-hydroxylation by using ligand **27**, 2 equivalents of copper(I) and 2,4-di-*tert*-butylphenol in the

presence of triethylamine and O_2. The formation of ~16 TN of 3,5-di-*tert*-butyl-*o*-quinone (per Cu_2O_2 unit) in one hour was accomplished. Shortly after this example, Casella and co-workers also reported catalytic behavior with compound $[Cu^{I}_2(\mathbf{21})]^{2+}$ on the oxidation of phenols containing electron-donating groups obtaining 1.2 TON of quinone.[78] Tuczek and co-workers reported in 2010 the first example of catalytic *ortho*-hydroxylation that started form a mononuclear copper(I) complex $[Cu^{I}(\mathbf{28})(MeCN)_2]^{+}$, NEt_3 and O_2 as oxidant. After the addition of 2,3-di-*tert*-butylphenol ~18 TN of 3,5-di-*tert*-butyl-*o*-quinone were produced,[79] albeit this system was around 10 times slower than Réglier's. More recent examples reported by Herres-Pawlis and co-workers[80] and Lumb and co-workers[81,82] showed great catalytic activity in *ortho*-hydroxylating a wide variety of phenols using Cu-polyamine complexes (bearing ligands **29** and **24** respectively) and O_2 as oxidant, in reactions with potential synthetic value.

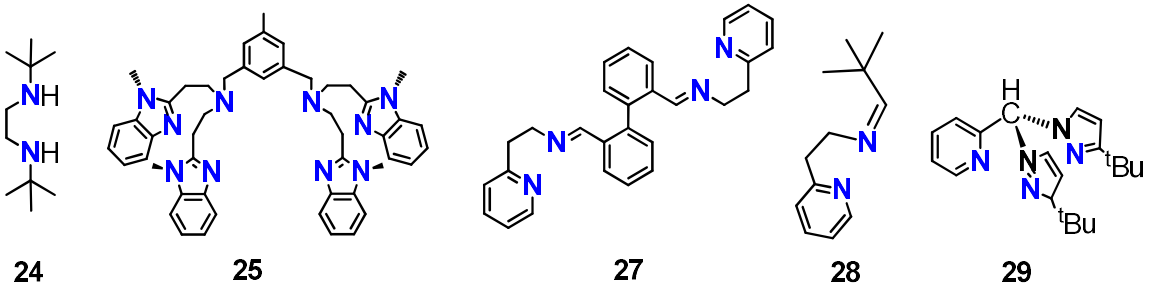

24 25 27 28 29

Figure I.8. Ligands used for catalytic phenol hydroxylation.

I.3.5 Oxygen activation through model systems for novel reactivities

A great amount of work has been directed towards the bioinspired oxidation/hydroxylation of C-H bonds, even though there is still a lot to be done to fully understand and control the mechanism of these transformations to give them synthetic use. Meanwhile, new parallel challenges have naturally emerged.

Carbon-fluorine bonds are often considered inert functionalities due to their high bond dissociation energy of 130 kcal mol^{-1}, representing the strongest single bond to carbon. Fluorinated organic products are commonly present in our everyday routine, representing up to 30% of agrochemical products and 20% of pharmaceuticals. Because of its inertness, fluorinated compounds show great thermal stability, enhanced lipophilicity and can suppress metabolic detoxification, thus increasing its *in vivo* residence time. Still, the large-scale production and application of these products has been increasing and nowadays they are subject of debate due to their potential toxicity, global warming potential, ozone depletion, environmental persistence, and bioaccumulation. For this reason, finding a way of degrading fluorinated organic compounds or even more interestingly, transforming C-F bonds into more

reactive functional groups, is a topic of current interest. However, such transformation constitutes a big challenge for conventional organic chemistry.[83,84]

Taking a look at natural systems, several enzymes are capable of cleaving C-F bonds[85] from both aromatic (e.g. fluorophenols or fluorobenzoates) and aliphatic substrates (e.g. fluoropyruvate, fluoroacetate). Cleavage and hydroxylation of aromatic C-F bonds normally occurs in aerobic organisms through the mediation of FAD-containing phenol hydroxylases, which convert 2-fluorophenols into catechols.[86,87] Cytochrome P450 and chloroperoxidase have been reported to oxidatively dehalogenate 4-fluorophenols[88], and methane monooxygenase can oxidize trifluoroethylene[89] In contrast, tyrosinase performs *ortho*-hydroxylation of phenols (section I.3.2.1), but fluorophenolates act as enzyme inhibitors.[90]

Regarding the use of model compounds, Karlin and co-workers reported in the early 90's the oxidative intramolecular dechlorination mediated by copper(I) complexes in the presence of a reducing agent and O_2 albeit in moderate yields (Scheme I.11 top).[91] Remarkably, the fluoro-substituted substrate analog only afforded traces of dehalogenated product. In the same line, one year later Feringa and co-workers reported intramolecular arene debromination of ligand **30** by copper-dioxygen species, yielding 80% of the hydroxylated ligand (Scheme I.11 bottom).[92]

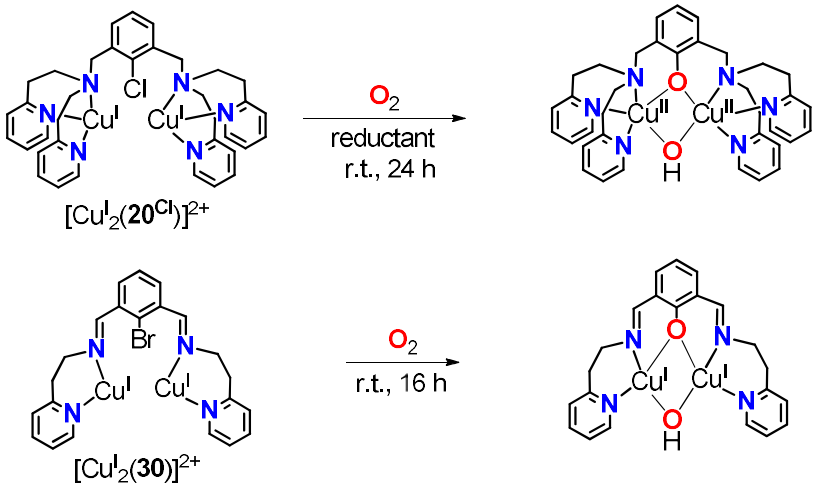

Scheme I.11. Intramolecular oxidative dehalogenation mediated by copper(I) complexes and O_2.

During the last couple of years, a few reports regarding the biomimetic functionalization of C-F bonds have been published. The first biomimetic example of defluorination reaction was reported in 2014 by us after observing that the bis(μ–oxo)dicopper(III) species [Cu$^{III}_2$(O)$_2$(**25**)]$^{2+}$ (**O**) was able to *ortho*-hydroxylate-defluorinate several fluorophenolates. These results will be further discussed in section VIII.2. Very recently three examples of iron-based model compounds proved to be competent for the cleavage of C-F bonds. Goldberg and co-workers reported the ability of a detectable nonheme pentadentate oxoiron(IV) to cleave an aromatic C-F bond from the ligand framework **31** through an electrophilic mechanism (Scheme I.12 top). In this context, Agapie and co-workers reported one year later an example of a tetranuclear iron complex that could intramolecularly cleave an aromatic C-F bond of ligand **32** (Scheme I.12

bottom). However, in this case no intermediate species could be observed and only the final reaction product was characterized.

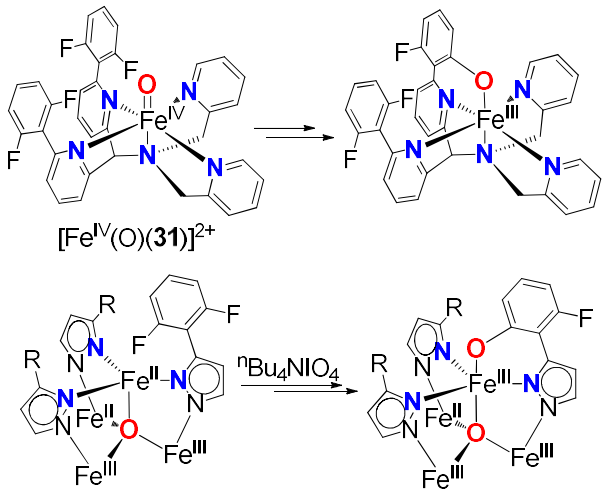

Scheme I.12. Intramolecular C-F cleavage by nonheme oxoiron(IV) compounds.

Finally, the first example of an iron-based complex capable of performing intermolecular aromatic C-F bond cleavage was reported by Sorokin and co-workers in 2014. A μ-nitrido diiron phthalocyanine complex [(**33**)Fe^{III}(μ-N)Fe^{IV}(**33**)]$^{4+}$ reacted with poly- and perfluorinated aromatics under mild conditions using H_2O_2 or tBuOOH as oxidant to give the hydroxylated-defluorinated product (Scheme I.13).[93] The reaction was proposed to occur via the generation of a high-valent diiron phthalocyanine radical cation complex with fluoride axial ligands.

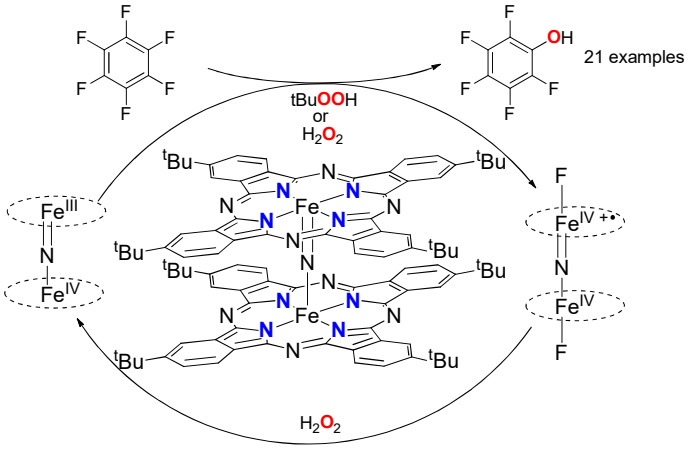

Scheme I.13. Intermolecular C-F cleavage by [(**33**)Fe^{III}(μ-N)Fe^{IV}(**33**)]$^{4+}$.

I.4 Oxidation reactions mediated by iron

I.4.1 Biological relevance of iron

Iron is the most abundant metal on earth. It is silver-white in pure form, but rusts easily. Iron is found in all living organisms, and while maybe it is best known for its task in O_2 transport in red blood cells (hemoglobin), it also plays other extremely important roles in a wide range of functions in natural systems. Iron is found in the active site of several enzymes in a wide range of oxidation states although the most common are Fe^{II} and Fe^{III}. Higher valent iron centers (Fe^{IV} and Fe^{V}) have been seldom detected but frequently postulated as reactive intermediate species in selected biological processes. Among all the functions associated with iron enzymes, especially interesting for the purpose of this thesis is the oxygenation of hydrocarbons. Oxygenation of nonactivated alkyl C-H bonds is a very challenging reaction owing to their notorious chemically inert character. Consequently, activation of such bonds requires highly reactive species. In nature, C-H hydroxylation is mainly performed by iron-dependent enzymes, which create highly electrophilic species via the finely controlled partial reduction of the O_2 molecule.

I.4.2 Dioxygen activation at iron proteins

Iron-containing metalloenzymes are found throughout the natural world and participate in vital catalytic oxidative processes and biosynthetic biological pathways involving O_2 activation.[94,95] As a result of the efforts of several research groups over the last decades, the structure of the active site of O_2-activating iron-containing metalloenzymes has been elucidated. In some cases, also the active iron-oxygen species have been trapped and spectroscopically characterized (Figure I.9). According to these studies, iron oxygenases can be classified in three main groups depending on the structure of the active site: heme (e.g. cytochrome P450), mononuclear nonheme (e.g. taurine dioxygenase, TauD) and dinuclear nonheme oxygenases (e.g. soluble methane monooxygenase, sMMO[96]) (Scheme I.14). Interestingly, most of the gathered knowledge on iron enzymes involved in dioxygen activation originates from the pioneering studies in heme enzymes, in which the iron center is coordinated to a porphyrin cavity. Over the last 20 years much effort has been directed towards the study of nonheme systems, which are of important biological relevance and it has been found that remarkable similarities exist in the reaction mechanism of heme and nonheme systems.[97-99]

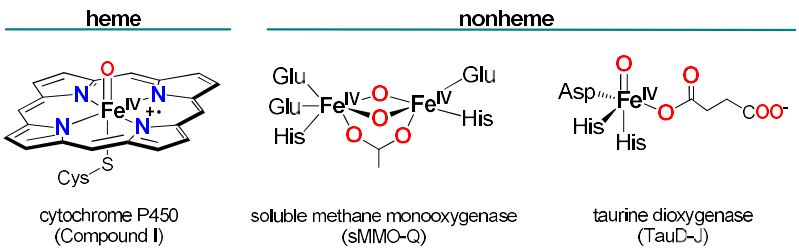

Figure I.9. Representative examples of spectroscopically characterized heme and nonheme iron-oxygen species in enzymes.

Heme and nonheme iron-dependent oxygenases catalyze an array of extremely challenging oxidative transformations with high catalytic efficiencies and selectivities.[100-102] Cytochrome P450 and Rieske oxygenases are probably the most studied examples within these two families of iron oxygenases and they will be discussed in more detail in the following sections.

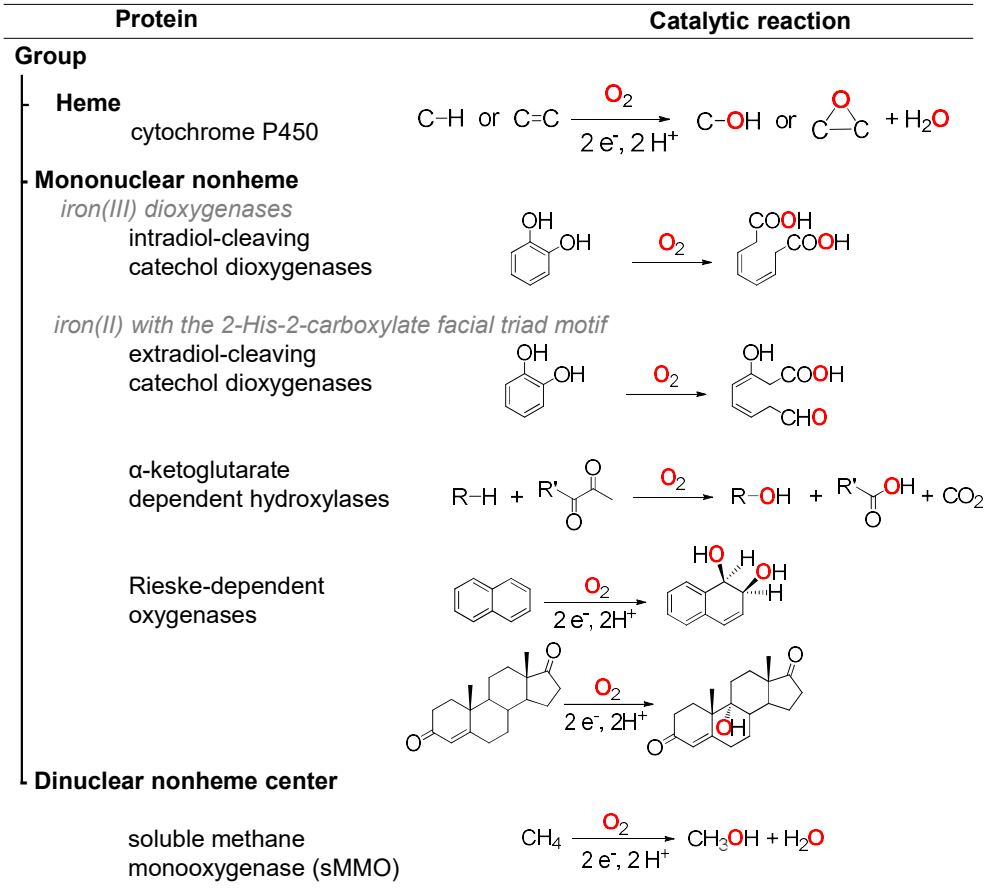

Scheme I.14. Representative examples of iron oxygenases and the reaction they catalyze.

I.4.2.1. Cytochrome P450

One of the most representative examples of heme enzymes is the cytochrome P450 family (cyt-P450), which is present in nearly all living systems. Cyt-P450s are capable of reductively activating O_2 to generate species that are active towards the oxidation of a wide range of organic substrates. X-ray analysis of their active site revealed that it is constituted by an iron center in an octahedral geometry bound to a porphyrin unit in the equatorial plane with axial positions occupied by a water (or hydroxide) molecule and a cysteinate ligand, which connects the active site to the protein backbone.[101] Cyt-P450s have been studied since the 1950s and nowadays their activity and catalytic cycle are quite well established (Scheme I.15a).[101,103-105] Starting from the hexacoordinate low spin iron(III) compound, binding of a substrate in the surroundings of the active site causes the dissociation of the water molecule leaving a high-spin

5-coordinate iron(III) complex which is then reduced by one electron to a Fe^{II} center.[106] At this point, the metal binds dioxygen leading to the formation of a superoxo unit which evolves to iron(III)-hydroperoxo after a second one-electron reduction and protonation. Then, a proton assists the heterolytic O-O bond cleavage to release a water molecule and form a highly reactive oxoiron(IV) cation radical $(Porph^{\bullet+})Fe^{IV}(O)$ (Compound I, Cpd I, Figure I.9) which is proposed to be the real active species. At this stage oxidation of the substrate occurs through the so-called "rebound mechanism" first proposed by Groves.[107,108] This is a two-step process that starts with the abstraction of the hydrogen atom of the substrate by the oxo moiety so that an alkyl radical (short-lived) is formed. This will then rapidly react with the Fe–OH moiety to afford the final product (*rebound*, Scheme I.15b). Release of the oxidized organic substrate regenerates the initial iron(III). Even though Cpd I was long being proposed as the final executor of the substrate oxidation, it was not until recently that Green and co-workers[109] could trap and spectroscopically characterize this species in a cyt-P450 mutant.

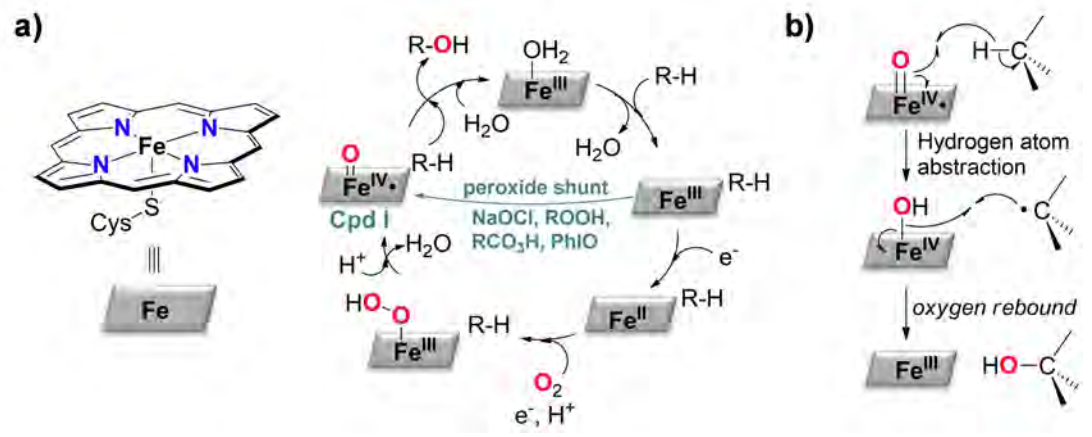

Scheme I.15. a) Proposed catalytic cycle for cyt-P450s. **b)** Postulated oxygen rebound mechanism for C-H hydroxylation in cyt-P450s.

I.4.2.2 Rieske oxygenases

In contrast to cyt-P450s, Rieske oxygenases are less understood. The ligand environment for these enzymes is more flexible compared to heme systems, thus allowing a more diverse chemistry. Indeed, they are involved in a wide range of reactions including sulfoxidation, desaturations, oxidative carboyclizations,[110] or O- and N-dealkylation.[111-113] Even more interestingly, they catalyze the selective C-H hydroxylation and stereo- and enantioselective *cis*-dihydroxylation of arenes and olefins, a reaction that is difficult to achieve through conventional organic synthesis and not observed for any other enzyme class.[114,115] Recently, it was found that Rieske oxygenases are also involved in the cholesterol catabolism and also in antibiotic biosynthetic pathways.[116]

Naphtalene 1,2-dioxygenase (NDO) is probably the most studied enzyme in this family, and its structure is representative for other enzymes such as benzoate 1,2-dioxygenase, toluene 2,3-dioxygenase, benzene dioxygenase, phthalate dioxygenase and dicamba monooxygenase.[113]

X-ray characterization of NDO isolated from *Pseudomonas putida* revealed that different components can be distinguished in its active site (Scheme I.16a).[117] The first one is the oxygenase component. It consists of an octahedral mononuclear nonheme iron(II) center which, in its resting state, is bound to two histidine residues and one aspartate occupying the same face of the octahedron.[117,118] This structural feature is known as the 2-His-1-carboxylate facial triad and it is characteristic of this class of enzymes.[119] It leaves three coordination sites on the metal available for interaction with exogenous molecules such as substrates and O_2. The coordination sphere of the iron in the resting state is completed by three water molecules. The other components of the active site are a Fe_2S_2 Rieske-type cluster that acts as a reductase and mediates electron transfer from NAD(P)H to the oxygenase site, and an aspartate residue that binds the oxygenase and reductase components.[116,117]

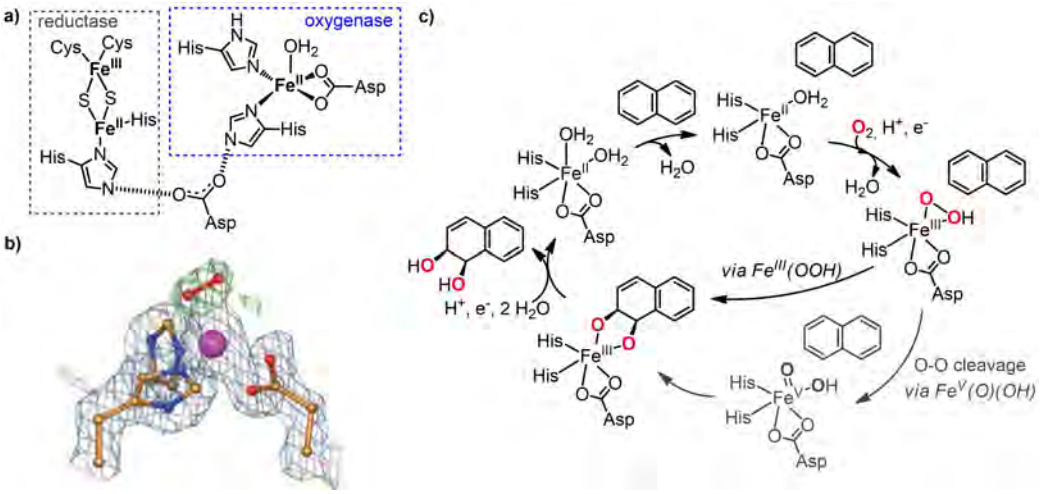

Scheme I.16. a) Schematic representation of the active site of napthalene 1,2-dioxygenase. **b)** X-ray structure of O_2-bound oxygenase component of NDO.[120] **c)** Proposed catalytic cycle of naphtalene 1,2-dioxygenase.

Despite considerable efforts have been directed towards gaining structural and spectroscopic insight into the catalytic cycle of Rieske oxygenases, not all reaction steps have been fully elucidated.[116] Ramaswamy and co-workers shed some light in 2003 by solving a nice set of crystal structures of NDO at different stages of its catalytic cycle: substrate bound in the active site cavity, oxygen coordinated to the metal center, and the final oxidized product ligated to the iron.[120] From these studies, a consensus has been reached about the mechanism of action of these enzymes (Scheme I.16c). In a first step, coordination of the substrate results in the loss of a water molecule leading to a 5-coordinated ferrous complex. O_2 then bounds to the metal and it is reduced to the peroxo state upon protonation to yield an (hydro)peroxoiron(III), as determined by X-ray analysis (Scheme I.16b).[115] Another crystallographically characterized example of hydroperoxoiron(III) species has recently been obtained for another Rieske-dependent oxygenase (carbazole 1,9a-dioxygenase).[121] This Fe^{III}(OOH) is the last detectable intermediate species before substrate oxidation occurs. At this point, there is an ongoing debate. This

species either directly attacks the arene double bond of the substrate or undergoes O-O cleavage, thus isomerizing to a very reactive high valent $Fe^{V}(O)(OH)$ that would be the real executor of the reaction. Even though a number of experimental and theoretical studies have been carried out, the discussion about whether $Fe^{III}(OOH)$ is directly responsible for substrate oxidation or not is still ongoing.[99,122,123] DFT calculations by Decker *et al*.[124] and Neese *et al*.[125] showed that $Fe^{III}(OOH)$ could be competent for the oxidation, while Kumar *et al.*[126] proposed that it is merely a precursor of the real active species. However, direct evidence for the high valent electromer has not been obtained in natural systems so far. On a last step, the oxidized substrate is uncoupled from the ferric center by protonation, regenerating the initial ferrous resting state.

I.4.3 Bioinspired nonheme iron complexes for oxidation catalysis

In contrast to copper-based model systems for O_2 activation, very few mononuclear iron(II) complexes are able to directly activate O_2 analogously to nonheme iron oxygenases. Indeed, iron(II) complexes coordinated to trispyrazolylborate (Tp, $\mathbf{3^R}$) ligands are the most successful compounds that carry out the reductive activation of O_2, akin to the activity of enzymes. They were first used for biomimetic purposes by Lippard and co-workers to mimic the tris(histidine) coordination environment found in the active site of hemerythrin, a diiron protein responsible for O_2 transport in some invertebrates.[127] This ligand system also allowed Kitajima and co-workers to trap relevant copper-dioxygen intermediate species (see section I.3.3.1). The basic Tp structure consists of an anionic tridentate and tripodal ligand bearing three pyrazole rings connected to a boron center (through one of the nitrogen atoms of the heterocycle). In order to accomplish O_2 activation, Tp-based iron(II) complexes often contain a complementary ligand that provides two electrons necessary for O_2 reduction (analogously to the cofactor in enzymes). Such strategy has been especially useful to mimic $(His)_3Fe$-type active sites such as those found in cysteine dioxygenase or acetyl acetone dioxygenase. Interestingly, Tp ligands have recently been used to structurally reproduce iron enzymes containing the 2His-1-carboxylate facial triad, particularly 1-aminocyclopropane-1-carboxylic acid oxidase, which produces ethylene from 1-amino-cyclopropane-1-carboxylic acid in the presence of ascorbate as reducing agent. The first model for this enzyme was provided by Limberg, Simaann and co-workers in 2015 (Scheme I.17), who observed that upon exposure of $[Fe^{II}(\mathbf{3^{Me,Ph}})(ACC)]$ to O_2 at 70ºC, 17% of ethylene was produced (with respect to the initial complex), which is a remarkable result taking into account that the enzyme produces only 35% under single turnover conditions.[128] The use of H_2O_2 enhanced the yield up to 68%. Even though Tp-based complexes nicely reproduce the structure of nonheme iron enzymes and their function, the application of such systems in oxidation catalysis has been scarce as they show limited turnover.

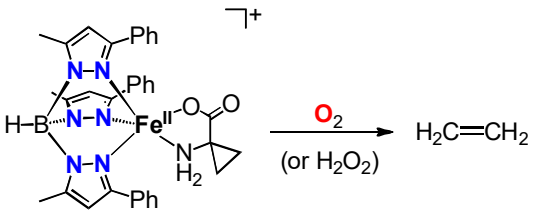

Scheme I.17. Reactivity of [Fe^{II}(**3**^{Me,Ph})(ACC)] with O_2 to give ethylene.

Interestingly, there is a wide library of other bioinspired iron-based model systems that reproduce the activity of iron oxygenases using O_2-activated forms such as peroxides or peracids in a catalytic fashion, albeit the structural similarities with the enzyme active sites are less accurate than in Tp-systems. In particular, mononuclear nonheme iron complexes with tetradentate nitrogen-based ligands act as efficient catalysts in the oxidation of alkanes and alkenes with high chemo- and stereoselectivities, thus reproducing the activity of Rieske oxygenases.

Sir Derek Barton reported during the 80's that the combination of iron salts and hydrogen peroxide (H_2O_2) in pyridine/acetic acid afforded hydrocarbon oxidation.[129] The involvement of a high-valent oxoiron(V) species was already proposed at that time by analogy to heme systems. This discovery was the starting point for the development of bioinspired nonheme iron complexes for hydrocarbon oxidation.

A breakthrough in the field was reported by Que and co-workers back in 1997: the first example of the well-defined nonheme iron(II) catalyst [Fe^{II}(**2**)$(CH_3CN)_2$]$^{2+}$ capable of performing the stereospecific oxidation of unactivated C-H bonds using H_2O_2 (see Figure I.10 for ligand structure).[130,131] After this remarkable precedent, the landscape of oxidations by nonheme iron complexes has grown to an extent that progressively more challenging oxidations have been achieved, which has resulted in significant improvements in both reaction selectivities and yields. This dramatic progress in the catalytic activity is, of course, directly related to a deeper knowledge on mechanistic aspects. In the following section, the most successful examples of bioinspired nonheme iron catalysts and details on their mechanism of action will be discussed.

I.4.3.1. Catalytic stereospecific C-H and C=C oxidation

Taking inspiration from nature, selected nonheme iron complexes have been developed that elicit site-selective and stereoretentive C-H bond oxidation upon reaction with H_2O_2. Selectivity and stereospecificity exhibited by these catalysts provide strong support in favor of the intermediacy of metal-based oxidants akin to those involved in iron-dependent oxygenases. Presumably because of their high reactivity, these oxidants do not accumulate in solution, and it is challenging to establish their nature.

The stereospecificity shown by the system presented by Que in 1997 was proposed to be induced by the nitrogen-based tetradentate ligand **2** (Figure I.10) that afforded an iron center with two free *cis*-oriented coordination sites.[132] After **2**, other iron complexes based on N-donor

tetradentate ligands that wrap around the metal center in a similar manner have been reported as efficient catalysts for the stereospecific C-H oxidation of alkanes to alcohols (see Figure I.10 for ligand structures described in this section).[5,98,133-135] Thus, excellent selectivities were obtained using $[Fe^{II}(L)(X)_2]^{2+}$ (L = **2**^{5Me} and **2**^{6Me},[97] **34**,[97] **35**,[131] **36**,[136] **37**,[137,138] or **38**,[139,140]), albeit these examples are far from being practical due to the large excess of substrate (relative to the oxidant) required to maximize oxidant conversion and minimize product overoxidation reactions.

A milestone work in the topic was reported by Chen and White in 2007.[140] By using $[Fe^{II}(\mathbf{39})(CH_3CN)_2]^{2+}$, H_2O_2 as oxidant and acetic acid as additive, hydroxylation of unactivated C-H bonds in synthetically useful yields and predictable selectivities was achieved. Moreover, the system was able to discriminate among multiple C-H bonds in complex molecules such as natural products, so that the most electron-rich and less sterically hindered C-H bond was preferentially hydroxylated.[140,141]

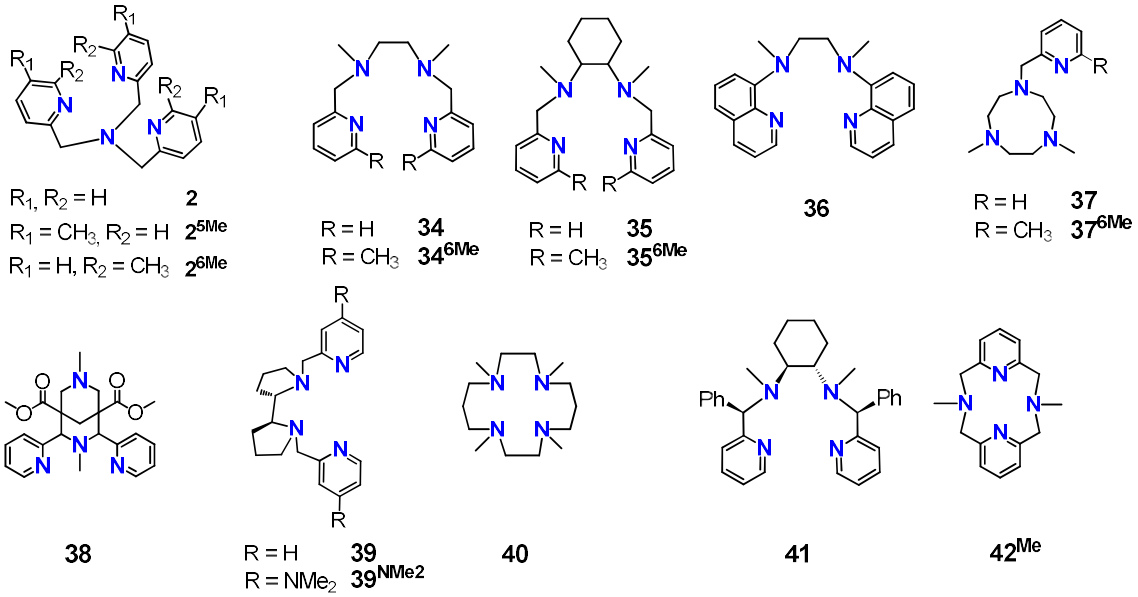

Figure I.10. Selected tetradentate nitrogen-based ligands used for iron-catalyzed C-H and/or C=C oxidation.

Synthetic nonheme model systems can also mediate the oxidation of olefins giving mainly two products, namely epoxides and *cis*-diols. Valentine and co-workers reported the first example of selective olefin epoxidation catalyzed by an iron complex $[Fe^{II}(\mathbf{40})(CH_3CN)_2]^{2+}$ and H_2O_2.[142] A remarkable work was reported by White and Jacobsen in 2001 using $[Fe^{II}(\mathbf{34})(CH_3CN)_2]^{2+}$ as catalyst, H_2O_2 as oxidant and acetic acid as a key additive.[143] This combination led to the production of epoxide from aliphatic olefins in high yields (up to 90%) and short reaction times (~5 min). Because of the growing interest in obtaining chiral compounds, the topic turned towards asymmetric epoxidation. Several works have showed that the use of chiral versions of the ligands can translate into the production of chiral epoxides with good enantioselectivities. The most successful family of iron catalysts developed so far for asymmetric epoxidation are

those based on tetradentate ligands with a bis-amine-bis-pyridine (or related heterocycle) structure.[144] Chiral modifications are commonly applied either in the backbone of the ligands or in the pyridine ring, which results in fine tuning of electronic or steric properties, that are determinant to decisive to reach high enantioselectivities. Following this strategy, Sun and co-workers reported the first remarkable example of enantioselective epoxidation of *trans*-chalcones using an iron(II) complex based on the N_4-ligand with a chiral cyclohexane diamine backbone $[Fe^{II}(\mathbf{41})(CH_3CN)_2]^{2+}$ and H_2O_2/AcOH, obtaining enantionmeric excesses up to 71%.[145] Later, Cussó *et al*. presented the system that so far affords the best performance in asymmetric epoxidation. They used $[Fe^{II}(\mathbf{39}^{NMe2})(CH_3CN)_2]^{2+}$ and H_2O_2 in the presence of carboxylic acids and obtained excellent enatioselectivities in synthetically valuable yields for the oxidation of different olefins.[146] Further studies by the same authors showed that this catalyst also tolerates protected amino acids instead of carboxylic acids as co-ligands thus representing a step forward towards the design of biologically inspired oxidation catalysts.[144]

As stated above, Rieske oxygenases perform the *cis*-dihydroxylation of C=C double bonds with very high selectivity and efficiency.[114] The combination of $[Fe^{II}(\mathbf{2}^{5Me})(CH_3CN)_2]^{2+}$ and H_2O_2 constitutes a good functional model of this transformation, as it catalyzes the oxidation of olefins to *cis*-diols under conditions of limiting substrate with high conversions and yields.[147] Prat *et al*. reported that the introduction of methyl groups in the α position of the pyridine ring in the pyridine-substituted 1,4,7-triazacyclonane ligand ($\mathbf{37}^{6Me}$) afforded olefin oxidation with a syn-diol:epoxide ratio of ~6:1 in synthetically useful yields.[148] Indeed, the development of chiral iron-based *cis*-dihydroxylation catalysts is also a topic of big interest. Que et *al.* reported in 2001 the first example of enantioselective *cis*-dihydroxylation of olefins in good enantiomeric excesses (ee) using $[Fe^{II}(\mathbf{34}^{6Me})(CH_3CN)_2]^{2+}$ and $[Fe^{II}(\mathbf{35}^{6Me})(CH_3CN)_2]^{2+}$, albeit the excess substrate used limited the synthetic utility of these systems.[149] In a later work Que and co-workers achieved up to 97% ee for the *cis*-diol in the oxidation of *trans*-2-heptene.[150]

Overall, these bio-inspired mononuclear nonheme iron(II) complexes for hydrocarbon oxidation using benign oxidants constitute an attractive environmentally friendly alternative to traditional stoichiometric oxidants. However, their use at industrial scale is still limited and one of the big challenges in this research area is the development of methodologies with improved catalytic performance, with the final aim of scaling-up these reactions and making them practical.[151] In this line, an encouraging result is the recent report by Che and co-workers which showed that $[Fe^{III}Cl_2(\mathbf{42}^{Me})]^{+}$ catalyzed in less than 10 min the *cis*-dihydroxylation of olefins at ~10 g scale using oxone as oxidant.[152] Gebbink and co-workers made progress in the same direction when they developed a more affordable epoxidation by scaling up the reaction using $[Fe^{II}(\mathbf{39})(CH_3CN)_2]^{2+}$ as catalyst. They carried out a multi-gram scale catalyst synthesis and they reduced the amount of acid to less than 2 mol% in the catalytic C=C oxidation, achieving ~1000 TON of epoxide as the single product.[153] Further understanding of why and how catalysts deactivate after certain activity will presumably be a key issue to further advance in this field.

I.4.3.2 Mechanism of action of nonheme iron catalysts in hydrocarbon oxidation

Basically two mechanisms have been proposed for catalytic hydrocarbon oxidation by synthetic nonheme iron compounds. In both cases the oxidant promotes the initial oxidation of the iron(II) precursor to iron(III)(OOR) (R = H, alkyl, acyl) species. This species then undergoes O-O cleavage (aided by either water or an acid) to form a high valent species, namely an oxoiron(V) species, which is responsible for substrate oxidation (Scheme I.18). Evidences for this mechanistic proposal have been gathered through the use of specific substrates that provide certain information of the catalytic system, the so-called mechanistic probes. Alternatively, despite being relatively poor catalysts, the use of iron complexes that stabilize the reactive species formed along the catalytic cycle of nonheme iron oxygenases has also resulted extremely informative.

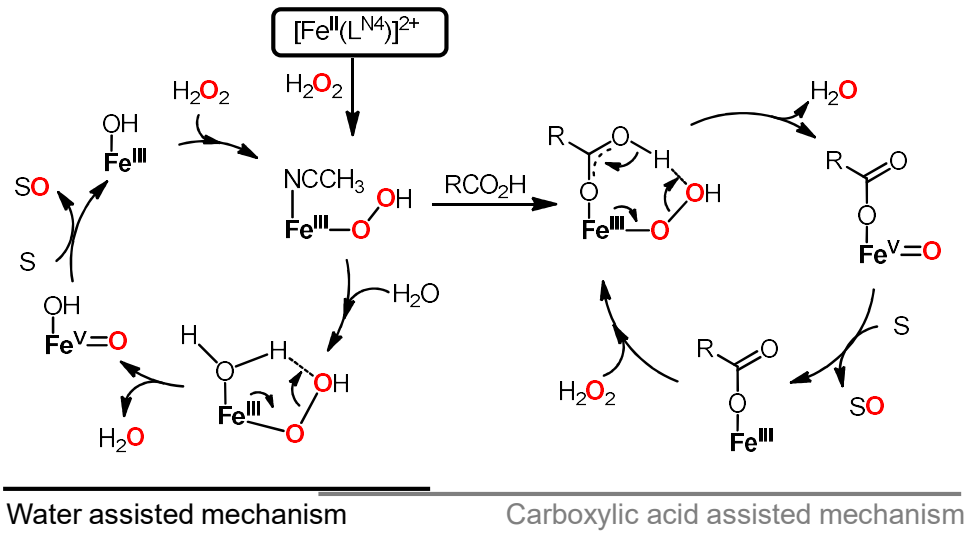

Scheme I.18. Water- and carboxylic acid-assisted mechanisms for hydrocarbon (alkanes or alkenes) oxidation by mononuclear nonheme iron enzymes. L^{N4} = nitrogen-based tetradentate ligand with *cis*-positions available (see Figure I.10 for ligand structures).

I.4.4 Gaining mechanistic insight into nonheme iron-oxygen oxidations: indirect and direct evidences

> *"The only way that we can explain these results is by a hypothesis that the reagent that oxidizes the hydrocarbon is present in a dormant form (Sleeping Beauty) until it collides with the saturated hydrocarbon (the Prince) and reacts with a saturated C-H bond (the kiss) to form the real reagent, which immediately gives the iron-carbon bond (…) The hydrocarbon should be inducing in the (formally) Fe^{V}=O species a change that makes possible such an unusual reaction."*
>
> D.H.R. Barton, 1992[129]

The best way of getting mechanistic insight about the species involved in a catalytic cycle is their separate characterization. This involves their detection and ideally isolation from the crude reaction mixture in order to submit the sample to an array of spectroscopic techniques or X-ray crystallography to unravel their nature.[154] Unfortunately, in most cases this is not possible because the catalytic intermediate species are unstable and rapidly react to form other compounds. Thus, they usually cannot be isolated and have to be studied while the reaction occurs. The improvement and development of several spectroscopic techniques has greatly contributed to trap and characterize iron-oxygen species that accumulate in solution (even if more than one species is present). Thus, electron paramagnetic resonance (EPR), Mössbauer, Raman, X-ray absorption spectroscopy (XAS) and mass spectrometry among others serve as excellent characterization tools of reactive catalytic intermediates. There is still another scenario, the one in which the given species does not accumulate in enough quantity in solution. If this is the case, no spectroscopic analysis can be performed to unravel its nature. Therefore, clues about the nature of the active species are acquired through indirect methods, such as the study of its reactivity using specific substrates (see section I.4.4.1) and/or computational methods. Such methodology is commonly used to get insight into the mechanism of hydrocarbon oxidation.

I.4.4.1 Mechanistic probes

The use of H_2O_2 in combination with iron is often associated to the formation of hydroxyl radicals (Fenton chemistry) which are highly reactive but also unselective oxidants, making them undesirable compared to the highly selective metal-based processes. *Mechanistic probes* are specially designed hydrocarbon substrates to provide insight into the nature of the oxidant species.[155] Analysis of the distribution of the oxidized products derived from these substrates at the end of the reaction affords valuable information about the oxidizing power of the active species and the participation or not of free diffusing radicals. Some examples of the most common mechanistic probes are listed below.

- Kinetic isotope effect (KIE)

Especially interesting for hydrogen-atom abstraction mechanisms, KIE experiments provide information about the involvement of the hydrogen atom in the rate determining step of the reaction. Determination of KIE values consists in a competition reaction between the substrate (*e.g.* cyclohexane, toluene,…) and its deuterated analog containing C-D bonds which are ~1.7 kcal mol^{-1} stronger than C-H (Scheme I.19). Because of their high oxidative power, reactions executed by hydroxyl radicals show KIE values between 1 and 2[156] whereas in metal-based oxidants higher values are obtained, with a theoretical maximum of 7.[155] However, larger KIEs have been reported for cyt-P450 (>11)[157] and methane monooxygenase (50-100),[158] which have been rationalized by invoking tunneling effects.

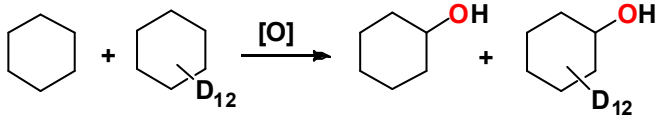

[O] species	KIE
·OH	1-2
cyt-P450	>11
MMO	50-100

Scheme I.19. Competition experiment between cyclohexane and deuterated cyclohexane for KIE determination.

- Regioselectivity

Adamantane is a suitable organic substrate for testing the regioselectivity of a given species because it contains both secondary and tertiary C-H bonds. The selectivity is calculated by quantifying the oxidized products and dividing the amount of 1-adamantanol by the sum of 2-adamantanol + 2-adamantanone (and multiplied by 3 to normalize the ratio of secondary C-H bonds with respect the tertiary). If free radicals are present, very low $3^{ary}/2^{ary}$ ratios are obtained (around 2 in the case of hydroxyl radicals), indicating that there is essentially no preference for the oxidation of the weaker 3^{ary} bonds (Scheme I.20). On the other hand, for metal-based oxidation reactions high $3^{ary}/2^{ary}$ ratios have been found (up to 48 in the case of cyt-P450[159]).

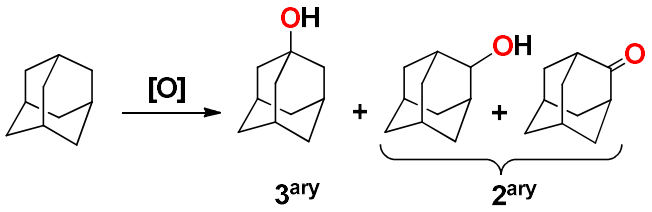

[O] species	$3^{ary}/2^{ary}$
·OH	2
cyt-P450	48

Scheme I.20. Possible products derived from adamantane oxidation.

- Alcohol/ketone ratio (A/K)

The oxidation of a secondary C-H bond, such as those of cyclohexane, can also give indications about the presence of long-lived free diffusing radicals. If a long-lived carbon radical is formed on the 2^{ary} carbon of the substrate, this is trapped by O_2 thus giving an alkylperoxyl radical. Reaction of two alkylperoxyl radicals results in a Russell-type termination step that affords equimolar amounts of alcohol and ketone.[160] In sharp contrast, short-lived alkyl radicals generated during a metal-based mechanism react immediately with the oxidant to form mainly the alcohol product (Scheme I.21).

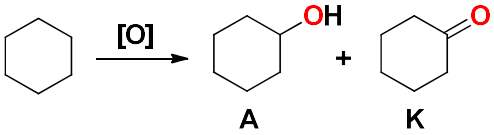

[O] species	A/K ratio
·OH	1
metal-based	mainly A

Scheme I.21. Oxidation of cyclohexane to give cyclohexanol and cyclohexanone.

- Stereospecificity: radical lifetime probes

The lifetime of an alkyl radical can be studied through the oxidation of substrates such as the *cis* and *trans* isomers of 1,2-dimethylcyclohexane and decalines. The radical on the 3^{ary} carbon of these substrates are known to epimerize.[155,161] Thus, reactions involving long-lived radicals afford both *cis* and *trans* alcohols (after C-O bond formation) in a ratio around 1.[161] In contrast, short-lived radicals, such as those involved in metal-based oxidations, give much faster rebound (or even concerted mechanisms), so that the radical in the 3^{ary} carbon of the substrate does not epimerize and the original configuration is retained upon alcohol formation (Scheme I.22). This experiment can also be performed for olefinic substrates using *cis*-alkenes and analyzing the *cis*- or *trans*- configuration in the epoxide products.

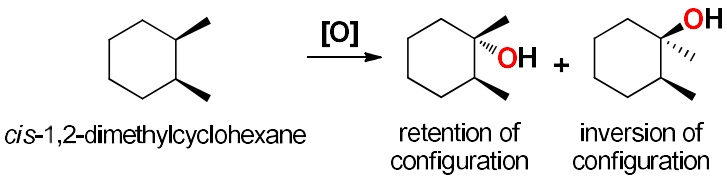

[O] species	retention of configuration
·OH	no
metal-based	yes

Scheme I.22. Isomers obtained in the tertiary C-H hydroxylation of *cis*-1,2-dimethylcylohexane.

- Electronic effects

In order to gain insight into the electro- or nucleophilicity of the species involved in the oxidation of C-H bonds, White and co-workers designed a series of 1-substituted 3,7-dimethyloctane alkane substrates.[162] These linear alkanes contain two 3^{ary} C-H bonds with different electronic properties because of the effect induced by the presence of an electronwithdrawing group X (X = Br, F, OAc) closer to one of them. Preferential oxidation of the remote 3^{ary} C-H (*distal*, D) rather than the one closer to the Br group (*proximal,* P) indicates the involvement of an electrophilic active species, and vice-versa (Scheme I.23). Indeed, when X = H, no preference for any of the two was observed.

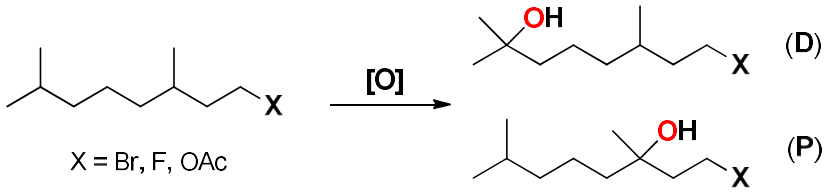

Scheme I.23. Alcohols obtained in the hydroxylation of tertiary C-H bonds of 1-substituted 3,7-dimethyloctane.

- Steric effects

Selectivity can also be induced by steric factors. 1,1-dimethylcyclohexane contains three energetically similar 2^{ary} C-H bonds, with markedly different steric hindrance. Analysis of the oxidation products after oxidation of this substrate gives information about the preference of the oxidant for attacking less sterically hindered positions (Scheme I.24).

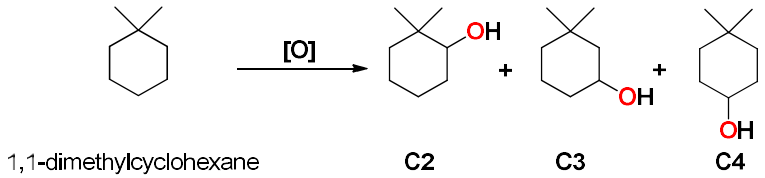

Scheme I.24. Possible alcohol products obtained in the hydroxylation of 1,1-dimethylcyclohexane.

- Labeling studies

Labeling experiments are used to unravel the origin of the oxygen atom in the final oxidized product, which may be directly related to the reaction mechanism. Since O_2 traps long-lived carbon-centered radicals at diffusion control rates, high levels of 18-oxygen incorporation into products when $^{18}O_2$ is present are associated with oxidants that produce free diffusing carbon-centered radicals. Interestingly, metal-oxo intermediates are known to exchange their oxygen atom with water through the so-called “oxo-hydroxo tautomerism” (Scheme I.25). This process consists in a rapid shift of two protons and one electron from a hydroxo ligand to the oxo group, thus the former ending up as an oxo moiety. If metal-oxo species are involved in the reaction, the oxidized product ends up partially labeled when ^{18}O-labeled water is present in the reaction

medium. Instead, if no labeling is observed, the involvement of such species cannot be ruled out, as the rate of water exchange with the oxo moiety might be slower than the oxidation event.[163]

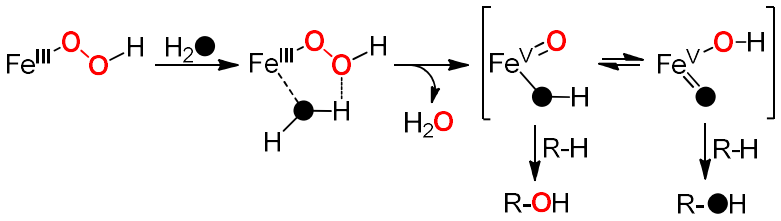

Scheme I.25. Incorporation of an oxygen atom fom water into hydroxylated products through an oxo-hydroxo tautomerism in an oxoiron(V) species.

I.4.4.2 Trapping mononuclear nonheme iron-oxygen species relevant to iron oxygenases

Over the last two decades the use of cryogenic methods has produced great advances towards the entrapment and characterization of novel iron-oxygen species. This has greatly contributed to unravel the nature of the reactive species involved in oxidation reactions. In this context, several mononuclear nonheme iron-oxygen species with various oxidation states at the iron (and different degrees of reduction of the oxidant) have been detected. Their relevance in oxidation reactions have been interrogated (Figure I.11)[99,100,164] and significant analogies between these compounds and iron oxygenases have also been established.

Formation of superoxoiron species is the first step proposed for the activation of O_2 by iron oxygenases. However, these species are generally regarded as pass-through points towards the generation of more oxidized metal species. In contrast to heme systems,[165] their characterization in nonheme enzymes has been scarce.[164,166,167] Similarly, very few synthetic models of nonheme superoxoiron species are available,[168-170] most probably because once formed, they undergo one-electron reduction to form peroxoiron(III) species. This event is often followed by protonation, which results in the formation of hydroperoxoiron(III) species (which have been directly detected in nonheme oxygenases, see section I.4.1). At this stage homolytic or heterolytic cleavage of the O-O bond results in the generation of higher valent compounds, namely oxoiron(IV) or oxoiron(V) species.

In the following section, the most relevant examples of iron-oxygen compounds obtained through the use of model systems will be discussed. Special attention will be paid to peroxoiron(III) compounds, with special focus on acylperoxoiron(III). However, because of their historical and inherent relevance, oxoiron(IV) and well defined oxoiron(V) compounds will also be discussed in detail.

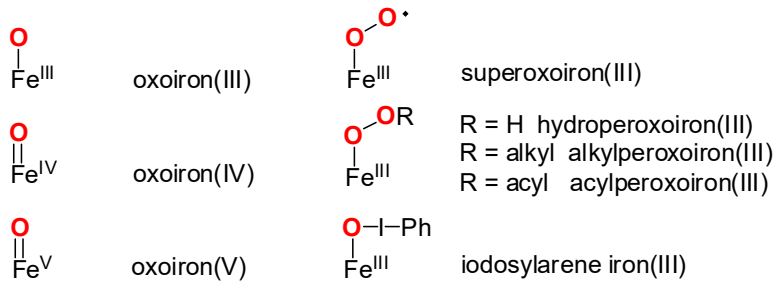

Figure I.11. Spectroscopically trapped mononuclear iron-oxygen species in model systems.

- **peroxoiron(III) species**

Bioinspired synthetic chemistry has produced a number of nonheme peroxoiron(III) compounds, $Fe^{III}(OOR)$ (R = H, alkyl, acyl).[100,113] In terms of reactivity, low spin $Fe^{III}(OOR)$ are usually described as sluggish oxidants that are not competent for the oxidation of strong C–H bonds.[171-173] However, such species can undergo homolytic or heterolytic O-O cleavage to form high valent species with greater oxidizing power.

Several examples of synthetic nonheme hydroperoxoiron(III) compounds, $Fe^{III}(OOH)$, have been obtained by reaction of iron(II) complexes with excess H_2O_2 at low temperatures.[113,174,175] In very few examples their generation was also achieved by using O_2 in the presence of a reducing agent.[176,177] Most synthetic nonheme hydroperoxoiron(III) compounds reported so far bear N-based pentadentate ligands,[175,178] but there are also a few cases in which the ligand employed is tetradentate.[113,174,179-182] Typically, low spin $Fe^{III}(OOH)$ compounds are deep purple with a characteristic UV-vis band at λ_{max} ~550 nm (ε ~1000 $M^{-1}cm^{-1}$) corresponding to the hydroperoxo-to-iron charge transfer transition. Excitation at ~ 550 nm in resonance Raman experiments gives resonance-enhanced features at ~800 cm^{-1} (downshifted ~20 cm^{-1} when ^{18}O is used) and 600 cm^{-1} (downshifted ~50 cm^{-1}) which are assigned to O-O and Fe-O stretching modes, respectively.

Strong evidences exist that the spin state of $Fe^{III}(OOH)$ affects its reactivity. Que and co-workers reported in 2011 the first example of a high-spin $[Fe^{III}(OOH)(\mathbf{40})]^{2+}$.[183] The authors observed that this compound could be quantitatively converted to an oxoiron(IV) species by addition of protons. Later, Nam, Shaik and co-workers reported that this high spin $[Fe^{III}(OOH)(\mathbf{40})]^{2+}$ was competent to perform OAT reactivity towards sulfides,[184] in contrast to low-spin analogs.

In selected examples, reaction of $Fe^{III}(OOH)$ with a base results in its deprotonation yielding the conjugated base $Fe^{III}(\eta^2\text{-}O_2)$ in which the peroxo moiety binds in a side-on fashion. As a representative example, $[Fe^{III}(OOH)(\mathbf{43})]^{2+}$ reacted with NEt_3 or NH_3 to form $[Fe^{III}(\eta^2\text{-}O_2)(\mathbf{43})]^{+}$ which presented different spectroscopic features (Scheme I.26a).[66,175] A similar deprotonation event was observed for $[Fe^{III}(OOH)(\mathbf{40})]^{2+}$. Interestingly, Nam and co-workers were able to crystallize the conjugated base $[Fe^{III}(\eta^2\text{-}O_2)(\mathbf{40})]^{2+}$ after reaction of the iron(II) precursor with

H_2O_2 (5 equiv) in the presence of triethylamine (2 equiv) at 0ºC (Figure I.26b).[171] Interestingly, some differences in reactivity were also observed for these two compounds: while the deprotonated $[Fe^{III}(\eta^2\text{-}O_2)(\mathbf{40})]^{2+}$ behaved as sluggish reagent in nucleophilic aldehyde deformylation and towards alkanes, the corresponding hydroperoxo $[Fe^{III}(OOH)(\mathbf{40})]^{2+}$ could perform both nucleophilic deformylation of aldehydes and electrophilic oxidation of weak C-H bonds such as xanthene or 9,10-dihydroanthracene.[171,185]

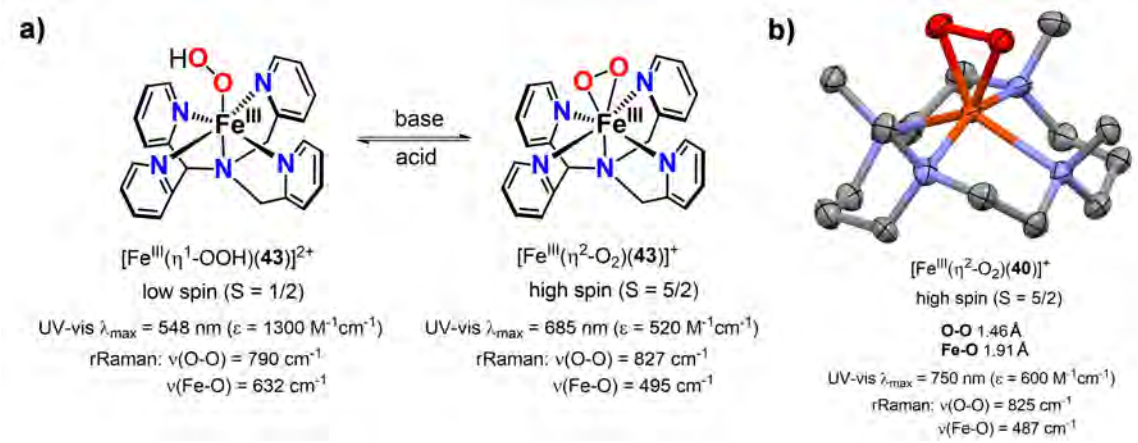

Scheme I.26. a) Reversible acid-base interconversion between hydroperoxoiron(III) and peroxoiron(III) using ligand **43**. **b)** X-ray structure and spectroscopic features of $[Fe^{III}(\eta^2\text{-}O_2)(\mathbf{40})]^{+}$ reported by Nam and co-workers.[171]

Acylperoxoiron(III) species

For the purpose of this thesis, a particularly interesting case of peroxide compounds are acylperoxoiron(III) species. These compounds are typically generated by reaction of an iron(II) precursor and H_2O_2 in the presence of acetic acid or by reaction with alkyl peracids. Very few examples of acylperoxoiron(III) compounds have been characterized and, except in one recently reported case,[186] these species are kinetically not competent for the oxidation of organic substrates. Furutachi and co-workers reported in 2011 the first (and so far the only) crystallographically characterized nonheme peracetatoiron(III) complex $[Fe^{II}(\mathbf{44})(CH_3CO_3)]^{2+}$ (Figure I.12a).[187] This compound was able to epoxidize cyclooctene and to oxidize weak C-H bonds such as those of adamantane albeit in very low yields.

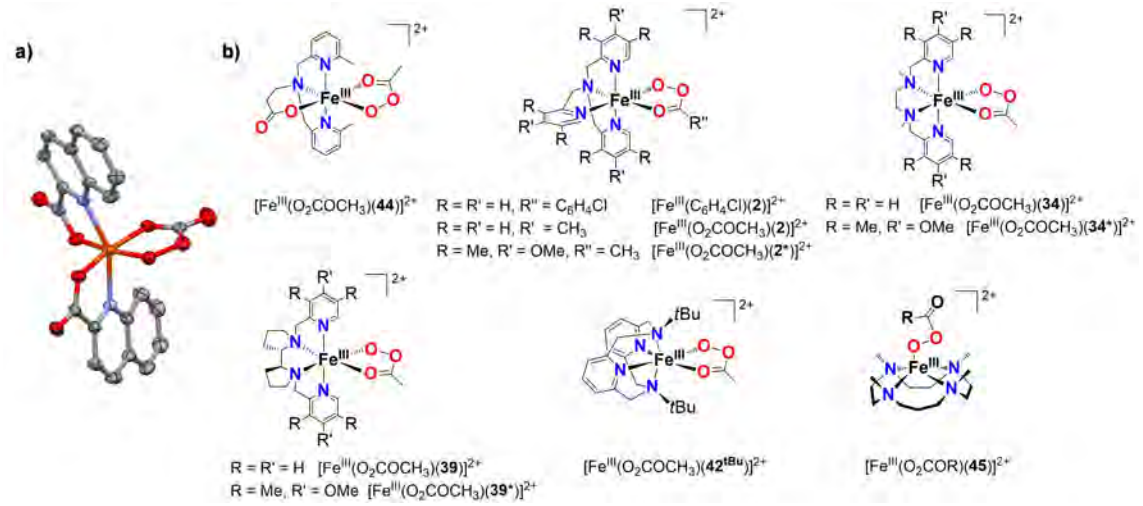

Figure I.12. a) X-ray structure of $[Fe^{II}(\mathbf{44})(O_2COCH_3)]^{2+}$ provided by Furutachi and co-workers. Hydrogen atoms have been ommited for clarity. **b)** Schematic representation of spectroscopically trapped acylperoxoiron(III) compounds.

Because of the poor thermal stability of most of these compounds, EPR spectroscopy has been commonly used as a tool for the identification of acylperoxoiron(III) species which are typically low spin (S = 1/2) (Figure I.12b). In some cases they have been detected by EPR in samples frozen after mixing an iron precursor and the desired oxidant, which can be either H_2O_2 in combination with a carboxylic acid or an alkyl peracid alone. Following this strategy, Richens and co-workers observed that by reacting $[Fe^{II}(\mathbf{2})(CH_3CN)_2]^{2+}$ and *m*CPBA (*meta*-chloroperbenzoic acid) at -40ºC a low spin S = 1/2 species was formed, which was assigned to an acylperoxoiron(III) species $[Fe^{III}(C_6H_4Cl)(\mathbf{2})]^{2+}$ (Scheme I.12b).[188] Upon decomposition the authors observed hydroxylation on the aromatic ring of the oxidant and they rationalized this observation by invoking the involvement of a higher valent electromer that would result from the O-O cleavage of the observed acylperoxoiron(III) compound. Talsi and co-workers studied in 2007 by EPR and ^{1}H-NMR the species generated after mixing $[Fe^{II}(L)(CH_3CN)_2]^{2+}$ (L = **2** or **34**) and H_2O_2/AcOH or peracetic acid at -50ºC in order to shed some light on the active species involved in nonheme iron oxidation catalysis. Their preliminary study concluded that an oxoiron(IV), formed after decay of an acylperoxoiron(III) precursor, was the active species in cyclohexene oxidation.[189] Two years later the same group reported the EPR analysis of a sample frozen 30 s after mixing the same complexes with excess *m*CPBA, peracetic acid or H_2O_2/HOAc at -60ºC.[190,191] The presence of a S = 1/2 rhombic species with *g*-values at 2.71, 2.42, 1.53 accounting for a 15% or 7% of the iron (using *m*CPBA and peracetic respectively) was detected. The decay rate of these species increased five-fold in the presence of cyclohexene compared to the self-decay, and the formation of cyclohexene oxide was observed. At that point, the authors assigned the g_{max} = 2.7 species to a low spin oxoiron(V) intermediate species.

Fortunately, in some cases the acylperoxoiron(III) species accumulated in higher yield paving the way for its characterization by several complementary techniques such as UV-vis, Mössbauer, rRaman, mass spectrometry, among others. Oloo *et al*. followed by UV-vis the formation of a metastable brown species (λ_{max} = 460 nm) upon reaction of $[Fe^{II}(\mathbf{2})(CH_3CN)_2]^{2+}$ with H_2O_2 in the presence of AcOH at -40ºC. EPR analysis revealed the presence of a S = 1/2 species accounting for 20% of Fe in the sample with similar *g* values to the ones observed by Talsi (see above) and that had been assigned to an oxoiron(V) species.[190,192] In order to increase the yield of this species the synthesis of a more electron rich version of the ligand achieved by introducing methoxy and methyl substituents in the pyridine rings was envisioned. Reaction of $[Fe^{II}(\mathbf{2^*})(CH_3CN)_2]^{2+}$ with excess H_2O_2 in the presence of acetic acid at -40ºC resulted again in the formation of a UV-vis chromophore at λ_{max} = 460 nm (ε ~ 4000 $M^{-1}cm^{-1}$) (Figure I.12b).[192] EPR analysis of a sample frozen at maximum formation of this chromophore revealed the presence of a S = 1/2 species (g-values 2.58, 2.38, 1.72) in this case in much higher yield (47% of the iron). Thanks to this higher purity, complementary spectroscopic analysis (electrospray mass spectrometry, Mössbauer and rRaman) were performed. All the acquired data taken together lead the authors to firmly assign the formed species as a low spin acylperoxoiron(III) and not oxoiron(V) as previously proposed by Talsi. Moreover, reactivity studies on this intermediate species were performed. After full formation, $[Fe^{III}(OOAc)(\mathbf{2^*})]^{2+}$ persisted in a steady-state phase at low temperatures during which oxidation products (OAT to 1-octene) were formed catalytically. The decay of the species occurred upon depletion of H_2O_2 at a rate independent of the nature of the substrate and its concentration. This kinetic behavior was an indication that $[Fe^{III}(O_2COCH_3)(\mathbf{2^*})]^{2+}$ was a precursor of the actual oxidant, a higher valent compound which resulted from O-O cleavage of the acylperoxide.[192]

With the same idea, Akimova and co-workers used electron rich versions of ligands **34** and **39** to stabilize similar acylperoxoiron(III) species.[193] Reaction of the corresponding iron(II) precursors $[Fe^{II}(\mathbf{34^*})(CH_3CN)_2]^{2+}$ or $[Fe^{II}(\mathbf{39^*})(CH_3CN)_2]^{2+}$ with H_2O_2 in the presence of acetic acid gave rise to the formation of the S = 1/2 EPR signal with g_{max} = 2.7 (Figure I.12b). Moreover, calculations performed by Shaik and co-workers in 2013 on the reaction of $[Fe^{II}(\mathbf{39})(CH_3CN)_2]^{2+}$ and H_2O_2 in the presence of AcOH pointed towards the formation of the cyclic peracetate complex, which would undergo O-O cleavage to form a high valent electromer.[194]

In 2013 the generation of an acylperoxoiron(III) intermediate species after reacting an iron(II) precursor in the tetradentate pyridinophane ligand $\mathbf{42^{tBu}}$ and peracetic acid at -35ºC was presented by Mirica and co-workers (Figure I.12b).[195] This species was characterized by UV-vis absorption spectroscopy, which showed a chromophore at λ_{max} = 535 nm (with a shoulder at ~850 nm), and by EPR, which revealed the presence of an S = 1/2 species with *g*-values at 2.15, 2.10, 1.96. Unfortunately, no information about the reactivity of this compound has been reported yet.

Interestingly, all the aforementioned acylperoxoiron(III) compounds are not kinetically competent for the oxidation of substrates, but they can be the precursors of higher valent

electromers. In sharp contrast, earlier this year Nam and co-workers reported the synthesis of a series of mononuclear high-spin (S = 5/2) acylperoxoiron(III) complexes by reaction of $[Fe^{II}(\mathbf{45})(CH_3CN)_2]^{2+}$ and 4 equiv of different peroxycarboxylic acids (phenylperoxyacetic acid, peroxybenzoic acid, *m*-chloroperbenzoic acid or peroxyacetic acid) (Figure I.12b).[186] These intermediate species were kinetically competent for oxidizing both olefins and alkanes with strong C-H bonds including cyclohexane. In order to reason the observed behavior the authors hypothesized that the high-spin state of this acylperoxide makes such compounds directly responsible for substrate oxidation.[186]

- **iodosylarene iron(III) species**

A few examples of iodosylarene iron(III) compounds, normally generated by reaction of an iron precursor and iodosylbenzene, have been described. McKenzie and co-workers reported in 2012 the first crystal structure of a nonheme iodosylbenzene iron(III) complex, $[Fe^{III}(\mathbf{46})(OIPh)]^{2+}$ (Figure I.13a) This compound was catalytically active in oxygen atom transfer (OAT) to thioanisole (~1600 TON). The authors proposed a left-lying equilibrium with a highly reactive Fe^{V} species (not observed) that would be the real oxidation agent.[196] Two years later Nam and co-workers characterized a high-spin iodosylarene iron(III) after the reaction of iodosylbenzene and an iron(II) precursor bearing an N-methylated cyclam ligand $[Fe^{II}(\mathbf{45})]^{2+}$ (Scheme I.13b). This species showed competence for the oxidation of strong C-H bonds of alkanes (e.g. cyclohexane) and it was also active in sulfoxidation reactions. In sharp contrast to the previous mechanistic proposal by McKenzie and co-workers, the authors in this work proposed the direct reaction of the iron(III) compound towards substrates.[197] Moreover, reaction of $[Fe^{II}(\mathbf{45})]^{2+}$ and a iodosylarene containing a chiral center at -60ºC generated and iron(III) compound that was able to epoxidize prochiral olefins with enantioselectivities up to 76%.[198]

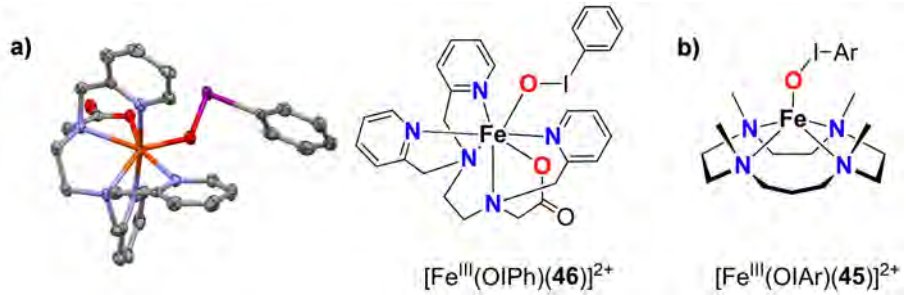

Figure I.13. Iodosylarene iron(III) compounds **a)** X-ray structure and schematic representation of $[Fe^{III}(OIPh)(\mathbf{46})]^{2+}$. Hydrogen atoms have been omitted for clarity. **b)** Schematic representation of $[Fe^{III}(OIAr)(\mathbf{45})]^{2+}$.

- **Oxoiron(IV) species**

Oxoiron(IV) species are so far the most studied iron-oxygen compounds through the use of synthetic models. These species have been detected and characterized in several mononuclear nonheme iron enzymes such as α-ketoglutarate-dependent taurine dioxygenase (TauD),[199-201] pterin dependent phenylalanine hydroxylase[202] and tyrosine hydroxylase,[203] halogenases CytC3[204] and SyrB2,[205] and prolyl 4-hydroxylase,[206] all of them presenting a high spin (S = 2) ground spin state. In contrast, the vast majority of the synthetic oxoiron(IV) complexes that have been reported are low spin (S = 1). Wieghardt and co-workers detected for the first time the formation of a synthetic oxoiron(IV) species after the reaction of a cylam-acetate iron(III) complex $[Fe^{III}(\mathbf{47})]^{2+}$ and ozone at -80ºC. Unfortunately, it was generated in very low yields, thus hampering thorough characterization.[207] Three years later a benchmark in the field of the synthetic models for nonheme iron oxygenases was the report of the first structurally characterized oxoiron(IV) compound by Que, Nam, Münck, and co-workers (Figure I.14).[208] Reaction of $[Fe^{II}(\mathbf{40})]^{2+}$ with iodosylbenzene (PhIO) afforded a pale green species with λ_{max} = 820 nm (ε = 400 $M^{-1}cm^{-1}$) that was stable at -40ºC for weeks. Full characterization by several spectroscopic techniques including Mössbauer analysis and rRaman confirmed the presence of a low spin (S = 1) iron(IV) center in >90% yield. After this precedent over 50 examples of other S = 1 oxoiron(IV) have been reported. They are typically prepared by reaction of iron(II) complexes containing tetra- or pentadentate ligands with oxygen-atom donors reagents such as PhIO, peracetic acid, *m*CPBA or hydroperoxides.[113,209-213] Most of them share some common spectroscopic features. For example, they show UV-vis absorption bands at λ_{max} ~ 750-850 (ε ~ 300-400 $M^{-1}cm^{-1}$) and they give rise to a Mössbauer quadrupole doublet with an isomer shift around δ = 0-0.2 mm s^{-1}. Only in selected cases, the X-ray structure has been obtained (Figure I.14).[214-217] In the reported structures, iron is six-coordinate in a pseudo-octahedral environment offered by pyridine- and tertiary amine-based ligands that provide a relatively strong field. A different case was the structure reported by Meyer and co-workers in 2013, which was the first example of an oxoiron(IV) complex in a tetracarbene environment provided by ligand **50** (Figure I.14).[214] In general, S = 1 oxoiron(IV) complexes can perform the oxidation of a wide range of organic substrates including OAT to different substrates such as triphenylphosphine, sulfides or olefins.[208,218-220] More interestingly, in some cases they have also been capable of C-H hydroxylation, albeit in slow rates.[221]

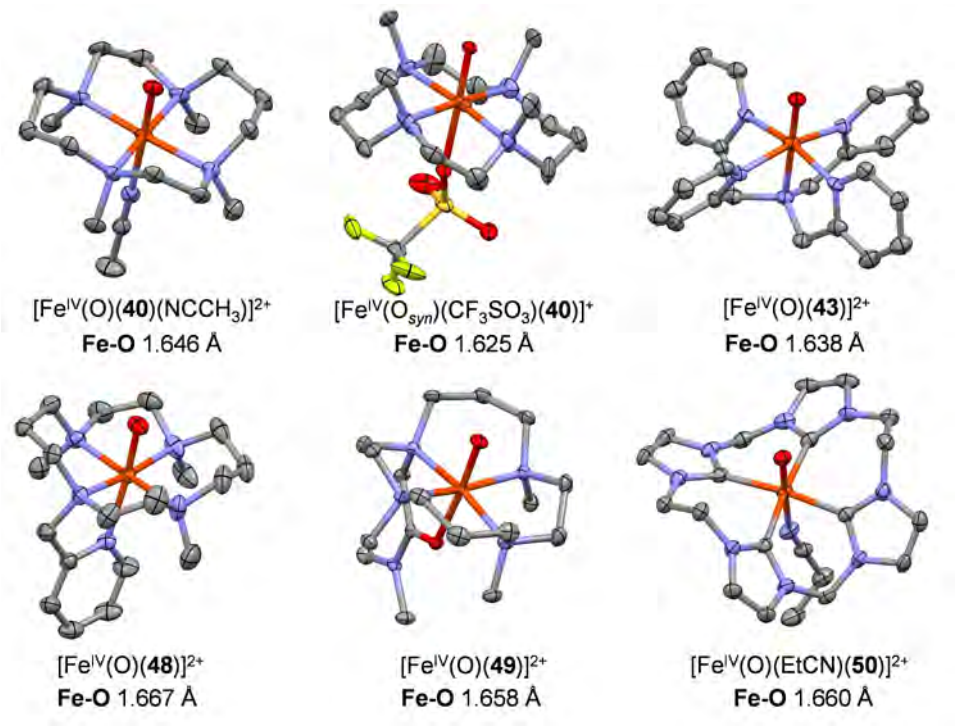

Figure I.14. Crystallographically characterized S = 1 oxoiron(IV) complexes.

Nam and co-workers reported in 2011 the synthesis of a S = 1 oxoiron(IV) compound [Fe^{IV}(O)(**51**)]$^{2+}$ that showed significant enhanced reactivity compared to its low-spin analogues (Figure I.15a).[222] For example, the oxidation rate measured for cyclohexane oxidation by this oxoiron(IV) at -40ºC was 3 orders of magnitude higher than for other S = 1 examples (even without correcting a 65-degree difference in some cases). In order to reason this extraordinary reactivity, [Fe^{IV}(O)(**51**)]$^{2+}$ was proposed to be in a very closely-lying equilibrium with the more reactive S = 2 spin state, that would be the real executor of the oxidation. Indeed, the Two-State-Reactivity (TSR) model developed by Shaik and co-workers postulates that the transition state in the S = 2 spin state lies lower than in the triplet ground state, so that globally the net barrier for C-H cleavage is lowered.[221-223]

As stated above, so far only the S = 2 ground state has been detected in oxoiron(IV) species in natural systems. Examples of synthetic oxorion(IV) complexes with quintet ground state (S = 2) remain much more scarce, with only six examples reported.[221,224] In order to reach the high spin state, a weakening of the ligand field is required, and this was successfully achieved in most cases by promoting trigonal-bipyramidal geometry enforced by C_3 symmetric bulky tripodal ligands (Figure I.15b).

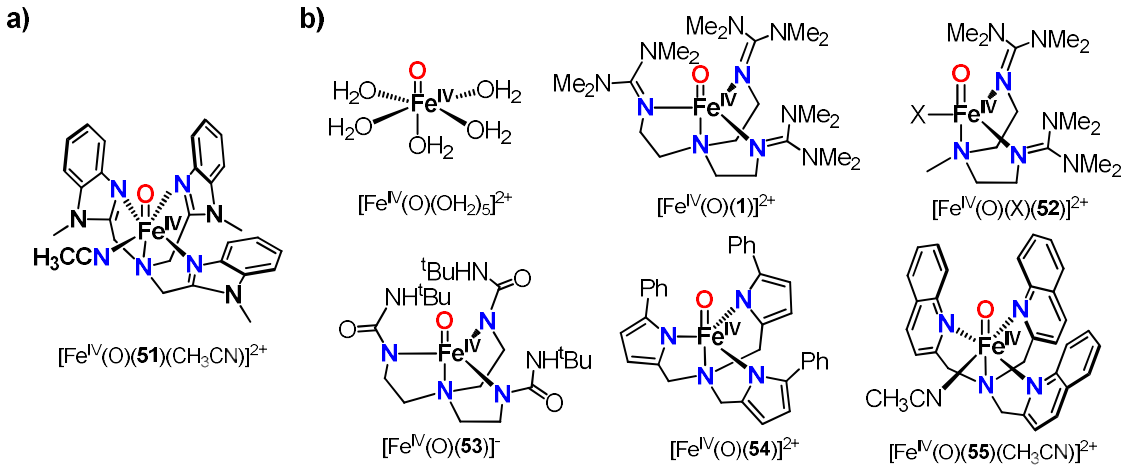

Figure I.15. a) S=1 $[Fe^{IV}(O)(\mathbf{51})]^{2+}$ complex, proposed to operate trough an S = 2 spin state. **b)** Crystallographically and/or spectroscopically characterized S = 2 oxoiron(IV) complexes.

Evidence for an S = 2 oxoiron(IV) compound was originally found in 2005 by Bakac and co-workers by reacting hexaaquoiron(II) and oxone in acidic conditions which yielded $[Fe^{IV}(O)(H_2O)_5]^{2+}$. It presented similar spectroscopic features to the oxorion(IV) species detected in the enzyme TauD (TauD-*J*) but its short half-life time of 7 s at 25ºC and the use of water as solvent limited further studies.[225] Que and co-workers reported four years later the first well-characterized synthetic nonheme oxoiron(IV) S = 2 compound $[Fe^{IV}(O)(\mathbf{1})]^{2+}$,[226] whose crystal structure was later published.[227] Even though this system was a good structural model of high-spin oxoiron(IV), it lacked oxidative reactivity against external substrates, presumably due to the steric hindrance around the oxo moiety provided by the bulky ligand **1**. Indeed, replacement of one of the tetramethylguanidiyl arms of the ligand by a methyl group gave a more reactive $[Fe^{IV}(O)(\mathbf{52})(CH_3CN)]^{2+}$ that still preserved the S = 2 spin state.[228] Structural models of high-spin oxoiron(IV) were also reported by Borovik and co-workers[229] and Chang and co-workers[230] by using tripodal **53** and **54** ligands respectively. In both cases the reactivity towards organic substrates was sluggish, which was again attributed to steric hindrance. Among all the examples of oxoiron(IV) compounds reported in the literature so far, probably the best example of *biomimetism* is the recently described $[Fe^{IV}(O)(\mathbf{55})(CH_3CN)]^{2+}$ by Que and co-workers.[231] Complete analysis revealed that this oxoiron(IV) corresponds to an S = 2 compound with spectroscopic features that closely resemble those obtained for the spectroscopically trapped enzymatic oxoiron(IV) TauD-*J* (Figure I.9).[232] Very remarkably, this compound was also found to be active in the oxidation of various hydrocarbons, showing an oxidation rate towards cyclohexane of 0.37 M^{-1} s^{-1} at -40ºC, which is of the same order of that calculated for TauD-*J*.

- **Oxoiron(V) species**

Intermediate species bearing iron in the oxidation state +5 have been proposed to be the active species in many oxidative enzymatic reactions. However, direct characterization of such compounds in natural systems remains elusive. The use of model systems has allowed the entrapment and characterization of a few oxoiron(V) species.

Collins and co-workers developed during the 90's different macrocyclic tetraamido ligands (TAML) used for the preparation of several examples of well-defined high valent iron compounds.[233] These ligands bear four amide groups that upon deprotonation provide exceptionally strong σ-donors amidate moieties. In 2007 the same group reported the first example of a well-defined oxoiron(V) by reacting the monomeric $[Fe^{III}(\mathbf{56})(H_2O)]^-$ with excess *m*CPBA at -60ºC (Figure I.16a).[234] Full characterization by UV-vis, EPR, Mössbauer, X-ray absorption and ESI-MS, as well as complementary DFT calculations, led the authors to unequivocally assign the compound as a d^3 oxoiron(V) complex with S = 1/2 ground state. By substituting a CMe_2 group by an N-Me group in the TAML architecture, some years later Gupta and co-workers could achieve the generation of an $Fe^V(O)$ complex $[Fe^V(O)(\mathbf{57})]^-$ stable at room temperature (Figure I.16a bottom).[235] The reactivity of $[Fe^V(O)(\mathbf{56})]^-$ was studied simultaneously by Nam and co-workers[236] and Collins and co-workers,[237] showing that this compound is competent for the oxidation of unactivated C-H bonds. Gupta's model $[Fe^V(O)(\mathbf{57})]^-$ could also perform C-H bond oxidation but at slower rates compared to TAML (one order of magnitude slower for the oxidation of cyclohexane).[235,237]

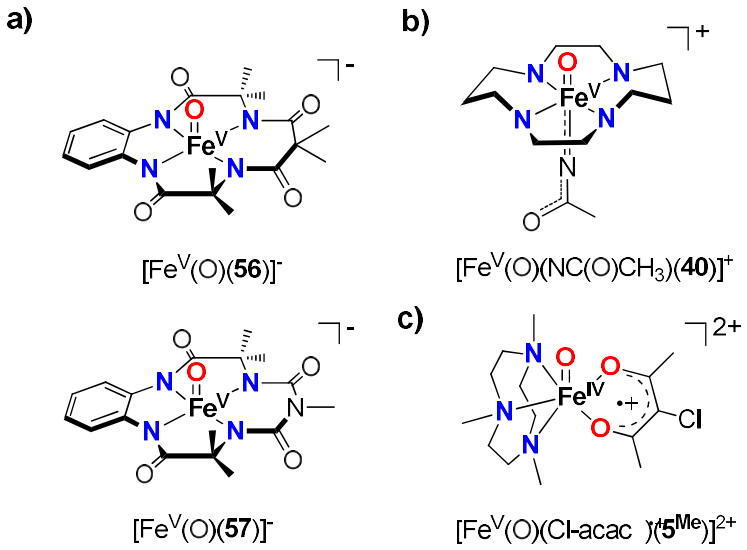

Figure I.16. Spectroscopically detected oxoiron(V) compounds **a)** with the TAML platform reported by Collins and co-workers (top) and Gupta and co-workers (bottom), **b)** generated from the one-electron oxidation of an oxoiron(IV) complex by Que and co-workers and **c)** generated by Che and co-workers after reaction of an iron(III) precursor and oxone. Cl-acac = 3-chloro-acetylacetonate.

Apart from TAML ligands (**56**, **57**), direct evidences of $Fe^V(O)$ species have also been obtained in other systems. Our group reported in 2011 the detection of $[Fe^V(O)(OH)(\mathbf{37})]^{2+}$ by means of

low-temperature mass-spectrometry.[210,238] The same technique allowed the detection of oxoiron(V) compounds during the catalysis of C-H oxidation reactions by a Fe^{III}-monoamidate complex.[239] Similarly, Chi-Ming Che and co-workers proposed the formation of an oxoiron(V) after reaction of $[Fe^{III}(Cl)_2(\mathbf{42^{Me}})]^+$ and oxone on the basis of mass spectrometry experiments and complementary DFT computations.[152]

Que and co-workers followed a different approach in order to synthesize an $Fe^{V}(O)$ compound. In that case, the strategy consisted in generating the oxoiron(IV) compound $[Fe^{IV}(O)(\mathbf{40})(CH_3CN)]^{2+}$ and then performing a one-electron oxidation with *t*BuOOH in the presence of a base. The resulting formally $[Fe^{V}(O)(NC(O)CH_3)(\mathbf{40})]^{2+}$ species (Figure I.16b) was characterized by several spectroscopic techniques including EPR, Mössbauer and rRaman.[240]

In a recent report, Che and co-workers presented an iron(III) compound in which the iron was bound to a strongly chelating tridentate ligand $\mathbf{5^{Me}}$ and an anionic bidentate ligand $[Fe^{III}(Cl\text{-}acac^{\bullet+})(\mathbf{42^{Me}})]^{2+}$. This compound mixed with oxone showed high activity towards the oxidation of typical alkanes such as cyclohexane but also the more challenging light alkanes propane and ethane at room temperature, and it was active for the epoxidation of several alkenes. Mass spectrometry studies revealed the presence of a peak that was consistent with the formulation as an oxoiron(V) compound (Figure I.16c)., which showed 60% ^{18}O incorporation from $H_2{}^{18}O$. EPR studies together with DFT were consistent with the presence of an oxoiron(IV) cation radical (formally Fe^{V}) compound, which was proposed to be the active species in the reaction.[241]

Finally, Talsi and co-workers claimed in 2009 to have detected an iron(V) species by EPR, albeit in low yields by reacting $[Fe^{II}(\mathbf{2})(CH_3CN)_2]^{2+}$ with peracetic acid.[190] A few years later Que and co-workers accumulated a higher yield of the same species and full spectroscopic analysis led to an iron(III) assignment (see discussion in section I.4.4.2). Very recently Talsi and co-workers reported the detection of another S = 1/2 with *g*-values = 2.07, 2.01, 1.96 by EPR after reaction of $[Fe^{II}(\mathbf{2^*})(CH_3CN)_2]^{2+}$ and H_2O_2 in the presence of AcOH that was assigned as an iron(V) species, even though it only accounted for 1% of the sample. Further characterization is needed to make a precise formulation of this species.[242]

I.5 References

(1) Que, L.; Tolman, W. B. *Nature* **2008**, *455*, 333.

(2) Punniyamurthy, T.; Velusamy, S.; Iqbal, J. *Chem. Rev.* **2005**, *105*, 2329.

(3) Crabtree, R. H. *Chem. Rev.* **2010**, *110*, 575.

(4) Schroeder, M. *Chem. Rev.* **1980**, *80*, 187.

(5) Oloo, W. N.; Que Jr, L. In *Comprehensive Inorganic Chemistry II (Second Edition)*; Elsevier: Amsterdam, 2013, p 763.

(6) Bertini, I.; Gray, H. B.; Stiefel, E. I.; Valentine, S. J. *Biological inorganic Chemistry: structure & reactivity*; University Science Books: Sausalito, California, 2007.

(7) Oldenburg, P. D.; Ke, C.-Y.; Tipton, A. A.; Shteinman, A. A.; Que, L. *Angew. Chem. Int. Ed.* **2006**, *45*, 7975.

(8) Ferraro, D. J.; Brown, E. N.; Yu, C.-L.; Parales, R. E.; Gibson, D. T.; Ramaswamy, S. *BMC Struct. Biol.* **2007**, *7*, 1.

(9) Cook, S. A.; Borovik, A. S. *Acc. Chem. Res.* **2015**, *48*, 2407.

(10) Garcia-Bosch, I.; Ribas, X.; Costas, M. *Eur J. Inorg. Chem.* **2012**, *2012*, 179.

(11) Sallmann, M.; Limberg, C. *Acc. Chem. Res.* **2015**, *48*, 2734.

(12) Mirica, L. M.; Ottenwaelder, X.; Stack, T. D. P. *Chem. Rev.* **2004**, *104*, 1013.

(13) http://copperalliance.org/history-of-copper.

(14) Solomon, E. I.; Heppner, D. E.; Johnston, E. M.; Ginsbach, J. W.; Cirera, J.; Qayyum, M.; Kieber-Emmons, M. T.; Kjaergaard, C. H.; Hadt, R. G.; Tian, L. *Chem. Rev.* **2014**, *114*, 3659.

(15) Balasubramanian, R.; Smith, S. M.; Rawat, S.; Yatsunyk, L. A.; Stemmler, T. L.; Rosenzweig, A. C. *Nature* **2010**, *465*, 115.

(16) Bollinger Jr, J. M. *Nature* **2010**, *465*, 40.

(17) Balasubramanian, R.; Rosenzweig, A. C. *Acc. Chem. Res.* **2007**, *40*, 573.

(18) Hakemian, A. S.; Kondapalli, K. C.; Telser, J.; Hoffman, B. M.; Stemmler, T. L.; Rosenzweig, A. C. *Biochemistry* **2008**, *47*, 6793.

(19) Smith, S. M.; Rawat, S.; Telser, J.; Hoffman, B. M.; Stemmler, T. L.; Rosenzweig, A. C. *Biochemistry* **2011**, *50*, 10231.

(20) Lieberman, R. L.; Rosenzweig, A. C. *Nature* **2005**, *434*, 177.

(21) Rompel, A.; Fischer, H.; Meiwes, D.; Büldt-Karentzopoulos, K.; Dillinger, R.; Tuczek, F.; Witzel, H.; Krebs, B. *J. Biol. Inorg. Chem.*, *4*, 56.

(22) Matoba, Y.; Kumagai, T.; Yamamoto, A.; Yoshitsu, H.; Sugiyama, M. *J. Biol. Chem.* **2006**, *281*, 8981.

(23) Solomon, E. I.; Sundaram, U. M.; Machonkin, T. E. *Chem. Rev.* **1996**, *96*, 2563.

(24) Decker, H.; Schweikardt, T.; Tuczek, F. *Angew. Chem. Int. Ed.* **2006**, *45*, 4546.

(25) Company, A. In *Ideas in Chemistry and Molecular Sciences*; Wiley-VCH Verlag GmbH & Co. KGaA: 2010, p 265.

(26) Rolff, M.; Schottenheim, J.; Decker, H.; Tuczek, F. *Chem. Soc. Rev.* **2011**, *40*, 4077.

(27) Cuff, M. E.; Miller, K. I.; van Holde, K. E.; Hendrickson, W. A. *J. Mol. Biol.* **1998**, *278*, 855.

(28) Sendovski, M.; Kanteev, M.; Ben-Yosef, V. S.; Adir, N.; Fishman, A. *J. Mol. Biol.* **2011**, *405*, 227.

(29) Gennis, R.; Ferguson-Miller, S. *Science* **1995**, *269*, 1063.

(30) Tainer, J. A.; Getzoff, E. D.; Beem, K. M.; Richardson, J. S.; Richardson, D. C. *J. Mol. Biol.* **1982**, *160*, 181.

(31) Siebert, X.; Eipper, B. A.; Mains, R. E.; Prigge, S. T.; Blackburn, N. J.; Amzel, L. M. *Biophys. J.* **2005**, *89*, 3312.

(32) Bradbury, A. F.; Finnie, M. D. A.; Smyth, D. G. *Nature* **1982**, *298*, 686.

(33) Hatcher, L. Q.; Karlin, K. D. *J. Biol. Inorg. Chem.* **2004**, *9*, 669.

(34) Lewis, E. A.; Tolman, W. B. *Chem. Rev.* **2004**, *104*, 1047.

(35) Kim, E.; Chufán, E. E.; Kamaraj, K.; Karlin, K. D. *Chem. Rev.* **2004**, *104*, 1077.

(36) Itoh, S. *Acc. Chem. Res.* **2015**, *48*, 2066.

(37) Prigge, S. T.; Eipper, B. A.; Mains, R. E.; Amzel, L. M. *Science* **2004**, *304*, 864.

(38) Kim, S.; Lee, J. Y.; Cowley, R. E.; Ginsbach, J. W.; Siegler, M. A.; Solomon, E. I.; Karlin, K. D. *J. Am. Chem. Soc.* **2015**, *137*, 2796.

(39) Würtele, C.; Gaoutchenova, E.; Harms, K.; Holthausen, M. C.; Sundermeyer, J.; Schindler, S. *Angew. Chem. Int. Ed.* **2006**, *45*, 3867.

(40) Cole, A. P.; Root, D. E.; Mukherjee, P.; Solomon, E. I.; Stack, T. D. P. *Science* **1996**, *273*, 1848.

(41) Meyer, F.; Pritzkow, H. *Angew. Chem. Int. Ed.* **2000**, *39*, 2112.

(42) Hakulinen, N.; Kiiskinen, L.-L.; Kruus, K.; Saloheimo, M.; Paananen, A.; Koivula, A.; Rouvinen, J. *Nat. Struct. Mol. Biol.* **2002**, *9*, 601.

(43) Messerschmidt, A.; Luecke, H.; Huber, R. *J. Mol. Biol.* **1993**, *230*, 997.

(44) Rosenzweig, A. C.; Sazinsky, M. H. *Curr. Opin. Struct. Biol.* **2006**, *16*, 729.

(45) Tyeklar, Z.; Jacobson, R. R.; Wei, N.; Murthy, N. N.; Zubieta, J.; Karlin, K. D. *J. Am. Chem. Soc.* **1993**, *115*, 2677.

(46) Jacobson, R. R.; Tyeklar, Z.; Farooq, A.; Karlin, K. D.; Liu, S.; Zubieta, J. *J. Am. Chem. Soc.* **1988**, *110*, 3690.

(47) Würtele, C.; Sander, O.; Lutz, V.; Waitz, T.; Tuczek, F.; Schindler, S. *J. Am. Chem. Soc.* **2009**, *131*, 7544.

(48) Hoppe, T.; Schaub, S.; Becker, J.; Würtele, C.; Schindler, S. *Angew. Chem. Int. Ed.* **2013**, *52*, 870.

(49) Kitajima, N.; Fujisawa, K.; Fujimoto, C.; Morooka, Y.; Hashimoto, S.; Kitagawa, T.; Toriumi, K.; Tatsumi, K.; Nakamura, A. *J. Am. Chem. Soc.* **1992**, *114*, 1277.

(50) Metz, M.; Solomon, E. I. *J. Am. Chem. Soc.* **2001**, *123*, 4938.

(51) Alsters, P. L.; Boersma, J.; van Koten, G. *Organometallics* **1993**, *12*, 1629.

(52) Litz, K. E.; Banaszak Holl, M. M.; Kampf, J. W.; Carpenter, G. B. *Inorg. Chem.* **1998**, *37*, 6461.

(53) Aboelella, N. W.; Lewis, E. A.; Reynolds, A. M.; Brennessel, W. W.; Cramer, C. J.; Tolman, W. B. *J. Am. Chem. Soc.* **2002**, *124*, 10660.

(54) Aboelella, N. W.; York, J. T.; Reynolds, A. M.; Fujita, K.; Kinsinger, C. R.; Cramer, C. J.; Riordan, C. G.; Tolman, W. B. *Chem. Commun.* **2004**, 1716.

(55) York, J. T.; Young, V. G.; Tolman, W. B. *Inorg. Chem.* **2006**, *45*, 4191.

(56) Kundu, S.; Pfaff, F. F.; Miceli, E.; Zaharieva, I.; Herwig, C.; Yao, S.; Farquhar, E. R.; Kuhlmann, U.; Bill, E.; Hildebrandt, P.; Dau, H.; Driess, M.; Limberg, C.; Ray, K. *Angew. Chem. Int. Ed.* **2013**, *52*, 5622.

(57) York, J. T.; Llobet, A.; Cramer, C. J.; Tolman, W. B. *J. Am. Chem. Soc.* **2007**, *129*, 7990.

(58) Donoghue, P. J.; Gupta, A. K.; Boyce, D. W.; Cramer, C. J.; Tolman, W. B. *J. Am. Chem. Soc.* **2010**, *132*, 15869.

(59) Nasir, M. S.; Karlin, K. D.; McGowty, D.; Zubieta, J. *J. Am. Chem. Soc.* **1991**, *113*, 698.

(60) Mahroof-Tahir, M.; Karlin, K. D. *J. Am. Chem. Soc.* **1992**, *114*, 7599.

(61) Tachi, Y.; Aita, K.; Teramae, S.; Tani, F.; Naruta, Y.; Fukuzumi, S.; Itoh, S. *Inorg. Chem.* **2004**, *43*, 4558.

(62) Ohtsu, H.; Itoh, S.; Nagatomo, S.; Kitagawa, T.; Ogo, S.; Watanabe, Y.; Fukuzumi, S. *Chem. Commun.* **2000**, 1051.

(63) Ohtsu, H.; Shimazaki, Y.; Odani, A.; Yamauchi, O.; Mori, W.; Itoh, S.; Fukuzumi, S. *J. Am. Chem. Soc.* **2000**, *122*, 5733.

(64) Chishiro, T.; Shimazaki, Y.; Tani, F.; Tachi, Y.; Naruta, Y.; Karasawa, S.; Hayami, S.; Maeda, Y. *Angew. Chem. Int. Ed.* **2003**, *42*, 2788.

(65) Garcia-Bosch, I.; Company, A.; Frisch, J. R.; Torrent-Sucarrat, M.; Cardellach, M.; Gamba, I.; Güell, M.; Casella, L.; Que, L.; Ribas, X.; Luis, J. M.; Costas, M. *Angew. Chem. Int. Ed.* **2010**, *49*, 2406.

(66) Y. N. Ho, R.; Que Jr, L.; Roelfes, G.; L. Feringa, B.; Hermant, R.; Hage, R. *Chem. Commun.* **1999**, 2161.

(67) Kieber-Emmons, M. T.; Ginsbach, J. W.; Wick, P. K.; Lucas, H. R.; Helton, M. E.; Lucchese, B.; Suzuki, M.; Zuberbühler, A. D.; Karlin, K. D.; Solomon, E. I. *Angew. Chem. Int. Ed.* **2014**, *53*, 4935.

(68) Karlin, K. D.; Hayes, J. C.; Gultneh, Y.; Cruse, R. W.; McKown, J. W.; Hutchinson, J. P.; Zubieta, J. *J. Am. Chem. Soc.* **1984**, *106*, 2121.

(69) Karlin, K. D.; Nasir, M. S.; Cohen, B. I.; Cruse, R. W.; Kaderli, S.; Zuberbuehler, A. D. *J. Am. Chem. Soc.* **1994**, *116*, 1324.

(70) Casella, L.; Monzani, E.; Gullotti, M.; Cavagnino, D.; Cerina, G.; Santagostini, L.; Ugo, R. *Inorg. Chem.* **1996**, *35*, 7516.

(71) Santagostini, L.; Gullotti, M.; Monzani, E.; Casella, L.; Dillinger, R.; Tuczek, F. *Chem. Eur. J.* **2000**, *6*, 519.

(72) Itoh, S.; Kumei, H.; Taki, M.; Nagatomo, S.; Kitagawa, T.; Fukuzumi, S. *J. Am. Chem. Soc.* **2001**, *123*, 6708.

(73) Citek, C.; Lyons, C. T.; Wasinger, E. C.; Stack, T. D. P. *Nat. Chem.* **2012**, *4*, 317.

(74) Mirica, L. M.; Vance, M.; Rudd, D. J.; Hedman, B.; Hodgson, K. O.; Solomon, E. I.; Stack, T. D. P. *Science* **2005**, *308*, 1890.

(75) Company, A.; Palavicini, S.; Garcia-Bosch, I.; Mas-Ballesté, R.; Que, L.; Rybak-Akimova, E. V.; Casella, L.; Ribas, X.; Costas, M. *Chem. Eur. J.* **2008**, *14*, 3535.

(76) Herres-Pawlis, S.; Verma, P.; Haase, R.; Kang, P.; Lyons, C. T.; Wasinger, E. C.; Flörke, U.; Henkel, G.; Stack, T. D. P. *J. Am. Chem. Soc.* **2009**, *131*, 1154.

(77) Reglier, M.; Jorand, C.; Waegell, B. *J. Chem. Soc., Chem. Commun.* **1990**, 1752.

(78) Casella, L.; Gullotti, M.; Radaelli, R.; Di Gennaro, P. *J. Chem. Soc., Chem. Commun.* **1991**, 1611.

(79) Rolff, M.; Schottenheim, J.; Peters, G.; Tuczek, F. *Angew. Chem. Int. Ed.* **2010**, *49*, 6438.

(80) Hoffmann, A.; Citek, C.; Binder, S.; Goos, A.; Rübhausen, M.; Troeppner, O.; Ivanović-Burmazović, I.; Wasinger, E. C.; Stack, T. D. P.; Herres-Pawlis, S. *Angew. Chem. Int. Ed.* **2013**, *52*, 5398.

(81) Esguerra, K. V. N.; Fall, Y.; Lumb, J.-P. *Angew. Chem. Int. Ed.* **2014**, *53*, 5877.

(82) Esguerra, K. V. N.; Fall, Y.; Petitjean, L.; Lumb, J.-P. *J. Am. Chem. Soc.* **2014**, *136*, 7662.

(83) Amii, H.; Uneyama, K. *Chem. Rev.* **2009**, *109*, 2119.

(84) Kuehnel, M. F.; Lentz, D.; Braun, T. *Angew. Chem. Int. Ed.* **2013**, *52*, 3328.

(85) Natarajan, R.; Azerad, R.; Badet, B.; Copin, E. *J. Fluorine Chem.* **2005**, *126*, 424.

(86) Peelen, S.; Rietjens, I. M. C. M.; Boersma, M. G.; Vervoort, J. *Eur. J. Biochem.* **1995**, *227*, 284.

(87) Bondar, V. S.; Boersma, M. G.; van Berkel, W. J. H.; Finkelstein, Z. I.; Golovlev, E. L.; Baskunov, B. P.; Vervoort, J.; Golovleva, L. A.; Rietjens, I. M. C. M. *FEMS Microbiol. Lett.* **1999**, *181*, 73.

(88) Osborne, R. L.; Raner, G. M.; Hager, L. P.; Dawson, J. H. *J. Am. Chem. Soc.* **2006**, *128*, 1036.

(89) Fox, B. G.; Borneman, J. G.; Wackett, L. P.; Lipscomb, J. D. *Biochemistry* **1990**, *29*, 6419.

(90) Battaini, G.; Monzani, E.; Casella, L.; Lonardi, E.; Tepper, A. W. J. W.; Canters, G. W.; Bubacco, L. *J. Biol. Chem.* **2002**, *277*, 44606.

(91) Nasir, M. S.; Cohen, B. I.; Karlin, K. D. *Inorg. Chim. Acta* **1990**, *176*, 185.

(92) Gelling, O. J.; Feringa, B. L. *Recl. Trav. Chim. Pays-Bas* **1991**, *110*, 89.

(93) Colomban, C.; Kudrik, E. V.; Afanasiev, P.; Sorokin, A. B. *J. Am. Chem. Soc.* **2014**, *136*, 11321.

(94) Groves, J. T. *J. Inorg. Biochem.* **2006**, *100*, 434.

(95) Kovacs, J. A. *Science* **2003**, *299*, 1024.

(96) Banerjee, R.; Proshlyakov, Y.; Lipscomb, J. D.; Proshlyakov, D. A. *Nature* **2015**, *518*, 431.

(97) Costas, M.; Que, J. L. *Angew. Chem. Int. Ed.* **2002**, *41*, 2179.

(98) Bryliakov, K. P.; Talsi, E. P. *Coord. Chem. Rev.* **2014**, *276*, 73.

(99) Kryatov, S. V.; Rybak-Akimova, E. V.; Schindler, S. *Chem. Rev.* **2005**, *105*, 2175.

(100) Costas, M.; Mehn, M. P.; Jensen, M. P.; Que, L. *Chem. Rev.* **2004**, *104*, 939.

(101) Poulos, T. L. *Chem. Rev.* **2014**, *114*, 3919.

(102) Costas, M. *Coord. Chem. Rev.* **2011**, *255*, 2912.

(103) Denisov, I. G.; Makris, T. M.; Sligar, S. G.; Schlichting, I. *Chem. Rev.* **2005**, *105*, 2253.

(104) Loew, G. H.; Harris, D. L. *Chem. Rev.* **2000**, *100*, 407.

(105) Sligar, S. G.; Makris, T. M.; Denisov, I. G. *Biochem. Biophys. Res. Commun.* **2005**, *338*, 346.

(106) Meunier, B.; de Visser, S. P.; Shaik, S. *Chem. Rev.* **2004**, *104*, 3947.

(107) Groves, J. T.; McClusky, G. A.; White, R. E.; Coon, M. J. *Biochem. Biophys. Res. Commun.* **1978**, *81*, 154.

(108) Groves, J. T.; McClusky, G. A. *J. Am. Chem. Soc.* **1976**, *98*, 859.

(109) Rittle, J.; Green, M. T. *Science* **2010**, *330*, 933.

(110) Sydor, P. K.; Barry, S. M.; Odulate, O. M.; Barona-Gomez, F.; Haynes, S. W.; Corre, C.; Song, L.; Challis, G. L. *Nat. Chem.* **2011**, *3*, 388.

(111) Gibson, D. T.; Resnick, S. M.; Lee, K.; Brand, J. M.; Torok, D. S.; Wackett, L. P.; Schocken, M. J.; Haigler, B. E. *Journal of Bacteriology* **1995**, *177*, 2615.

(112) Mohammadi, M.; Viger, J.-F.; Kumar, P.; Barriault, D.; Bolin, J. T.; Sylvestre, M. *J. Biol. Chem.* **2011**, *286*, 27612.

(113) Company, A.; Lloret-Fillol, J.; Costas, M. In *Comprehensive Inorganic Chemistry II (Second Edition)*; Elsevier: Amsterdam, 2013, p 487.

(114) Ferraro, D. J.; Gakhar, L.; Ramaswamy, S. *Biochem. Biophys. Res. Commun.* **2005**, *338*, 175.

(115) Neibergall, M. B.; Stubna, A.; Mekmouche, Y.; Münck, E.; Lipscomb, J. D. *Biochemistry* **2007**, *46*, 8004.

(116) Barry, S. M.; Challis, G. L. *ACS Catal.* **2013**, *3*, 2362.

(117) Kauppi, B.; Lee, K.; Carredano, E.; Parales, R. E.; Gibson, D. T.; Eklund, H.; Ramaswamy, S. *Structure* **1998**, *6*, 571.

(118) Koehntop, K. D.; Emerson, J. P.; Que, L. *J. Biol. Inorg. Chem.* **2005**, *10*, 87.

(119) Bruijnincx, P. C. A.; van Koten, G.; Klein Gebbink, R. J. M. *Chem. Soc. Rev.* **2008**, *37*, 2716.

(120) Karlsson, A.; Parales, J. V.; Parales, R. E.; Gibson, D. T.; Eklund, H.; Ramaswamy, S. *Science* **2003**, *299*, 1039.

(121) Ashikawa, Y.; Fujimoto, Z.; Usami, Y.; Inoue, K.; Noguchi, H.; Yamane, H.; Nojiri, H. *BMC Struct. Biol.* **2012**, *12*, 1.

(122) Thibon, A.; Jollet, V.; Ribal, C.; Sénéchal-David, K.; Billon, L.; Sorokin, A. B.; Banse, F. *Chem. Eur. J.* **2012**, *18*, 2715.

(123) Chakrabarty, S.; Austin, R. N.; Deng, D.; Groves, J. T.; Lipscomb, J. D. *J. Am. Chem. Soc.* **2007**, *129*, 3514.

(124) Decker, A.; Chow, M. S.; Kemsley, J. N.; Lehnert, N.; Solomon, E. I. *J. Am. Chem. Soc.* **2006**, *128*, 4719.

(125) Neese, F.; Zaleski, J. M.; Loeb Zaleski, K.; Solomon, E. I. *J. Am. Chem. Soc.* **2000**, *122*, 11703.

(126) Kumar, D.; Hirao, H.; Shaik, S.; Kozlowski, P. M. *J. Am. Chem. Soc.* **2006**, *128*, 16148.

(127) Armstrong, W. H.; Lippard, S. J. *J. Am. Chem. Soc.* **1983**, *105*, 4837.

(128) Sallmann, M.; Oldenburg, F.; Braun, B.; Réglier, M.; Simaan, A. J.; Limberg, C. *Angew. Chem. Int. Ed.* **2015**, *54*, 12325.

(129) Barton, D. H. R.; Doller, D. *Acc. Chem. Res.* **1992**, *25*, 504.

(130) Kim, C.; Chen, K.; Kim, J.; Que, L. *J. Am. Chem. Soc.* **1997**, *119*, 5964.

(131) Chen, K.; Que, L. *J. Am. Chem. Soc.* **2001**, *123*, 6327.

(132) Chen, K.; Costas, M.; Que, J. L. *J. Chem. Soc., Dalton Trans.* **2002**, 672.

(133) Sun, C.-L.; Li, B.-J.; Shi, Z.-J. *Chem. Rev.* **2011**, *111*, 1293.

(134) Oloo, W. N.; Que, L. *Acc. Chem. Res.* **2015**, *48*, 2612.

(135) Lindhorst, A. C.; Haslinger, S.; Kuhn, F. E. *Chem. Commun.* **2015**, *51*, 17193.

(136) England, J.; Britovsek, G. J. P.; Rabadia, N.; White, A. J. P. *Inorg. Chem.* **2007**, *46*, 3752.

(137) Company, A.; Gómez, L.; Güell, M.; Ribas, X.; Luis, J. M.; Que, L.; Costas, M. *J. Am. Chem. Soc.* **2007**, *129*, 15766.

(138) Company, A.; Gómez, L.; Fontrodona, X.; Ribas, X.; Costas, M. *Chem. Eur. J.* **2008**, *14*, 5727.

(139) Bukowski, M. R.; Comba, P.; Lienke, A.; Limberg, C.; Lopez de Laorden, C.; Mas-Ballesté, R.; Merz, M.; Que, L. *Angew. Chem. Int. Ed.* **2006**, *45*, 3446.

(140) Bautz, J.; Comba, P.; Lopez de Laorden, C.; Menzel, M.; Rajaraman, G. *Angew. Chem. Int. Ed.* **2007**, *46*, 8067.

(141) Chen, M. S.; White, M. C. *Science* **2010**, *327*, 566.

(142) Nam, W.; Ho, R.; Valentine, J. S. *J. Am. Chem. Soc.* **1991**, *113*, 7052.

(143) White, M. C.; Doyle, A. G.; Jacobsen, E. N. *J. Am. Chem. Soc.* **2001**, *123*, 7194.

(144) Cusso, O.; Ribas, X.; Costas, M. *Chem. Commun.* **2015**, *51*, 14285.

(145) Wu, M.; Miao, C.-X.; Wang, S.; Hu, X.; Xia, C.; Kühn, F. E.; Sun, W. *Adv. Synth. Catal.* **2011**, *353*, 3014.

(146) Cussó, O.; Garcia-Bosch, I.; Ribas, X.; Lloret-Fillol, J.; Costas, M. *J. Am. Chem. Soc.* **2013**, *135*, 14871.

(147) Ryu, J. Y.; Kim, J.; Costas, M.; Chen, K.; Nam, W.; Que Jr, L. *Chem. Commun.* **2002**, 1288.

(148) Prat, I.; Font, D.; Company, A.; Junge, K.; Ribas, X.; Beller, M.; Costas, M. *Adv. Synth. Catal.* **2013**, *355*, 947.

(149) Costas, M.; Tipton, A. K.; Chen, K.; Jo, D.-H.; Que, L. *J. Am. Chem. Soc.* **2001**, *123*, 6722.

(150) Suzuki, K.; Oldenburg, P. D.; Que, L. *Angew. Chem. Int. Ed.* **2008**, *47*, 1887.

(151) Enthaler, S.; Junge, K.; Beller, M. *Angew. Chem. Int. Ed.* **2008**, *47*, 3317.

(152) Chow, T. W.-S.; Wong, E. L.-M.; Guo, Z.; Liu, Y.; Huang, J.-S.; Che, C.-M. *J. Am. Chem. Soc.* **2010**, *132*, 13229.

(153) Yazerski, V. A.; Spannring, P.; Gatineau, D.; Woerde, C. H. M.; Wieclawska, S. M.; Lutz, M.; Kleijn, H.; Klein Gebbink, R. J. M. *Org. Biomol. Chem.* **2014**, *12*, 2062.

(154) Casitas, A.; Krause, H.; Goddard, R.; Fürstner, A. *Angew. Chem. Int. Ed.* **2015**, *54*, 1521.

(155) Costas, M.; Chen, K.; Que Jr, L. *Coord. Chem. Rev.* **2000**, *200–202*, 517.

(156) Buxton, G. V.; Greenstock, C. L.; Helman, W. P.; Ross, A. B. *J. Phys. Chem. Ref. Data* **1988**, *17*, 513.

(157) Sono, M.; Roach, M. P.; Coulter, E. D.; Dawson, J. H. *Chem. Rev.* **1996**, *96*, 2841.

(158) Nesheim, J. C.; Lipscomb, J. D. *Biochemistry* **1996**, *35*, 10240.

(159) Groves, J. T.; Nemo, T. E. *J. Am. Chem. Soc.* **1983**, *105*, 6243.

(160) Russell, G. A. *J. Am. Chem. Soc.* **1957**, *79*, 3871.

(161) Miyajima, S.; Simamura, O. *Bull. Chem. Soc. Jpn.* **1975**, *48*, 526.

(162) Chen, M. S.; White, M. C. *Science* **2007**, *318*, 783.

(163) Bernadou, J.; Meunier, B. *Chem. Commun.* **1998**, 2167.

(164) Kovaleva, E. G.; Neibergall, M. B.; Chakrabarty, S.; Lipscomb, J. D. *Acc. Chem. Res.* **2007**, *40*, 475.

(165) Meunier, B.; de Visser, S. P.; Shaik, S. *Chemical Reviews* **2004**, *104*, 3947.

(166) Xing, G.; Diao, Y.; Hoffart, L. M.; Barr, E. W.; Prabhu, K. S.; Arner, R. J.; Reddy, C. C.; Krebs, C.; Bollinger, J. M. *Proc. Natl. Acad. Sci. U.S.A.* **2006**, *103*, 6130.

(167) Jeoung, J.-H.; Bommer, M.; Lin, T.-Y.; Dobbek, H. *Proc. Natl. Acad. Sci. U.S.A.* **2013**, *110*, 12625.

(168) Shan, X.; Que, L. *Proc. Natl. Acad. Sci. U.S.A.* **2005**, *102*, 5340.

(169) Zhao, M.; Helms, B.; Slonkina, E.; Friedle, S.; Lee, D.; DuBois, J.; Hedman, B.; Hodgson, K. O.; Fréchet, J. M. J.; Lippard, S. J. *J. Am. Chem. Soc.* **2008**, *130*, 4352.

(170) Chiang, C.-W.; Kleespies, S. T.; Stout, H. D.; Meier, K. K.; Li, P.-Y.; Bominaar, E. L.; Que, L.; Münck, E.; Lee, W.-Z. *J. Am. Chem. Soc.* **2014**, *136*, 10846.

(171) Cho, J.; Jeon, S.; Wilson, S. A.; Liu, L. V.; Kang, E. A.; Braymer, J. J.; Lim, M. H.; Hedman, B.; Hodgson, K. O.; Valentine, J. S.; Solomon, E. I.; Nam, W. *Nature* **2011**, *478*, 502.

(172) Park, M. J.; Lee, J.; Suh, Y.; Kim, J.; Nam, W. *Journal of the American Chemical Society* **2006**, *128*, 2630.

(173) Seo, M. S.; Kamachi, T.; Kouno, T.; Murata, K.; Park, M. J.; Yoshizawa, K.; Nam, W. *Angew. Chem. Int. Ed.* **2007**, *46*, 2291.

(174) Oloo, W. N.; Fielding, A. J.; Que, L. *J. Am. Chem. Soc.* **2013**, *135*, 6438.

(175) Roelfes, G.; Vrajmasu, V.; Chen, K.; Ho, R. Y. N.; Rohde, J.-U.; Zondervan, C.; la Crois, R. M.; Schudde, E. P.; Lutz, M.; Spek, A. L.; Hage, R.; Feringa, B. L.; Münck, E.; Que, L. *Inorg. Chem.* **2003**, *42*, 2639.

(176) Thibon, A.; England, J.; Martinho, M.; Young, V. G.; Frisch, J. R.; Guillot, R.; Girerd, J.-J.; Münck, E.; Que, L.; Banse, F. *Angew. Chem. Int. Ed.* **2008**, *47*, 7064.

(177) Hong, S.; Lee, Y.-M.; Shin, W.; Fukuzumi, S.; Nam, W. *J. Am. Chem. Soc.* **2009**, *131*, 13910.

(178) Bukowski, M. R.; Comba, P.; Limberg, C.; Merz, M.; Que, L.; Wistuba, T. *Angew. Chem. Int. Ed.* **2004**, *43*, 1283.

(179) Ho, R. Y. N.; Roelfes, G.; Feringa, B. L.; Que, L. *Journal of the American Chemical Society* **1999**, *121*, 264.

(180) Mekmouche, Y.; Hummel, H.; Ho, R. Y. N.; Que, J. L.; Schünemann, V.; Thomas, F.; Trautwein, A. X.; Lebrun, C.; Gorgy, K.; Leprêtre, J.-C.; Collomb, M.-N.; Deronzier, A.; Fontecave, M.; Ménage, S. *Chemistry – A European Journal* **2002**, *8*, 1196.

(181) Mikhalyova, E. A.; Makhlynets, O. V.; Palluccio, T. D.; Filatov, A. S.; Rybak-Akimova, E. V. *Chem. Commun.* **2012**, *48*, 687.

(182) He, Y.; Goldsmith, C. R. *Chem. Commun.* **2012**, *48*, 10532.

(183) Li, F.; Meier, K. K.; Cranswick, M. A.; Chakrabarti, M.; Van Heuvelen, K. M.; Münck, E.; Que, L. *J. Am. Chem. Soc.* **2011**, *133*, 7256.

(184) Kim, Y. M.; Cho, K.-B.; Cho, J.; Wang, B.; Li, C.; Shaik, S.; Nam, W. *J. Am. Chem. Soc.* **2013**, *135*, 8838.

(185) Annaraj, J.; Suh, Y.; Seo, M. S.; Kim, S. O.; Nam, W. *Chem. Commun.* **2005**, 4529.

(186) Wang, B.; Lee, Y.-M.; Clémancey, M.; Seo, M. S.; Sarangi, R.; Latour, J.-M.; Nam, W. *J. Am. Chem. Soc.* **2016**, *138*, 2426.

(187) Zhang, X.; Furutachi, H.; Tojo, T.; Tsugawa, T.; Fujinami, S.; Sakurai, T.; Suzuki, M. *Chem. Lett.* **2011**, *40*, 515.

(188) Guisado-Barrios, G.; Zhang, Y.; Harkins, A. M.; Richens, D. T. *Inorg. Chem. Commun.* **2012**, *20*, 81.

(189) Duban, E. A.; Bryliakov, K. P.; Talsi, E. P. *Eur. J. Inorg. Chem.* **2007**, *2007*, 852.

(190) Lyakin, O. Y.; Bryliakov, K. P.; Britovsek, G. J. P.; Talsi, E. P. *J. Am. Chem. Soc.* **2009**, *131*, 10798.

(191) Lyakin, O. Y.; Bryliakov, K. P.; Talsi, E. P. *Inorg. Chem.* **2011**, *50*, 5526.

(192) Oloo, W. N.; Meier, K. K.; Wang, Y.; Shaik, S.; Münck, E.; Que, L. *Nat. Commun.* **2014**, *5*.

(193) Makhlynets, O. V.; Oloo, W. N.; Moroz, Y. S.; Belaya, I. G.; Palluccio, T. D.; Filatov, A. S.; Muller, P.; Cranswick, M. A.; Que, L.; Rybak-Akimova, E. V. *Chem. Commun.* **2014**, *50*, 645.

(194) Wang, Y.; Janardanan, D.; Usharani, D.; Han, K.; Que, L.; Shaik, S. *ACS Catal.* **2013**, *3*, 1334.

(195) Khusnutdinova, J. R.; Luo, J.; Rath, N. P.; Mirica, L. M. *Inorg. Chem.* **2013**, *52*, 3920.

(196) Lennartson, A.; McKenzie, C. J. *Angew. Chem. Int. Ed.* **2012**, *51*, 6767.

(197) Hong, S.; Wang, B.; Seo, M. S.; Lee, Y.-M.; Kim, M. J.; Kim, H. R.; Ogura, T.; Garcia-Serres, R.; Clémancey, M.; Latour, J.-M.; Nam, W. *Angew. Chem. Int. Ed.* **2014**, *53*, 6388.

(198) Wang, B.; Lee, Y.-M.; Seo, M. S.; Nam, W. *Angew. Chem. Int. Ed.* **2015**, *54*, 11740.

(199) Price, J. C.; Barr, E. W.; Glass, T. E.; Krebs, C.; Bollinger, J. M. *J. Am. Chem. Soc.* **2003**, *125*, 13008.

(200) Proshlyakov, D. A.; Henshaw, T. F.; Monterosso, G. R.; Ryle, M. J.; Hausinger, R. P. *J. Am. Chem. Soc.* **2004**, *126*, 1022.

(201) Sinnecker, S.; Svensen, N.; Barr, E. W.; Ye, S.; Bollinger, J. M.; Neese, F.; Krebs, C. *J. Am. Chem. Soc.* **2007**, *129*, 6168.

(202) Panay, A. J.; Lee, M.; Krebs, C.; Bollinger, J. M.; Fitzpatrick, P. F. *Biochemistry* **2011**, *50*, 1928.

(203) Eser, B. E.; Barr, E. W.; Frantom, P. A.; Saleh, L.; Bollinger, J. M.; Krebs, C.; Fitzpatrick, P. F. *J. Am. Chem. Soc.* **2007**, *129*, 11334.

(204) Galonic, D. P.; Barr, E. W.; Walsh, C. T.; Bollinger, J. M.; Krebs, C. *Nat. Chem. Biol.* **2007**, *3*, 113.

(205) Matthews, M. L.; Krest, C. M.; Barr, E. W.; Vaillancourt, F. H.; Walsh, C. T.; Green, M. T.; Krebs, C.; Bollinger, J. M. *Biochemistry* **2009**, *48*, 4331.

(206) Hoffart, L. M.; Barr, E. W.; Guyer, R. B.; Bollinger, J. M.; Krebs, C. *Proc. Natl. Acad. Sci. U.S.A.* **2006**, *103*, 14738.

(207) Grapperhaus, C. A.; Mienert, B.; Bill, E.; Weyhermüller, T.; Wieghardt, K. *Inorg. Chem.* **2000**, *39*, 5306.

(208) Rohde, J.-U.; In, J.-H.; Lim, M. H.; Brennessel, W. W.; Bukowski, M. R.; Stubna, A.; Münck, E.; Nam, W.; Que, L. *Science* **2003**, *299*, 1037.

(209) Hohenberger, J.; Ray, K.; Meyer, K. *Nat. Commun.* **2012**, *3*, 720.

(210) McDonald, A. R.; Que, L. *Nat. Chem.* **2011**, *3*, 761.

(211) Wang, D.; Ray, K.; Collins, M. J.; Farquhar, E. R.; Frisch, J. R.; Gomez, L.; Jackson, T. A.; Kerscher, M.; Waleska, A.; Comba, P.; Costas, M.; Que, L. *Chem. Sci.* **2013**, *4*, 282.

(212) Que, L. *Acc. Chem. Res.* **2007**, *40*, 493.

(213) Nam, W.; Lee, Y.-M.; Fukuzumi, S. *Acc. Chem. Res.* **2014**, *47*, 1146.

(214) Meyer, S.; Klawitter, I.; Demeshko, S.; Bill, E.; Meyer, F. *Angew. Chem. Int. Ed.* **2013**, *52*, 901.

(215) Klinker, E. J.; Kaizer, J.; Brennessel, W. W.; Woodrum, N. L.; Cramer, C. J.; Que, L. *Angew. Chem. Int. Ed.* **2005**, *44*, 3690.

(216) Prakash, J.; Rohde, G. T.; Meier, K. K.; Münck, E.; Que, L. *Inorg. Chem.* **2015**, *54*, 11055.

(217) England, J.; Bigelow, J. O.; Van Heuvelen, K. M.; Farquhar, E. R.; Martinho, M.; Meier, K. K.; Frisch, J. R.; Munck, E.; Que, L. *Chem. Sci.* **2014**, *5*, 1204.

(218) Lim, M. H.; Rohde, J.-U.; Stubna, A.; Bukowski, M. R.; Costas, M.; Ho, R. Y. N.; Münck, E.; Nam, W.; Que, L. *Proc. Natl. Acad. Sci. U.S.A.* **2003**, *100*, 3665.

(219) Sastri, C. V.; Sook Seo, M.; Joo Park, M.; Mook Kim, K.; Nam, W. *Chem. Commun.* **2005**, 1405.

(220) Company, A.; Sabenya, G.; González-Béjar, M.; Gómez, L.; Clémancey, M.; Blondin, G.; Jasniewski, A. J.; Puri, M.; Browne, W. R.; Latour, J.-M.; Que, L.; Costas, M.; Pérez-Prieto, J.; Lloret-Fillol, J. *J. Am. Chem. Soc.* **2014**, *136*, 4624.

(221) Kleespies, S. T.; Oloo, W. N.; Mukherjee, A.; Que, L. *Inorg. Chem.* **2015**, *54*, 5053.

(222) Seo, M. S.; Kim, N. H.; Cho, K.-B.; So, J. E.; Park, S. K.; Clemancey, M.; Garcia-Serres, R.; Latour, J.-M.; Shaik, S.; Nam, W. *Chem. Sci.* **2011**, *2*, 1039.

(223) Hirao, H.; Kumar, D.; Que, L.; Shaik, S. *Journal of the American Chemical Society* **2006**, *128*, 8590.

(224) Puri, M.; Que, L. *Acc. Chem. Res.* **2015**, *48*, 2443.

(225) Pestovsky, O.; Stoian, S.; Bominaar, E. L.; Shan, X.; Münck, E.; Que, L.; Bakac, A. *Angew. Chem. Int. Ed.* **2005**, *44*, 6871.

(226) England, J.; Martinho, M.; Farquhar, E. R.; Frisch, J. R.; Bominaar, E. L.; Münck, E.; Que, L. *Angew. Chem. Int. Ed.* **2009**, *48*, 3622.

(227) England, J.; Guo, Y.; Farquhar, E. R.; Young Jr, V. G.; Münck, E.; Que Jr, L. *J. Am. Chem. Soc.* **2010**, *132*, 8635.

(228) England, J.; Guo, Y.; Van Heuvelen, K. M.; Cranswick, M. A.; Rohde, G. T.; Bominaar, E. L.; Münck, E.; Que, L. *J. Am. Chem. Soc.* **2011**, *133*, 11880.

(229) Lacy, D. C.; Gupta, R.; Stone, K. L.; Greaves, J.; Ziller, J. W.; Hendrich, M. P.; Borovik, A. S. *J. Am. Chem. Soc.* **2010**, *132*, 12188.

(230) Bigi, J. P.; Harman, W. H.; Lassalle-Kaiser, B.; Robles, D. M.; Stich, T. A.; Yano, J.; Britt, R. D.; Chang, C. J. *J. Am. Chem. Soc.* **2012**, *134*, 1536.

(231) Biswas, A. N.; Puri, M.; Meier, K. K.; Oloo, W. N.; Rohde, G. T.; Bominaar, E. L.; Münck, E.; Que, L. *J. Am. Chem. Soc.* **2015**, *137*, 2428.

(232) Sinnecker, S.; Svensen, N.; Barr, E. W.; Ye, S.; Bollinger, J. M.; Neese, F.; Krebs, C. *Journal of the American Chemical Society* **2007**, *129*, 6168.

(233) Chanda, A.; Popescu, D.-L.; de Oliveira, F. T.; Bominaar, E. L.; Ryabov, A. D.; Münck, E.; Collins, T. J. *J. Inorg. Biochem.* **2006**, *100*, 606.

(234) de Oliveira, F. T.; Chanda, A.; Banerjee, D.; Shan, X.; Mondal, S.; Que, L.; Bominaar, E. L.; Münck, E.; Collins, T. J. *Science* **2007**, *315*, 835.

(235) Ghosh, M.; Singh, K. K.; Panda, C.; Weitz, A.; Hendrich, M. P.; Collins, T. J.; Dhar, B. B.; Sen Gupta, S. *J. Am. Chem. Soc.* **2014**, *136*, 9524.

(236) Kwon, E.; Cho, K.-B.; Hong, S.; Nam, W. *Chem. Commun.* **2014**, *50*, 5572.

(237) Kundu, S.; Thompson, J. V. K.; Shen, L. Q.; Mills, M. R.; Bominaar, E. L.; Ryabov, A. D.; Collins, T. J. *Chem. Eur. J.* **2015**, *21*, 1803.

(238) Prat, I.; Mathieson, J. S.; Güell, M.; Ribas, X.; Luis, J. M.; Cronin, L.; Costas, M. *Nat. Chem.* **2011**, *3*, 788.

(239) Hitomi, Y.; Arakawa, K.; Funabiki, T.; Kodera, M. *Angew. Chem. Int. Ed.* **2012**, *51*, 3448.

(240) Van Heuvelen, K. M.; Fiedler, A. T.; Shan, X.; De Hont, R. F.; Meier, K. K.; Bominaar, E. L.; Münck, E.; Que, L. *Proc. Natl. Acad. Sci. U.S.A.* **2012**, *109*, 11933.

(241) Tse, C.-W.; Chow, T. W.-S.; Guo, Z.; Lee, H. K.; Huang, J.-S.; Che, C.-M. *Angew. Chem. Int. Ed.* **2014**, *53*, 798.

(242) Lyakin, O. Y.; Zima, A. M.; Samsonenko, D. G.; Bryliakov, K. P.; Talsi, E. P. *ACS Catal.* **2015**, *5*, 2702.

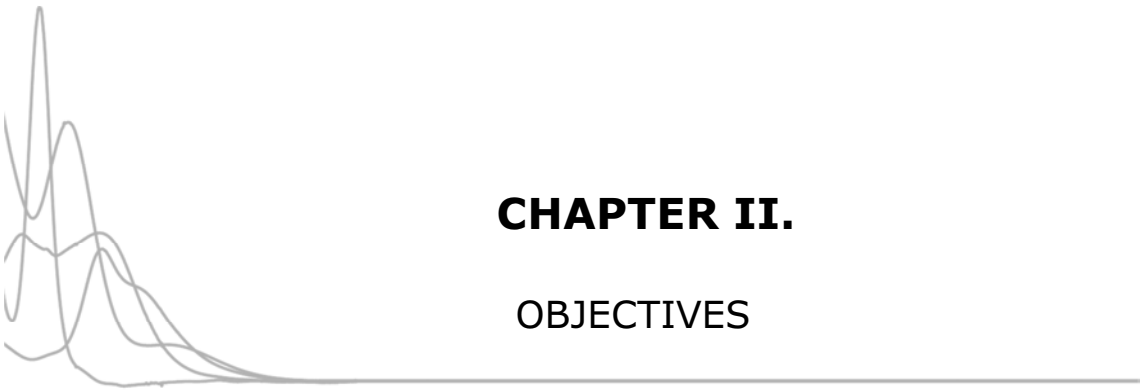

CHAPTER II.

OBJECTIVES

II. OBJECTIVES

The use of synthetic model systems is an excellent tool in order to get insight on the structure and reactivity of enzymes. Especially interesting is the study of O_2-activating proteins. In nature, this class of enzymes, which often contain copper and/or iron in their active site, carries out oxidative processes in a highly selective manner and using O_2 as oxidant. With the idea of designing oxidative transformations that operate in an environmentally friendly manner, much effort has been devoted to develop low molecular weight complexes to reproduce the chemical activity of a given enzyme. Even though we are still far from optimal processes, great advances have been achieved over the last decades. In this context, this thesis will be focused in the preparation of copper and nonheme iron-based complexes for O_2 activation. Special attention will be given to the characterization of highly elusive metal based oxidizing species, which are the key reaction intermediates in oxidation catalysis, and to the study of their reactivity.

To date, the development of unsymmetric complexes for oxygen activation has remained scarce due to the complexity of building pure heterometallic compounds. In this line, in **Chapter III** we will synthesize a carefully designed ligand, L^{N3N4} (Scheme II.1), which contains two markedly different coordinating sites. L^{N3N4} is an aminopyridine-based ligand designed in order to mimic the nitrogen-rich environment found in the active site of enzymes. We will synthesize the dicopper complex and explore its reactivity towards O_2 at low temperatures in order to trap and characterize possible copper-dioxygen adducts. More interestingly, we will study the abilities of L^{N3N4} in holding heterometallic complexes, using copper(I) and a complementary metal, and we will also study their reactivity towards O_2.

In **Chapter IV** we will explore further the reactivity of a high valent copper-dioxygen species generated after reaction of a dicopper(I) precursor at cryogenic temperatures (Scheme II.1). This compound has been reported capable of performing *ortho*-hydroxylation of phenols, thus mimicking the activity of the enzyme tyrosinase. The oxidative power of such species towards the cleavage of *ortho*-substituted fluorophenolates is explored. This is a much more challenging reaction, since fluorine forms the strongest single bond to carbon and highly reactive species are needed to break it.

In **Chapters V-VII** our attention will be turned into modelling iron-based enzymes. A novel iron(II) complex based on a tetradentate ligand is described (Scheme II.1). This complex structurally resembles other complexes that have been described as successful catalysts for the oxidation of hydrocarbons in combination with peroxides or peracids as oxidants. Even though we will also be interested in developing catalytic activity, the main aim of this thesis is to trap and characterize the active species in the catalytic cycle of such oxidations. In order to do so, reaction of the designed ferrous complex with oxidants will be studied. Full spectroscopic characterization of the resulting species and the study of their reactivity will be the main focus in

this part of the thesis with the final goal of unraveling their relevance in oxidation processes, both in enzymes and in synthetic oxidations.

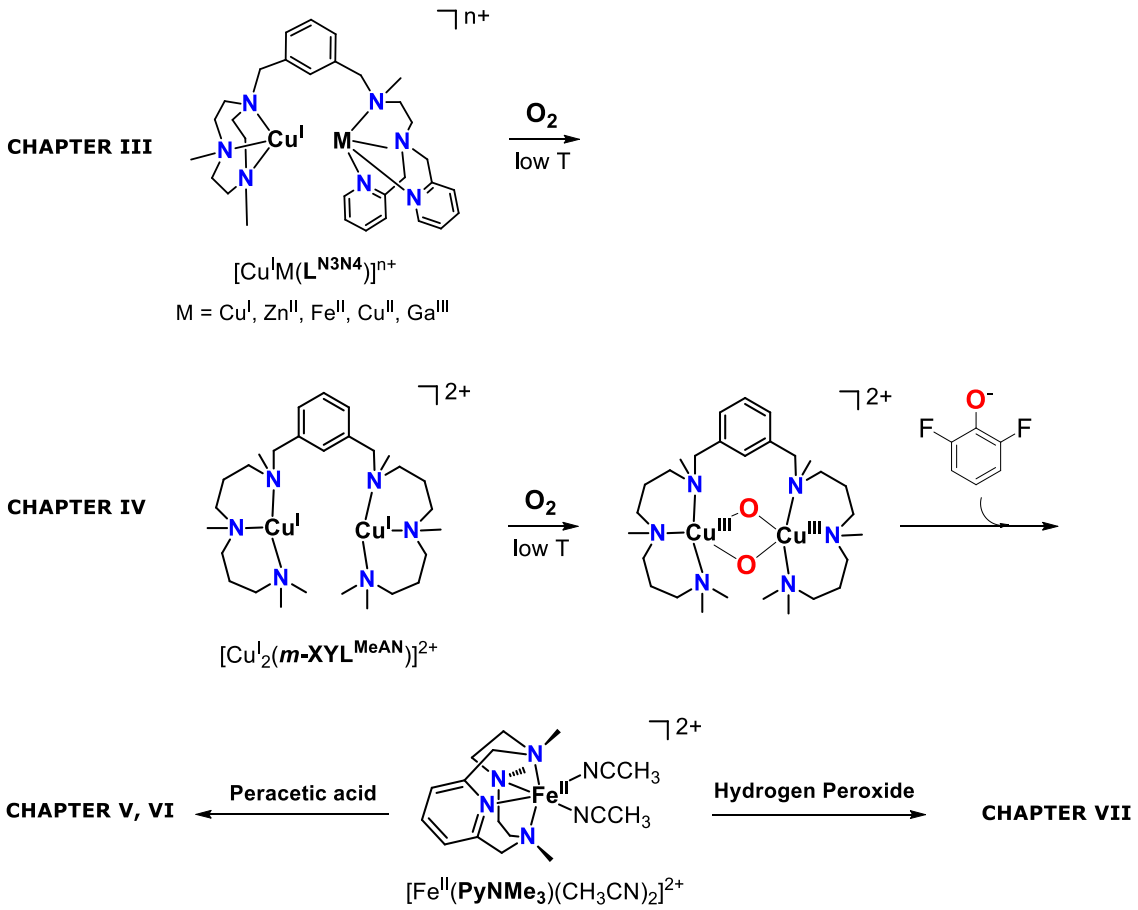

Scheme II.1 Schematic representation of the objectives of this thesis.

CHAPTER III.

Building Complexity in O_2 Binding Copper Complexes. Site-selective Metalation and Intermolecular O_2-Binding at Dicopper and Heterometallic Complexes Derived from an Unsymmetric Ligand

This chapter corresponds to the following publication:

Joan Serrano-Plana, Miquel Costas,* and Anna Company*

Inorg. Chem., **2014**, *53*, 12929-12938

For this publication, J.S.-P. synthesized and characterized all the reported ligands and complexes, and he also performed the reactivity studies. Besides, J.S.-P. contributed in writing the manuscript and was involved in argumentations and discussions.

Inorganic Chemistry

Article

pubs.acs.org/IC

Building Complexity in O_2-Binding Copper Complexes. Site-Selective Metalation and Intermolecular O_2-Binding at Dicopper and Heterometallic Complexes Derived from an Unsymmetric Ligand

Joan Serrano-Plana, Miquel Costas,* and Anna Company*

Grup de Química Bioinorgànica, Supramolecular i Catàlisi (QBIS-CAT), Institut de Química Computacional i Catàlisi (IQCC), Departament de Química, Universitat de Girona, Campus Montilivi, E17071 Girona, Catalonia, Spain

Supporting Information

ABSTRACT: A novel unsymmetric dinucleating ligand (L^{N3N4}) combining a tridentate and a tetradentate binding sites linked through a *m*-xylyl spacer was synthesized as ligand scaffold for preparing homo- and dimetallic complexes, where the two metal ions are bound in two different coordination environments. Site-selective binding of different metal ions is demonstrated. L^{N3N4} is able to discriminate between Cu^I and a complementary metal (M′ = Cu^I, Zn^{II}, Fe^{II}, Cu^{II}, or Ga^{III}) so that pure heterodimetallic complexes with a general formula $[Cu^IM'(L^{N3N4})]^{n+}$ are synthesized. Reaction of the dicopper(I) complex $[Cu^I_2(L^{N3N4})]^{2+}$ with O_2 leads to the formation of two different copper-dioxygen (Cu_2O_2) intermolecular species (**O** and ^{T}**P**) between two copper atoms located in the same site from different complex molecules. Taking advantage of this feature, reaction of the heterodimetallic complexes $[CuM'(L^{N3N4})]^{n+}$ with O_2 at low temperature is used as a tool to determine the final position of the Cu^I center in the system because only one of the two Cu_2O_2 species is formed.

INTRODUCTION

Unsymmetric dinuclear active centers are commonly found in metalloproteins.[1] They can be either dimetallic centers where two metal ions of different nature act together to afford activity (e.g., FeZn purple acid phosphatases[2]) or homometallic sites in which the asymmetry originates from a markedly different coordination environment around each of the metal sites (hemerythrin[3]). Especially remarkable is the structural diversity found in O_2-activating enzymes relying on copper.[4,5] Some copper-containing dinuclear proteins have a heterometallic active site, so that a Cu center shares the active site with a second metal such as iron (cytochrome *c* oxidase)[6] or zinc (superoxide dismutase).[7] In addition, enzymes such as peptidylglicine-α-hydroxylating monooxygenase (PHM),[8] dopamine-β-hydroxylase (DβH),[8,9] and tyrosinase[10] bear two copper atoms in distinct coordination environments. While for PHM and DβH the residues coordinated to each of the copper ions are different, in the case of tyrosinase, the differences of the second coordination sphere render the two metal ions inequivalent. The lack of equivalence enables the two metals to perform different essential tasks in the enzymatic reaction.[8,9,11,12] The development of well-defined synthetic models with unsymmetrical bimetallic centers is highly desirable to understand these enzymatic processes, and it may be relevant for the development of catalytic systems.[13−18]

Modeling copper−dioxygen chemistry occurring in enzymes has attracted the attention of many research groups over the last three decades, and it is well-stablished that the ligand architecture surrounding the copper center determines the structure of the resulting Cu−dioxygen species.[5,19−24] However, the number of model systems featuring unsymmetric dinuclear sites is rather limited, most likely due to the difficulty in establishing control over the distribution of the two types of metals in the system.[1,13,25,26] Apart from the inherent difficulty in the challenging synthesis of unsymmetric dinucleating ligands, the preparation of heterometallic complexes might be hampered by the formation of homometallic complexes during the synthesis. One efficient strategy to overcome this problem is the design of dinucleating ligands with two differentiated binding sites that exhibit markedly distinctive affinities for the two metals involved.[26,27] Although the synthesis of these ligands is not straightforward, unsymmetric dicopper systems[28−30] and synthetic models of cytochrome c oxidase have been successfully prepared following this methodology.[31]

In this line, we recently described the preparation of a dicopper(I) complex bearing a dinucleating ligand that confers different coordination environments to the two metal centers.[32] Reaction of this dicopper complex toward O_2 afforded an unsymmetric *trans*-1,2-peroxodicopper(II) core, which exhibits reactivity patterns distinct from symmetric analogues.[33] Following these studies, in the present work we explore the coordination chemistry of a novel polyamine ligand scaffold designed with the aim to provide two distinct binding sites. The ligand was devised suitable for preparing well-defined heterometallic complexes combining copper(I) and another metal.

Received: August 14, 2014
Published: November 26, 2014

ACS Publications © 2014 American Chemical Society

Scheme 1. Synthetic Route toward the Preparation of L^{N3N4} and Schematic Representation of L^{N4N4}

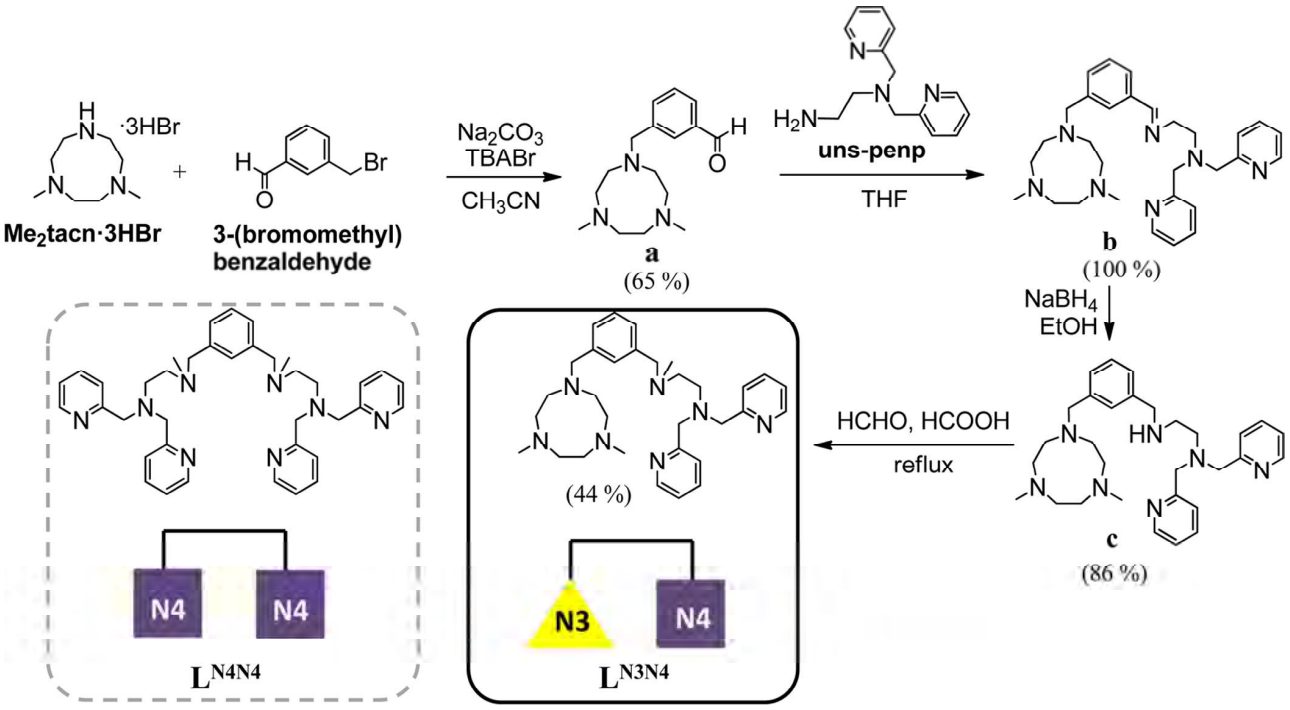

The designed ligand (L^{N3N4}) contains two distinct binding sites (N_3 and N_4) connected through a *meta*-xylyl moiety (Scheme 1). Both donor sets were used independently to support Cu^I/O_2 chemistry. The tridentate binding site (N_3) corresponds to a triazacyclononane ring (tacn), which forms highly stable complexes with a number of metals, which are chemically robust and resistant to oxidative degradation.[34] In this coordination environment, copper(I) is facially bound through the three aliphatic amines, and free coordination sites are available for interaction with other molecules. Tolman et al. have shown that the alkyl substituents in the nitrogen atoms of the triazacyclonane ring determine the outcome of the reaction of copper(I) with O_2. While *i*Pr-substituted tacn (iPr_3tacn) leads to a mixture of bis(μ-oxo)dicopper(III) (**O**) and μ–η^2:η^2-peroxodicopper(II) (^{s}**P**) species,[35] the less bulky benzyl or methyl substituents (Bn_3tacn and Me_3tacn) afford exclusively bis(μ-oxo)dicopper(III) (**O**) intermediates.[36−38] The second site (N_4) offers a tetracoordinating environment composed of two aliphatic nitrogen atoms and two pyridines (uns-penp). In contrast to tacn, uns-penp supports the formation of *trans*-1,2-peroxodicopper(II) (^{T}**P**) species upon reaction with O_2,[39,40] as occurs with other N-based tetradentate ligands.[41−44] The markedly different denticity of the two binding sites in L^{N3N4} is envisioned to translate into different binding constants that in turn should the preparation of heterobimetallic complexes combining copper(I) and another metal without contamination by the homometallic analogues.

Thus, in this work, we report the synthesis of the dinucleating ligand L^{N3N4} and we explore its ability to coordinate to copper(I) together with a second metal ion to give the corresponding heterobimetallic complexes $[Cu^IM'(L^{N3N4})]^{n+}$ (M′ = Cu^I, Zn^{II}, Fe^{II}, Cu^{II}, or Ga^{III}). Heterometallic complexes $[Cu^IM'(L^{N3N4})]^{n+}$ exhibit fast reactivity with O_2 to form tetrametallic $[(L^{N3N4})M'Cu(O_2)$-$CuM'(L^{N3N4})]^{2n+}$ species where the O_2 molecule binds two copper centers. The nature of the Cu_2O_2 unit can be interrogated by its distinctive spectroscopic properties, and this in turn can be used to identify which is the binding site (N_3 or N_4) of Cu^I and M′ in the heterometallic complex. This analysis demonstrates that metal binding in L^{N3N4} is site-selective.

RESULTS AND DISCUSSION

Synthesis of L^{N3N4} and L^{N4N4}. L^{N3N4} was obtained after four reaction steps with moderate yields starting from Me_2tacn·3HBr and 3-(bromomethyl)benzaldehyde (Scheme 1, see Experimental Section for details). The *meta*-xylyl linker was chosen because it has been successfully applied in the past for the preparation of dicopper complexes that intramolecularly bind O_2 and that can be seen as models of O_2-activating dicopper proteins.[5] The use of the unsymmetric platform 3-(bromomethyl)benzaldehyde, prepared by reductive hydrolysis of the commercially available 3-(bromomethyl)benzonitrile,[45] enables the connection of two differentiated donor sets in the same molecule. The linkage of the N_3 set (tacn) occurs by reaction of 3-(bromomethyl)benzaldehyde with equimolar amounts of Me_2tacn·3HBr through a nucleophilic substitution reaction to give compound **a**. The N_4 coordination site is introduced by a condensation reaction between the aldehyde functionality and the primary amine of uns-penp to give an imine (**b**). Its hydrogenation and posterior methylation affords the final ligand L^{N3N4}, which is purified by column chromatography.

For the sake of comparison, we also synthesized the symmetric ligand L^{N4N4} (Scheme 1 and Supporting Information, Scheme S1) bearing two identical tetracoordinating binding sites connected through a *meta*-xylyl moiety. L^{N4N4} was prepared through a similar synthetic route as the one followed to obtain L^{N3N4} (see Supporting Information for further details).

dx.doi.org/10.1021/ic501951f | Inorg. Chem. 2014, 53, 12929−12938

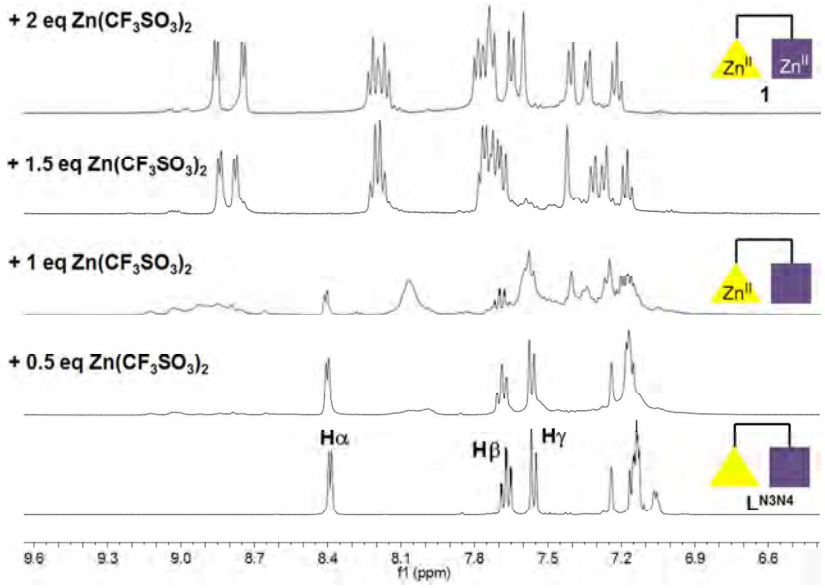

Figure 1. ^{1}H NMR monitoring of the titration of L^{N3N4} with $Zn(CF_3SO_3)_2$ in acetone-d_6 at 240 K. For clarity, only the aromatic region of the ^{1}H NMR spectrum is shown. The aliphatic region of the spectra is shown in Supporting Information, Figure S1. The tridentate and tetradentate sites are represented by a yellow triangle and a purple square, respectively.

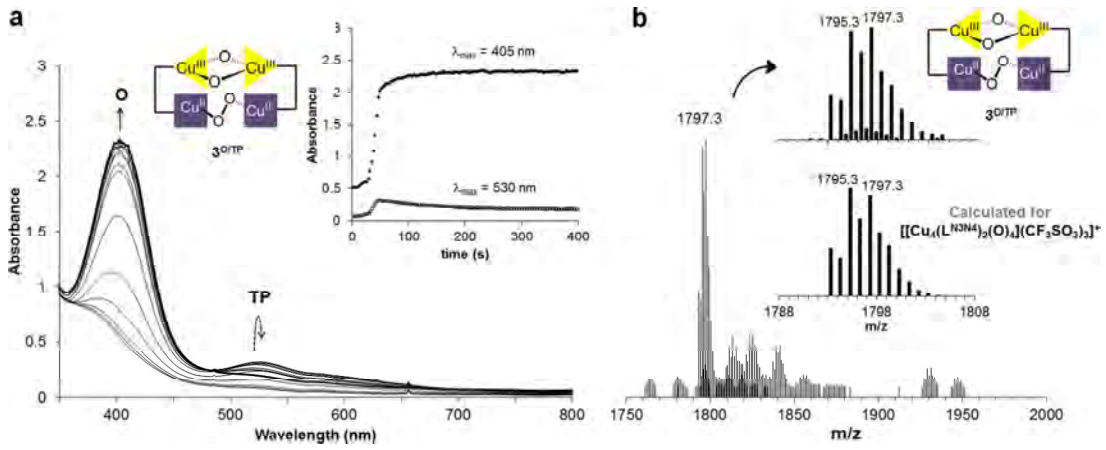

Figure 2. (a) UV−vis absorption spectra for the reaction of $[Cu^I_2(L^{N3N4})]^{2+}$ (**3**) (0.30 mM) and O_2 at −90 °C in acetonitrile/acetone 1:19. (inset) Time traces at 405 and 530 nm ($\mathbf{3}^{O/TP}$). (b) CSI-MS spectra at −90 °C for the reaction of **3** with O_2 in acetonitrile:acetone 1:19 leading to the formation of a dimeric species ($\mathbf{3}^{O/TP}$).

Homodimetallic Complexes. *Titration of L^{N3N4} with $Zn(CF_3SO_3)_2$.* To explore the ability of L^{N3N4} to selectively bind a metal ion in one of its two binding sites, we performed a ^{1}H NMR titration of the ligand in deuterated acetone (acetone-d_6) by adding small amounts of a metal salt (Figure 1). In particular, we chose $Zn(CF_3SO_3)_2$ because of its diamagnetic character and its stability under air enables its manipulation in the open atmosphere. The ^{1}H NMR spectrum of the free ligand (L^{N3N4}) in acetone-d_6 shows readily identifiable signals in the aromatic region corresponding to the two equivalent pyridine units in the tetradentate N_4 site (α, β, and γ protons) along with the less well-defined signals of the *meta*-xylyl moiety. Addition of 0.5 equiv of $Zn(CF_3SO_3)_2$ causes a broadening of these signals, but no apparent shift is observed, which suggests that Zn^{II} preferentially binds to the N_3 site and not to N_4. Addition of 0.5 equiv more of Zn^{II} causes severe broadening of the NMR lines, so that most likely some exchange of this metal ion is occurring between N_3 and N_4 sites. When more than 1 equiv of Zn^{II} is added the signals corresponding to H_α, H_β, and H_γ of the free ligand (L^{N3N4}) completely disappear, and new well-defined signals clearly arise (8.85, 8.74, and 8.18 ppm, Figure 1). Similar information can be extracted by analyzing the aliphatic region of the NMR spectrum (Supporting Information, Figure S1). Addition of a total of 2 equiv of Zn^{II} affords the homodimetallic complex $[Zn^{II}_2(L^{N3N4})]^{4+}$ (**1**), which was further characterized by high-resolution mass spectrometry (HR-MS) (Figure 1 and Supporting Information, Figure S2). Remarkably, the aromatic region of the ^{1}H NMR spectrum of **1** resembles that of the complex with the symmetric ligand $[Zn^{II}_2(L^{N4N4})](CF_3SO_3)_4$ (**2**) (Supporting Information, Figure S4). Thus, it seems that the first equivalent of zinc preferentially binds to the tacn ring (N_3) of L^{N3N4} and that the second equivalent binds to the N_4 binding site to form **1**. This observation suggests that L^{N3N4} can be potentially used to hold

dx.doi.org/10.1021/ic501951f | Inorg. Chem. 2014, 53, 12929−12938

heterobimetallic complexes generated by sequential addition of two different metals.

Synthesis of $[Cu^{I}_2(L^{N3N4})]^{2+}$ (3) and Its Reactivity with O_2. The dicopper(I) complex $[Cu^{I}_2(L^{N3N4})]^{2+}$ (**3**) was prepared in the glovebox by reaction of L^{N3N4} with 2 equiv of $[Cu^{I}(CH_3CN)_4](CF_3SO_3)$ in acetonitrile affording a bright yellow solution. All attempts to isolate this compound by precipitation or crystallization using diethyl ether were unsuccessful due to the tendency of the resulting complex to disproportionate, as evidenced by a color change to deep green (Cu^{II}) and the formation of copper mirror (Cu^0) upon addition of diethyl ether into solutions of **3**. Synthesis of **3** in any solvent different from acetonitrile such as CH_2Cl_2, tetrahydrofuran (THF), or acetone also led to its immediate disproportionation. Thus, characterization of **3** was carried out in solution in acetonitrile-containing mixtures. The ^{1}H NMR spectrum of **3** exhibits broad signals even at 240 K (Supporting Information, Figure S5),[46] while HR-MS shows the expected peaks for this dicopper(I) complex (Supporting Information, Figure S6).

As **3** could not be isolated, studies of its reaction with O_2 were carried out starting from freshly prepared solutions by mixing L^{N3N4} with 2 equiv of the copper(I) source. A concentrated stock solution of **3** in acetonitrile (18 mM) was prepared, and after a 60-fold dilution with dry acetone, the reaction with O_2 was monitored by UV–vis spectroscopy at −90 °C. Upon exposure to O_2, two intense absorption bands concurrently developed within 1 min (Figure 2a): the absorption at λ_{max} 530 nm (ε = 2000 M^{-1} cm^{-1}) reached its maximum absorbance after 45 s of reaction, and then it decayed, while another band at λ_{max} 405 nm (ε = 15 000 M^{-1} cm^{-1}) was formed approximately over the same period of time, but it remained stable for at least 15 min at −90 °C. Remarkably, the latter quickly decomposed upon warming the solution, and none of the bands were detected when the reaction of **3** with O_2 was performed at room temperature. Finally, it is worth highlighting that the oxygenation of **3** was irreversible, as recovery of the starting dicopper(I) complex was not achieved when vacuum was applied after reaction with O_2.

The fact that these two bands follow completely different decomposition time courses indicates that they arise from two independent chromophores. The reported **O** species obtained upon reaction of two mononuclear $[Cu^{I}(Me_3tacn)]^+$ units with O_2 exhibits very characteristic absorption bands at 307 nm (ε = 16 000 M^{-1} cm^{-1}) and 412 nm (ε = 18 000 M^{-1} cm^{-1}),[37] while ^{T}**P** species originating from the reaction of $[Cu^{I}(uns\text{-}penp)]^+$ with O_2 presents a UV–vis absorption at 535 nm (ε = 7000 M^{-1} cm^{-1}).[40] Comparison of these reported data with the observed reactivity of **3** with O_2 suggests that the unstable intermediate with λ_{max} = 530 nm may correspond to a ^{T}**P** species formed by interaction of two copper centers coordinated to the N_4 sites of two different molecules. Similarly, the intense band observed at 405 nm suggests the formation of an **O** species by interaction of copper centers located in the N_3 sites of two different molecules, giving rise to a complex structure containing two different Cu_2O_2 cores ($\mathbf{3}^{O/TP}$). Because of the intermolecular character of O_2 binding in **3**, both a dimeric species or an oligomeric/polymeric structure are plausible structures for $\mathbf{3}^{O/TP}$ (Scheme 2a,b, respectively). Cryospray ionization mass spectrometry (CSI-MS) turned out to provide conclusive information to distinguish between the two possibilities. Analysis of the initial stages of the reaction of **3** with O_2 by CSI-MS at 183 K (Figure 2b) clearly showed a major peak at *m*/*z* 1795.3 with a mass

Scheme 2. Representation of the Possible Structures of $\mathbf{3}^{O/TP}$ [a]

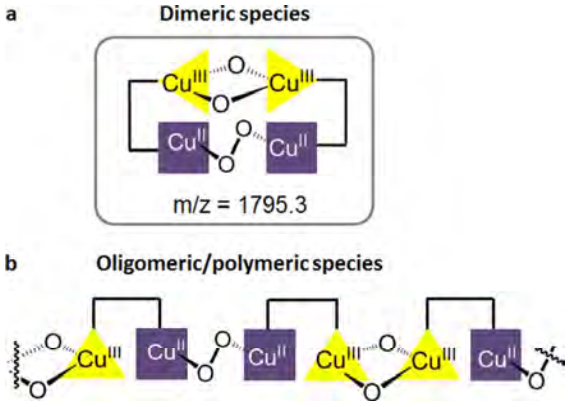

[a](a) Dimeric species. (b) Oligomeric/polymeric species.

value and an isotopic pattern corresponding to $\{[(L^{N3N4})\text{-}Cu^{II}Cu^{III}(\mu\text{-}O)_2(\mu\text{-}1,2\text{-}O_2)Cu^{II}Cu^{III}(L^{N3N4})](CF_3SO_3)_3\}^+$, which is consistent with the formation of a dimeric species in $\mathbf{3}^{O/TP}$ (Scheme 2a). No peak that could be attributed to an oligomeric/polymeric species was detected.

To gain more evidence about the formation of a putative ^{T}**P** species by interaction of two copper(I) centers in two different N_4 sites, we synthesized the symmetric dicopper(I) complex using L^{N4N4} $[Cu^{I}_2(L^{N4N4})]^{2+}$ (**4**) (Scheme 1 and Supporting Information, Figure S7). Indeed, upon reaction of **4** with O_2 at −90 °C in acetonitrile/acetone 1:19 the exclusive formation of the band at λ_{max} = 530 nm (ε = 4400 M^{-1} cm^{-1}) was observed (Supporting Information, Figure S8).

Heterobimetallic Complexes. Despite the fact that both binding sites in L^{N3N4} are nitrogen-based, the coordination number, donor set, and binding constants were envisioned to be different enough to enable the preparation of heterobimetallic complexes in which each of the metal ions is selectively coordinated to one of the binding sites, that is, N_3 or N_4. In this line and as shown above, titration of L^{N3N4} with Zn^{II} indicates that this ligand is potentially a good candidate to hold heterobimetallic complexes.

Synthesis of $[M^{II}Cu^{I}(L^{N3N4})]^{3+}$ (M = Zn (5), Cu (6), Fe (7)) and Their Reactivity with O_2. To test the ability of L^{N3N4} to give well-defined heterobimetallic complexes, initial experiments were carried out by combining copper(I) and zinc(II). The use of these diamagnetic metal ions enables the proper characterization of the resulting complexes by ^{1}H NMR spectroscopy.

$[Zn^{II}Cu^{I}(L^{N3N4})]^{3+}$ (**5**) was prepared in the glovebox by sequential addition of 1 equiv of $[Cu^{I}(CH_3CN)_4](CF_3SO_3)$ and 1 equiv of $Zn(CF_3SO_3)_2$ in an acetonitrile solution of L^{N3N4}. No matter the order of addition of the two metals, in any case the ^{1}H NMR spectrum of the product was the same. The aromatic region of the ^{1}H NMR spectrum of **5** presents a great similarity with that of **1** and **2** (Figure 3 and Supporting Information, Figure S4), meaning that zinc coordinates to the N_4 site. If, instead, Cu^{I} were located in the pyridine site, broader NMR signals, like those observed in the ^{1}H NMR spectrum of **3** or **4**, would be observed (Figure 3 and Supporting Information, Figure S5). Thus, according to ^{1}H NMR, in compound **5** zinc binds to the N_4 site, while copper is bound to the N_3 unit. It is worth highlighting that the addition

dx.doi.org/10.1021/ic501951f | Inorg. Chem. 2014, 53, 12929−12938

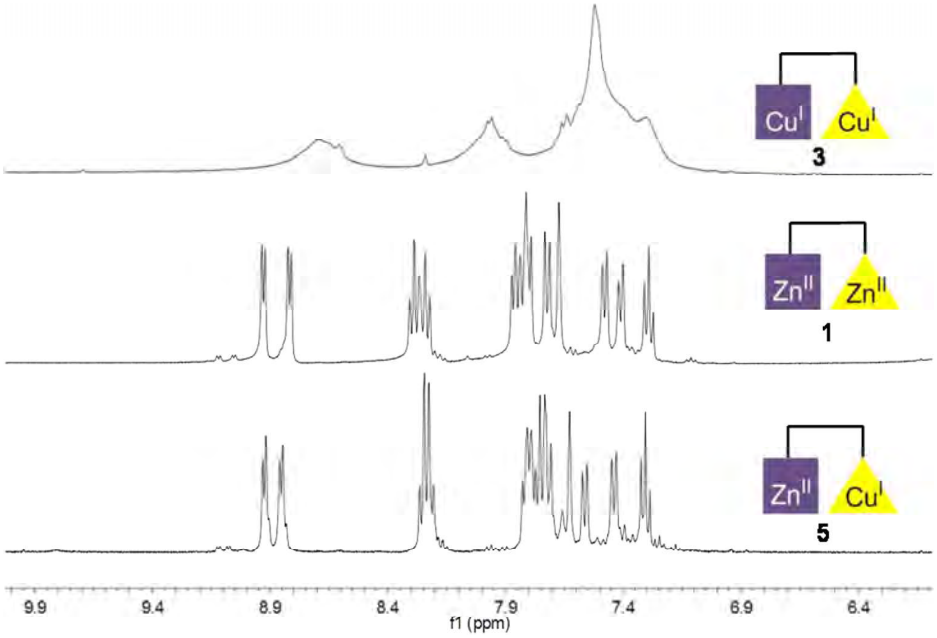

Figure 3. ^{1}H NMR spectrum of **1**, **3**, and **5** in CD_3CN/acetone-d_6 1:5 at 240 K. Only the aromatic region is shown for clarity.

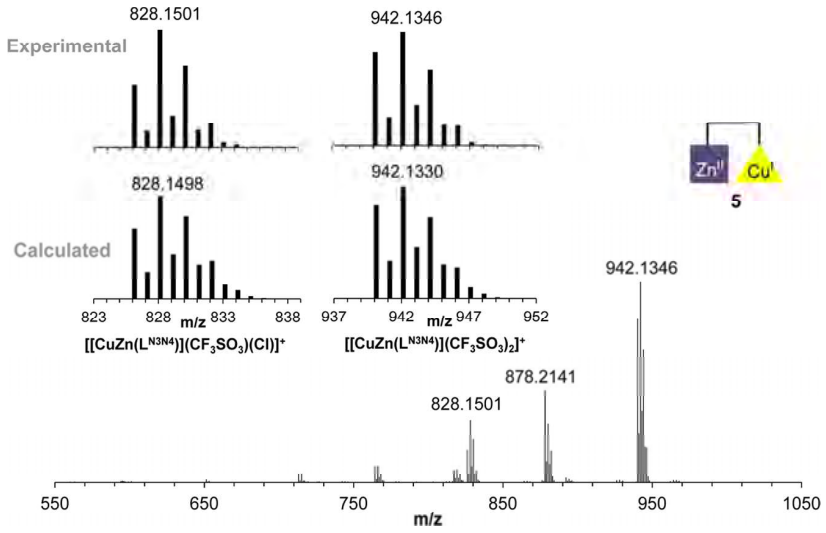

Figure 4. HR-MS spectrum of **5**. The peak at 878.2141 corresponds to the mononuclear $\{[Zn(L^{N3N4})](CF_3SO_3)_2H\}^+$ complex ($L^{N3N4} = C_{31}H_{45}N_7$).

of 1 equiv of Cu^I after the addition of 1 equiv of Zn^{II} displaces the latter from the N_3 site to the N_4 site (as ascertained in the titration experiment, the first equivalent of zinc coordinates to N_3 site).

Compound **5** was also characterized by HR-MS (Figure 4). Two main peaks were observed at m/z = 828.1501 and 942.1346 with mass values and isotopic patterns fully consistent with the pure heterodimetallic species $\{[Cu^IZn^{II}(L^{N3N4})](CF_3SO_3)(Cl)\}^+$ and $\{[Cu^IZn^{II}(L^{N3N4})](CF_3SO_3)_2\}^+$. Remarkably, no peaks of the possible homodimetallic dizinc(II) or dicopper(I) complexes **1** and **3**, respectively, were detected.

To obtain more experimental evidence in favor of the heterobimetallic complex **5**, we studied its reactivity with O_2 at cryogenic temperatures. UV−vis monitoring of the reaction of **5** with O_2 at −90 °C in acetonitrile/acetone 1:19 showed the formation within 20 min of a new band at 405 nm (ε = 11 900 M^{-1} cm^{-1}) corresponding to the intermolecular **O** species $[(L^{N3N4})Zn^{II}Cu^{III}(\mu\text{-}O)_2Cu^{III}Zn^{II}(L^{N3N4})]^{6+}$ ($\mathbf{5^O}$). No growth of any band at 530 nm characteristic of the ^{T}**P** species was observed, meaning that all the copper is located in the tacn tridentate binding site (Figure 5a). Remarkably, formation of $\mathbf{5^O}$ was observed independently of the order of addition of the two metallic salts to L^{N3N4} during the complex synthesis, which agrees with the formation of the same species as ascertained by NMR (see above).

The formation of $\mathbf{5^O}$ was further confirmed by CSI-MS at 183 K, which afforded a spectrum with peaks at m/z 2065.2049, 1951.2226, and 1839.2400 whose mass value and distribution pattern were consistent with $\{[(L^{N3N4})Zn^{II}Cu^{III}(\mu\text{-}O)_2Cu^{III}Zn^{II}(L^{N3N4})(CF_3SO_3)_5\}^+$, $\{[(L^{N3N4})Zn^{II}Cu^{III}(\mu\text{-}O)_2Cu^{III}Zn^{II}(L^{N3N4})](CF_3SO_3)_4Cl\}^+$, and $\{[(L^{N3N4})Zn^{II}Cu^{III}(\mu\text{-}O)_2Cu^{III}Zn^{II}(L^{N3N4})](CF_3SO_3)_3Cl_2\}^+$, respectively

dx.doi.org/10.1021/ic501951f | Inorg. Chem. 2014, 53, 12929−12938

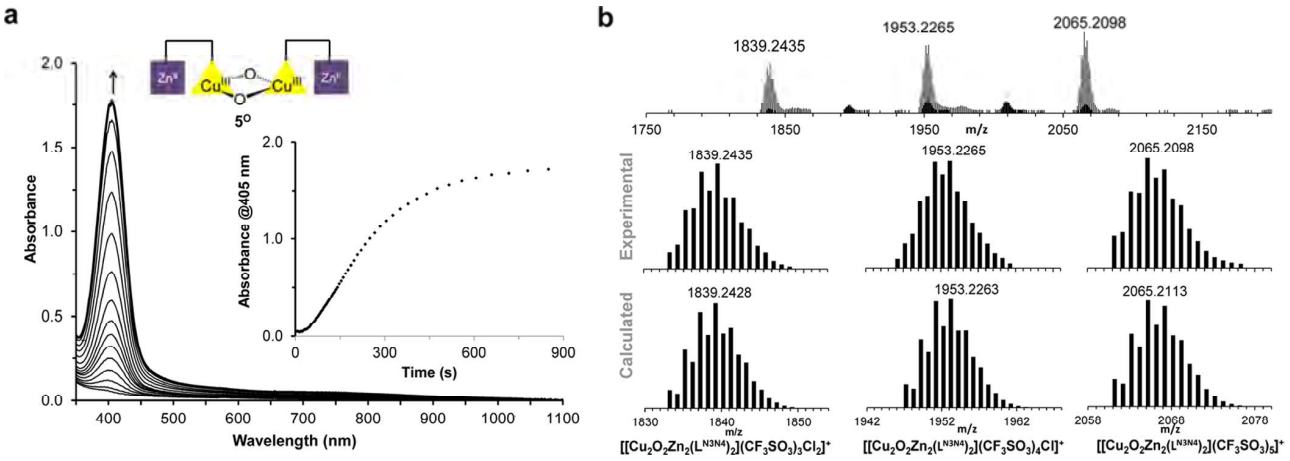

Figure 5. (a) UV−vis absorption spectra for the reaction of **5** (0.3 mM) with O_2 in acetonitrile/acetone 1:19 at −90 °C. (inset) Time trace at 405 nm. (b) CSI-MS spectra at −90 °C corresponding to the reaction of **5** with O_2 in acetonitrile/acetone 1:19 to give $\mathbf{5}^{O}$ ($L^{N3N4} = C_{31}H_{45}N_7$).

(Figure 5b). Remarkably all the identified peaks in the ESI-MS spectrum corresponded to pure heterobimetallic species containing both copper and zinc, which further renders L^{N3N4} as a privileged platform to selectively hold two different metals. Since both Zn^{II} and Cu^{I} have a d^{10} electronic configuration, none of them has stabilization of the crystal field according to the crystal field theory. Thus, it is remarkable that Cu^{I} is located in only one site, avoiding mixtures of **O** and ^{T}**P** species upon reaction with O_2.

Preparation of $[Cu^{II}Cu^{I}(L^{N3N4})]^{3+}$ (**6**) and $[Fe^{II}Cu^{I}(L^{N3N4})]^{3+}$ (**7**) was also achieved through the sequential addition of 1 equiv of $[Cu^{I}(CH_3CN)_4](CF_3SO_3)$ and then 1 equiv of $Cu^{II}(CF_3SO_3)_2$ or $[Fe^{II}(CF_3SO_3)_2(CH_3CN)_2]$ to L^{N3N4} in acetonitrile. These compounds could be characterized by HR-MS (Supporting Information, Figures S9 and S10). Attempts to characterize **6** and **7** by means of ^{1}H NMR proved unsuccessful, as only broad, not informative bands were observed in the spectra. UV−vis monitoring of the reaction of **6** and **7** with O_2 at −90 °C in acetonitrile/acetone 1:19 at −90 °C indicated the exclusive formation in both cases of an **O** species, $\mathbf{6}^{O}$ (λ_{max} = 405 nm, ε = 12 000 M^{-1} cm^{-1}), and $\mathbf{7}^{O}$ (λ_{max} = 405 nm, ε = 12 300 M^{-1} cm^{-1}), most likely arising from the intermolecular interaction between two copper(I) centers coordinated to N_3 sites of two different molecules (Figure 6 and Supporting Information, Figure S11). Interestingly, no heterometallic intramolecular O_2 activation occurred in $[Fe^{II}Cu^{I}(L^{N3N4})]^{3+}$ (**7**), where the redox active iron(II) center could potentially be involved in such activation processes.[47] Instead, formation of the intermolecular **O** species seems to be the thermodynamic driving force that dictates the fate of the O_2 activation. Overall, divalent metals such as Zn^{II}, Fe^{II} or Cu^{II} coordinate to the N_4 site in L^{N3N4} leaving the N_3 site available for copper(I), which gives intermolecular **O** species upon reaction with O_2.

Comparison of the formation and decay rates of the four bis(μ-oxo) species described in this manuscript ($\mathbf{3}^{O/TP}$, $\mathbf{5}^{O}$, $\mathbf{6}^{O}$, and $\mathbf{7}^{O}$) might give insight into the influence of the second metal in the formation of this Cu_2O_2 species. Interestingly, compounds **5**, **6**, and **7**, which contain Cu^{I} in the trivalent site (N_3) together with a divalent spectator metal such as Zn^{II}, Cu^{II}, and Fe^{II} in the tetradentate site (N_4), behave in an analogous fashion, and full formation of the corresponding bis(μ-oxo) species ($\mathbf{5}^{O}$, $\mathbf{6}^{O}$, and $\mathbf{7}^{O}$) is achieved after 10 min at −75 °C. In

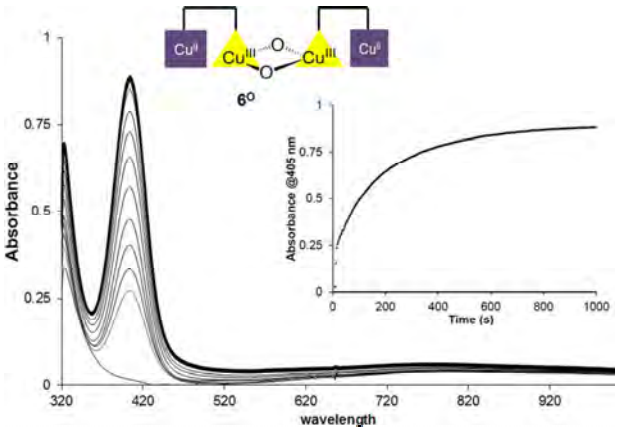

Figure 6. UV−vis absorption spectra for the reaction of $[Cu^{I}Cu^{II}(L^{N3N4})]^{3+}$ (**6**) (0.15 mM) and O_2 at −90 °C in acetonitrile/acetone 1:19. (inset) Time trace at 405 nm ($\mathbf{6}^{O}$).

sharp contrast, formation of $\mathbf{3}^{O/TP}$ is much faster, and this species is fully developed only 1 min after starting the reaction of **3** with O_2 (Supporting Information, Figure S12a). On the other hand, the decay rates of $\mathbf{5}^{O}$, $\mathbf{6}^{O}$, and $\mathbf{7}^{O}$ are small (only 15% decomposition after 2 h at −60 °C) compared to the bis(μ-oxo) unit in $\mathbf{3}^{O/TP}$, which decomposes in only 20 min at −60 °C (Supporting Information, Figure S12b). The acceleration in the decay rate of $\mathbf{3}^{O/TP}$ might be related to the strain exerted by a putative interaction between the Cu^{II} centers resulting from the decomposition of the thermally unstable *trans*-peroxide unit. Such acceleration in the formation and decay rates of Cu_2O_2 species has been previously documented in Cu_2O_2 species derived from strained dinucleating ligands.[48] ESI-MS analyses of the final species derived from the thermal decomposition of $\mathbf{3}^{O/TP}$, $\mathbf{5}^{O}$, $\mathbf{6}^{O}$, and $\mathbf{7}^{O}$ showed the exclusive formation of metal-hydroxide species coordinated to the intact L^{N3N4} ligand. No ligand oxidation was detected in any case.

*Synthesis of $[Ga^{III}Cu^{I}(L^{N3N4})]^{4+}$ (**8**) and Its Reactivity with O_2.* The use of Ga^{III} completely changes the position of the copper center within ligand L^{N3N4}. $[Ga^{III}Cu^{I}(L^{N3N4})]^{4+}$ (**8**) was prepared analogously to the previously described heterometallic complexes but using $GaCl_3$ as the complementary metal source

dx.doi.org/10.1021/ic501951f | Inorg. Chem. 2014, 53, 12929−12938

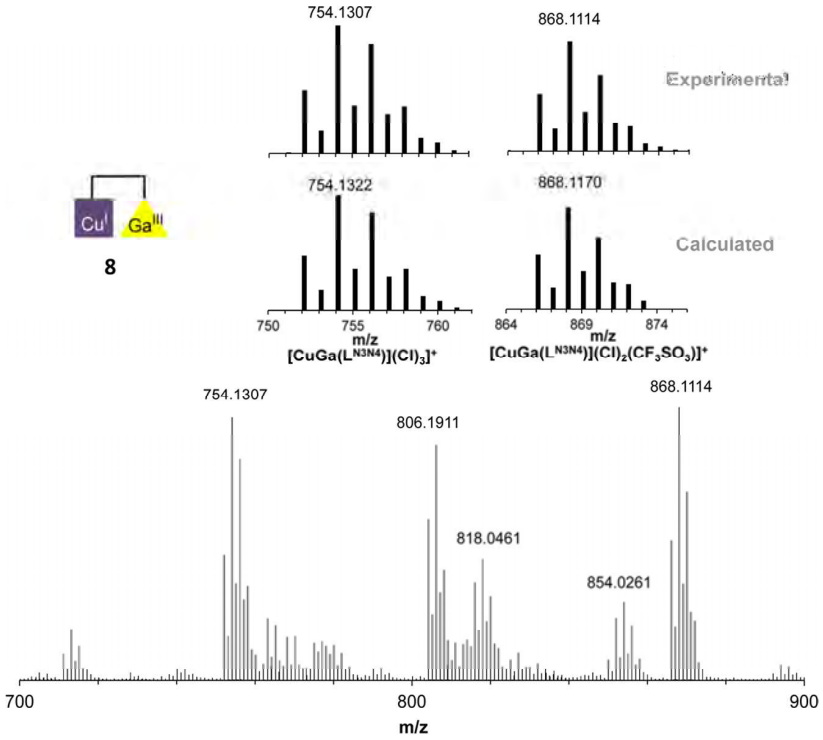

Figure 7. HR-MS spectrum of **8**. Peaks at 806.1911 and 818.0461 correspond to mononuclear Ga^{III} species ($L^{N3N4} = C_{31}H_{45}N_7$).

to copper(I). In the HR-MS spectrum of **8** peaks at *m/z* 754.1316 and 868.1114 corresponding to the heterodimetallic complex $\{[Cu^{I}Ga^{III}(L^{N3N4})](Cl)_3\}^+$ and $\{[Cu^{I}Ga^{III}(L^{N3N4})](Cl)_2(CF_3SO_3)\}^+$ were observed (Figure 7).

Interestingly, UV–vis monitoring of the reaction of this complex with O_2 at low temperature only exhibited the formation of the characteristic bands of ^{T}**P** species ($\mathbf{8}^{TP}$) with an absorption band centered at 530 nm (Figure 8). No trace of

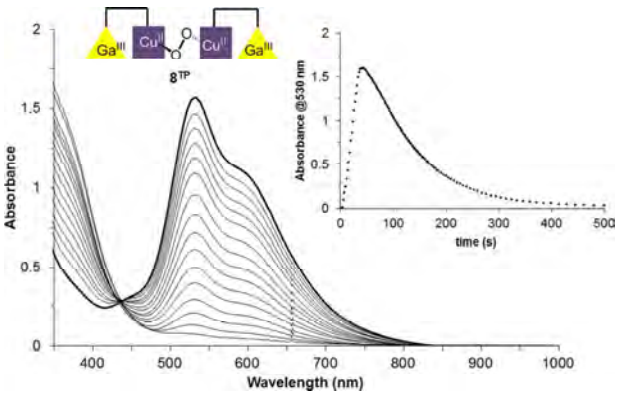

Figure 8. UV–vis absorption spectra for the reaction of $[Ga^{III}Cu^{I}(L^{N3N4})]^{4+}$ (**8**, 0.79 mM) with O_2 in acetonitrile/acetone 1:19 at −90 °C. (inset) Time trace at 530 nm ($\mathbf{8}^{TP}$).

the band at 405 nm characteristic of the **O** compound was detected. Such result indicates that the trivalent metal is tightly bound to the tacn site blocking the access of copper(I) in the starting material, which is displaced to the N_4 site. Remarkably, the use of redox active trivalent metals such as Fe^{III} caused the immediate oxidation of the copper(I) site to copper(II), thus preventing further studies of O_2 activation.

CONCLUSIONS

In this work we have developed a novel dinuclear unsymmetric ligand scaffold (L^{N3N4}) that contains two highly differentiated coordination environments: a tridentate site (N_3) composed of a tacn ring and a tetradentate environment (N_4) offered by two aliphatic amines and two pyridines. It is shown that L^{N3N4} is potentially a good candidate for the synthesis of heterodimetallic complexes (Scheme 3). Reaction of the homodinuclear copper(I) complex (**3**) with O_2 at low temperature affords a mixture of **O** and ^{T}**P** species arising from the intermolecular interaction between two copper centers in the same binding environment but placed in two different complex molecules (Table 1). Taking advantage of the ligand asymmetry, a set of heterodimetallic complexes containing Cu^{I} and a divalent or trivalent complementary metal has been prepared as ascertained by ^{1}H NMR and HR-MS analyses. Since Cu^{I} forms kinetically labile complexes, its binding site in the heterometallic complexes is finally dictated by the donor set preferences of the complementary metal. Divalent metals such as Zn^{II}, Cu^{II}, or Fe^{II} bind preferentially at the N_4 site and force the coordination of Cu^{I} to the N_3 site. Instead, a trivalent metal such as Ga^{III} preferentially bind to the tacn site, thus positioning Cu^{I} in the N_4 site. Since the nature of the O_2-bound species at copper sites depends in their ligand donor set,[5,19,20] it follows that reaction between the heterodimetallic complexes (**5**–**8**) and O_2 afforded the exclusive formation of either **O** or ^{T}**P**, depending on the donor set of the Cu^{I} site (Scheme 3, Table 1). When Cu^{I} is bound at the tridentate site **O** species form upon reaction with O_2, while formation of ^{T}**P** species occurs upon reaction of O_2 with complexes where Cu^{I} is bound at the N_4 site. Indeed, the exclusive formation of **O** or ^{T}**P** when **5**–**8** react with O_2 could be regarded as evidence for site-selective binding to L^{N3N4}. Furthermore, the position of the

dx.doi.org/10.1021/ic501951f | Inorg. Chem. 2014, 53, 12929–12938

Scheme 3. Representation of the Complexes and the O_2-Bound Species Generated upon Reaction with O_2 Described in This Work

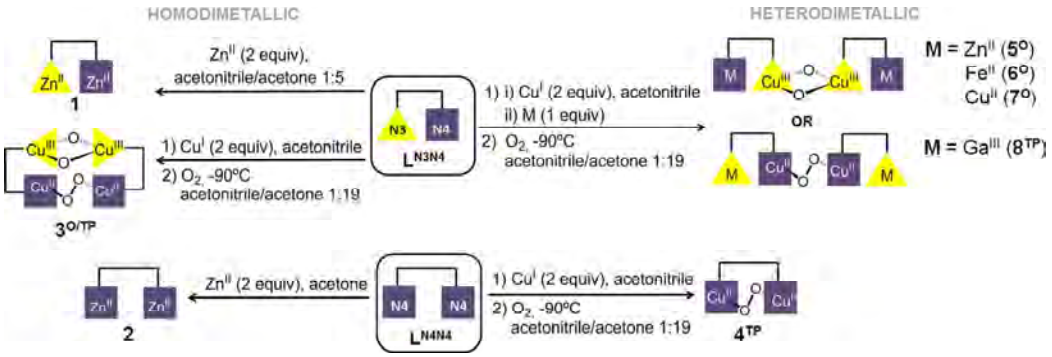

Table 1. Summary of the Spectroscopic Features of the O and ^{T}P Species Formed upon Reaction of $[M^{II/III}Cu^{I}(L)]^{3+/4+}$ with O_2 at −90°C in Acetonitrile/Acetone 1:19

ligand	compound	N_4 site	N_3 site	UV−vis features λ_{max}, nm (ε, M^{-1} cm^{-1})[a]	Cu_2O_2 species
L^{N3N4}	3	Cu^{I}	Cu^{I}	405 (15 000), 530 (2000)	O + ^{T}P
	5	Zn^{II}	Cu^{I}	405 (11 900)	O
	6	Cu^{II}	Cu^{I}	405 (12 000)	O
	7	Fe^{II}	Cu^{I}	405 (12 300)	O
	8	Cu^{I}	Ga^{III}	530 (4050)	^{T}P
L^{N4N4}	4	Cu^{I}	Cu^{I}	530 (4400), 600 (sh)	^{T}P

[a] ε values were calculated taking into account the expected maximum concentration of Cu_2O_2 unit.

copper(I) center within the ligand framework can be tuned by the complementary metal.

Thus, ligand L^{N3N4} has been proven to be a good platform for the synthesis of heterodimetallic complexes. The reactivity of some of the **O** and ^{T}**P** species described in this work is currently being investigated in our lab. Moreover, synthetic efforts are devoted to the preparation of new asymmetric ligand scaffolds that can force the intramolecular O_2 activation performed by two different metals akin to the reactivity exhibited by some enzymes.

EXPERIMENTAL SECTION

Instrumentation. All the spectroscopic and chromatographic analyses were carried out in Unitat d'Anàlisi Química i Estructural (UAQiE) or in the laboratories of the Bioinorganic and Supramolecular Chemistry Group (QBIS) at the University of Girona.

Elemental analyses were performed using a CHNS-O EA-1108 elemental analyzer from Fiscons. High-resolution mass spectra (HR-MS) were recorded on a Bruker MicrOTOF-Q II instrument using electrospray ionization (ESI) or cryospray ionization (CSI) sources at Serveis Tècnics of the University of Girona. Samples were introduced into the mass spectrometer ion source by direct infusion using a syringe pump and were externally calibrated using sodium formate. A cryospray attachment was used for CSI-MS. Temperature of the nebulizing and drying gases was set at −90 °C. The capillary voltage was set at −4500 V, and the collision energy at 8−10 eV. The instrument was operated in both positive and negative ion modes. NMR experiments were performed on a Bruker Ultrashield Avance III400 and Ultrashield DPX300 spectrometers. UV−vis spectroscopy was performed with an Agilent 50 Scan (Varian) UV−vis spectrophotometer with 1 cm quartz cells. Low-temperature control was achieved with a cryostat from Unisoku Scientific Instruments, Japan

Materials and Synthesis. Only the synthesis of the unsymmetric ligand L^{N3N4} is described below. A detailed synthesis procedure for the symmetric ligand L^{N4N4} can be found in the Supporting Information. Reagents and solvents used were of commercially available reagent quality unless otherwise stated. Solvents were purchased from Scharlab, Acros, or Sigma-Aldrich and were used without further purification.

Synthesis of L^{N3N4}. L^{N3N4} was obtained as a yellow oil after a total of four reaction steps with moderate yields starting from 1,4-dimethyl-1,4,7-triazacyclononane trihydrobromide salt (Me_2tacn·3HBr), (2-aminoethyl)bis(2-pyridylmethyl)amine (uns-penp), and 3-(bromomethyl)benzaldehyde. Me_2tacn·3HBr was synthesized after three reaction steps starting from 1,4,7-tritosyl-1,4,7-triazacyclononane. 3-(bromomethyl)benzaldehyde and uns-penp were synthesized from commercially available reagents after one and two steps, respectively, following previously described procedures.[49,50] See Supporting Information for the correspondence of ^{1}H NMR and ^{13}C NMR signal assignments.

Synthesis of ***a***. Me_2tacn·3HBr (1.26 g, 6.3 mmol) and 3-(bromomethyl)benzaldehyde (2.53 g, 6.3 mmol) were mixed in a two-necked flask in anhydrous CH_3CN (40 mL), leading to a yellow mixture. Na_2CO_3 (4.69 g, 44 mmol) and tetrabutylammonium bromide (TBABr, 0.05 g, 0.16 mmol) were then added directly as solids. Nitrogen atmosphere was established, and the mixture was refluxed for 20 h. Then it was cooled to room temperature, and a yellow solution with a suspended white solid was obtained. The solution was filtered to remove unreacted Na_2CO_3, and the filter cake was washed with CH_2Cl_2. The solvent from the combined filtrates was removed under reduced pressure, and an orange oil was obtained. NaOH (1 M, 15 mL) was added, and the product was extracted with CH_2Cl_2 (3 × 10 mL). The organic layers were combined and dried over $MgSO_4$, and the solvent was removed under reduced pressure. *n*-Pentane (50 mL) was added, and the mixture was stirred overnight. After filtration the solvent from the filtrates was removed under reduced pressure, and 1.13 g (4.1 mmol, 65%) of **a** were obtained. ^{1}H NMR ($CDCl_3$, 400 MHz, 298 K) δ, ppm: 10.02 (s, 1H, $\mathbf{H_i}$), 7.86 (s, 1H, $\mathbf{H_i}$), 7.76 (d, J = 7.6 Hz, 1H, $\mathbf{H_h}$), 7.66 (d, J = 7.6 Hz,1H, $\mathbf{H_f}$), 7.46 (t, J = 7.6 Hz, 1H, $\mathbf{H_g}$), 3.74 (s, 2H, $\mathbf{H_e}$), 2.80 (s, 4H, $\mathbf{H_b}$), 2.77−2.75 (m, 4H, $\mathbf{H_d}$), 2.68−2.65 (m, 4H, $\mathbf{H_c}$), 2.35 (s, 6H, $\mathbf{H_a}$). ^{13}C NMR ($CDCl_3$, 100 MHz, 298 K) δ, ppm: 192.55 ($\mathbf{C_l}$), 141.55 ($\mathbf{C_h}$), 136.43 ($\mathbf{C_f}$), 135.26 ($\mathbf{C_k}$), 130.14 ($\mathbf{C_g}$), 128.88 ($\mathbf{C_j}$), 128.45 ($\mathbf{C_i}$), 62.82 ($\mathbf{C_e}$), 57.11, 56.92 ($\mathbf{C_d}$,$\mathbf{C_c}$), 56.02 ($\mathbf{C_a}$), 46.66 ($\mathbf{C_b}$). ESI-MS (m/z): 276.2 $[M + H]^+$

Synthesis of ***b***. A measured quantity of uns-penp (786 mg, 3.2 mmol) was dissolved in THF (5 mL) and cooled to 0 °C. A solution of **a** (893 mg, 3.2 mmol) in THF (5 mL) was added dropwise. The mixture was left to attain room temperature, and it was stirred for 15 h. The solvent was removed under reduced pressure, and 1.95 g (3.88 mmol, >100%) of a pale yellow oil were obtained and used in the next step without further purification. ^{1}H NMR ($CDCl_3$, 400 MHz, 298 K)

dx.doi.org/10.1021/ic501951f | Inorg. Chem. 2014, 53, 12929−12938

δ, ppm:8.52 (d, J = 4.8 Hz, 2H, $\mathbf{H_q}$), 8.25 (s, 1H, $\mathbf{H_j}$), 7.66 (s, 1H, $\mathbf{H_f}$), 7.61−7.52 (m, 3H, $\mathbf{H_o}$+$\mathbf{H_n}$+$\mathbf{H_g}$), 7.45 (d, J = 7.8 Hz, 1H, $\mathbf{H_i}$), 7.37 (t, J = 7.8 Hz, 1H, $\mathbf{H_h}$), 7.14−7.11 (m, 2H, $\mathbf{H_p}$), 3.93 (s, 4H, $\mathbf{H_m}$), 3.83−3.78 (m, 2H, $\mathbf{H_k}$), 3.72 (s, 2H, $\mathbf{H_e}$), 2.98−2.92 (m, 6H, $\mathbf{H_l}$+$\mathbf{H_b}$), 2.78 (br. s., 8H, $\mathbf{H_d}$+$\mathbf{H_c}$), 2.40 (s, 6H, $\mathbf{H_a}$). ^{13}C NMR ($CDCl_3$, 100 MHz, 298 K) δ, ppm: 161.95 ($\mathbf{C_p}$), 159.84 ($\mathbf{C_i}$), 149.04 ($\mathbf{C_t}$), 140.15 ($\mathbf{C_h}$), 136.44 ($\mathbf{C_q}$/$\mathbf{C_r}$), 131.57 ($\mathbf{C_k}$), 128.71, 128.45, 127.15 ($\mathbf{C_j}$, $\mathbf{C_g}$, $\mathbf{C_i}$), 125.53 ($\mathbf{C_f}$), 122.93 ($\mathbf{C_q}$/$\mathbf{C_r}$), 122.02 ($\mathbf{C_i}$), 62.92 ($\mathbf{C_e}$), 60.79 ($\mathbf{C_o}$), 59.49 ($\mathbf{C_m}$), 56.42 ($\mathbf{C_n}$), 55.77 ($\mathbf{C_c}$+$\mathbf{C_d}$), 54.89 ($\mathbf{C_b}$), 45.83 ($\mathbf{C_a}$). ESI-MS (m/z): 500.3 $[M + H]^+$, 276.2 [a+H]$^+$, 243.1 [uns-penp+H]$^+$.

Synthesis of **c**. Compound **b** (1.95 g, 3.9 mmol) was dissolved in absolute ethanol (50 mL), and sodium borohydride (0.16 g, 4.2 mmol) was added as a solid in little portions. The reaction was stirred for 12 h at room temperature, and then 10 mL of water was added to remove the unreacted $NaBH_4$. After removal of the solvent under reduced pressure, CH_2Cl_2 (15 mL) and H_2O (4 mL) were added. The mixture was treated with CH_2Cl_2 (2 × 8 mL). The organic layers were dried over $MgSO_4$, and the solvent was removed under reduced pressure to obtain 1.68 g (3.3 mmol, 86%) of a pale yellow oil. ^{1}H NMR ($CDCl_3$, 400 MHz, 298 K) δ, ppm: 8.51 (d, 2H, J = 4.3 Hz, $\mathbf{H_q}$), 7.64−7.60 (m, 2H, $\mathbf{H_o}$), 7.45 (d, 2H, J = 7.7 Hz, $\mathbf{H_n}$), 7.24−7.21 (m, 3H, $\mathbf{H_f}$+$\mathbf{H_i}$+$\mathbf{H_h}$), 7.15−7.12 (m, 3H, $\mathbf{H_g}$+$\mathbf{H_p}$), 3.83 (s, 4H, $\mathbf{H_m}$), 3.66 (s, 2H, $\mathbf{H_j}$), 3.62 (s, 2H, $\mathbf{H_e}$), 2.79 (s, 4H, $\mathbf{H_b}$), 2.77−2.70 (m, 8H, $\mathbf{H_k}$+$\mathbf{H_l}$+$\mathbf{H_d}$), 2.65−2.63 (m, 4H, $\mathbf{H_c}$), 2.34 (s, 6H, $\mathbf{H_a}$). ^{13}C NMR ($CDCl_3$, 100 MHz, 298 K) δ, ppm: 159.67 ($\mathbf{C_p}$), 149.08 ($\mathbf{C_t}$), 140.26 ($\mathbf{C_f}$+$\mathbf{C_h}$), 136.37 ($\mathbf{C_r}$), 128.75, 128.12, 127.63 ($\mathbf{C_g}$+$\mathbf{C_j}$+$\mathbf{C_k}$), 126.47 ($\mathbf{C_i}$), 122.94 ($\mathbf{C_q}$), 121.96 ($\mathbf{C_s}$), 63.26 ($\mathbf{C_e}$), 60.71 ($\mathbf{C_o}$), 57.07 ($\mathbf{C_c}$), 56.81 ($\mathbf{C_b}$), 55.90 ($\mathbf{C_d}$), 54.101 ($\mathbf{C_m}$), 53.80 ($\mathbf{C_l}$), 46.68 ($\mathbf{C_n}$). ESI-MS (m/z): 502.4 $[M + H]^+$, 251.6 $[M+2H]^{2+}$

Synthesis of L^{N3N4}. Compound **c** (1.68 g, 3.3 mmol) was dissolved in formic acid 98% (13 mL); formaldehyde 37% (25 mL) was added, and the mixture was refluxed for 24 h. The solvent was then removed under reduced pressure, and NaOH 3 M (5 mL) was added to the resultant yellow solid. The product was extracted with CH_2Cl_2 (3 × 50 mL). The organic phases were dried over $MgSO_4$, and the solvent was removed under reduced pressure. The resulting yellow oil was extracted with hexane overnight. After filtration, the solvent from the filtrates was removed under reduced pressure. The resulting yellow oil was purified by column chromatography over silica using a mixture of CH_2Cl_2/MeOH/NH_3 80:20:4 as eluent. 770 mg (1.49 mmol, 44%) of a yellow oil was obtained. ^{1}H NMR ($CDCl_3$, 400 MHz, 298 K) δ, ppm: 8.52 (d, J = 4.6 Hz, 2H, $\mathbf{H_q}$), 7.63 (td, J = 7.9 Hz, J' = 1.8 Hz, 2H, $\mathbf{H_o}$), 7.52 (d, J = 7.9 Hz, 2H, $\mathbf{H_n}$), 7.23−7.20 (m, 3H, $\mathbf{H_f}$+$\mathbf{H_i}$+$\mathbf{H_h}$), 7.15−7.11 (m, 3H, $\mathbf{H_p}$+$\mathbf{H_g}$), 3.84 (s, 4H, $\mathbf{H_m}$), 3.61 (s, 2H, $\mathbf{H_e}$), 3.44 (s, 2H, $\mathbf{H_j}$), 2.79 (s, 4H, $\mathbf{H_b}$), 2.75 (t, J = 6.4 Hz, 2H, $\mathbf{H_l}$), 2.72−2.68 (m, 4H, $\mathbf{H_d}$), 2.65−2.58 (m, 6H, $\mathbf{H_c}$+$\mathbf{H_k}$), 2.34 (s, 6H, $\mathbf{H_a}$), 2.12 (s, 3H, $\mathbf{H_r}$). ^{13}C NMR ($CDCl_3$, 100 MHz, 298 K) δ, ppm: 160.07 ($\mathbf{C_p}$), 149.11 ($\mathbf{C_t}$), 140.15, 138.98 ($\mathbf{C_f}$,$\mathbf{C_h}$), 136.46 ($\mathbf{C_r}$), 129.90, 128.10, 127.87, 127.63 ($\mathbf{C_i}$, $\mathbf{C_j}$, $\mathbf{C_k}$, $\mathbf{C_g}$), 123.00 ($\mathbf{C_q}$), 121.99 ($\mathbf{C_s}$), 63.44 ($\mathbf{C_e}$), 62.77 ($\mathbf{C_l}$), 60.95 ($\mathbf{C_o}$), 57.11 ($\mathbf{C_c}$), 56.83 ($\mathbf{C_b}$), 56.02 ($\mathbf{C_d}$), 55.58 ($\mathbf{C_m}$), 52.36 ($\mathbf{C_n}$), 46.62 ($\mathbf{C_a}$), 42.65 ($\mathbf{C_u}$). HR-MS (ESI time-of-flight) m/z calc. for $[M + H]^+$ 516.3809, found 516.3807.

Synthesis of Dimetallic Complexes. All the complexes containing copper(I) used in this work were synthesized in acetonitrile at room temperature under anaerobic conditions in a glovebox to avoid the oxidation of the initial Cu^I centers. Because of the high instability of these Cu^I centers, all the attempts to isolate the copper complexes failed. Thus, every day freshly prepared solutions of the complexes (∼18 mM) were used. NMR samples were prepared in an analogous way directly in deuterated solvent in the glovebox. For the preparation of heterodimetallic complexes, a general procedure was followed: L^{N3N4} was dissolved inside the glovebox in acetonitrile, and 1 equiv of $[Cu(CH_3CN)_4](CF_3SO_3)$ was added directly as a solid. After 10 min of stirring, 1 equiv of the desired metallic salt ($Zn(CF_3SO_3)_2$, $Cu(CF_3SO_3)_2$, $Fe(CF_3SO_3)_2(CH_3CN)_2$, or $GaCl_3$) was directly added as a solid, leading to an 18 mM solution of the complex with the general formula of $[M^{II}/^{III}Cu^I(L^{N3N4})]^{3+/4+}$. From this solution, the desired concentration for characterization or reactivity experiments was obtained after dilutions with the appropriate amount of acetonitrile or acetone.

UV−vis Spectroscopy: Sample Preparation and Monitoring of the Formed Species at Low Temperature. All the UV−vis experiments were performed in acetonitrile/acetone 1:19 as the solvent mixture. The final complex concentration ranged between 0.3 and 0.9 mM. For the preparation of a 0.9 mM sample, a UV−vis cell was charged with 100 μL of the acetonitrile complex solution (∼18 mM) and 1.9 mL of dry acetone in the glovebox. The quartz cell was capped with a septum, taken out of the box, and placed in a Unisoku thermostated cell holder designed for low-temperature experiments at 183 K. After reaching thermal equilibrium, a UV−vis spectrum of the starting complex was recorded. Dioxygen was injected into the cell with a balloon and a needle through the septum causing immediate reaction. For lower concentrations, the sample preparation was the same as described before, but in this case, the appropriate volume of the complex solution (∼18 mM) was taken, and CH_3CN was added until the total volume of the aliquot was 100 μL.

■ ASSOCIATED CONTENT

Supporting Information

Detailed synthesis of L^{N4N4}, NMR spectra of the different steps in the synthetic routes of L^{N3N4} and L^{N4N4}, aliphatic region of the ^{1}H NMR monitoring of the titration of L^{N3N4} with $Zn(CF_3SO_3)_2$, HR-MS spectra of **1**−**4**, **6**, and **7**, UV−vis monitoring of the reaction of **4** and **7** with O_2, comparison of the formation/decay rates of bis(μ-oxo) species ($\mathbf{3^{O/TP}}$, $\mathbf{5^O}$, $\mathbf{6^O}$, $\mathbf{7^O}$). This material is available free of charge via the Internet at http://pubs.acs.org.

■ AUTHOR INFORMATION

Corresponding Authors

*Phone: +34 972 41 98 42. Fax: +34 972 41 81 50. E-mail: miquel.costas@udg.edu. (M.C.)

*E-mail: anna.company@udg.edu. (A.C.)

Notes

The authors declare no competing financial interest.

■ ACKNOWLEDGMENTS

Financial support for this work was provided by the European Commission (FP7-PEOPLE-2011-CIG-303522 to A.C. and ERC-2009-StG-239910 to M.C.), MINECO (CTQ2012-37420-C02-01/BQU and CSD2010-00065 to M.C.) and Generalitat de Catalunya (ICREA Academia Award to M.C.). The Spanish Ministry of Science is acknowledged for a Ramón y Cajal contract to A.C. We are thankul to Dr. X. Ribas for financial support from INNPLANTA Project No. INP-2011-0059-PCT-420000-ACT1. We also thank Dr. L. Gómez (Serveis Tècnics de Recerca, Universitat de Girona) for helpful advice in setting up the HR-MS experiments and for fruitful discussions. We thank Catexel for a generous gift of 1,4,7-tritosyl-1,4,7-triazacyclononane.

■ REFERENCES

(1) Belle, C.; Pierre, J.-L. *Eur. J. Inorg. Chem.* **2003**, 4137−4146.

(2) Mitić, N.; Smith, S. J.; Neves, A.; Guddat, L. W.; Gahan, L. R.; Schenk, G. *Chem. Rev.* **2006**, *106*, 3338−3363.

(3) Stenkamp, R. E. *Chem. Rev.* **1994**, *94*, 715−726.

(4) Bento, I.; Carrondo, M. A.; Lindley, P. F. *J. Biol. Inorg. Chem.* **2006**, *11*, 539−547.

(5) Mirica, L. M.; Ottenwaelder, X.; Stack, T. D. P. *Chem. Rev.* **2004**, *104*, 1013−1045.

(6) Kaila, V. R. I.; Verkhovsky, M. I.; Wikström, M. *Chem. Rev.* **2010**, *110*, 7062−7081.

(7) Tainer, J. A.; Getzoff, E. D.; Richardson, J. S.; Richardson, D. C. *Nature* **1983**, *306*, 284−287.

(8) Chen, P.; Solomon, E. I. *Proc. Nat. Acad. Sci. U.S.A.* **2004**, *101*, 13105−13110.
(9) Blackburn, N. J.; Pettingill, T. M.; Seagraves, K. S.; Shigeta, R. T. *J. Biol. Chem.* **1990**, *265*, 15383−15386.
(10) Matoba, Y.; Kumagai, T.; Yamamoto, A.; Yoshitsu, H.; Sugiyama, M. *J. Biol. Chem.* **2006**, *281*, 8981−8990.
(11) Klinman, J. P. *Chem. Rev.* **1996**, *96*, 2541−2561.
(12) Prigge, S. T.; Kolhekar, A. S.; Eipper, B. A.; Mains, R. E.; Amzel, L. M. *Science* **1997**, *278*, 1300−1305.
(13) Garcia-Bosch, I.; Ribas, X.; Costas, M. *Eur. J. Inorg. Chem.* **2012**, 179−187.
(14) York, J. T.; Llobet, A.; Cramer, C. J.; Tolman, W. B. *J. Am. Chem. Soc.* **2007**, *129*, 7990−7999.
(15) Aboelella, N. W.; Lewis, E. A.; Reynolds, A. M.; Brennessel, W. W.; Cramer, C. J.; Tolman, W. B. *J. Am. Chem. Soc.* **2002**, *124*, 10660−10661.
(16) Fujita, K.; Schenker, R.; Gu, W.; Brunold, T. C.; Cramer, S. P.; Riordan, C. G. *Inorg. Chem.* **2004**, *43*, 3324−3326.
(17) Yao, S.; Herwig, C.; Xiong, Y.; Company, A.; Bill, E.; Limberg, C.; Driess, M. *Angew. Chem., Int. Ed.* **2010**, *49*, 7054−7058.
(18) Kundu, S.; Pfaff, F. F.; Miceli, E.; Zaharieva, I.; Herwig, C.; Yao, S.; Farquhar, E. R.; Kuhlmann, U.; Bill, E.; Hildebrandt, P.; Dau, H.; Driess, M.; Limberg, C.; Ray, K. *Angew. Chem., Int. Ed.* **2013**, *52*, 5622−5626.
(19) Hatcher, L. Q.; Karlin, K. D. *J. Biol. Inorg. Chem.* **2004**, *9*, 669−683.
(20) Hatcher, L. Q.; Karlin, K. D. In *Advances in Inorganic Chemistry;* Eldik, R. v., Reedijk, J., Eds.; Academic Press: Waltham, MA, 2006; Vol. Vol. *58*, p 131−184.
(21) Dalle, K. E.; Gruene, T.; Dechert, S.; Demeshko, S.; Meyer, F. *J. Am. Chem. Soc.* **2014**, *136*, 7428−7434.
(22) Mandal, S.; Mukherjee, J.; Lloret, F.; Mukherjee, R. *Inorg. Chem.* **2012**, *51*, 13148−13161.
(23) Park, G. Y.; Qayyum, M. F.; Woertink, J.; Hodgson, K. O.; Hedman, B.; Narducci Sarjeant, A. A.; Solomon, E. I.; Karlin, K. D. *J. Am. Chem. Soc.* **2012**, *134*, 8513−8524.
(24) Matsumoto, J.; Kajita, Y.; Masuda, H. *Eur. J. Inorg. Chem.* **2012**, *2012*, 4149−4158.
(25) Uyeda, C.; Peters, J. C. *Chem. Sci.* **2013**, *4*, 157−163.
(26) Halvagar, M. R.; Neisen, B.; Tolman, W. B. *Inorg. Chem.* **2013**, *52*, 793−799.
(27) Roth, A.; Spielberg, E. T.; Plass, W. *Inorg. Chem.* **2007**, *46*, 4362−4364.
(28) Tachi, Y.; Aita, K.; Teramae, S.; Tani, F.; Naruta, Y.; Fukuzumi, S.; Itoh, S. *Inorg. Chem.* **2004**, *43*, 4558−4560.
(29) Tachi, Y.; Matsukawa, Y.; Teraoka, J.; Itoh, S. *Chem. Lett.* **2009**, *38*, 202−203.
(30) Murthy, N. N.; Mahroof-Tahir, M.; Karlin, K. D. *Inorg. Chem.* **2001**, *40*, 628−635.
(31) Kim, E.; Chufán, E. E.; Kamaraj, K.; Karlin, K. D. *Chem. Rev.* **2004**, *104*, 1077−1134.
(32) Garcia-Bosch, I.; Company, A.; Frisch, J. R.; Torrent-Sucarrat, M.; Cardellach, M.; Gamba, I.; Güell, M.; Casella, L.; Q, L., Jr.; Ribas, X.; Luis, J. M.; Costas, M. *Angew. Chem., Int. Ed.* **2010**, 2406−2409.
(33) Kieber-Emmons, M. T.; Ginsbach, J. W.; Wick, P. K.; Lucas, H. R.; Helton, M. E.; Lucchese, B.; Suzuki, M.; Zuberbühler, A. D.; Karlin, K. D.; Solomon, E. I. *Angew. Chem., Int. Ed.* **2014**, *53*, 4935−4939.
(34) Wainwright, K. P. *Coord. Chem. Rev.* **1997**, *166*, 35−90.
(35) Halfen, J. A.; Mahapatra, S.; Wilkinson, E. C.; Kaderli, S.; Young, V. G.; Que, L.; Zuberbühler, A. D.; Tolman, W. B. *Science* **1996**, *271*, 1397−1400.
(36) Mahapatra, S.; Halfen, J. A.; Wilkinson, E. C.; Pan, G.; Cramer, C. J.; Que, L., Jr.; Tolman, W. B. *J. Am. Chem. Soc.* **1995**, *117*, 8865−8866.
(37) Cole, A. P.; Mahadevan, V.; Mirica, L. M.; Ottenwaelder, X.; Stack, T. D. P. *Inorg. Chem.* **2005**, *44*, 7345−7364.
(38) Mahadevan, V.; Hou, Z.; Cole, A. P.; Root, D. E.; Lal, T. K.; Solomon, E. I.; Stack, T. D. P. *J. Am. Chem. Soc.* **1997**, *119*, 11996−11997.
(39) Weitzer, M.; Schatz, M.; Hampel, F.; Heinemann, F. W.; Schindler, S. *J. Chem. Soc., Dalton Trans.* **2002**, 686−694.
(40) Schatz, M.; Leibold, M.; Foxon, S. P.; Weitzer, M.; Heinemann, F. W.; Hampel, F.; Walter, O.; Schindler, S. *Dalton Trans.* **2003**, 1480−1487.
(41) Comba, P.; Haaf, C.; Helmle, S.; Karlin, K. D.; Pandian, S.; Waleska, A. *Inorg. Chem.* **2012**, *51*, 2841−2851.
(42) Börzel, H.; Comba, P.; Katsichtis, C.; Kiefer, W.; Lienke, A.; Nagel, V.; Pritzkow, H. *Chem.—Eur. J.* **1999**, *5*, 1716−1721.
(43) Henson, M. J.; Vance, M. A.; Zhang, C. X.; Liang, H.-C.; Karlin, K. D.; Solomon, E. I. *J. Am. Chem. Soc.* **2003**, *125*, 5186−5192.
(44) Lee, D.-H.; Wei, N.; Murthy, N. N.; Tyeklar, Z.; Karlin, K. D.; Kaderli, S.; Jung, B.; Zuberbuehler, A. D. *J. Am. Chem. Soc.* **1995**, *117*, 12498−12513.
(45) Wagner, R. W.; Johnson, T. E.; Lindsey, J. S. *Tetrahedron* **1997**, *53*, 6755−6790.
(46) Costas, M.; Xifra, R.; Llobet, A.; Solà, M.; Robles, J.; Parella, T.; Stoeckli-Evans, H.; Neuburger, M. *Inorg. Chem.* **2003**, *42*, 4456−4468.
(47) Kim, E.; Chufán, E. E.; Kamaraj, K.; Karlin, K. D. *Chem. Rev.* **2004**, *104*, 1077−1134.
(48) Karlin, K. D.; Lee, D.-H.; Kaderli, S.; Zuberbühler, A. K. *Chem. Commun.* **1997**, 475−476.
(49) Wagner, R. W.; Johnson, T. E.; Lindsey, J. S. *Tetrahedron* **1997**, *53*, 6755−6790.
(50) Schatz, M.; Leibold, M.; Foxon, S. P.; Weitzer, M.; Heinemann, F. W.; Hampel, F.; Walter, O.; Schindler, S. *Dalton. Trans.* **2003**, 1480−1487.

CHAPTER IV.

Selective O*rtho*-Hydroxylation-Defluorination of 2-Fluorophenolates with a Bis(μ-oxo)dicopper(III) Species.

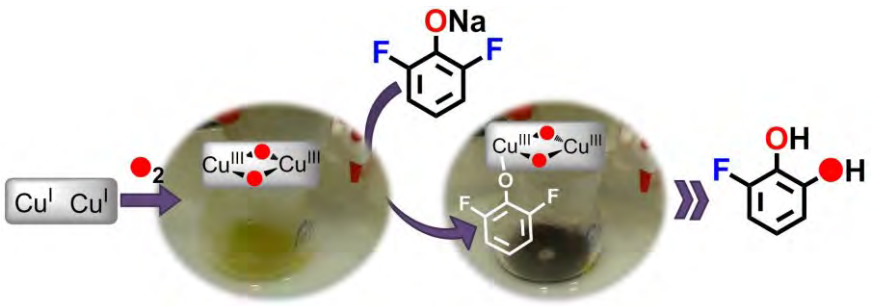

This chapter corresponds to the following publication:

Joan Serrano-Plana, Isaac Garcia-Bosch, Ryosuke Miyake, Miquel Costas,* and Anna Company*

Angew. Chem. Int. Ed. **2014**, *53*, 9608-9612

For this publication, J.S.-P. synthesized and characterized all the reported ligands and complexes, and he also performed the reactivity studies. Besides, J.S.-P. contributed in writing the manuscript and was involved in argumentations and discussions.

O_2 Activation

DOI: 10.1002/anie.201405060

Selective *Ortho*-Hydroxylation–Defluorination of 2-Fluorophenolates with a Bis(μ-oxo)dicopper(III) Species**

Joan Serrano-Plana, Isaac Garcia-Bosch, Ryosuke Miyake, Miquel Costas, and Anna Company**

Dedicated to Prof. Lawrence Que, Jr. on the occasion of his 65th birthday

Abstract: *The bis(μ-oxo)dicopper(III) species $[Cu^{III}_2(\mu\text{-}O)_2(m\text{-}XYL^{MeAN})]^{2+}$ (**1**) promotes the electrophilic ortho-hydroxylation–defluorination of 2-fluorophenolates to give the corresponding catechols, a reaction that is not accomplishable with a $(\eta^2{:}\eta^2\text{-}O_2)$dicopper(II) complex. Isotopic labeling studies show that the incoming oxygen atom originates from the bis(μ-oxo) unit. Ortho-hydroxylation–defluorination occurs selectively in intramolecular competition with other ortho-substituents such as chlorine or bromine.*

Fluorine forms the strongest single bond to carbon (bond dissociation energy up to 130 kcal mol^{-1}) and thus, C–F bonds are considered the most inert organic functionalities. This arises from the electronegativity of fluorine, which confers reinforcing ionic forces through the strong polarization of this bond.[1] Fluorinated organic compounds are renowned for their unique properties such as thermal stability, enhanced lipophilicity and ability to suppress metabolic detoxification, thus increasing the in vivo residence time.[2] Owing to these properties, fluorinated chemicals represent 20% of all pharmaceuticals and up to 30% of all agrochemicals.[3] In spite of their stability, the large-scale production and application of anthropogenic organofluorines have increasingly become subjects of debate due to the toxicity, global warming potential, ozone depletion, environmental persistence, and bioaccumulation of these compounds.[4] For this reason, the degradation of fluorinated organic compounds or activation and transformation of C–F bonds into more reactive functional groups is of current interest.[5]

In nature, several microbial enzymes can break C–F bonds,[6] and a wide range of fluorinated substrates including aliphatics (e.g. fluoroacetate, fluoropyruvate) and aromatics (e.g. fluorobenzoates, fluorophenols) can be defluorinated. Focusing on aromatics, the defluorination of fluorophenols usually occurs in aerobic organisms through the mediation of FAD-containing phenol hydroxylases, which convert 2-fluorophenols into catechols.[7] The oxidative dehalogenation of 4-fluorophenols has also been reported for cytochrome P450 and chloroperoxidase.[8]

Tyrosinase is a ubiquitous dicopper enzyme that catalyzes the *ortho*-hydroxylation of phenols to catechols and the subsequent oxidation to quinones using dioxygen as oxidant,[9] in an overall reaction analogous to that taking place in FAD-dependent phenol hydroxylases.[7] Tyrosinase operates via a $(\eta^2{:}\eta^2$-peroxo)dicopper(II) species (**P**), that undergoes electrophilic attack over the arene. However, in contrast to FAD-dependent hydroxylases, tyrosinase is incapable of hydroxylating 2-fluorophenols, which indeed are inhibitors of this enzyme.[10] Studies with model compounds have shown that the **P** species are usually in equilibrium with a highly electrophilic bis(μ-oxo)dicopper(III) species (**O**), which may open the door to novel oxidative reactivity hitherto not attained by the peroxide isomer. Herein, we indeed show that **O** species promote the defluorination of 2-fluorophenols to give the corresponding catechols, thus selectively transforming a C_{Ar}–F into a C_{Ar}–OH functional group. The reaction shows a remarkable selectivity, opening a bioinspired alternative to multistep transformations involving reactions that are most commonly associated with highly reactive organometallic compounds.[11]

$[Cu^{III}_2(\mu\text{-}O)_2(m\text{-}XYL^{MeAN})]^{2+}$ (**1**; Scheme 1) has been described as a thermally unstable compound, which can be generated at low temperatures (−90 °C) in acetone or THF by reaction of the dicopper(I) precursor $[Cu^{I}_2(m\text{-}XYL^{MeAN})]^{2+}$ with O_2.[12] It has been previously established that this compound can bind to phenolates and perform their *ortho*-hydroxylation, thus mimicking the reactivity exhibited by the dicopper enzyme tyrosinase.[13] Therefore, the activity of **1** resembles that found for other **P** and **O** type dicopper

[*] J. Serrano-Plana, Dr. I. Garcia-Bosch, Dr. M. Costas, Dr. A. Company
Grup de Química Bioinorgànica i Supramolecular (QBIS)
Institut de Química Computacional i Catàlisi (IQCC)
Departament de Química, Universitat de Girona
Campus Montilivi, 17071 Girona (Catalonia) (Spain)
E-mail: anna.company@udg.edu
miquel.costas@udg.edu

Dr. I. Garcia-Bosch
Department of Chemistry, The Johns Hopkins University
Baltimore, MD 21218 (USA)

Dr. R. Miyake
Department of Chemistry and Biochemistry, Graduate School of Humanities and Sciences, Ochanomizu University
2-1-1 Otsuka, Bunkyo-Ku, Tokyo 112-8610 (Japan)

[**] Financial support for this work was provided by the European Commission (FP7-PEOPLE-2011-CIG-303522 to A.C.; ERC-2009-StG-239910 to M.C., and Marie Curie IOF to I.G.-B.), MINECO (CTQ2012–37420-C02-01/BQU and CSD2010-00065 to M.C.), Generalitat de Catalunya (ICREA Academia Award to M.C.), Spanish Ministry of Science (Ramón y Cajal contract to A.C.), and the INNPLANTA project INP-2011-0059-PCT-420000-ACT1 (Dr. X. Ribas). We also thank Dr. Laura Gómez (Serveis Tècnics de Recerca, Universitat de Girona) for helpful advice in setting up the HR-MS experiments, and for fruitful discussions.

Supporting information for this article is available on the WWW under http://dx.doi.org/10.1002/anie.201405060.

 © 2014 Wiley-VCH Verlag GmbH & Co. KGaA, Weinheim

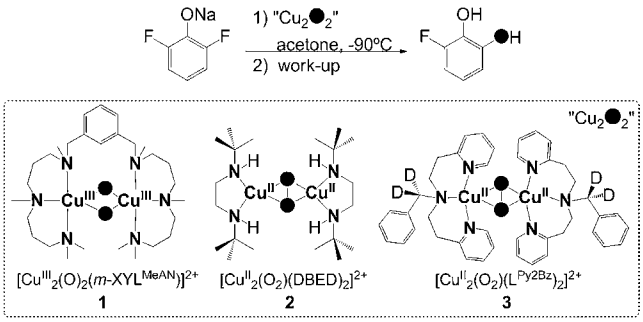

Scheme 1. *Ortho*-hydroxylation–defluorination reaction of sodium 2,6-difluorophenolate to give 3-fluorocatechol along with the schematic representation of Cu_2O_2 species **1**–**3**.

complexes.[14] The **P** species in tyrosinase has been shown to bind fluorophenolates, but the hydroxylation does not occur in *ortho*-substituted phenolates.[10] To our surprise, the reaction of **1** (2 mM) with 3 equiv sodium 2,6-difluorophenolate (Na(DFP)) at −90 °C caused the rapid decay of **1**, as shown by monitoring the reaction by UV/Vis spectroscopy. Following the complete decay of **1** and subsequent work-up, ^{1}H NMR and HPLC analyses evidenced that the reaction afforded 3-fluorocatechol in 21 % yield (with respect to **1**), indicating that *ortho*-hydroxylation and defluorination had taken place (Scheme 2). The yield was unaffected by the use

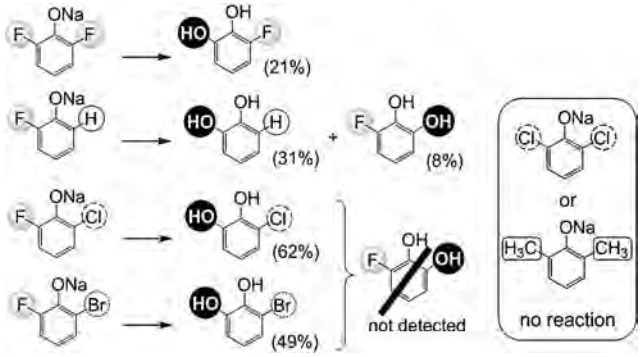

Scheme 2. Selective *ortho*-hydroxylation–defluorination reactions promoted by **1**. Reaction conditions: 1) **1**, sodium phenolate (3 equiv), acetone, −90 °C 2) acidic work-up. See the Supporting Information for further details.

of higher amounts of substrate (10 equiv) or by lowering the initial concentration of **1** (0.2 mM) (Table S1).

Isotope labeling experiments were performed by reacting Na(DFP) with ^{18}O-labeled **1** (generated by initial reaction of the dicopper(I) precursor with $^{18}O_2$, subsequent removal of the excess $^{18}O_2$, and placing the reaction under N_2) affording 3-fluorocatechol with 86 % ^{18}O label, thereby demonstrating that the oxygen atom incorporated into the catechol product originated from the Cu_2O_2 unit. Moreover, this dehalogenation reaction was regioselective for the *ortho* position of the phenolate, as no defluorination occurred upon reaction of **1** with 4-fluorophenolate (only 4-fluorocatechol was detected as product).

The *ortho*-defluorination reaction also occurred when unsymmetric phenolates bearing only one *ortho*-fluorine substituent were used as substrates. Thus, reaction of **1** with 3 equiv of sodium 2-fluorophenolate afforded 31 % of 1,2-dihydroxybenzene along with 8 % of 3-fluorocatechol (Scheme 2). Complex **1** proved to be highly selective in the defluorination of unsymmetric phenolates bearing other halogen substituents at the *ortho* position, such as sodium 2-chloro-6-fluorophenolate or sodium 2-bromo-6-fluorophenolate. Upon reaction with **1**, they both afforded exclusively 3-chlorocatechol and 3-bromocatechol in 62 % and 49 % yield, respectively (Scheme 2). Finally, no *ortho*-hydroxylation occurred upon reaction of **1** with phenolates bearing substituents in the *ortho* position different from fluorine or hydrogen. Thus, reaction with sodium 2,6-dichlorophenolate or sodium 2,6-dimethylphenolate only afforded the recovery of the starting material (Scheme 2). In conclusion, the *ortho*-C_{arene}–F bond is especially reactive against **O**, even in the presence of presumably weaker and/or more nucleophilic *ortho*-C_{arene}–R bonds. This result is especially remarkable, because the oxidative dehalogenation of C_{arene}–Br and C_{arene}–Cl bonds has been observed upon reacting binuclear copper(I) complexes with O_2,[15] whereas defluorination has never been reported for such systems.

It is well established that **O** species are usually in a nearly degenerate equilibrium with their corresponding **P** isomer.[16] Thus, it is not clear which one of the two isomers is the real executor of the phenol *ortho*-hydroxylation reaction. To determine the necessity of the bis(μ-oxo) core for the *ortho*-hydroxylation–defluorination reaction, we studied two **P** complexes that are known to promote the *ortho*-hydroxylation of phenolates. In particular, we chose the complexes $[Cu^{II}_2(\mu\text{-}\eta^2\text{:}\eta^2\text{-}O_2)(DBED)_2]^{2+}$ (**2**)[14b,c] and $[Cu^{II}_2(\mu\text{-}\eta^2\text{:}\eta^2\text{-}O_2)(L^{Py2Bz})_2]^{2+}$ (**3**),[14d] which have been previously described by the groups of Stack and Itoh, respectively (Scheme 1). Whereas for complex **3** only the **P** isomer is observed along the reaction with phenolates,[14d] for complex **2**, **P** converts into **O** upon phenolate coordination. In this respect, O is the real executor of the hydroxylation reaction.[14c] When **2** reacted with Na(DFP) (3 equiv), 3-fluorocatechol was obtained in 23 % yield (with respect to **2**). More interestingly, under analogous reaction conditions, **3** was unable to cleave the C–F bond and only trace amounts of catechol were observed (< 3 %, Table S1). Control experiments with $[Cu^{I}(MeCN)_4]CF_3SO_3$ as the copper source and O_2 as oxidant only afforded trace amounts of the defluorinated product. From these results it may be concluded that an **O** species is necessary to achieve this unprecedented *ortho*-hydroxylation–defluorination reaction of phenols by a Cu_2O_2 species.

A deeper insight into the mechanism of this *ortho*-hydroxylation–defluorination reaction was gained by means of low temperature UV/Vis spectroscopy. Acetone solutions of **1** at −90 °C exhibited an intense absorption band at 413 nm ($\varepsilon = 21\,000\,M^{-1}cm^{-1}$), which remained relatively stable at this temperature. Addition of 3 equiv of a particular phenolate led to an immediate color change from yellow to deep purple. This was readily evident in the UV/Vis spectrum, which showed the immediate formation of a novel species exhibiting two new bands in the range of 357–414 nm and 516–639 nm

 © 2014 Wiley-VCH Verlag GmbH & Co. KGaA, Weinheim

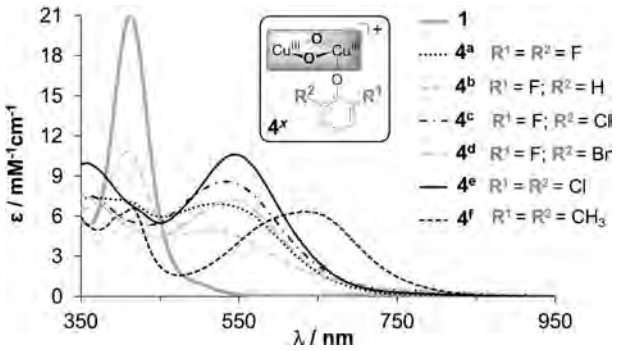

Figure 1. UV/Vis spectra of **1** and **4^x** in acetone at −90 °C. Compounds **4^x** were obtained by reaction of **1** with 3 equiv of the corresponding sodium phenolate.

depending on the nature of the phenolate (Figure 1 and S1). Previous rRaman studies on the purple intermediate resulting from the reaction of **1** with *p*-chlorophenolate[13] indicate that this species corresponds to the adduct that results from binding of the phenolate to the bis(μ-oxo) core of **1** (**4^x**, Figure 1). Cryospray mass spectrometry (CMS) at −90 °C was performed to further substantiate the proposed nature of **4^a**. The CMS spectrum of a freshly prepared sample of **4^a** is dominated by two intense peaks at *m*/*z* 783.2571 and *m*/*z* 763.3194 (Figure 2). Mass values and isotopic patterns of

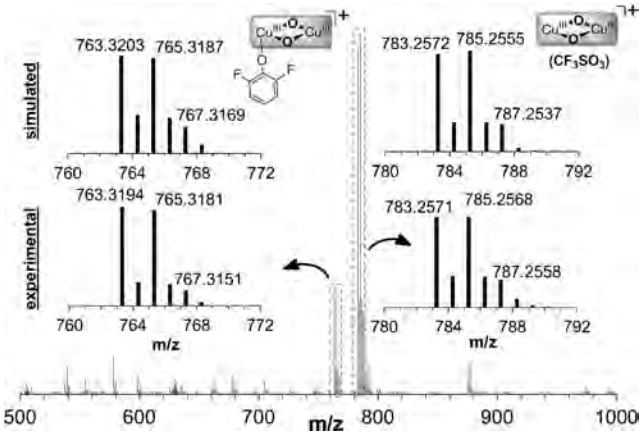

Figure 2. Spectra of cryospray mass spectrometry (CMS) experiments at −90 °C corresponding to the reaction of **1** with 3 equiv of Na(DFP) in acetone.

these peaks are consistent with their formulation as $\{[Cu^{III}_2(\mu\text{-}O)_2(m\text{-}XYL^{MeAN})](OTf)\}^+$ and $\{[Cu^{III}_2(\mu\text{-}O)_2(C_6H_3F_2O)(m\text{-}XYL^{MeAN})]\}^+$. In agreement with this interpretation, collision-induced dissociation experiments conducted over the *m*/*z* 763.3 species produced a new peak at *m*/*z* 634.3 corresponding to the loss of a phenolate ligand (*m*/*z* 129.0; Figure S3). This experiment further confirmed the nature of **4^a** as a phenolate-bound **O** species.

Kinetic analysis indicated that the formation of **4^x** was too fast to be studied by conventional benchtop UV/Vis spectroscopic techniques but its decay was substantially slower followinga first-order process that could be adjusted to a single exponential. The decay rates of complexes **4$^{g–k}$**, obtained by reaction of **1** with 10 equiv of the appropriate *para*-substituted sodium 2-fluorophenolates, were studied by UV/Vis spectroscopy and they were fitted to a single exponential function by nonlinear regression methods. Interestingly, plotting the logarithm of the rate of decay (k_{obs}) against the corresponding Hammett *meta*-substituent constants (σ^+) afforded a linear correlation ($R^2 = 0.98$) that gave a negative slope ($\rho = -2.4$) (Figure 3) indicating that the reaction

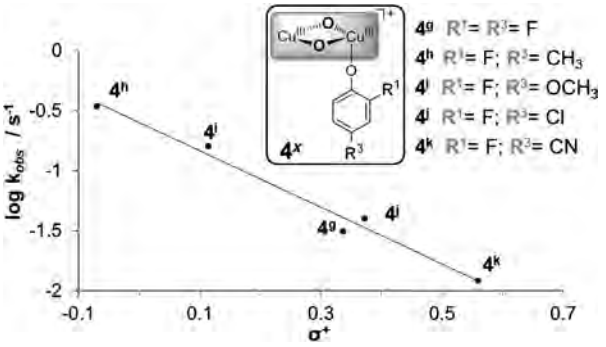

Figure 3. Hammett plot for the thermal decay of **4$^{g–k}$** at −90 °C in acetone.

occurred through an electrophilic attack on the aromatic ring of the phenolate. Remarkably, the hydroxylation reaction of nonfluorinated phenolates catalyzed by tyrosinase and some model compounds is also of electrophilic nature, and exhibits ρ values that are similar to the value found for this *ortho*-hydroxylation–defluorination reaction.[13,14,17] This data provides strong experimental support that the reaction of **1** with Na(DFP) entails an initial binding of the phenolate moiety to one of the copper centers, and then proceeds through an electrophilic attack of one of the oxo ligands at the *ortho*-C_{arene}–F site, akin to that occurring in the hydroxylation of phenolates.

At this point, we aimed to improve the reaction yield, which remained moderate for most substrates (Table S1, Scheme 2). By definition, the observed *ortho*-hydroxylation–defluorination reaction does not involve a neat gain or loss of electrons, but experimentally it is observed that the oxidation state of copper changes from +3 to +2 at the end of the reaction. We speculated that the source of the electrons, which reduce the metal center, could originate from a reaction with a second Cu_2O_2 unit releasing O_2, from an oxidative degradation of the ligand, or from a combination of both. Since the *m*-XYL^{MeAN} ligand was recovered intact after the complete decay of **4^x**, substoichiometric reactions most likely originate from an intermolecular reaction with a second Cu_2O_2 unit. Following this reasoning, the addition of a reducing agent was envisioned to provide the necessary electrons from an external source, thus facilitating the reaction and increasing the yields. Indeed this strategy has been previously successfully applied for the intramolecular oxidative aromatic dechlorination by a **P** species.[15b] Unfortunately, in the present case, the addition of $[Cu^I(MeCN)_4]CF_3SO_3$, sodium ascorbate, or zinc dust as reducing agent caused the rapid

 © 2014 Wiley-VCH Verlag GmbH & Co. KGaA, Weinheim

decomposition of **1**, which was previously reported for other **O** species.[14e] However, we observed that **2** (which is a **P** species in the absence of a phenolate substrate) could be generated in the presence of sodium ascorbate. Most remarkably, whereas the reaction of **2** in acetone at −90 °C with sodium 2-chloro-6-fluorophenolate and sodium 2-bromo-6-fluorophenolate afforded 41 % of 3-chlorocatechol and 34 % of 3-bromocatechol, respectively, the presence of sodium ascorbate (2 equiv with respect to **2**) raised the yields to 83 % in both cases.

From all these results a mechanistic picture of the *ortho*-hydroxylation–defluorination can be drawn. 2-fluorophenolates bind rapidly to one of the copper(III) centers in **1** to afford $\mathbf{4}^{x}$ (step a, Scheme 3), which evolves through a first-order intramolecular process, in which the bis(μ-oxo) core performs an electrophilic attack on the aromatic ring (step c). This attack is translated to a selective *ortho*-hydroxylation–defluorination reaction. It is especially remarkable that the reaction occurs exclusively at the *ortho*-fluorine atom, even in the presence of competing substituents with weaker C–X bonds (X = Cl, Br) at the other *ortho* position of the phenolate (Scheme 2). This selectivity may be tentatively reasoned by the establishment of a putative interaction between an unpaired pair of electrons of the *ortho*-fluorine atom and the adjacent copper(III) center, so that the carbon atom of the C–F bond becomes properly oriented to be attacked by the bis(μ-oxo) core (step b, Scheme 3). Coordination bond interactions between a lone pair of electrons from fluorine ligands with copper(III) centers have not been reported, but such interactions are well-established for other metals such as alkaline and alkaline earth metals, Ag, Pd, Pt, Ru, or Ir, among others.[18] An electrophilic attack on the aromatic ring (step c, Scheme 3) affords the catecholate product. In the absence of a reducing agent, the $2e^-$ reduction of the copper centers from oxidation state +3 to +2 is achieved by an intermolecular decomposition involving a second Cu_2O_2 complex (step d, Scheme 3).

In conclusion, this work constitutes the first example of an *ortho*-hydroxylation–defluorination reaction of phenolates with oxygen as a sacrificial oxidant by means of a synthetic metal complex. This reaction finds precedent in FAD-dependent hydroxylase enzymes in biological systems. It constitutes a fascinating transformation from a basic chemical point of view not only because of the strength of the C–F bond but also because of the rather unusual selectivity properties it exhibits.[19] Even though product yields are still far from practical for synthetic purposes, this work points towards the involvement of **O** species in the *ortho*-hydroxylation of 2-fluorophenolates by cleaving the C–F bond, thus obtaining the corresponding catechol. Moreover, this reaction is also interesting from the perspective of environmental science, because it enables the transformation of the inert C–F bonds of common persistent pollutants into a more reactive C–OH unit. Studies regarding the catalytic version of this transformation are currently underway in our lab.

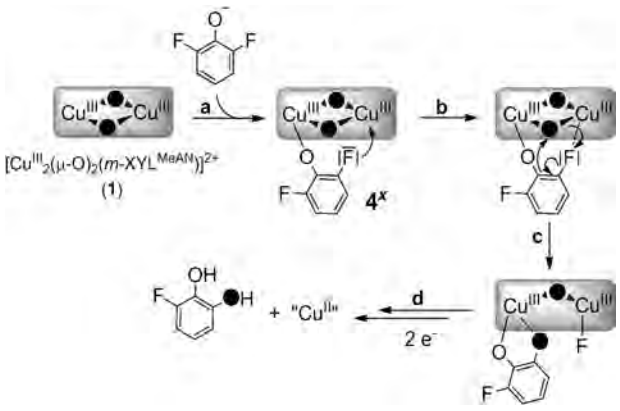

Scheme 3. Proposed mechanism of the *ortho*-hydroxylation–defluorination reaction of 2-fluorophenolates promoted by **1**.

Received: May 7, 2014
Published online: July 9, 2014

Keywords: aromatic defluorination · copper · dioxygen · hydroxylation

[1] D. M. Lemal, *J. Org. Chem.* **2004**, *69*, 1 – 11.
[2] B. E. Smart, *J. Fluorine Chem.* **2000**, *109*, 3 – 11.
[3] K. Müller, C. Faeh, F. Diederich, *Science* **2007**, *317*, 1881 – 1886.
[4] a) B. D. Key, R. D. Howell, C. S. Criddle, *Environ. Sci. Technol.* **1997**, *31*, 2445 – 2454; b) M. Houde, J. W. Martin, R. J. Letcher, K. R. Solomon, D. C. G. Muir, *Environ. Sci. Technol.* **2006**, *40*, 3463 – 3473.
[5] a) H. Amii, K. Uneyama, *Chem. Rev.* **2009**, *109*, 2119 – 2183; b) M. F. Kuehnel, D. Lentz, T. Braun, *Angew. Chem.* **2013**, *125*, 3412 – 3433; *Angew. Chem. Int. Ed.* **2013**, *52*, 3328 – 3348.
[6] a) R. Natarajan, R. Azerad, B. Badet, E. Copin, *J. Fluorine Chem.* **2005**, *126*, 425 – 436; b) C. D. Murphy, *Biotechnol. Lett.* **2010**, *32*, 351 – 359.
[7] a) V. S. Bondar, M. G. Boersma, E. L. Golovlev, J. Vervoort, W. J. H. Van Berkel, Z. I. Finkelstein, I. P. Solyanikova, L. A. Golovleva, I. Rietjens, *Biodegradation* **1998**, *9*, 475 – 486; b) S. Peelen, I. Rietjens, M. G. Boersma, J. Vervoort, *Eur. J. Biochem.* **1995**, *227*, 284 – 291; c) V. S. Bondar, M. G. Boersma, W. J. H. van Berkel, Z. I. Finkelstein, E. L. Golovlev, B. P. Baskunov, J. Vervoort, L. A. Golovleva, I. Rietjens, *FEMS Microbiol. Lett.* **1999**, *181*, 73 – 82.
[8] a) A. Harkey, H. J. Kim, S. Kandagatla, G. Raner, *Biotechnol. Lett.* **2012**, *34*, 1725 – 1731; b) R. L. Osborne, G. M. Raner, L. P. Hager, J. H. Dawson, *J. Am. Chem. Soc.* **2006**, *128*, 1036 – 1037.
[9] a) Y. Matoba, T. Kumagai, A. Yamamoto, H. Yoshitsu, M. Sugiyama, *J. Biol. Chem.* **2006**, *281*, 8981 – 8990; b) E. I. Solomon, U. M. Sundaram, T. E. Machonkin, *Chem. Rev.* **1996**, *96*, 2563 – 2605; c) M. Rolff, J. Schottenheim, H. Decker, F. Tuczek, *Chem. Soc. Rev.* **2011**, *40*, 4077 – 4098.
[10] a) G. Battaini, E. Monzani, L. Casella, E. Lonardi, A. W. J. W. Tepper, G. W. Canters, L. Bubacco, *J. Biol. Chem.* **2002**, *277*, 44606 – 44612; b) A. Spada, S. Palavicini, E. Monzani, L. Bubacco, L. Casella, *Dalton Trans.* **2009**, 6468 – 6471.
[11] a) L. I. Goryunov, V. D. Steingarts, *Russ. J. Org. Chem.* **1999**, *35*, 246 – 251; b) L. Keyes, J. A. Love in *C-H and C-X Bond Functionalization* (Ed.: X. Ribas), RSC Publishing, Cambridge, **2013**, pp. 159 – 189.
[12] A. Company, D. Lamata, A. Poater, M. Sola, E. V. Rybak-Akimova, L. Que, X. Fontrodona, T. Parella, A. Llobet, M. Costas, *Inorg. Chem.* **2006**, *45*, 5239 – 5241.

 © 2014 Wiley-VCH Verlag GmbH & Co. KGaA, Weinheim

[13] A. Company, S. Palavicini, I. Garcia-Bosch, R. Mas-Balleste, L. Que, E. V. Rybak-Akimova, L. Casella, X. Ribas, M. Costas, *Chem. Eur. J.* **2008**, *14*, 3535 – 3538.
[14] a) S. Palavicini, A. Granata, E. Monzani, L. Casella, *J. Am. Chem. Soc.* **2005**, *127*, 18031 – 18036; b) L. M. Mirica, M. Vance, D. J. Rudd, B. Hedman, K. O. Hodgson, E. I. Solomon, T. D. P. Stack, *J. Am. Chem. Soc.* **2002**, *124*, 9332 – 9333; c) L. M. Mirica, M. Vance, D. J. Rudd, B. Hedman, K. O. Hodgson, E. I. Solomon, T. D. P. Stack, *Science* **2005**, *308*, 1890 – 1892; d) S. Itoh, H. Kumei, M. Taki, S. Nagatomo, T. Kitagawa, S. Fukuzumi, *J. Am. Chem. Soc.* **2001**, *123*, 6708 – 6709; e) S. Herres-Pawlis, P. Verma, R. Haase, P. Kang, C. T. Lyons, E. C. Wasinger, U. Florke, G. Henkel, T. D. P. Stack, *J. Am. Chem. Soc.* **2009**, *131*, 1154 – 1169; f) K. D. Karlin, M. S. Nasir, B. I. Cohen, R. W. Cruse, S. Kaderii, A. D. Zuberbiihlert, *J. Am. Chem. Soc.* **1994**, *116*, 1324 – 1336.
[15] a) O. J. Gelling, B. L. Feringa, *Recl. Trav. Chim. Pays-Bas* **1991**, *110*, 89 – 91; b) M. S. Nasir, B. I. Cohen, K. D. Karlin, *Inorg. Chim. Acta* **1990**, *176*, 185 – 187.
[16] W. B. Tolman, *Acc. Chem. Res.* **1997**, *30*, 227 – 237.
[17] S. Yamazaki, S. Itoh, *J. Am. Chem. Soc.* **2003**, *125*, 13034 – 13035.
[18] a) H. Plenio, *Chem. Rev.* **1997**, *97*, 3363 – 3384; b) H. Takemura, N. Kon, M. Kotoku, S. Nakashima, K. Otsuka, M. Yasutake, T. Shinmyozu, T. Inazu, *J. Org. Chem.* **2001**, *66*, 2778 – 2783; c) K. Stanek, B. Czarniecki, R. Aardoom, H. Rüegger, A. Togni, *Organometallics* **2010**, *29*, 2540 – 2546.
[19] The origin of the remarkable selectivity is currently explored by means of computational DFT analyses.

 © 2014 Wiley-VCH Verlag GmbH & Co. KGaA, Weinheim

CHAPTER V.

Trapping a Highly Reactive Non-heme Iron Intermediate That Oxygenates Strong C-H Bonds with Stereoretention.

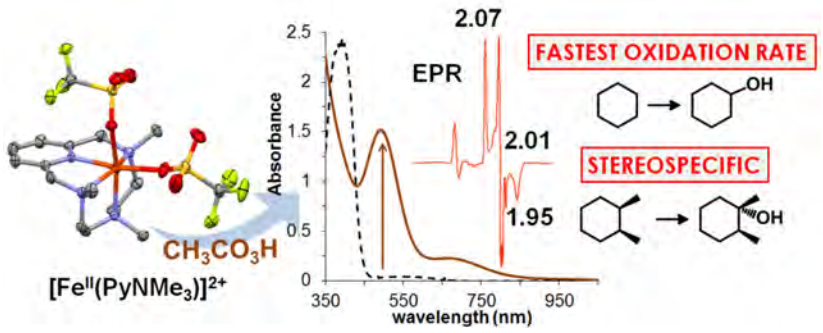

This chapter corresponds to the following publication:

Joan Serrano-Plana, Williamson N. Oloo, Laura Acosta-Rueda, Katlyn K. Meier, Begoña Verdejo, Enrique Garcia-España, Manuel G. Basallote,* Eckard Münck,* Lawrence Que, Jr.,* Anna Company,* and Miquel Costas*

J. Am. Chem. Soc. **2015**, *137*, 15833-15842

For this publication, J.S.-P. synthesized and fully characterized ligand $PyNMe_3$ and the iron(II) complex. He also performed the reactivity studies towards substrates and was involved in the generation of samples for EPR analysis. Besides, J.S.-P. contributed in writing the manuscript and was involved in argumentations and discussions.

JACS
JOURNAL OF THE AMERICAN CHEMICAL SOCIETY
Article
pubs.acs.org/JACS

Trapping a Highly Reactive Nonheme Iron Intermediate That Oxygenates Strong C—H Bonds with Stereoretention

Joan Serrano-Plana,[†] Williamson N. Oloo,[‡] Laura Acosta-Rueda,[§] Katlyn K. Meier,[∥] Begoña Verdejo,[⊥] Enrique García-España,[⊥] Manuel G. Basallote,*[,§] Eckard Münck,*[,∥] Lawrence Que, Jr.,*[,‡] Anna Company,*[,†] and Miquel Costas*[,†]

[†]Grup de Química Bioinspirada, Supramolecular i Catàlisi (QBIS-CAT), Institut de Química Computacional i Catàlisi (IQCC), Departament de Química, Universitat de Girona, Campus de Montilivi, Girona E17071, Catalonia, Spain

[‡]Department of Chemistry and Center for Metals in Biocatalysis, University of Minnesota, Minneapolis, Minnesota 55455, United States

[§]Universidad de Cádiz, Facultad de Ciencias, Departamento de Ciencia de los Materiales e Ingeniería Metalúrgica y Química Inorgánica, Apdo. 40, Puerto Real, Cádiz 11510, Spain

[∥]Department of Chemistry, Carnegie Mellon University, 4400 Fifth Avenue, Pittsburgh, Pennsylvania 15213, United States

[⊥]Instituto de Ciencia Molecular (ICMol), Universidad de Valencia, C/Catedrático José Beltrán, Paterna, Valencia 2 46980, Spain

Supporting Information

ABSTRACT: An unprecedentedly reactive iron species (**2**) has been generated by reaction of excess peracetic acid with a mononuclear iron complex $[Fe^{II}(CF_3SO_3)_2(PyNMe_3)]$ (**1**) at cryogenic temperatures, and characterized spectroscopically. Compound **2** is kinetically competent for breaking strong C—H bonds of alkanes (BDE ≈ 100 kcal·mol^{-1}) through a hydrogen-atom transfer mechanism, and the transformations proceed with stereoretention and regioselectively, responding to bond strength, as well as to steric and polar effects. Bimolecular reaction rates are at least an order of magnitude faster than those of the most reactive synthetic high-valent nonheme oxoiron species described to date. EPR studies in tandem with kinetic analysis show that the 490 nm chromophore of **2** is associated with two $S = 1/2$ species in rapid equilibrium. The minor component **2a** (~5% iron) has g-values at 2.20, 2.19, and 1.99 characteristic of a low-spin iron(III) center, and it is assigned as $[Fe^{III}(OOAc)(PyNMe_3)]^{2+}$, also by comparison with the EPR parameters of the structurally characterized hydroxamate analogue $[Fe^{III}(t\text{BuCON(H)O})(PyNMe_3)]^{2+}$ (**4**). The major component **2b** (~40% iron, g-values = 2.07, 2.01, 1.95) has unusual EPR parameters, and it is proposed to be $[Fe^{V}(O)(OAc)(PyNMe_3)]^{2+}$, where the O—O bond in **2a** has been broken. Consistent with this assignment, **2b** undergoes exchange of its acetate ligand with CD_3CO_2D and very rapidly reacts with olefins to produce the corresponding *cis*-1,2-hydroxoacetate product. Therefore, this work constitutes the first example where a synthetic nonheme iron species responsible for stereospecific and site selective C—H hydroxylation is spectroscopically trapped, and its catalytic reactivity against C—H bonds can be directly interrogated by kinetic methods. The accumulated evidence indicates that **2** consists mainly of an extraordinarily reactive $[Fe^{V}(O)(OAc)(PyNMe_3)]^{2+}$ (**2b**) species capable of hydroxylating unactivated alkyl C—H bonds with stereoretention in a rapid and site-selective manner, and that exists in fast equilibrium with its $[Fe^{III}(OOAc)(PyNMe_3)]^{2+}$ precursor.

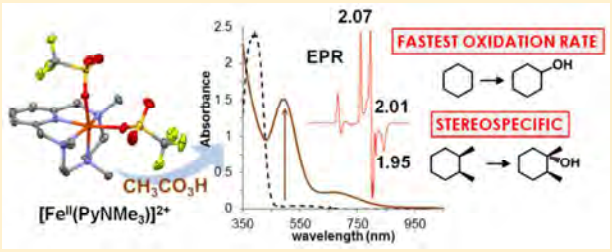

INTRODUCTION

The oxygenation of nonactivated alkyl C—H bonds is a very challenging reaction owing to their notorious chemically inert character. Consequently, highly reactive species are necessary to break these bonds.[1] However, because of their high reactivity, these species can only rarely be detected. In nature, C—H hydroxylation is mainly performed by iron-dependent enzymes, which create highly electrophilic species via finely controlled partial reduction of the O_2 molecule. Although it is now well established that the oxidation of C—H bonds can be carried out by oxoiron(IV) species generated in the catalytic cycles of both heme (e.g., cytochrome P450)[2,3] and nonheme enzymes (e.g., α-ketoglutarate-dependent enzymes),[4,5] an Fe^{III}—OOH species has been observed and implicated as the C—H oxidizing species in the catalytic cycle of the antibiotic anticancer drug bleomycin, and in naphthalene dioxygenase, an enzyme that belongs to the Rieske oxygenase family.[6,7]

In parallel, biomimetic synthetic chemistry has produced a number of Fe^{III}—OOR (R = H, alkyl, acyl) compounds,[4,8] but not one has been shown capable of directly attacking strong alkyl C—H bonds.[9−12] Taking inspiration from nature, selected

Received: September 21, 2015
Published: November 24, 2015

ACS Publications © 2015 American Chemical Society

DOI: 10.1021/jacs.5b09904
J. Am. Chem. Soc. 2015, 137, 15833−15842

nonheme iron complexes have been developed that elicit site-selective and stereoretentive C—H bond oxidation upon reaction with H_2O_2. Selectivity and stereospecificity exhibited by these catalysts provide strong support in favor of the intermediacy of metal-based oxidants akin to those involved with iron-dependent oxygenases. Presumably because of their high reactivity, these oxidants do not accumulate in solution, and it is challenging to establish their nature.

Herein we report the trapping and spectroscopic characterization of a metastable iron species that is kinetically and catalytically competent to attack strong alkane C—H bonds and can carry out this transformation at unprecedentedly fast reaction rates and with stereospecificity. This reagent also proves to be sensitive to the strength of the C—H bond, polar effects, and steric constraints, and therefore it bears the characteristics of a selective C—H hydroxylating agent. We propose this catalytically competent oxidant to be an $[Fe^{V}(O)(OAc)(L)]^{2+}$ species.

RESULTS AND DISCUSSION

Ferrous complex $[Fe^{II}(CF_3SO_3)_2(PyNMe_3)]$ (**1**) (Figure 1) was prepared and characterized in the solid state by X-ray

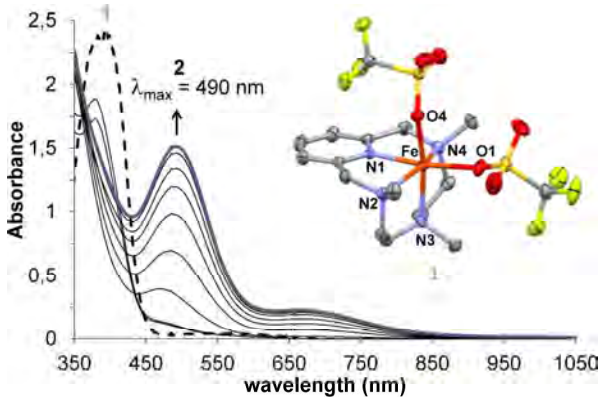

Figure 1. UV—vis spectra of **1** (1 mM, dashed line) and **2** (violet line). Solid black lines show the progressive formation of **2** upon addition of 4 equiv peracetic acid to **1** at −41 °C in acetonitrile over the course of 1 min. Inset: the thermal ellipsoid plot (50% probability) of $[Fe^{II}(CF_3SO_3)_2(PyNMe_3)]$ (**1**). Hydrogen atoms have been omitted for clarity.

crystallography and in solution by ^{1}H NMR spectroscopy (see the Supporting Information, SI, for details). X-ray analysis shows an octahedral ferrous center coordinated to the four nitrogen atoms of the macrocyclic ligand ($PyNMe_3$) and to two triflates disposed *cis* to each other. The average Fe—N distance is 2.2 Å, indicating the presence of a high-spin iron(II) center.[13,14] The ^{1}H NMR spectrum of **1** in acetonitrile-d_3 at 298 K reveals broad bands that span from 80 to −30 ppm, demonstrating that the iron center remains in the high-spin configuration ($S = 2$) in solution. This is further confirmed by a magnetic moment of 4.94 μ_B measured by the Evans' method. The basic chemical features of **1**, namely the presence of a tetradentate aminopyridine ligand with two *cis*-labile coordination sites, are the same as those of iron complexes with general formula $[Fe^{II}(^{N4}L)(X)_2]^{n+}$ (representative cases are ^{N4}L = BPMEN, BPMCN, TPA, PDP, PyTACN;[15] X = CH_3CN or CF_3SO_3) that mediate selective and stereoretentive C—H hydroxylation. While mechanistic studies on these catalysts have implicated oxoiron(V) species as the oxidants responsible for their catalytic activity, the characterization of such species has remained elusive because they do not accumulate in solution.[16−19]

Treatment of **1** with 10 equiv peracetic acid (AcOOH) in the presence of excess cyclohexane at 25 °C under air resulted in the formation of cyclohexanol and cyclohexanone in a 5:1 ratio with a total turnover number of 9.5. Under analogous conditions, adamantane oxidation occurs with a high selectivity for the tertiary C—H site (normalized 3°/2° ratio = 23), while hydroxylation of the tertiary C—H bonds of *cis*-1,2-dimethylcyclohexane occurs with a high degree of stereoretention (92%). The sum of these observations suggests that the combination of **1** and peracetic acid generates a metal-centered oxidant capable of attacking strong C—H bonds. Furthermore, the regio- and stereospecificity of the reactions excludes the involvement of unselective HO$^\bullet$ or related species and long-lived carbon-centered radicals.[20] To gain insight into the nature of the oxidant, we monitored the reaction of **1** with 4 equiv peracetic acid at −41 °C in acetonitrile by UV—vis spectroscopy and observed the rapid formation of a metastable brown species **2** ($t_{1/2}$ = 70 s) with visible absorption features at 490 and 660 nm having a 7:1 relative absorbance ratio (Figure 1).

Kinetic Analysis of the Formation of 2 by Stopped-Flow UV—vis Spectroscopy. To get more information on the formation of intermediate **2**, detailed cryo-stopped-flow experiments were carried out using a diode-array detector. The reaction of **1** with peracetic acid in acetonitrile solution at −35 °C shows spectral changes that clearly reveal multiphasic kinetics in which intermediate **2** forms and then decays (Figures S6—S7). Global fitting analysis requires the involvement of another intermediate (**B**) preceding formation of **2** in order to obtain a satisfactory fit of the spectral changes, but **B** has no visible absorption (Figure S8). The kinetic model consists of three consecutive steps (**A** → **B** → **C** → **D**), where **A** = **1**, **C** = **2**, and **D** is the species formed upon decay of **2**.

Under pseudo-first order conditions of excess oxidant, the rate constant for the first resolved step (**A** → **B**) shows a linear dependence on the concentration of AcOOH (Figure S9), which yields a second order rate constant $k_{A\to B}$ = 54 ± 1 M^{-1} s^{-1} at −35 °C. The appearance of a band at 330 nm and the absence of spectral features in the visible region suggest that this step consists of the oxidation of the starting complex to form an Fe^{III} species that corresponds to intermediate **B**. **B** then converts to **2** with a rate constant that does not show a clear dependence on the concentration of the oxidant ($k_{B\to C}$ = 0.12 ± 0.06 s^{-1}). The large uncertainty associated with $k_{B\to C}$ value is probably due to the existence of some parallel reaction of intermediate **B**, as revealed by the small deviation of the experimental kinetic traces at the absorption maximum of **2** from those expected for the 3-step kinetic model. Nevertheless, conversion of **B** to **2** requires the presence of more oxidant, as **2** does not form unless supra-stoichiometric amounts of AcOOH are added. The rate constant for the third step, which leads to decomposition of intermediate **2**, is also independent of the concentration of oxidant and shows a value of $k_{C\to D}$= 0.007 ± 0.001 s^{-1}.

Because peracetic acid solutions contain additional species (H_2O_2, acetic acid, water), it cannot be ruled out that some of the observed kinetic features may be caused by those additional species. To clarify this potential ambiguity, some kinetic experiments in acetonitrile solution were also carried out with

DOI: 10.1021/jacs.5b09904
J. Am. Chem. Soc. 2015, 137, 15833−15842

pernonanoic acid, which can be obtained as a pure solid. Reaction of **1** with 10 equiv of pernonanoic acid in acetonitrile at −35 °C produced a metastable species **2′** with analogous spectroscopic features as **2** (see SI for details). Again, an adequate fit of the spectral changes observed during the reaction of the starting complex **1** with the oxidant requires a model with three consecutive kinetic steps, the first one showing a second order rate constant of $k_{A\rightarrow B} = 11.9 \pm 0.6\ M^{-1}\ s^{-1}$ (Figure S13a) and the third one being independent of the concentration of pernonanoic acid, $k_{C\rightarrow D} = (2.3 \pm 0.3) \times 10^{-3}\ s^{-1}$. Importantly, unlike with peracetic acid, the rate of the second step in this case does show a dependence on the concentration of the oxidant ($k_{B\rightarrow C} = 1.1 \pm 0.1\ M^{-1}\ s^{-1}$, Figure S13b), supporting our suspicion that the second step in the peracetic acid reaction is complicated by one or more of the additional species present in solution. Importantly, the second order rate constants for the reactions of alkanes with **2** generated from either peracetic or pernonanoic acid are congruent.

Kinetic Analysis of the Reaction of 2 with Alkanes by Stopped-Flow UV−vis Spectroscopy. The decay of **2** is significantly accelerated by the addition of cyclohexane (Figure S14), requiring the use of stopped-flow UV−vis methods to follow the disappearance of **2** (490 nm) as a function of cyclohexane concentration (Figure 2a). The kinetic traces show

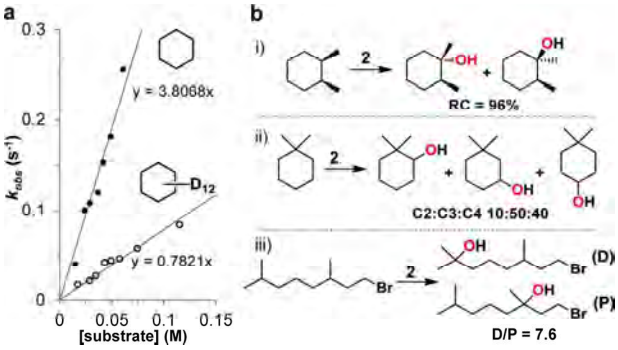

Figure 2. (a) Kinetic data for the reaction of **2** with cyclohexane at −35 °C (cyclohexane, filled circles; cyclohexane-d_{12}, open circles). (b) Reactivity of **2** with various substrates demonstrating its selectivity.

pseudo-first order behavior and can be fitted with single exponentials. The corresponding k_{obs} values are in turn found to be linearly dependent on substrate concentration (Figure 2a), affording a second order rate constant (k_2) of 2.8 ± 0.1 $M^{-1}\ s^{-1}$ at −41 °C. Analysis of the reaction rates of **2** with cyclohexane as a function of temperature (Figure S15) reveal an activation barrier with a relatively small activation enthalpy ($\Delta H^{\ddagger}$ = 37 ± 3 KJ·mol^{-1}) and a negative activation entropy ($\Delta S^{\ddagger}$ = −76 ± 8 J·K^{-1}·mol^{-1}), consistent with a bimolecular reaction. Comparison of the k_2 values for substrates with weaker C—H bonds show an inverse correlation between the logarithms of second order kinetic constants (normalized by the number of equivalent C—H bonds that can be cleaved) versus BDE_{C-H} (bond dissociation energy) of the weakest C—H bond of the hydrocarbon (Figure S18). *These results demonstrate that C—H bond cleavage by* **2** *is an important component of the rate-determining step and that even unactivated C—H bonds can be cleaved by* **2** *at fast* reaction *rates.*

Figure 2b shows that **2** exhibits significant selectivity in its reactions with various substrates. For the oxidation of cyclohexane, cyclohexanol (A) and cyclohexanone (K) products were obtained with an A/K ratio of 4.5. In the case of adamantane, 1-adamantanol and 2-adamantanol/one were produced with a normalized 3°/2° selectivity of 29, while the hydroxylation of *cis*-1,2-dimethylcyclohexane to *trans*-1,2-dimethylcyclohexanol occurred with >95% retention of configuration. In addition, the oxidation of 1,1-dimethylcyclohexane yielded a mixture of C2, C3, and C4 alcohols and ketones in a relative ratio of 10:50:40, which showed that the sterically more congested C2 site was less prone to attack. Lastly, the hydroxylation of 1-bromo-3,7-dimethyloctane resulted in the preferential attack of the more electron-rich C7—H bond over the C3—H bond by a factor of 8. Taken together, these observations demonstrate a metal-based oxidant that discriminates among multiple C—H bonds based not only on the C—H bond strength but also on steric and polar factors.[21−26]

The significance of the ability of **2** to react with substrates having strong C—H bonds becomes more obvious when its reaction rates are compared with those determined for other iron-based oxidants. Thus far, hydroperoxoiron(III) species have only been shown capable of attacking weak C—H bonds such as those of xanthene.[11,27] Cleavage of much stronger C—H bonds such as those of cyclohexane has been described only for a few high-valent nonheme oxoiron complexes. Surprisingly, as shown in Figure 3 and Table 1, **2** is by far

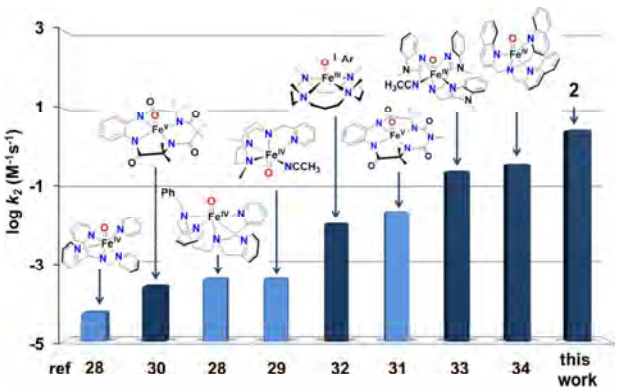

Figure 3. Cyclohexane oxidation rates (k_2) obtained at −40 or 25 °C for various nonheme iron complexes. Dark blue bars represent k_2 values at −40 °C, while light blue bars correspond to k_2 values at 25 °C.

the most reactive of such species. The reaction of **2** with cyclohexane at −41 °C is at least 4 orders of magnitude faster than several S = 1 oxoiron(IV) complexes.[28,29] Also, when compared to the two previously reported oxoiron(V) complexes supported by tetraamido macrocyclic ligands (TAML), the reaction rates for **2** are respectively 4 and 2 orders of magnitude faster,[30,31] even without correcting the 65-degree difference in temperature in the second case. Furthermore, **2** is more than 200 times more reactive than an iron(III)-iodosylarene adduct, which can be construed as a masked oxoiron(V) species.[32] The complexes that most closely approach **2** in C—H bond cleavage reactivity are the S = 1 complex $[Fe^{IV}(O)(Me_3NTB)]^{2+}$ (which is proposed to operate through a highly reactive high spin (S = 2) excited state) and the recently described S = 2 complex $[Fe^{IV}(O)(TQA)(NCMe)]^{2+}$; both react with cyclohexane an order of

DOI: 10.1021/jacs.5b09904
J. Am. Chem. Soc. 2015, 137, 15833−15842

Table 1. Alkane Oxidation Reactions by Selected Non-Heme Iron High-Valent Species

high-valent species	k_2 (cyclohexane) (M^{-1} s^{-1}) (T)[a]	A/K[b] (cyclohexane)	KIE[c]	ref
2	2.8(1) (−40 °C)	1/0.2	5 (cyclohexane)	this work
$[Fe^{IV}(O)(TQA)(NCMe)]^{2+}$	0.37 (−40 °C)	0/0.35	25 (cyclohexane)	34
$[Fe^{IV}(O)(Me_3NTB)]^{2+}$	0.25 (−40 °C)		26 (PhEt)	33
Fe^{III}(13-TMC)/OIAr adduct	0.011 (−40 °C)	0.11/0.04	10 (cumene)	32
$[Fe^{V}(O)(TAML)]^{-}$	0.00026 (−40 °C)		26 (PhEt)	30
$[Fe^{V}(O)(bTAML)]^{-}$	0.023 (25 °C)	0.4/0.02	9 ($PhCH_3$)	31
$[Fe^{IV}(O)(PyTACN)]^{2+}$	0.0004 (25 °C)		27 (DHA)	29
$[Fe^{IV}(O)(BnTPEN)]^{2+}$	0.00039 (25 °C)	0.03/0.13	50 (PhEt)	28
$[Fe^{IV}(O)(N4Py)]^{2+}$	0.000055 (25 °C)	0.03/0.04	27 (PhEt)	28

[a]Second-order rate constant determined in cyclohexane oxidation. [b]Equivalents of cyclohexanol (A) and cyclohexanone (K) with respect to Fe obtained in the oxidation of cyclohexane. [c]KIE = kinetic isotope effect. Ligand abbreviations: TQA = tris(2-quinolylmethyl)amine; Me_3NTB = tris((*N*-methyl-benzimidazol-2-yl)methyl)amine; TAML = tetraamido macrocyclic ligand; bTAML = biuret tetraamidate macrocyclic ligand; 13-TMC = 1,4,7,10-tetramethyl-1,4,7,10-tetraazacyclotridecane; PyTACN = 1,4-dimethyl-7-(2-pyridylmethyl)-1,4,7-triazacyclononane; BnTPEN = *N*-benzyl-*N*,*N*′,*N*′-tris(2-pyridylmethyl)-1,2-diaminoethane; N4Py = *N*,*N*-bis(2-pyridylmethyl)-*N*-(bis-2-pyridylmethyl)amine.

magnitude more slowly than **2** (Table 1).[33,34] Thus, **2** is the most effective species observed to date in solution that can oxidize cyclohexane.

Intermediate **2** stands out from the other complexes in Figure 3 in yet another respect. As shown in Figure 2a, **2** oxidizes cyclohexane and cyclohexane-d_{12} at different rates, exhibiting a classical kinetic isotope effect (KIE) of **5**. This value is obtained as well from the product analysis of competitive oxidations of cyclohexane and cyclohexane-d_{12}, corroborating that **2** is in fact the actual C—H bond cleaving agent. In contrast, the other complexes in Figure 3 carry out C—H bond cleavage with large nonclassical KIE values. The subset consisting of the oxoiron(IV) complexes exhibits KIE values of 25−50 that have been attributed to H atom tunneling,[28,35] while the other subset comprising the two oxoiron(V) complexes and the iron(III)-iodosylarene adduct exhibit lower values of 9−26 (Table 1). As KIE values can depend on temperature and the nature of the substrate, the best comparison is for the oxidation of cyclohexane at −40 °C between **2** and $[Fe^{IV}(O)(TQA)(NCMe)]^{2+}$ where the KIE values differ by a factor of 5. What this difference tells us about the distinct natures of the oxidants and how they cleave C—H bonds remains to be uncovered, but it is clear that there is a difference. However, the classical KIE value of 5 found for **2** matches those found for nonheme-iron-catalyzed hydroxylation of cyclohexane by H_2O_2. For these catalysts, there is strong indirect evidence for an $Fe^{V}(O)$ oxidant, but it has not yet been spectroscopically identified.[16,36] In at least three cases, evidence for the $Fe^{V}(O)$ oxidant has been obtained in the gas phase by electrospray ionization mass spectrometry.[16,18,37] In a few cases, hydroperoxy- or acylperoxyiron(III) intermediates have been observed and spectroscopically characterized;[38−41] unlike **2**, these intermediates persist in a steady-state phase at −40 °C, during which oxidation products are formed catalytically. The decay occurs upon depletion of H_2O_2 at a rate independent of the nature of the substrate and its concentration. This kinetic behavior makes them precursors to the actual oxidant. In contrast, **2** is unique as the only catalytic intermediate shown to effect C—H bond cleavage directly.

EPR Insights into the Nature of 2. EPR spectroscopy turned out to be an excellent tool to characterize the nature of the iron center in **2**. We have studied a series of EPR samples prepared at −50 °C using a 1:3 (v/v) acetonitrile:acetone glassing solvent mixture.[42] This procedure yielded well resolved EPR features in the g = 2 region that could be monitored concurrent with the growth and decay of the 490 nm chromophore (Figure 4a and Figures S28−S32). At maximum accumulation of this visible chromophore, three major EPR-active species can be observed. There is a high-spin iron(III) species with signals in the g = 9 and 4−6 regions that account for ∼40% of total Fe; this species exhibits a time course that does not correlate at all with the kinetic behavior of **2**, suggesting that it is associated with side reactions often observed in this kind of chemistry. This high-spin iron(III) species can also be observed in the Mössbauer spectrum of the same sample (Figure S33) and represents ∼40% of the total Fe in the sample as well.

There are also two S = 1/2 species. The minor component, representing 5% of total Fe, exhibits g values at 2.20, 2.19, and 1.99 (**2a**, g_{max} = 2.20 species), and its simulated spectrum is shown in blue in Figure 4a. The major component, representing ∼40% of total Fe, has g-values at 2.07, 2.01, and 1.95 (**2b**, g_{max} = 2.07 species); its simulation is shown in red in Figure 4a. Significantly, the growth and decay of both EPR species closely track the time course of the 490 nm chromophore (Figure 4b). More importantly, addition of 50 equiv cyclohexane at −50 °C accelerated the decay of the 490 nm chromophore, in tandem with the decay of both **2a** and **2b**. Upon complete decay of the 490 nm chromophore, a new low-spin iron(III) center with g values at 2.21, 2.14, and 1.97 (labeled the g_{mid} = 2.14 species) was observed, which represents 28% of total Fe. However, its formation is not directly connected with the decay of the 490 nm chromophore either in the absence or the presence of cyclohexane (Table S6). The most important observation from this study is that both **2a** and **2b** are kinetically connected with the 490 nm chromophore and are therefore likely to be species that are in equilibrium with each other. (For more detailed discussion, see text associated with Table S6 and Figures S28−S32.)

At near maximal development of the 490 nm chromophore, the two isomeric S = 1/2 species in equilibrium with each other account for ∼45% of the Fe. If only the g_{max} = 2.20 species (**2a**) contributes to the 490 nm band, it would have an unreasonably large ε_{490} of 36 000 $M^{-1}cm^{-1}$, whereas a more reasonable $\varepsilon_{490} \approx$ 4500 $M^{-1}cm^{-1}$ results if only the 2.07 species (**2b**) contributes to the absorption band. Clearly, **2b** must be associated with the 490 nm band, if not alone then in concert with **2a**. It is interesting to note that an $\varepsilon_{490} \approx$ 4000 $M^{-1}cm^{-1}$ (assuming that both **2a** and **2b** contribute to the chromophore) would compare well with that of the 460 nm chromophore ($\varepsilon_{460} \approx$

DOI: 10.1021/jacs.5b09904
J. Am. Chem. Soc. 2015, 137, 15833−15842

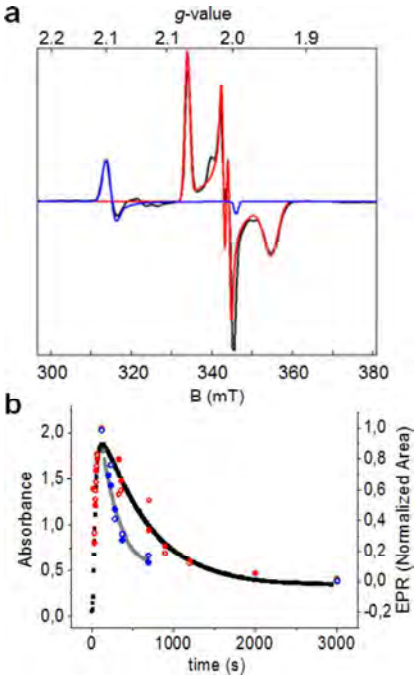

Figure 4. (A) X-band EPR spectrum of a 1 mM solution of **1** in 1:3 (v/v) acetonitrile/acetone reacted with 5 equiv AcOOH at −50 °C and frozen at t = 120 s. EPR conditions: T = 20 K, 0.2 mW microwave power, 1 mT modulation. Shown is the g = 2 region of the experimental spectrum (black). The theoretical curves (red and blue) are S = 1/2 SpinCount simulations. Blue: g_{max} = 2.20 species (**2a**) simulated with g = 2.20, 2.19, 1.99 (5% of Fe). Red: g_{max} = 2.07 species (**2b**) simulated with g = 2.07, 2.01, 1.95 (40% of Fe). The sharp feature at g = 2.00 belongs to an unknown minor species (<2%). Spectra along the time course that also include the low field region are shown in the Figures S28−S32. (B) Time course of **2** generated by adding 5 equiv AcOOH to a 1 mM solution of **1** in 1:3 (v/v) acetonitrile/acetone at −50 °C. Black squares: formation and self-decay of the 490 nm chromophore. Gray line shows the decay of the chromophore after the addition of cyclohexane (50 equiv) upon maximum formation of **2** (near 120 s). Red open and filled circles represent the respective amounts of the g_{max} = 2.20 and g_{max} = 2.07 species (**2a** and **2b**) during the formation and self-decay of the 490 chromophore. Blue open and filled circles respectively mark the time course of the g_{max} = 2.20 and 2.07 species (**2a** and **2b**) during the decay of **2** after the addition of 50 equiv of cyclohexane.

4000 $M^{-1}cm^{-1}$) recently found in the reaction of $[Fe^{II}(TPA^*)]^{2+}$ with H_2O_2/AcOH or AcOOH at −40 °C, which is associated with an S = 1/2 acylperoxoiron(III) intermediate $[Fe^{III}(OOAc)(TPA^*)]^{2+}$ (**3**, TPA* = tris(3,5-dimethyl-4-methoxy-2-pyridylmethyl)amine), even though the latter has a much greater EPR anisotropy (g = 2.58, 2.38, 1.72).[40] It should also be noted that Talsi et al. have recently found a similar transient species in epoxidation reactions with the [Fe(TPA*)] catalyst performed at −85 °C with g-values like those of the g_{max} = 2.07 species.[43] However, this species accumulates to only ∼1% of total Fe in the [Fe(TPA*)] sample.

By analogy to the 460 nm chromophore **3** derived from the Fe(TPA*) catalyst, we first considered the assignment of the 490 nm intermediate **2** to a low-spin $[Fe^{III}(OOAc)(PyNMe_3)]^{2+}$ complex. In previous work, we reported that the Mössbauer and EPR data of **3**, having g = (2.58, 2.38, 1.72), fit well to the Griffith−Taylor model, which generally describes the g-values of low-spin Fe^{III} complexes quite well.[44,45] This model considers spin−orbit coupling within a T_{2g} set that is energetically well separated from the E_g set and low-lying charge transfer states. The assignment of **3** as a low-spin S = 1/2 acylperoxoiron(III) species was corroborated by resonance Raman and ESI−MS experiments.[40] To serve as an analog for the putative $[Fe^{III}(\kappa^2\text{-OOAc})(PyNMe_3)]^{2+}$ species, the $[Fe^{III}(t\text{BuCON(H)O})(PyNMe_3)]^{2+}$ complex (**4**) has been synthesized and structurally characterized, where a hydroxamate replaces the bidentate peracetate ligand (see SI for details). Complex **4** exhibits an axial EPR spectrum with g = 2.21 and 1.94 (Figure S25) that is similar to that of **2a**, suggesting that the latter arises from the $[Fe^{III}(\kappa^2\text{-OOAc})(PyNMe_3)]^{2+}$ complex.

In stark contrast, the g-values of **2b** do not fit to the Griffith−Taylor model. To obtain the observed g values would require T_{2g} splittings in excess of 10 000 cm^{-1}, and the resonance at g = 2.01 would be especially troublesome to fit.[44,45] While this argument does not necessarily rule out the possibility of **2b** as a low-spin Fe^{III} complex, the small spread of its g-values (2.07, 2.01, 1.95) would indicate a very unusual nonheme low-spin iron(III) center that has not yet been observed.[35] So, an alternative description needs to be considered.

Comparison of the g-values of **2b** with those reported for a handful of $Fe^{V}(O)(L)$[31,43,46,50] and $Fe^{IV}(O)(L^{\bullet+})$[52−54] species (where $L^{\bullet+}$ stands for a ligand radical cation) suggests a possible solution (Table 2). In particular, the g-values of **2b** and $[Fe^{V}(O)(NC(O)Me)(TMC)]^{+}$ **5** (g = 2.053, 2.010, 1.971), closely resemble each other.[46] Furthermore, both exhibit highly anisotropic ^{57}Fe A-tensors. Examination of the EPR spectrum of an ^{57}Fe-enriched sample of **2** revealed a large magnetic hyperfine interaction of 47 MHz at $g_{mid} = g_y$ = 2.01 and two much smaller components at g_{max} and g_{min} (see Figure S34). For comparison, the EPR spectrum of an ^{57}Fe-enriched sample of **5** also showed a large component of 47 MHz, but this was observed along the direction of $g_{max} = g_x$ = 2.05 (the unpaired electron of the Fe^{V} is in d_{yz}),[47] suggesting some (possibly significant) differences between **2b** and **5**. Nevertheless, these two complexes are clearly different from the S = 1/2 $Fe^{IV}(O)(L^{\bullet+})$ species such as Compound I of horseradish peroxidase, chloroperoxidase, and cytochrome P450 (Table 2),[48,49] which all have *axial* ^{57}Fe A-tensors with $|A_x| \approx |A_y| \gg A_z$. Both the d_{yz} and d_{xz} orbitals of the S = 1 $Fe^{IV}(O)$ complexes are singly occupied, in contrast to the S = 1/2 $Fe^{V}(O)$ centers, which have only one unpaired electron in either the d_{xz} or d_{yz} orbital (with d_{xy} doubly occupied). An x/y anisotropy is also observed for $[Fe^{V}(O)(TAML)]^{-}$, the first characterized example of a bona fide oxoiron(V) complex (Table 2).[50] We can thus safely conclude that **2b** cannot arise from an $Fe^{IV}(O)(L^{\bullet+})$ complex. However, the presence of a highly anisotropic ^{57}Fe A-tensor does not allow us to distinguish between an S = 1/2 peroxoiron(III) and an S = 1/2 oxoiron(V) center, as similar anisotropies of the ^{57}Fe A-tensor have been observed for some low-spin iron(III) complexes having g-values close to g = 2.0, such as the S = 1/2 $[Fe^{III}(\eta^1\text{-OOH})(N4Py)]^{2+}$ complex (Table 2).[51]

At this point, our usual strategy would have been to carry out a complementary Mössbauer analysis in order to distinguish between an S = 1/2 peroxoiron(III) and an S = 1/2 oxoiron(V) center. However, our attempts to identify unique Mössbauer features associated with the g_{max}= 2.07 species (**2b**) were stymied by the spectral complexity of samples (Figure S33) that have at least four EPR-active species, all of which would be

DOI: 10.1021/jacs.5b09904
J. Am. Chem. Soc. 2015, 137, 15833−15842

Table 2. *g*- and A-values of Established and Proposed $Fe^{V}(O)(L)$ and $Fe^{IV}(O)(L^{\bullet+})$ Complexes and Related $S = 1/2$ Peroxoiron(III) Species

complex[a]	$g_{x,y,z}$	^{57}Fe $A_{x,y,z}$ (MHz)	ref
$[Fe^{V}(O)(TAML)]^{-}$	1.99, 1.97. 1.74	−67, −2, −22	50
$[Fe^{V}(O)(bTAML)]^{-}$	1.98, 1.94, 1.73		31
$[Fe^{V}(O)(NC(O)Me)(TMC)]^{+}$ (**5**)	2.05, 2.01, 1.97	−47, −17, 0	46
$[Fe^{V}(O)(TPA^{*})]^{3+}$[b]	2.07, 2.01, 1.96		43
$[Fe^{IV}(O)(Cl\text{-}acac^{\bullet+})(Me_3TACN)]^{2+}$[c]	1.97, 1.93, 1.91		52
$[Fe^{IV}(O)(TBP_8Cz^{\bullet+})]$	2.09, 2.05, 2.02		53
$[Fe^{IV}(NTs)(TBP_8Cz^{\bullet+})]$	2.1, 2.1, 2		54
HRP-Cpd I	1.99 (broad)	−26, −26, −8[d]	48
CPO-Cpd I	1.72, 1.61, 2.00	−42, −41, −3	49
CYP119-Cpd I	2.00, 1.96, 1.86	−38, −44, −4	49
$[Fe^{III}(\kappa^2\text{-}OOAc)(TPA^{*})]^{2+}$ (**3**)	2.58, 2.38, 1.72	−62, +26, +42	40
$[Fe^{III}(\eta^1\text{-}OOH)(N4Py)]^{2+}$	2.16, 2.11, 1.98	−9, −53, +6	51
2a	2.20, 2.19, 1.99	not determined	this work
2b	2.07, 2.01, 1.95	$A_x \ll A_y = 47 \gg A_z$	this work

[a]Abbreviations used: TAML = tetraamidate macrocyclic ligand, bTAML = biuret tetraamidate macrocyclic ligand, TMC = tetramethylcyclam, TPA* = tris(3,5-dimethyl-4-methoxy-pyridyl-2-methyl)amine, Me_3TACN = 1,4,7-trimethyl-1,4,7-triazacyclononane, Cl-acac =3-chloro-acetylacetonate, TBP_8Cz = octakis(4-*tert*-butylphenyl)corrolazine, HRP = horseradish peroxidase; CPO = chloroperoxidase, CYP119 = cytochrome P-450 from *Sulfolobus acidocaldarius*, N4Py = bis(2-pyridylmethyl)-bis(2-pyridyl)methylamine. [b]This species has the same *g*-values as **2b** but represents only ca. 1% of the iron in the sample. The iron(V) oxidation state proposed for this species has not been established. [c]The proposed formulation for this intermediate needs further spectroscopic corroboration. [d]Quoted for the local $S = 1$ Fe^{IV} site in a coupled system.

expected to exhibit Mössbauer spectra with magnetic hyperfine features even without an applied magnetic field (see SI for further comments). What emerges from our EPR studies is that **2b** must have an unusual electronic structure, either in an $S = 1/2$ iron(III) description with a small spread of *g*-values that has yet to be observed for a nonheme low-spin iron(III) center[35] or an $S = 1/2$ oxoiron(V) description for which there are only three well characterized examples for comparison, namely the TMC complex and the two TAML complexes listed in Table 2.

The insights derived from the EPR analysis must be interpreted within the context of the kinetic results, which show that **2a** and **2b** both rise and fall in concert with the 490 nm chromophore and are thus in equilibrium with each other. If **2b** is assigned to a low-spin iron(III) center with an unusual electronic structure, it would most likely be a geometric isomer of the acylperoxoiron(III) center associated with **2a**. Such a geometric isomer would presumably have the bidentate acylperoxo ligand bound trans to different N atoms of the supporting $PyNMe_3$ macrocycle. However, it is unlikely that such an equilibrium would be facile at −40 °C. Furthermore, the subsequent rate determining cleavage of the strong substrate C—H bond would have to be effected by an acylperoxoiron(III) center, which is thus far unprecedented. However, assignment of **2b** to an $S = 1/2$ $Fe^{V}(O)$ center would make it an electromer of the acylperoxoiron(III) center associated with **2a** that would form by a reversible O—O bond cleavage step (Scheme 1). There is experimental precedent for such equilibria as well as DFT calculations showing that higher-valent electromers of acylperoxoiron(III) species are energetically accessible (see subsequent sections for discussion of these topics). The proposed oxoiron(V) species that we favor for the assignment of the $g_{max} = 2.07$ species (**2b**) would certainly have the oxidative power required to cleave strong C—H bonds directly, as demonstrated in this paper for the 490 nm chromophore.

Scheme 1. Reversible O—O Bond Cleavage of Acylperoxoiron(III) Species 2a to Oxoiron(V) Species 2b

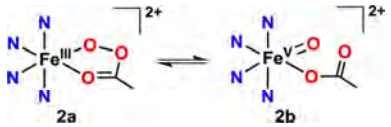

Mass Spectroscopic Insights into the Nature of 2. Additional experimental evidence has been obtained in solution at −40 °C, corroborating the formation of a $Fe^{V}(O)(O_2CR)$ derivative that is in equilibrium with the acylperoxoiron(III) intermediate. High-resolution cryospray mass spectrometry (CSI–MS) experiments at −40 °C showed **2** to exhibit a major peak at m/z 528.0893 with an associated isotopic pattern fully consistent with its formulation as $\{Fe(OOAc)(PyNMe_3)](CF_3SO_3)\}^{+}$ (Figure 5a) or either of its higher-valent electromers. CD_3COOD was added into the **1**/AcOOH reaction mixture during the formation of **2** at −40 °C. This experiment resulted in the appearance of a new feature at m/z 531 (Figure 5b), indicating the substitution of the acetate (CH_3CO_2) by d_3-acetate (CD_3CO_2). Control experiments showed that CD_3CO_2D and AcOOH did not exchange under the reaction conditions (see SI), so there must be a pathway for the incorporation of labeled acetate into the primary mass peak associated with **2**. We propose carboxylate exchange with the $Fe^{V}(O)$ electromer as representing the most facile pathway that rationalizes the observed deuterium incorporation into **2** from CD_3COOD.

Corroboration for carboxylate exchange with **2** was obtained by investigating the reactions of **1**/AcOOH with cyclooctene in the presence of CD_3COOD. In room temperature reactions with 20 equiv AcOOH and no added CD_3COOD, cyclooctene was converted to cyclooctene oxide as the major product (17 TON) and *cis*-2-acetoxycyclooctanol as the minor product (2 TON). The latter has been reported in cyclooctene oxidations catalyzed by Fe(TPA) and Fe(BPMCN) with H_2O_2 in the presence of AcOH[15,55,56] and was proposed to arise from a [3 + 2] cycloaddition of a fleeting $Fe^{V}(O)(OAc)$ oxidant to the C=C bond of the olefin substrate. It should be noted that the

DOI: 10.1021/jacs.5b09904
J. Am. Chem. Soc. 2015, 137, 15833−15842

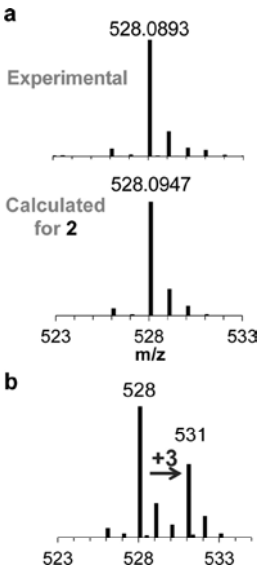

Figure 5. Cryospray mass spectral (CSI–MS) experiments. (a) Experimental and calculated patterns of **2** generated by reaction of **1** with 4 equiv peracetic acid in acetonitrile at −40 °C. (b) Spectrum of **2** generated with 4 equiv peracetic acid in the presence of 20 equiv acetic acid-d_4 at −40 °C. An M+3 ion was observed at m/z = 528, indicating that the CD_3CO_2 can be incorporated into this species. See Figures S35–S36 for full spectra.

exclusive *syn*-stereochemistry observed for the product is consistent with this scenario but not with a two-step mechanism involving initial epoxidation followed by epoxide ring opening. A control experiment in the absence of **1** afforded ~5 times less epoxide product, but, importantly, there was no trace of *cis*-2-acetoxycyclooctanol. The *cis*-2-acetoxycyclooctanol product observed was 10% trideuterated in reactions of **1** and AcOOH with 200 equiv cyclooctene in the presence of 200 equiv CD_3COOD, both at −40 °C and at 25 °C, and also upon addition of 200 equiv CD_3COOD and 200 equiv cyclooctene after maximal formation of **2** at −40 °C, indicating that the acetate exchange in **2** occurs very fast (see Section VII of SI). Up to 29% of the labeled product was obtained after increasing the CD_3COOD amount to 500 equiv at 25 °C. These results clearly demonstrate that there must be a mechanism for the incorporation of deuterated acetate into the oxidant generated from **1** and AcOOH.

Comparison with Literature Precedents for Acylperoxoiron(III) Complexes. Intermediate **2** resembles in several respects the closely related low-spin acylperoxoiron(III) intermediate **3** recently characterized at −40 °C in the reaction of Fe^{II}(TPA*) with H_2O_2/AcOH[40] but differs in others. Both **2** and **3** exhibit similarly intense visible chromophores in the 450–500 nm region that are associated with S = 1/2 EPR signals and undergo self-decay in MeCN at −40 °C with k_{obs} values of 0.02 s^{-1}. However, the reactivity of **2** significantly differs from that of **3**. Upon its generation, **3** persists in a steady state phase and undergoes rate-determining O—O bond cleavage that is substrate-independent. In contrast, **2** decays at a rate that depends on the nature of the substrate and its concentration, indicating that, unlike **3**, **2** directly reacts with alkanes. Moreover, the substrate-dependent decay of **2** is associated with two S = 1/2 species with g_{max} = 2.20 and 2.07 (**2a** and **2b**), respectively. These two species maintain a constant intensity ratio as **2** decays at different rates in the course of oxidizing various substrates. To accommodate these observations, we propose the possibility of a reversible O—O bond cleavage equilibrium between the $[Fe^{III}(OOAc)(PyNMe_3)]^{2+}$ (**2a**, g_{max} = 2.20) and the highly oxidizing high-valent iron-oxo species $[Fe^{V}(O)(OAc)(PyNMe_3)]^{2+}$ (**2b**, g_{max} = 2.07) which acts as the actual oxidant (Scheme 2). Reversible cleavage of the O—O bond has in fact been demonstrated for a peroxocarbonatoiron(III) complex by Suzuki and co-workers, resulting in the incorporation of labeled water into the bound peroxocarbonate moiety and label scrambling.[57] It is highly unlikely that the observed incorporation of deuterated acetate into **2** occurs by direct exchange with the acylperoxoiron(III) species **2a**, but it could easily come about by ligand exchange of CD_3COOD with the $Fe^{V}(O)(OAc)$ electromer **2b**. Our experimental results thus support the notion of energetically accessible higher-valent electromers in equilibrium with the acylperoxoiron(III) species, a notion first proposed by Shaik and co-workers based on DFT calculations on related systems.[17,40] The existence of this equilibrium allows **2** to attack strong C—H bonds directly and rapidly, a kinetic behavior that makes **2** unique among the few characterized first-row transition metal acylperoxo complexes reported so far including iron,[58,59] copper,[60–62] and nickel,[63] which are generally much more stable and sluggish in cleaving C—H bonds.

Comparison of the C—H Bond Cleavage Reactivities of 2 and Cpd I. In Figure 3, **2** was shown to be at least an order of magnitude faster with respect to HAT from cyclohexane than the most reactive nonheme iron-oxo complex

Scheme 2. Proposed Mechanism for the Reaction of 1/AcOOH with Substrates

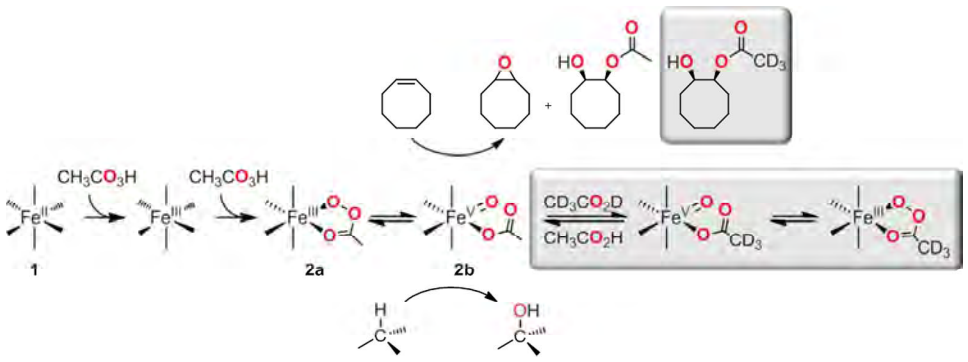

DOI: 10.1021/jacs.5b09904
J. Am. Chem. Soc. 2015, 137, 15833–15842

described to date. A comparison can be also made between **2** and Cpd I, the highly reactive oxoiron(IV) oxidant in heme chemistry. The second order rate constant (k_2) of 2.8 M^{-1} s^{-1} for the reaction of **2** with cyclohexane at 232 K is 25-fold faster than that measured for the Cpd I model $[Fe^{IV}(O)(TDCPP^{\bullet})]^+$ (TDCPP = tetrakis(2,6-dichlorophenyl)porphyrin) at the same temperature.[33] However, the k_2 value for the reaction of **2** with toluene at 298 K of 6 × 10^3 M^{-1} s^{-1}, as estimated from the Eyring parameters obtained at lower temperature ($\Delta H^{\ddagger}$ = 27(1) kJ mol^{-1}, $\Delta S^{\ddagger}$ = −82(5) J K^{-1} mol^{-1}, Figure S19), is only 2 orders of magnitude smaller than the k_2 value for *p*-toluic acid oxidation recently determined by Groves for the highly reactive Cpd I intermediate of a heme-thiolate peroxygenase.[64] When the toluene oxidation rate of **2** is mapped onto a plot of log k_2 values of different oxidants toward toluene vs the strength of the O—H bond formed,[65] an estimate of ∼101 kcal·mol^{-1} can be made for the FeO—H bond that forms in the HAT reaction by **2** (Figure S20), which is substantially larger than those determined for $Fe^{III}O(R)$ (∼85 kcal·mol^{-1}) and heme $Fe^{IV}(O)$ oxidants (∼90 kcal·mol^{-1})[66,67] and just 2 kcal·mol^{-1} smaller than the 103 kcal·mol^{-1} value associated with the heme-thiolate peroxygenase Cpd I.[64]

CONCLUSIONS

We have thus collected a set of spectroscopic and reactivity data on **2** that shed light on a remarkable oxidant **2** that is generated at −40 °C by the reaction of peracetic acid with the nonheme iron catalyst **1**. Oxidant **2** is an order of magnitude faster at cleaving the C—H bonds of cyclohexane than the most reactive nonheme oxoiron(IV) complexes reported thus far[33,34] and 4 orders of magnitude faster than oxoiron(V) TAML complexes at the same temperature.[30] Oxidant **2** is also capable of catalytic turnover, unlike the latter complexes, which at best can only carry out stoichiometric substrate oxidation. Furthermore, despite its high reactivity, **2** effects site-selective C—H bond functionalization that is responsive to electronic and steric parameters. Most significantly, in stark contrast to the reactivity of several nonheme oxoiron(IV) and oxoiron(V) complexes that can cleave strong C—H bonds but generate long-lived carbon-centered radicals,[28,29,31,68] **2** carries out C—H hydroxylations with high stereoretention. This observation is especially remarkable because structurally related iron complexes catalyze this challenging reaction with reactivity patterns analogous to those exhibited by **2**.[24,25,69] Selectivity in C—H bond reactivity converts them into very interesting tools for synthetic organic chemistry, yet the active species that account for this selectivity have not been directly observed. Therefore, this work constitutes the first case where the species responsible for stereospecific and site selective C—H hydroxylation with this class of catalysts is spectroscopically trapped, and its catalytic reactivity against C—H bonds could be directly demonstrated. Results presented here identify the major component of **2**, namely **2b**, as a species having unusual electronic structure. The *g* values of this $S = 1/2$ species exhibit a small *g* anisotropy that is not observed thus far for a nonheme low-spin iron(III) center but resembles that of a recently described oxoiron(V) complex **5**. We thus favor the latter formulation as a rationale for the unprecedentedly C—H bond cleavage reactivity found in the reaction of **1** with peracetic acid.

EXPERIMENTAL SECTION

Materials. Reagents and solvents used were of commercially available reagent quality, unless otherwise stated. Solvents were purchased from Scharlab, Acros, or Sigma-Aldrich and used without further purification. Peracetic acid was purchased from Aldrich as a 32 wt % solution in acetic acid containing less than 6% H_2O_2. Preparation and handling of air-sensitive materials were carried out in a N_2 drybox (Jacomex) with O_2 and H_2O concentrations <1 ppm. Synthesis of compound **1** is detailed in the SI.

Physical Methods. High resolution mass spectra (HR—MS) were recorded on a Bruker MicrOTOF-Q IITM instrument using ESI or Cryospray ionization sources at Serveis Tècnics of the University of Girona. Samples were introduced into the mass spectrometer ion source by direct infusion using a syringe pump and were externally calibrated using sodium formate. A cryospray attachment was used for CSI—MS (cryospray mass spectrometry). The temperature of the nebulizing and drying gases was set at −40 °C. The instrument was operated in positive ion mode. NMR experiments were performed on a Bruker Ultrashield Avance III400 and Ultrashield DPX300 spectrometers. UV—vis spectroscopy was performed with an Agilent 50 Scan (Varian) UV—vis spectrophotometer with 1 cm quartz cells. Low temperature control was achieved with a cryostat from Unisoku Scientific Instruments, Japan. GC product analyses were performed on an Agilent 7820A gas chromatograph equipped with an HP-5 capillary column 30m × 0.32 mm × 0.25 μm and a flame ionization detector. Stopped-flow experiments were carried out using an SFM4000 Biologic instrument provided with a cryo-stopped-flow accessory fitted to a Huber CC-905 bath.

Mössbauer spectra were recorded with two spectrometers, using Janis Research (Wilmington, MA) SuperVaritemp dewars that allow studies in applied magnetic fields up to 8.0 T in the temperature range from 1.5 to 200 K. Mössbauer spectral simulations were performed using the WMOSS software package (WEB Research, Minneapolis). Perpendicular (9.63 GHz) mode X-band EPR spectra were recorded on a Bruker EPP 300 spectrometer equipped with an Oxford ESR 910 liquid helium cryostat and an Oxford temperature controller. The quantification of the signals was relative to a Cu-EDTA spin standard. Software for EPR analysis was provided by Dr Michael P. Hendrich of Carnegie Mellon University.

Generation of 2. In a typical experiment, a 1 mM solution of **1** in dry acetonitrle was prepared inside the glovebox and 2 mL of this solution were placed in a UV—vis cuvette (2 μmols of **1**). The quartz cell was capped with a septum and taken out of the box, placed in the Unisoku cryostat of the UV—vis spectrophotometer and cooled down to 238 K. After reaching thermal equilibrium an UV—vis spectrum of the starting complex was recorded. Then, 50 μL of a solution containing 66 μL of 32% peracetic acid in 2 mL of dry acetonitrile were added (8 μmols). The formation of a band at λ_{max} = 490 nm and a shoulder at λ_{max} = 660 nm was observed. Compound **2** was fully formed after 70 s. In the reactions where the intermediate species is generated in acetone, a 4 mM solution of the complex in acetonitrile was prepared and then further diluted with the corresponding amount of dry acetone.

Kinetic Analysis of Reactions against Alkanes. The experiments were carried out by mixing thermostated acetonitrile solutions of **1** and peracetic acid (1:4 ratio) in a delay line. The resulting solution was aged for the time required to achieve the maximum concentration of **2**, and then it was mixed with a solution of the substrate. The concentration of the substrate in the observation cell was changed by using different ratios of the volumes in the second mixing. In any case, the substrate concentration was always in pseudo-first order excess with respect to **2**, and the kinetics of reaction was monitored by measuring the spectral changes with time using a diode-array detector. The data acquired after the second mixing were analyzed using the standard software of the stopped-flow instrument. In all cases, a satisfactory fit was obtained for the disappearance of 2 using a single exponential.

Analysis of the Oxidation Products. Once **2** was fully formed, 100 μL of a solution containing the corresponding equivalents of the desired substrate were added in the cuvette. The decay of the band at λ = 490 nm was monitored and after complete decay the cuvette was let to attain room temperature. Biphenyl was added as internal standard, and the iron complex was removed by passing the solution through a

DOI: 10.1021/jacs.5b09904
J. Am. Chem. Soc. 2015, 137, 15833−15842

short path of silica. The products were then eluted with ethyl acetate and then analyzed by GC.

Catalytic Experiments at Room Temperature with 1/AcOOH. In a typical experiment, 2 mL of a 1 mM solution of **1** in acetonitrile were placed in a 20 mL vial together with the appropriate amount of the desired substrate. Then, the corresponding amount of peracetic acid solution diluted in acetonitrile was added over 30 min. The solution was stirred for extra 15 min. For alkane oxidation, an internal standard (biphenyl) was added after the reaction was completed. The iron complex was removed by passing the solution through a short path of silica followed by elution with ethyl acetate (2 mL). Finally, the solution was subjected to GC analysis. For the oxidation of cyclooctene, the sample was treated with acetic anhydride (1 mL) together with 1-methylimidazole (0.1 mL), stirred for 15 min at r.t. to esterify the alcohol products. Then 3 mL of ice were added and stirred for 10 min. Biphenyl was added as an internal standard at that point, and then the organic products were extracted with $CHCl_3$ (2 mL). The organic layer was extracted and washed with H_2SO_4 (2 mL, 1M), saturated aq. $NaHSO_3$ (2 mL) and water (2 mL). The organic layer was dried over $MgSO_4$, filtered through a short path of diatomaceous earth and subjected to GC or GC–MS analysis.

■ ASSOCIATED CONTENT

Supporting Information

The Supporting Information is available free of charge on the ACS Publications website at DOI: 10.1021/jacs.5b09904.

Experimental details for the preparation and characterization of ligand $PyNMe_3$, and compounds **1**, **2′** and **4**; UV–vis stopped-flow experiments for the generation and reactivity of **2**; details on EPR and Mössbauer experiments; carboxylate exchange experiments of **2** with acetic acid-d_4 (PDF)

X-ray data for **1** (CIF)

X-ray data for **4** (CIF)

■ AUTHOR INFORMATION

Corresponding Authors

*manuel.basallote@uca.es

*emunck@cmu.edu

*larryque@umn.edu

*anna.company@udg.edu

*miquel.costas@udg.edu

Notes

The authors declare no competing financial interest.

■ ACKNOWLEDGMENTS

Financial support for this work was provided by the European Commission (2011-CIG-303522 to A.C. and ERC-2009-StG-239910 to M.C.), the Spanish Ministry of Science (CTQ2012-37420-C02-01/BQU to M.C., CTQ2012-37821-C02-02 to M.G.B., CTQ2013-43012-P to A.C., and CSD2010-00065 to M.C., M.G.B., and E.G.E) and Generalitat de Catalunya (ICREA Academia Award to M.C.). The Spanish Ministry of Science is acknowledged for a Juan de la Cierva contract to B.V. (JCI-2011-09302) and for a Ramón y Cajal contract to A.C. (RYC-2011-08683). We are thankful for the financial support from INNPLANTA project INP-2011-0059-PCT-420000-ACT1 to Dr. Xavi Ribas. We also thank Dr. Laura Gómez (Serveis Tècnics de Recerca, Universitat de Girona) for helpful advice in setting up the HR–MS experiments and helpful discussions. The work at the University of Minnesota and Carnegie Mellon University was respectively supported by grants from the U.S. Department of Energy, Office of Basic Energy Sciences (Grant DE-FG02-03ER15455 to L.Q.) and the US National Science Foundation (CHE-1305111 to E.M.).

■ REFERENCES

(1) Dyker, G. *Handbook of C-H Transformations*; Wiley-VCH: Weinheim, 2005.

(2) Meunier, B.; de Visser, S. P.; Shaik, S. *Chem. Rev.* **2004**, *104*, 3947–3980.

(3) Montellano, P. R. O. d. *Cytochrome P450: Structure, Mechanism, and Biochemistry*; Springer: New York, 2005.

(4) Costas, M.; Mehn, M. P.; Jensen, M. P.; Que, L. *Chem. Rev.* **2004**, *104*, 939–986.

(5) Abu-Omar, M. M.; Loaiza, A.; Hontzeas, N. *Chem. Rev.* **2005**, *105*, 2227–2252.

(6) Kovaleva, E. G.; Lipscomb, J. D. *Nat. Chem. Biol.* **2008**, *4*, 186–193.

(7) Barry, S. M.; Challis, G. L. *ACS Catal.* **2013**, *3*, 2362–2370.

(8) Company, A.; Lloret-Fillol, J.; Costas, M. In *Comprehensive Inorganic Chemistry II*; Reedijk, J., Poeppelmeier, K., Eds.; Elsevier: Oxford, 2013; Vol. 3, pp 487–564.

(9) Park, M. J.; Lee, J.; Suh, Y.; Kim, J.; Nam, W. *J. Am. Chem. Soc.* **2006**, *128*, 2630–2634.

(10) Seo, M. S.; Kamachi, T.; Kouno, T.; Murata, K.; Park, M. J.; Yoshizawa, K.; Nam, W. *Angew. Chem., Int. Ed.* **2007**, *46*, 2291–2294.

(11) Cho, J.; Jeon, S.; Wilson, S. A.; Liu, L. V.; Kang, E. A.; Braymer, J. J.; Lim, M. H.; Hedman, B.; Hodgson, K. O.; Valentine, J. S.; Solomon, E. I.; Nam, W. *Nature* **2011**, *478*, 502–505.

(12) Thibon, A.; Jollet, V.; Ribal, C.; Sénéchal-David, K.; Billon, L.; Sorokin, A. B.; Banse, F. *Chem. - Eur. J.* **2012**, *18*, 2715–2724.

(13) Prat, I.; Company, A.; Corona, T.; Parella, T.; Ribas, X.; Costas, M. *Inorg. Chem.* **2013**, *52*, 9229–9244.

(14) Britovsek, G. J. P.; England, J.; White, A. J. P. *Inorg. Chem.* **2005**, *44*, 8125–8134.

(15) BPMEN = *N*,*N*′-dimethyl-*N*,*N*′-bis(2-pyridylmethyl)ethane-1,2-diamine; BPMCN = *N*,*N*′-dimethyl-*N*,*N*′-bis(2-pyridylmethyl)-*trans*-1,2-diaminocyclohexane; TPA = *tris*(2-pyridylmethyl)amine; PDP = *N*,*N*′-Bis(2-pyridylmethyl)-2,2′-bipyrrolidine; PyTACN = 1,4-Dimethyl-7-(2-pyridylmethyl)-1,4,7-triazacyclononane.

(16) Chen, K.; Que, L. *J. Am. Chem. Soc.* **2001**, *123*, 6327–6337.

(17) Wang, Y.; Janardanan, D.; Usharani, D.; Han, K.; Que, L., Jr.; Shaik, S. *ACS Catal.* **2013**, *3*, 1334–1341.

(18) Prat, I.; Mathieson, J. S.; Güell, M.; Ribas, X.; Luis, J. M.; Cronin, L.; Costas, M. *Nat. Chem.* **2011**, *3*, 788–793.

(19) Oloo, W. N.; Que, L. *Acc. Chem. Res.* **2015**, *48*, 2612–2621.

(20) Costas, M.; Chen, K.; Que, L. *Coord. Chem. Rev.* **2000**, *200*, 517–544.

(21) Even though the BDE_{C-H} of CH_3CN (93 kcal·mol^{-1}) is lower than that of some of the hydrocarbon substrates used in this work (e.g., BDE_{C6H12} = 99.3 kcal·mol^{-1}), acetonitrile oxidation does not take place due to polar effects. See: Roberts, B. P. *Chem. Soc. Rev.* **1999**, *28*, 25.

(22) Gomez, L.; Canta, M.; Font, D.; Prat, I.; Ribas, X.; Costas, M. *J. Org. Chem.* **2013**, *78*, 1421–1433.

(23) Canta, M.; Font, D.; Gomez, L.; Ribas, X.; Costas, M. *Adv. Synth. Catal.* **2014**, *356*, 818–830.

(24) Chen, M. S.; White, M. C. *Science* **2007**, *318*, 783–787.

(25) Chen, M. S.; White, M. C. *Science* **2010**, *327*, 566–571.

(26) Oloo, W. N.; Que, L. In *Comprehensive Inorganic Chemistry II*; Reedijk, J., Poeppelmeier, K., Eds.; Elsevier: Oxford, 2013; Vol. 6, pp 763–778.

(27) Liu, L. V.; Hong, S.; Cho, J.; Nam, W.; Solomon, E. I. *J. Am. Chem. Soc.* **2013**, *135*, 3286–3299.

(28) Kaizer, J.; Klinker, E. J.; Oh, N. Y.; Rohde, J.-U.; Song, W. J.; Stubna, A.; Kim, J.; Münck, E.; Nam, W.; Que, L. *J. Am. Chem. Soc.* **2004**, *126*, 472–473.

(29) Company, A.; Prat, I.; Frisch, J. R.; Mas-Balleste, R.; Guell, M.; Juhasz, G.; Ribas, X.; Munck, E.; Luis, J. M.; Que, L.; Costas, M. *Chem. - Eur. J.* **2011**, *17*, 1622–1634.

DOI: 10.1021/jacs.5b09904
J. Am. Chem. Soc. 2015, 137, 15833–15842

(30) Kundu, S.; Thompson, J. V. K.; Shen, L. Q.; Mills, M. R.; Bominaar, E. L.; Ryabov, A. D.; Collins, T. J. *Chem. - Eur. J.* **2015**, *21*, 1803−1810.
(31) Ghosh, M.; Singh, K. K.; Panda, C.; Weitz, A.; Hendrich, M. P.; Collins, T. J.; Dhar, B. B.; Gupta, S. S. *J. Am. Chem. Soc.* **2014**, *136*, 9524−9527.
(32) Hong, S.; Wang, B.; Seo, M. S.; Lee, Y.-M.; Kim, M. J.; Kim, H. R.; Ogura, T.; Garcia-Serres, R.; Clémancey, M.; Latour, J.-M.; Nam, W. *Angew. Chem., Int. Ed.* **2014**, *53*, 6388−6392.
(33) Seo, M. S.; Kim, N. H.; Cho, K.-B.; So, J. E.; Park, S. K.; Clemancey, M.; Garcia-Serres, R.; Latour, J.-M.; Shaik, S.; Nam, W. *Chem. Sci.* **2011**, *2*, 1039−1045.
(34) Biswas, A. N.; Puri, M.; Meier, K. K.; Oloo, W. N.; Rohde, G. T.; Bominaar, E. L.; Münck, E.; Que, L. *J. Am. Chem. Soc.* **2015**, *137*, 2428−2431.
(35) Sastri, C. V.; Lee, J.; Oh, K.; Lee, Y. J.; Lee, J.; Jackson, T. A.; Ray, K.; Hirao, H.; Shin, W.; Halfen, J. A.; Kim, J.; Que, L.; Shaik, S.; Nam, W. *Proc. Natl. Acad. Sci. U. S. A.* **2007**, *104*, 19181−19186.
(36) Company, A.; Gómez, L.; Güell, M.; Ribas, X.; Luis, J. M.; Que, L.; Costas, M. *J. Am. Chem. Soc.* **2007**, *129*, 15766−15767.
(37) Hitomi, Y.; Arakawa, K.; Funabiki, T.; Kodera, M. *Angew. Chem., Int. Ed.* **2012**, *51*, 3448−3452.
(38) Makhlynets, O. V.; Oloo, W. N.; Moroz, Y. S.; Belaya, I. G.; Palluccio, T. D.; Filatov, A. S.; Muller, P.; Cranswick, M. A.; Que, L.; Rybak-Akimova, E. V. *Chem. Commun.* **2014**, *50*, 645−648.
(39) Oloo, W. N.; Fielding, A. J.; Que, L. *J. Am. Chem. Soc.* **2013**, *135*, 6438−6441.
(40) Oloo, W. N.; Meier, K. K.; Wang, Y.; Shaik, S.; Munck, E.; Que, L. *Nat. Commun.* **2014**, *5*, 4041−4049.
(41) Makhlynets, O. V.; Rybak-Akimova, E. V. *Chem. - Eur. J.* **2010**, *16*, 13995−14006.
(42) The EPR of **2** in MeCN shows broad signals and it is difficult to integrate. Thus, **2** was generated in the glassy 1:3 MeCN/acetone solvent mixture to afford dramatically sharpened EPR signals.
(43) Lyakin, O. Y.; Zima, A. M.; Samsonenko, D. G.; Bryliakov, K. P.; Talsi, E. P. *ACS Catal.* **2015**, *5*, 2702−2707.
(44) McGarvey, B. R. *Coord. Chem. Rev.* **1998**, *170*, 75−92.
(45) Taylor, C. P. S. *Biochim. Biophys. Acta, Protein Struct.* **1977**, *491*, 137−148.
(46) Van Heuvelen, K. M.; Fiedler, A. T.; Shan, X.; De Hont, R. F.; Meier, K. K.; Bominaar, E. L.; Münck, E.; Que, J. L. *Proc. Natl. Acad. Sci. U. S. A.* **2012**, *109*, 11933−11938.
(47) For the extreme octahedral case, for which the tetragonal and rhombic distortions are small compared to the spin-orbit coupling constant ($\lambda \approx 380$ cm^{-1}), the *g*-values are close to $g = 2.00$; see for instance Figure 3 in Telser, J. *J. Braz. Chem. Soc.* **2006**, *17*, 1501−1515 for $A^2 \approx 1/3$. This, perhaps unlikely, case would be recognizable by Mössbauer spectroscopy, as the ^{57}Fe magnetic hyperfine tensor would differ considerably from that observed for the other region for which the *g*-values are close to $g = 2$, namely when the tetragonal distortion is large compared to λ..
(48) Schulz, C. E.; Rutter, R.; Sage, J. T.; Debrunner, P. G.; Hager, L. P. *Biochemistry* **1984**, *23*, 4743−4754.
(49) Rittle, J.; Green, M. T. *Science* **2010**, *330*, 933−937.
(50) de Oliveira, F. T.; Chanda, A.; Banerjee, D.; Shan, X.; Mondal, S.; Que, L.; Bominaar, E. L.; Münck, E.; Collins, T. J. *Science* **2007**, *315*, 835−838.
(51) Roelfes, G.; Vrajmasu, V.; Chen, K.; Ho, R. Y. N.; Rohde, J.-U.; Zondervan, C.; la Crois, R. M.; Schudde, E. P.; Lutz, M.; Spek, A. L.; Hage, R.; Feringa, B. L.; Münck, E.; Que, L. *Inorg. Chem.* **2003**, *42*, 2639−2653.
(52) Tse, C.-W.; Chow, T. W.-S.; Guo, Z.; Lee, H. K.; Huang, J.-S.; Che, C.-M. *Angew. Chem., Int. Ed.* **2014**, *53*, 798−803.
(53) McGown, A. J.; Kerber, W. D.; Fujii, H.; Goldberg, D. P. *J. Am. Chem. Soc.* **2009**, *131*, 8040−8048.
(54) Leeladee, P.; Jameson, G. N. L.; Siegler, M. A.; Kumar, D.; de Visser, S. P.; Goldberg, D. P. *Inorg. Chem.* **2013**, *52*, 4668−4682.
(55) Mas-Balleste, R.; Fujita, M.; Que, L., Jr. *Dalton Trans.* **2008**, 1828−1830.
(56) Iyer, S. R.; Javadi, M. M.; Feng, Y.; Hyun, M. Y.; Oloo, W. N.; Kim, C.; Que, L. *Chem. Commun.* **2014**, *50*, 13777−13780.
(57) Furutachi, H.; Hashimoto, K.; Nagatomo, S.; Endo, T.; Fujinami, S.; Watanabe, Y.; Kitagawa, T.; Suzuki, M. *J. Am. Chem. Soc.* **2005**, *127*, 4550−4551.
(58) Zhang, X.; Furutachi, H.; Tojo, T.; Tsugawa, T.; Fujinami, S.; Sakurai, T.; Suzuki, M. *Chem. Lett.* **2011**, *40*, 515−517.
(59) Khusnutdinova, J. R.; Luo, J.; Rath, N. P.; Mirica, L. M. *Inorg. Chem.* **2013**, *52*, 3920−3932.
(60) Ghosh, P.; Tyeklar, Z.; Karlin, K. D.; Jacobson, R. R.; Zubieta, J. *J. Am. Chem. Soc.* **1987**, *109*, 6889−6891.
(61) Sanyal, I.; Ghosh, P.; Karlin, K. D. *Inorg. Chem.* **1995**, *34*, 3050−3056.
(62) Kitajima, N.; Fujisawa, K.; Moro-oka, Y. *Inorg. Chem.* **1990**, *29*, 357−358.
(63) Nakazawa, J.; Terada, S.; Yamada, M.; Hikichi, S. *J. Am. Chem. Soc.* **2013**, *135*, 6010−6013.
(64) Wang, X.; Peter, S.; Kinne, M.; Hofrichter, M.; Groves, J. T. *J. Am. Chem. Soc.* **2012**, *134*, 12897−12900.
(65) Mayer, J. M. *Acc. Chem. Res.* **1998**, *31*, 441−450.
(66) Wolak, M.; van Eldik, R. *Chem. - Eur. J.* **2007**, *13*, 4873−4883.
(67) Groves, J. T.; Gross, Z.; Stern, M. K. *Inorg. Chem.* **1994**, *33*, 5065−5072.
(68) Kwon, E.; Cho, K.-B.; Hong, S.; Nam, W. *Chem. Commun.* **2014**, *50*, 5572−5575.
(69) Gómez, L.; Garcia-Bosch, I.; Company, A.; Benet-Buchholz, J.; Polo, A.; Sala, X.; Ribas, X.; Costas, M. *Angew. Chem., Int. Ed.* **2009**, *48*, 5720−5723.

DOI: 10.1021/jacs.5b09904
J. Am. Chem. Soc. 2015, 137, 15833−15842

CHAPTER VI.

Exceedingly Fast Oxygen Atom Transfer to Olefins via a Catalytically Competent Nonheme Iron Species.

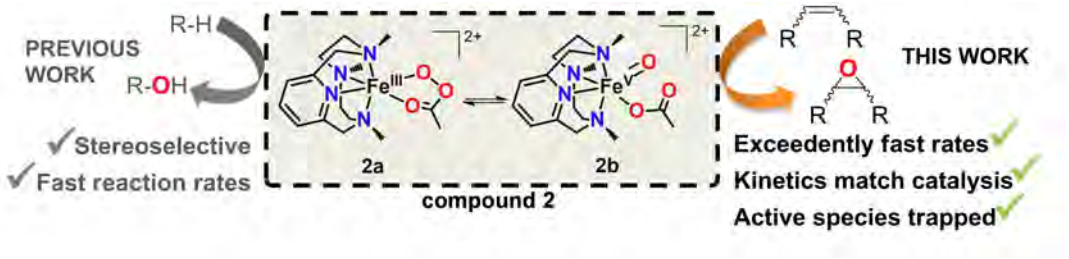

This chapter corresponds to the following publication:

Joan Serrano-Plana, Almudena Aguinaco, Raquel Belda, Enrique García-España, Manuel G. Basallote,* Anna Company,* and Miquel Costas*

Angew. Chem. Int. Ed. **2016** doi: 10.1002/anie.201601396

For this publication, J.S.-P. synthesized ligand $PyNMe_3$ and the iron(II) complex. He also performed the oxidation catalysis experiments. Besides, J.S.-P. contributed in writing the manuscript and was involved in argumentations and discussions.

Iron–Oxygen Species Hot Paper

International Edition: DOI: 10.1002/anie.201601396
German Edition: DOI: 10.1002/ange.201601396

Exceedingly Fast Oxygen Atom Transfer to Olefins via a Catalytically Competent Nonheme Iron Species

Joan Serrano-Plana[+], Almudena Aguinaco[+], Raquel Belda, Enrique García-España, Manuel G. Basallote, Anna Company,* and Miquel Costas**

Abstract: *The reaction of $[Fe(CF_3SO_3)_2(PyNMe_3)]$ with excess peracetic acid at −40 °C leads to the accumulation of a metastable compound that exists as a pair of electromeric species, $[Fe^{III}(OOAc)(PyNMe_3)]^{2+}$ and $[Fe^{V}(O)(OAc)(PyNMe_3)]^{2+}$, in fast equilibrium. Stopped-flow UV/Vis analysis confirmed that oxygen atom transfer (OAT) from these electromeric species to olefinic substrates is exceedingly fast, forming epoxides with stereoretention. The impact of the electronic and steric properties of the substrate on the reaction rate could be elucidated, and the relative reactivities determined for the catalytic oxidations could be reproduced by kinetic studies. The observed fast reaction rates and high selectivities demonstrate that this metastable compound is a truly competent OAT intermediate of relevance for nonheme iron catalyzed epoxidations.*

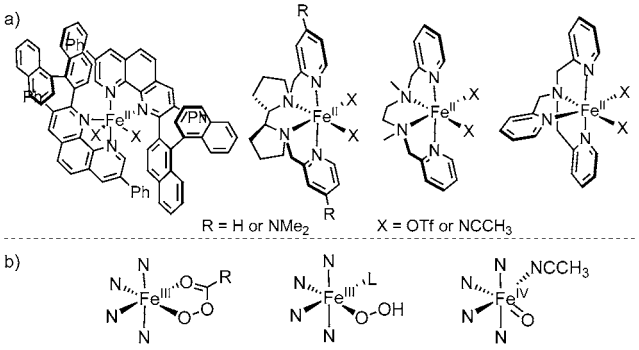

Scheme 1. a) Representative iron epoxidation catalysts. b) Metastable reaction intermediates spectroscopically characterized after the reaction of iron complexes with H_2O_2/AcOH or peracids.

The epoxidation of olefins is a valuable reaction in organic synthesis,[1,2] and catalytic variants relying on base metals and peroxides have recently received increasing attention because of cost and sustainability considerations. Among them, a biologically inspired approach entails the iron-catalyzed activation of hydrogen peroxide. Selected iron complexes with strong-field N_4 donor ligands have been described as particularly efficient and selective homogeneous catalysts for epoxidation, providing good product yields in short reaction times under very mild reaction conditions (Scheme 1 a).[3–7] Some of these complexes are also highly stereoselective catalysts, which renders them powerful tools in fine chemistry. A key aspect for the development of these systems as catalysts for practical organic synthesis was the discovery that the combination of hydrogen peroxide with acetic acid substantially improved their efficiency.[7] Alternatively, excellent activities and selectivities could be attained by the use of peracetic acid and other peracids.[4–9]

The elucidation of the mechanistic details of these reactions is challenging because the active species operating in this class of highly reactive systems most often do not accumulate in solution. Furthermore, the few iron species that have been spectroscopically trapped and characterized under cryogenic conditions related to catalysis (Scheme 1 b) either do not exhibit kinetic competence consistent with catalysis,[6,10] or their kinetic competence has not been proven presumably because they are formed in very small amounts (ca. 1 %).[11] Therefore, reaction mechanisms have been mainly interrogated by product analysis, isotopic labelling, and computational methods. Together, these studies suggest that a $Fe^{V}(O)(O_2CR)$ intermediate is the oxidizing species when either peracetic acid or a combination of H_2O_2 and a carboxylic acid is employed.[4,6,10,11] Recent computational studies have also suggested that a $Fe^{V}(O)(O_2CR)$ species may reversibly evolve in the formation of a cyclic percarboxylate moiety, $Fe^{III}(O_2C(O)R)$, thus alleviating the high reactivity associated with highly electrophilic Fe^{V} centers.[12]

We have recently shown that the reaction of alkyl peracids with $[Fe^{II}(CF_3SO_3)_2(PyNMe_3)]$ (**1**) in acetonitrile at low temperature (−40 °C) led to a transient species **2** that is kinetically competent for oxidizing strong C–H bonds of alkanes (with bond dissociation energies of up to 100 kcal mol^{-1}) through an initial hydrogen atom transfer (HAT) mechanism.[13] Compound **1** contains an iron center ligated, with a distorted octahedral geometry, to a strong-field

[*] J. Serrano-Plana,[+] Dr. A. Company, Dr. M. Costas
Grup de Química Bioinorgànica
Supramolecular i Catàlisi (QBIS-CAT)
Institut de Química Computacional I Catàlisi (IQCC)
Departament de Química, Universitat de Girona
Campus Montilivi, 17071 Girona (Catalonia, Spain)
E-mail: anna.company@udg.edu
miquel.costas@udg.edu
Dr. A. Aguinaco,[+] Dr. M. G. Basallote
Universidad de Cádiz, Facultad de Ciencias
Departamento de Ciencia de los Materiales e Ingeniería Metalúrgica y Química Inorgánica
Apdo. 40, 11510 Puerto Real, Cádiz (Spain)
E-mail: manuel.basallote@uca.es
Dr. R. Belda, Dr. E. García-España
Instituto de Ciencia Molecular (ICMol)
Universidad de Valencia
C/Catedrático José Beltrán, Paterna, Valencia 2 46980 (Spain)
[+] These authors contributed equally to this work.
Supporting information and the ORCID identification number(s) for the author(s) of this article can be found under http://dx.doi.org/10.1002/anie.201601396.

 © 2016 Wiley-VCH Verlag GmbH & Co. KGaA, Weinheim

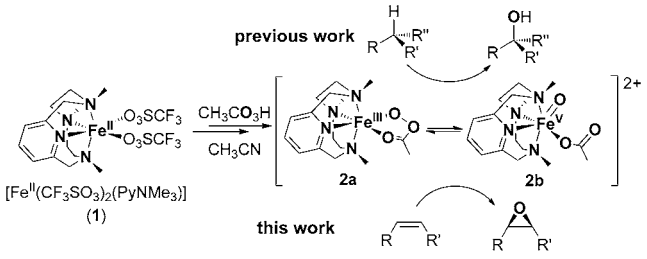

Scheme 2. Species **2** formed upon reaction of **1** with peracetic acid in acetonitrile.

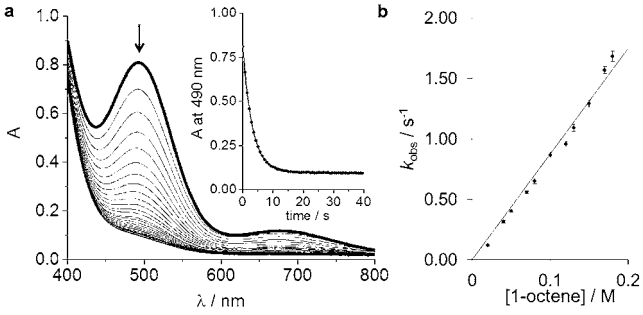

Figure 1. a) UV/Vis monitoring of the reaction of **2** with 1-octene in acetonitrile/acetone (1:3) at −60 °C. Inset: Decay of the 490 nm chromophore fitted to a single exponential. b) Plot of k_{obs} against the 1-octene concentration for the reaction of **2** with 1-octene at −60 °C in acetonitrile/acetone (1:3).

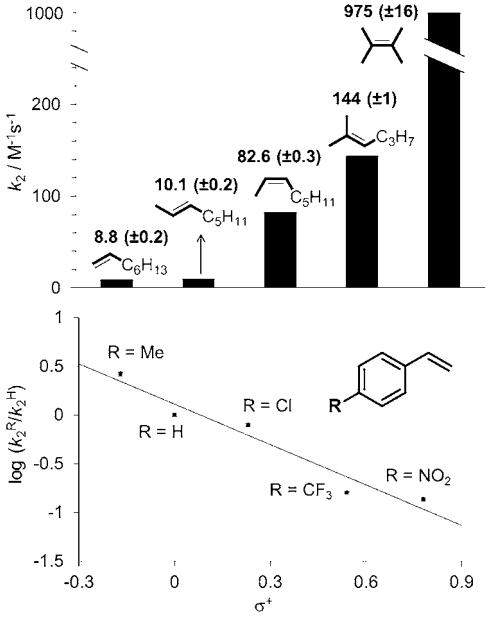

Figure 2. Top: Second-order rate constants (k_2 in $M^{-1}\,s^{-1}$) for the reaction of **2** towards selected alkenes at −60 °C in acetonitrile/acetone (1:3). Bottom: Hammett plot for the reaction of **2** with a series of *para*-substituted styrenes at −60 °C in acetonitrile/acetone (1:3).

tetradentate aminopyridine macrocyclic ligand, and also to two labile triflate anions that are *cis* to each other (Scheme 2). Therefore, **1** bears the chemical and structural properties associated with iron complexes that behave as powerful C–H and C=C oxidation catalysts.[3,14,15] EPR analyses have shown that **2** actually consists of two components, a major ($[Fe^{V}(O)(OAc)(PyNMe_3)]^{2+}$; 40 %, **2b**) and a minor species ($[Fe^{III}(OOAc)(PyNMe_3)]^{2+}$; 5 %, **2a**), in fast equilibrium, thus reproducing the reactivity that was predicted earlier for a related system on the basis of DFT calculations.[10] Remarkably, the reaction of **2** towards alkanes occurred at unprecedentedly fast reaction rates compared to all previously spectroscopically characterized iron-based oxidants.

Motivated by the discovery of the extraordinary reactivity of **2** towards alkanes, we herein explored its ability to engage in oxygen atom transfer (OAT) reactions with olefins. By doing so, this work provides direct experimental evidence that a $[Fe^{V}(O)(OAc)(L^{N4})]^{2+}$ species is the OAT agent in catalytic epoxidation reactions with this class of catalysts, and establishes the role of steric and electronic factors in defining its reactivity.

The thermally unstable compound **2** was prepared by the reaction of **1** with 4 equiv peracetic acid at −41 °C in acetonitrile. This reaction was monitored by UV/Vis spectroscopy, showing the appearance of two absorption features in the visible region at 490 and 660 nm that are characteristic of **2**.[13] Once maximized, the addition of cyclooctene (50 equiv) resulted in the immediate decay of the UV/Vis features associated with **2**. After the reaction, product analysis indicated that 1.3 equiv of the epoxide and 0.06 equiv of *cis*-2-acetoxycyclooctanol with respect to **2** had been formed.

The reaction of **2** towards olefinic substrates was very fast, and in order to determine the reaction rates, kinetic analyses required the performance of sequential stopped-flow experiments under cryogenic conditions at −60 °C using a 1:3 acetonitrile/acetone mixture as the solvent. The kinetics were monitored by following the decay of the 490 nm band, which is characteristic of **2**, upon addition of excess olefin (Figure 1 a). The time traces were satisfactorily fitted to a single exponential to obtain the observed rate constants (k_{obs}), which showed a linear dependence on substrate concentration (Figure 1 b; see also the Supporting Information, Figure S7), affording second-order rate constants (k_2; Figure 2, top and Tables S1 and S2). Interestingly, the second-order reaction rates were independent of the peracid concentration (2–16 equiv with respect to **1**) employed to form **2**, indicating that neither the peracid nor the acetic acid that inevitably goes with it are responsible for the extraordinary reactivity of **2**. Moreover, activation parameters were obtained for the reaction of **2** with 1-octene by performing experiments at different temperatures (Figure S8, Table S3). A small activation enthalpy ($\Delta H^{\neq} = 28.4 \pm 0.5\ kJ\,mol^{-1}$) and a negative activation entropy ($\Delta S^{\neq} = -90 \pm 2\ J\,K^{-1}mol^{-1}$) were found, which are characteristic of a bimolecular process with a low enthalpic barrier. It is interesting to note that OAT from **2** towards sulfides was so fast that proper kinetic data could not be obtained with our stopped-flow equipment (see the Supporting Information).

The basic structural and electronic aspects that determine the relative reactivity of **2** towards olefins were also inter-

 © 2016 Wiley-VCH Verlag GmbH & Co. KGaA, Weinheim

rogated. The oxidation rate of **2** toward olefins (k_2) increased as the degree of olefin substitution increased (Figure 2, top). Thus the rate for the oxidation of 2,3-dimethyl-2-butene with **2** was $975 \pm 16\,M^{-1}s^{-1}$, almost seven times higher than that for 2-methyl-2-hexene ($k_2 = 144 \pm 1\,M^{-1}s^{-1}$), which in turn reacted around two and fourteen times faster than *cis*- and *trans*-2-octene, respectively. The lowest rate was observed for 1-octene ($8.8 \pm 0.2\,M^{-1}s^{-1}$). Most probably this is related to the increase in the electron density of the double bond, which is due to inductive effects of the substituents,[1] which supports the hypothesis that **2** acts as an electrophile. Interestingly, these results indicate that electronic effects dominate over steric factors in determining the reactivity of **2** towards olefins. It is also particularly interesting that the relative reactivity was configuration-dependent and that the *cis* isomer was more prone to oxidation than the *trans* analogue, and reacted up to eight times faster in the case of 2-octene.

The impact of electronic effects in defining the relative reactivity of olefins with **2** was further studied in a systematic manner by analyzing the reaction rates for the reaction of **2** with several *para*-substituted styrenes. The logarithm of the second-order rate constants of the decay was plotted against the Hammett *para* substituent constants, σ^+, affording a good correlation ($R = 0.95$) and a negative slope (ρ) of -1.4 ± 0.2 (Figure 2, bottom; see also Table S4). The negative ρ value confirms the electrophilic character of **2** in OAT reactions,[16,17] which is in agreement with the increase in reactivity with increased olefin substitution (Figure 2, top).

Compound **1** acts as a catalyst in the epoxidation of olefins. The catalytic oxidation of excess 1-octene (100 equiv) at room temperature with peracetic acid (20 equiv) as the oxidant and **1** as the catalyst afforded 1-octene oxide as the major product (12 TON; TON = turnover number) and the corresponding hydroxyacetate as the minor product (3 TON). Both compounds are proposed to be formed by the reaction of in situ generated **2** with the olefin. Comparison of the catalytic results obtained with the **1**/AcOOH system (1:10:100, **1**/AcOOH/substrate, −60 °C) with the kinetic data gathered for the reaction of **2** with alkenes demonstrates the relevance of **2** in catalytic epoxidation reactions. The selectivities of the **1**/AcOOH catalytic reactions could be extracted from the competitive epoxidation of pairs of olefins (alkene^A and alkene^B) in acetonitrile/acetone (1:3) at −60 °C. Three different competition experiments were performed: styrene vs. 1-octene, *cis*-cyclooctene vs. *cis*-2-octene, and *cis*- vs. *trans*-2-octene (Figure 3). Blank experiments showed that under these experimental conditions, uncatalyzed epoxidation is negligible (< 3% with respect to the oxidant). Interestingly, the reactions occurred with stereoretention, and the relative amounts of the two epoxides formed after each competition reaction (epoxide^A/epoxide^B) reasonably matched the ratios of the corresponding k_2 values measured individually for the reaction of **2** with each olefin (k_2^A/k_2^B). This remarkable agreement provides strong evidence that **2** constitutes the active species responsible for OAT in these catalytic epoxidations.

Aside from its selectivity, the fast reactivity of **2** is also consistent with a catalytically competent intermediate. The reaction rates of **2** towards alkenes are especially impressive

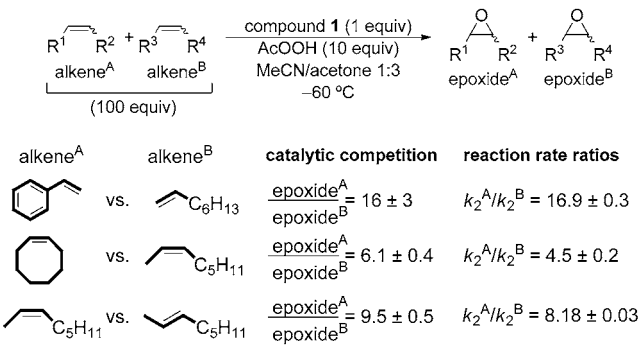

Figure 3. Intermolecular competitive epoxidation of pairs of olefins (alkene^A and alkene^B) by the **1**/AcOOH catalytic system. Epoxide^A/epoxide^B: ratio of the epoxide^A and epoxide^B products determined by GC analysis. k_2^A/k_2^B: ratio of the second-order rate constants for the reaction of **2** with alkene^A (k_2^A) and alkene^B (k_2^B) in acetonitrile/acetone (1:3) at −60 °C determined by stopped-flow analysis.

when compared to other iron–oxygen species. It must be kept in mind that comparison with these compounds is not straightforward, as the oxidation state of the metal and the ligands, oxidants, and reaction conditions employed are not equivalent. Furthermore, a cautious note is warranted; iron-catalyzed epoxidations using other tetra- or pentadentate ligands have been studied, and alternative reaction mechanisms have been proposed. In most of these cases, the lack of accumulation of the OAT species, which is presumably very reactive, prevents comparison.[3,4,6,15,24] With these limitations in mind, **2** can be ranked among the different types of iron–oxygen species for which second-order reaction rates for OAT reactions have been determined (Table 1, Figure 4). The

Table 1: Second-order rate constants (k_2) for the reaction of **2** and selected mononuclear iron–oxygen species with 1-octene, styrene, and *cis*-cyclooctene (see Figure 4 for the structures of compounds **3**–**9**).

Catalyst	T [°C]	k_2 [$M^{-1}s^{-1}$]			Ref.
		1-octene	styrene	cyclooctene	
2	−60	8.8 ± 0.2	149 ± 3	375 ± 15	this work
3	0	–	–	0.45	[18]
4	20	–	–	0.032	[19]
5	25	–	0.026	–	[20]
6[a]	25	–	0.043 ± 0.003	–	[21]
7	−40	5.3	–	3.3	[22]
8	RT	–	148 ± 8.1	29 ± 3.6	[17]
9	−60	–	0.4	–	[23]

[a] Proton-coupled electron transfer (PCET) in the presence of HOTf. Compound **6** itself cannot oxidize styrene.

iron(IV) oxo complexes **3**[18] and **4**,[19] bearing pyridine-containing macrocyclic ligands, and **5** with a N_2S_2 thioether ligand[20] exhibit rates that are three to four orders of magnitude lower than **2**, but these reactions were carried out at much higher temperatures. The same difference in reactivity was observed for the iron(IV) oxo complex **6**, which bears a pentadentate N4Py ligand, in the presence of triflic acid.[21] Compound **2** also shows higher reaction rates than the more reactive $S = 2$ iron(IV) oxo complex **7**, which was

 © 2016 Wiley-VCH Verlag GmbH & Co. KGaA, Weinheim

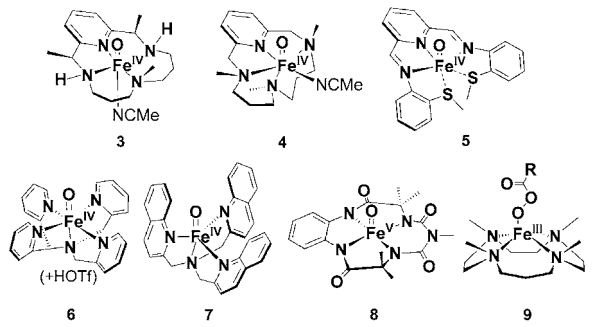

Figure 4. Spectroscopically detected nonheme iron–oxygen species for which alkene epoxidation rates have been determined.

recently reported by Que and co-workers, and shows an oxidation rate for 1-octene ($5.4\,M^{-1}s^{-1}$ at −40 °C) that is of the same order of magnitude as that for **2** ($8.8\,M^{-1}s^{-1}$ at −60 °C). However, the rate of *cis*-cyclooctene oxidation by **3** is two orders of magnitude lower than for **2**.[22] The rate obtained for *cis*-cyclooctene oxidation by the TAML oxo iron(V) species **8** ($29\,M^{-1}s^{-1}$ at 25 °C)[17] is still ten times lower than that for **2** at −60 °C ($375\,M^{-1}s^{-1}$ at −60 °C) without correcting for the 80 °C difference, meaning that **2** reacts much faster than **8**. Interestingly, the recently reported high-spin iron(III) acylperoxo complex **9** oxidizes styrene almost 400 times slower than **2**.[23] This reactivity difference is especially striking because it further highlights that the cleavage of the O–O bond is crucial for creating a uniquely powerful oxidation agent. Other iron(III) acylperoxo species have been reported but they proved to be either sluggish oxidants in OAT,[25] kinetically incompetent to perform this chemistry,[10] or no reactivity studies have been undertaken.[26–28] The latter include Fe complexes based on pyridinophane ligands structurally related to $PyNMe_3$, for which no direct evaluation of the reactivity of the spectroscopically trapped iron–oxygen species was reported, and no direct comparison can be established with the current system.[28,29] Finally, the superior reactivity of **2** is also illustrated by its faster reaction (2 or 3 orders of magnitude) when compared to synthetic iron(IV) oxo porphyrin radical species, which reproduce the electronic structure of compound I of cytochrome P450 and related enzymes (see the Supporting Information).[30,31]

Overall, compound **2** stands out amongst all previously reported iron–oxygen species for olefin oxidation. Furthermore, our observations provide experimental support for the proposal that the acetic acid effect in iron-catalyzed epoxidations is (at least partially) due to facilitating the O–O heterolytic cleavage to form a highly reactive iron(V) oxo acetato complex such as **2**.[32]

In conclusion, **2** is an exceedingly reactive compound with second-order reaction rate constants that, to the best of our knowledge, render this molecule the fastest OAT agent described to date. Most significantly, the agreement between the reaction rates determined by stopped-flow analysis and the selectivity properties of **2** under catalytic epoxidation conditions provide solid evidence that it is a truly competent intermediate and a plausible OAT agent with broad relevance in biologically inspired nonheme iron oxidation catalysis.

Acknowledgements

Financial support for this work was provided by the European Commission (2011-CIG-303522 to A.C. and ERC-2009-StG-239910 to M.C.), the Spanish Ministry of Science (CTQ2012-37420-C02-01/BQU to M.C., CTQ2012-37821-C02-02 to M.G.B., CTQ2013-43012-P to A.C., CTQ2013-48917-C3-1-P to R.B. and E.G.-E.), the Unidad de Excelencia (MDM 2015-0038 and CSD2010-00065 to M.C., M.G.B., R.B., and E.G.-E), the Generalitat Valenciana (PROMETEOII 2015/002t to R.B. and E.G.-E.), and the Generalitat de Catalunya (ICREA Academia Award to M.C. and 2014SGR-862). The Spanish Ministry of Science is also acknowledged for a Ramón y Cajal contract to A.C. (RYC-2011-08683). Prof. Lawrence Que, Jr. from the University of Minnesota is acknowledged for fruitful discussions.

Keywords: epoxidation · kinetics · nonheme iron complexes · olefins · oxidation

How to cite: *Angew. Chem. Int. Ed.* **2016**, *55*, 6310–6314
Angew. Chem. **2016**, *128*, 6418–6422

[1] E. A. Mikhalyova, O. V. Makhlynets, T. D. Palluccio, A. S. Filatov, E. V. Rybak-Akimova, *Chem. Commun.* **2012**, *48*, 687–689.
[2] S. Huber, M. Cokoja, F. E. Kühn, *J. Organomet. Chem.* **2014**, *751*, 25–32.
[3] K. P. Bryliakov, E. P. Talsi, *Coord. Chem. Rev.* **2014**, *276*, 73–96.
[4] O. Cussó, I. Garcia-Bosch, X. Ribas, J. Lloret-Fillol, M. Costas, *J. Am. Chem. Soc.* **2013**, *135*, 14871–14878.
[5] Y. Nishikawa, H. Yamamoto, *J. Am. Chem. Soc.* **2011**, *133*, 8432–8435.
[6] R. Mas-Ballesté, L. Que, Jr., *J. Am. Chem. Soc.* **2007**, *129*, 15964–15972.
[7] M. C. White, A. G. Doyle, E. N. Jacobsen, *J. Am. Chem. Soc.* **2001**, *123*, 7194–7195.
[8] G. Dubois, A. Murphy, T. D. P. Stack, *Org. Lett.* **2003**, *5*, 2469–2472.
[9] C. Marchi-Delapierre, A. Jorge-Robin, A. Thibon, S. Menage, *Chem. Commun.* **2007**, 1166–1168.
[10] W. N. Oloo, K. K. Meier, Y. Wang, S. Shaik, E. Münck, L. Que, Jr., *Nat. Commun.* **2014**, *5*, 3046.
[11] O. Y. Lyakin, A. M. Zima, D. G. Samsonenko, K. P. Bryliakov, E. P. Talsi, *ACS Catal.* **2015**, *5*, 2702–2707.
[12] Y. Wang, D. Janardanan, D. Usharani, K. Han, L. Que, Jr., S. Shaik, *ACS Catal.* **2013**, *3*, 1334–1341.
[13] J. Serrano-Plana, W. N. Oloo, L. Acosta-Rueda, K. K. Meier, B. Verdejo, E. García-España, M. G. Basallote, E. Münck, L. Que, Jr., A. Company, M. Costas, *J. Am. Chem. Soc.* **2015**, *137*, 15833–15842.
[14] O. Cussó, X. Ribas, M. Costas, *Chem. Commun.* **2015**, *51*, 14285–14298.
[15] W. N. Oloo, L. Que, Jr., *Acc. Chem. Res.* **2015**, *48*, 2612–2621.
[16] C. V. Sastri, M. S. Seo, M. J. Park, K. M. Kim, W. Nam, *Chem. Commun.* **2005**, 1405–1407.
[17] K. K. Singh, M. k. Tiwari, B. B. Dhar, K. Vanka, S. Sen Gupta, *Inorg. Chem.* **2015**, *54*, 6112–6121.
[18] W. Ye, D. M. Ho, S. Friedle, T. D. Palluccio, E. V. Rybak-Akimova, *Inorg. Chem.* **2012**, *51*, 5006–5021.
[19] W. Ye, R. J. Staples, E. V. Rybak-Akimova, *J. Inorg. Biochem.* **2012**, *115*, 1–12.

 © 2016 Wiley-VCH Verlag GmbH & Co. KGaA, Weinheim

[20] J. Annaraj, S. Kim, M. S. Seo, Y.-M. Lee, Y. Kim, S.-J. Kim, Y. S. Choi, H. G. Jang, W. Nam, *Inorg. Chim. Acta* **2009**, *362*, 1031 – 1034.
[21] J. Park, Y.-M. Lee, K. Ohkubo, W. Nam, S. Fukuzumi, *Inorg. Chem.* **2015**, *54*, 5806 – 5812.
[22] A. N. Biswas, M. Puri, K. K. Meier, W. N. Oloo, G. T. Rohde, E. L. Bominaar, E. Münck, L. Que, Jr., *J. Am. Chem. Soc.* **2015**, *137*, 2428 – 2431.
[23] B. Wang, Y.-M. Lee, M. Clémancey, M. S. Seo, R. Sarangi, J.-M. Latour, W. Nam, *J. Am. Chem. Soc.* **2016**, *138*, 2426 – 2436.
[24] J. Bautz, P. Comba, C. Lopez de Laorden, M. Menzel, G. Rajaraman, *Angew. Chem. Int. Ed.* **2007**, *46*, 8067 – 8070; *Angew. Chem.* **2007**, *119*, 8213 – 8216.
[25] X. Zhang, H. Furutachi, T. Tojo, T. Tsugawa, S. Fujinami, T. Sakurai, M. Suzuki, *Chem. Lett.* **2011**, *40*, 515 – 517.
[26] O. V. Makhlynets, W. N. Oloo, Y. S. Moroz, I. G. Belaya, T. D. Palluccio, A. S. Filatov, P. Müller, M. A. Cranswick, L. Que, Jr., E. V. Rybak-Akimova, *Chem. Commun.* **2014**, *50*, 645 – 648.
[27] G. Guisado-Barrios, Y. Zhang, A. M. Harkins, D. T. Richens, *Inorg. Chem. Commun.* **2012**, *20*, 81 – 85.
[28] J. R. Khusnutdinova, J. Luo, N. P. Rath, L. M. Mirica, *Inorg. Chem.* **2013**, *52*, 3920 – 3932.
[29] T. W.-S. Chow, E. L.-M. Wong, Z. Guo, Y. Liu, J.-S. Huang, C.-M. Che, *J. Am. Chem. Soc.* **2010**, *132*, 13229 – 13239.
[30] L. Ji, A. Franke, M. Brindell, M. Oszajca, A. Zahl, R. van Eldik, *Chem. Eur. J.* **2014**, *20*, 14437 – 14450.
[31] N. Hessenauer-Ilicheva, A. Franke, D. Meyer, W.-D. Woggon, R. van Eldik, *J. Am. Chem. Soc.* **2007**, *129*, 12473 – 12479.
[32] A reviewer suggested that the acetic acid may be the reason for the high reaction rates observed for **2**. However, we note that the second-order rate constants are independent of the amount of peracid employed for its generation.

Received: February 8, 2016
Revised: March 21, 2016
Published online: April 13, 2016

 © 2016 Wiley-VCH Verlag GmbH & Co. KGaA, Weinheim

CHAPTER VII.

Evidence for acid-triggered heterolytic O-O cleavage in a nonheme Fe^{III}-OOH species

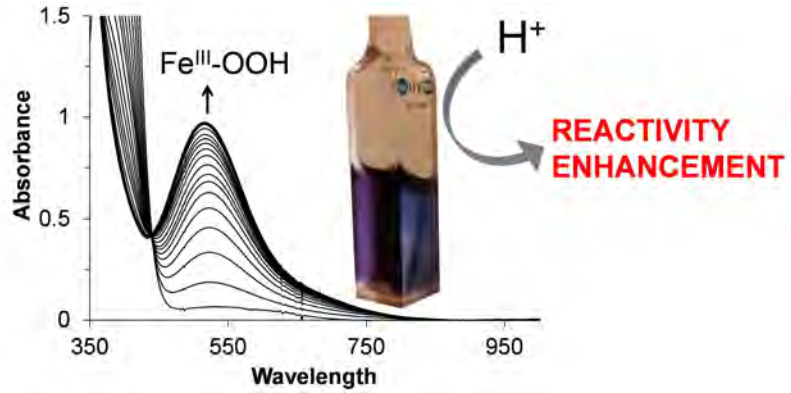

This chapter corresponds to the following publication:

Joan Serrano-Plana, Williamson N. Oloo, Vlad Martin-Diaconsescu, Lawrence Que, Jr., Anna Company, Miquel Costas

Manuscript in preparation

For this publication, J.S.-P. synthesized ligand $PyNMe_3$ and the iron(II) complex. He also performed the oxidation catalysis experiments. Besides, J.S.-P. contributed in writing the manuscript and was involved in argumentations and discussions.

Evidence for acid-triggered heterolytic O-O cleavage in a nonheme Fe^{III}-OOH species

Joan Serrano-Plana,[a] Williamson N. Oloo,[b] Vlad Martin-Diaconsescu,[a] Lawrence Que Jr.,*[,b] Anna Company, [a,]* Miquel Costas [a,]*

[a]Grup de Química Bioinspirada, Supramolecular i Catàlisi (QBIS-CAT), Institut de Química Computacional i Catàlisi (IQCC), Departament de Química, Universitat de Girona. Campus de Montilivi, E17071, Girona (Catalonia, Spain). E-mail: anna.company@udg.edu, miquel.costas@udg.edu

[b]Department of Chemistry and Center for Metals in Biocatalysis, University of Minnesota, Minneapolis, MN 55455 (United States). E-mail: larryque@umn.edu

Abstract

A novel iron(III)-hydroperoxo species $[Fe^{III}(OOH)(S)(PyNMe_3)]^{2+}$ S = MeCN or H_2O (**3**) has been generated by reaction of its ferrous precursor $[Fe^{II}(CF_3SO_3)_2(PyNMe_3)]$ with hydrogen peroxide at low temperatures. This species has been fully characterized by several spectroscopic techniques (EPR, rRaman, XAS, EXAFS) and cryospray mass spectrometry. Similarly to most of the previously described low-spin iron(III)-hydroperoxo compounds, **3** behaves as a sluggish oxidant and it is not kinetically competent for breaking the weak C-H bond of dihydroanthreacene or transferring the oxygen atom to sulfides. Instead, the putative iron(IV)-oxo species (**4**) formed along the self-decay of **3** is responsible for the observed oxygen-atom transfer to thioanisoles. The addition of stoichiometric amounts of triflic acid causes the rapid bleaching of the UV-vis features associated with **3**. Interestingly, the reactivity of **3** towards organic substrates upon triflic acid addition is radically different from that observed in its absence, showing enhanced reactivity towards unactivated C-H bonds with high stereospecificity and an increase in the electrophilic character in sulfide oxidation. Such effect has been previously observed for heme systems, where protonation of the hydroperoxo leads to the formation of the high-valent (Porf•)Fe^{IV}(O) (Compound I). Thus, the addition of acid to **3** presumably assists the heterolytic cleavage of the O-O bond to form a high valent iron(V)-oxo species that behaves as a strong oxidizing agent.

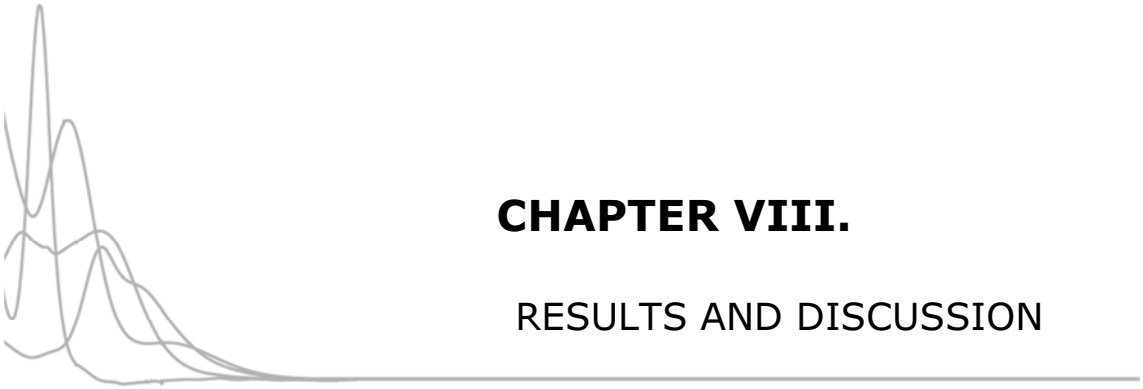

CHAPTER VIII.

RESULTS AND DISCUSSION

VIII. RESULTS AND DISCUSSION

(Note: For ligand nomenclature of this section, see Annex p.171)

The activation of O_2 has been a topic of interest over the last decades. An array of synthetic model systems has been developed in order to understand how natural systems use O_2 to perform highly effective and selective oxidations. At the same time these model systems have contributed to design biologically inspired methodologies for more sustainable oxidative reactions traditionally performed with toxic reagents. Due to the biological relevance of iron and copper, most efforts have been directed towards the investigation of coordination complexes based on these metals. This thesis focuses on the development of coordination compounds that could reproduce oxidation reactions performed by copper and nonheme iron oxygenases (Scheme VIII.1).

Chapter VIII.1 and VIII.2 depict our progress in developing copper-based complexes for oxygen activation. In the former, the synthesis of a novel unsymmetric ligand is discussed, together with the preparation of the corresponding dicopper(I) complex and also heterodimetallic compounds combining copper(I) and a second metal. The reactivity of these complexes towards O_2 at low temperature, in order to identify metastable O_2-bound species, is discussed. Chapter VIII.2 deals with the reactivity studies of a bis(μ-oxo)dicopper(III) species (**O**) that had been previously described in the group. While in the previous work from 2008 this species was proven to hydroxylate phenolates mimicking tyrosinase activity, in this thesis the reactivity was extended towards C-F cleavage and hydroxylation of fluorophenolates.

In Chapters VIII.3, and VIII.4 we will turn our attention towards nonheme iron models for oxygen activation. We present a novel iron(II) complex bearing a tetradentate ligand ($PyNMe_3$) that allows us to trap different iron-oxygen species after reaction with peracids and hydrogen peroxide. Such species are most likely generated in the catalytic cycle of nonheme iron catalysts employed in oxidation reactions, but they are normally very difficult to observe. Very remarkably, the use of this novel complex allowed us to generate different metastable species and explore their reactivity towards different organic substrates. Especially interesting is the reaction of the ferrous precursor with peracids, which led to the formation of a highly reactive compound that was kinetically competent for the stereospecific oxidation of alkanes with strong C-H bonds and alkenes (Chapter VIII.3), exhibiting unprecedented reaction rates. The spectroscopic characterization of this compound pointed towards an acylperoxoiron(III) compound that undergoes O-O bond cleavage leading to the formation of a high valent species that is the real executor of the oxidative transformation. This high valent species has been proposed along the mechanistic cycle of nonheme iron catalysis, and for the first time we were able to trap it and kinetically interrogate its behavior towards substrates. Lastly, the reaction of the ferrous compound with hydrogen peroxide formed a low spin peroxoiron(III) species which

was a seemingly sluggish oxidant. Very interestingly, the addition of acid triggered the O-O cleavage and generated a highly active and selective reagent (Chapter VIII.4).

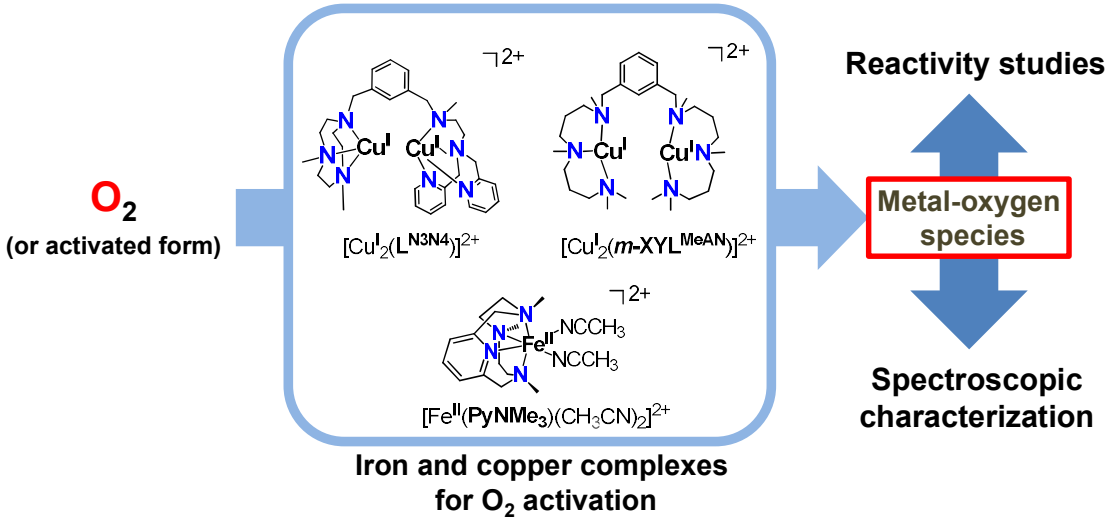

Scheme VIII.1. O_2 activation by the bioinspired copper- and iron-based models studied in this thesis.

VIII.1 Building complexity in O_2-binding copper complexes. Site-selective metalation and intermolecular O_2-binding at dicopper and heterometallic complexes derived from an unsymmetric ligand

This section corresponds to the contents of the manuscript by Serrano-Plana *et al. Inorg. Chem.*, **2014**, *53*, 12929-12938, which can be found in **Chapter III** of this thesis.

VIII.1.1 Ligand design and synthesis

We designed a novel ligand L^{N3N4} (**1**) that contains two distinct coordination sites connected through a *meta*-xylyl moiety (Scheme VIII.2a). This linker has been previously used in copper-dioxygen model chemistry, as it places the two binding sites at an ideal distance so that intramolecular interactions between the two metals located in each site are likely to occur upon reaction with O_2.[1,2] For comparison, the use of *para*-substituted xylyl linkers significantly increases the distance between the two substituents, which prevents the interaction between the metallic centers. In order to imitate the nitrogen-rich environment of the metal centers in the active site of O_2-activating copper enzymes, both sites in **1** are nitrogen-based. The first site consists of a triazacyclononane (tacn) ring (tridentate, N_3), which is chemically robust and forms highly stable complexes with a number of metals. In this moiety three aliphatic amines facially bind the metal leaving free coordination sites to interact with external molecules. The second site offers a tetradentate environment (N_4) provided by two tertiary aliphatic nitrogen atoms and two pyridines (uns-penp). Thus, the coordination properties of the two sites are markedly different.

Indeed, both donor sets had been independently previously used in the literature to support Cu^I/O_2 chemistry (Scheme VIII.2b).[3] Tolman et al. showed that reaction of cuprous N-alkylated tacn complexes [Cu^I(**3**^{R})] formed μ–η^2:η^2–peroxodicopper(II) (**^{S}P**) or bis(μ-oxo)dicopper(III) (**O**) species upon reaction with oxygen.[4,5] The outcome depended on the steric hindrance of the alkyl groups, affording **O** when less bulky substituents such as methyl or benzyl were used. Specifically, the Me_3tacn-based complex [Cu^I(**3**)]$^+$ reacted with O_2 forming **O** species (Scheme VIII.2b left) with spectroscopic features at λ_{max} = 307 nm (16000 M^{-1} cm^{-1}) and 412 nm (λ = 18000 M^{-1} cm^{-1}).[6] On the other hand, the copper(I) complex of the monomeric ligand uns-penp [Cu^I(**4**)]$^+$ reacted with O_2 to form *trans*-μ-1,2-peroxodicopper(II) (**^{T}P**) species (Scheme VIII.2b right) which showed a chromophore at 535 nm (ε = 7000 M^{-1} cm^{-1}),[7] analogously to other N-based tetradentate systems.[3,7,8] With the notable structural differences between the two binding sites, and the different O_2 reactivity described for the two monomeric copper complexes introduced above, we aimed at the study of the Cu^I/O_2 chemistry of [Cu^I_2(**1**)]$^{2+}$. Moreover, we envisioned that the unsymmetry of **1** would allow us to prepare a set of homo- and heterobimetallic complexes combining copper(I) and a complementary metal.

The synthetic strategy to prepare **1** (Scheme VIII.2a) consisted of a total of four reaction steps starting from Me_2tacn·3HBr (prepared from tritosyl 1,4,7-triazacyclononane) and 3-(bromomethyl)benzaldehyde (prepared from the commercially available 3-(bromomethyl)benzonitrile). Stoichiometric reaction of these two compounds through a nucleophilic substitution mechanism gave compound **a** (Scheme VIII.2a), in which the tridentate site (tacn) is already present. The N_4 coordination site was introduced later by reaction of the aldehyde unit in **a** with the primary amine of uns-penp giving **b**. The hydrogenation of the imine and posterior methylation afforded **1**, which needed to be purified by column chromatography. Even though the synthesis consisted of many reaction steps, moderated to good yields were obtained along the synthetic route. The symmetric ligand bearing two N_4 sites L^{N4N4} (**2**) was also prepared following a similar synthetic route starting from uns-penp and isophthalaldehyde (see annex).

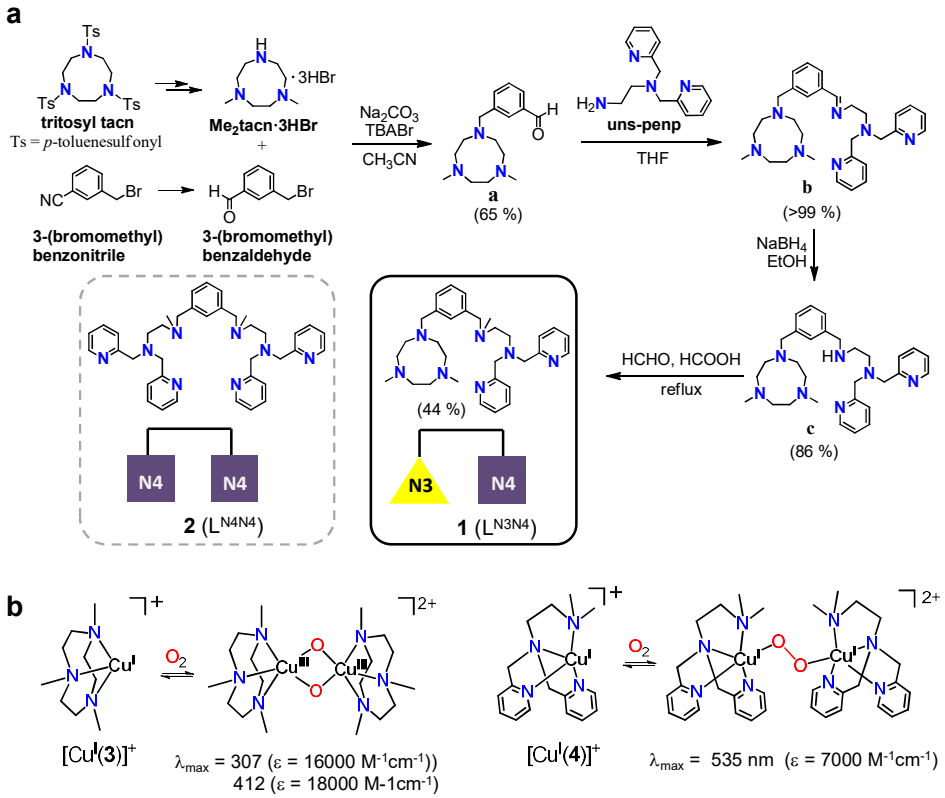

Scheme VIII.2. a) Synthetic route for the preparation of **1** and schematic representation of **2**. **b)** Schematic representation of **3** and **4**, previously used for copper-dioxygen chemistry.

VIII.1.2. Synthesis of homodimetallic complexes

The selective binding of metal ions in only one of the two binding sites in a dinucleating system is a challenging goal, since often mixtures between both sites are obtained. In order to explore whether **1** was an adequate platform to support heterometallic systems we monitored by ^{1}H-NMR the formation of homodimetallic zinc(II) by four sequential additions of 0.5 equiv of $Zn(OTf)_2$ (Figure VIII.1). The aromatic region of the ^{1}H-NMR spectrum of free **1** in acetone-d_6

showed readily identifiable signals that belong to the two equivalent pyridines in the N_4 site (α, β and γ protons). After the first addition of Zn^{II} (0.5 equiv), no substantial changes were observed in the aromatic region, thus suggesting that the N_4 site remained free. Instead, after the addition of the first Zn^{II} equivalent severe broadening was observed, indicating that most likely some exchange was occurring between both binding sites. However, remarkably, when more than one equivalent of Zn^{II} was added new well-defined sharp features clearly arose in the aromatic region (8.85, 8.74 and 8.18 ppm), and the original signals completely disappeared. The homodimetallic complex $[Zn^{II}_2(\mathbf{1})]^{4+}$ was obtained and further characterized by HR-MS after addition of a total 2 equiv of Zn^{II}. Similar sharp signals were also observed in the ^{1}H-NMR spectrum of the homodimetallic Zn^{II} complex $[Zn^{II}_2(\mathbf{2})]^{4+}$ bearing the symmetric ligand with two N_4 sites. Overall, this titration experiment suggested that zinc preferentially binds in the N_3 binding site, and it leaves the other binding unit available to coordinate a second metal ion. Because of the different nature of sites N_3 and N_4, we envisioned that **1** would be a good candidate for the preparation of heterometallic complexes.

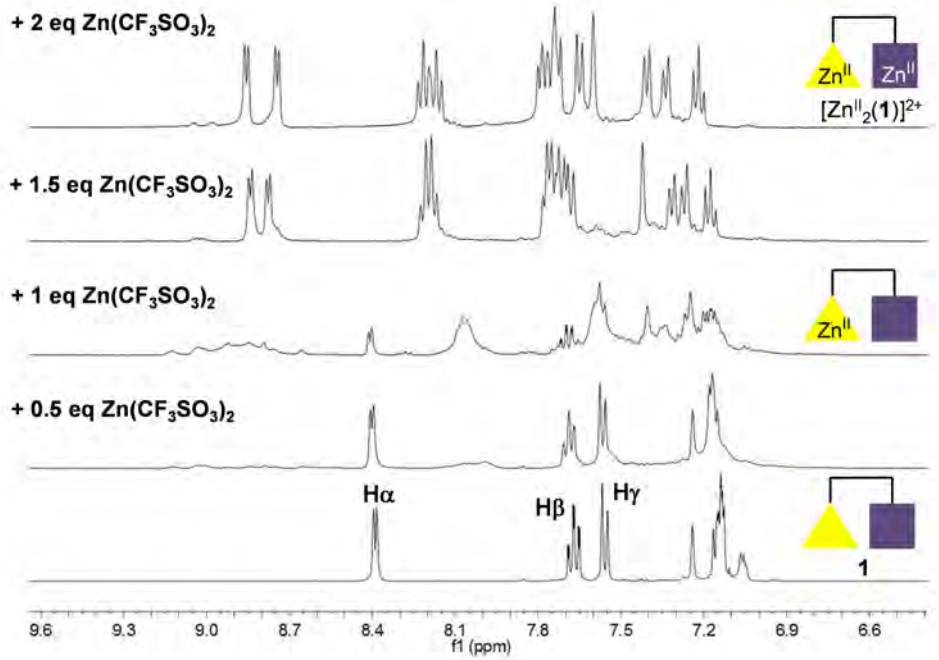

Figure VIII.1. ^{1}H-NMR titration of **1** with $Zn^{II}(CF_3SO_3)_2$ in acetone-d_6 at 243 K.

The homodimetallic copper(I) complex $[Cu^{I}_2(\mathbf{1})]^{2+}$ was prepared in the glovebox by adding two equivalents of $[Cu^{I}(CH_3CN)_4](OTf)$ to **1** in acetonitrile. This complex could not be isolated due to its tendency to disproportionate and it could only be synthesized in acetonitrile, since the formation of a green solution (Cu^{II}) and copper mirror (Cu^0) was observed for any other solvent, indicating that copper(I) disproportionation was occurring. Thus, characterization of $[Cu^{I}_2(\mathbf{1})]^{2+}$ was performed exclusively in solution in acetonitrile-containing mixtures by ^{1}H-NMR (broad peaks were observed even at 240 K) and HR-MS. As $[Cu^{I}_2(\mathbf{1})]^{2+}$ could not be isolated, we

studied its reaction with O_2 using freshly prepared concentrated solutions in acetonitrile and diluting a sample in dry acetone under anaerobic conditions (final solvent mixture: acetonitrile/acetone 1:19). When the sample was exposed to O_2 at -90ºC the formation of two chromophores in the UV-vis was observed within 1 min (Figure VIII.2a). On one hand, a band at λ_{max} = 530 nm (ε = 2000 M^{-1} cm^{-1}) was formed in ~45 s and then started decaying. At the same time, a band at 405 nm (ε = 15000 M^{-1} cm^{-1}) formed and remained stable at least 15 min at -90ºC but disappeared upon warming up the sample. None of the two species was detected when the reaction was monitored at room temperature.

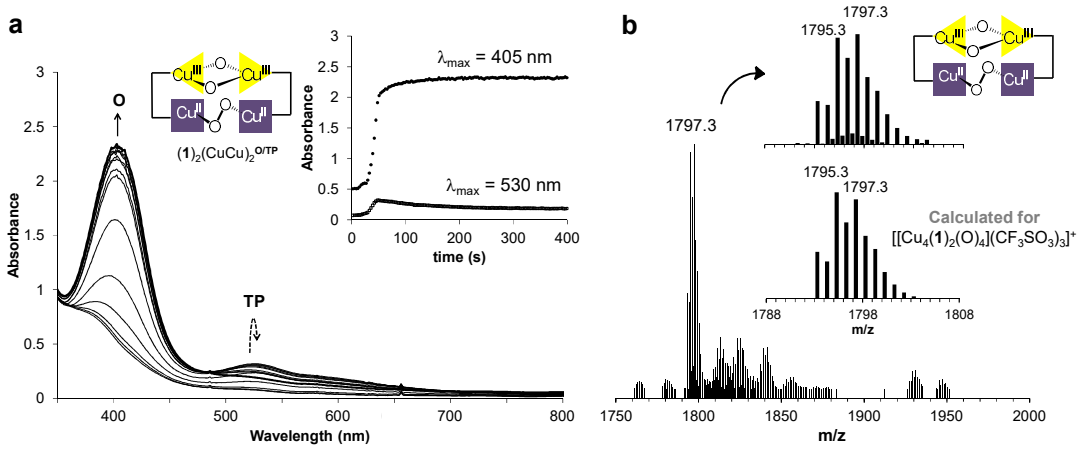

Figure VIII.2. a) Spectral changes observed upon reaction of $[Cu^{I}_2(\mathbf{1})]^{2+}$ (0.3 mM) and O_2 at -90ºC in acetonitrile/acetone 1:19. Inset: time traces at 405 and 530 nm. **b)** CSI-MS spectrum for $(\mathbf{1})(CuCu)_2^{O/TP}$ generated at -90ºC.

The fact that the two bands follow different time courses indicated that they belong to different species. Interestingly, the cuprous complex bearing a symmetric ligand with two N_4 sites, $[Cu^{I}_2(\mathbf{2})]^{2+}$, exclusively formed $^{T}\mathbf{P}$ species (λ_{max} = 530 nm, ε = 4400 M^{-1} cm^{-1}) when exposed to O_2 at low temperature. Moreover, as detailed in VIII.1.1, the monomeric complexes $[Cu^{I}(\mathbf{3})]$ and $[Cu^{I}(\mathbf{4})]$ formed **O** and $^{T}\mathbf{P}$ species respectively upon reaction with O_2 (Scheme VIII.2). All these observations taken together suggested that in the case of $[Cu^{I}_2(\mathbf{1})]^{2+}$ the Cu^{I} centers located in the N_4 site of **1** were responsible for the formation of $^{T}\mathbf{P}$ species and the Cu^{I} centers placed in the N_3 site gave rise to the **O** species. Thus, we speculated that formation of intramolecular species was not taking place but instead reaction between two different $[Cu^{I}_2(\mathbf{1})]^{2+}$ complex molecules was occurring. In that case, a dimeric species $[(\mathbf{1})Cu^{II}Cu^{III}(\mu\text{-}O)_2(\mu\text{-}1,2\text{-}O_2)Cu^{III}Cu^{II}(\mathbf{1})]^{4+}$ ($(\mathbf{1})_2(CuCu)_2^{O/TP}$) or a polymeric compound would be formed after reaction with O_2. Indeed, cryospray ionization mass spectrometry (CSI-MS) experiments performed at -90ºC further supported this idea. A major peak at m/z = 1795.3 with an isotopic pattern consistent with $[(\mathbf{1})_2(CuCu)_2^{O/TP}(CF_3SO_3)_3]^{+}$ was clearly observed (Figure VIII.2b), indicating that polymeric structures were unlikely in this system.

VIII.1.3 Synthesis of heterodimetallic complexes

Initial experiments for the preparation of heterodimetallic complexes were performed using Cu^{I} and Zn^{II}, as both metals allow diamagnetic ^{1}H-NMR characterization. Thus, 1 equiv of $[Cu^{I}(CH_3CN)_4](CF_3SO_3)$ and 1 equiv of $Zn^{II}(CF_3SO_3)_2$ were sequentially added to a solution of **1** in acetonitrile. No matter the order of addition of the two metals, in any case the same final complex was obtained ($[Cu^{I}Zn^{II}(\mathbf{1})]^{3+}$). Sharp signals were observed in the aromatic region, very similar to the ones obtained for $[Zn^{II}_2(\mathbf{1})]^{2+}$, indicating that Zn^{II} is coordinating to the N_4 site (Figure VIII.3). If instead copper(I) had been located in this site, broad NMR signals such as those in $[Cu^{I}_2(\mathbf{1})]^{2+}$ would have been observed (Figure VIII.3). Indeed, while broad signals were observed in the ^{1}H-NMR spectra of $[Cu^{I}_2(\mathbf{2})]^{2+}$, for $[Zn^{II}_2(\mathbf{2})]^{4+}$ only sharp signals were observed (Figure VIII.3). Compound $[Cu^{I}Zn^{II}(\mathbf{1})]^{3+}$ was further characterized by HR-MS, which showed two main peaks at m/z = 828.1501 and m/z = 942.1346, fully consistent with the pure heterodimetallic species $\{[Cu^{I}Zn^{II}(\mathbf{1})](CF_3SO_3)(Cl)\}^{+}$ and $\{[Cu^{I}Zn^{II}(\mathbf{1})](CF_3SO_3)_2\}^{+}$. Very remarkably, no peaks of the possible homodimetallic complexes $[Cu^{I}Cu^{I}(\mathbf{1})]^{2+}$ or $[Zn^{II}Zn^{II}(\mathbf{1})]^{4+}$ were detected.

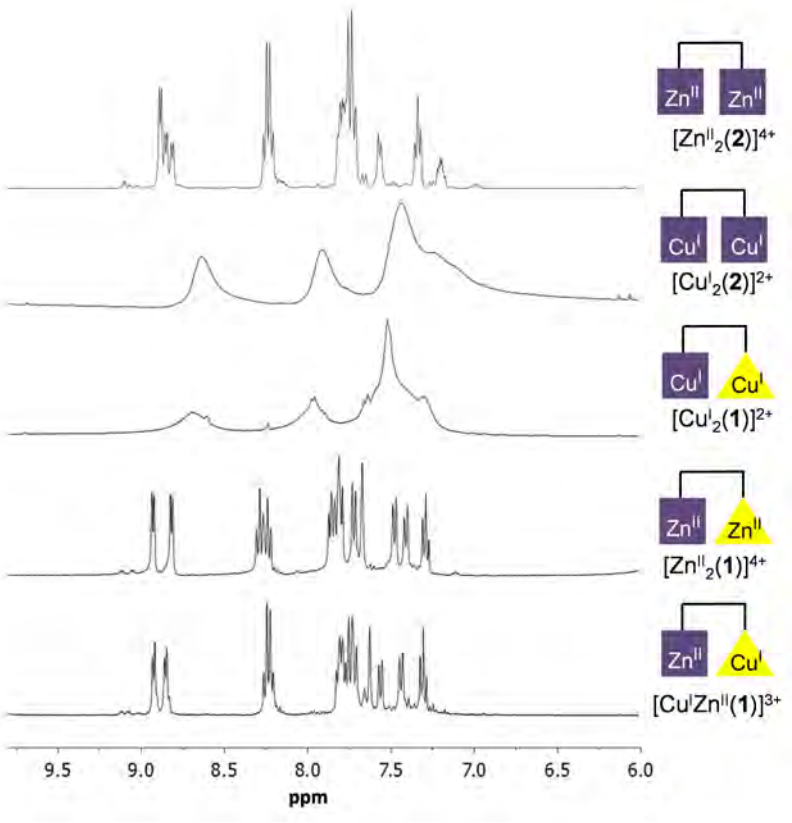

Figure VIII.3. Aromatic region of the ^{1}H-NMR spectra of $[Zn^{II}Cu^{I}(\mathbf{1})]^{3+}$, $[Zn^{II}_2(\mathbf{1})]^{4+}$, $[Cu^{I}(\mathbf{1})]^{2+}$, $[Cu^{I}_2(\mathbf{2})]^{4+}$ and $[Zn^{II}_2(\mathbf{2})]^{4+}$ in CD_3CN/acetone-d_6 1:5 at 240 K.

The reactivity of $[Cu^{I}Zn^{II}(\mathbf{1})]^{3+}$ with O_2 was also used to obtain further experimental evidence about its heterometallic character. UV-Vis monitoring of the reaction of $[Cu^{I}Zn^{II}(\mathbf{1})]^{3+}$ with O_2 at -90ºC in acetonitrile/acetone 1:19 afforded in ~900 s the formation of only the **O** species

[(**1**)$Zn^{II}Cu^{III}(\mu\text{-}O)_2Cu^{III}Zn^{II}$(**1**)] ((**1**)$_2$(CuZn)$_2^{O}$, Scheme VIII.3a) with λ_{max} = 405 nm (ε = 11900 $M^{-1}cm^{-1}$). No formation of ^{T}**P** was observed, indicating that no copper was bound in the N_4 site. Again, independently of the order of addition of the two metallic salts, only the formation of **O** species was observed upon reaction with O_2 at low temperatures. (**1**)$_2$(CuZn)$_2^{O}$ was also further characterized by CSI-MS experiments performed at -90ºC (Scheme VIII.3b). Major peaks at m/z = 2065.2049, 1951.2226, 1839.2400 showed mass values and isotopic patterns fully consistent with {[(**1**)$_2$(CuZn)$_2^{O}$](CF$_3$SO$_3$)$_5$}$^+$, {[(**1**)$_2$(CuZn)$_2^{O}$](CF$_3$SO$_3$)$_4$Cl}$^+$, and {[(**1**)$_2$(CuZn)$_2^{O}$](CF$_3$SO$_3$)$_3$Cl$_2$}$^+$ (Scheme VIII.3b). Again no peaks that would correspond to homobimetallic species were observed, thus corroborating that **1** is a privileged platform to selectively locate two different metals in distinct binding sites.

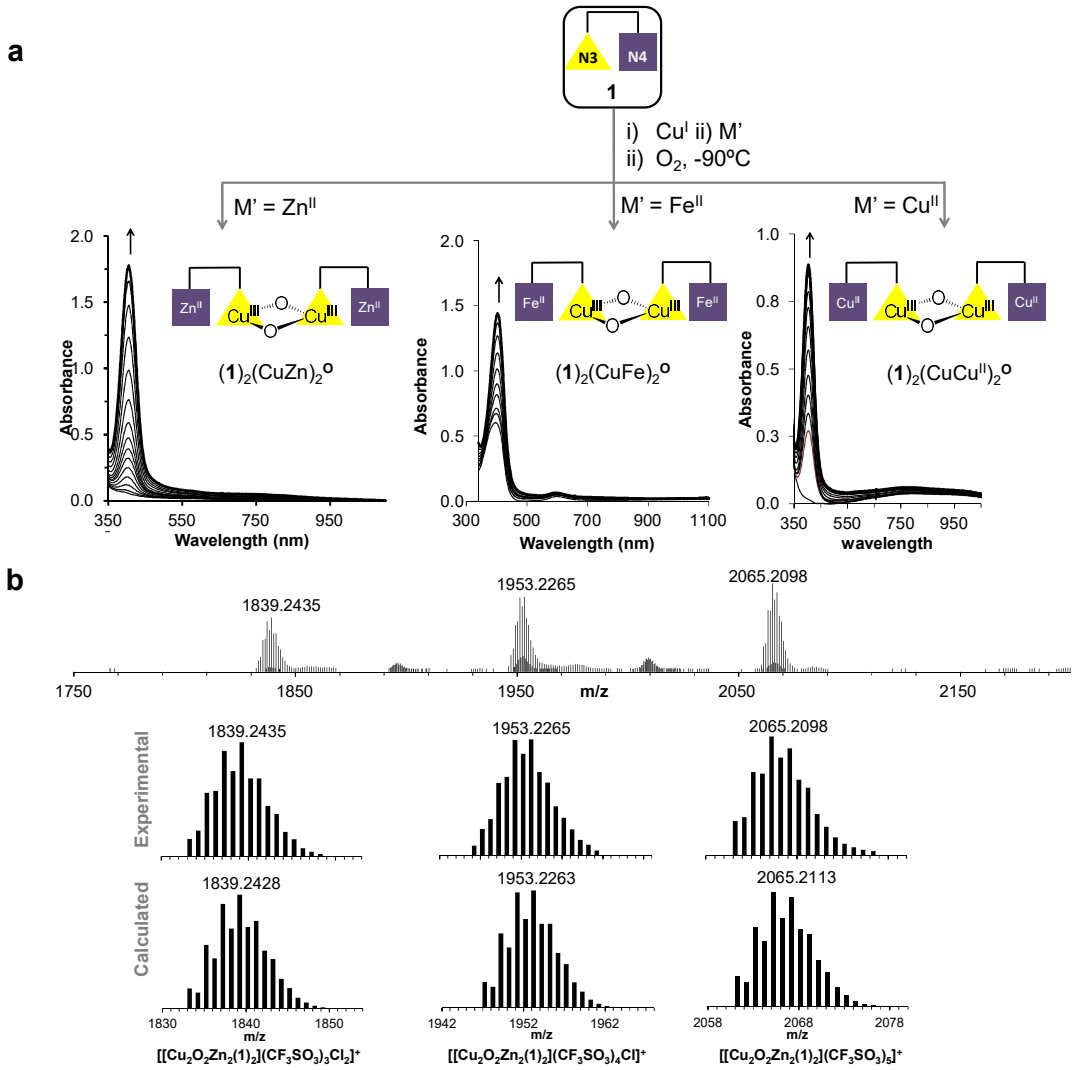

Scheme VIII.3. a) Synthesis and reactivity of [Cu^{I}M'(**1**)]$^{3+}$ (M' = Zn^{II}, Fe^{II}, Cu^{II}; complex concentration 0.3 mM, 0.2 mM and 0.15 mM respectively) towards O_2 at -90ºC in acetonitrile/acetone 1:19. **b)** CSI-MS characterization of (**1**)$_2$(CuZn)$_2^{O}$ at -90ºC.

Other heterometallic complexes were also prepared using Cu^{I} and Fe^{II} ([Cu^{I}Fe^{II}(**1**)]$^{3+}$), Cu^{II} ([Cu^{I}Cu^{II}(**1**)]$^{3+}$) or Ga^{III} ([Cu^{I}Ga^{III}(**1**)]$^{4+}$) as complementary metals. As a general strategy, 1 equiv

of Cu^{I} was added to a solution of **1** in acetonitrile, and then 1 equiv of the complementary salt ($[Fe^{II}(CF_3SO_3)_2(CH_3CN)_2$, $Cu^{II}(CF_3SO_3)_2$ or $GaCl_3$ respectively) was added.

$[Cu^{I}Fe^{II}(\mathbf{1})]^{3+}$ and $[Cu^{I}Cu^{II}(\mathbf{1})]^{3+}$ were characterized by HR-MS, as attempts to analyze them by ^{1}H-NMR were unsuccessful, because only non-informative broad bands were obtained, most likely caused by the paramagnetism of the Fe^{II} and Cu^{II} centers. Interestingly, both compounds reacted with O_2 in acetonitrile/acetone 1:19 at -90ºC to form exclusively the **O** species (Scheme VIII.3a) $(\mathbf{1})_2(CuFe)^{\mathbf{O}}$ (λ_{max} = 405 nm, ε = 12000 M^{-1} cm^{-1}), and $(\mathbf{1})_2(CuCu^{II})^{\mathbf{O}}$ (λ_{max} = 405 nm, ε = 12300 M^{-1} cm^{-1}). Again these compounds are most likely generated from the intermolecular interaction between copper(I) centers bound to the N_3 site of two different complex molecules. It is important to note that $^{\mathbf{T}}\mathbf{P}$ species was not formed in any of the two cases. Unfortunately, no heterometallic intramolecular oxygen activation occurred in the reaction of $[Cu^{I}Fe^{II}(\mathbf{1})]^{3+}$ with O_2, for which the redox active iron(II) center was expected to be involved in an O_2 activating process together with Cu^{I}.

Overall these experiments show that divalent metals Zn^{II}, Fe^{II} and Cu^{II} coordinate to the N_4 site in L^{N3N4} leaving the Cu^{I} in the N_3 site, so that it reacts with O_2 forming **O** species. Interestingly, the formation of the **O** species after reaction of the three heterodimetallic complexes $[Cu^{I}M'(\mathbf{1})]^{3+}$ (M' = Zn^{II}, Fe^{II}, Cu^{II}) and O_2 was achieved after ~ 10 min at -75ºC (Figure VIII.4a). In sharp contrast, the **O** species generated after reaction of the homodimetallic complex $[Cu^{I}Cu^{I}(\mathbf{1})]^{2+}$ with O_2 was complete in less than one minute under the same reaction conditions. Thus, the nature of the secondary metal has a great influence on the reaction rate.

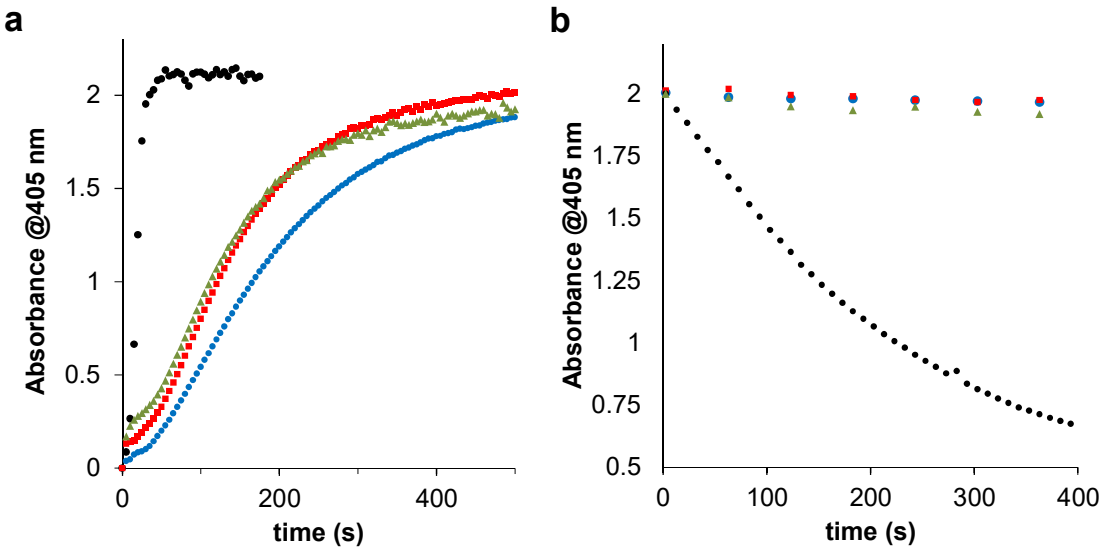

Figure VIII.4. a) Time traces for the formation of the **O** species (λ_{max} = 405 nm) after reaction of O_2 and $[Cu^{I}_2(\mathbf{1})]^{2+}$ (black dots), $[Cu^{I}Zn^{II}(\mathbf{1})]^{3+}$ (blue dots), $[Cu^{I}Cu^{II}(\mathbf{1})]^{3+}$ (red squares) or $[Cu^{I}Fe^{II}(\mathbf{1})]^{3+}$ (green triangles) in a solvent mixture acetonitrile/acetone 1:19 at -75ºC. **b)** Decay of the previous **O** species at -60ºC. While only 15% decomposition after 2 h at this temperature was observed for the heterodimetallic compounds, the **O** species in $(\mathbf{1})_2(CuCu)_2^{\mathbf{O/TP}}$ was fully decayed after 20 min.

Moreover, the decay of the **O** species in $(\mathbf{1})_2(CuCu)_2^{O/TP}$ at -60ºC was much faster than in $(\mathbf{1})_2(CuZn)_2^{O}$, $(\mathbf{1})_2(CuFe)_2^{O}$ and $(\mathbf{1})_2(CuCu^{II})_2^{O}$ (Figure VIII.4b). This is probably due to the fact that the prior formation and decay of the $^{T}\mathbf{P}$ species of the same dimeric unit in $(\mathbf{1})_2(CuCu)_2^{O/TP}$ caused some strain which destabilized the **O** species. Analysis of decayed samples of the **O** species $(\mathbf{1})_2(CuCu)_2^{O/TP}$, $(\mathbf{1})_2(CuZn)_2^{O}$, $(\mathbf{1})_2(CuFe)_2^{O}$ and $(\mathbf{1})_2(CuCu^{II})_2^{O}$ by ESI-MS showed the formation of metal-hydroxide species, without ligand oxidation being detected.

To our delight, the use of the trivalent Ga^{III} as complementary metal source changed the position of the copper(I) center. Compound $[Cu^{I}Ga^{III}(\mathbf{1})]^{4+}$ was prepared in an analogous way to the previously heterodimetallic complexes and analyzed by HR-MS, showing peaks with an isotopic pattern fully consistent with the formation of the heterodimetallic complex at m/z 754.1316 and 878.1114 that were assigned to $\{[Cu^{I}Ga^{III}(\mathbf{1})](Cl)_3\}^{+}$ and $\{[Cu^{I}Ga^{III}(\mathbf{1})](CF_3SO_3)(Cl)_2\}^{+}$. Very interestingly, reaction of $[Cu^{I}Ga^{III}(\mathbf{1})]^{4+}$ with O_2 at -90ºC afforded the exclusive formation of a band at λ_{max} = 530 nm ($\varepsilon \sim 4000\ M^{-1}\ cm^{-1}$) corresponding to $^{T}\mathbf{P}$ species $(\mathbf{1})_2(CuGa)_2^{TP}$ and UV-vis features associated to **O** species were not observed (Figure VIII.5). This indicated that the copper(I) center in $[Cu^{I}Ga^{III}(\mathbf{1})]^{4+}$ was located in the N_4 site, while Ga^{III} was tightly bound to the tacn ring in N_3. The preparation of other heterodimetallic complexes using trivalent metals such as Fe^{III} proved unsuccessful due to the oxidation of the copper(I) to copper(II), thus hampering further reactivity with O_2.

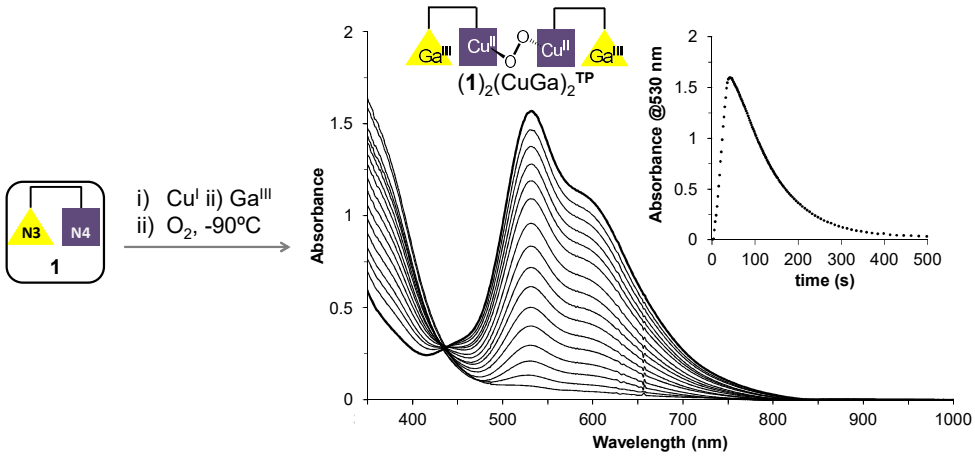

Figure VIII.5. Synthesis and reactivity of $[CuGa(\mathbf{1})]^{4+}$ towards oxygen at -90ºC.

Table VIII.1. Summary of the spectroscopic features of the **O** and ^{T}**P** species formed upon reaction of $[MCu^{I}(\mathbf{1})]^{n+}$ (M = Cu^{I}, Cu^{II}, Zn^{II}, Fe^{II}, Ga^{III}; n= 2, 3, 4) or $[Cu^{I}_{2}(\mathbf{2})]^{2+}$ with O_2 at -90ºC in acetonitrile/acetone 1:19.

Ligand	compound	N_4 site	N_3 site	UV-Vis features λ_{max}, nm (ε, $M^{-1}cm^{-1}$)[a]	Cu_2O_2 species
1 ($\mathbf{L^{N3N4}}$)	$[Cu^{I}Cu^{I}(\mathbf{1})]^{2+}$	Cu^{I}	Cu^{I}	405 (15000), 530 (2000)	**O** + ^{T}**P**
	$[Cu^{I}Zn^{II}(\mathbf{1})]^{3+}$	Zn^{II}	Cu^{I}	405 (11900)	**O**
	$[Cu^{I}Cu^{II}(\mathbf{1})]^{3+}$	Cu^{II}	Cu^{I}	405 (12000)	**O**
	$[Cu^{I}Fe^{II}(\mathbf{1})]^{3+}$	Fe^{II}	Cu^{I}	405 (12300)	**O**
	$[Cu^{I}Ga^{III}(\mathbf{1})]^{4+}$	Cu^{I}	Ga^{III}	530 (4050)	^{T}**P**
2 ($\mathbf{L^{N4N4}}$)	$[Cu^{I}Cu^{I}(\mathbf{2})]^{2+}$	Cu^{I}	Cu^{I}	530 (4400), 600 (sh)	^{T}**P**

[a] ε values were calculated taking into account the expected maximum concentration of Cu_2O_2 unit.

In summary, ligand **1** served as an excellent platform for the synthesis of heterometallic complexes. We successfully prepared heterometallic copper-based complexes that were able to reductively activate O_2, giving raise to the formation of different Cu_2O_2 species. Very interestingly, the reactivity of the heterometallic systems was defined by the complementary metal used during the complex synthesis.

VIII.2 Selective *ortho*-hydroxylation-defluorionation of 2-fluorophenolates with a bis(μ-oxo)dicopper(III) species

This section corresponds to the contents of the manuscript by Serrano-Plana *et al. Angew. Chem. Int. Ed.* **2014**, *53*, 9608-9612, which can be found in **Chapter IV** of this thesis.

Our group described in 2008 the formation and characterization of a bis(μ-oxo)dicopper(III) species $(\mathbf{5})(CuCu)^{O}$ after the reaction between a dicopper(I) complex $[Cu^{I}_{2}(\mathbf{5})]^{2+}$ and O_2 at low temperatures (-90ºC) in non-coordinating solvents such as acetone or THF.[9] Upon addition of selected phenolates, this species performed *ortho*-hydroxylation to give the corresponding catechols. With this precedent in mind, we aimed at further developing the reactivity of $(\mathbf{5})(CuCu)^{O}$ with phenolates that contained fluorine substituents in the *ortho* position. Since the carbon-fluorine bond represents the strongest single bond to carbon,[10] the species needed to break it must be highly reactive.

Reaction of $[Cu^{I}_{2}(\mathbf{5})]^{2+}$ with O_2 in acetone at -90ºC was monitored by UV-vis absorption spectroscopy. Formation of the previously described chromophore at λ_{max} = 413 nm (ε = 21000 $M^{-1}cm^{-1}$) corresponding to the **O** species $(\mathbf{5})(CuCu)^{O}$ was observed,[9] which remained relatively stable at this temperature. The addition of 3 equiv of sodium 2,6-difluorophenolate (Na(DFP)) to the pre-formed $(\mathbf{5})(CuCu)^{O}$ caused drastic color changes in the reaction mixture. The yellow

color of the **O** species (Figure VIII.6a) immediately disappeared changing to deep purple (Figure VIII.6b). Consequently, by monitoring the UV-vis spectral changes for this reaction, instant bleaching of the λ_{max} = 413 nm chromophore and formation of new features at λ_{max} = 520 and λ_{max} ~ 400 nm was observed upon addition of Na(DFP) (see figure VIII.6). rRaman studies performed in a previous work on a sample obtained after the addition of *p*-chlorophenolate to (**5**)(CuCu)^{O} concluded that such violet species corresponded to phenolate-coordinated **O** species.[9]

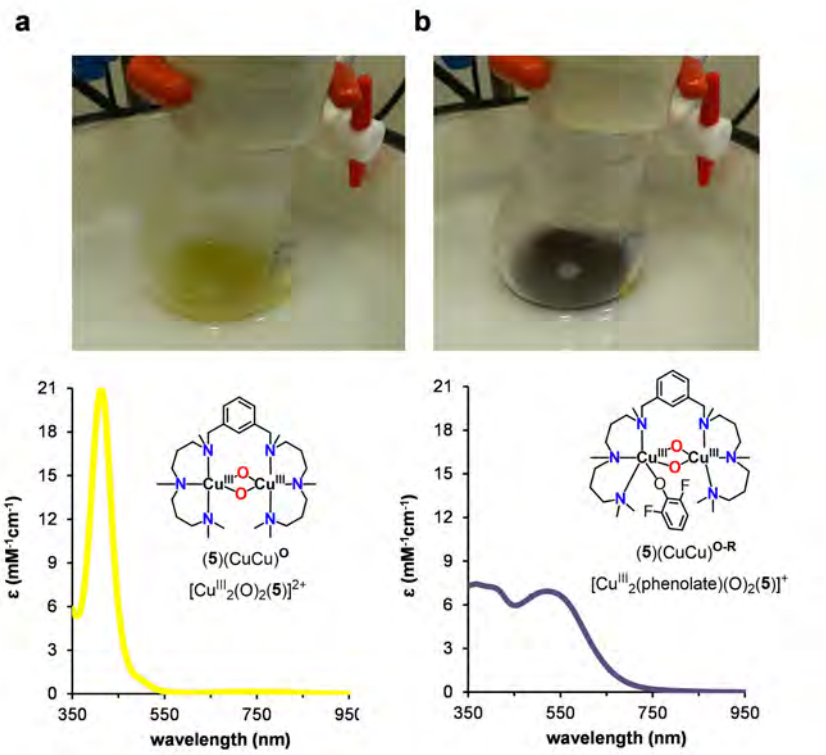

Figure VIII.6. Visual color changes observed during the reaction of $[Cu^{I}_{2}(\mathbf{5})]^{2+}$ with O_2 and sodium phenolates in acetone at -90ºC along with the UV-vis spectra recorded at -90ºC and the schematic representation of the compounds. **a)** Fully formed bis(μ-oxo)dicopper(III) species (**5**)(CuCu)^{O}. **b)** Sudden color change to intense purple upon addition of sodium phenolates to (**5**)(CuCu)^{O} to form (**5**)(CuCu)$^{O\text{-}R}$.

Cryospray mass spectrometry (CSI-MS) experiments at -90ºC were performed to gain further insight into the nature of this purple species. The CSI-MS spectrum right after the addition of Na(DFP) to (**5**)(CuCu)^{O} consisted mainly of two intense peaks at m/z = 783.2571 and m/z = 763.3194 (Figure VIII.7a). These mass values together with the isotopic pattern of the two peaks were fully consistent with their formulation as $\{[Cu^{III}_{2}(\mu\text{-}O)_2(\mathbf{5})](OTf)\}^{+}$ and $\{[Cu^{III}_{2}(\mu\text{-}O)_2(C_6H_3F_2O)(\mathbf{5})]\}^{+}$. Collision-induced dissociation experiments conducted on the m/z = 763.3 peak produced a new peak at m/z = 634.3 corresponding to the loss of a phenolate ligand (m/z = 129.0). Overall, this was in agreement with the formulation of the purple species as the phenolate bound to the **O** core, namely (**5**)(CuCu)$^{O\text{-}A}$ (Figure VIII.7b).

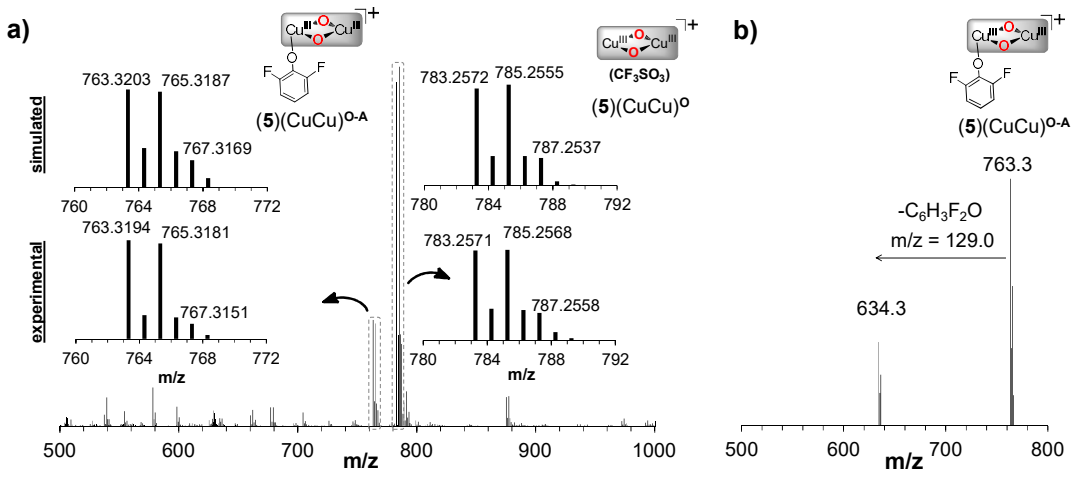

Figure VIII.7. a) Cryospray mass spectrometry (CSI-MS) experiments performed at -90ºC corresponding to the reaction of (**5**)(CuCu)^{O} with 3 equiv Na(DFP) in acetone. b) Collision-induced dissociation experiment conducted at -90ºC on the m/z = 763.3 species resulting on a loss of a phenolate ligand (m/z = 129.0).

To our surprise, analysis of the reaction mixture after acidic work up once (**5**)(CuCu)$^{O\text{-}A}$ had vanished ($t_{1/2}$ ~ 40 s at -90ºC) indicated the production of 3-fluorocatechol in 21 % yield (with respect to (**5**)(CuCu)^{O}). The addition of higher amounts of substrate or lowering the initial concentration of $[Cu^{I}_{2}(\mathbf{5})]^{2+}$ did not affect the reaction yield. Very importantly, labeling experiments performed by generating (**5**)(CuCu)^{O} with $^{18}O_2$ afforded 3-fluorocatechol with 86% ^{18}O label, thus confirming that indeed the Cu_2O_2 core is responsible for the *ortho*-hydroxylation-defluorination reaction (Scheme VIII.4).

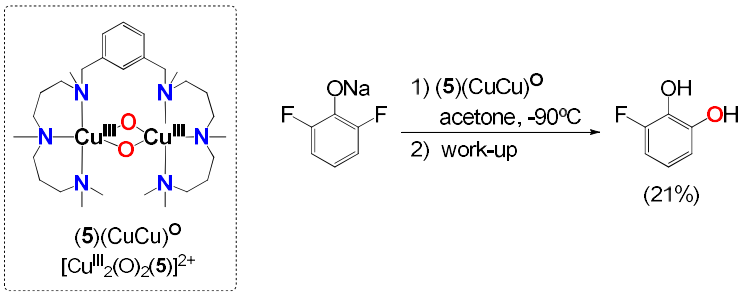

Scheme VIII.4. *Ortho*-hydroxylation-defluorination reaction of sodium 2,6-difluorophenolate to give 3-fluorocatechol along with the schematic representation of (**5**)(CuCu)^{O}.

Interestingly, the reaction was found to be regioselective for the *ortho* position of the phenolate: only the production of 4-fluorocatechol was observed upon addition of sodium 4-fluorophenolate to (**5**)(CuCu)^{O} (Scheme VIII.5a). At this point, the reaction towards unsymmetric phenolates bearing a fluorine atom and a different substituent in the two *ortho* positions was also studied. In all cases, the addition of the corresponding sodium phenolate caused the immediate decay of the (**5**)(CuCu)^{O} features giving raise to the formation of new chromophores in the range of 357-414 nm and 516-639 nm (depending on the nature of the phenolate, Figure VIII.8) indicative of the formation of the phenolate-bound species (**5**)(CuCu)$^{O\text{-}X}$.

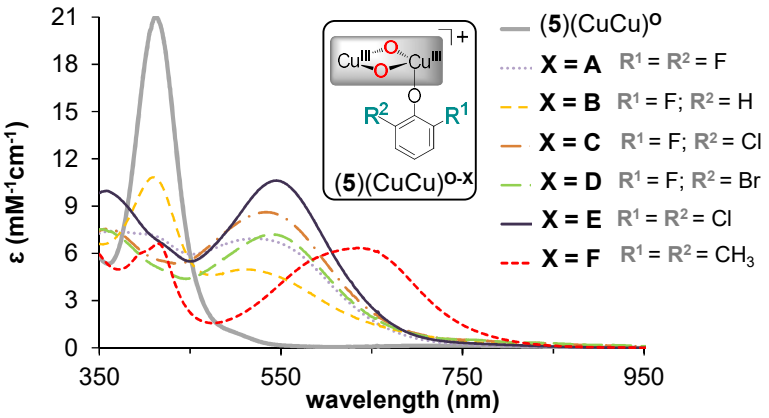

Figure VIII.8. UV-Vis features of the different (**5**)(CuCu)$^{O\text{-}X}$ species generated after the addition of the corresponding sodium phenolate to (**5**)(CuCu)^{O}.

To our delight, work up after complete decay of (**5**)(CuCu)$^{O\text{-}X}$ revealed that the reaction was selective for cleaving the C-F bond. Thus, reaction of (**5**)(CuCu)^{O} with 3 equiv Na(DFP) afforded 31% of 1,2-dihydroxybenzene together with 8% of 3-fluorocatechol (Figure VIII.5b). Exquisite selectivity was observed for substrates bearing another halogen in the *ortho* position, such as sodium 2-choro-6-fluorophenolate and 2-bromo-6-fluorophenolate. In this case, the *ortho*-hydroxylated-defluorinated product was the only one observed in 62% and 49% yield respectively. Thus, *ortho*-hydroxylation-defluorination occurred even though presumably weaker C_{arene}-R bonds (R = Cl, Br, CH_3) were present. Interestingly, only recovery of the starting material was observed when phenolates bearing substituents different from hydrogen and fluorine in the *ortho* position were used (such as sodium 2,6-dichlorophenolate or sodium 2,6-dimethylphenolate). This *ortho*-hydroxylation-defluorination reaction is unique in the sense that whereas oxidative dehalogenation of C_{arene}-X (X = Cl, Br) had previously been described to occur by reaction of binuclear copper(I) complexes and O_2,[11] no examples of defluorination by Cu_2O_2 species were known.

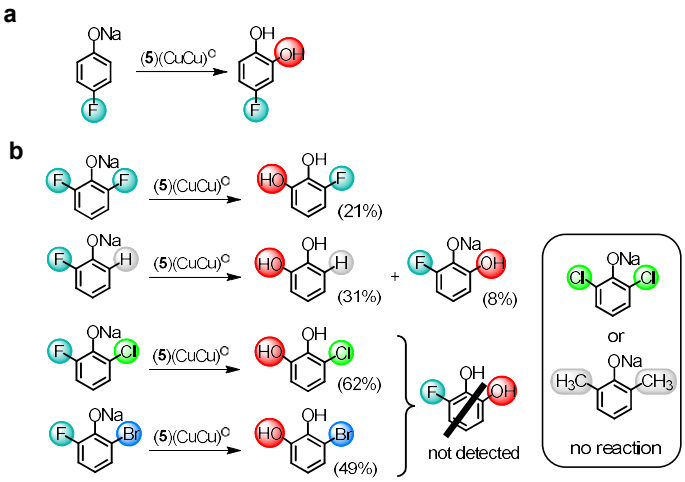

Scheme VIII.5. Selective *ortho*-hydroxylation-defluorination upon reaction of (**5**)(CuCu)^{O} and *ortho*-substituted sodium fluorophenolates at -90ºC.

Further mechanistic studies were performed in order to gain more insight about this remarkable reactivity. Specifically, we performed the reaction with a series of *para*-substituted sodium-fluorophenolates. While the formation of the corresponding (**5**)(CuCu)$^{\mathbf{O\text{-}X}}$ species was too fast to be measured by conventional UV-vis spectroscopic techniques, their decay was slower following a first-order process that could be fitted to a single exponential function by nonlinear regression methods. Then the logarithm of the rate of decay (k_{obs}) was plotted against the corresponding Hammett *meta*-substituent constant (σ^+) affording a linear correlation (R^2 = 0.98) with a negative slope (ρ = -2.4). The negative value is indicative of an electrophilic attack on the aromatic ring of the phenolate (faster reaction when the substituent is electron-donating). Very interestingly, the *ortho*-hydroxylation of phenolates by tyorinase (and its model compounds) is also of electrophilic nature, exhibiting similar ρ values.[9,12-15] Thus, all the accumulated mechanistic data taken together indicated that the reaction starts with the binding of the sodium fluorophenolate to one of the copper centers in (**5**)(CuCu)$^{\mathbf{O}}$, and then it proceeds through an electrophilic attack of one of the oxo ligands of the Cu_2O_2 core at the *ortho*-C_{arene}-F bond.

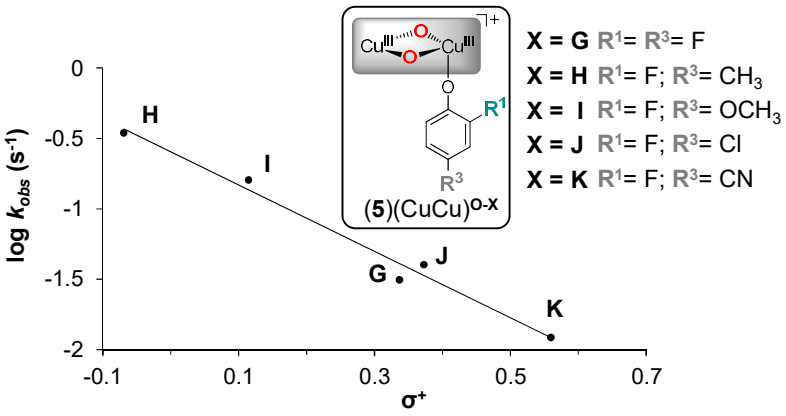

Figure VIII.9. Hammett plot for the thermal decay of (**5**)(CuCu)$^{\mathbf{O\text{-}X}}$ at -90ºC in acetone.

As it has been discussed in the introduction (see section I.3.3.1), there is an open debate in the field of copper-dioxygen chemistry about the nature of the active species in the phenol *ortho*-hydroxylation reaction. Even though such species has only been observed in model systems so far, it is well known that **O** species are usually in a nearly degenerate equilibrium with the corresponding $^{\mathbf{S}}$**P** isomers.[16] Indeed, both can promote *ortho*-hydroxylation of phenolates as observed in model chemistry.[17,18] We decided to study the capacity of both species to *ortho*-hydroxylate-defluorinate 2-fluorophenolates. In order to do so, we selected two functional models previously described for the *ortho*-hydroxylation of phenolates, [Cu$^{\mathrm{I}}$(**6**)]$^+$ and [Cu$^{\mathrm{I}}$(**7**)]$^+$.[13,14,19] Both mononuclear copper(I) complexes react with oxygen at low temperatures to form $^{\mathbf{S}}$**P** species (**6**)$_2$(CuCu)$^{\mathbf{SP}}$ and (**7**)$_2$(CuCu)$^{\mathbf{SP}}$, respectively (Scheme VIII.6). However, whereas for the latter direct decomposition was observed upon phenolate addition,[19] for (**6**)$_2$(CuCu)$^{\mathbf{SP}}$ substrate addition caused the conversion of $^{\mathbf{S}}$**P** species into **O**, which was the real executor of the oxidation.[14] Interestingly, product analyses after the addition of 3 equiv of Na(DFP) to (**6**)$_2$(CuCu)$^{\mathbf{SP}}$, revealed formation of 3-fluorocatechol in 23 % yield (with respect to

Cu_2O_2) thus closely resembling the result obtained with (**5**)(CuCu)^{O}. Even more interestingly, when the same reaction was performed with the pre-formed (**7**)$_2$(CuCu)^{SP}, only recovery of the starting material was observed (<3 % of catechol product). All these observations taken together suggested that the involvement of **O** species was key to achieve the *ortho*-hydroxylation-defluorination reaction. Control experiments performed with $[Cu^{I}(CH_3CN)_4](CF_3SO_3)$ produced only trace amounts of the defluorinated product.

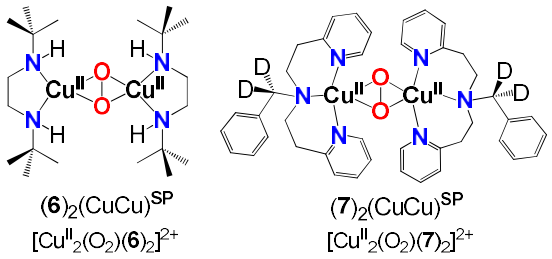

Scheme VIII.6. Schematic representation of (**6**)$_2$(CuCu)^{SP} and (**7**)$_2$(CuCu)^{SP}.

The next goal was trying to improve the reaction yield, which in most cases remained moderate (Scheme VIII.5b). The observed *ortho*-hydroxylation-defluorination itself does not involve a neat gain or loss of electrons, but experimentally it was observed that the Cu^{III} was reduced to Cu^{II}. We speculated that the ligand could undergo oxidative degradation to provide these reducing equivalents, but **5** was recovered intact after reaction of (**5**)(CuCu)^{O} with Na(DFP) so that an alternative explanation was needed. The electrons could also originate from a reaction with a second (**5**)(CuCu)^{O} unit releasing O_2, thus recovering the initial Cu^{I} complex and releasing electrons. If this was the case, we envisioned that the addition of an external reducing agent would provide the necessary electrons and yields would increase. Such strategy had already been used to enhance the dechlorination yield by a ^{S}**P** species.[11] Unfortunately, and as previously reported for other **O** species, the addition of sodium ascorbate, zinc dust or a copper(I) salt caused the immediate decomposition of (**5**)(CuCu)^{O}. However, we found that (**6**)(CuCu)^{SP} could be generated in the presence of sodium ascorbate. Very remarkably, whereas the reaction of this compound with sodium 2-chloro-6-fluorophenolate and sodium 2-bromo-6-fluorophenolate at -90ºC afforded 41 % and 34 % of the respective catechols, the presence of sodium ascorbate (2 equiv with respect to (**6**)(CuCu)^{SP}) raised both yields up to 83%.

From all the accumulated data, a mechanism for the *ortho*-hydroxylation-defluorination reaction could be depicted (Scheme VIII.7). In the first place, the 2-fluorophenolate binds to one of the copper(III) centers in (**5**)(CuCu)^{O} to afford (**5**)(CuCu)$^{O\text{-}X}$ (step a). This species decays following a first order intramolecular mechanism after an electrophilic attack of the **O** species on the aromatic ring (step b). We propose that this step is the origin of the exquisite selectivity for the *ortho*-fluorine atom, which is selectively cleaved even in the presence of in principle weaker C-X bonds (X = Cl, Br) that a priori could be regarded as competing cleavage sites. We hypothesize in the establishment of a putative interaction between an unpaired pair of electrons of the *ortho*-

fluorine and the adjacent copper(III) center in (**5**)(CuCu)^{O} species, so that the C-F bond becomes properly oriented to suffer the electrophilic attack by the Cu_2O_2 core. It is worth noticing that such interaction has never been described for copper(III) centers but it is well established for other metals such as alkaline and alkaline earth metals such as Ag, Pd, Pt, Ru, or Ir.[20-22] After the electrophilic attack, the catecholate product is formed (step c) and then the copper centers are reduced by two electrons to Cu^{II}. In the absence of a reducing agent, O_2 release from another (**5**)(CuCu)^{O} affords the necessary two electrons.

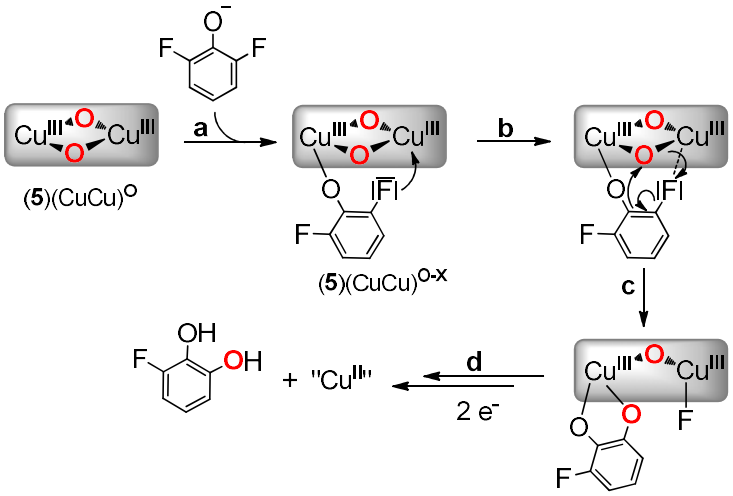

Scheme VIII.7. Proposed mechanism of *ortho*-hydroxylation-defluorination of 2-fluorophenolates by (**5**)(CuCu)^{O}.

Overall, this work represented the first example of an *ortho*-hydroxylation-defluorination of 2-fluorophenolates using O_2 as sacrificial oxidant by means of a synthetic metal complex, a reaction that finds precedent in FAD-dependent hydroxylase enzymes in biological systems. The involvement of **O** species seems to be a key issue to perform such reaction. The product yields obtained in the reaction are still far from practical for synthetic purposes and even though it would be of a great interest, we have not been able to develop the catalytic version of such reaction so far. Most probably the Cu-F bond formed at the end of the reaction is too strong to allow further regeneration of the **O** species. Still, this reaction constitutes a fascinating transformation from a basic chemical point of view not only because of the inherent interest of cleaving a strong C-F bond, but also due to the rather unusual selectivity properties it exhibits. Finally, this reaction is also interesting from the perspective of environmental science, as it proves that the transformation of inert C-F bonds of common persistent pollutants into a more reactive C-OH unit is doable.

VIII.3 Trapping a highly reactive nonheme iron-oxygen species: stereoselective oxygenation of strong C-H bonds and C=C bonds

This section corresponds to the contents of the manuscripts by Serrano-Plana *et al. J. Am. Chem. Soc.* **2015**, *137*, 15833-15842 and Serrano-Plana *et al. Angew. Chem. Int. Ed.* **2016**, *55*, 6310-6314 which can be found in **Chapters V** and **VI** of this thesis.

Oxygenation of nonactivated alkyl C-H bonds constitutes a very challenging reaction owing to their notorious chemically inert character. Consequently, highly reactive species are necessary to break these bonds. Moreover, the epoxidation of olefins is a valuable reaction in organic synthesis since these products are building blocks used in the synthesis of value-added chemical products. In nature, C-H hydroxylation and C=C epoxidation are mainly performed by iron-dependent enzymes, which create electrophilic iron-oxygen species via finely controlled partial reduction of the O_2 molecule to form peroxoiron species.[23] The oxidative reactivity of synthetic mononuclear peroxoiron compounds against organic substrates has proven to be sluggish at best, and they are not capable of attacking strong C-H bonds or olefins (see section I.4.4.2).[23-25] Instead, the reactivity observed for such systems is proposed to operate through the generation of high-valent species after O-O cleavage. Indeed, quite often oxoiron(V) species have been invoked as the active species generated during the catalytic cycle of the aforementioned compounds. As detailed in the introduction (section I.4.3), the reaction of ferrous complexes with peracids or hydrogen peroxide in the presence of acetic acid affords highly active systems for the catalytic oxidation of alkanes or olefins. The mechanism behind these transformations is unclear but it is proposed the formation of an acylperoxoiron(III) that is the precursor of the real active species. However, such species rarely accumulate in solution and direct evidence of their existence remains scarce.

VIII.3.1 Synthesis and characterization of a novel tetradentate ferrous complex

In this thesis we contribute to the synthetic bioinspired iron-oxygen chemistry with the preparation of a novel ferrous complex $[Fe^{II}(CF_3SO_3)_2(\mathbf{8})]$ synthesized from $[Fe(CF_3SO_3)_2(CH_3CN)_2]$ and a novel tetradentate macrocyclic nitrogen-based ligand **8** (Figure VIII.10a). Most of the reported iron complexes that selectively and stereoretentively oxidize C-H and C=C bonds bear similar basic chemical features, and they are based on tetradentate amino- and pyridine-based ligands that leave two *cis*-labile coordination positions available for interaction with other molecules. Representative examples of these iron complexes $[Fe^{II}(^{N4}L)(X)_2]^{2+}$ (^{N4}L = tetradentate aminopyridine ligand; X = CH_3CN or CF_3SO_3) have been presented in the introduction (section I.3.3.1, Figure I.10).

We fully characterized $[Fe^{II}(CF_3SO_3)_2(\mathbf{8})]$ by several techniques. By analogy to structurally related systems,[26] dissolution of $[Fe^{II}(CF_3SO_3)_2(\mathbf{8})]$ in acetonitrile causes a displacement of the

bound triflate groups so that the corresponding bis-solvato cationic complex $[Fe^{II}(\mathbf{8})(CH_3CN)_2]^{2+}$ is formed. In solution, broad bands spanning from 80 to -30 ppm were observed in its ^{1}H-NMR spectrum in CD_3CN at 243 K (Figure VIII.10b). A magnetic moment of 4.94 μ_B was measured by the Evans' method, consistent with 4 unpaired electrons as expected for an iron(II) high spin center. High-resolution mass spectrum was dominated by a peak at m/z = 453.0882 with a mass and isotopic pattern fully consistent with $\{[Fe^{II}(\mathbf{8})](CF_3SO_3)\}^+$. $[Fe^{II}(CF_3SO_3)_2(\mathbf{8})]$ was also characterized in the solid state by elemental analysis and X-ray crystallography. The latter showed that the iron center was six-coordinated in an octahedral fashion, so that ligand **8** occupied four positions in a tripodal fashion with an average iron-nitrogen distance of ~2.2 Å. Two triflate anions completed the coordination sphere and were disposed *cis* to each other (Figure VIII.10a). All collected data indicated that the iron(II) center was high-spin (S = 2) both in solution and in the solid state.

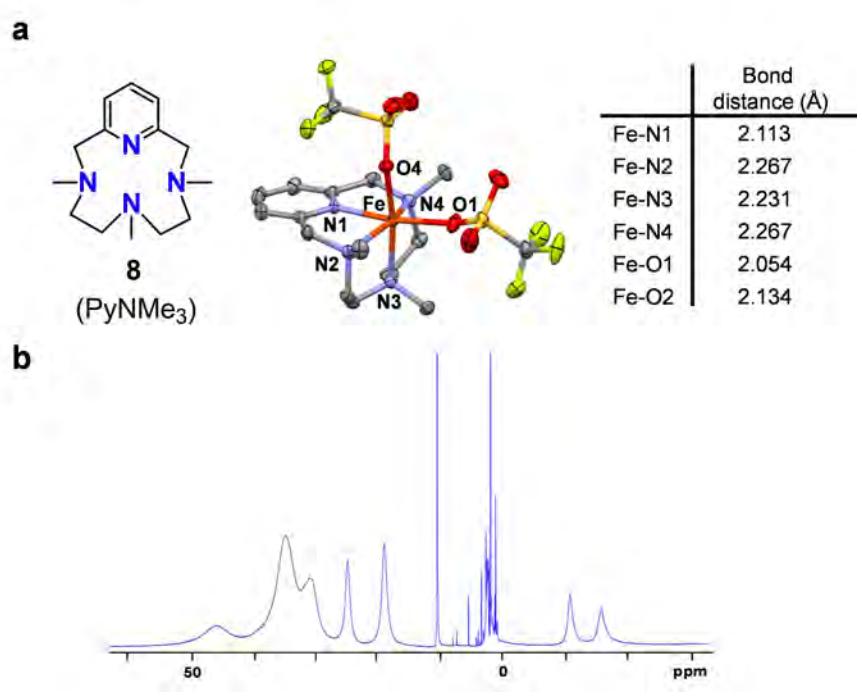

Figure VIII.10. a) Schematic representation of ligand **8** together with the X-ray structure (50% probability) of $[Fe^{II}(CF_3SO_3)_2(\mathbf{8})]$ and selected bond distances. Hydrogen atoms have been omitted for clarity. **b)** ^{1}H-NMR spectrum of $[Fe^{II}(\mathbf{8})(CD_3CN)_2]^{2+}$ in CD_3CN at 243 K.

VIII.3.2 Reactivity towards alkanes: oxygenation of strong C-H bonds with stereoretention

The catalytic activity of $[Fe^{II}(\mathbf{8})(CH_3CN)_2]^{2+}$ was tested towards alkane substrates that provide mechanistic information (mechanistic probes, see section I.4.4.1 in the introduction). The addition of peracetic acid (AcOOH, 10 equiv) to an acetonitrile solution of $[Fe^{II}(\mathbf{8})(CH_3CN)_2]^{2+}$ in the presence of excess cyclohexane at 25ºC produced a total of 9.5 turnovers of cyclohexanol and cyclohexanone in a 5:1 ratio. The oxidation of adamantane resulted in a high selectivity for the tertiary C-H bonds (normalized $3^{ary}/2^{ary}$ ratio = 23), and a high degree of stereoretention

(92%) was obtained in the oxidation of *cis*-1,2-dimethylcyclohexane. These results clearly pointed towards the involvement of a metal-based oxidant in these oxidation reactions rather than unselective free diffusing hydroxyl radicals that would afford lower $3^{ary}/2^{ary}$ ratios (~2) and no retention of configuration.

Intrigued by the nature of the oxidant involved in these transformations, we monitored the reactivity of the ferrous precursor with the oxidant at cryogenic temperatures by UV-vis absorption spectroscopy. The addition of peracetic acid (4 equiv) to a 1 mM solution of $[Fe^{II}(\mathbf{8})(CH_3CN)_2]^{2+}$ in acetonitrile caused the formation of a new species (referred as α in this section), which consists of two absorption bands at λ_{max} = 490 nm and λ_{max} = 660 in a 7:1 relative absorbance ratio, and reached its maximum formation after ~1 min (Figure VIII.11). Compound α was not stable at this temperature and it quickly decayed with a half-life time ($t_{1/2}$) of ~ 70 s.

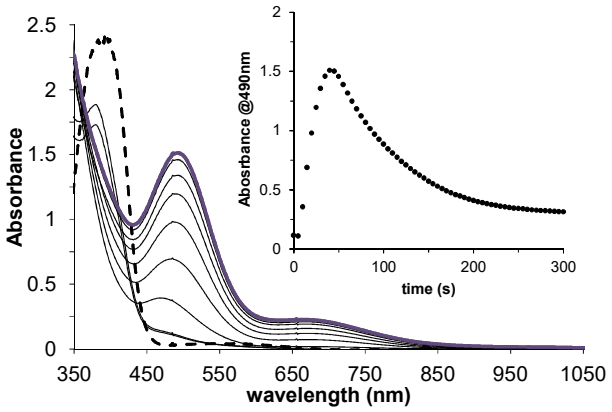

Figure VIII.11. Progressive formation of α (violet line) upon addition of peracetic acid (4 equiv) to $[Fe^{II}(\mathbf{8})(CH_3CN)_2]^{2+}$ (1mM, dashed line) in acetonitrile at -40ºC. Inset: time trace for the 490 nm absorption band.

Global fitting analysis indicated that the formation of α was not straightforward and it consisted of at least two reaction steps (A → B → C), requiring the involvement of an intermediate species between $[Fe^{II}(\mathbf{8})(CH_3CN)_2]^{2+}$ (A) and compound α (C), which did not have any visible absorption. Species B most likely corresponds to the initial one electron oxidation of the Fe^{II} center to Fe^{III} by the oxidant.

Very interestingly, the addition of cyclohexane accelerated the decay of α as a function of cyclohexane concentration. The kinetic trace for the decay of α showed pseudo-first order behavior and it could be fitted to single exponentials to obtain the corresponding observed reaction rate (k_{obs}). The different k_{obs} showed a linear dependence on the concentration of substrate, affording a second order rate constant (k_2) of 2.8 ± 0.1 $M^{-1}s^{-1}$ at -41ºC. Moreover, analysis of the reaction rates of α with cyclohexane as a function of temperature (see annex) revealed an activation barrier with a relatively small activation enthalpy ($\Delta H^{\neq}$ = 37 ± 3 $KJ{\cdot}mol^{-1}$) and a negative activation entropy ($\Delta S^{\neq}$ = -76 ± 8 $J{\cdot}K^{-1}{\cdot}mol^{-1}$), consistent with a bimolecular

reaction. The k_2 value was also measured for substrates with weaker C–H bonds. An inverse correlation was observed when the logarithm of these k_2 values (after normalization by the number of equivalent C-H bonds than can be cleaved) was plotted versus the C-H bond dissociation energy (BDE_{C-H}) of the weakest C–H bond of the hydrocarbon, so that the oxidation rate was faster for weaker C-H bonds. Such correlation is usually found in reactions with hydrogen atom abstraction (HAT) as the rate determining step.

The selectivity of α towards the oxidation of different C-H bonds was again tested using mechanistic probes (Scheme VIII.8). Thus, excess cyclohexane to pre-formed α at -40ºC afforded cyclohexanol and cyclohexanone in a 9:2 ratio. Compound α also showed a kinetic isotope effect (KIE) of 5, which matches those found for nonheme iron-catalyzed hydroxylations of cyclohexane by H_2O_2.[27,28] Very interestingly, this KIE value was obtained from direct measurement of the reaction rates of α with the substrate or its deuterated analogue (k_H/k_D) and also from the product analysis of a competitive oxidation of cyclohexane and d_{12}-cyclohexane under catalytic conditions by $[Fe^{II}(\mathbf{8})(CH_3CN)_2]^{2+}$ and peracetic acid. This observation corroborates that indeed α is the actual active species. High selectivity for the oxidation of 3^{ary} C-H bonds of adamantane was observed ($3^{ary}/2^{ary}$ ratio = 29), and high retention of configuration (>95 %) was observed for the oxidation of the 3^{ary} C-H bonds of *cis*-1,2-dimethylcyclohexane. Moreover, compound α was also selective for the oxidation of the less sterically hindered positions. This was clearly observed in the oxidation of 1,1-dimethylcyclohexane, which yielded a mixture of C2, C3 and C4 alcohols and ketones in a relative ratio 10:50:40, significantly different from the statistically 40:40:20 expected if all C-H bonds were equally oxidized. Finally, this oxidant also responded to polar factors and the preferential oxidation of the more electron-rich 3^{ary} C-H bond was observed when 1-bromo-3,7-dimethyloctane was used as substrate.

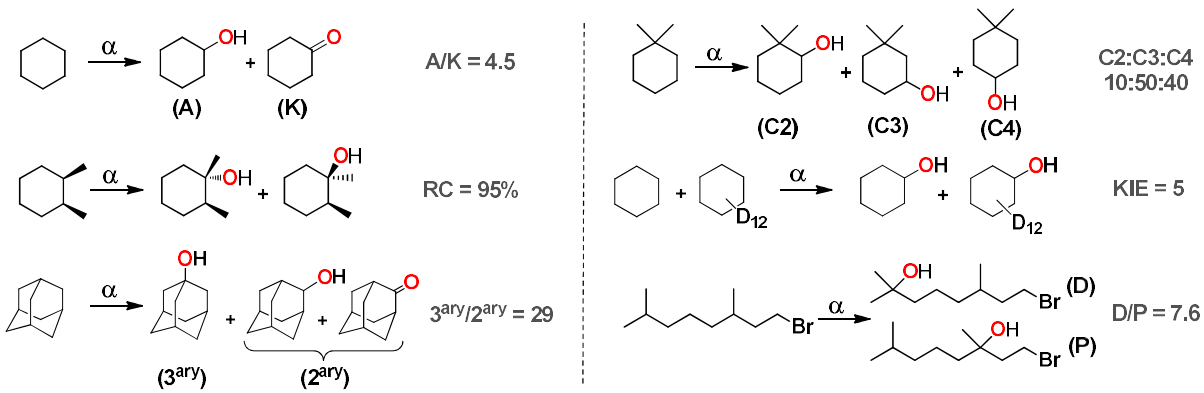

Scheme VIII.8. Oxidation products found after reaction of α and mechanistic probes substrates.

Thus, all the accumulated experimental evidences showed that indeed α was a strong oxidant capable of cleaving unactivated strong C-H bonds with high selectivites, being able to discriminate among different C-H bonds in the same molecule on the basis of not only the C-H bond strength but also responding to steric and polar factors.

In the literature there are just a few trapped iron-oxygen species able to react with substrates bearing unactivated C-H bonds such as those of cyclohexane. In order to put into context the oxidizing power of α, we compared the obtained k_2 value for the oxidation of cyclohexane with all the other previously reported iron-oxygen species for which the rate of this reaction had been measured (Figure VIII.12).[29-36] This included oxoiron(IV), oxoiron(V), iodosylareneiron(III) and a recently reported high spin acylperoxoiron(III). To our delight, among these compounds, α showed the highest rate described so far.

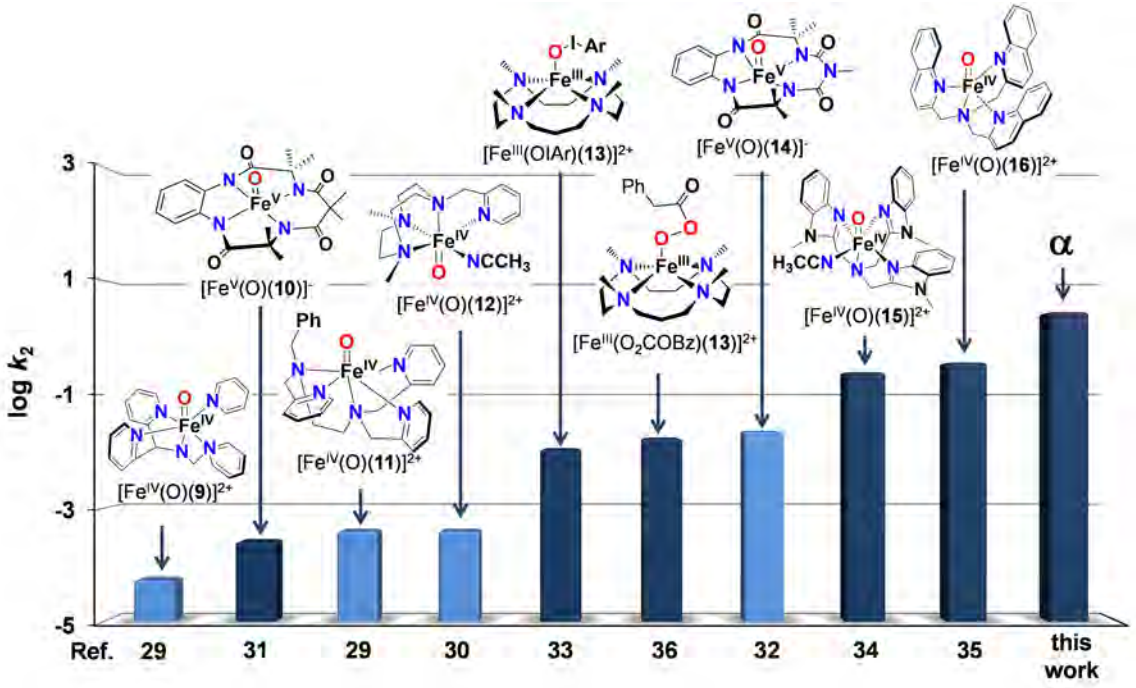

Figure VIII.12. Cyclohexane oxidation rates (k_2) obtained at -40ºC (dark blue) or 25ºC (light blue) for various nonheme iron-oxygen compounds.

The differences in reaction rates towards cyclohexane were especially remarkable (at least 4 orders of magnitude) when the reaction rate of α was compared to several S = 1 oxoiron(IV) complexes [Fe^{IV}(O)(L)]$^{2+}$ (L = **9**, **11**, **12**, Figure VIII.12).[29,30] It was also four and two orders of magnitude faster than for the two well-defined oxoiron(V) stabilized by TAML systems [Fe^{V}(O)(**10**)]$^{-}$ and [Fe^{V}(O)(**14**)]$^{-}$ reported by Collins and Gupta respectively (even without correcting the 65-degree difference for the latter).[31,32] A 200-fold difference was found with the iodosylareneiron(III) adduct [Fe^{III}(OIAr)(**13**)]$^{2+}$,[33] which can be considered as a masked oxoiron(V), while the high-spin acylperoxoiron(III)- [Fe^{III}(O$_2$COBz)(**13**)]$^{2+}$ reported by Nam and coworkers was around 150 times slower.[36] There are two examples that more closely approach the rate obtained for α. One is the S = 1 oxoiron(IV) [Fe^{IV}(O)(**15**)]$^{2+}$ that was proposed to be in equilibrium with a highly reactive S = 2 spin state[34] and the other is the recently described well-defined S = 2 oxoiron(IV) [Fe^{IV}(O)(**16**)]$^{2+}$ by Que and co-workers.[35] Both compounds show rates that are *just* one order of magnitude slower than that measured for α.

VIII.3.3 Reactivity towards alkenes: exceedingly fast oxygen atom transfer

Motivated by the extraordinary reactivity of α towards alkanes, we decided to explore further its oxygen-atom transfer (OAT) ability towards olefins. Upon addition of peracetic acid (20 equiv) to a mixture of $[Fe^{II}(\mathbf{8})(CH_3CN)_2]^{2+}$ and excess cyclooctene (200 equiv) at room temperature, cyclooctene oxide was obtained as the major product (17 TON) but very remarkably *cis*-2-acetoxycyclooctanol was also detected (2 TON). It must be noted that the latter product was found exclusively in *syn*-stereochemistry so that it could not derive from epoxide ring opening. A blank experiment in the absence of the iron complex afforded ~5 times less of epoxide but importantly no traces of the minor product were detected. Under similar conditions, the catalytic oxidation of excess 1-octene (100 equiv) at room temperature using $[Fe^{II}(\mathbf{8})(CH_3CN)_2]^{2+}$ as catalyst and peracetic acid (20 equiv) as oxidant afforded 12 TON of 1-octene as the major product and also 3 TON of *cis*-2-acetoxyoctanol. Both the epoxide and the diol products are proposed to be formed by reaction of the *in situ* generated α with the olefin.

The addition of cyclooctene (50 equiv) to α (generated by adding 4 equiv peracetic acid to $[Fe^{II}(\mathbf{8})(CH_3CN)_2]^{2+}$ at -40ºC in acetonitrile) caused the immediate decay of the characteristic 490 nm chromophore. Analysis of the oxidation products revealed that 1.3 equiv of epoxide and 0.06 equiv of *cis*-2-acetoxycyclooctanol (with respect to iron) had been formed, indicating that α is also kinetically competent for the oxidation of olefinic substrates. Because of the very fast decay of α in the presence of alkenes, the use of sequential cryo-stopped-flow at -60ºC with an acetonitrile/acetone 1:3 mixture was required to get accurate reaction rates. Kinetics were monitored by adding excess olefin and monitoring the decay of the 490 nm chromophore. The time trace could be fitted to a single exponential to obtain observed rate constants (k_{obs}) which depended linearly on substrate concentration, so that second-order rate constants (k_2) could be obtained. A small activation enthalpy ($\Delta H^{\neq}$ = 28.4 ± 0.5 kJ mol^{-1}) and a negative activation entropy ($\Delta S^{\neq}$ = -90 ± 2 J K^{-1} mol^{-1}) were determined by performing experiments with α and 1-octene at different temperatures. This data is consistent with a bimolecular process with a low enthalpic barrier. We also attempted to measure OAT rates of α towards sulfides but surprisingly the reactions were too fast to be measured with our stopped-flow equipment.

In order to have a general idea about the basic structural and electronic aspects that determine the relative reactivity of α against olefins, we measured the rates towards different olefins. As a general rule, the reaction rate (k_2) increased with the degree of substitution (Figure VIII.13a), most probably related to the increase in the electron density of the double bond caused by substituent inductive effects,[37] which supports the electrophilic character of α. Consequently, the fastest rate was obtained for the oxidation of 2,3-dimethyl-2-butene (k_2 = 975 ± 16 $M^{-1}s^{-1}$), almost 7 times faster than for 2-methyl-2-hexene (144 ± 1 $M^{-1}s^{-1}$), which in turn was around 2 and 14 times faster than *cis* and *trans*-2-octene, respectively. The slowest rate was observed for 1-octene (8.8 ± 0.2 $M^{-1}s^{-1}$). These results indicated that electronic effects dominated over

sterics in determining the reactivity of α against olefins. It is also remarkable that the relative reactivity was configuration dependent and the *cis* isomer was more prone to be oxidized than the *trans* (8 times faster in the case of 2-octene).

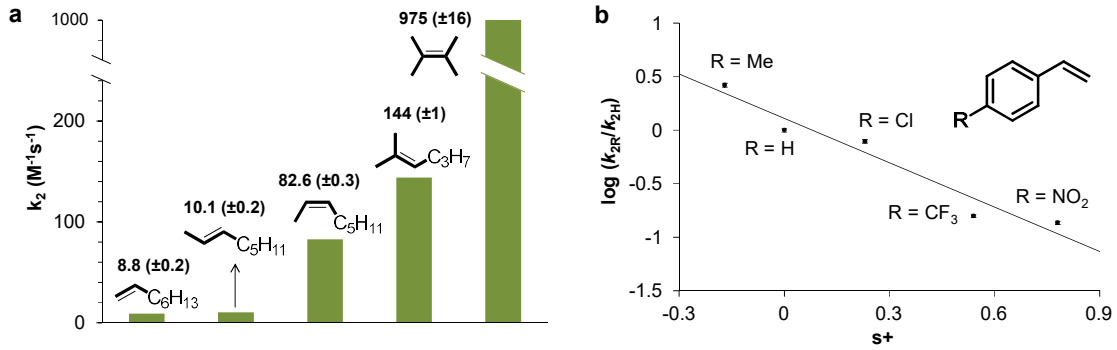

Figure VIII.13. a) Second-order rate constants for the oxidation of olefinic substrates by α at -60ºC in acetonitrile/acetone 1:3. **b)** Hammett plot for the reaction of α with a series of *para*-substituted styrenes at -60ºC in acetonitrile/acetone 1:3.

We further investigated the influence of electronic effects in determining the reactivity of olefins in a systematic manner. Specifically, we measured reaction rates towards different *para*-substituted styrenes. Then the logarithm of the corresponding k_2 was plotted against the Hammett *para*-substituent constant (σ^+), affording a good correlation (R = 0.95) and a negative slope (ρ) of -1.4 ± 0.2 (Figure VIII.13b). The negative ρ value is indicative of the electrophilic character of α in OAT reactions.[38,39]

The catalytic relevance of α was evaluated in a competition experiment in which two different olefins were reacted at the same time under catalytic conditions in a $[Fe^{II}(\mathbf{8})(CH_3CN)_2]^{2+}$/AcOOH system (1:10:100, Fe/AcOOH/substrate, in a mixture acetonitrile/acetone 1:3 at -60 ºC). The relative amounts of the two epoxide products produced from the catalytic oxidation were compared with the kinetic rate constants gathered for the reaction of α with alkenes (measured by stopped flow at -60ºC). Specifically, three pairs of olefins ($alkene^A$ and $alkene^B$) were used: styrene vs 1-octene, *cis*-cyclooctene vs *cis*-2-octene, and *cis*- vs *trans*-2-octene (Figure VIII.9). Blank experiments showed that under these experimental conditions, uncatalyzed epoxidation was negligible (<3% with respect to the oxidant). Very interestingly, reactions occurred with stereoretention and the relative amount of the two epoxides formed after each competition reaction ($epoxide^A/epoxide^B$) reasonably matched the ratio of the corresponding k_2 values measured individually for the reaction of α with each olefin (k_2^A/k_2^B). This result provided strong evidence that α was a relevant intermediate in catalytic epoxidation reactions.

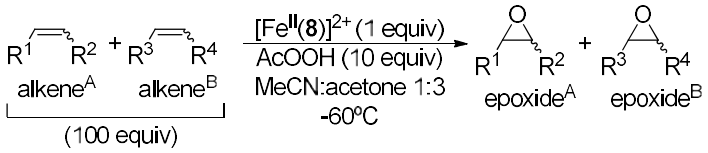

alkene^A		alkene^B	catalytic competition	reaction rate ratios
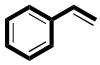	vs.	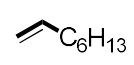	$\frac{\text{epoxide}^A}{\text{epoxide}^B} = 16 \pm 3$	$k_2^A/k_2^B = 16.9 \pm 0.3$
	vs.	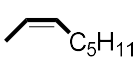	$\frac{\text{epoxide}^A}{\text{epoxide}^B} = 6.1 \pm 0.4$	$k_2^A/k_2^B = 4.5 \pm 0.2$
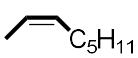	vs.	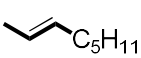	$\frac{\text{epoxide}^A}{\text{epoxide}^B} = 9.5 \pm 0.5$	$k_2^A/k_2^B = 8.18 \pm 0.03$

Scheme VIII.9. Schematic representation of the intermolecular competitive epoxidation of pairs of olefins (alkene^A and alkene^B) by $[Fe^{II}(\mathbf{8})(CH_3CN)_2]^{2+}$/AcOOH catalytic system. Epoxide^A/epoxide^B: ratio of epoxide^A and epoxide^B products determined by GC. k_2^A/k_2^B: ratio of second order rate constants for the reaction of α with alkene^A (k_2^A) and alkene^B (k_2^B) in acetonitrile/acetone 1:3 at -60 ºC determined by stopped-flow.

With the precedent of the fast rate obtained for α for the oxidation of cyclohexane, we proceeded to rank the OAT rates towards olefins observed for this compound with the available rates for the same reaction by other iron-oxygen species (Table VIII.2, Figure VIII.14). In this line, *cis*-cyclooctene is often used to compare oxidizing abilities of different compounds. For this substrate, α exhibited a k_2 = 375 $M^{-1}s^{-1}$ at -60ºC. This rate was especially impressive when compared to previously reported values for well-defined iron-oxygen species. For example, rates between 3 and 4 orders of magnitude slower were exhibited by the oxoiron(IV) complexes $[Fe^{IV}(O)(\mathbf{17})]^{2+}$ and $[Fe^{IV}(O)(\mathbf{18})]^{2+}$ (which also bear an aminopyridine-based macrocycle) and $[Fe^{IV}(O)(\mathbf{19})]^{2+}$ (with a N_2S_2 thioether ligand), even though the rates were measured at much higher temperatures.[40,41] The same rate difference was measured for $[Fe^{IV}(O)(\mathbf{9})]^{2+}$ (which bears a pentadentate ligand), in the presence of triflic acid.[42] The S = 2 oxoiron(IV) complex $[Fe^{IV}(O)(\mathbf{16})]^{2+}$ recently reported by Que and co-workers showed a rate for the oxidation of 1-octene (5.4 $M^{-1}s^{-1}$ at -40 ºC) which was of the same order of magnitude compated to that for α (8.8 $M^{-1}s^{-1}$ at -60 ºC).[35] However, it exhibited a rate for *cis*-cyclooctene oxidation two orders of magnitude slower. The TAML-oxoiron(V) species $[Fe^{V}(O)(\mathbf{14})]^{-}$ (29 $M^{-1}s^{-1}$ at 25ºC) was still 10 times slower than α at -60ºC, even without correcting for the 80ºC difference, meaning that in fact α reacted much faster.[38] Interestingly, the recently reported high-spin acylperoxoiron(III) complex $[Fe^{III}(O_2COR)(\mathbf{13})]^{2+}$ oxidized styrene almost 400 times slower than α.[36] This data is especially striking because it further highlights that the cleavage of the O-O bond is crucial for creating a uniquely powerful oxidation agent. Finally, other acylperoxoiron(III) species have been reported but they proved to be either sluggish oxidants in OAT,[43] kinetically incompetent to perform this chemistry,[44] or no reactivity studies were undertaken.[45-47] The latter include Fe complexes based on pyridinophane ligands structurally related to **8** for which no direct

evaluation of the reactivity of the spectroscopically trapped iron-oxygen species was reported, so that no direct comparison could be established with the current system.

Table VIII.2. Second order rate constants (k_2) for the reaction of α and selected mononuclear iron-oxygen species towards 1-octene, styrene and *cis*-cyclooctene (See Figure VIII.14 for the structures of compounds).

Compound	T, ºC	k_2, $M^{-1}s^{-1}$			ref.
		1-octene	styrene	cyclooctene	
α	-60	8.8 ± 0.2	149 ± 3	375 ± 15	this work
$[Fe^{IV}(O)(\mathbf{9})]^{2+}$ [a]	25	-	0.043 ± 0.003	-	42
$[Fe^{III}(O_2COBz)(\mathbf{13})]^{2+}$	-60	-	0.4	-	36
$[Fe^{V}(O)(\mathbf{14})]^{+}$	r.t.	-	148 ± 8.1	29 ± 3.6	38
$[Fe^{IV}(O)(\mathbf{16})]^{2+}$	-40	5.3	-	3.3	35
$[Fe^{IV}(O)(\mathbf{17})]^{2+}$	0	-	-	0.45	41
$[Fe^{IV}(O)(\mathbf{18})]^{2+}$	20	-	-	0.032	41
$[Fe^{IV}(O)(\mathbf{19})]^{2+}$	25	-	0.026	-	40

[a] Proton-coupled electron transfer (PCET) in the presence of HOTf. $[Fe^{IV}(O)(\mathbf{9})]^{2+}$ itself cannot oxidize styrene.

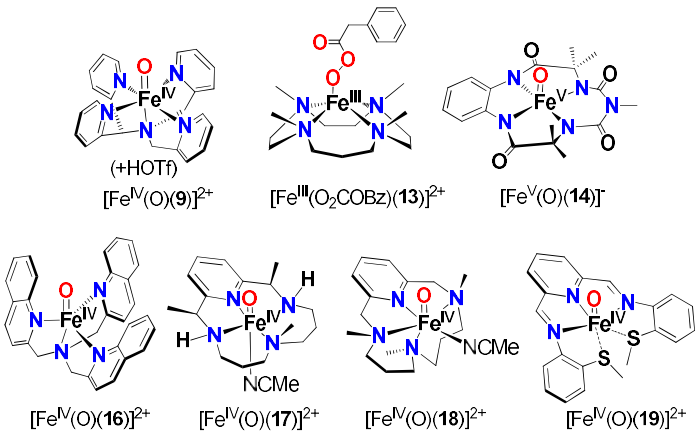

Figure VIII.14. Spectroscopically detected nonheme iron-oxygen species competent for olefin epoxidation.

VIII.3.4 Spectroscopic analysis of α

EPR spectroscopy was found to be an excellent technique to study the nature of α. Initial analysis of frozen samples of α generated in acetonitrile at -40ºC was complicated because of the presence of broad signals difficult to integrate. However, a sample frozen upon maximum formation of α generated in an acetonitrile/acetone 1:3 glassing solvent mixture at -50ºC showed well-resolved EPR features. At maximum formation of the 490-nm chromophore three major EPR-active species could be observed. There was a high-spin iron(III) species with signals in the g = 9 and g = 4-6 regions that accounted for ~40% of total Fe. This high-spin iron(III) species was also present in the Mössbauer spectrum of the same sample, representing

40% of the iron as well. However, formation of this species did not follow the kinetic behavior of the 490 nm chromophore associated to α, suggesting that most likely it was formed in a side reaction not related to α.

Two S = 1/2 species were also observed in the low spin region of the EPR spectrum. A minor component accounted for 5% of total Fe with *g* values 2.20, 2.19, and 1.99 (α_A), and a major component with *g* values 2.07, 2.01 and 1.95 (α_B) represented 40% of the iron content (Figure VIII.15 a)**.** Very interestingly, EPR analysis of several samples frozen during the formation and decay of the 490 nm chromophore revealed that both α_A and α_B species closely tracked the time trace of the 490 nm chromophore. More importantly, addition of 50 equiv cyclohexane at maximum formation of the chromophore caused its faster decay in tandem with both α_A and α_B species (figure VIII.15b). These observations were an indication that these compounds were either the active oxidant species or it existed a rapìd equilibrium between them. A sample frozen upon complete decay of the 490 nm chromophore showed the presence of a new low-spin iron(III) species with *g* values at 2.21, 2.14 and 1.97 accounting for 28% of the total iron. Its formation was not directly dependent on the decay of the 490 nm chromophore.

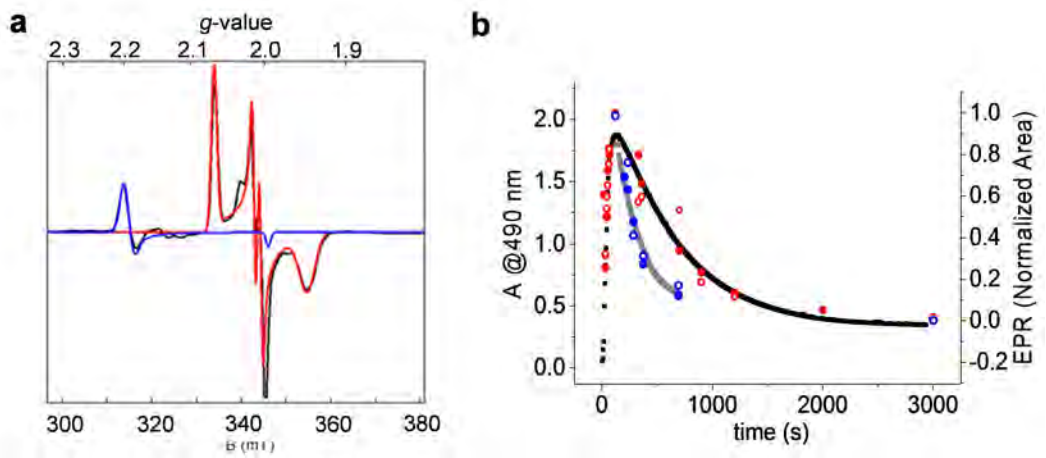

Figure VIII.15. a) EPR spectrum of a sample taken at maximum formation of α after reaction of $[Fe^{II}(\mathbf{8})(CH_3CN)_2]^{2+}$ and peracetic acid (5 equiv) in acetonitrile/acetone 1:3 solvent mixture at -50ºC EPR conditions: T = 20 K, 0.2 mW microwave power, 1 mT modulation. Shown is the *g* = 2 region of the spectrum (black). The theoretical curves (red and blue) are SpinCount simulations. Blue: α_A simulated with *g* = 2.20, 2.19, 1.99 (5% of Fe). Red: α_B simulated with *g* = 2.07, 2.01, 1.95 (40% of Fe). Spectra along the time course can be found in the annex. **b)** Time course of α generated by adding 5 equiv. AcOOH to $[Fe^{II}(\mathbf{8})(CH_3CN)_2]^{2+}$ (1 mM) in acetonitrile/acetone 1:3 solvent mixture at -50 ºC. Black squares: formation and self-decay of the 490-nm chromophore. Grey line shows the decay of the chromophore after the addition of cyclohexane (50 equiv) upon maximum formation of α (near 120 s). Red open and filled circles represent the respective amounts of α_A (g_{max} = 2.20) and α_B (g_{max} = 2.07) during the formation and self-decay of the 490 chromophore. Blue open and filled circles respectively mark the time course of the α_A and α_B species during the decay of α after the addition of 50 equivalents of cyclohexane.

At that point we aimed at unravelling the nature of α_A and α_B. Que and co-workers recently reported the reaction of a structurally related system $[Fe^{II}(\mathbf{20})(CH_3CN)_2]^{2+}$ with H_2O_2/AcOH or AcOOH at -40ºC giving raise to the formation of a metastable UV-Vis chromophore at λ_{max} = 460 nm.[48] This compound could unequivocally be characterized by several spectroscopic techniques including EPR, resonance Raman, Mössbauer and also by ESI-MS experiments as a low spin acylperoxoiron(III) $[Fe^{III}(\kappa^2\text{-OOAc})(\mathbf{20})]^{2+}$ (Figure VIII.16b) (see section I.4.4.2 in the introduction). Other well-defined iron(III) compounds such as $[Fe^{III}(OOH)(\mathbf{9})]$ showed similar *g*-values (2.16, 2.11, 1.98) (Figure VIII.16b).[49] Thus, by analogy, we initially considered α as an acylperoxoiron(III). A structurally related compound of such species was obtained by reaction of $[Fe^{II}(\mathbf{8})(CH_3CN)_2]^{2+}$ with an hydroxamic acid, affording a thermally stable hydroxomate-iron(III) species $[Fe^{III}(\kappa^2\text{-}t\text{BuCON(H)O})(\mathbf{8})]^{2+}$ that could be characterized by several techniques including single crystal X-ray diffraction (Figure VIII.16a, see annex for full characterization). In this compound, a hydroxamate ligand replaces the bidentate peracetate ligand expected for an acylperoxoiron(III) species. Interestingly its *g*-values (2.21, 1.94) were close to those determined for α_A, thus reinforcing its formulation as an $[Fe^{III}(OOAc)(PyNMe_3)]^{2+}$.

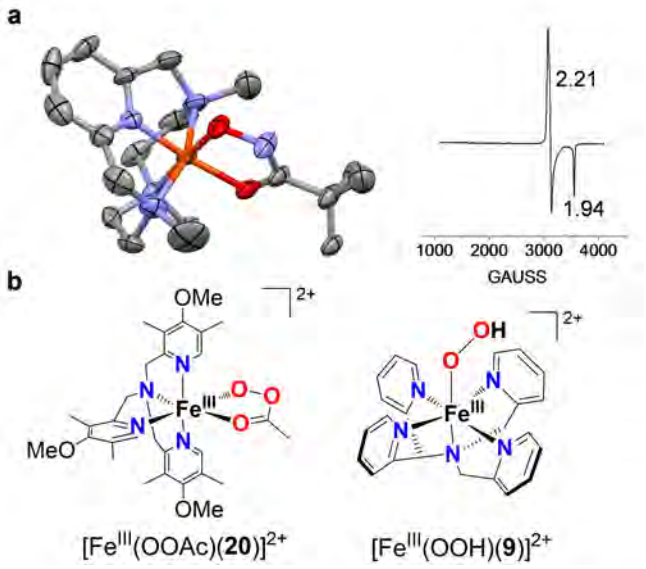

Figure VIII.16. a) Left: Thermal ellipsoid plot (30% probability) of $[Fe^{III}(t\text{BuCON(H)O})(\mathbf{8})]^{2+}$. Perchlorate anions and hydrogen atoms have been omitted for clarity. Right: EPR spectrum of $[Fe^{III}(\kappa^2\text{-}t\text{BuCON(H)O})(\mathbf{8})]^{2+}$ showing signals at g = 2.21 and 1.94. **b)** Schematic representation of the iron(III) compounds $[Fe^{III}(\kappa^2\text{-OOAc})(\mathbf{20})]^{2+}$ and $[Fe^{III}(OOH)(\mathbf{9})]^{2+}$.

The formulation of α_B was somewhat more problematic. The *g*-values obtained for this compound could not be fitted to the Griffith-Taylor model, which was developed to describe low spin iron(III) compounds.[50,51] Thus, while an iron(III) species cannot be completely ruled out, it would consist of a very unusual nonheme iron(III) center that has not been observed so far. Thus, alternative descriptions were considered.

When we compared the *g* values of α_B with the ones obtained for high valent heme and nonheme oxoiron compounds ($Fe^{V}(O)(L)$ or $Fe^{IV}(O)(L^{\bullet+})$, where $L^{\bullet+}$ stands for a ligand radical cation) important analogies were found (Table VIII.3). Particularly, a great similarity was found with the *g* = 2.053, 2.010, 1.971 values previously reported for the 1,4,8,11-tetraazacyclotetradecane-based compound $[Fe^{V}(O)(NC(O)Me)(\mathbf{21})]^{+}$. Moreover, Talsi et al. recently reported the detection of a transient species with *g* values at 2.07, 2.01, 1.95 after the reaction of $[Fe^{II}(\mathbf{20})(CH_3CN)_2]^{2+}$ with hydrogen peroxide in the presence of acetic acid and was formulated as an $[Fe^{V}(O)(\mathbf{20})]^{3+}$ albeit it only represented ~1% of the sample. Thus, further evidences were needed to confirm such assignment.

Table VIII.3. *g*-values of established and proposed $Fe^{V}(O)(L)$ and $Fe^{IV}(O)(L^{\bullet+})$ complexes and related S = 1/2 peroxoiron(III) species.

Complex [a]	EPR *g* values	ref
$[Fe^{V}(O)(\mathbf{10})]^{-}$	1.99, 1.97. 1.74	52
$[Fe^{V}(O)(\mathbf{14})]^{-}$	1.98, 1.94, 1.73	53
$[Fe^{V}(O)(NC(O)CH_3)(\mathbf{21})]^{+}$	2.05, 2.01, 1.97	54
$[Fe^{V}(O)(OC(O)CH_3)(\mathbf{20})]^{3+}$ [b]	2.07, 2.01, 1.96	55
$[Fe^{IV}(O)(Cl\text{-}acac^{\bullet+})(\mathbf{3})]^{2+}$ [c]	1.97, 1.93, 1.91	56
$[Fe^{IV}(O)(\mathbf{22})]$	2.09, 2.05, 2.02	57
$[Fe^{IV}(NTs)(\mathbf{22})]$	2.1, 2.1, 2	58
HRP-Cpd I	1.99 (broad)	59
CPO-Cpd I	2.00, 1.72, 1.61	60
CYP119-Cpd I	2.00, 1.96, 1.86	60
$[Fe^{III}(\kappa^2\text{-}OOAc)(\mathbf{20})]^{2+}$	2.58, 2.38, 1.72	48
$[Fe^{III}(\eta^1\text{-}OOH)(\mathbf{9})]^{2+}$	2.16, 2.11, 1.98	49
α_B	2.07, 2.01, 1.95	
α_A	2.20, 2.19, 1.99	

[a]See compound structures in Figure VIII.17. Abbreviations used: HRP = horseradish peroxidase; CPO = chloroperoxidase, CYP119 = cytochrome P-450 from Sulfolobus acidocaldarius, [b]This species has the same *g*-values as α_B but represents only ca. 1% of the iron in the sample. The iron(V) oxidation state proposed for this species has not been established. [c]The proposed formulation for this intermediate needs further spectroscopic corroboration.

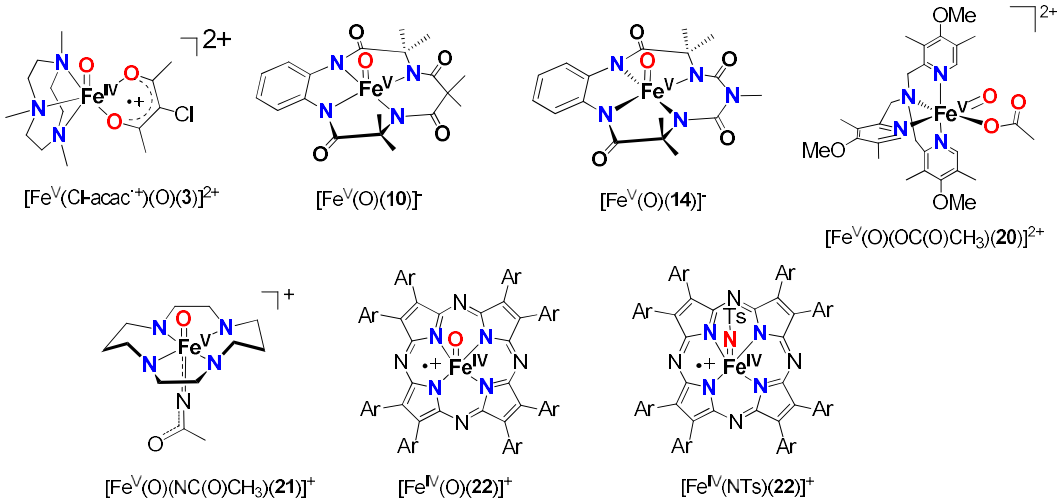

Figure VIII.17. Schematic representation of established and proposed $Fe^{V}(O)(L)$ and $Fe^{IV}(O)(L^{\bullet+})$.

We considered Mössbauer spectrometry in order gain more insight about the nature of α. Unfortunately, the presence of multiple species complicated the analysis. As stated above, a sample frozen upon maximum formation of the 490 nm chromophore indicated that 40% of the Fe in the sample was represented by iron(III) high spin species (see above), which partially obscured the region where the contribution of α_B would fall. Consequently, no isomer shift for the latter could be obtained (see annex). A promising future strategy would be to generate *difference* spectra of samples frozen at different points along the time course, cancelling features that are constant. Moreover, another strategy consisting in the achievement of a higher yield of α_B through the use of other alkyl peracids was also envisioned (experiments currently ongoing).

It is also interesting to note that in the EPR of α_B generated from the ^{57}Fe enriched ferrous precursor $[^{57}Fe^{II}(\mathbf{8})(CH_3CN)_2]^{2+}$ only a broadening in the g_{mid} signal was observed. Interestingly, the EPR spectrum of $[^{57}Fe^{V}(O)(NC(O)Me)(TMC)]^{+}$ also revealed hyperfine interaction in only one of the signals, as it only contains one unpaired electron in its d orbitals. This observation is in sharp contrast with previously described S = 1/2 oxoiron(IV) cation radical from Compound I of horsereadish peroxidase, chloroperoxidase, and cytochrome P450 that contain two unpaired electrons in their d orbitals and thus two signals were shifted.[59,60]

In order to accumulate more experimental data, we performed high resolution cryospray mass experiments at -40ºC (Figure VIII.18). The spectra of the reaction of $[Fe^{II}(\mathbf{8})(CH_3CN)_2]^{2+}$ with peracetic acid at maximum accumulation of the 490 nm chromophore showed the presence of a major peak at m/z = 528.0893 with an isotopic pattern fully consistent with its formulation as $\{[Fe(OOAc)(\mathbf{8})](CF_3SO_3)\}^{+}$ or its higher-valent electromers after O-O cleavage. Very interestingly, the appearance of a new feature at m/z = 531 was observed after adding CD_3COOD to the reaction mixture, indicating the substitution of an acetate (CH_3CO_2) by d_3-acetate (CD_3CO_2). Thus, there must be a pathway for the incorporation of labeled acetate into the molecule associated with the 528 mass peak. This carboxylate exchange can be explained

by invoking an $Fe^{V}(O)(OAc)$ species, which would provide a nice rationale for this observation. Blank experiments consisting in mixing peracetic acid and acetic acid-d_4 (20 equiv) in acetonitrile at room temperature for 30 min did not afford the formation of peracetic acid-d_4, even when the reaction was performed in the presence of Lewis acidic compounds such as $Sc^{III}(OTf)_3$ and $Ga(NO_3)_3$ (see annex).

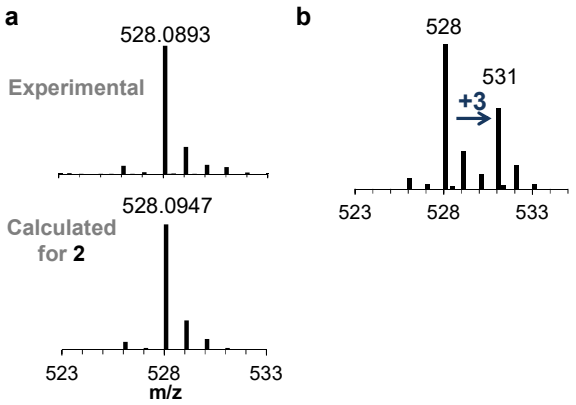

Figure VIII.18. Cryospray mass spectrometry (CSI-MS) experiments at -40ºC. Experimental and calculated pattern of α generated **a)** after reaction of $[Fe^{II}(\mathbf{8})(CH_3CN)_2]^{2+}$ and peracetic acid (4 equiv) in acetonitrile at -40ºC and **b)** after reaction of $[Fe^{II}(\mathbf{8})(CH_3CN)_2]^{2+}$ and peracetic acid (4 equiv) in acetonitrile at -40ºC in the presence of 20 equiv acetic acid-d_4 at -40ºC. The appearance of a new peak shifted 3 mass units was observed, indicating the incorporation of deuterated acetate in α.

Further evidences about the presence of this species and the putative carboxylate exchange were obtained by reaction of α with olefins. The formation of the diol product in *syn*-stereochemistry was proposed to come from the [3+2] cycloaddition of an $Fe^{V}(O)(OAc)$ to the C=C bond of the olefin and it had been previously reported for olefin oxidations catalyzed by structurally related iron(II) complexes with H_2O_2 in the presence of AcOH.[61,62] Remarkably, when this catalytic reaction was performed in the presence of a large excess of deuterated acetic acid, up to 29% of the *cis*-2-acetoxycyclooctanol was found to be trideuterated.

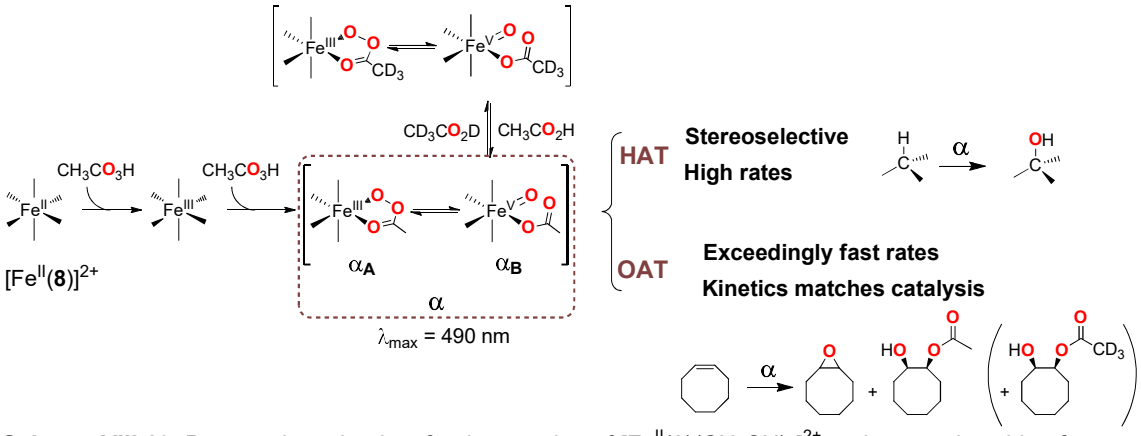

Scheme VIII.10. Proposed mechanism for the reaction of $[Fe^{II}(\mathbf{8})(CH_3CN)_2]^{2+}$ and peracetic acid to form α, which is kinetically competent for performing HAT and OAT reactions with stereoretention and high reaction rates.

After all the accumulated data, we proposed a mechanistic scenario in which the iron(II) precursor $[Fe^{II}(\mathbf{8})(CH_3CN)_2]^{2+}$ reacts with peracetic acid to give an acylperoxoiron(III) α_A that is in equilibrium with α_B via O-O bond cleavage-formation. The latter is responsible for the high reaction rates observed towards both C-H and C=C bonds. α constitutes the first example of a kinetically competent intermediate of a nonenzymatic nonheme iron system that mediates a stereospecific C-H hydroxylation reaction. Despite the fact that selected nonheme iron complexes can catalyze this transformation and have become tools for organic synthesis, until now the active species had not been directly observed. Moreover, α is an exceedingly reactive oxygen atom transfer agent. The rates that this compound exhibits for the oxidation of olefins are, to the best of our knowledge, the fastest described to date. Even more importantly, the agreement between reaction rates determined by stopped-flow and the selectivity properties of α under catalytic epoxidation conditions provide solid evidence that it is a true competent intermediate and a plausible OAT agent with broad relevance in biologically inspired nonheme iron oxidation catalysis.

VIII.5 REFERENCES

(1) Karlin, K. D.; Hayes, J. C.; Gultneh, Y.; Cruse, R. W.; McKown, J. W.; Hutchinson, J. P.; Zubieta, J. *J. Am. Chem. Soc.* **1984**, *106*, 2121.

(2) Karlin, K. D.; Nasir, M. S.; Cohen, B. I.; Cruse, R. W.; Kaderli, S.; Zuberbuehler, A. D. *J. Am. Chem. Soc.* **1994**, *116*, 1324.

(3) Mirica, L. M.; Ottenwaelder, X.; Stack, T. D. P. *Chem. Rev.* **2004**, *104*, 1013.

(4) Halfen, J. A.; Mahapatra, S.; Wilkinson, E. C.; Kaderli, S.; Young, V. G.; Que, L.; Zuberbühler, A. D.; Tolman, W. B. *Science* **1996**, *271*, 1397.

(5) Mahapatra, S.; Halfen, J. A.; Wilkinson, E. C.; Pan, G.; Cramer, C. J.; Que, L., Jr.; Tolman, W. B. *J. Am. Chem. Soc.* **1995**, *117*, 8865.

(6) Cole, A. P.; Mahadevan, V.; Mirica, L. M.; Ottenwaelder, X.; Stack, T. D. P. *Inorg. Chem.* **2005**, *44*, 7345.

(7) Schatz, M.; Leibold, M.; Foxon, S. P.; Weitzer, M.; Heinemann, F. W.; Hampel, F.; Walter, O.; Schindler, S. *Dalton Trans.* **2003**, 1480.

(8) Weitzer, M.; Schatz, M.; Hampel, F.; Heinemann, F. W.; Schindler, S. *J. Chem. Soc., Dalton Trans.* **2002**, 686.

(9) Company, A.; Palavicini, S.; Garcia-Bosch, I.; Mas-Ballesté, R.; Que, L.; Rybak-Akimova, E. V.; Casella, L.; Ribas, X.; Costas, M. *Chem. Eur. J.* **2008**, *14*, 3535.

(10) Lemal, D. M. *J. Org. Chem.* **2004**, *69*, 1.

(11) Nasir, M. S.; Cohen, B. I.; Karlin, K. D. *Inorg. Chim. Acta* **1990**, *176*, 185.

(12) Palavicini, S.; Granata, A.; Monzani, E.; Casella, L. *Journal of the American Chemical Society* **2005**, *127*, 18031.

(13) Mirica, L. M.; Vance, M.; Rudd, D. J.; Hedman, B.; Hodgson, K. O.; Solomon, E. I.; Stack, T. D. P. *Journal of the American Chemical Society* **2002**, *124*, 9332.

(14) Mirica, L. M.; Vance, M.; Rudd, D. J.; Hedman, B.; Hodgson, K. O.; Solomon, E. I.; Stack, T. D. P. *Science* **2005**, *308*, 1890.

(15) Herres-Pawlis, S.; Verma, P.; Haase, R.; Kang, P.; Lyons, C. T.; Wasinger, E. C.; Florke, U.; Henkel, G.; Stack, T. D. P. *Journal of the American Chemical Society* **2009**, *131*, 1154.

(16) Tolman, W. B. *Acc. Chem. Res.* **1997**, *30*, 227.

(17) Serrano-Plana, J.; Garcia-Bosch, I.; Company, A.; Costas, M. *Acc. Chem. Res.* **2015**, *48*, 2397.

(18) Rolff, M.; Schottenheim, J.; Decker, H.; Tuczek, F. *Chemical Society Reviews* **2011**, *40*, 4077.

(19) Itoh, S.; Kumei, H.; Taki, M.; Nagatomo, S.; Kitagawa, T.; Fukuzumi, S. *Journal of the American Chemical Society* **2001**, *123*, 6708.

(20) Plenio, H. *Chem. Rev.* **1997**, *97*, 3363.

(21) Takemura, H.; Kon, N.; Kotoku, M.; Nakashima, S.; Otsuka, K.; Yasutake, M.; Shinmyozu, T.; Inazu, T. *J. Org. Chem.* **2001**, *66*, 2778.

(22) Stanek, K.; Czarniecki, B.; Aardoom, R.; Rüegger, H.; Togni, A. *Organometalllics* **2010**, *29*, 2540.

(23) Costas, M.; Mehn, M. P.; Jensen, M. P.; Que, L. *Chem. Rev.* **2004**, *104*, 939.

(24) Park, M. J.; Lee, J.; Suh, Y.; Kim, J.; Nam, W. *Journal of the American Chemical Society* **2006**, *128*, 2630.

(25) Nam, W. *Acc. Chem. Res.* **2015**, *48*, 2415.

(26) Prat, I.; Company, A.; Corona, T.; Parella, T.; Ribas, X.; Costas, M. *Inorg. Chem.* **2013**, *52*, 9229.

(27) Chen, K.; Que, L. *J. Am. Chem. Soc.* **2001**, *123*, 6327.

(28) Company, A.; Gómez, L.; Güell, M.; Ribas, X.; Luis, J. M.; Que, L.; Costas, M. *J. Am. Chem. Soc.* **2007**, *129*, 15766.

(29) Kaizer, J.; Klinker, E. J.; Oh, N. Y.; Rohde, J.-U.; Song, W. J.; Stubna, A.; Kim, J.; Münck, E.; Nam, W.; Que, L. *J. Am. Chem. Soc.* **2004**, *126*, 472.

(30) Company, A.; Prat, I.; Frisch, J. R.; Mas-Balleste, R.; Guell, M.; Juhasz, G.; Ribas, X.; Munck, E.; Luis, J. M.; Que, L.; Costas, M. *Chem. Eur. J.* **2011**, *17*, 1622.

(31) Kundu, S.; Thompson, J. V. K.; Shen, L. Q.; Mills, M. R.; Bominaar, E. L.; Ryabov, A. D.; Collins, T. J. *Chem. Eur. J.* **2015**, *21*, 1803.

(32) Ghosh, M.; Singh, K. K.; Panda, C.; Weitz, A.; Hendrich, M. P.; Collins, T. J.; Dhar, B. B.; Sen Gupta, S. *J. Am. Chem. Soc.* **2014**, *136*, 9524.

(33) Hong, S.; Wang, B.; Seo, M. S.; Lee, Y.-M.; Kim, M. J.; Kim, H. R.; Ogura, T.; Garcia-Serres, R.; Clémancey, M.; Latour, J.-M.; Nam, W. *Angew. Chem. Int. Ed.* **2014**, *53*, 6388.

(34) Seo, M. S.; Kim, N. H.; Cho, K.-B.; So, J. E.; Park, S. K.; Clemancey, M.; Garcia-Serres, R.; Latour, J.-M.; Shaik, S.; Nam, W. *Chem. Sci.* **2011**, *2*, 1039.

(35) Biswas, A. N.; Puri, M.; Meier, K. K.; Oloo, W. N.; Rohde, G. T.; Bominaar, E. L.; Münck, E.; Que, L. *J. Am. Chem. Soc.* **2015**, *137*, 2428.

(36) Wang, B.; Lee, Y.-M.; Clémancey, M.; Seo, M. S.; Sarangi, R.; Latour, J.-M.; Nam, W. *J. Am. Chem. Soc.* **2016**, *138*, 2426.

(37) Mikhalyova, E. A.; Makhlynets, O. V.; Palluccio, T. D.; Filatov, A. S.; Rybak-Akimova, E. V. *Chemical Communications* **2012**, *48*, 687.

(38) Singh, K. K.; Tiwari, M. k.; Dhar, B. B.; Vanka, K.; Sen Gupta, S. *Inorganic Chemistry* **2015**, *54*, 6112.

(39) Sastri, C. V.; Sook Seo, M.; Joo Park, M.; Mook Kim, K.; Nam, W. *Chemical Communications* **2005**, 1405.

(40) Annaraj, J.; Kim, S.; Seo, M. S.; Lee, Y.-M.; Kim, Y.; Kim, S.-J.; Choi, Y. S.; Jang, H. G.; Nam, W. *Inorg. Chim. Acta* **2009**, *362*, 1031.

(41) Ye, W.; Staples, R. J.; Rybak-Akimova, E. V. *Journal of Inorganic Biochemistry* **2012**, *115*, 1.

(42) Park, J.; Lee, Y.-M.; Ohkubo, K.; Nam, W.; Fukuzumi, S. *Inorganic Chemistry* **2015**, *54*, 5806.

(43) Zhang, X.; Furutachi, H.; Tojo, T.; Tsugawa, T.; Fujinami, S.; Sakurai, T.; Suzuki, M. *Chem. Lett.* **2011**, *40*, 515.

(44) Oloo, W. N.; Meier, K. K.; Wang, Y.; Shaik, S.; Münck, E.; Que, L. *Nat. Commun.* **2014**, *5*.

(45) Makhlynets, O. V.; Oloo, W. N.; Moroz, Y. S.; Belaya, I. G.; Palluccio, T. D.; Filatov, A. S.; Muller, P.; Cranswick, M. A.; Que, L.; Rybak-Akimova, E. V. *Chem. Commun.* **2014**, *50*, 645.

(46) Khusnutdinova, J. R.; Luo, J.; Rath, N. P.; Mirica, L. M. *Inorg. Chem.* **2013**, *52*, 3920.

(47) Guisado-Barrios, G.; Zhang, Y.; Harkins, A. M.; Richens, D. T. *Inorg. Chem. Commun.* **2012**, *20*, 81.

(48) Oloo, W. N.; Meier, K. K.; Wang, Y.; Shaik, S.; Münck, E.; Que, L. *Nat. Commun.* **2014**, *5*, 4046.

(49) Roelfes, G.; Vrajmasu, V.; Chen, K.; Ho, R. Y. N.; Rohde, J.-U.; Zondervan, C.; la Crois, R. M.; Schudde, E. P.; Lutz, M.; Spek, A. L.; Hage, R.; Feringa, B. L.; Münck, E.; Que, L. *Inorg. Chem.* **2003**, *42*, 2639.

(50) Taylor, C. P. S. *BBA Protein Struct.* **1977**, *491*, 137.

(51) McGarvey, B. R. *Coord Chem. Rev.* **1998**, *170*, 75.

(52) de Oliveira, F. T.; Chanda, A.; Banerjee, D.; Shan, X.; Mondal, S.; Que, L.; Bominaar, E. L.; Münck, E.; Collins, T. J. *Science* **2007**, *315*, 835.

(53) Ghosh, M.; Singh, K. K.; Panda, C.; Weitz, A.; Hendrich, M. P.; Collins, T. J.; Dhar, B. B.; Gupta, S. S. *J. Am. Chem. Soc.* **2014**, *136*, 9524.

(54) Van Heuvelen, K. M.; Fiedler, A. T.; Shan, X.; De Hont , R. F.; Meier, K. K.; Bominaar, E. L.; Münck, E.; Que, J. L. *Proc. Natl. Acad. Sci. USA* **2012**, *109*, 11933.

(55) Lyakin, O. Y.; Zima, A. M.; Samsonenko, D. G.; Bryliakov, K. P.; Talsi, E. P. *ACS Catal.* **2015**, *5*, 2702.

(56) Tse, C.-W.; Chow, T. W.-S.; Guo, Z.; Lee, H. K.; Huang, J.-S.; Che, C.-M. *Angewandte Chemie International Edition* **2014**, *53*, 798.

(57) McGown, A. J.; Kerber, W. D.; Fujii, H.; Goldberg, D. P. *Journal of the American Chemical Society* **2009**, *131*, 8040.

(58) Leeladee, P.; Jameson, G. N. L.; Siegler, M. A.; Kumar, D.; de Visser, S. P.; Goldberg, D. P. *Inorganic Chemistry* **2013**, *52*, 4668.

(59) Schulz, C. E.; Rutter, R.; Sage, J. T.; Debrunner, P. G.; Hager, L. P. *Biochemistry* **1984**, *23*, 4743.

(60) Rittle, J.; Green, M. T. *Science* **2010**, *330*, 933.

(61) Mas-Balleste, R.; Fujita, M.; Que, J. L. *Dalton Trans.* **2008**, 1828.

(62) Iyer, S. R.; Javadi, M. M.; Feng, Y.; Hyun, M. Y.; Oloo, W. N.; Kim, C.; Que, L. *Chem. Commun.* **2014**, *50*, 13777.

(63) Nam, W.; Han, H. J.; Oh, S.-Y.; Lee, Y. J.; Choi, M.-H.; Han, S.-Y.; Kim, C.; Woo, S. K.; Shin, W. *J. Am. Chem. Soc.* **2000**, *122*, 8677.

(64) Denisov, I. G.; Makris, T. M.; Sligar, S. G.; Schlichting, I. *Chem. Rev.* **2005**, *105*, 2253.

(65) Company, A.; Lloret-Fillol, J.; Costas, M. In *Comprehensive Inorganic Chemistry II (Second Edition)*; Elsevier: Amsterdam, 2013, p 487.

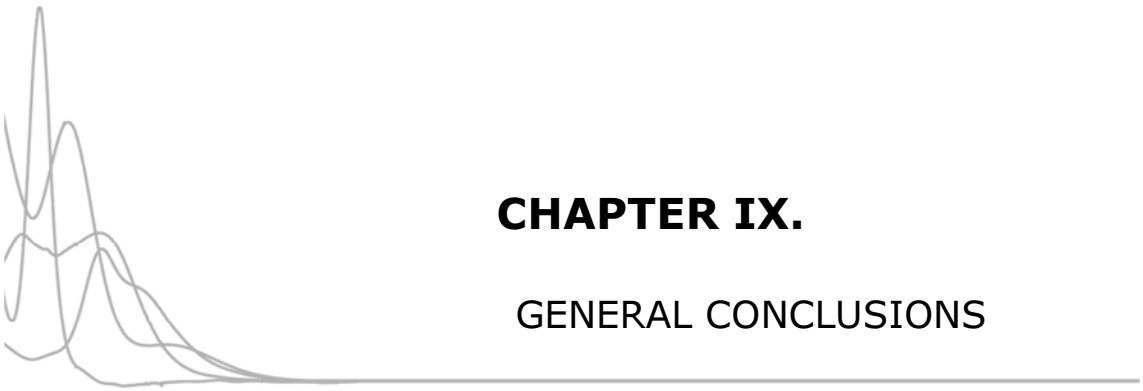

CHAPTER IX.

GENERAL CONCLUSIONS

IX. GENERAL CONCLUSIONS

The activation of small molecules, especially O_2, has been a topic of interest over the last decades. Many synthetic models of enzymes have been developed in order to understand how natural systems use O_2 to perform highly effective selective oxidations. Most efforts have been directed towards the investigation of iron and copper complexes because these are the two prevalent metals found in O_2-activating enzymes.

The active site of copper-based enzymes that are capable of activating O_2 often present an unsymmetric active site. Inspired on that idea, **Chapter III** is focused on the development of a novel dinucleating unsymmetric ligand scaffold. This nitrogen-based ligand bears two markedly distinct coordination sites. We have prepared the dicopper(I) complex and studied its reactivity towards O_2 at cryogenic temperatures. Two different intermediate species, formed between two copper centers in the same coordination environment from different complex molecules, have been characterized. More interestingly, the unsymmetry of the ligand has allowed us to prepare different copper-based heterodimetallic complexes. In this case, site selective metalation is observed, being the site dependent on the nature of the metal ion and ligand site denticity. These heterometallic complexes react with O_2 at low temperatures forming exclusively only one of the two copper-dioxygen species observed for the dicopper complex. Remarkably, the nature of the complementary metal used for the synthesis of the heterodimetallic complex is crucial in order to determine the site where the copper is bound and thus the formed species after reaction with O_2.

In **Chapter IV** we turned our attention towards the development of reactivity never observed before for Cu_2O_2 species. Our group reported in 2008 a copper complex that served as a tyrosinase model, as it was capable of *ortho*-hydroxylating phenols to the corresponding catechol using O_2 as sacrificial oxidant. A high valent bis(μ-oxo)dicopper(III) species was responsible for the oxidation. In this thesis we have shown that indeed such intermediate species is not only capable of hydroxylation aromatic C-H bonds but can also defluorinate and hydroxylate aromatic C-F bonds, which constitutes a much more challenging reaction because of the bond strength of the latter. Interestingly, the reaction is selective for the cleavage of C-F bonds when a second substituent X, which a priori forms a weaker C-X bond, is present in the other equivalent *ortho* position of the phenol ring.

In **Chapters V**, **VI** and **VII** we have turned our attention in studying a novel iron-based model for mimicking the oxygenating species of nonheme iron enzymes (e.g. Rieske oxygenases).

In **Chapter V and VI** we have shown that reaction of a new ferrous complex with peracetic acid at low temperatures gives raise to the formation of a metastable species. This species is competent for the oxidation of alkanes with strong C-H bonds with stereoretention and it exhibits

the fastest rates reported so far for the oxidation of cyclohexane among previously reported iron-oxygen compounds. Additionally, this compound performs fast oxygen atom transfer towards olefinic substrates. Very interestingly, we have observed that the kinetic behavior towards alkenes matches the catalytic behavior observed upon mixing the iron(II) precursor and peracetic acid, meaning that the trapped compound is indeed the true competent oxidant species along the catalytic cycle. Spectroscopic characterization points towards the generation of an acylperoxoiron(III) after reaction of peracetic acid and the ferrous precursor. This compound undergoes O-O bond cleavage to generate a high valent electromer oxoiron species that is the final executor of the oxidative transformation. The formation of such high valent oxoiron species has been proposed in the catalytic cycle of nonheme iron complexes, even though its detection and characterization had remained elusive so far. Very remarkably, the work detailed in **Chapters V** and **VI** constitutes the first example in which such species has been spectroscopically trapped and directly interrogated by kinetic methods.

In **Chapter VII** the reactivity of the same ferrous precursor towards hydrogen peroxide has been studied. A metastable compound has been trapped and fully characterized as an hydroperoxoiron(III) by comparison with previously reported examples that show similar spectroscopic features (including UV-vis, EPR, rRaman). This compound was kinetically not competent for the oxidation of strong C-H bonds, and most likely the observed oxidation chemistry derives from free diffusing hydroxyl radicals generated along the decay of the hydroperoxoiron(III). Interestingly, the addition of stoichiometric amounts of triflic acid caused the immediate bleaching of the visible features of the latter. The reactivity observed after the addition of the acid is markedly different and points towards the involvement of a selective metal-based oxidant. Most probably, proton addition assists O-O cleavage and leads to the formation of a high-valent oxoiron species responsible for the observed chemistry, in a process similar to that observed in heme and non-heme iron enzymes.

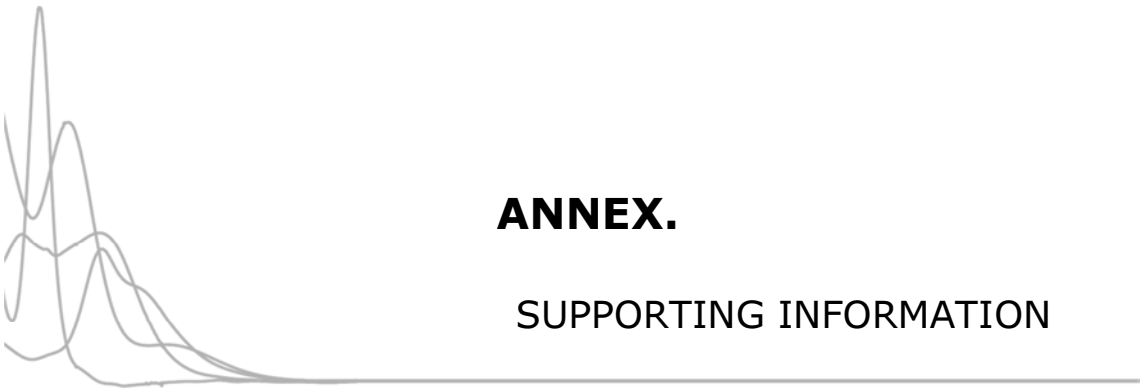

ANNEX.

SUPPORTING INFORMATION

LIGAND NOMENCLATURE FOR CHAPTER I

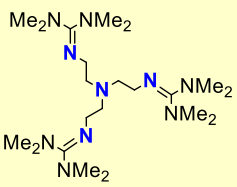

1

(TMG$_3$tren)

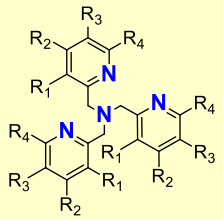

$R_1 = R_2 = R_3 = R_4 = H$ **2**
$R_1 = R_2 = R_3 = H$, $R_4 = CH_3$ **2^{6Me}**
$R_1 = R_2 = R_4 = H$, $R_3 = CH_3$ **2^{5Me}**
$R_1 = R_3 = CH3$, $R_2 = OCH_3$, $R_4 = H$ **2***

(TPA)

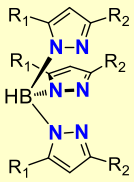

$R_1 = R_2 = i$Pr **3^{iPr}**
$R_1 = CH_3$, $R_2 = Ph$ **3^{Me,Ph}**

(Tp)

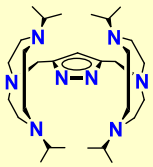

4

(HLPzTACN)

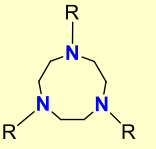

R = benzyl **5^{Bz}**
R = Me **5^{Me}**
R = iPr **5^{iPr}**

(R_3tacn)

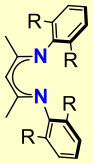

R = iPr **6^{iPr}**
R = Me **6^{Me}**

(NacNac, HMe_2L^{R2})

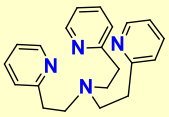

7

(TEPA)

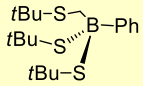

8

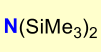

9

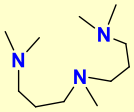

10

11

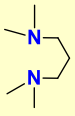

12

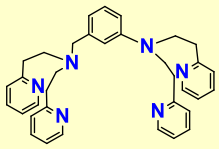

13

(UN)

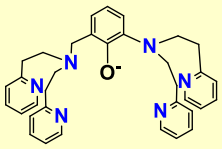

14

(UNO$^-$)

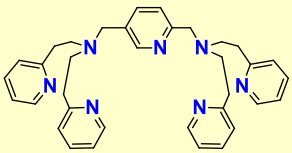

15

(PyPye2)

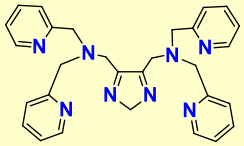

16

(bdpi)

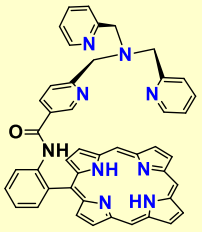

17

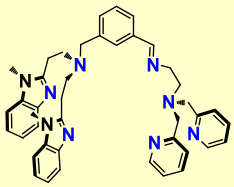

18

(*m*-XYL^{N3N4})

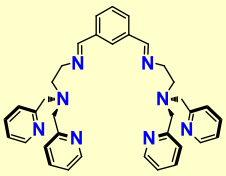

19

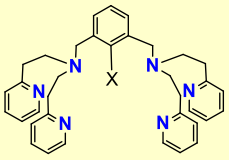

X = H **20^{H}**
X = Cl **20^{Cl}**
X = F **20^{F}**

(XYL-X)

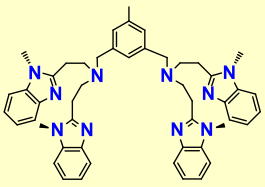

21

(MeL66)

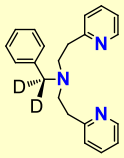

22

(L^{Py2Bz})

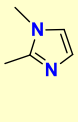

23

(Im)

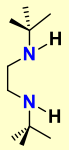

24

(DBED)

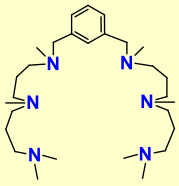

25

(*m*-XYL^{MeAN})

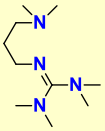

26

(L^{AG})

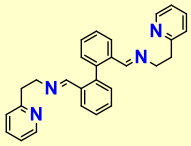

27

(BiPh-(impy)$_2$)

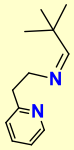

28

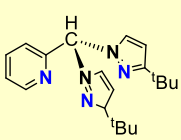

29

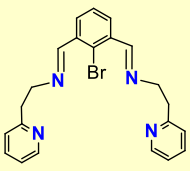

30

(2,6-BPB-1-Br)

LIGAND NOMENCLATURE FOR CHAPTER I

(CONTINUATION)

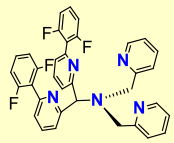

31

(N_4Py^{2PhF2})

32

(F_2ArPz)

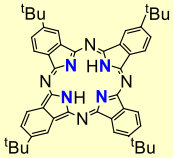

33

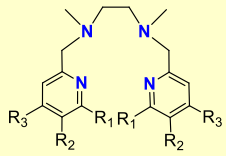

$R_1 = R_2 = R_3 =$ H **34**

$R_1 = CH_3$, $R_2 = R_3 =$ H **34^{6Me}**

$R_1 = R_3 = CH_3$, $R_2 = OCH_3$ **34***

(BPMEN)

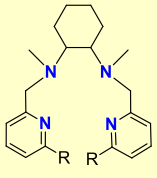

R = H **35**

R = CH_3 **35^{6Me}**

(BPMCN)

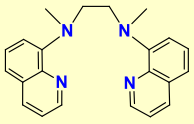

36

(bqen)

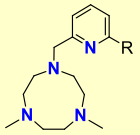

R = H **37**

R = CH_3 **37^{6Me}**

(Pytacn)

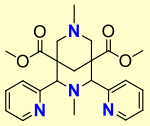

38

(N_2Py_2)

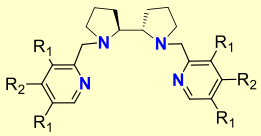

$R_1 = R_2 =$ H **39**

$R_1 =$ H, $R_2 = N(CH_3)_2$ **39^{NMe2}**

$R_1 = CH_3$, $R_2 = OCH_3$ **39***

(pdp)

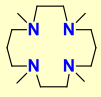

40

(TMC)

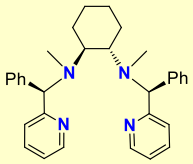

41

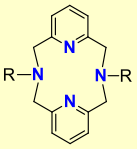

R = Me **42^{Me}**

R = *t*Bu **42^{tBu}**

(L-N_4Me_2 and $^{tBu}N_4$)

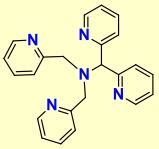

43

(N4Py)

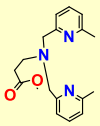

44

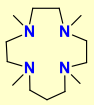

45

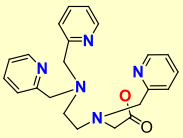

46

(13-TMC)

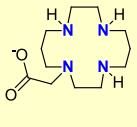

47

(cyclam-acetate)

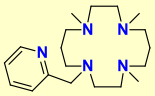

48

(TMC-Py)

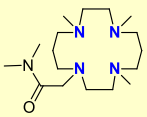

49

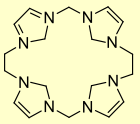

50

(L^{NHC})

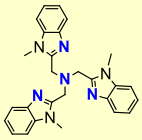

51

(Me3NTB)

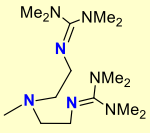

52

(TMG_2dien)

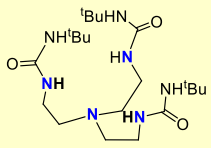

53

(H_3buea)

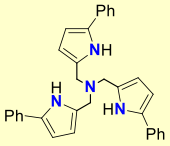

54

(tpa^{Ph})

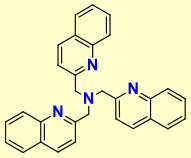

55

(TQA)

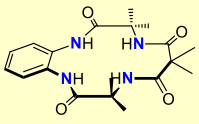

56

(TAML)

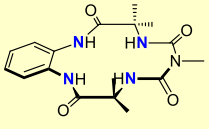

57

(bTAML)

LIGAND NOMENCLATURE FOR CHAPTER VIII

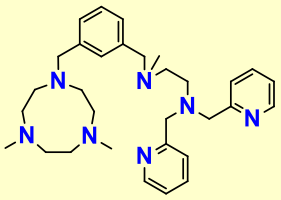

1
L^{N3N4}

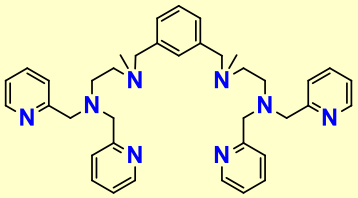

2
L^{N4N4}

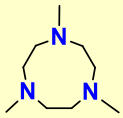

3
Me_3tacn

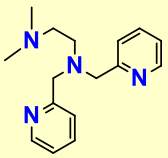

4
uns-penp

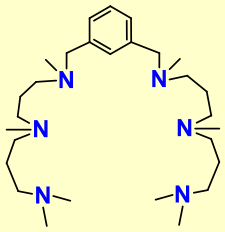

5
(*m*-XYL^{MeAN})

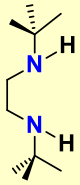

6
(DBED)

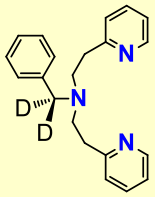

7
(L^{Py2Bz})

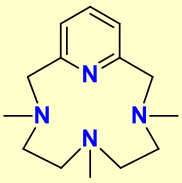

8
($PyNMe_3$)

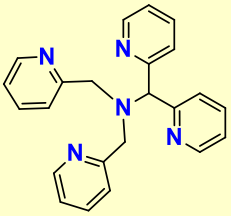

9
(N4Py)

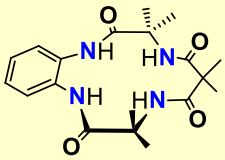

10
(TAML)

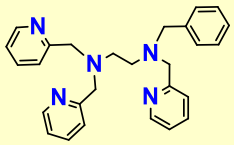

11
(BzTPEN)

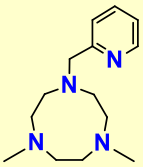

12
(Pytacn)

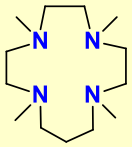

13
(13-TMC)

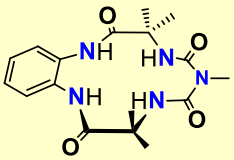

14
(bTAML)

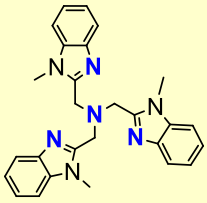

15
(Me_3NTB)

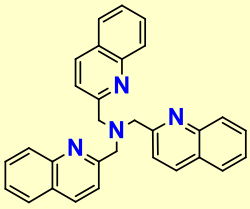

16
(TQA)

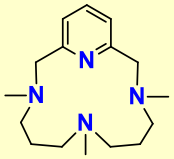

17

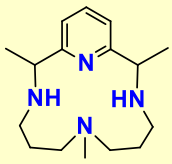

18

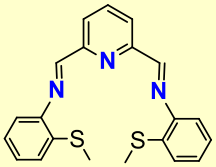

19

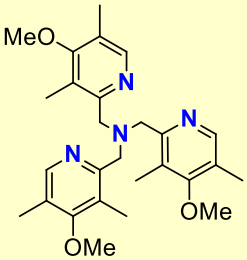

20
(TPA*)

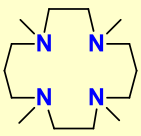

21
(TMC)

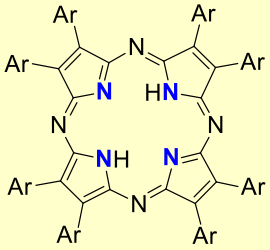

22
(TBP_8Cz)

Supporting Information Chapter III

Building complexity in O_2-binding Copper Complexes. Site-selective Metallation and Intermolecular O_2-Binding at Dicopper and Heterometallic Complexes Derived from an Unsymmetric Ligand

Synthesis of L^{N4N4}

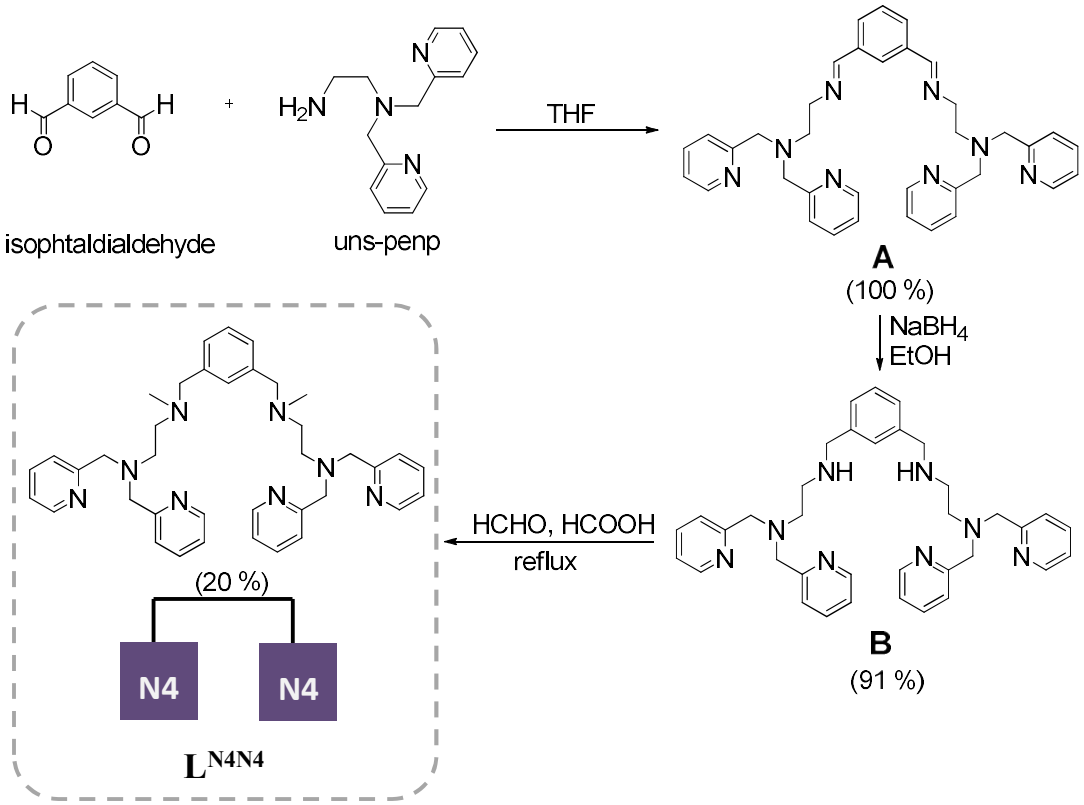

Scheme S1 Synthetic route towards the preparation of L^{N4N4}.

Synthesis of A: uns-penp (960 mg, 3.9 mmols) was dissolved in THF (15 mL) and cooled down to 0ºC. A solution of isophtaldialdehyde (266 mg, 1.9 mmols) in THF (5 mL) was added dropwise. The mixture was left to attain room temperature and it was stirred for 15 hours. The solvent was removed under reduced pressure and 1.4 g (2.4 mmols, >100%) of a pale yellow oil were obtained and used in the next step without further purification. ^{1}H-NMR ($CDCl_3$, 400 MHz, 298K) δ, ppm: 8.50 (d, J=4.0 Hz, 4H, $\mathbf{H_a}$), 8.31 (s, 2H, $\mathbf{H_h}$), 8.00 (s, 1H, $\mathbf{H_i}$), 7.77 (d, J=7.5, 2H, $\mathbf{H_j}$), 7.61-7.50 (m, 8H, $\mathbf{H_c}$+$\mathbf{H_d}$), 7.45 (t, J=7.6 Hz, 1H, $\mathbf{H_k}$), 7.10 (td, J=4.0 Hz, J'=1.5 Hz, 4H, $\mathbf{H_b}$), 3.93 (s, 8H, $\mathbf{H_e}$), 3.82 (t, J=6.6 Hz, 4H, $\mathbf{H_g}$), 2.97 (t, J=6.6 Hz, 4H, $\mathbf{H_f}$).

Synthesis of B: A (1.4 g, 2.4 mmols) was dissolved in absolute ethanol (40 mL) and sodium borohydride (0.2 g, 5.2 mmols) was added as a solid in little portions. The reaction was stirred for 12 hours at room temperature and then 10 mL of water were added to remove the unreacted $NaBH_4$. After removal of the solvent under reduced pressure, CH_2Cl_2 (15 mL) and H_2O (4 mL) were added. The mixture was treated with CH_2Cl_2 (2x8 mL). The organic layers were dried over $MgSO_4$ and the solvent was removed under reduced pressure to obtain 1.32 g (2.2 mmols, 91%) of a pale yellow oil. ^{1}H-NMR ($CDCl_3$, 400 MHz, 298K) δ, ppm: 8.51 (d, J=4.8 Hz, 4H, $\mathbf{H_a}$), 7.61 (td, J=7.8 Hz, J'=1.8 Hz, 4H, $\mathbf{H_c}$), 7.45 (d, J=7.8 Hz, 4H, $\mathbf{H_d}$), 7.23-7.10 (m, 8H, $\mathbf{H_b}$+$\mathbf{H_i}$+$\mathbf{H_k}$+$\mathbf{H_j}$), 3.82 (s, 8H, $\mathbf{H_e}$), 3.62 (s, 4H, $\mathbf{H_h}$), 2.75-2.72 (m, 8H, $\mathbf{H_f}$+$\mathbf{H_g}$). ^{13}C-NMR ($CDCl_3$, 100 MHz, 298K) δ, ppm: 159.67 ($\mathbf{C_E}$), 149.09 ($\mathbf{C_A}$), 136.38 ($\mathbf{C_C}$), 126.51 ($\mathbf{C_J}$), 122.94 ($\mathbf{C_K}$), 121.96 ($\mathbf{C_M}$), 122.94 ($\mathbf{C_D}$), 121.96 ($\mathbf{C_B}$), 60.71 ($\mathbf{C_F}$), 54.09 ($\mathbf{C_G}$), 53.77 ($\mathbf{C_i}$), 46.75 ($\mathbf{C_H}$). ESI-MS (m/z)= 587.4 $[M+H]^+$, 294.2 $[M+2H]^{2+}$

Synthesis of L^{N4N4}: B (1.32 g, 2.2 mmols) was dissolved in formic acid 98% (34 mL), formaldehyde 37% (18 mL) was added and the mixture was refluxed for 24 h. The solvent was then removed under reduced pressure and NaOH 3M (10 mL) was added to the resultant yellow solid. The product was extracted with CH_2Cl_2 (3 x 50 mL). The organic phases were dried over $MgSO_4$ and the solvent was removed under reduced pressure. The resulting yellow oil was purified by column chromatography over silica using a mixture of CH_2Cl_2:MeOH:NH_3 85:15:2 as eluent. 260 mg (0.43 mmols, 20 %) of a yellow

oil were obtained. ^{1}H-NMR ($CDCl_3$, 400 MHz, 298K) δ, ppm: 8.50 (d, J=4.8 Hz, 4H, $\mathbf{H_a}$), 7.60 (td, J=7.9 Hz, J'=2.0 Hz, 4H, $\mathbf{H_c}$), 7.50 (d, J=7.9 Hz, 4H, $\mathbf{H_d}$), 7.16-7.10 (m, 8H, $\mathbf{H_b}$+$\mathbf{H_i}$+$\mathbf{H_j}$+$\mathbf{H_k}$), 3.83 (s, 8H, $\mathbf{H_e}$), 3.40 (s, 4H, $\mathbf{H_h}$), 2.73 (t, J= 6.5 Hz, 4H, $\mathbf{H_f}$), 2.57 (t, J= 6.5 Hz, 4H, $\mathbf{H_g}$), 2.09 (s, 6H, $\mathbf{H_l}$). ^{13}C-NMR ($CDCl_3$, 100 MHz, 298K) δ, ppm: 159.81 ($\mathbf{C_E}$), 148.98 ($\mathbf{C_A}$), 136.37 ($\mathbf{C_C}$), 129.78, 128.15, 127.86 ($\mathbf{C_K}$, $\mathbf{C_M}$, $\mathbf{C_J}$), 122.91 ($\mathbf{C_D}$), 121.91 ($\mathbf{C_B}$), 62.39 ($\mathbf{C_I}$), 60.74 ($\mathbf{C_F}$), 55.33 ($\mathbf{C_G}$), 51.99 ($\mathbf{C_H}$), 42.33 ($\mathbf{C_N}$). HR-MS (ESI-TOF, $[M+Na]^+$) *m/z* calc. for $[C_{38}H_{47}N_8]^+$ 615.3918 found 516.3955; $[C_{38}H_{46}N_8Na]^+$ 637.3738 found 637.3764

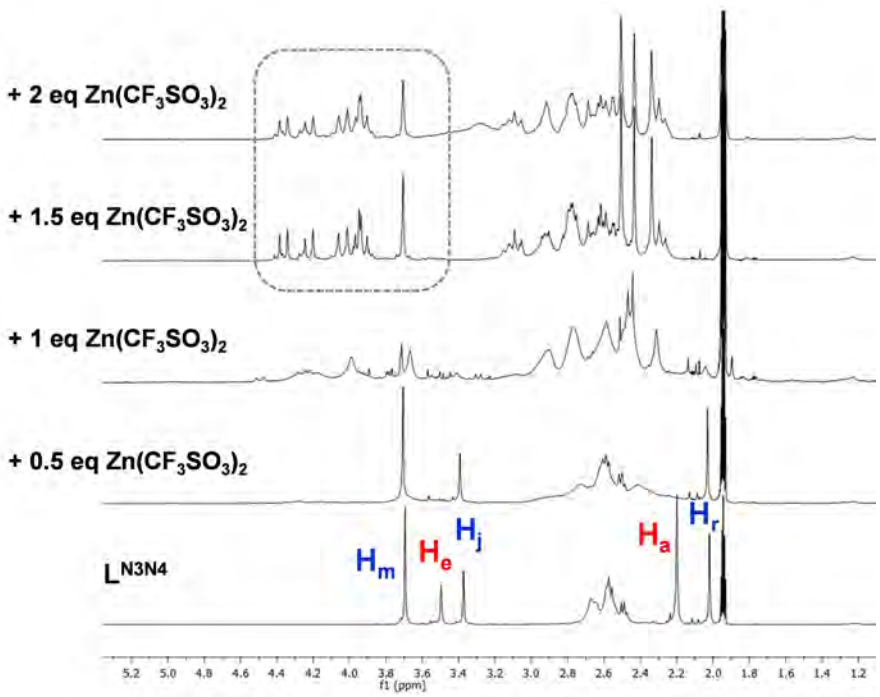

Figure S1 Aliphatic region of the ^{1}H-NMR monitored (see Figure 1 for the aromatic region) titration of L^{N3N4} with $Zn^{II}(CF_3SO_3)_2$ in acetone-d_6 at 240 K. Protons in blue ($\mathbf{H_m}$, $\mathbf{H_j}$ and $\mathbf{H_r}$) are located around the N_4 site and the red ones ($\mathbf{H_a}$ and $\mathbf{H_e}$) belong to the N_3 triazacyclonane ring site of L^{N3N4}. $\mathbf{H_a}$ and $\mathbf{H_e}$, which are assigned to N_{tacn}-C$\mathbf{H}_3$ and benzylic protons respectively (see Scheme S2), readily disappear upon addition of 0.5 equiv $Zn^{II}(CF_3SO_3)_2$, while $\mathbf{H_m}$, $\mathbf{H_j}$ and $\mathbf{H_r}$ can still be identified at that point. The NMR shows severe broadening upon addition of 1 equiv of $Zn^{II}(CF_3SO_3)_2$. However, when more than 1 equiv is added sharp signals in the 4.5-3.8 ppm region are clearly observed.

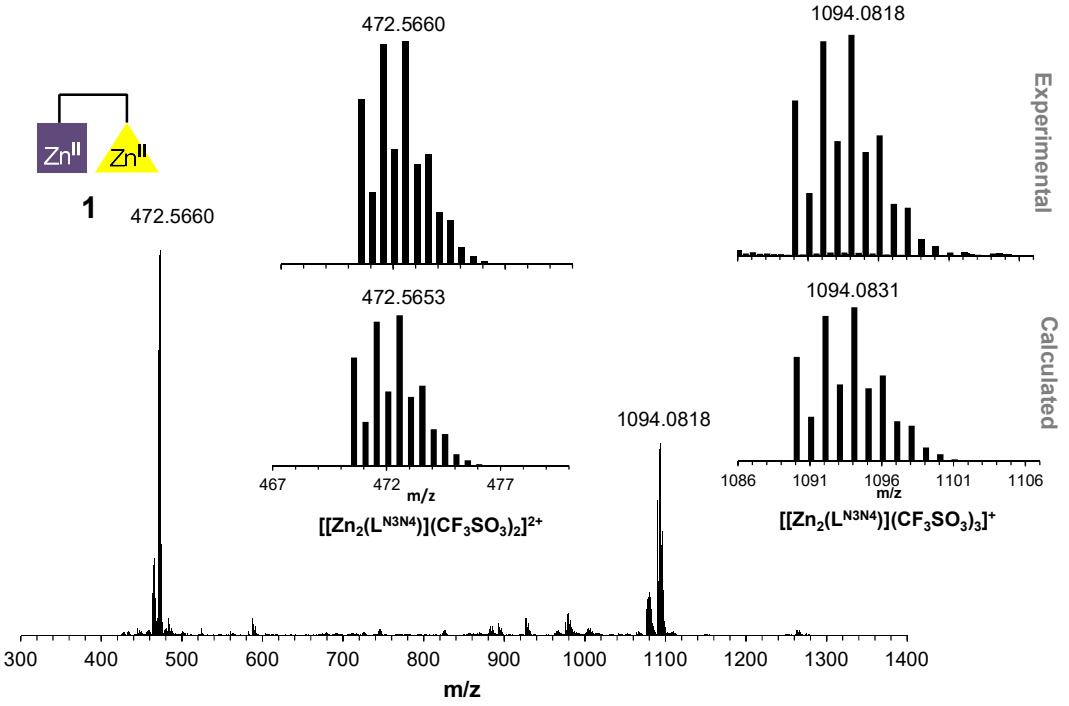

Figure S2 HR-MS spectrum of **1** ($C_{31}H_{45}N_7 = L^{N3N4}$).

HR-MS (*m/z*): calc. for $[[Zn_2(L^{N3N4})](CF_3SO_3)_2]^{2+}$ 472.5653, found 472.5660; calc. for $[[Zn_2(L^{N3N4})](CF_3SO_3)_3]^{+}$ 1094.0831, found 1094.0818.

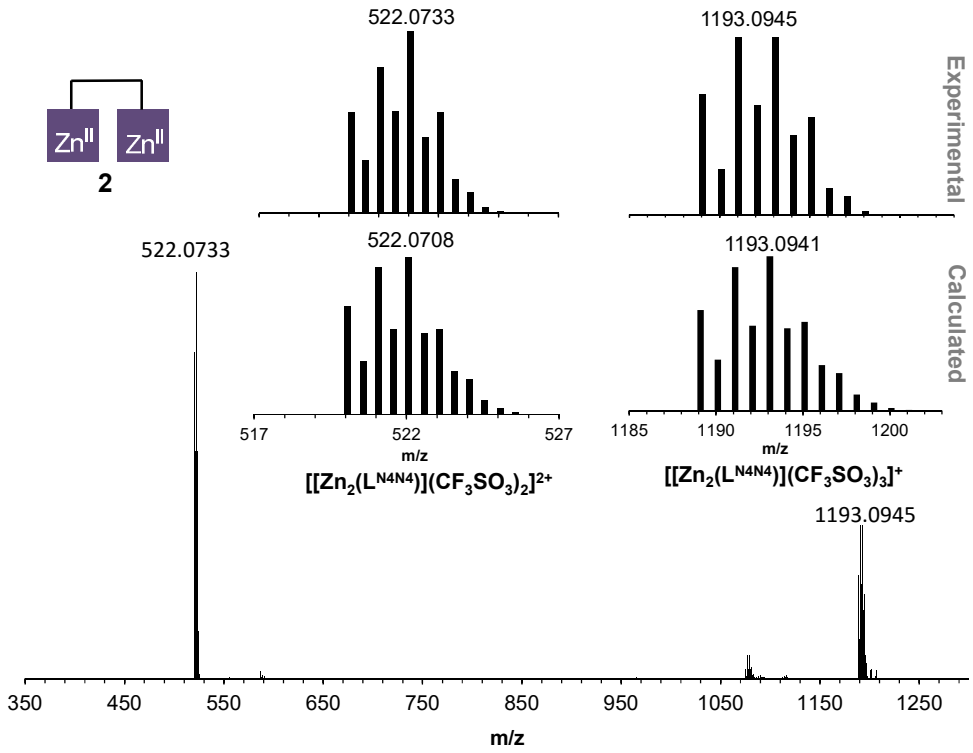

Figure S3 HR-MS spectrum of **2** ($L^{N4N4} = C_{38}H_{46}N_8$).

HR-MS (*m/z*): calc. for $[[Zn_2(L^{N4N4})](CF_3SO_3)_2]^{2+}$ 522.0708, found 522.0733; calc. for $[[Zn_2(L^{N4N4})](CF_3SO_3)_3]^{+}$ 1193.0941, found 1193.0945.

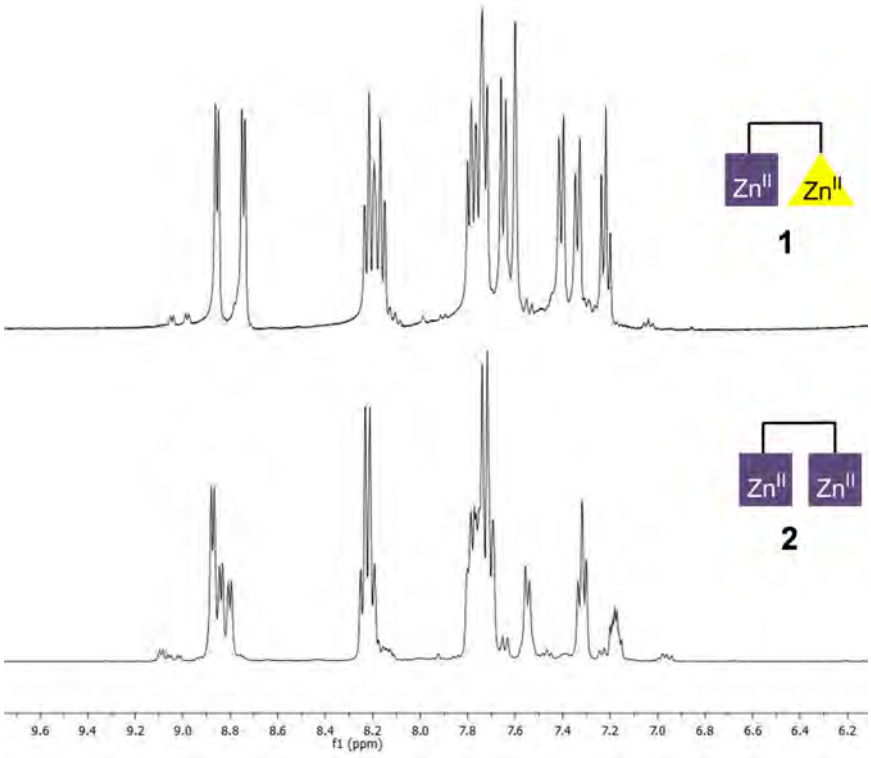

Figure S4 Comparison between the aromatic region of the ^{1}H-NMR spectrum of **1** and **2** in acetone-d_6 at 240K.

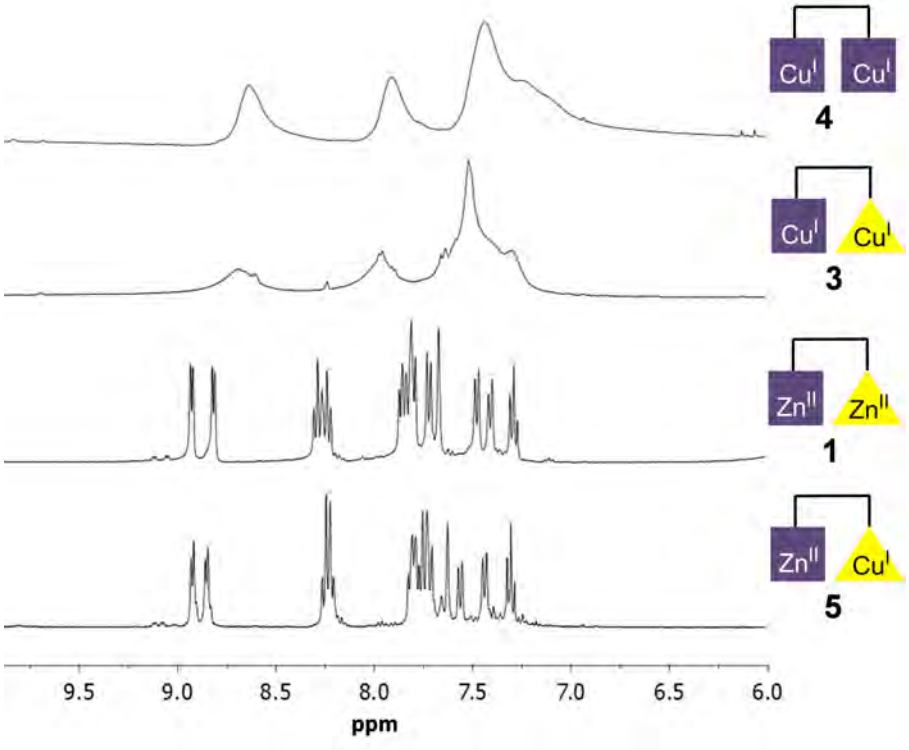

Figure S5 Comparison between the aromatic region of the ^{1}H-NMR spectra of **1**, **3**, **4** and **5** in acetonitrile-d_3:acetone-d_6 1:5 at 240 K. When Cu^{I} is located in the N_4 site broad signals are observed, while sharp signals arise when Zn^{II} is coordinated to this site.

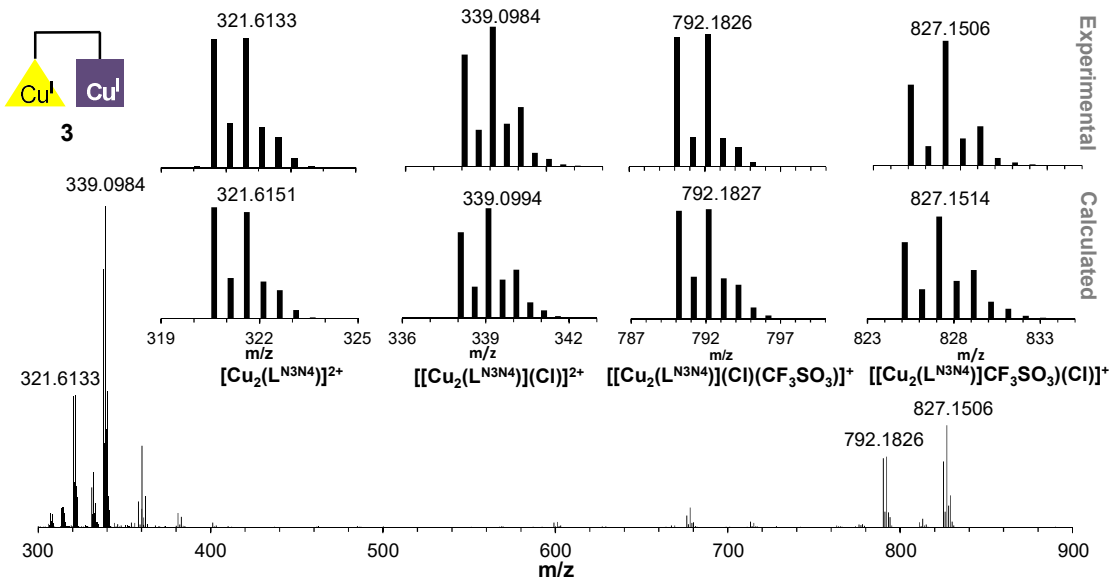

Figure S6 HR-MS spectrum of **3** ($L^{N3N4} = C_{31}H_{45}N_7$).

HR-MS (*m/z*): calc. for $[Cu_2(L^{N3N4})]^{2+}$ 321.6151, found 321.6133; calc. for $[[Cu_2(L^{N3N4})](Cl)]^{2+}$ 339.0994, found 339.0984; calc. for $[[Cu_2(L^{N3N4})](CF_3SO_3)]^{+}$ 792.1827, found 792.1826; calc. for $[[Cu_2(L^{N3N4})](CF_3SO_3)Cl_2]^{+}$ 827.1514, found 827.1506.

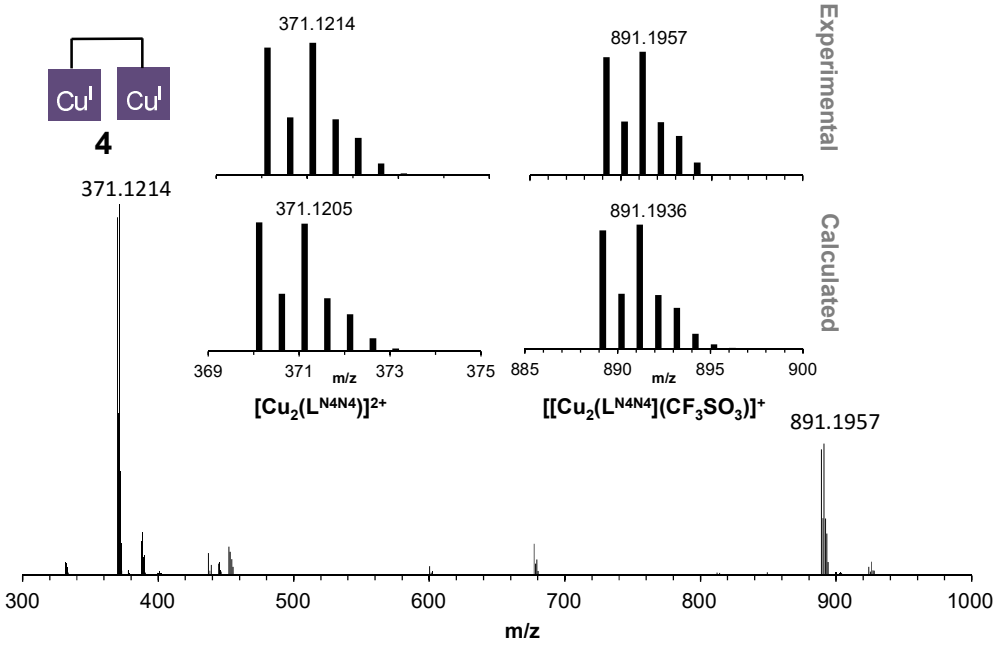

Figure S7 HR-MS spectrum of **4** ($L^{N4N4} = C_{38}H_{46}N_8$).

HR-MS (*m/z*): calc. for $[Cu_2(L^{N4N4})]^{2+}$ 371.1205, found 371.1214; calc. for $[[Cu_2(L^{N4N4})](CF_3SO_3)]^{+}$ 891.1936, found 891.1957.

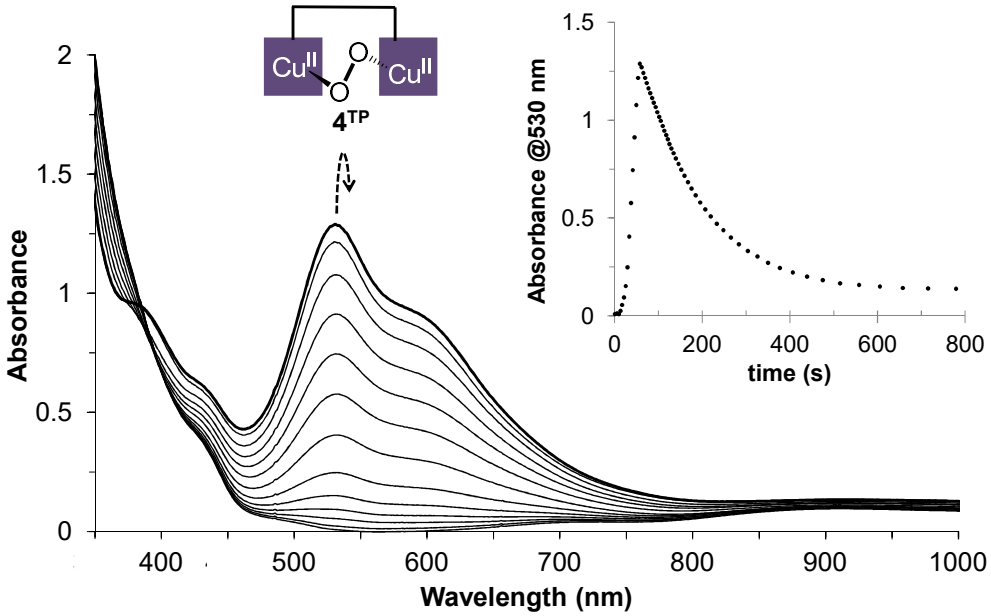

Figure S8 UV-Vis absorption spectra for the reaction of $[Cu^{I}_{2}(L^{N4N4})]^{2+}$ (**4**) (0.6 mM) and O_2 at -90°C in acetonitrile:acetone 1:19. Inset: Kinetic trace at 530 nm ($\mathbf{4}^{TP}$).

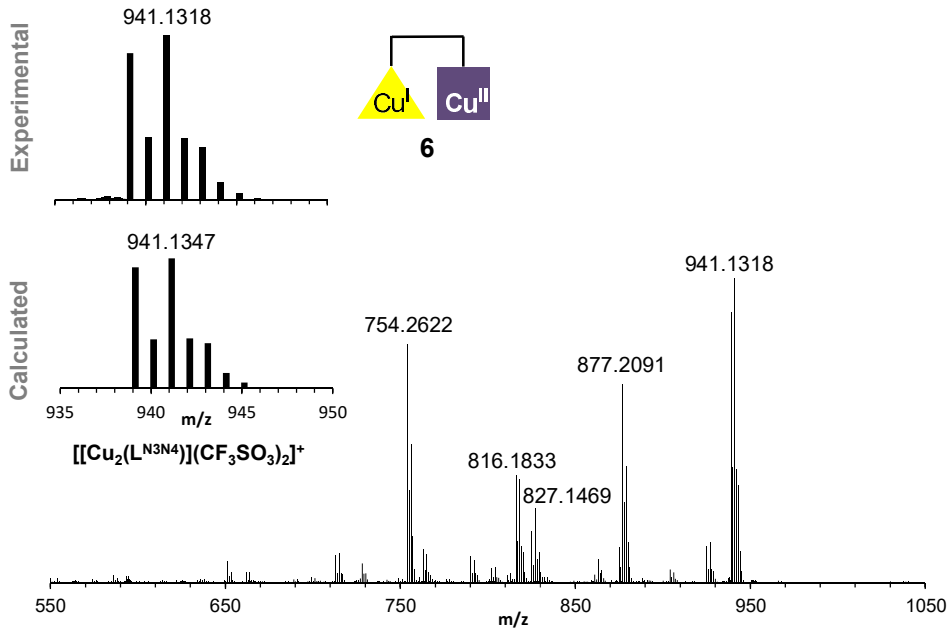

Figure S9 HR-MS spectrum of **6** ($L^{N3N4} = C_{31}H_{45}N_7$).

HR-MS (*m/z*): calc. for $[[Cu(L^{N3N4})](CF_3SO_3)(CN)(H)]^+$ 754.2656, found 754.2622; calc. for $[[Cu_2(L^{N3N4})](CF_3SO_3)CN]^+$ 816.1874, found 816.1833; calc. for $[[Cu(L^{N3N4})](CF_3SO_3)(Cl)]^+$ 827.1514, found 827.1469; calc. for $[[Cu(L^{N3N4})](CF_3SO_3)_2(H)]^+$ 877.2146, found 877.2091; calc. for $[[Cu_2(L^{N3N4})](CF_3SO_3)_2]^+$ 941.1347, found 941.1318.

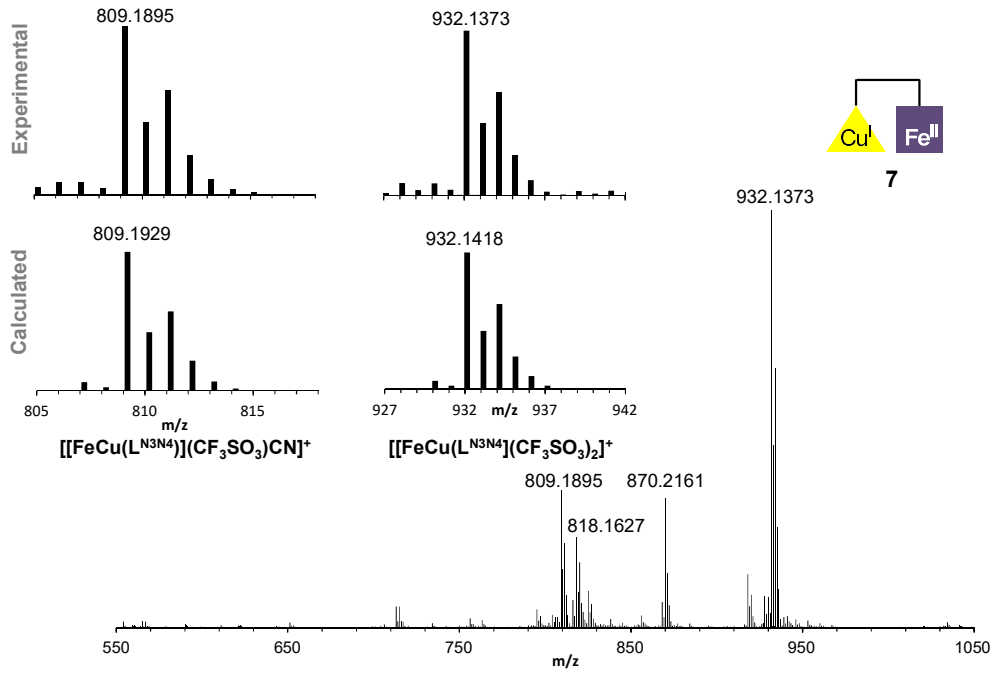

Figure S10 HR-MS spectrum of **7** ($L^{N3N4} = C_{31}H_{45}N_7$).

HR-MS (*m/z*): calc. for $[[FeCu(L^{N3N4})](CF_3SO_3)CN]^+$ 809.1929, found 809.1895; calc. for $[[FeCu(L^{N3N4})](CF_3SO_3)(Cl)]^+$ 818.1587, found 818.1627; calc. for $[[Fe(L^{N3N4})](CF_3SO_3)_2H]^+$ 870.2200, found 870.2161; calc. for $[[FeCu(L^{N3N4})](CF_3SO_3)_2]^+$ 932.1418, found 932.1373.

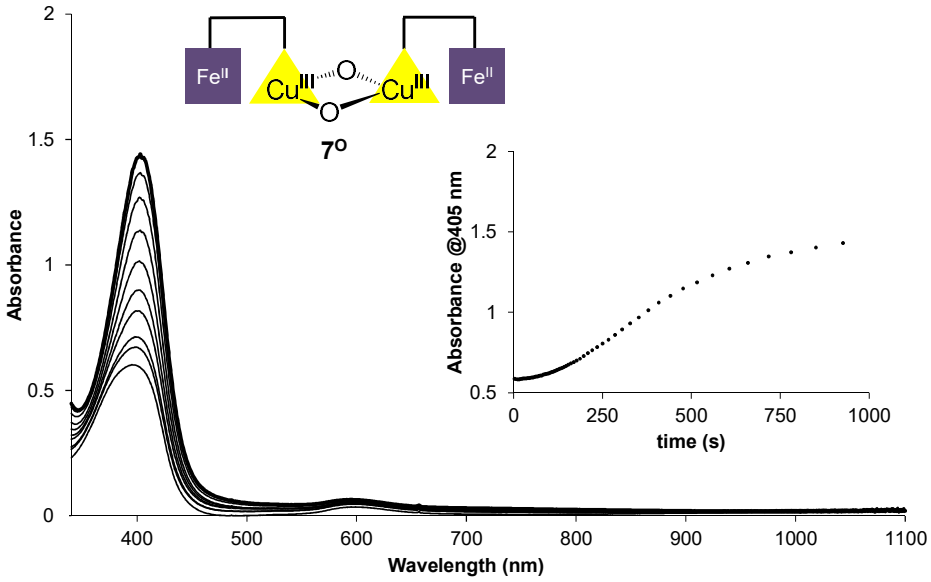

Figure S11 UV-Vis absorption spectra for the reaction of $[Cu^IFe^{II}(L^{N3N4})]^{3+}$ (**7**) (0.25 mM) and O_2 at -90°C in acetonitrile:acetone 1:19. Inset: time trace at 405 nm ($\mathbf{7^O}$).

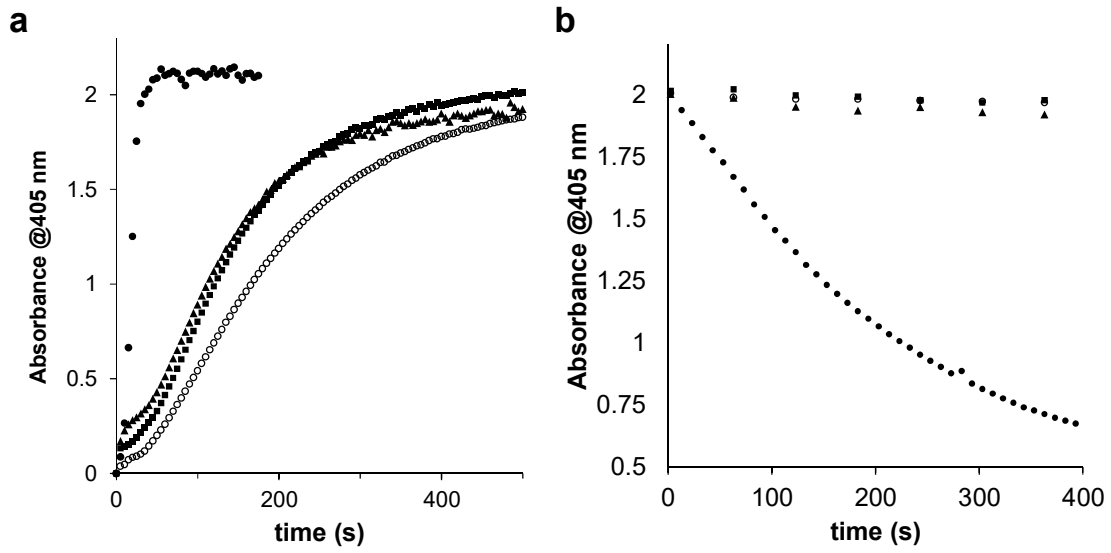

Figure S12. a) Normalized time trace at 405 nm for the formation of $\mathbf{3}^{O}$ (dots), $\mathbf{5}^{O}$ (circles), $\mathbf{6}^{O}$ (squares) and $\mathbf{7}^{O}$ (triangles) upon reaction of **3**, **5**, **6** or **7** with O_2 in acetonitrile:acetone 1:19 at -75ºC. Compounds $\mathbf{5}^{O}$, $\mathbf{6}^{O}$ and $\mathbf{7}^{O}$ reach full formation after 10 min at -75ºC. In sharp contrast, formation of $\mathbf{3}^{O}$ is much faster and maximum absorbance is achieved only after 1 min at -75ºC. b) Normalized time trace at 405 nm for the decay of $\mathbf{3}^{O}$ (dots), $\mathbf{5}^{O}$ (circles), $\mathbf{6}^{O}$ (squares) and $\mathbf{7}^{O}$ (triangles) in acetonitrile:acetone 1:19 at -60ºC. While for $\mathbf{5}^{O}$, $\mathbf{6}^{O}$ and $\mathbf{7}^{O}$ only 15% decomposition is observed after 2 h at -60ºC, UV-vis features of $\mathbf{3}^{O}$ are completely depleted after 20 min.

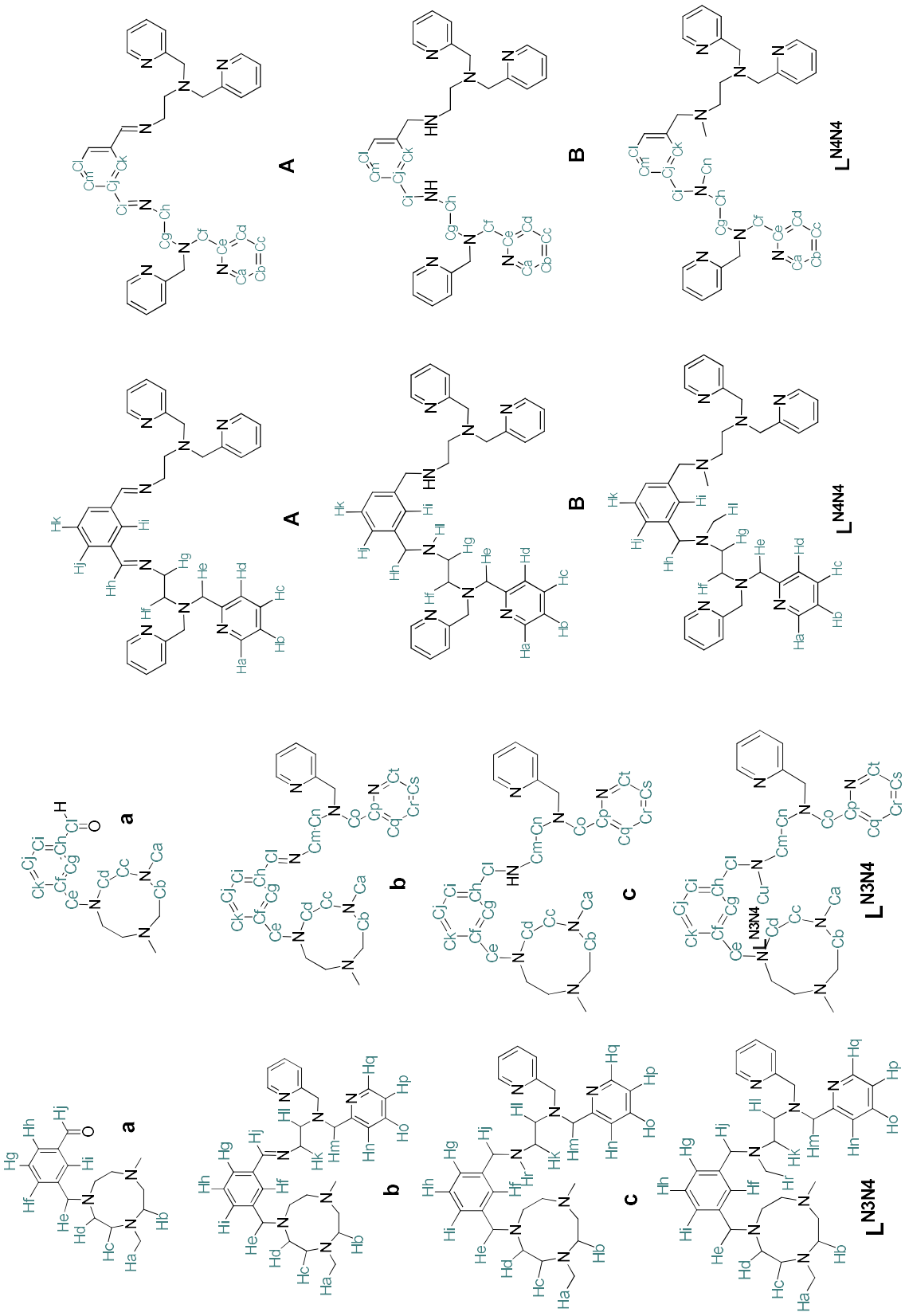

Scheme S2 Nomenclature for the full ^{1}H-NMR and ^{13}C-NMR assignment.

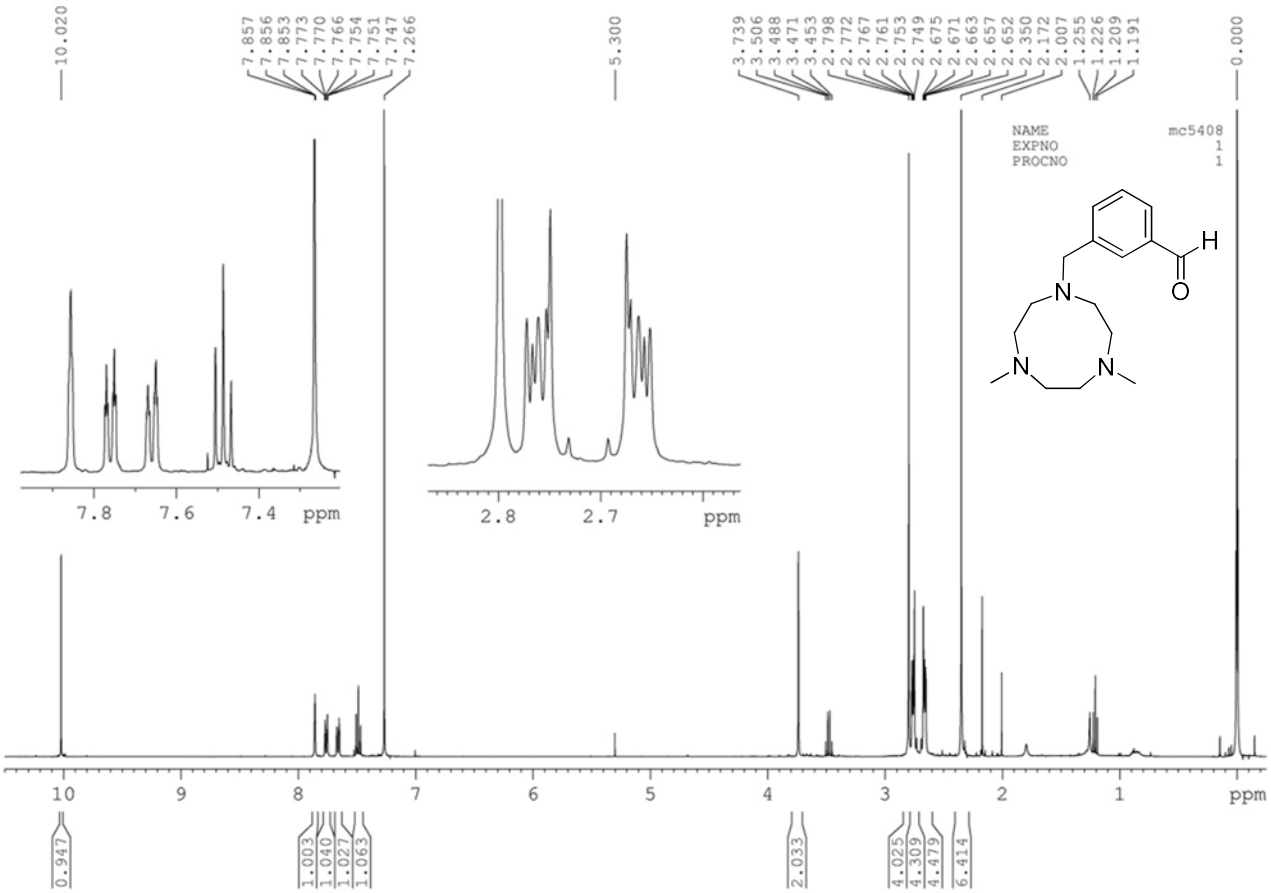

Figure S13 ^{1}H-NMR (400 MHz, $CDCl_3$, 298 K) of **a.**

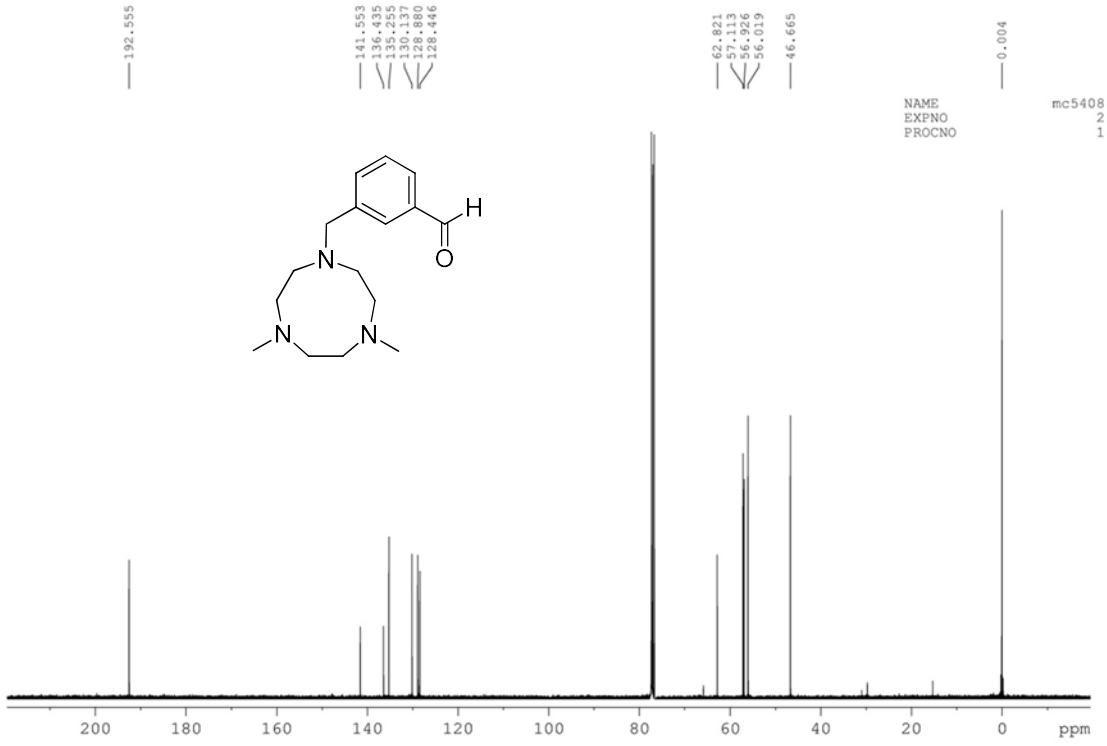

Figure S14 ^{13}C-NMR (400MHz, $CDCl_3$, 298 K) of **a**.

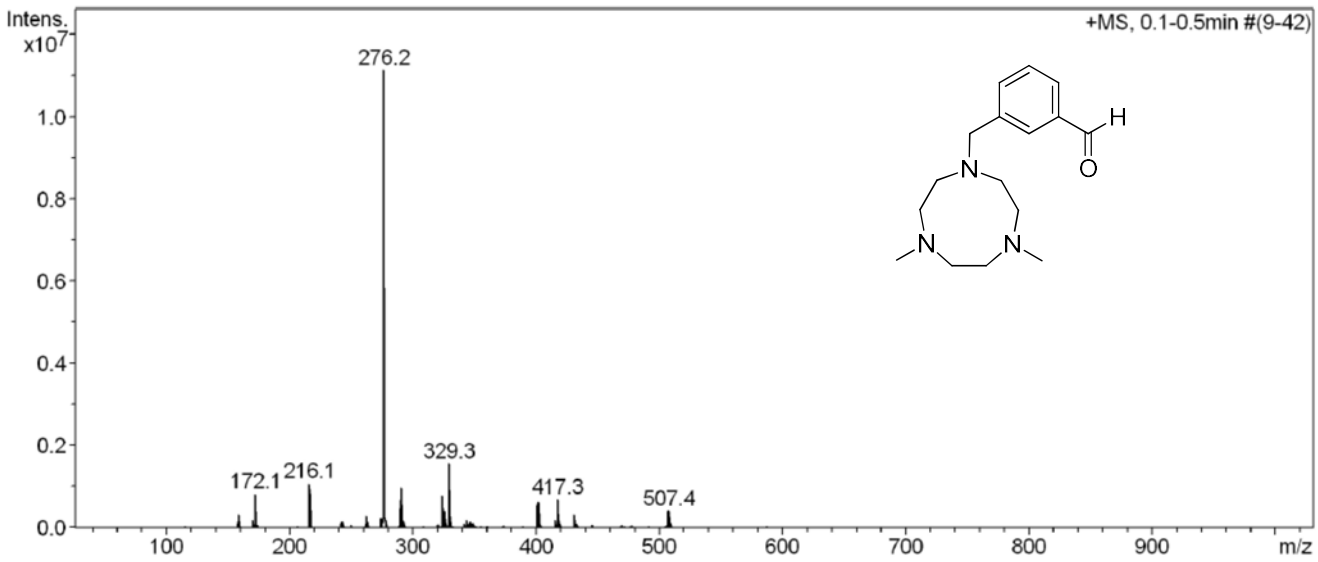

Figure S15 ESI-MS of **a**.

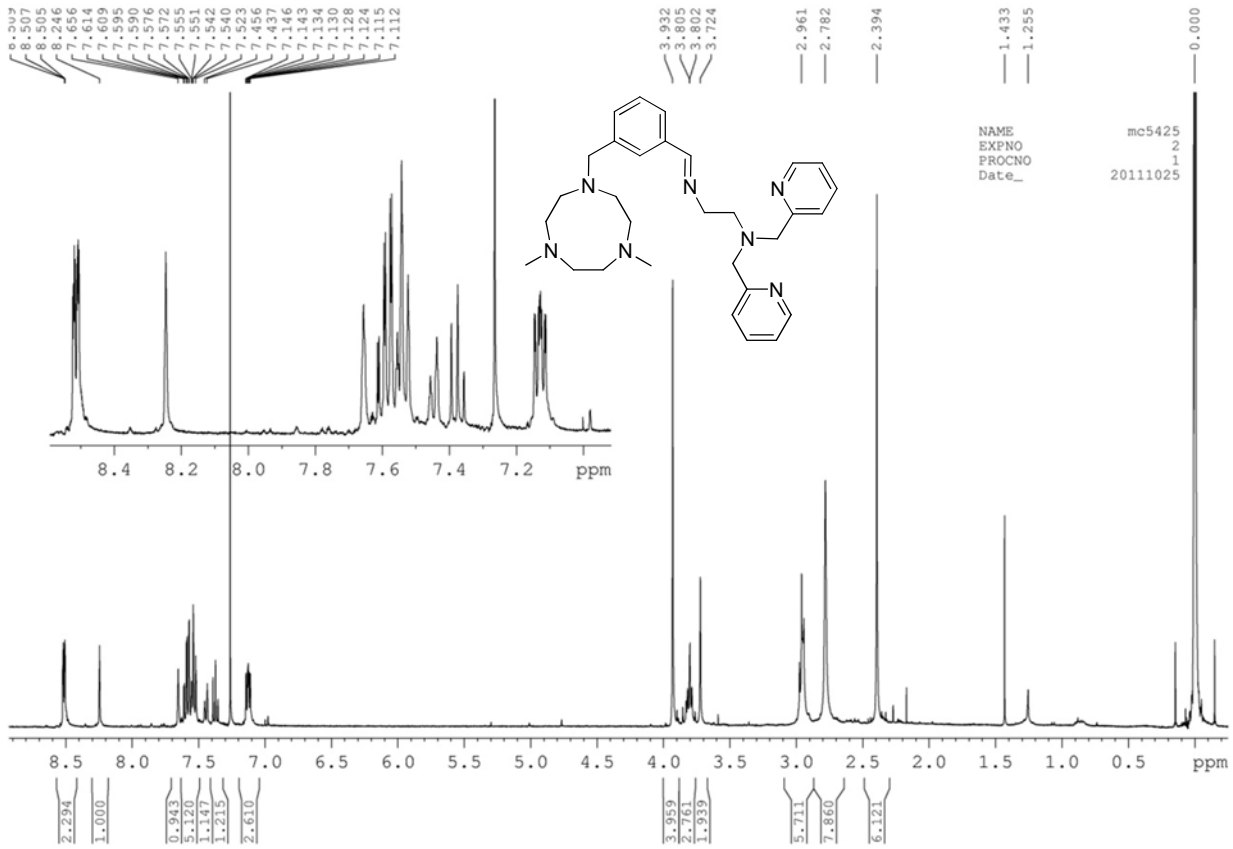

Figure S16 ^{1}H-NMR (400MHz, $CDCl_3$, 298 K) of **b**.

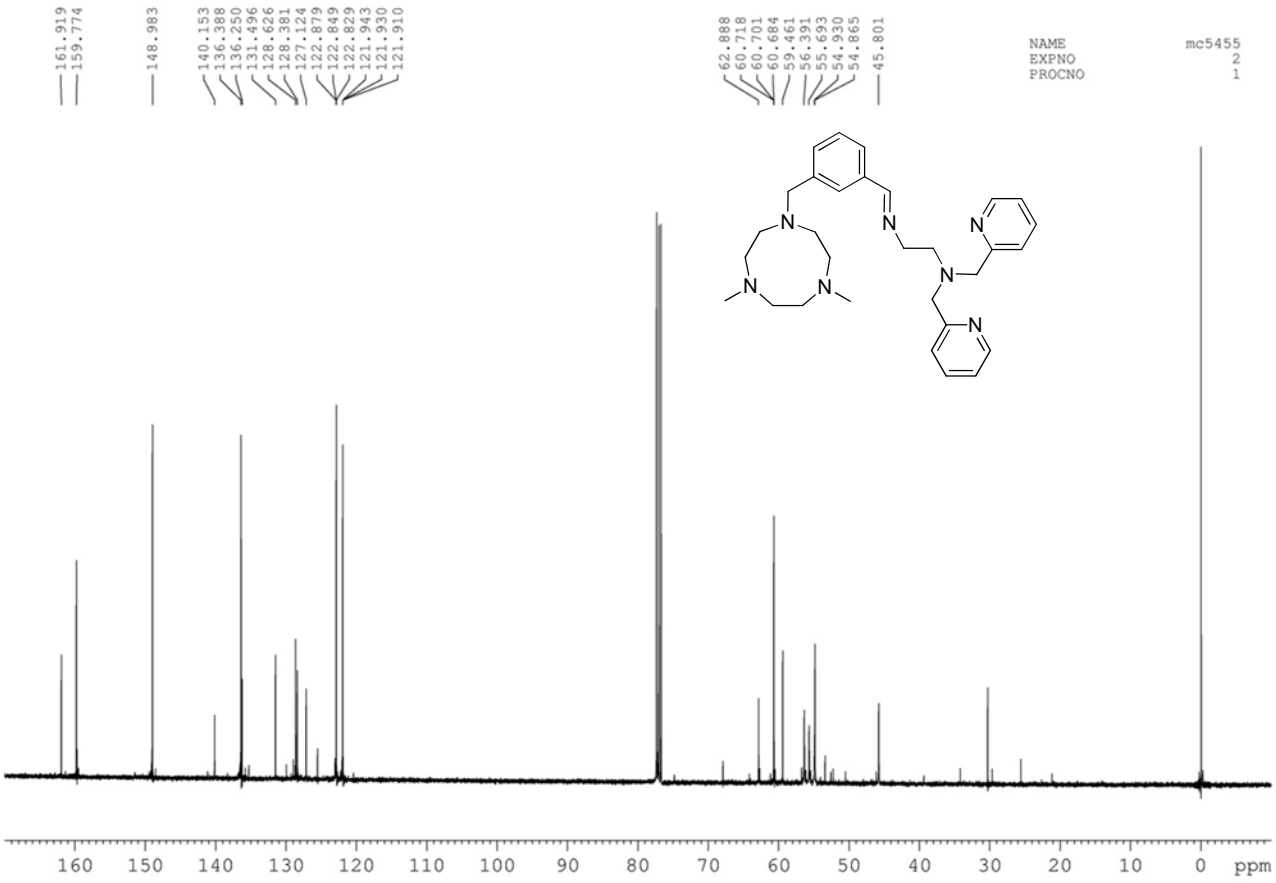

Figure S17 ^{13}C-NMR (400MHz, $CDCl_3$, 298 K) of **b**.

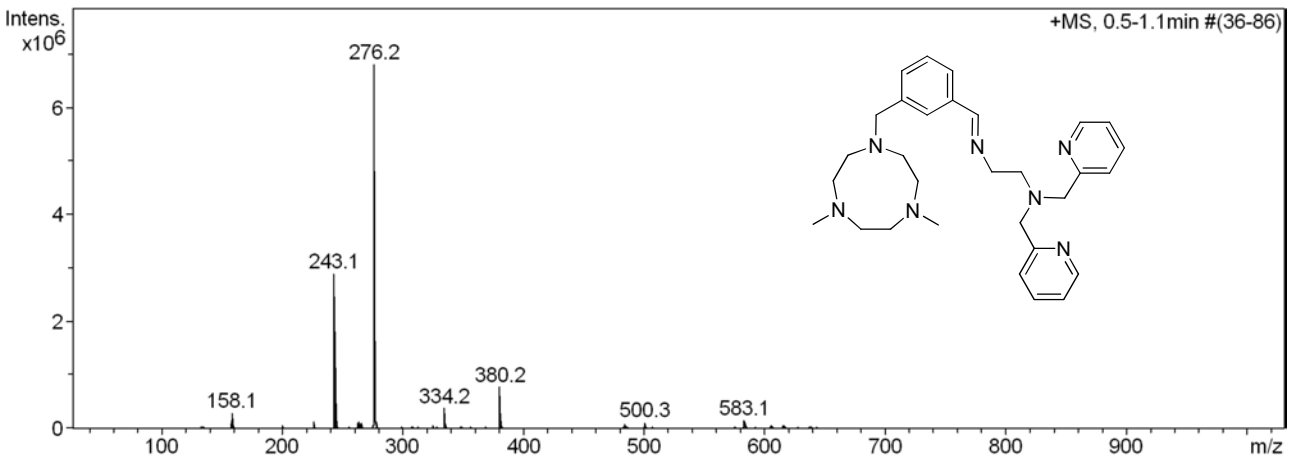

Figure S18 ESI-MS of **b**.

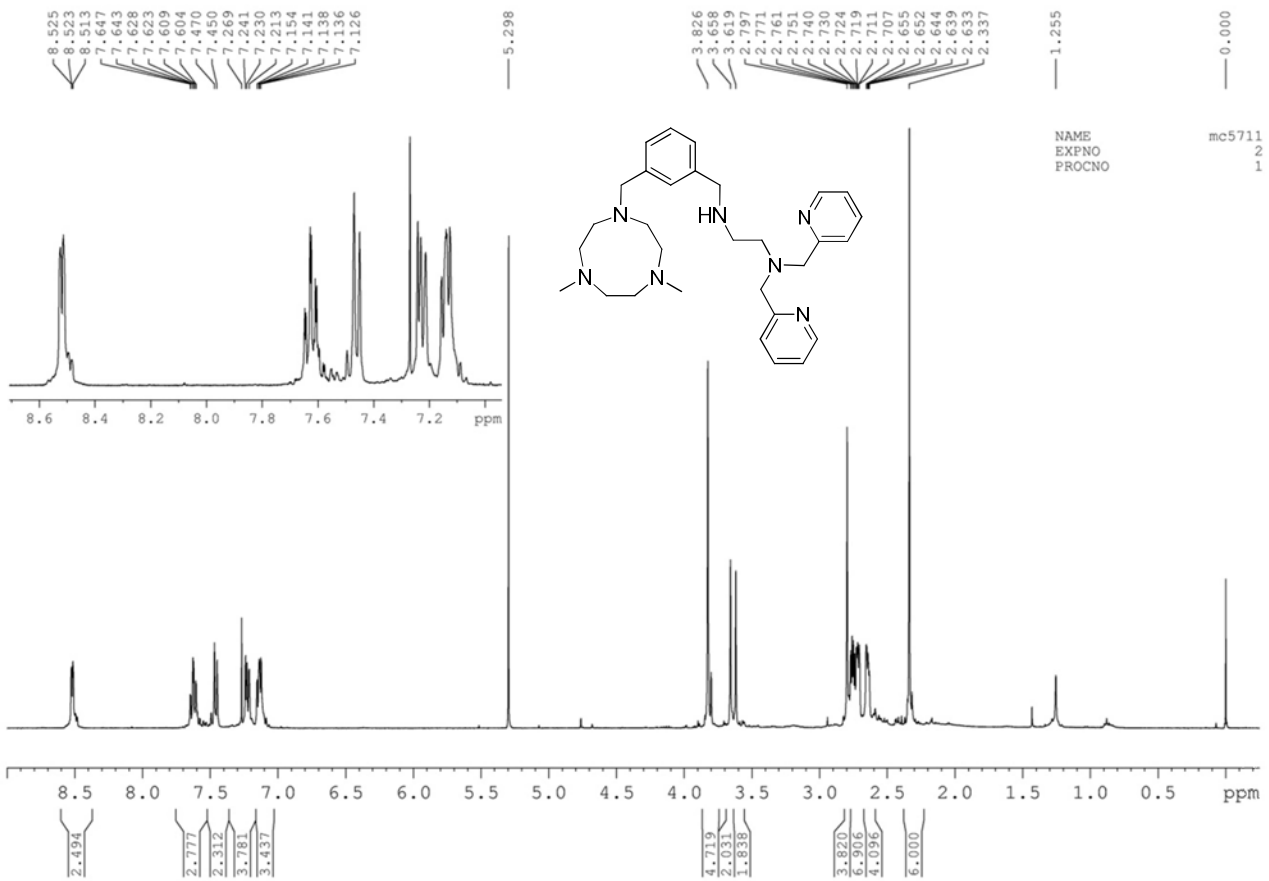

Figure S19 ^{1}H-NMR (400MHz, $CDCl_3$, 298 K) of **c**.

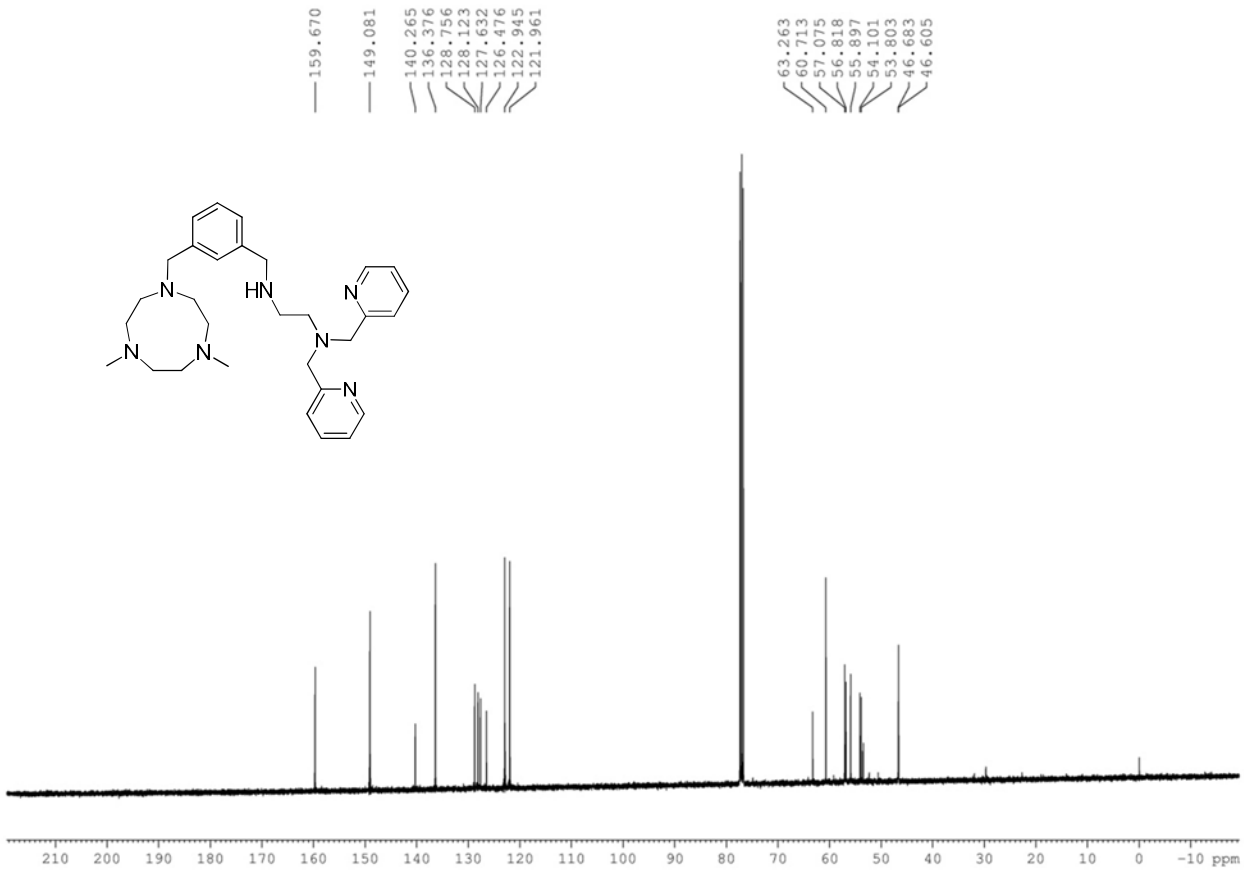

Figure S20 ^{13}C-NMR (400MHz, $CDCl_3$, 298 K) of **c**.

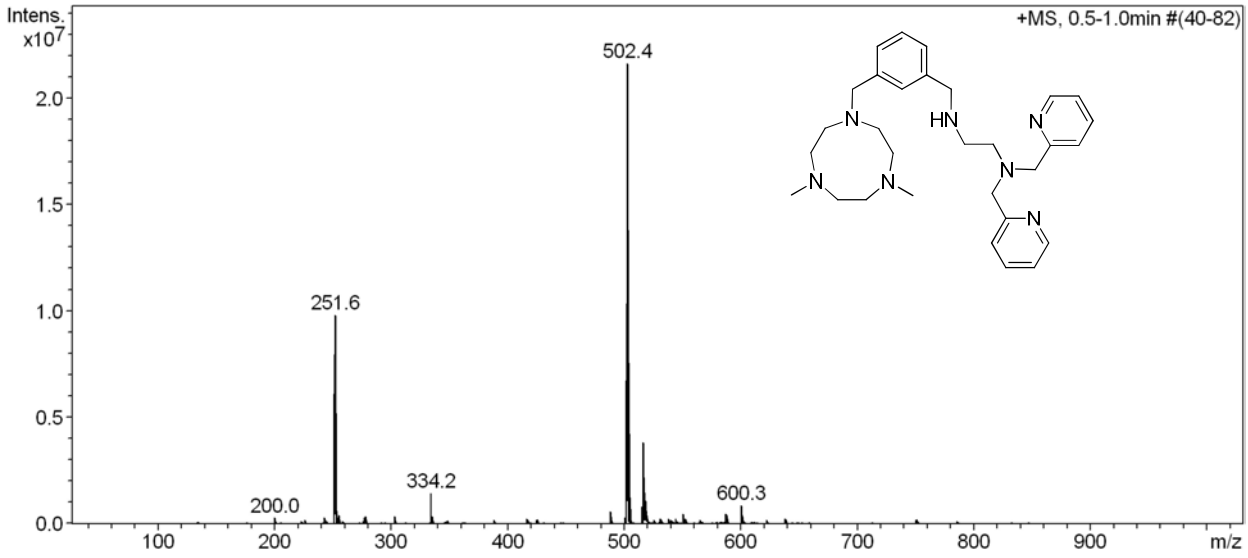

Figure S21 ESI-MS of **c**.

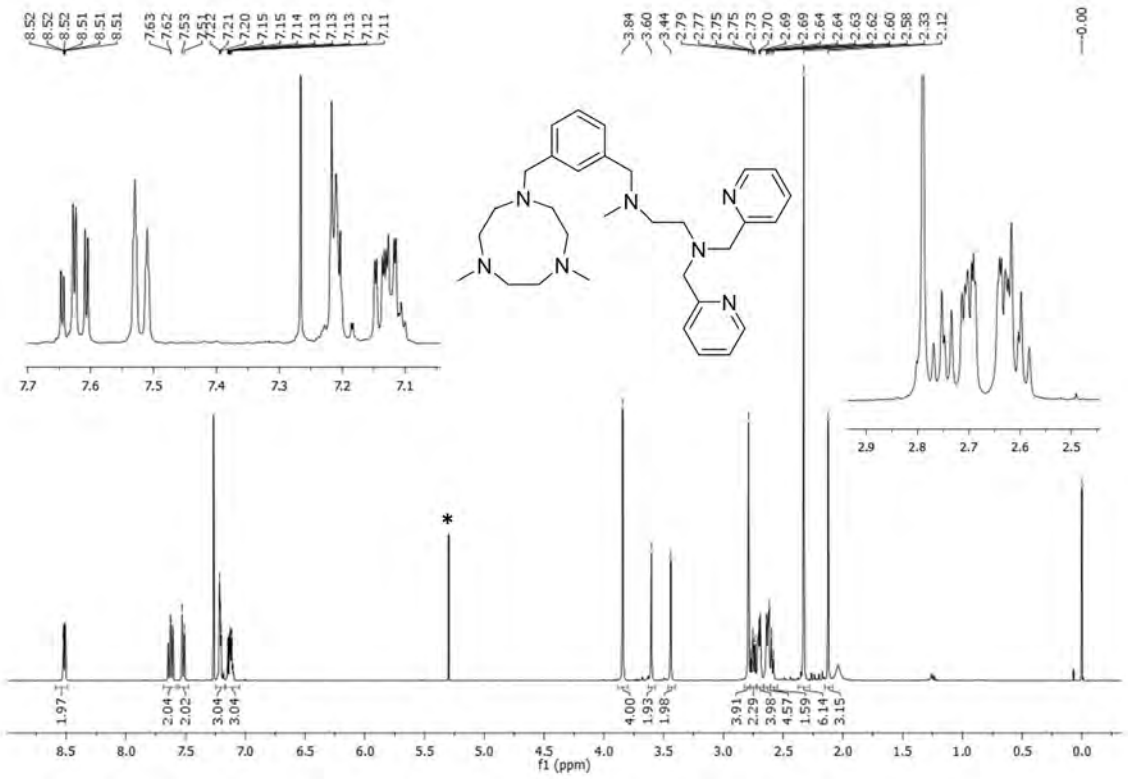

Figure S22 ^{1}H-NMR (400MHz, $CDCl_3$, 298 K) of L^{N3N4}.

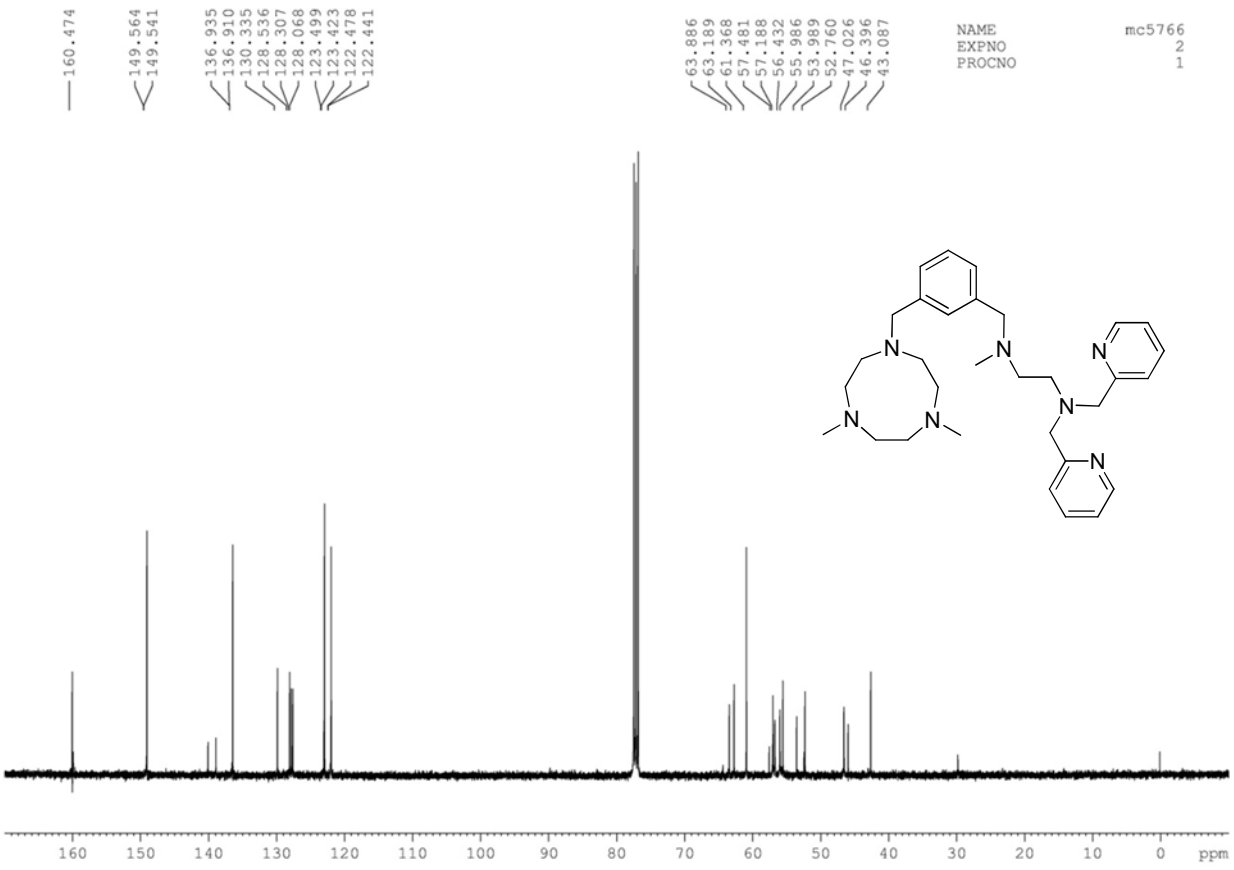

Figure S23 ^{13}C-NMR (400MHz, $CDCl_3$, 298 K) of L^{N3N4}.

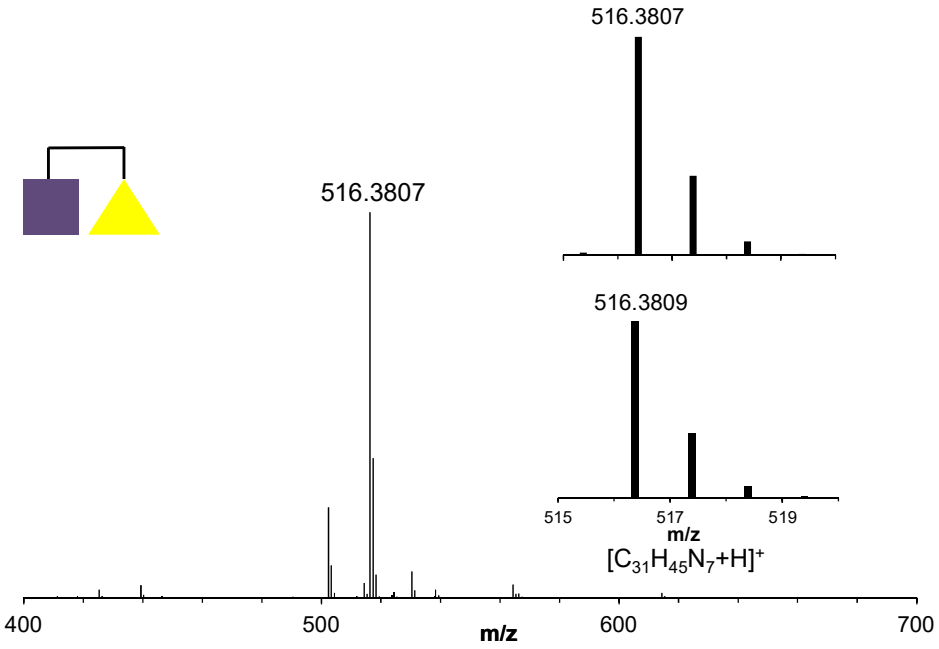

Figure S24 HR-MS of L^{N3N4}.

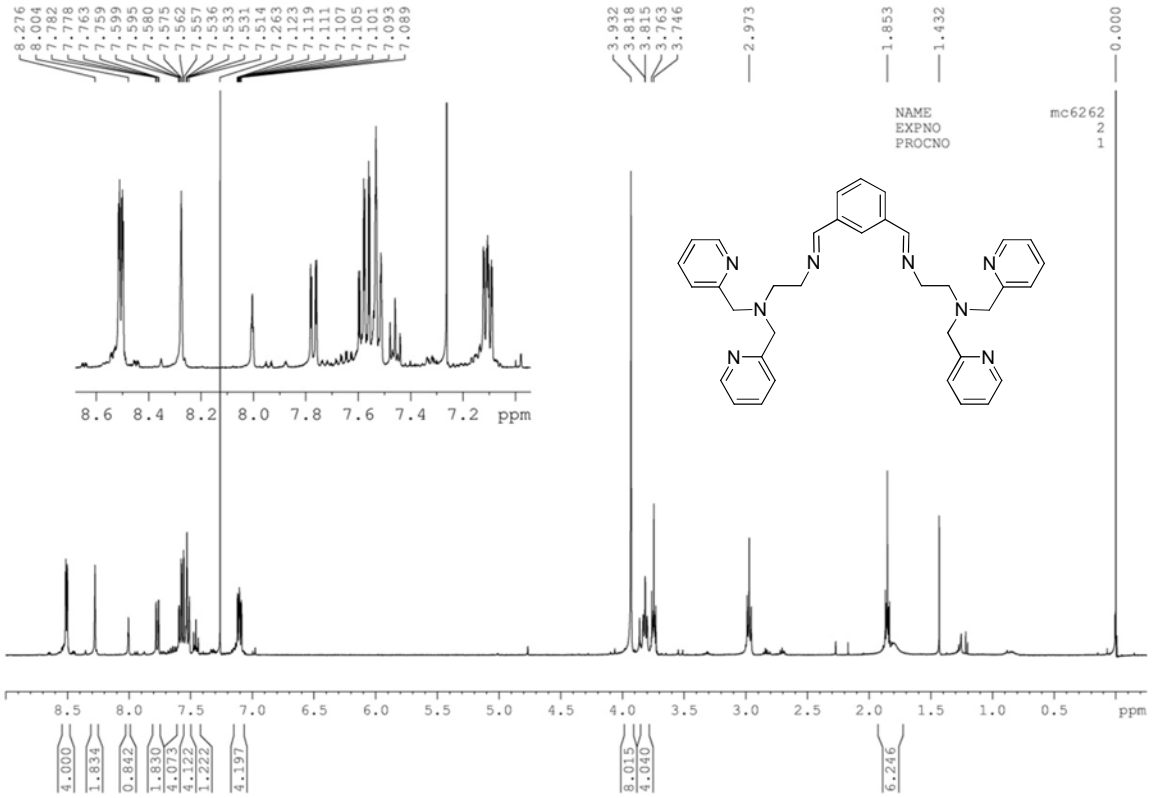

Figure S25 ^{1}H-NMR (400MHz, $CDCl_3$, 298 K) of **A**.

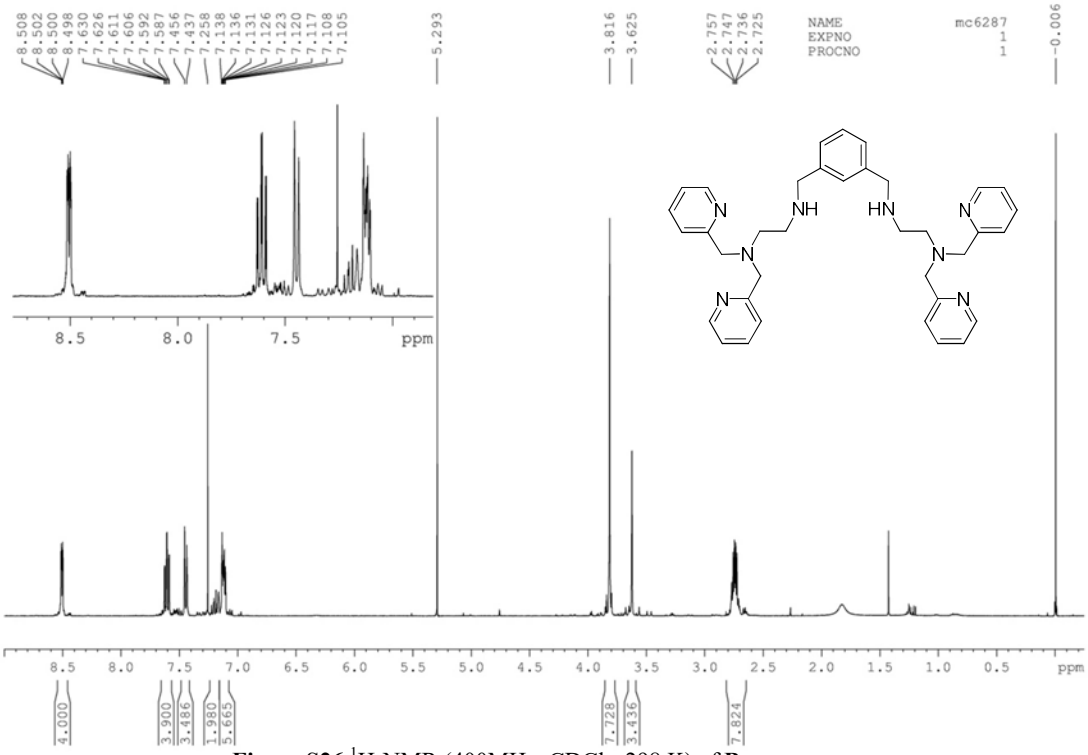

Figure S26 ^{1}H-NMR (400MHz, $CDCl_3$, 298 K) of **B**.

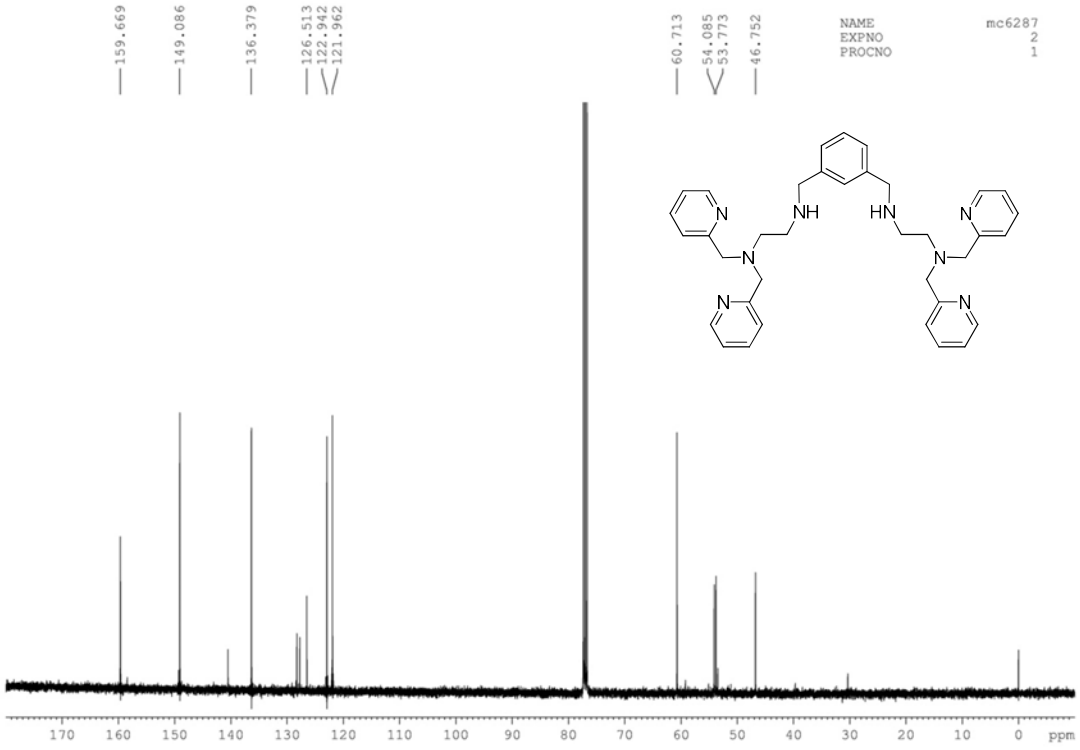

Figure S27 ^{13}C-NMR (400MHz, $CDCl_3$, 298 K) of **B**.

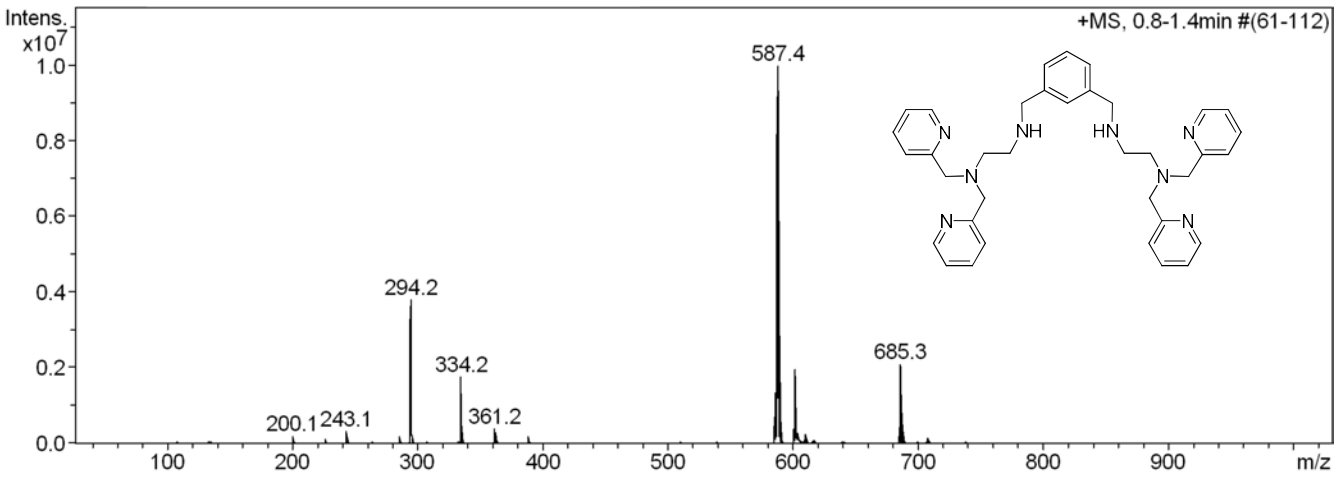

Figure S28 ESI-MS of **B**.

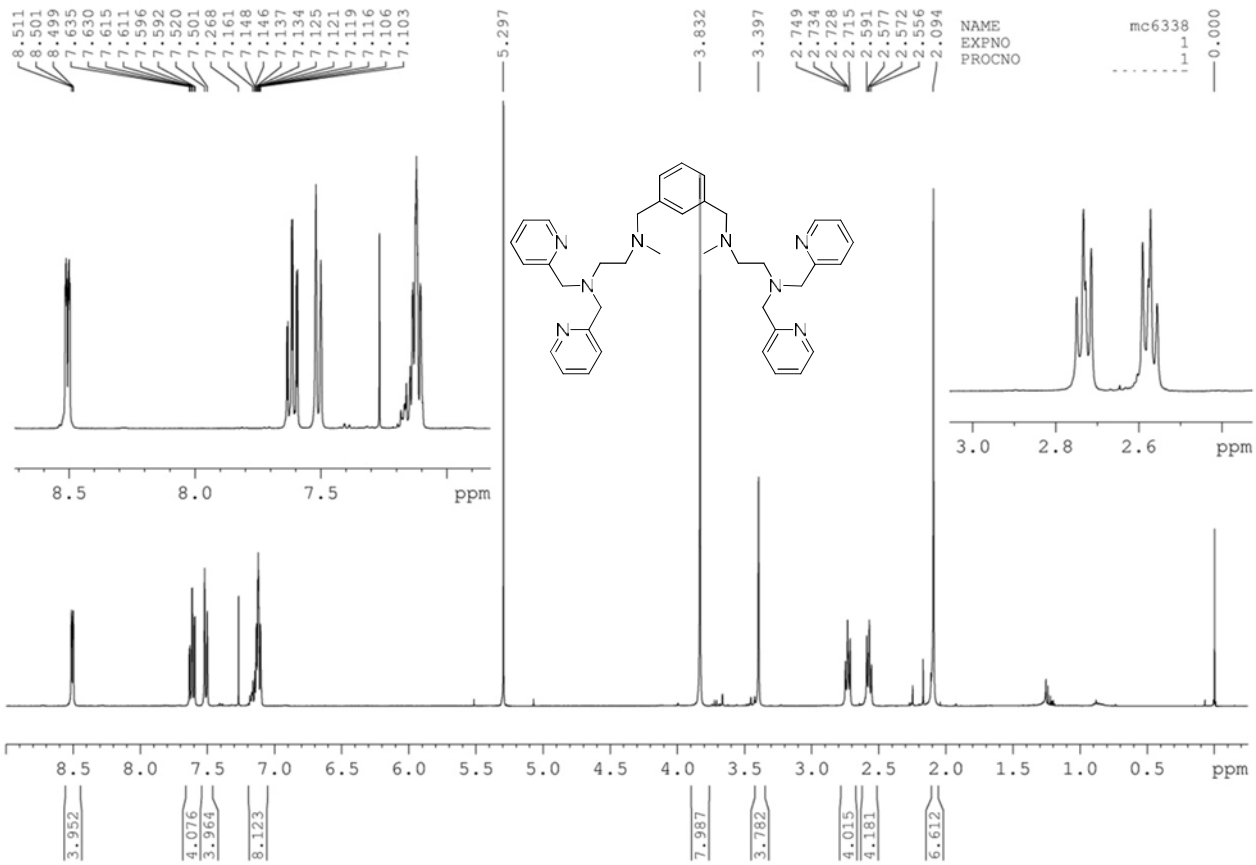

Figure S29 ^{1}H-NMR (400MHz, $CDCl_3$, 298 K) of L^{N4N4}.

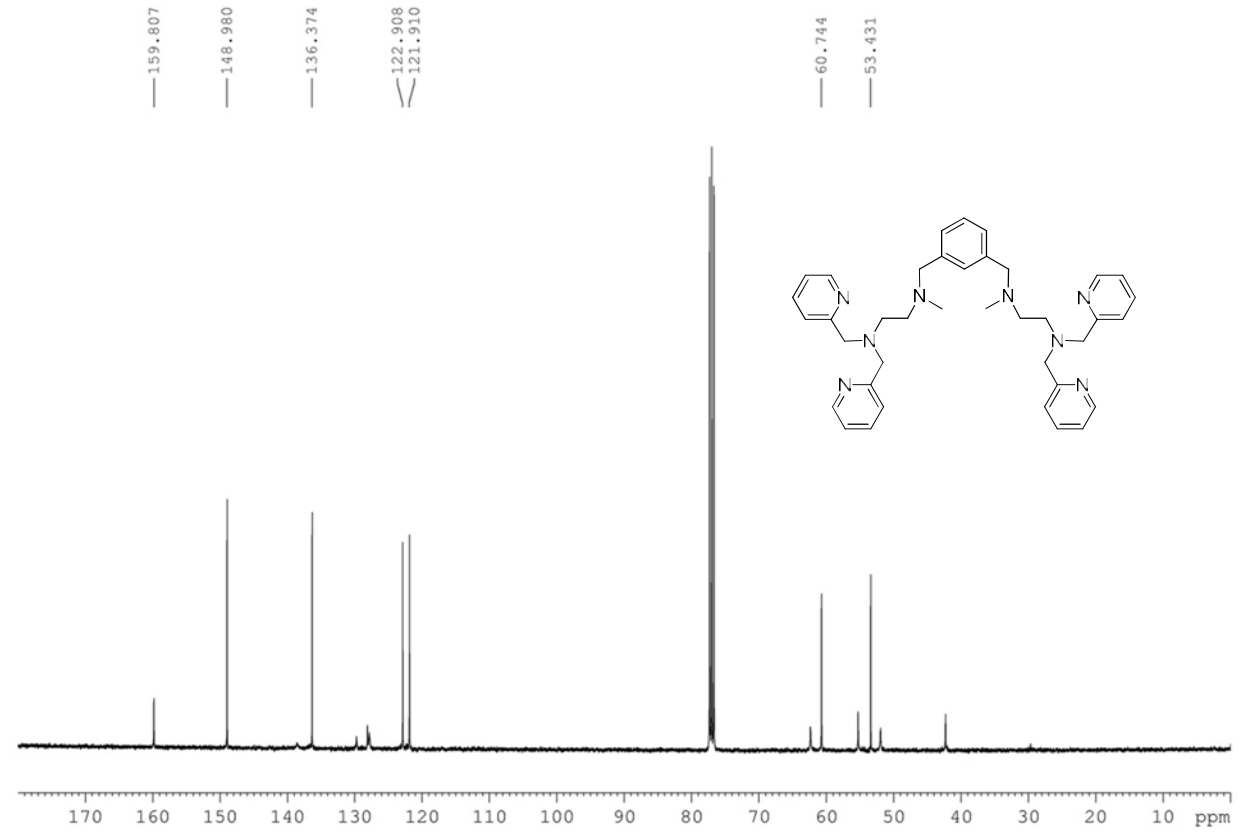

Figure S30 ^{13}C-NMR (400MHz, $CDCl_3$, 298 K) of L^{N4N4}.

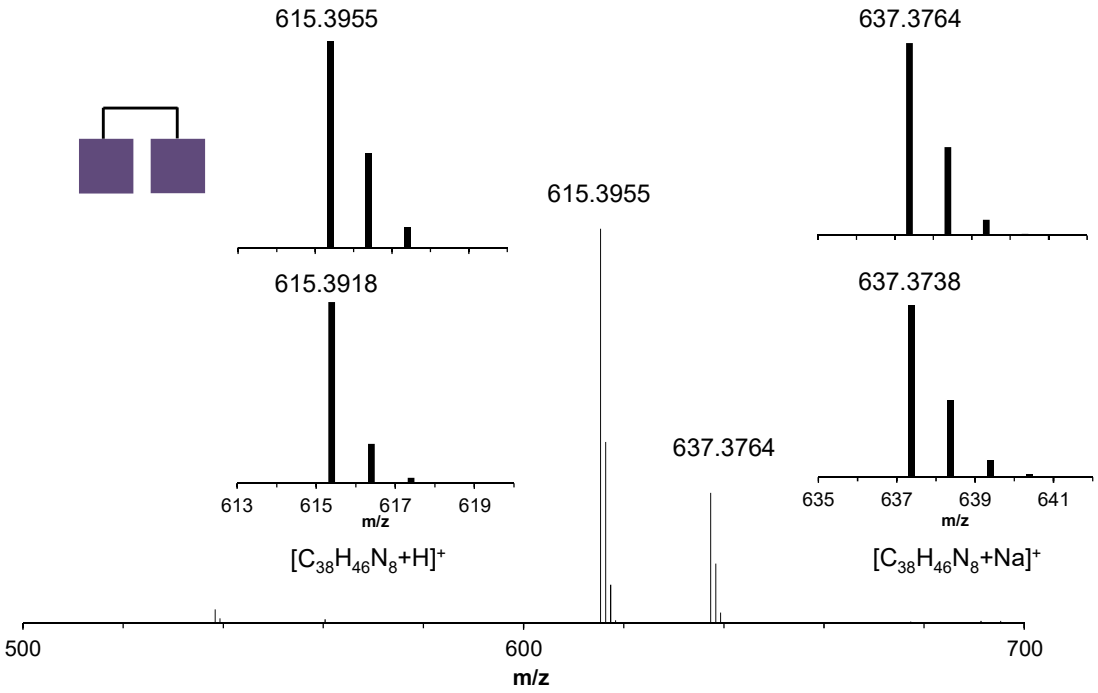

Figure S31 HR-MS of L^{N4N4}.

Supporting Information Chapter IV

Selective *ortho*-hydroxylation-defluorination of 2-fluorophenolates with a bis(μ-oxo)dicopper(III) Species

Contents

I. Instrumentation

All the spectroscopic and chromatographic analyses were carried out in *Unitat d'Anàlisi Química i Estructural* (UAQiE) or in the laboratories of the Bioinorganic and Supramolecular Chemistry Group (QBIS) at the University of Girona.

Elemental analyses were performed using a CHNS-O EA-1108 elemental analyzer from Fiscons. High resolution mass spectra (HRMS) were recorded on a Bruker MicrOTOF-Q II™ instrument using ESI or Cryospray ionization sources at Serveis Tècnics of the University of Girona. Samples were introduced into the mass spectrometer ion source by direct infusion using a syringe pump and were externally calibrated using sodium formate. A cryospray attachment was used for CMS (cryospray mass spectrometry). Temperature of the nebulizing and drying gases was set at -90ºC. The instrument was operated in both positive and negative ion modes. NMR experiments were performed on a Bruker Ultrashield Avance III400 and Ultrashield DPX300 spectrometers. UV/Vis spectroscopy was performed with an Agilent 50 Scan (Varian) UV/Vis spectrophotometer with 1 cm quartz cells. Low temperature control was achieved with a cryostat from Unisoku Scientific Instruments, Japan. HPLC analyses were performed on an Agilent Technologies LC 1200 series using an Eclipse XDB - C18 analytical column (150 x 4.6 mm, 5 µm Agilent Technologies). Spectrophotometric detection of the HPLC elution profile in the range 190-400 nm was performed with an Agilent 1200 Series G1315D diode array detector. Quantification of the catechol in the reaction mixtures was performed at 215 nm and using 1,3,5-trimethoxybenzene as internal standard. All HPLC-MS spectra were obtained on an Agilent Technologies 6120 Quadrupole LC/MS in electrospray positive ionization (ESI+) mode. For HPLC-DAD analyses elution was carried out using 0.1% H_3PO_4 in milliQ water (solvent A) and methanol (solvent B), with a flow rate of 0.5 mL/min. Elution started with 30% solvent A, the eluting solvent decreased to 20% A over 5 min, and to 0% A over additional 5 min. Finally returned to 30% A over 5 min and remained stable for 15 min. For HPLC-MS analyses elution was carried out using 0.1% HCOOH in Milli-Q water (solvent A) and methanol (solvent B), with a flow rate of 0.5 mL/min. Elution started with 30% solvent A for 5 min, over an additional 5 min the eluting solvent decreased to 20%. Then it returned to 30% A over 5 min and remained stable for 10 min.

II. Materials and Synthesis

Reagents and solvents used were of commercially available reagent quality unless otherwise stated. Solvents were purchased from Scharlab, Acros or Sigma-Aldrich and used without further purification. $^{18}O_2$ was purchased from CortecNet (min 99 atom % ^{18}O). Preparation and handling of air-sensitive materials were carried out in a N_2 drybox (Jacomex) with O_2 and H_2O concentrations < 1 ppm. ***m*-XYL^{MeAN}** and N,N-Bis[2-(2-pyridyl)ethyl]-α,α-dideuterio-benzylamine (**L^{Py2Bz}**) and their corresponding Cu^I complexes, $[Cu^I_2(m\text{-}XYL^{MeAN})]^{2+}$ and $[Cu^I(L^{PyBz})]^+$, were prepared following previously described procedures.[1] N,N′-di-tert-Butyl-ethylenediamine (**DBED**) was purchased from Aldrich and used without further purification. All phenols and catechols used were commercially available and they were used without any further purification except for 2-bromocatechol and 2-chlorocatechol, which were synthesized following previously described procedures.[2]

Preparation of sodium salts of phenolates

Sodium substituted phenolates were obtained from the corresponding commercially available phenols by reaction with 1 equivalent of NaOH in MeOH under an inert atmosphere, as exemplified for sodium 2,6-difluorophenolate. These compounds are highly hygroscopic and must be manipulated under a dry atmosphere.

Sodium 2,6-difluorophenolate: 2,6-difluorophenol (1.66 g, 12.8 mmols) was dissolved in methanol (25 mL) in a 50 mL schlenk flask. An inert atmosphere was established by several vacuum/N_2 cycles. Sodium hydroxide (0.51 g, 12.8 mmols) was added directly as a solid. The mixture was let stirring overnight and afterwards the solvent was removed under vacuum to yield 1.77 g (11.6 mmols, 91%) of a white solid. Anal Calcd. for $C_6H_3F_2NaO$: C,47.39; H, 1.99 %. Found: C, 47.16; H, 1.71 %. ^{1}H-NMR (D_2O, 300 MHz, 298 K): 6.81 – 6.72 (m, 2H, Ar**H**), 6.39 – 6.27 (m, 1H, Ar-**H**).

Sodium 2-fluorophenolate: White solid (yield = 90 %). Anal Calcd. for $C_6H_3F_2NaO{\cdot}0.2H_2O$: C, 52.34; H, 3.22 %. Found: C, 52.67; H, 2.84 %. ^{1}H-NMR (D_2O, 300 MHz, 298 K): 7.00 - 6.83 (m, 2H, Ar**H**), 6.73 – 6.64 (m, 1H, Ar**H**), 6.50 – 6.41 (m, 1H, Ar-**H**).

Sodium 2-chloro-6-fluorophenolate: Grey solid (yield = 87 %). Anal Calcd. for $C_6H_3ClFNaO$: C, 42.76; H, 1.79 %. Found: C, 43.16; H, 1.38 %. ^{1}H-NMR (D_2O, 300 MHz, 298 K): 7.05 - 6.98 (m, 1H, Ar**H**), 6.94 – 6.83 (m, 1H, Ar**H**), 6.43 – 6.33 (m, 1H, Ar-**H**).

Sodium 2-bromo-6-fluorophenolate: White solid (yield = 93%). Anal Calcd. for $C_6H_3BrFNaO$: C, 33.84 %; H, 1.42 %. Found: C, 33.89 %; H, 1.38 %. ^{1}H-NMR (D_2O, 300 MHz, 298 K): 7.09 (dt, J = 8.0 Hz, J' = 1.8 Hz, 1H, Ar**H**), 6.88-6.79 (m, 1H, Ar**H**), 6.22 (td, J = 5.3 Hz, J' = 8.0 Hz, 1H, Ar**H**)

Sodium 2,6-dichlorophenolate: White solid (yield = 82 %). Anal Calcd. for $C_6H_3Cl_2NaO$: C, 38.96; H, 1.63 %. Found: C, 39.10; H, 1.33 %. ^{1}H-NMR (D_2O, 300 MHz, 298 K): 7.07 (d, J = 7.8 Hz, 2H, Ar**H**), 6.27 (t, J = 7.8 Hz, 1H, Ar**H**).

Sodium 2,6-dimethylphenolate: Grey solid (yield = 97 %). Anal Calcd. for $C_8H_9NaO \cdot 1.1H_2O$: C, 58.60; H, 6.88 %. Found: C, 58.85; H, 6.78 %. ^{1}H-NMR (D_2O, 300 MHz, 298 K): 6.80 (d, J = 7.3 Hz, 2H, Ar**H**), 6.28 (t, J = 7.3 Hz, 1H, Ar**H**), 1.96 (s, 6H, C**H**$_3$).

Sodium 4-fluorophenolate: White solid (yield = 87 %). Anal Calcd. for $C_6H_4FNaO \cdot 1.3H_2O$: C, 45.75; H, 4.22 %. Found: C, 45.51; H, 3.98 %. ^{1}H-NMR (D_2O, 300 MHz, 298 K): 6.77 – 6.66 (m, 2H, Ar**H**), 6.44 – 6.34 (m, 2H, Ar**H**).

Sodium 2,4-difluorophenolate: White solid (yield = 96 %). Anal Calcd. for $C_6H_3F_2NaO$: C, 47.39; H, 1.99 %. Found: C, 47.00; H, 1.75 %. ^{1}H-NMR (D_2O, 300 MHz, 298 K): 6.74 - 6.62 (m, 1H, Ar**H**), 6.59 – 6.42 (m, 2H, Ar**H**).

Sodium 2-chloro-6-fluorophenolate: Reddish solid (yield = 98 %). Anal Calcd. for $C_6H_3ClFNaO$: C, 42.76; H, 1.79 %. Found: C, 42.25; H, 1.39 %. ^{1}H-NMR (D_2O, 300 MHz, 298 K): 6.92 – 6.84 (m, 1H, Ar**H**), 6.77 – 6.71 (m, 1H, Ar**H**), 6.55 – 6.46 (m, 1H, Ar-**H**).

Sodium 2-fluoro-4-methoxyphenolate: Pale brown solid (yield = 84 %). Anal Calcd. for $C_7H_6FNaO_2 \cdot 0.8H_2O$: C, 47.09; H, 4.29 %. Found: C, 47.04; H, 3.99 %. ^{1}H-NMR (D_2O, 300 MHz, 298 K): 6.64 – 6.39 (m, 3H, Ar**H**), 3.57 (s, 3H, OC**H**$_3$).

Sodium 2-fluoro-4-methylphenolate: White solid (yield = 93 %). Anal Calcd. for C_7H_6FNaO: C, 56.77; H, 4.08 %. Found: C, 56.57; H, 4.00 %.^{1}H-NMR (D_2O, 300 MHz, 298 K): 6.75 – 6.406 (m, 3H, Ar**H**), 2.01 (s, 3H, C**H**$_3$).

Sodium 4-cyano-2-fluorophenolate: White solid (yield = 77 %). Anal Calcd. for $C_7H_3FNNaO \cdot 0.1H_2O$: C, 52.25; H, 2.00; N, 8.70. Found: C, 51.43; H, 1.4; N, 8.55. ^{1}H-NMR (D_2O, 300 MHz, 298 K): 7.20 – 7.10 (m, 2H, Ar**H**), 6.58 – 6.51 (m, 1H, Ar**H**).

III. Preparation and reactivity of Cu_2O_2 species

1. Generation of Cu_2O_2 species (1-3) for UV-Vis experiments

Generation of $[Cu^{III}_2(\mu\text{-}O)_2(m\text{-}XYL^{MeAN})]^{2+}$ (**1**)[3]

In a typical experiment, a 1.5 mM solution of $[Cu^{I}_2(m\text{-}XYL^{MeAN})](CF_3SO_3)_2$ in dry acetone was prepared inside the glovebox. 100 µL of this solution were placed in a UV-Vis cuvette together with 1.9 mL of dry acetone, leading to a final concentration of the complex of 0.07 mM. The quartz cell was capped with a septum and taken out of the box, placed in the Unisoku cryostat of the UV-Vis spectrophotometer and cooled down to 183K. After reaching thermal equilibrium an UV-Vis spectrum of the starting complex was recorded. Dioxygen was injected into the cell with a balloon and a needle through the septum causing immediate reaction. The formation of a band at λ = 413 nm was observed. Full formation of the Cu_2O_2 species **1** (ε = 21000 $M^{-1}cm^{-1}$) was reached after 600 seconds.

Generation of $[Cu^{II}_2(\mu\text{-}\eta^2\text{:}\eta^2\text{-}O_2)(DBED)_2]^{2+}$ (**2**)[4]

10 mL of a 6 mM solution of $[Cu^{I}(MeCN)(DBED)](CF_3SO_3)$ in anhydrous acetone was prepared in the glovebox by mixing equimolar amounts of $[Cu^{I}(MeCN)_4](CF_3SO_3)$ and DBED. 50 µL of this solution were placed in a UV-Vis cuvette together with 2.5 mL of dry acetone, leading to a final concentration of the complex of 0.1 mM. The quartz cell was capped with a septum and taken out of the box, placed in the Unisoku cryostat of the UV-Vis spectrophotometer and cooled down to 183K. After reaching thermal equilibrium an UV-Vis spectrum of the starting complex was recorded. Dioxygen was injected into the cell with a balloon and a needle through the septum causing immediate reaction. The formation of a band at λ = 350 nm was observed. Full formation of $[Cu^{II}_2(\mu\text{-}\eta^2\text{:}\eta^2\text{-}O_2)(DBED)_2]^{2+}$ (**2**) (ε = 28000 $M^{-1}cm^{-1}$) was reached after 400 seconds.

Generation of $[Cu^{II}_2(\mu\text{-}\eta^2\text{:}\eta^2\text{-}O_2)(L^{Py2Bz})_2]^{2+}$ (**3**)[5]

5 mL of a 1.5 mM solution of $[Cu^{I}(L^{Py2Bz})](PF_6)$ in acetone was prepared in the glovebox by mixing equimolar amounts of $[Cu^{I}(MeCN)_4]PF_6$ and L^{Py2Bz}. 200 µL of this solution were placed in a UV-Vis cuvette together with 1.8 mL of anhydrous acetone, leading to a final concentration of the complex of 0.14 mM. The quartz cell was then capped with a septum and taken out of the glovebox, placed in the Unisoku cryostat of the UV-Vis spectrophotometer and cooled down to 183K. After reaching thermal equilibrium an UV-Vis spectrum of the starting complex was recorded. Dioxygen was injected into the cell with a balloon and a needle through the septum causing immediate reaction. The formation of a band at λ = 390 nm was observed. Full formation of $[Cu^{II}_2(\mu\text{-}\eta^2\text{:}\eta^2\text{-}O_2)(L^{Py2Bz})_2]^{2+}$ (**3**) (ε = 18000 $M^{-1}cm^{-1}$) was reached after 6000 seconds.

2. Reaction of Cu_2O_2 species (1-3) with 2-fluorophenolates

2.1 UV-Vis monitoring

To the pre-formed $[Cu^{III}_2(\mu\text{-}O)_2(m\text{-}XYL^{MeAN})]^{2+}$ (**1**) (see section III.1), 100 µL of a solution containing 3 equivalents of the desired phenolate in acetone were added at 183 K. This caused the immediate disappearance of the charactersitc band of **1** at λ = 413 nm, and it was accompanied by the formation of a new species (**4**^{x}, see Figure 1) with absorption bands between 500 and 700 nm depending on the added phenolate. These new species were not stable even at this low temperature and decomposed as shown by the kinetic traces (Figure S1).

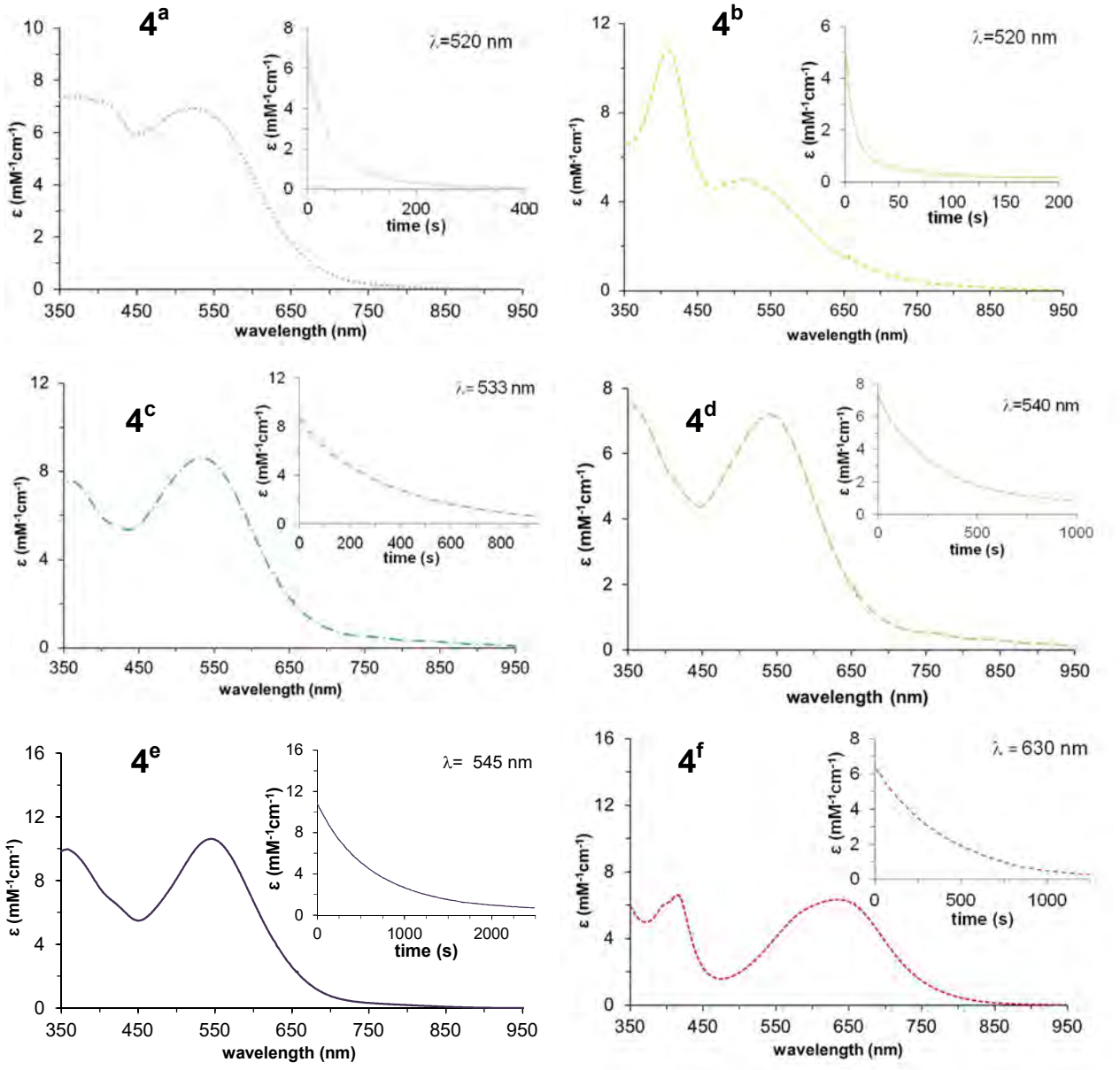

Figure S1 UV-Vis spectra of 4^{X} obtained upon reaction of 1 with 3 equiv of the corresponding sodium phenolate at -90ºC in acetone. Inset: kinetic trace of the decay of 4^{X} species at their maximum wavelength at -90ºC.

2.2 Analysis and quantification of the final oxidized products

a) Oxidations of 2-fluorophenolates by $[Cu^{III}_2(\mu\text{-}O)_2(m\text{-}XYL^{MeAN})]^{2+}$ (**1**). In a typical preparation, $[Cu^{I}_2(m\text{-}XYL^{MeAN})](CF_3SO_3)_2$ (20 mg, 22 µmols) was dissolved in anhydrous acetone (11 mL) in a 50 mL schlenk flask in the glovebox. The flask was capped with a septum, taken out from the glovebox and placed in an acetone/N_2 bath at -90ºC. After reaching thermal equilibrium, O_2 atmosphere was established using a balloon filled with this gas, so that the initial colorless solution turned deep yellow, indicative of the formation of **1**. The solution was stirred at -90ºC for 20 minutes to ensure full formation of **1**. Afterwards, excess O_2 was removed by several vacuum/N_2 cycles. 0.5 mL of a solution containing the desired equivalents of the corresponding phenolate in acetone was then added, which caused an immediate color change from dark yellow to purple corresponding to $\mathbf{4^x}$. The mixture was stirred for 20 minutes at -90ºC, quenched with $HClO_4$ (10 mL of a 0.5 M solution), and then it was taken out from the cold bath to attain room temperature. At this point, 1,3,5-trimethoxybenzene was added as an internal standard. Acetone was removed under vacuum and the resulting aqueous mixture was extracted with CH_2Cl_2 (3x15 mL). The organic layers were combined and dried over $MgSO_4$. The solvent was removed under reduced pressure to obtain the final sample, which was analyzed by ^{1}H-NMR or HPLC to quantify the amount of oxidized products (catechols).

b) Oxidations of 2-fluorophenolates by $[Cu^{II}_2(\mu\text{-}\eta^2\text{:}\eta^2\text{-}O_2)(DBED)_2]^{2+}$ (**2**) and $[Cu^{II}_2(\mu\text{-}\eta^2\text{:}\eta^2\text{-}O_2)(L^{Py2Bz})_2]^{2+}$ (**3**). In a typical experiment, 20 mL of a 2 mM solution of the starting copper(I) complex $[Cu^{I}(MeCN)(DBED)](OTf)$ or $[Cu^{I}(L^{Py2Bz})](PF_6)$ was prepared in situ in a glovebox by mixing equimolar amounts of ligand and copper(I) salt (see section III.1). This solution was placed in a 50 mL Schlenk flask which was capped with a septum. This flask was then taken out from the glovebox and cooled down to 183 K in an acetone/N_2 bath. An O_2 atmosphere was established using a balloon filled with O_2, leading to the formation of $[Cu^{II}_2(\mu\text{-}\eta^2\text{:}\eta^2\text{-}O_2)(DBED)_2]^{2+}$ (**2**) and $[Cu^{II}_2(\mu\text{-}\eta^2\text{:}\eta^2\text{-}O_2)(L^{Py2Bz})_2]^{2+}$ (**3**). Once these species had been fully formed (400 min for **2** and 6000 min for **3**, see section III.1), excess dioxygen was removed and the desired amount of phenolate was added. Isolation and quantification of the oxidized products was carried out following the work-up procedure described above for compound **1**.

2.3 Optimization of the reaction conditions

The optimal reaction conditions were established using sodium 2,6-difluorophenolate (Na(DFP)) as substrate, following the previously described experimental procedure (see section III.2.2)

Table S1. Reaction of compounds **1-3** with Na(DFP) (substrate) to give 3-fluorocatechol.

compound	$[Cu_2O_2]$ (mM)	equiv 2,6-difluorophenolate	yield (%)[c]
$[Cu^{III}_2(\mu\text{-}O)_2(m\text{-}XYL^{MeAN})]^{2+}$ (**1**)	2.1	3	21
$[Cu^{III}_2(\mu\text{-}O)_2(m\text{-}XYL^{MeAN})]^{2+}$ (**1**)	0.2	3	20
$[Cu^{III}_2(\mu\text{-}O)_2(m\text{-}XYL^{MeAN})]^{2+}$ (**1**)	2.2	1	15
$[Cu^{III}_2(\mu\text{-}O)_2(m\text{-}XYL^{MeAN})]^{2+}$ (**1**)	2.2	10	22
$[Cu^{I}_2(m\text{-}XYL^{MeAN})]^{2+} + O_2$ [a]	2.2	3	9
$[Cu^{II}_2(\mu\text{-}\eta^2\text{:}\eta^2\text{-}O_2)(DBED)_2]^{2+}$ (**2**)	2.0	3	23
$[Cu^{II}_2(\mu\text{-}\eta^2\text{:}\eta^2\text{-}O_2)(L^{Py2Bz})_2]^{2+}$ (**3**)	2.1	3	2.5
$[Cu^{I}_2(m\text{-}XYL^{MeAN})]^{2+}$ [b]	2.3	3	<0.1
$[Cu^{I}(MeCN)_4](CF_3SO_3) + O_2$	2.4	3	3
$[Cu^{I}(MeCN)_4](CF_3SO_3)$ [b]	2.4	3	<0.1

[a]Reaction at room temperature. [b]Reaction in the absence of O_2. [c]Yield of 3-fluorocatechol with respect to Cu_2O_2.

3. Labeling experiments with $^{18}O_2$

Labeling experiments wih $^{18}O_2$ were carried out following an experimental procedure similar to that described above for the oxidation of 2-fluorophenolates by $[Cu^{III}_2(\mu\text{-}O)_2(m\text{-}XYL^{MeAN})]^{2+}$ (**1**) (section III.2.2). Inside the glovebox, $[Cu^{I}_2(m\text{-}XYL^{MeAN})](OTf)_2$ (14.5 mg, 8.5 μmols) was dissolved in acetone (6 mL) and placed in a 10 mL round flask in order to minimize the headspace volume. The flask was then capped with a septum, taken out from the glovebox and cooled down to -90ºC in an acetone/N_2 bath. Vacuum was applied to remove all the N_2 from the atmosphere and then a $^{18}O_2$ atmosphere was established. The mixture was stirred for 20 minutes at -90ºC and then excess $^{18}O_2$ was removed by applying several vacuum/N_2 cycles. 3 equiv of Na(DFP) were added (25.6 μmols in 0.5 mL acetone) and the mixture was sitrred for 20 min at -90ºC. Finally the reaction was quenched with $HClO_4$. Isolation of 3-fluorocatechol product was carried out following the work-up procedure described in section III.2.2. The amount of ^{18}O-labeled 3-fluorocatechol was established by HPLC-MS analysis (Figure S2).

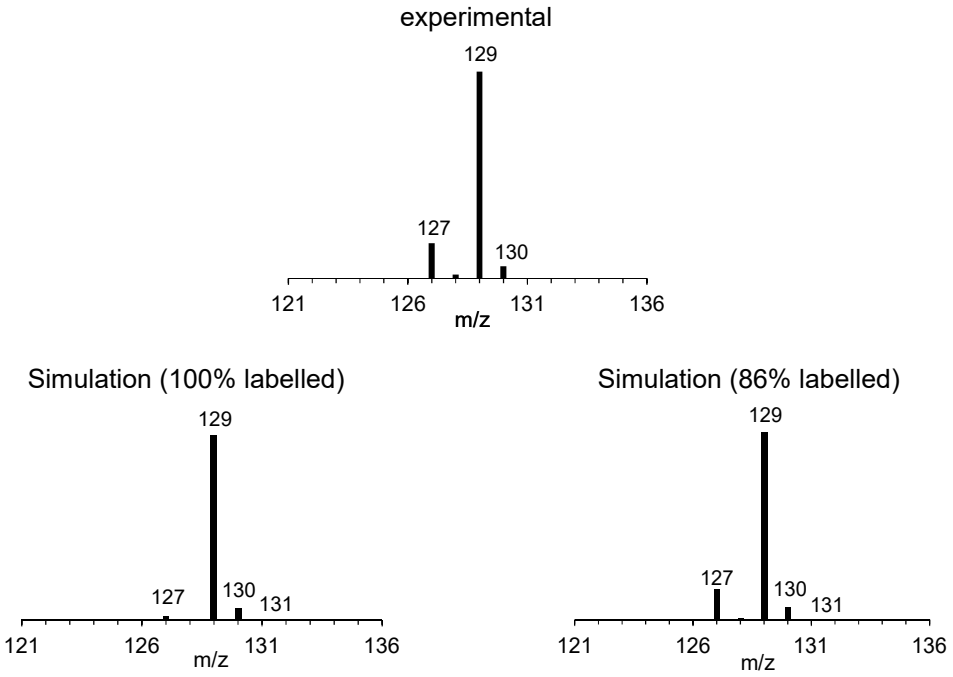

Figure S2 MS spectrum of 3-fluorocatechol obtained upon reaction of ^{18}O-labeled **1** with 3 equiv sodium 2,6-difluorophenolate at -90ºC in acetone (top). Mass spectrium simulations for 100% and 86% labeled 3-fluorocatechol (bottom)

4. Collision induced dissociation experiments of 4[a]

4[a] was generated in the cryospray mass spectrometer and the corresponding peak at m/z = 763.3 was isolated. After a collision energy of 8 eV a loss of 129 units corresponding to a 2,6-difluorophenolate moiety was observed (Figure S3).

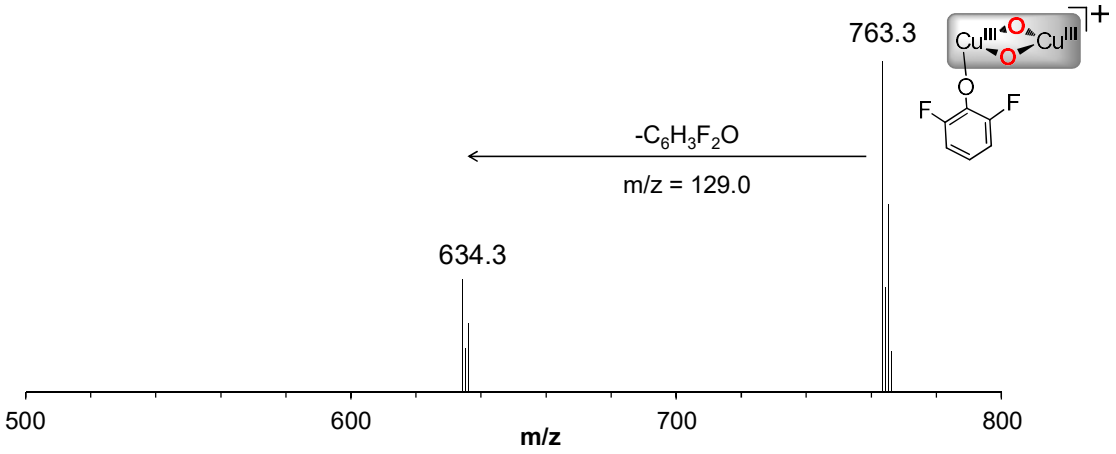

Figure S3 Collision induced dissociation of the peak at m/z = 763.3 formed in the reaction of **1** with 3 equiv sodium 2,6-difluorophenolate

5. Detection of 4^e by high resolution mass spectrometry with a cryospray ionization (CMS)

Given the relatively long $t_{1/2}$ for $\mathbf{4^x}$ when 2,6-dichlorophenolate was used as substrate ($\mathbf{4^e}$), cyrospray mass spectrometry at -90ºC was undertaken in order to gain information about the nature of this species. ESI-MS analysis of the reaction of **1** with 3 equiv sodium 2,6-dichlorophenolate at -90ºC afforded a clean mass spectrum with predominant peaks at m/z = 783.2571 and m/z = 785.2568 corresponding to $[Cu^{III}_2(\mu\text{-}O)_2(CF_3SO_3)(m\text{-}XYL^{MeAN})]^+$ (**1**) and m/z = 797.2567 corresponding to $[Cu^{III}_2(\mu\text{-}O)_2(2,6\text{-}Cl_2\text{-}C_6H_3O)(m\text{-}XYL^{MeAN})]^+$. Thus, $\mathbf{4^e}$ corresponds to the coordination of 2,6-dichlorophenolate to the bis(μ-oxo) core in **1**.

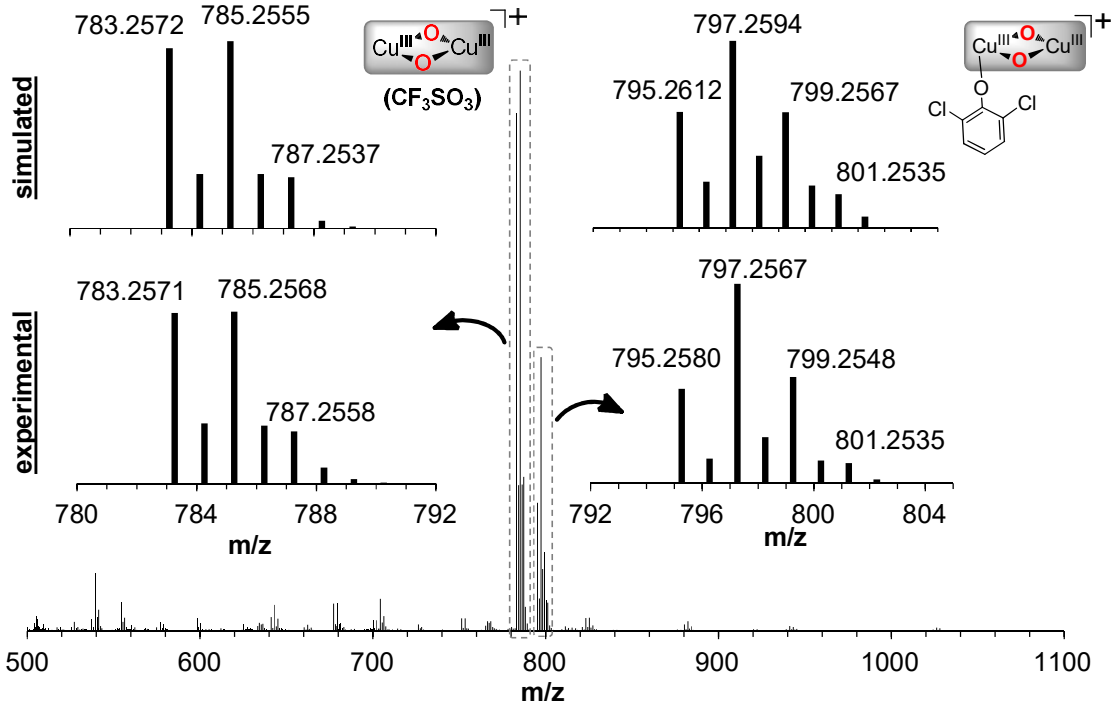

Figure S4 Cryospray mass spectrometry at -90ºC corresponding to the reaction of **1** with 3 equiv sodium 2,6-dichlorophenolate in acetone.

6. Extraction of *m*-XYL^{MeAN}

After the decay of 4^a was complete, basic work-up was performed by adding $NH_{3(aq)}$ (2 mL) and extracting the ligand with CH_2Cl_2 (3 x 5 mL). The organic layers were combined and dried over $MgSO_4$. Then the solvent was removed under reduced pressure, leading to the recovery of *m*-XYL^{MeAN} as ascertained by ^{1}H-NMR and ESI-MS.[1]

IV. References

[1] a) A. Company, D. Lamata, P. A, S. M, E. V. Rybak-Akimova, L. Que, X. Fontrodona, P. T, L. A, C. M, *Inorg Chem* **2006**, *45*, 5239-5241; b) I. Sanyal, M. Mahroof-Tahir, M. S. Nasir, P. Ghosh, B. I. Cohen, Y. Gultneh, R. W. Cruse, A. Farooq, K. D. Karlin *Inorg Chem* **1992**, *31*, 4322-4332.

[2] a) T. V. Hansen, L. Skattebøl, *Tetrahedron Lett.* **2005**, *46*, 3357-3358; b) N. U. Hofslokken, L. Skattebol, *Acta Chem Scand* **1999**, *53*, 258-262.

[3] A. Company, S. Palavicini, I. Garcia-Bosch, R. Mas-Balleste, L. Que, E. V. Rybak-Akimova, L. Casella, X. Ribas, M. Costas, *Chem.-Eur. J.* **2008**, *14*, 3535-3538.

[4] a) L. M. Mirica, M. Vance, D. J. Rudd, B. Hedman, K. O. Hodgson, E. I. Solomon, T. D. P. Stack, *Science* **2005**, *308*, 1890-1892; b) L. M. Mirica, M. Vance, D. J. Rudd, B. Hedman, K. O. Hodgson, E. I. Solomon, T. D. P. Stack, *J. Am. Chem. Soc.* **2002**, *124*, 9332-9333.

[5] S. Itoh, H. Kumei, M. Taki, S. Nagatomo, T. Kitagawa, S. Fukuzumi, *J. Am. Chem. Soc.* **2001**, *123*, 6708-6709.

Supporting Information Chapter V

Trapping a Highly Reactive Non-heme Iron Intermediate That Oxygenates Strong C-H Bonds with Stereoretention

Contents

I. Synthesis and characterization of $[Fe(CF_3SO_3)_2(PyNMe_3)]$ (1)

3,6,9,15-tetraazabicyclo[9.3.1]pentadeca-1(15),11,13-triene (**$PyNH_3$**, Scheme S1) was prepared following previously described procedures.[1]

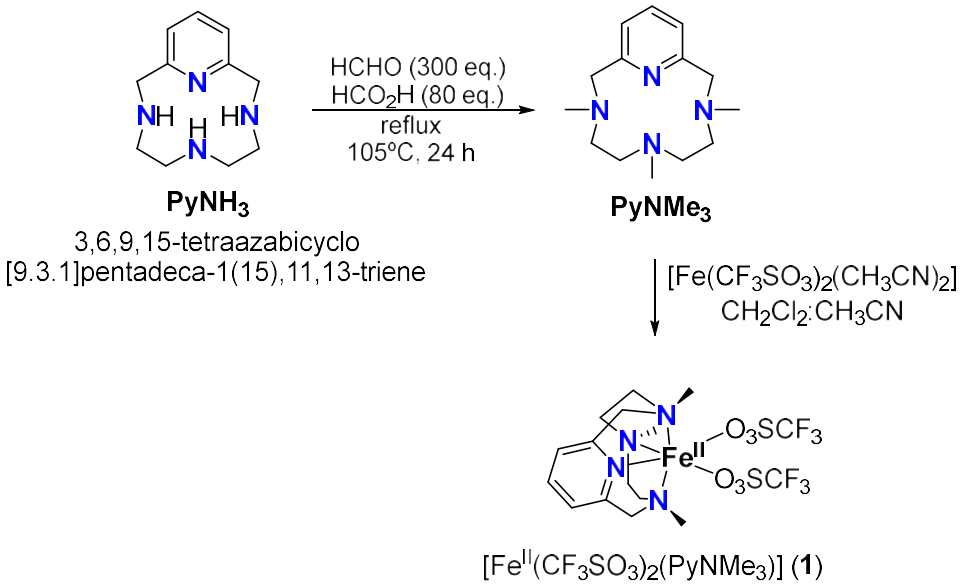

Scheme S1 Synthesis of $PyNMe_3$ and $[Fe(CF_3SO_3)_2(PyNMe_3)]$ (**1**).

Synthesis of $PyNMe_3$. $PyNH_3$ (497 mg, 2.41 mmols) was dissolved in formaldehyde 37% (54.0 mL, 723 mmols) and formic acid (7.4 mL, 192 mmols) in a 100 mL round flask, and the resulting mixture was then refluxed for 24 hours. Following reflux, the solvent was removed under reduced pressure and NaOH 30% (20 mL) was added. The product was then extracted with CH_2Cl_2 (4x20 mL), and the organic phase was dried over $MgSO_4$ and then filtered, and the solvent was removed under reduced pressure. A yellow oil was obtained, which was purified by column chromatography over silica using a mixture CH_2Cl_2:MeOH:NH_3 80:20:5. 373 mg of **$PyNMe_3$** (1.50 mmols, 62% yield) were obtained as a yellow oil. ^{1}H-NMR ($CDCl_3$, 400 MHz, 298K) δ, ppm: 7.57 (t, J= 7.7 Hz, 1H, py**H**$_\gamma$), 7.09 (d, J= 7.7 Hz, 2H, py**H**$_\beta$), 3.77 (s, 4H, py-C**H**$_2$), 2.55-2.47 (m, 14H, **H**$_3$C-N-C**H**$_2$-C**H**$_2$), 2.21 (s, 3H, N-C**H**$_3$); ^{13}C-NMR ($CDCl_3$, 100 MHz, 298K) δ, ppm: 157.6 (py**C**$_q$), 136.80 (pyC$_\gamma$), 122.2 (pyC$_\beta$), 62.8 (py-**C**H$_2$), 53.2, 52.4 (N-**C**H$_2$-**C**H$_2$), 45.2 (N-**C**H$_3$), 44.7 (N-**C**H$_3$); HR-MS (ESI-TOF) *m/z*: calc for $[C_{14}H_{24}N_4+H]^+$ 249.2074 found 249.2044.

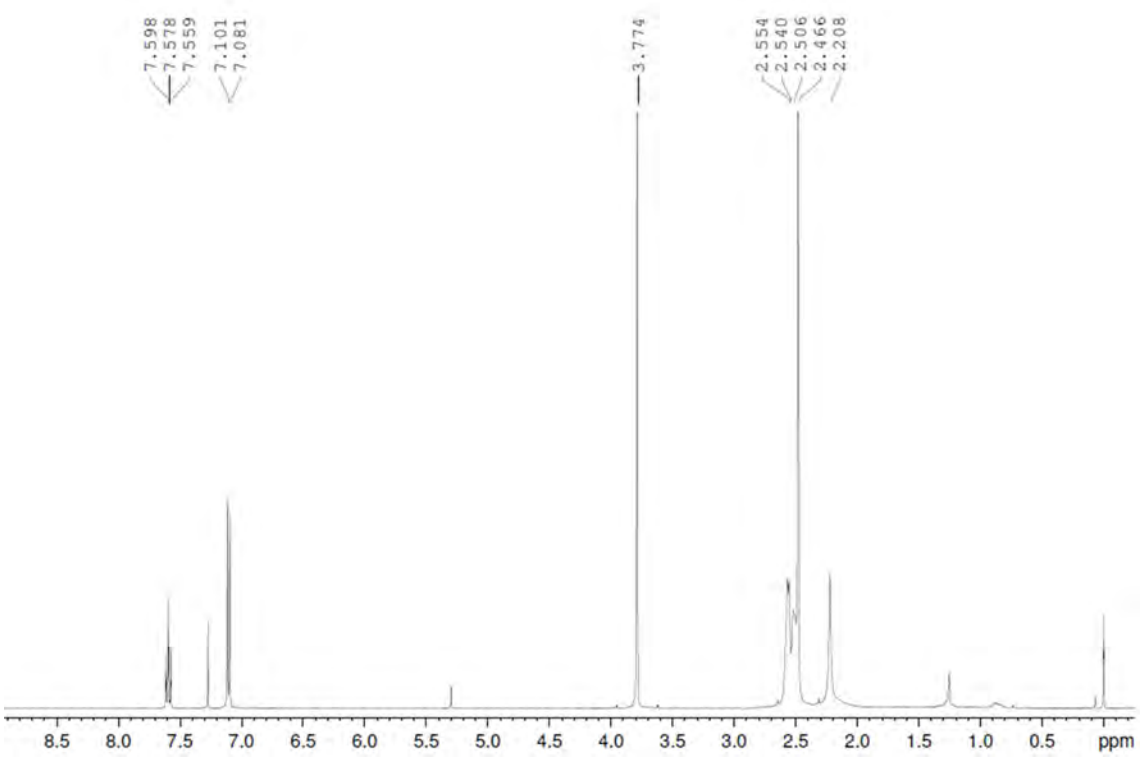

Figure S1 ^{1}H-NMR spectrum of $PyNMe_3$ in $CDCl_3$ at 298 K.

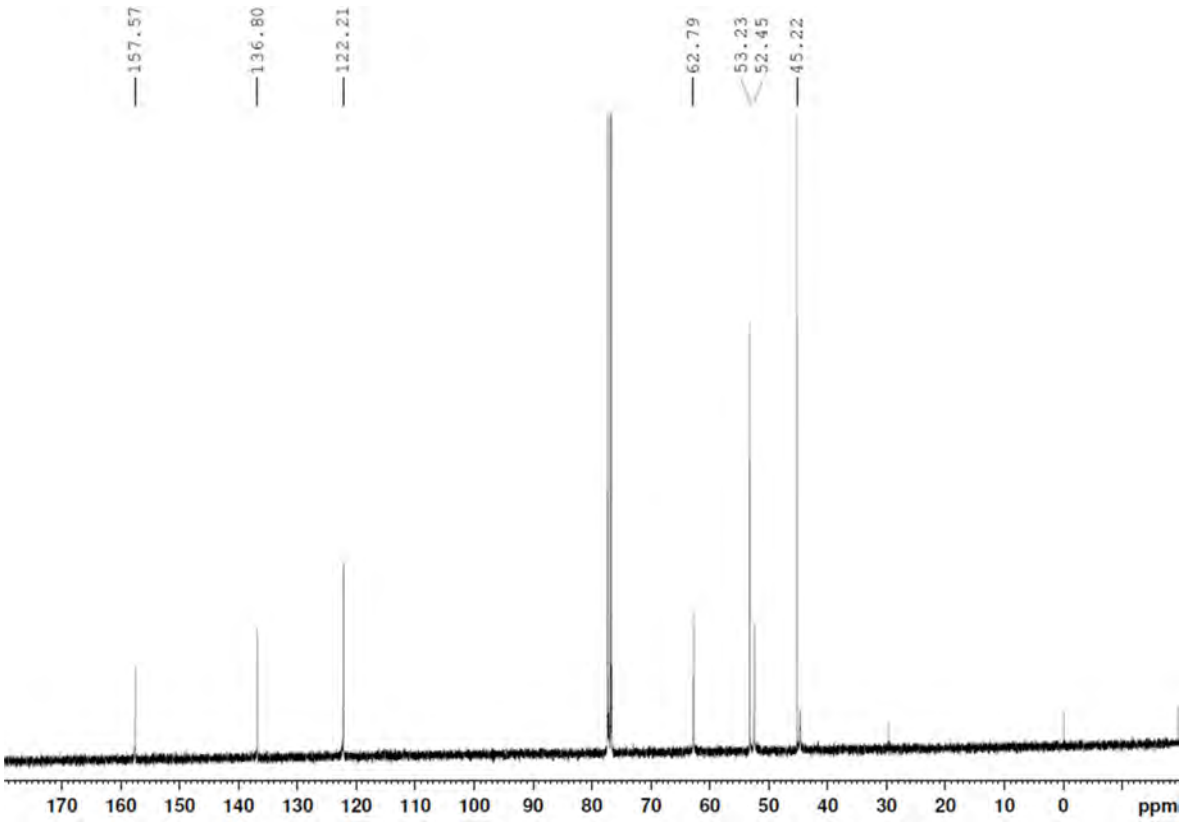

Figure S2 ^{13}C-NMR spectrum of $PyNMe_3$ in $CDCl_3$ at 298 K.

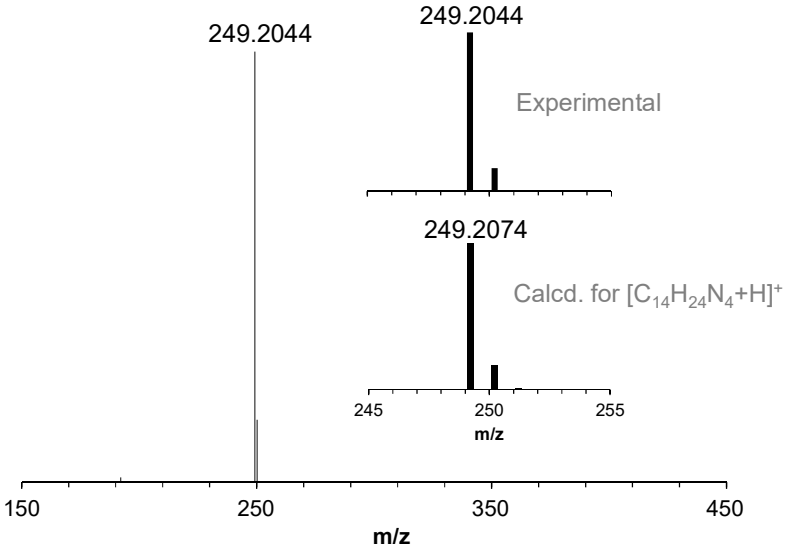

Figure S3 High resolution mass spectrum (HR-MS) of $PyNMe_3$.

Synthesis of $[Fe(CF_3SO_3)_2(PyNMe_3)]$ (1). $[Fe(CF_3SO_3)_2(CH_3CN)_2]$ (28.5 mg, 0.065 mmol) was added directly as a solid to a vigorously stirred solution of $PyNMe_3$ (16.2 mg, 0.065 mmol) in CH_2Cl_2 (2 mL). The solution turned from a pale color to an intense yellow color. Acetonitrile (0.2 mL) was added to ensure the complete solubilization of the complex. The mixture was stirred for 20 minutes and then filtered through celite. Slow diethyl ether diffusion over the resulting solution afforded 30.8 mg (0.051 mmol, 79 %) of yellow crystals. ^{1}H-NMR (CD_3CN, 298 MHz, 298 K) δ, ppm = 124.4, 118.7, 105.3, 91.1, 84.4, 78.6, 68.7, 65.2, 60.6, -9.5, -21.6. HR-MS (ESI-TOF) *m/z*: calc for $[[Fe(C_{14}H_{24}N_{4)}](CF_3SO_3)]^+$ 453.0865 found 453.0882. Anal Calcd. for **1** calcd. C, 32.09; N, 9.35; H, 3.89 %. Found C, 31.90; N, 9.30; H, 4.02 %.

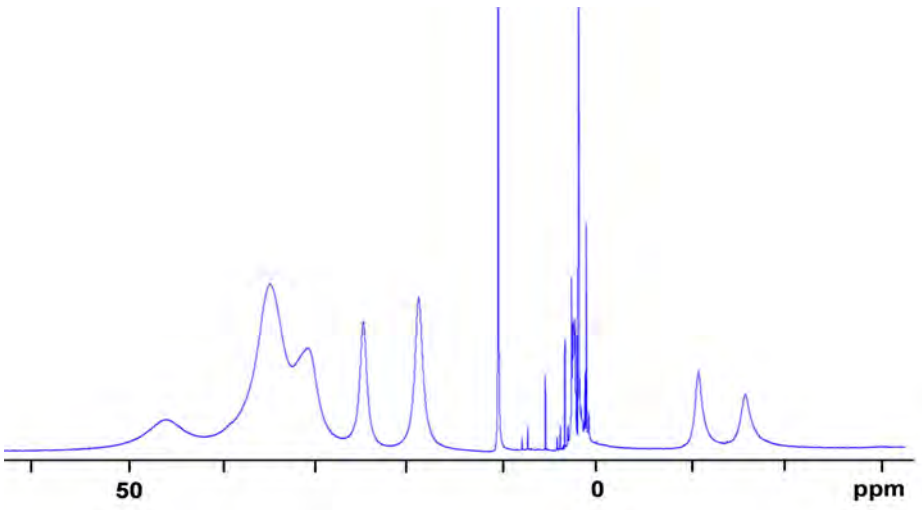

Figure S4 ^{1}H-NMR spectrum of **1** in CD_3CN at 243 K.

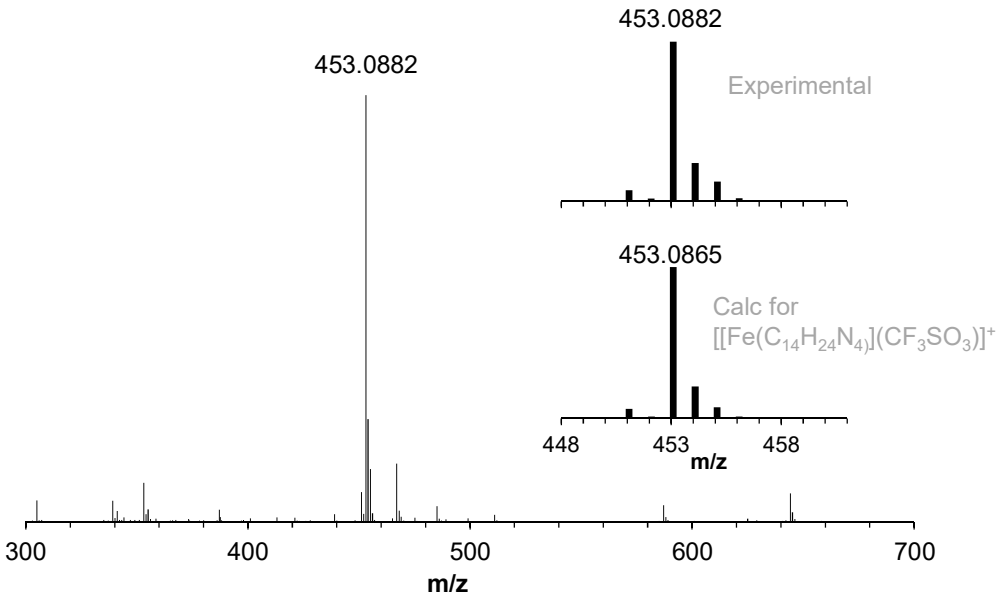

Figure S5 High resolution mass spectrum (HR-MS) of **1**.

Crystal Structure Determination for 1. Crystals of $C_{16}H_{24}F_6FeN_4O_6S_2$ were grown from slow diffusion of diethyl ether in a 10:1 (v/v) dichloromethane:acetonitrile solution of the compound, and used for low temperature (120(2) K) X-ray structure determination. A single crystal of **1** was measured in an Enraf Nonius Kappa CCD diffractometer using MoKα radiation at 120 K respectively. The structure was solved by direct methods using SIR97[2] and refined by full-matrix least-squares on all F^2 using SHELXL97[3] with the WinGX suite.[4] The non-hydrogen atoms were refined anisotropically and hydrogen atoms were placed in calculated positions and refined using a riding model. Hydrogen bonds have been analyzed with SHELXL97.

Table S1 Crystal data for [Fe(CF_3SO_3)$_2$($PyNMe_3$)] (**1**).

Empirical Formula	$C_{16}H_{24}F_6FeN_4O_6S_2$	
Formula weight	602,36	
Temperature	120(2) K	
Wavelength	0,71069 Å	
Crystal system, space group	Monoclinic, P c	
Unit cell dimensions	a = 9.349(5) Å	$\alpha = 90^o$
	b = 9.148(5) Å	$\beta = 123.32(2)^o$
	c = 16.448(6) Å	$\gamma = 90^o$
Volume	1175.5(10) $Å^3$	
Density (calculated)	1.702 g/cm^3	
Absorption coefficient	0.908 mm^{-1}	
F(000)	616	
Cell formula units_Z	2	
Crystal size	0.12 x 0.11 x 0.06 mm	
Θ range for data collection	2.226 to 27.471^o	
Limiting índices	-12<=h<=12, -11<=k<=11, -21<=l<=19	
Reflections collected / unique	8126 / 4828 [R(int) = 0.0407]	
Completeness to Θ	100 % (Θ =25.24^o)	
Refinement method	Full-matrix least-squares on F^2	
Data / restraints / parameters	4828/2/319	
Goodness-of-fit on F^2	1.105	
Final R indices [I>2σ(I)]	R1 = 0.0410, wR2 = 0.0965	
R indices (all data)	R1 = 0.0535, wR2 = 0.1182	
Largest diff. peak and hole	0.527 and -0.843 $e.Å^{-3}$	

Table S2 Selected bond lengths (Å) and angles (^{o}) for [Fe(CF_3SO_3)$_2$($PyNMe_3$)] (**1**).

Fe-N1 2.113(4)	O1-Fe-O4 89.16(13)
Fe-N2 2.267(4)	N1-Fe-N2 77.14(14)
Fe-N3 2.231(4)	N1-Fe-N3 88.21(13)
Fe-N4 2.267(4)	N1-Fe-O4 88.93(13)
Fe-O1 2.054(3)	N1-Fe-N4 76.99(14)
Fe-O4 2.135(3)	N3-Fe-N2 80.99(13)
O1-Fe-N3 95.83(13)	N3-Fe-N4 80.62(13)
O1-Fe-N2 114.28(15)	O4-Fe-N4 109.60(13)
O1-Fe-N4 92.81(15)	O4-Fe-N2 87.46(13)

II. Generation of 2: UV/vis stopped-flow experiments

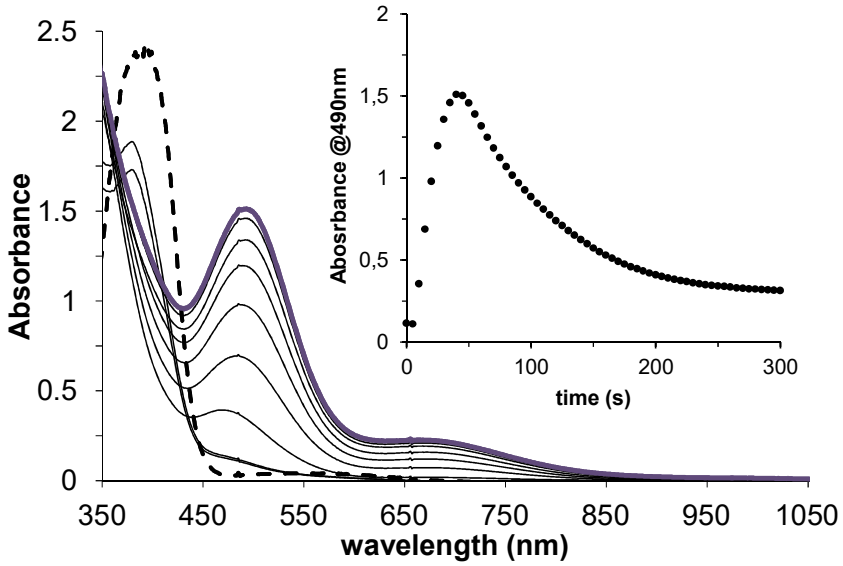

Figure S6 UV-Vis spectra of **1** (1 mM, dashed line), **2** (violet line). Solid black lines show the progressive formation of **2** upon addition of 4 equiv peracetic acid to **1** at -41 °C in acetonitrile over the course of 1 minute. Inset: time trace at 490 nm.

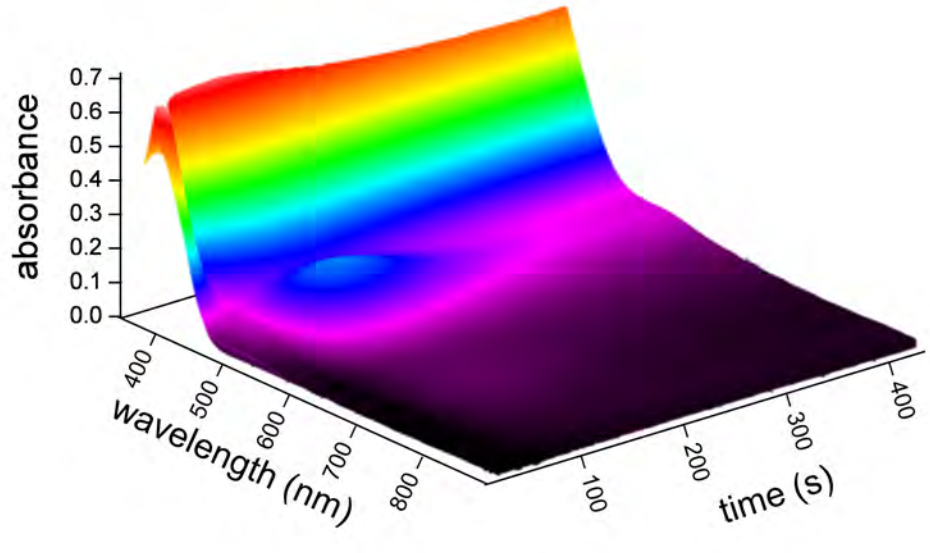

Figure S7 Tridimensional representation of the spectral changes observed for the reaction of **1** with peracetic acid in acetonitrile solution at -35ºC using stopped-flow equipment.

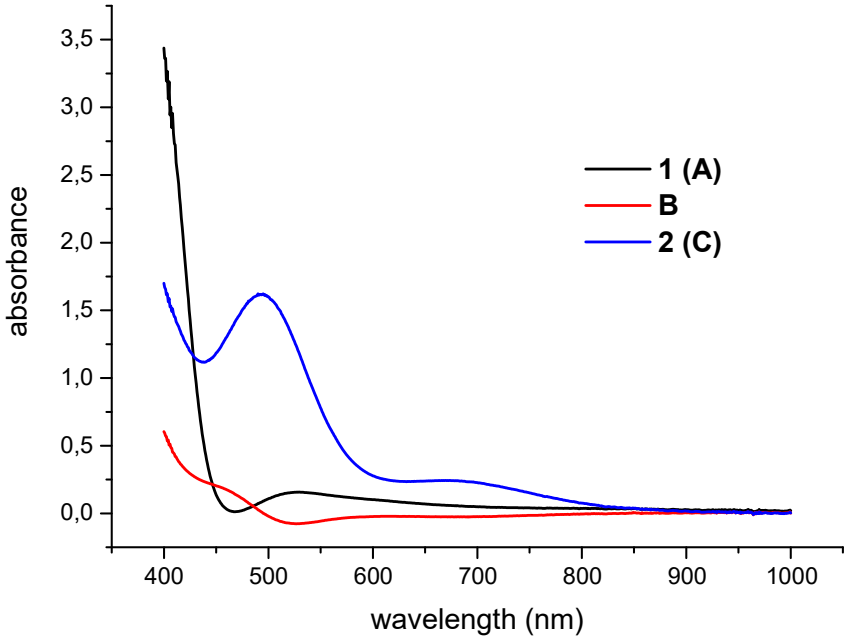

Figure S8 Spectra calculated from the fit of the spectral changes in Figure S7 to a kinetic model with three consecutive kinetic steps (A→B→C→D). A is the starting compound (**1**), C is intermediate **2** and B is an intermediate formed at the early stages of the reaction.

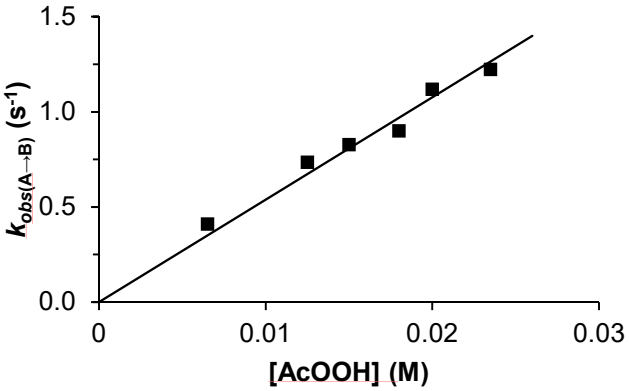

Figure S9 Dependence of $k_{obs(A\rightarrow B)}$ with the concentration of peracetic acid in acetonitrile at -35ºC.

III. Synthesis and characterization of 2 generated with pernonanoic acid (2')

Synthesis of pernonanoic acid[5]

Hydrogen peroxide (0.5 mL, 50%, 8.7 mmol) was added dropwise to a stirred suspension of nonanoic (1.02 g, 6.4 mmol) in MsOH (2 mL) at 40 ºC. After 4.5 h, the colorless solution was cooled, treated with ice (3 g), followed by saturated aqueous $(NH_4)_2SO_4$ solution (3 mL). The resulting mixture was extracted with CH_2Cl_2 (3 x 4 mL), the combined extracts were washed with saturated aqueous $(NH_4)_2SO_4$ (3 x 4 mL), dried ($MgSO_4$), and concentrated by rotary evaporation at room temperature (it is important not warming it up at this point). The desired product, pernonanoic acid, was obtained as a white crystalline solid (0.99 g, 88 % yield). υ_{max}/cm^{-1} 3256 (s), 2917 (s), 2846 (s), 1732 (s), 1466 (s), 1419 (s), 1306 (m), 1257 (m), 1215 (s), 1154 (s), 1103 (s), 1055 (m), 940 (m), 885 (s), 754 (s), 722 (s), 497 (m), 469 (m), 417 (m). ^{1}H-NMR ($CDCl_3$, 400 MHz, 298K) δ, ppm: 11.38 (s br, 1H, O**H**), 2.40 (t, J = 7.68 Hz, 2H, $\mathbf{H_a}$), 1.68 (m, 2H, $\mathbf{H_b}$), 1.26 (m, 10H, $\mathbf{H_c}$), 0.87 (m, 3H, $\mathbf{H_d}$). ^{13}C-NMR ($CDCl_3$, 100 MHz, 298K) δ, ppm: 174.67, 31.72, 30.42, 28.99, 28.91, 24.62, 22.59, 14.03.

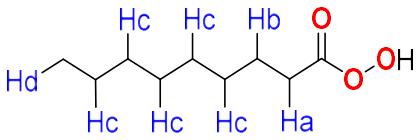

Figure S10 Pernonanoic acid structure.

Generation of 2'

2' was generated in an analogous way than **2**. In a typical experiment, a 1 mM solution of **1** in dry acetonitrle was prepared inside the glovebox. 2 mL of this solution were placed in a UV-Vis cuvette (2 μmols of **1**). The quartz cell was capped with a septum and taken out of the box, placed in the Unisoku cryostat of the UV-Vis spectrophotometer and cooled down to 238 K. After reaching thermal equilibrium, a UV-Vis spectrum of the starting complex was recorded. Then, 50 μL of a solution containing pernonanoic acid in dry acetonitrile were added (10 μmols). The formation of a band at λ_{max} = 490 nm and a shoulder at λ_{max} = 660 nm was observed (Figure S11).

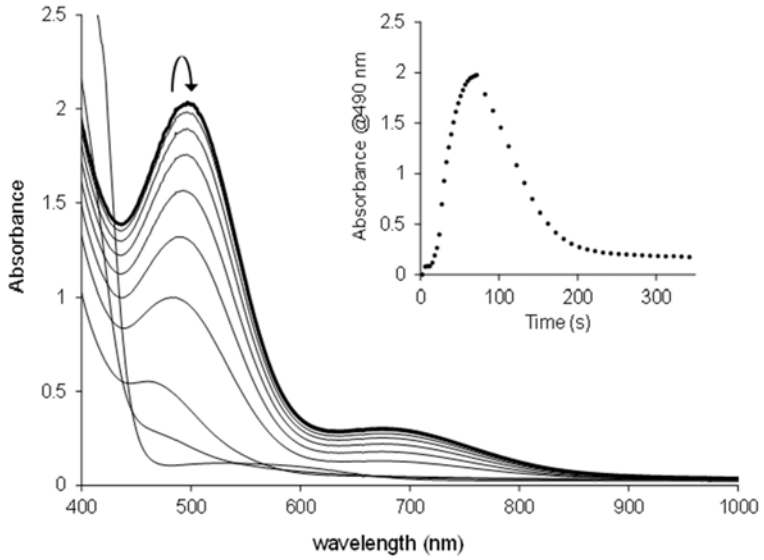

Figure S11 UV-Vis monitoring of the reaction of **1** (1.26 mM) with pernonanoic acid (10 equiv) in acetonitrile at -40ºC to generate **2'**. Inset: time trace of the 490 nm chromophore.

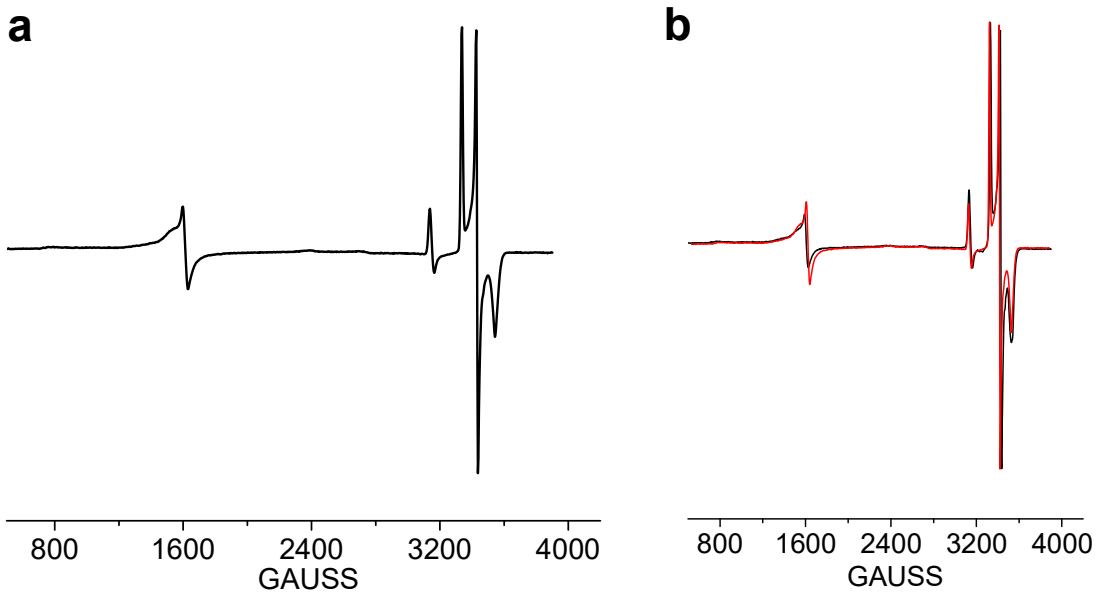

Figure S12 a) EPR spectrum of **1** in 1:3 (v/v) acetonitrile:acetone reacted with 10 equiv nonanoic peracid at -60ºC and frozen at maximum accumulation of **2'**. EPR conditions: T = 20 K, 0.2 mW, microwave power, 1 mT modulation. b) Overlay of the EPR spectra of **2** and **2'** generated by reacting **1** in 1:3 (v/v) acetonitrile:acetone with peracetic acid (5 equiv) and pernonanoic acid (10 equiv), respectively.

Kinetic analysis for the formation of 2'

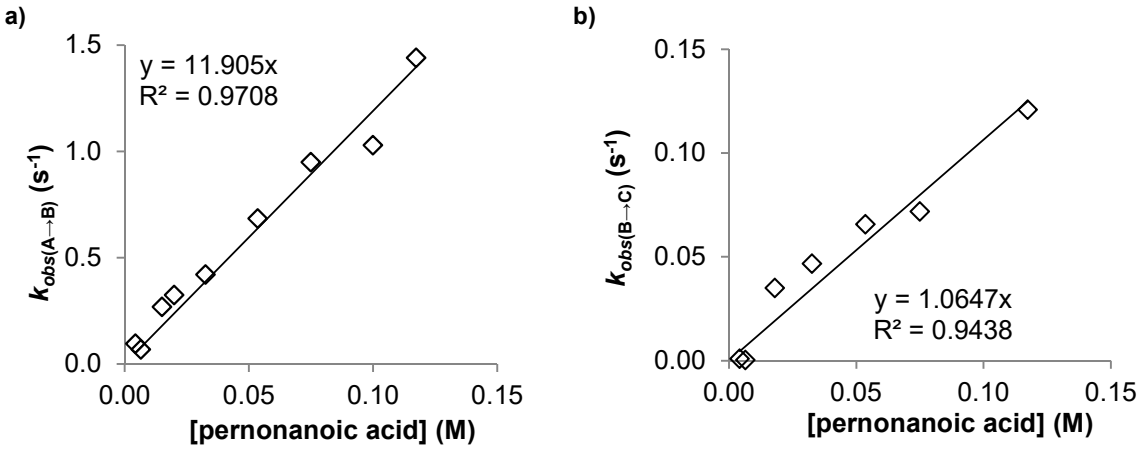

Figure S13 a) Dependence of $k_{obs(A\rightarrow B)}$ with the concentration of pernonanoic acid in acetonitrile at -35ºC. b) Dependence of $k_{obs(B\rightarrow C)}$ with the concentration of pernonanoic acid in acetonitrile at -35ºC.

IV. Reactivity of 2 towards organic substrates: UV/vis stopped-flow experiments

The kinetics of reactions of intermediate **2** with substrates was measured in sequential cryo-stopped-flow experiments at -35 ºC. In these experiments, the starting complex and peracetic acid were mixed and the mixture was allowed to react in a delay line maintained at low temperature for the time required to achieve the maximum concentration of intermediate **2**. At this time, the solution in the delay line was mixed with another acetonitrile solution containing an excess of substrate. The concentration of the different species participating in the process were optimized in preliminary experiments; the concentrations of AcOOH and the starting complex were finally kept in a 4:1 molar ratio, and the substrate concentration was selected in each case to achieve adequate reaction times while maintaining pseudo-first order conditions of substrate excess with respect to intermediate **2**. The kinetics of reaction with the substrates was evaluated from the decay of the absorbance at 490 nm following the second mixing, so that they correspond to the disappearance of intermediate **2**. In all cases the kinetic traces could be satisfactorily fitted by a single exponential over the entire course of the reaction (see Figure S14), and the values derived for the observed rate constants show a linear dependence on the substrate concentration (Figure 2a), so that under the experimental conditions used the rate law is k_s[**2**][substrate].

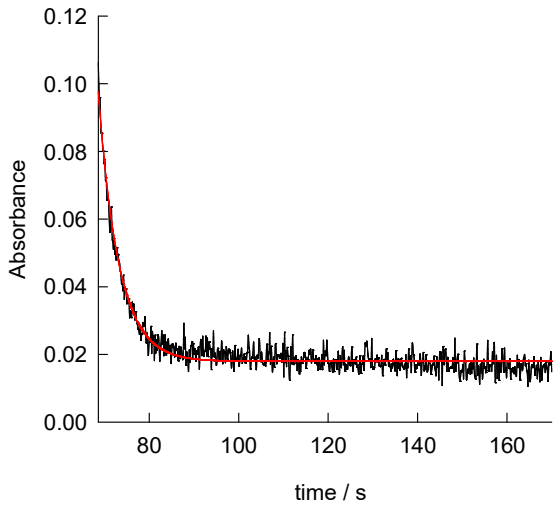

Figure S14 Typical experimental and calculated kinetic traces observed for the reaction of **2** with substrates. The present curve corresponds to reaction of **2** with cyclohexane (0,061 mM, black) and the calculated trace (red) corresponds to the fit by a single exponential.

This rate law can be accommodated by the catalytic mechanism shown in equations 1-2, in which **2** is assumed to react initially with the substrate to form the oxidized substrate (SO) and an intermediate (I) that regenerates **2** upon reaction with the excess of AcOOH. However, because of the very small excess of oxidant used in these experiments (part of the oxidant has been consumed for the generation of **2** from **1**), regeneration of **2** is limited at the very early stages of the reaction. Once the oxidant excess is consumed the kinetic traces show the decay of **2** with an observed rate constant $k_{obs} = k_2$ [S].

2 + S → I + SO k_2 (1)

I + CH_3CO_3H → **2** fast (2)

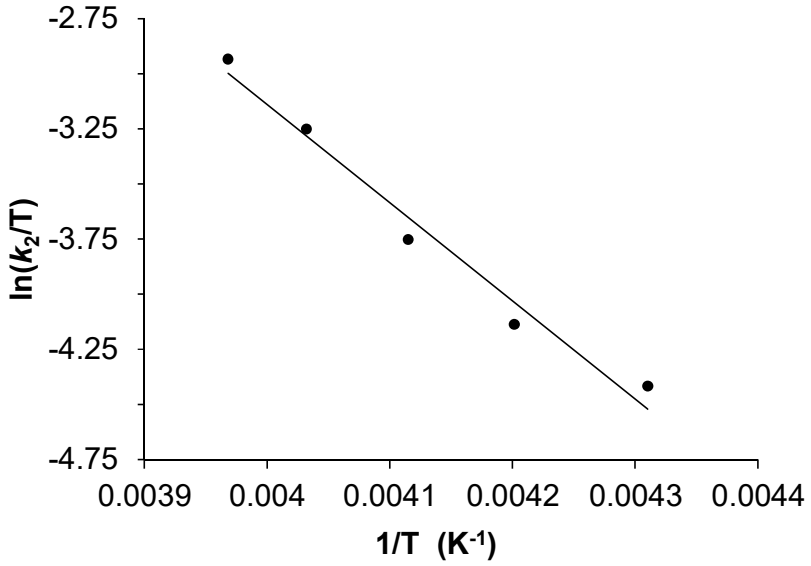

Figure S15 Eyring plot for the reaction of **2** with cyclohexane in acetonitrile.

Species **2'**reacts with cyclohexane with a rate constant k_2 = 4.8 ± 0.4 $M^{-1}s^{-1}$ at -35 º C (Figure S16), very close to that observed for **2**.

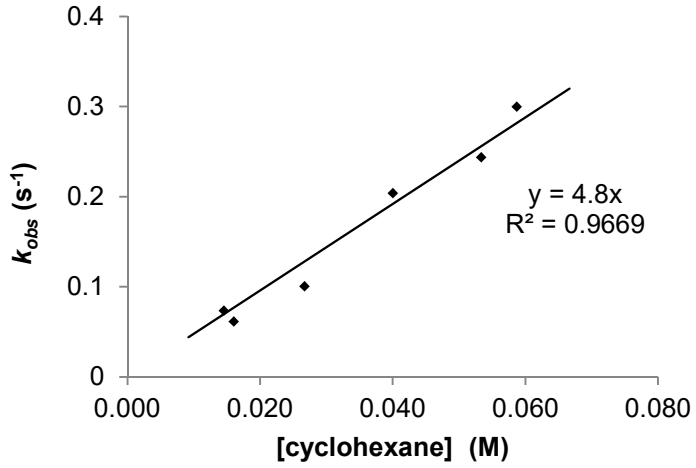

Figure S16 Observed reaction rates (k_{obs}) for the reaction of **2'** with different amounts of cyclohexane at -35ºC in acetonitrile.

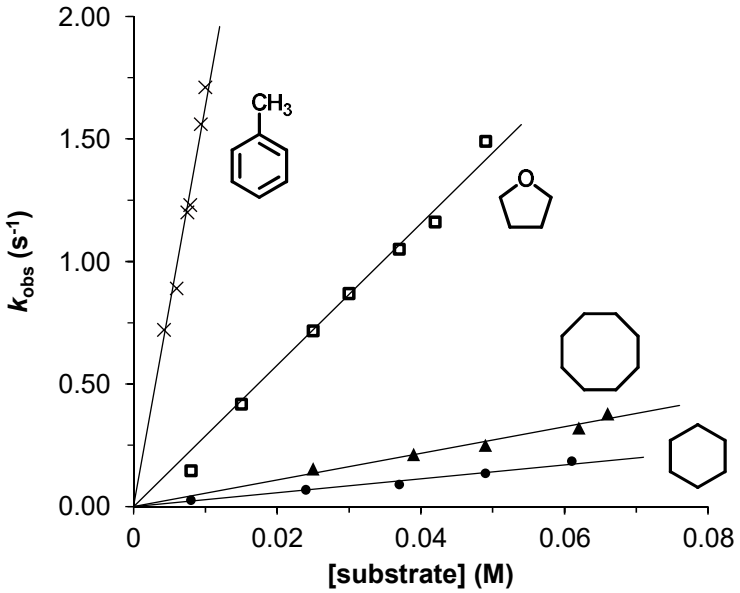

Figure S17 Plot of kinetic data at -41ºC for the reaction of **2** with different organic substrates in acetonitrile (circles: cyclohexane; triangles: cyclooctane; squares: tetrahydrofuran; crosses: toluene).

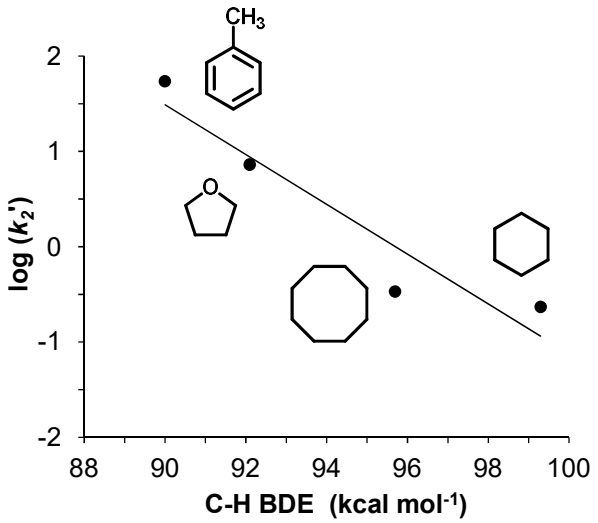

Figure S18 Plot of log k_2' (determined at -41°C in acetonitrile) versus the C-H BDE of different substrates.

Table S3 Rate constants for the reaction of **2** with different substrates in acetonitrile.

Substrate	T (ºC)	k_2 ($M^{-1}s^{-1}$)
Cyclohexane	-35	3.8±0.1[a]
Cyclohexane-d_{12}	-35	0.78±0.03
Cyclohexane	-21	13.4±0.1
Cyclohexane	-25	9.6±0.2
Cyclohexane	-30	5.7±0.3
Cyclohexane	-41	2.8±0.1
Cyclooctane	-41	5.4±0.1
Tetrahydrofuran	-41	28.9±0.6
Toluene	-41	163.6±3.3

[a]A value of 4.8 ± 0.4 $M^{-1}s^{-1}$ at -35 º C was obtained using intermediate **2'** formed with pernonanoic acid (Figure S16).

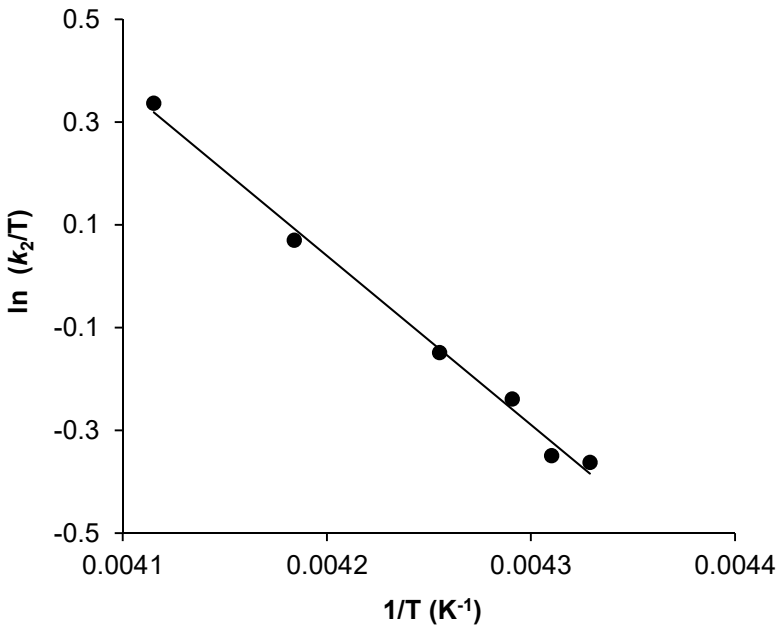

Figure S19 Eyring plot for the reaction of **2** with toluene in acetonitrile.

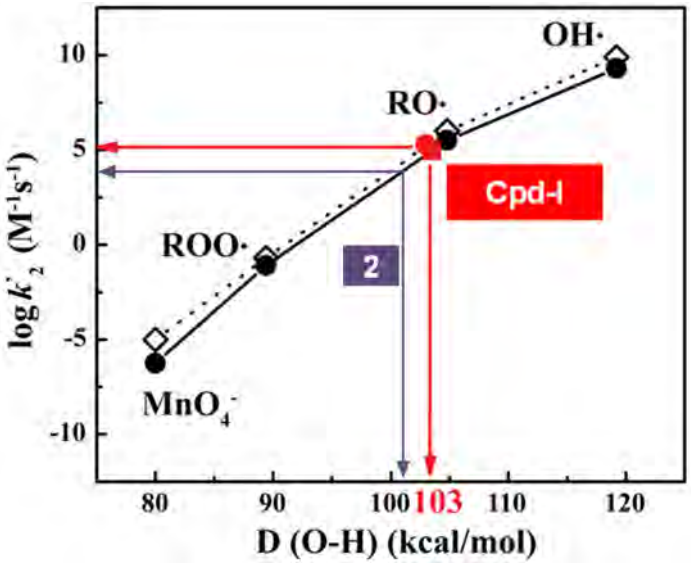

Figure S20 Plot of log k_2 of different oxidants towards toluene vs. the strength of the O-H bond formed at room temperature. Plotting rate constants for hydrogen atom abstraction by **2** and Cpd-I with toluene gives a Fe^{IV}O-H bond strength of ≈101 and 103 kcal·mol^{-1} respectively.[6]

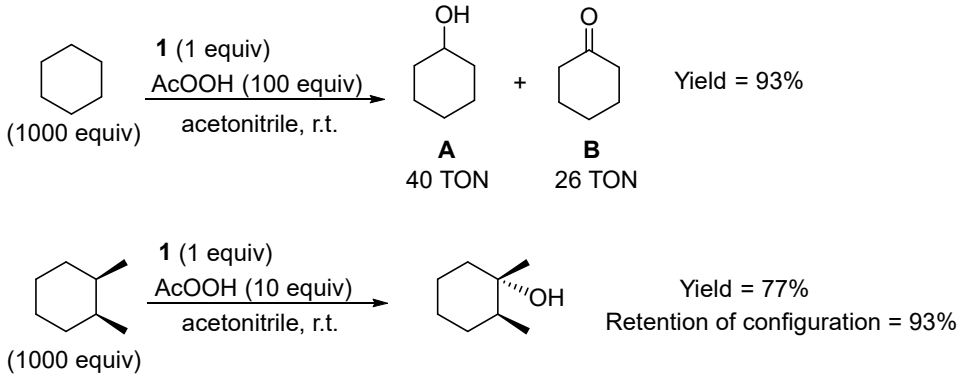

Scheme S2 Oxidation of cyclohexane and *cis*-1,2-dimethylcyclohexane catalyzed by **1** using AcOOH as oxidant and acetonitrile as solvent at room temperature.

V. Synthesis and characterization of the Fe^{III}-hydroxamate analog (4)

Synthesis of N-hydroxypivalamide

N-hydroxypivalamide (*t*BuCON(H)OH) was prepared following a procedure similar to Reddy *et al.* starting from pivalic acid.[7]

Ethyl chloroformate (1.3 g, 12 mmols) was added together with N-methylmorpholine (1.3 g, 13 mmols) to a solution of pivalic acid (1.02 g, 10 mmols) in diethyl ether (30 mL) at 0ºC. The solution was stirred for 10 minutes at this temperature and then freshly prepared hydroxylamine (15 mmols) in methanol was added. The reaction was stirred at room temperature for 15 minutes and then the solvent was removed under pressure. A white solid was obtained after recrystallization with CH_2Cl_2. HR-MS (ESI-TOF) *m/z*: calc for $[C_5H_{11}NO_2Na]^+$ 140.0682, found 140.0683; $[(C_5H_{11}NO_2)_2Na]^+$ 257.1472, found 257.1481. ^{1}H-NMR (400 MHz, D_2O, 298K): 1.19 (s, 9H). ^{13}C-NMR (100MHz, D_2O, 298K) 178.94 (C_q), 37.38 (C_{tBu}), 26.28 (CH_3).

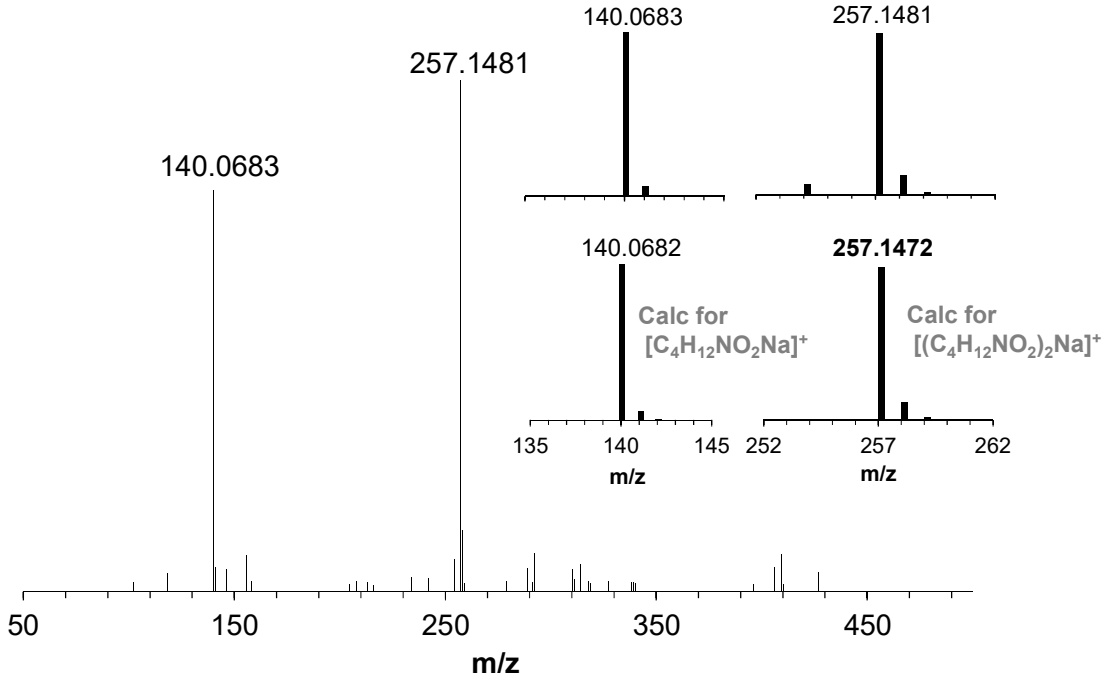

Figure S21 High resolution mass spectrum (HR-MS) of N-hydroxypivalamide.

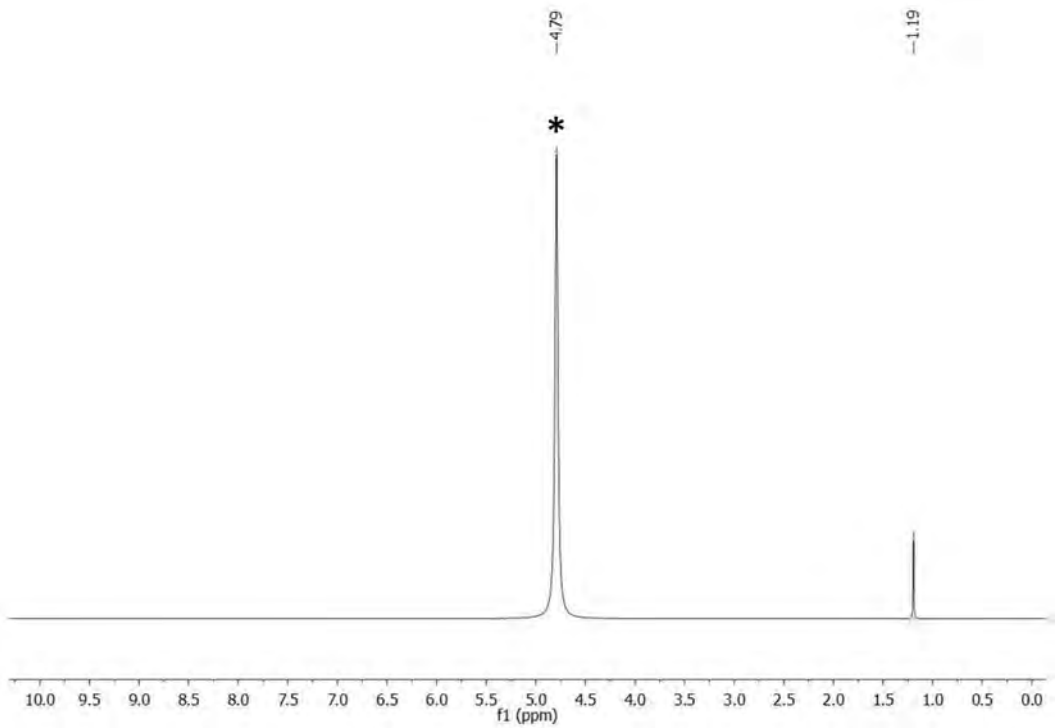

Figure S22 ^{1}H-NMR (400 MHz, D_2O, 298 K) of N-hydroxypivalamide.

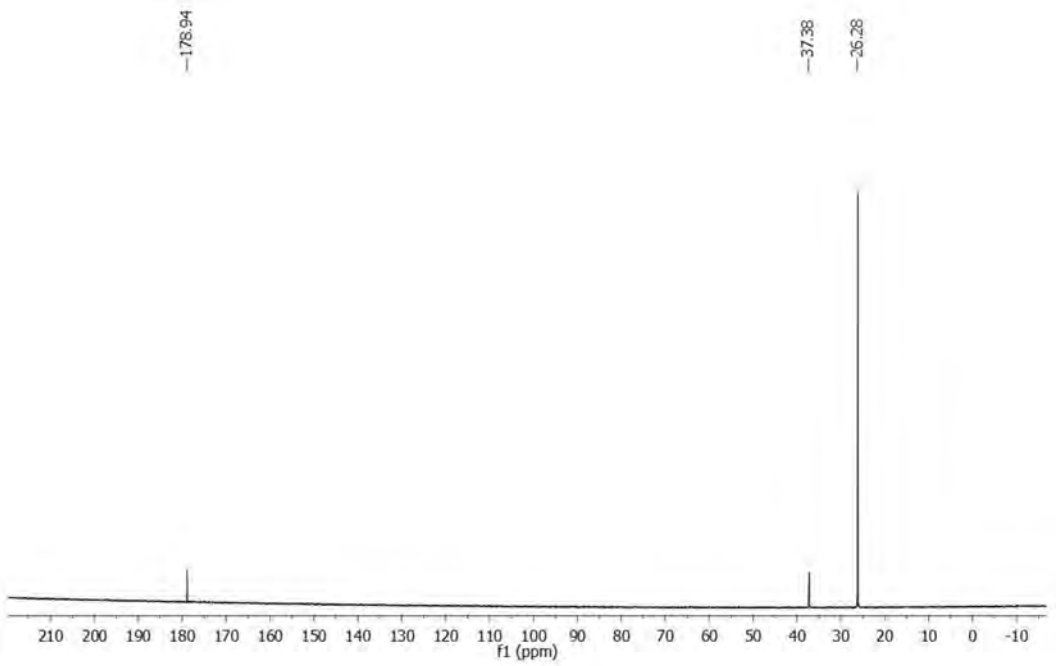

Figure S23 ^{13}C-NMR (100 MHz, D_2O, 298 K) of N-hydroxypivalamide.

Synthesis of $[Fe^{III}(tBuCON(H)O)(PyNMe_3)](X)_2$ ($4X_2$, X = CF_3SO_3 or ClO_4)

$[Fe^{III}(tBuCON(H)O)(PyNMe_3)](CF_3SO_3)_2$ (**$4(CF_3SO_3)_2$**) was prepared by adding N-hydroxypivalamide (4.3 mg, 36 mmols) to **1** (22 mg, 36 mmols) in acetonitrile (1 mL) in an open air atmosphere. The mixture was left stirring for 30 minutes and it changed from dark yellow to reddish-brown. The solution was filtered through a celite plug and solid material (21.1 mg, 83 %) was obtained after slow diffusion of diethyl ether for some days. No crystals suitable for X-ray diffraction could be obtained, for this reason the perchlorate analogue was synthesized (see below). HR-MS (ESI-TOF) *m/z*: calc for $[Fe(C_5H_{10}NO_2)(C_{14}H_{24}N_4)]^{2+}$ 210.1026, found 210.1013; calc for $[C_{14}H_{24}N_4]^+$ 249.2074, found 249.2058; calc for $[Fe(C_5H_{10}NO_2)(CF_3SO_3)(C_{14}H_{24}N_4)]^+$ 569.1577, found 569.1531.

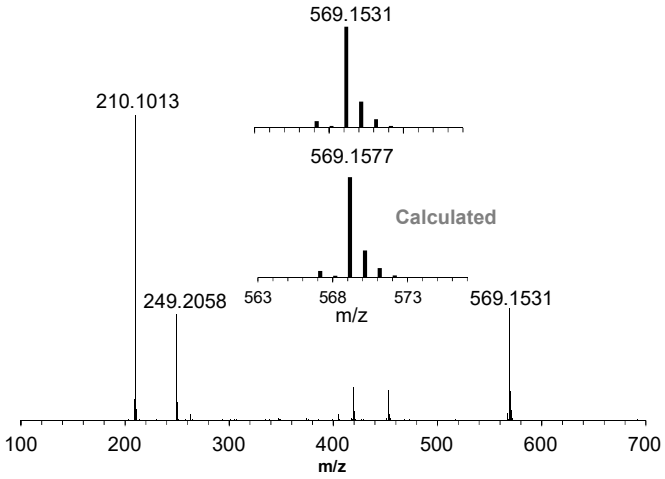

Figure S24 High resolution mass spectrum of **$4(CF_3SO_3)_2$**.

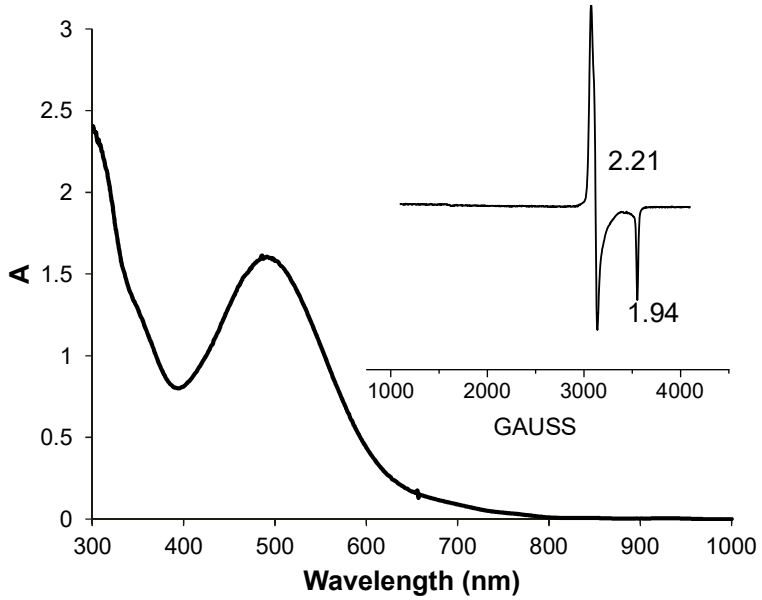

Figure S25 UV-Vis of a 1 mM **$4(CF_3SO_3)_2$** solution in acetonitrile at -40ºC that exhibits a λ_{max} = 490 nm and (inset) its axial EPR spectrum showing signals at *g* = 2.21 and 1.94.

$[Fe^{III}(t\text{BuCON(H)O})(PyNMe_3)](ClO_4)_2$ (**4(ClO$_4$)$_2$**) was prepared by adding $FeCl_2$ (12.5 mg, 98 mmols) to a solution of $PyNMe_3$ (24.5 mg, 98 mmols) in acetonitrile (1 mL) under inert atmosphere. After stirring for two hours, $AgClO_4$ (40.9 mg, 197 mmols) was added directly as a solid and the solution was left stirring for another 2 hours. The yellow solution was filtered through an Acrodisc® in order to remove the precipitated AgCl and N-hydroxypivalamide (11.5 mg, 98 mmols) was added to the solution directly as a solid. At this point an O_2 atmosphere was established and the solution was stirred overnight, turning into intense red. The solvent was evaporated and the precipitate was redissolved in dichloromethane (2 mL) and acetonitrile (100 μL). The solution was filtered through a celite plug and single crystals suitable for X-ray diffraction (43 mg, 70 %) were obtained after slow diffusion of diethyl ether. HR-MS (ESI-TOF) *m/z*: calc for $[Fe(C_5H_{10}NO_2)(C_{14}H_{24}N_4)]^{2+}$ 210.1026, found 210.1019; calc for $\{[Fe(C_{14}H_{24}N_4)](ClO_4)\}^+$ 403.0830, found 403.0833. calc for $\{[Fe(C_5H_{10}NO_2)(C_{14}H_{24}N_4)](ClO_4)\}^+$ 519.1542, found 519.1538;

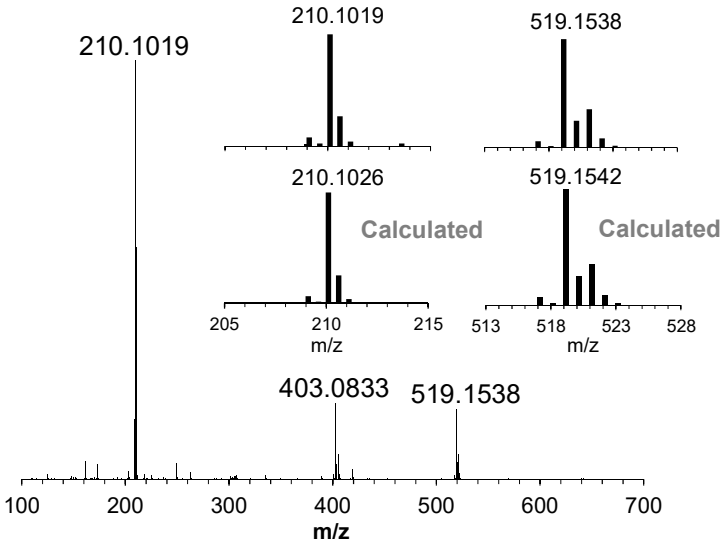

Figure S26 High resolution mass spectrum (HR-MS) of **4(ClO$_4$)$_2$**.

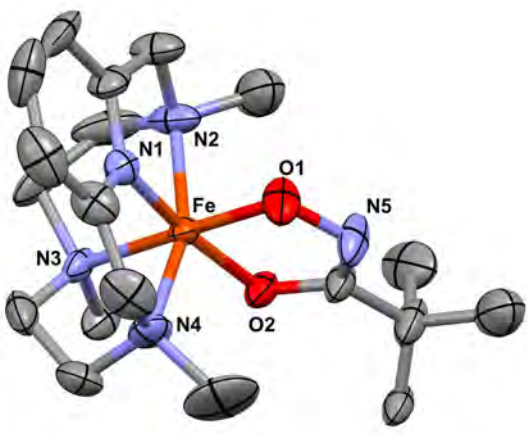

Figure S27 Thermal ellipsoid plot (30% probability) of **4(ClO$_4$)$_2$**. Perchlorate anions and hydrogen atoms have been omitted for clarity.

Table S4 Crystal data for **4(ClO$_4$)$_2$**.

Empirical Formula	$C_{19}H_{34}Cl_2FeN_5O_{10}$	
Formula weight	619,26	
Temperature	130(2) K	
Wavelength	0.71073 Å	
Crystal system, space group	Monoclinic, P 21/c	
Unit cell dimensions	a = 12.875(4) Å	$\alpha = 90^o$
	b = 10.538(3) Å	$\beta = 93.329(6)^o$
	c = 21.741(7) Å	$\gamma = 90^o$
Volume	2944.8(16) Å^3	
Density (calculated)	1.397 g/cm^3	
Absorption coefficient	0.748 mm^{-1}	
F(000)	1292	
Cell formula units_Z	4	
Crystal size	0.35 x 0.30 x 0.1 mm	
Θ range for data collection	1.877 to 28.289^o	
Limiting indices	-15<=h<=14, -13<=k<=13, -28<=l<=26	
Reflections collected / unique	11887 / 5675 [R(int) = 0.0711]	
Completeness to Θ	ACTA 50 %	
Refinement method	Full-matrix least-squares on F^2	
Data / restraints / parameters	5675/0/340	
Goodness-of-fit on F^2	1.026	
Final R indices [I>2σ(I)]	R1 = 0.1179, wR2 = 0.3203	
R indices (all data)	R1 = 0.2100, wR2 = 0.3844	
Largest diff. peak and hole	0.863 and -0.535 e.Å^{-3}	

Table S5 Selected bond lengths (Å) and angles (^{o}) for **4(ClO$_4$)$_2$**.

Fe-N1	1.916(8)	O2-Fe1-N3	93.1(3)
Fe-N2	2.041(9)	O1-Fe1-N4	97.0(4)
Fe-N3	2.020(8)	N1-Fe1-N4	82.2(4)
Fe-N4	2.036 (9)	O2-Fe1-N4	99.5(4)
Fe-O1	1.812(8)	N3-Fe1-N4	83.7(4)
Fe-O2	1.923(7)	O1-Fe1-N2	95.7(4)
O1-Fe1-N1	87.2(3)	N1-Fe1-N2	82.6(4)
O1-Fe-O2	85.1(3)	O2-Fe1-N2	97.4(4)
N1-Fe1-N3	94.6(3)	N3-Fe1-N2	84.1(4)

VI. Characterization of 2

VI.1 Additional EPR spectra

In the following we show a variety of EPR spectra collected along the time course of the rise and decay of the 490 nm chromophore. Figure S28 shows the *g* = 2 region of spectra of samples frozen between t = 30 s and t = 120 s after addition of 5 equivalents of peracetic acid to a 1 mM solution of **1** at -50 °C in a 1:3 (v/v) acetonitrile:acetone solvent mixture. In this time interval we observed the increase of the g_{max} = 2.20 (**2a**) and g_{max} = 2.07 (**2b**) species; respective *g*-values are at (2.20, 2.19, 1.99) and (2.07, 2.01, 1.95). These two signals reach their maximal intensity near t = 120 s. Figure S29 shows the decline of these signals in the time interval from 120 s to 3000 s. Spectral simulations using the SpinCount software yielded the concentration of **2a** and **2b** at each time point; these simulations yielded the data points entered into Figure 4b of the main text (solid and open red circles). Figure S30 shows the time course of the decay (120 s - 2900 s) after addition of 50 equiv cyclohexane at t = 120 s. The resulting concentrations are also plotted in Figure 4b (solid and open blue circles).

The EPR spectra of Figures S28-S30 reveal a third S = ½ species whose time course is not correlated with the kinetics of the 490 nm chromophore. This species has *g* values at 2.21, 2.14 and 1.97; we label it as the g_{mid} = 2.14 species, because its g_{mid} feature can be observed unobscured over the whole time course. Figure S31 shows time traces of the development of this species in the presence and absence of cyclohexane, showing that its rate of formation is not affected by the addition of cyclohexane. At the endpoint, the g_{mid} = 2.14 species has accumulated to ≈ 28 % of the Fe in the sample. It can be seen that its kinetic behavior does not correlate at all with the kinetics of the 490-nm chromophore that correlates with **2a** and **2b**. The g_{mid} = 2.14 signal clearly represents a low-spin Fe^{III} complex and fits well to the Griffith-Taylor model. Its chemical nature still needs to be determined. Table S6 lists the rate constants (in s^{-1}) of the three S = ½ species, as determined by fitting the time course of the signal to first-order expressions.

Table S6 First-order rate constants (s^{-1}) at -50 °C for the formation or decay of the two S = 1/2 species that correlate with the kinetics of the 490 nm chromophore (**2a** and **2b**), and for the formation of the g_{mid} = 2.14 species (row 3). Numbers in italics are decay rates.

EPR species	upon formation of the 490-nm chromophore	upon decay of the 490-nm chromophore	upon decay of the 490-nm chromophore with added C_6H_{12}
***g* = 2.20, 2.19, 1.99 (2a)**	0.030	*0.0019*	*0.0045*
***g* = 2.07, 2.01, 1.95 (2b)**	0.030	*0.0019*	*0.0049*
***g* = 2.21, 2.14, 1.97**	-	0.0013	0.0013

All samples also contained a considerable amount of poorly resolved high-spin (S = 5/2) Fe^{III} species, but the time course of these signals did not correlate with the decay of the 490-nm chromophore. Figure S32 shows two wide sweep traces taken at the t = 120 s and t = 3000 s time points. Besides the low-spin signals mentioned above there are at least two high-spin Fe^{III} species: one broad feature with E/D ≈ 0.15-0.20 and a sharper one with E/D near 1/3 (the feature at g ≈ 4.3). Although a glance at Figure S32 would suggest a substantial intensity increase of the high-spin species, spectral simulations suggest that the sum of the high-spin signals accounts for about 40% of the total Fe at t = 120 s and about 50 % of Fe at 3000 s. The fraction of high-spin species seen at t = 120 s agrees well with our Mössbauer quantification (see below) which is quite precise (± 2%) for the high-spin species.

We have observed various minority EPR species, among them one with a sharp negative-going resonance at g = 2.00 (and perhaps the bump at g = 2.03). This signal is not necessarily associated with Fe. There are two broader features at g ≈ 2.28 (positive peak) and g ≈ 1.89 (negative peak). These signals, of unknown nature, were present in all samples along the time course with the same amplitude.

It should be mentioned that we have no evidence that **2a** and **2b** decay into EPR active complexes, although some iron associated with the chromophore may end up, with some delay, as high-spin Fe^{III}.

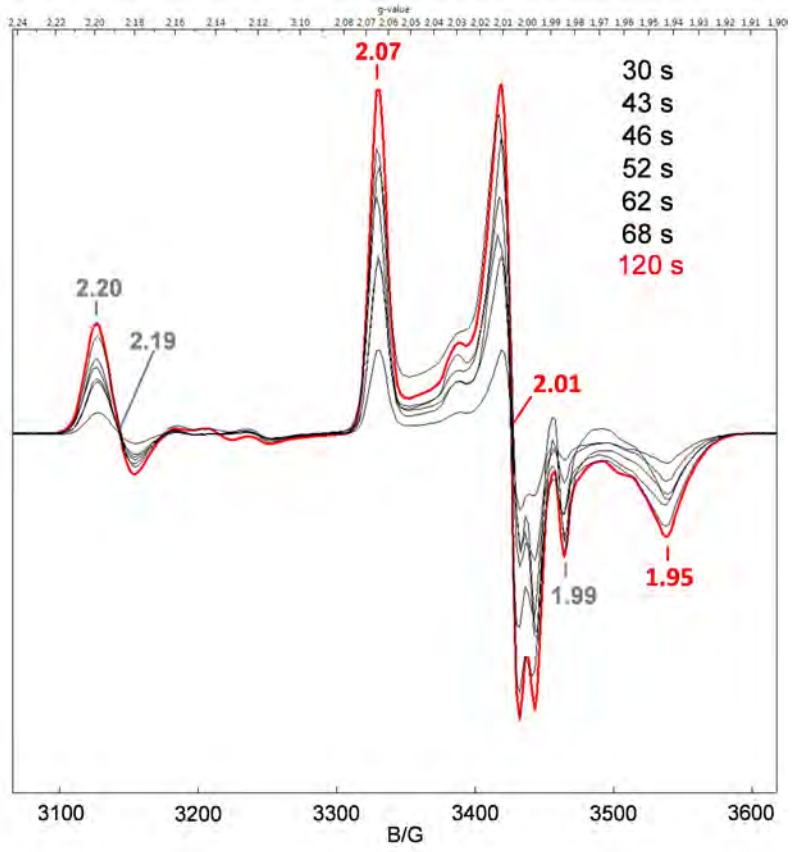

Figure S28 EPR spectra of samples collected during the formation of the 490-nm chromophore **2** after addition of peracetic acid (5 equiv) to a 1 mM solution of **1** at -50 °C in a 1:3 (v/v) acetonitrile:acetone solvent mixture. Only the *g* = 2 region is shown. At least three species are present, namely the *g* = (2.20, 2.19, 1.99) species (**2a**, 5% of total Fe at maximal concentration at 120 s), the *g* = (2.07, 2.01, 1.95) species (**2b**, 40% of total Fe at maximal concentration at 120 s), and a minority species (≈ 2% at maximal concentration) that produces the sharp downward feature at *g* = 2.00 (the bump at *g* = 2.03 may also belong to this species). EPR conditions: T = 20 K, 0.2 mW microwave power, 1 mT modulation.

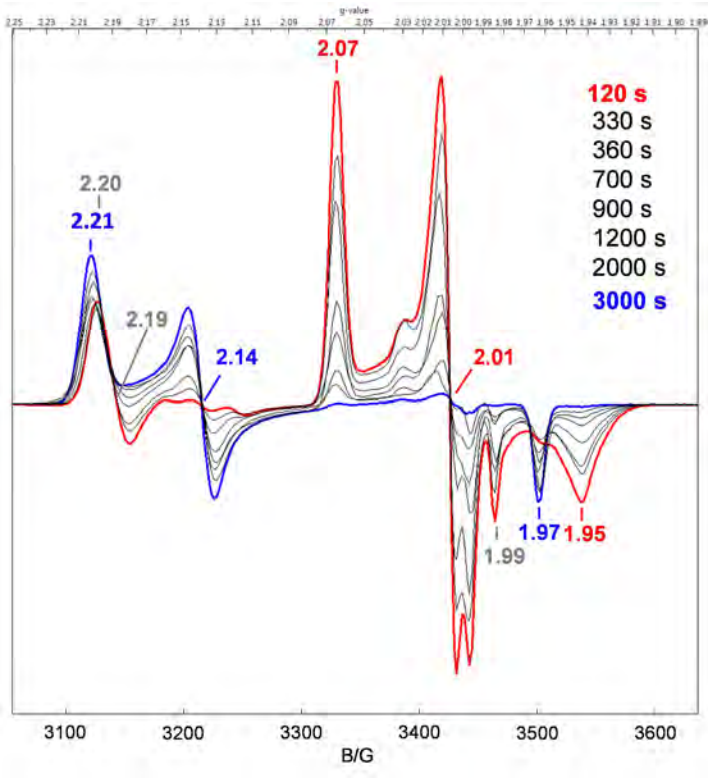

Figure S29 EPR spectra of samples collected during the decay of the 490-nm chromophore **2**, generated after addition of peracetic acid (5 equiv) to a 1 mM solution of **1** at -50 °C in a 1:3 (v/v) acetonitrile:acetone solvent mixture. During the decay of the *g* = (2.20, 2.19, 1.99) (**2a**) and *g* = (2.07, 2.01, 1.95) (**2b**) species, a new feature with *g* values at *g* = 2.21, 2.14, and 1.97 arises. The g_{mid} = 2.14 signal is kinetically not related the decay of the **2a** and **2b**, and its rate of appearance did not change upon addition of cyclohexane (see Figure S31 and Table S6). At t = 3000 s the blue spectrum was observed.

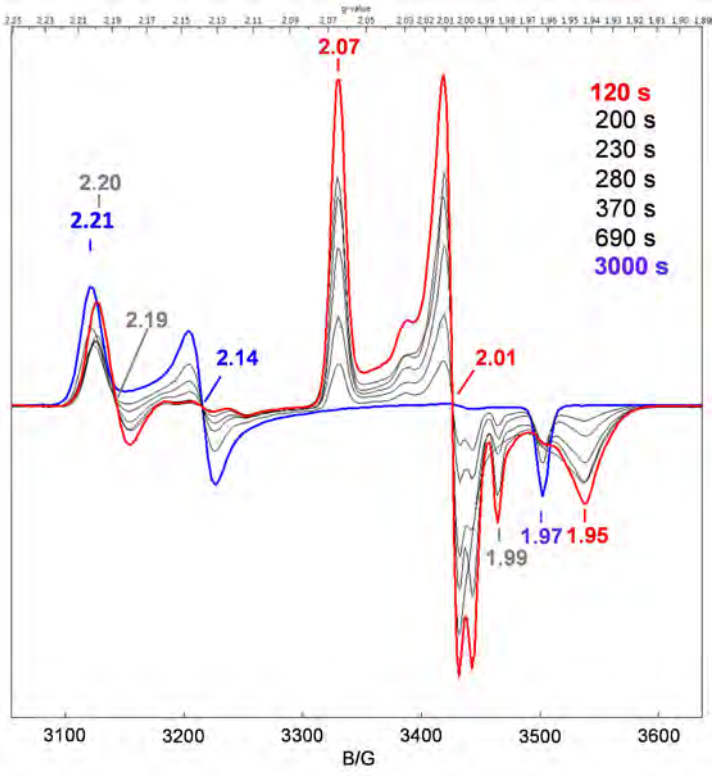

Figure S30 EPR spectra for samples collected during the decay of **2** after addition of cyclohexane (50 equiv) at t = 120 s in a 1:3 (v/v) acetonitrile:acetone solvent mixture at -50 ºC. In the presence of 50 equivalents cyclohexane, the pseudo first-order decay rates of the g_{max} = 2.20 and 2.07 species (**2a** and **2b**) both increased by a factor 2.5.

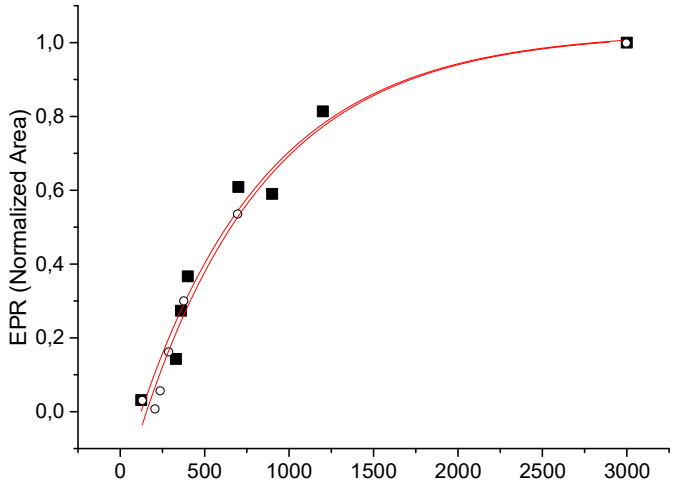

Figure S31 Kinetic time trace for the formation of the S = 1/2 signal (g_{mid} = 2.14 species) with g = 2.21, 2.14, 1.97 during the decay of **2** (generated by adding peracetic acid (5 equiv) to a 1 mM solution of **1** in a 1:3 (v/v) acetonitrile:acetone solvent mixture at -50 ºC) in the absence (filled squares) and the presence (open circles) of 50 equiv of cyclohexane. Red lines represent the exponential fitting for the kinetic traces, showing that the rate of formation of the g_{mid} = 2.14 species is unaffected by addition of cyclohexane (see also Table S6).

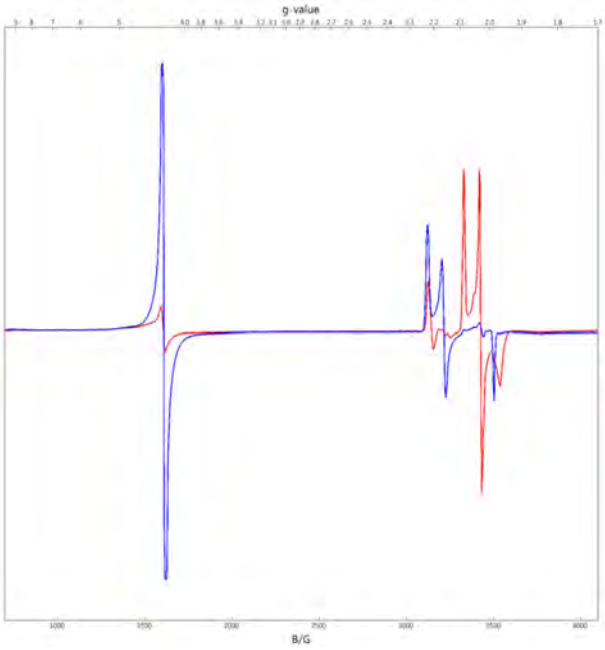

Figure S32 X-band EPR spectra in 1:3 (v/v) acetonitrile:acetone collected for samples frozen at t = 120 s (red) and 3000 s (blue) after reaction of **1** with 5 equivalents of AcOOH at -50 °C. The spectra shown were recorded at 20 K under non-saturating conditions. While the 490-nm chromophore decays, the g_{max} = 2.20 and the g_{max} = 2.07 species (**2a** and **2b**) concurrently disappear, and a new species with g values 2.21, 2.14 and 1.97 (g_{mid} = 2.14) and the high spin Fe^{III} species at $g \approx 4.3$ appears (but not with the rate corresponding to the decay rate of **2a** and **2b**) (see also Table S6).

VI.2 Mössbauer spectra

In the early phases of this study we prepared a Mössbauer sample of **2** at T = - 60 °C (rather than at -50 °C as for the samples described above) frozen at a time where the 490-nm chromophore is near its maximum concentration. This sample was prepared to assess whether Mössbauer spectroscopy might yield valuable information about intermediate **2**. Not surprisingly, Mössbauer spectra are immensely complex due to the presence of multiple paramagnetic species (there are at least five EPR active species), thereby precluding a spectral decomposition at this time. A recent, second Mössbauer sample prepared at -50 °C yielded a spectrum essentially identical to that shown in Figure S33A. The 7.5 T Mössbauer spectrum of Figure S33B indicates that 40% of the Fe in the sample is represented by two (or more) high-spin Fe^{III} species. Spectral simulations indicate that the *major* high-spin ferric species (>30% of the Fe) has a rhombicity parameter E/D ~ 0.15 - 0.20. There is a species with E/D ≈ 1/3 (g = 4.3) that must be a minority species, accounting for less than 10% of the Fe in the sample, in agreement with quantification of the EPR data. Various S = ½ species (g_{max} = 2.07, g_{max} = 2.20 and g_{mid} = 2.14 species) will contribute absorption between + 4 mm/s and – 4 mm/s Doppler velocity. Unfortunately, contributions from the middle Kramers doublets of the high-spin Fe^{III} species and other S = ½ species partially obscure the region where one would expect to see the contribution of the g_{max} = 2.07 species (**2b**). Moreover, the spectrum of Figure S33A suggests to us that the sample may contain some diiron(III) species (indicated by the doublet feature in the center of the spectrum); such a species would be EPR silent (diiron(III) species are often the thermodynamic sink in this sort of oxidation chemistry). We have recorded Mössbauer spectra at T = 120 K and 150 K (not shown) with the goal of observing a quadrupole doublet associated with **2b**. We would observe such a doublet if the electronic relaxation rate of **2** were fast compared to the nuclear precession frequencies. This, however, was not the case: **2** is in the intermediate relaxation regime at these temperatures, yielding broad and unresolved features. A promising future strategy would be to generate *difference* spectra of samples frozen at different points along the time course, canceling features that are constant, or nearly so. Such studies have to be carried out at ≈1.5 K and 4.2 K in variable applied magnetic fields with good signal/noise (NB: At 1.5 K the middle Kramers doublets of the high-spin Fe^{III} species become essentially depopulated, clearing a window to observe the low-spin features). Such experiments are rather demanding in data accumulation (weeks of running time at 4.2 K and 1.5 K) and manpower, and are beyond the scope of the present study.

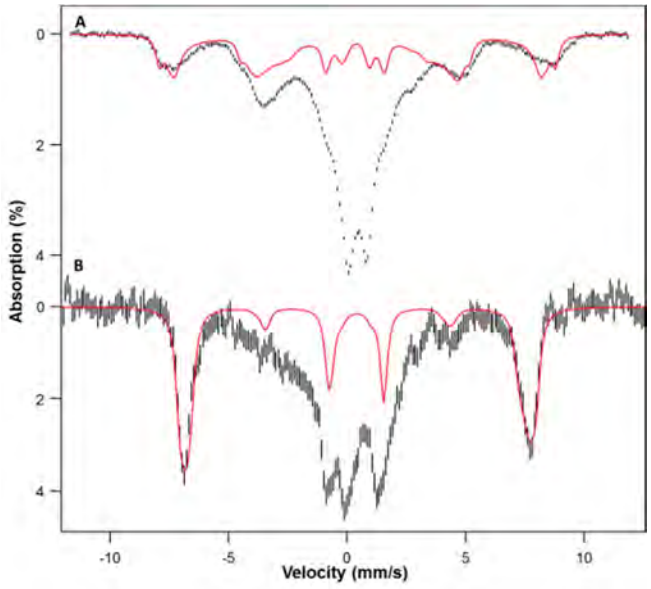

Figure S33 4.2 K Mössbauer spectra (hashed) of a sample (1.89 mM ^{57}Fe) prepared by reacting **1** with 5 equivalents AcOOH in a 1:3 (v/v) acetonitrile:acetone at -60 °C, and freezing at the time point corresponding to maximum accumulation of the 490-nm species. Spectra were collected in variable, parallel applied magnetic fields of (A) 45 mT and (B) 7.5 T. The red curves are simulations for a high-spin Fe^{III} species accounting for 40% of total iron in the sample and were prepared using an S = 5/2 spin Hamiltonian with D = 0.50 cm^{-1}, E/D = 0.18, ΔE_Q = 0.20 mm s^{-1}, η = -3, A_x = -20.0 T, A_y = -22.0 T, A_z = -21.0 T, δ = 0.40 mm s^{-1}. The simulated spectra are meant to indicate the contribution of high-spin ferric species.

VI.3 EPR spectrum of 2 for a ^{57}Fe enriched sample

Using the material prepared for the Mössbauer study of Figure S33 we have studied a parallel sample by EPR. The g = 2 region of a recorded spectrum is shown in Figure S34. The experimental data in panels (A) and (B) (black curves) are the same. The experimental spectrum shows a ^{57}Fe magnetic hyperfine splitting at g_y = 2.01 and hardly any broadening at g_x = 2.07 and g_z = 1.95. We have modeled the g_y splitting by assuming $A_y(^{57}Fe)$ = 47 MHz. To illustrate the nature of this feature we have simulated in (B, blue line) a spectrum with a too large $A_y(^{57}Fe)$ = 80 MHz. It can be seen that the g_y derivative-type feature of the unenriched sample splits into two derivative-type components. The 47 MHz in (A) is not sufficient for a clear separation. Note that the g_y = 2.01 region contains a ≈ 2% contaminant that yields a sharp feature at g = 2.00 and perhaps the bump at g = 2.03. Our simulations also show that $A_x(^{57}Fe)$ < 15 MHz in magnitude; the feature at g_z = 1.95 is difficult to simulate because our sample displays contributions from minor contaminants in the wings of this feature.

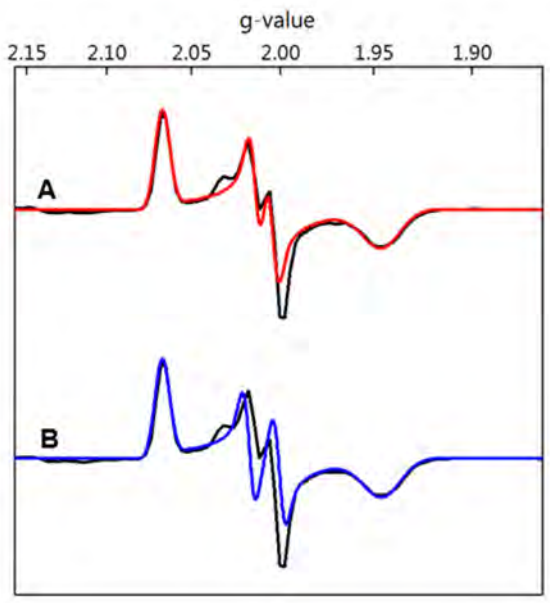

Figure S34 g = 2 region of the EPR spectrum of a ^{57}Fe enriched sample of **2** prepared by reacting **1** with 5 equivalents AcOOH in a 1:3 (v/v) solvent mixture of acetonitrile:acetone at -60°C, and freezing at the time point corresponding to maximum accumulation of the 490 nm chromophore. The spectrum was recorded at T = 17 K; shown in (A) and (B) is the same experimental spectrum (black line). The red line in (A) is a SpinCount simulation of **2** for the g_x = 2.07, g_y = 2.01 and g_z = 1.95 using A_x = 0 MHz, A_y = 47 MHz and A_z = 0 MHz for the ^{57}Fe magnetic hyperfine tensor. For the simulation (blue curve) in (B) we have deliberately used a too large A_y (= 80 MHz); this simulation illustrates how the observed features of the split middle resonance come about when A_y is reduced to the correct ≈ 47 MHz. For the simulations we have used the same line width parameters as for the simulation of the natural abundance (2.2% ^{57}Fe) sample of Figure 4a.

VI.4 Cryospray-MS experiments (CSI-MS)

Two solutions of $[Fe^{II}(CF_3SO_3)_2(PyNMe_3)]$ (**1**) (0.6 mM) and peracetic acid (2.43 mM, 4 eq with respect to iron) in acetonitrile were cooled down to -40ºC. By using a T-connector equal amounts of these two solutions were mixed and directly infused in the CSI-MS (cryospray ionization mass spectrometer). The mixture was injected into the spectrometer in continuous flow by using a syringe pump (180 μL/h) and the spectrum was recorded (Figure S35).

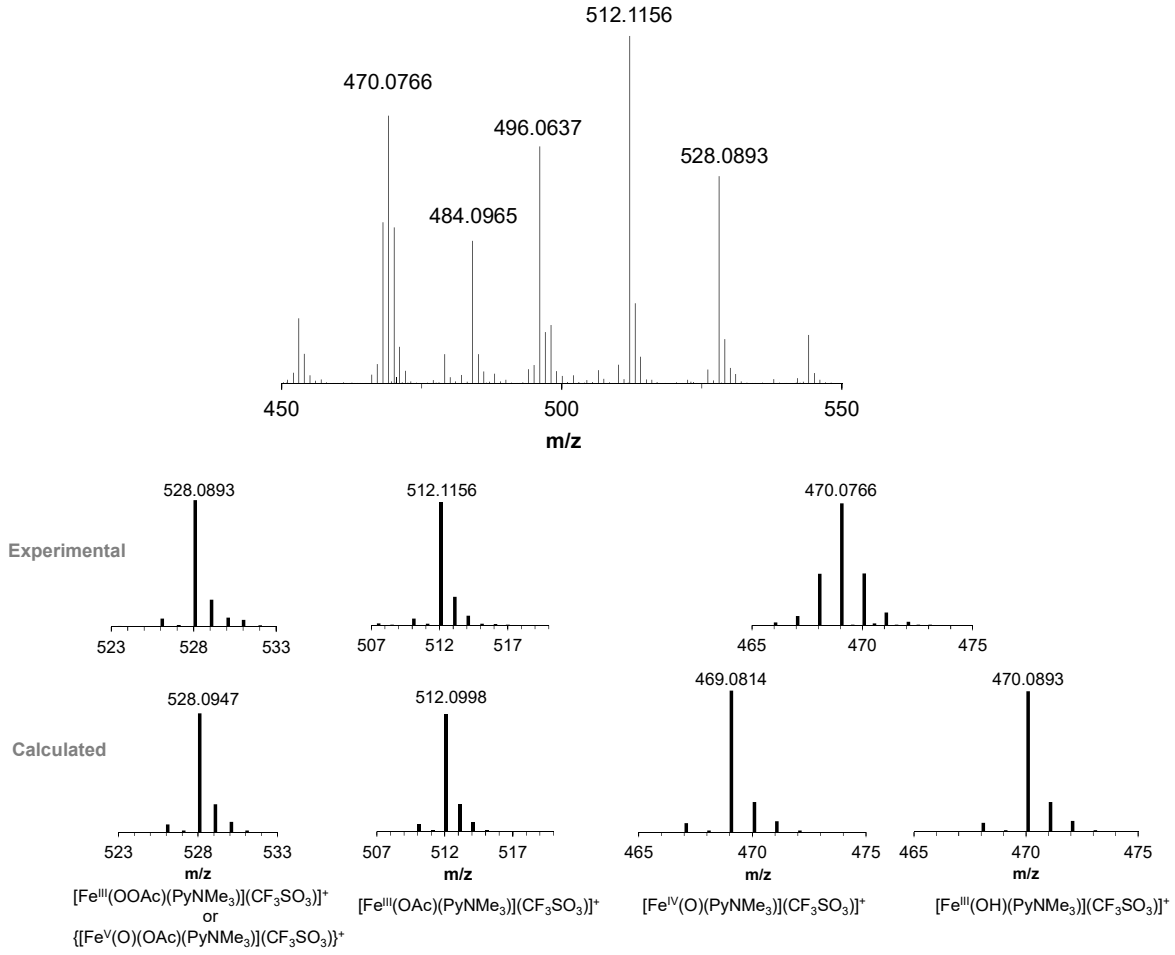

Figure S35 CSI-MS at -40ºC of **2** (generated by reaction of **1** with 4 equiv peracetic acid) in acetonitrile.

VII. Carboxylate exchange of 2 with acetic acid-d_4

VII.1 CSI-MS evidence

A solution of [$Fe^{II}(CF_3SO_3)_2(PyNMe_3)$] (**1**) (0.6 mM) at -40ºC in acetonitrile was mixed with a solution containing peracetic acid (2.43 mM, 4 equiv with respect to iron) and acetic acid-d_4 (12.15 mM, 20 equiv with respect to iron) in acetonitrile at -40ºC by using a T-connector. Equal amounts of these two solutions were mixed and directly infused in the CSI-MS (cryospray ionization mass spectrometer). The mixture was injected into the spectrometer in continuous flow by using a syringe pump (180 μL/h) and the spectrum was recorded (Figure S36).

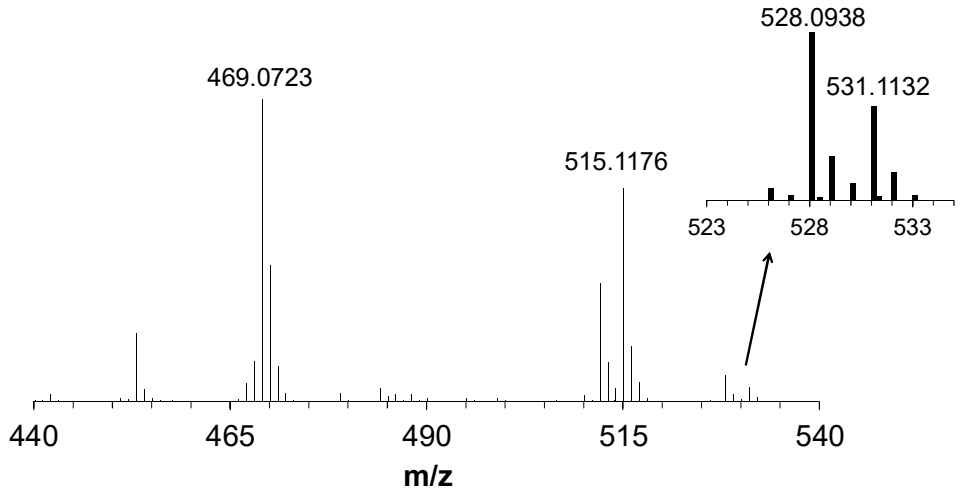

Figure S36 CSI-MS at -40ºC of **2** (generated by reaction of **1** with 4 equiv peracetic acid in the presence of 20 equiv acetic acid-d_4) in acetonitrile.

VII.2 Control experiments

A possible exchange between AcOOH and CD_3CO_2D was considered. In order to discard this option, control experiments were performed.

AcOOH and CD_3CO_2D (20 equiv) were mixed in CD_3CN at room temperature and the mixture was stirred for 30 min. After that period, the mixture was analyzed by ^{1}H-NMR spectroscopy and no exchange was detected.

In the reaction between **1** and peracetic acid, lewis acidic species are generated. These species might promote an exchange between AcOOH and CD_3CO_2D. Thus, the experiment described above was repeated in the presence of $Sc^{III}(OTf)_3$ and $Ga^{III}(NO_3)_3$. No exchange between AcOOH and CD_3CO_2D was observed.

VII.3 Exchange into the *syn*-2-acetoxycyclooctanol product

Three different reactivity experiments were conducted in order to determine the rate of exchange of **2** and CD_3CO_2D:

a) **1** was dissolved in acetonitrile and cyclooctene (200 equiv) and acetic acid-d_4 (200 equiv) were added to the solution. The mixture was cooled down to -40 ºC and then peracetic acid (20 equiv) was added. The mixture was stirred for 30 minutes, worked up and the products were analyzed by GC-MS. 8% of the *syn*-2-acetoxycyclooctanol reaction product had incorporated CD_3CO_2.

b) **2** was generated by adding peracetic (20 equiv) to a 1 mM solution of **1** in acetonitrile at -40 ^{o}C. Upon maximum formation of the intermediate species, cyclooctene (200 equiv) and acetic acid-d_4 (200 equiv) were added together to the reaction mixture. The mixture was let stirring for 30 min at -40 ºC, then worked up and the products were analyzed by GC-MS. 12% of the *syn*-2-acetoxycyclooctanol reaction product had incorporated CD_3CO_2.

c) **2** was generated by adding peracetic acid (20 equiv) to a 1 mM solution of **1** in acetonitrile at -40 ^{o}C. Upon maximum formation of the intermediate species, acetic acid-d_4 (200 equiv) was added and the mixture was let stirring for 1 minute at -40 ºC. Then, cyclooctene (200 equiv) was added. After decay of the cromophore, the mixture was worked up and the products were analyzed by GC-MS. 10% of the *syn*-2-acetoxycyclooctanol reaction product had incorporated CD_3CO_2.

Taken together, the results of these three experiments lead us to the conclusion that the exchange between **2** and acetic acid-d_4 is immediate.

VIII. References

1 Wang, Z., Yin, Y., Geng, Z. & Wen, J. *Inorganic Chemistry Communications* **21**, 16-20 (2012).

2 Giacovazzo, C. J. *Appl. Cryst.* **32**, 115-119 (1999).

3 Sheldrick, G. M. *Acta Cryst. A* **64**, 112-122 (2008).

4 Farrugia, L. *J. Appl. Cryst.* **32**, 837-838 (1999).

5 Harman, D. G., Ramachandran, A., Gracanin, M. & Blanksby, S. J. The Loss of Carbon Dioxide from Activated Perbenzoate Anions in the Gas Phase: Unimolecular Rearrangement via Epoxidation of the Benzene Ring. *The Journal of Organic Chemistry* **71**, 7996-8005 (2006).

6 Mayer, J. M. Hydrogen Atom Abstraction by Metal-Oxo Complexes: Understanding the Analogy with Organic Radical Reactions. *Acc. Chem. Res.* **3**, 441-450 (1998).

7 Reddy, A. S., Kumar, M. S. & Reddy, G. R. A convenient method for the preparation of hydroxamic acids. *Tetrahedron Letters* **41**, 6285-6288 (2000).

Supporting Information Chapter VI

Exceedingly fast oxygen atom transfer to olefins via a catalytically competent nonheme iron species

Table of contents

I. Materials and methods

Materials. Reagents and solvents used were of commercially available reagent quality unless otherwise stated. Solvents were purchased from Scharlab, Acros or Sigma-Aldrich and used without further purification. Peracetic acid was purchased from Aldrich as a 32 wt% solution in acetic acid containing less than 6% H_2O_2. Preparation and handling of air-sensitive materials were carried out in a N_2 drybox (Jacomex) with O_2 and H_2O concentrations < 1 ppm. $[Fe(CF_3SO_3)_2(PyNMe_3)]$ (**1**) was prepared from $PyNMe_3$ and $[Fe(CF_3SO_3)_2(MeCN)_2]$ following the experimental procedure previously reported.[1] **$PyNMe_3$** was prepared following a slightly modified procedure than the previously reported.[1] Dientt was prepared following previously described procedures.[2]

Physical methods. UV/Vis spectroscopy was performed with an Agilent 50 Scan (Varian) UV/Vis spectrophotometer with 1 cm quartz cells. Low temperature control was achieved with a cryostat from Unisoku Scientific Instruments, Japan. GC product analyses were performed on an Agilent 7820A gas chromatograph equipped with a HP-5 capillary column 30mx0.32mmx0.25µm and a flame ionization detector. Stopped-flow experiments were carried out using an SFM4000 Bio-logic instrument provided with a cryo-stopped-flow accessory fitted to a Huber CC-905 bath and the spectral changes were recorded with a diode array detector and analyzed with Specfit.

II. Synthesis of $PyNMe_3$: modified procedure

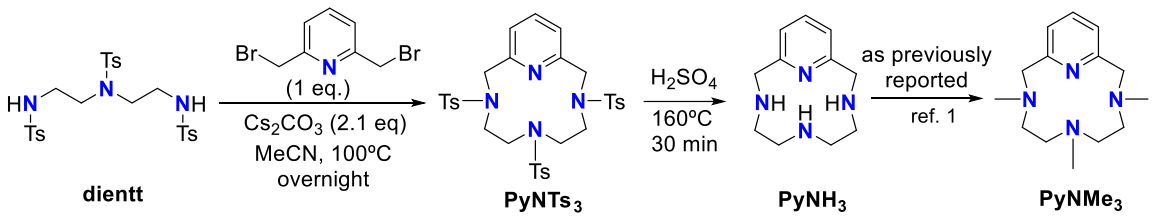

Scheme S1. Synthetic route for the preparation of **$PyNMe_3$**.

Synthesis of $PyNTs_3$: Dientt (N,N',N''-tris(*p*-toluensulfonyl)diethylentriamine, 7.11 g, 12.57 mmol) and cesium carbonate (8.69 g, 26.40 mmol) were introduced in a two-necked 500mL round-bottoom flask and MeCN (300 mL) was added. After heating the mixture to reflux (100 ºC), a solution of 2,6-bis(bromomethyl)pyridine (3.04 g, 12.57 mmol) in MeCN (100 mL) was added dropwise over a period of 3 hours. The mixture was stirred at 100 ºC overnight and then cooled down to room temperature. After filtration, the solvent of the filtrate was removed under reduced pressure, obtaining a yellow solid. The product was purified by column chromatography over silica using a mixture 90:10 CH_2Cl_2:AcOEt. **$PyNTs_3$** (6.61 g, 9.87 mmol, 79% yield) was obtained pure as a white solid. ^{1}H-NMR ($CDCl_3$, 300MHz, 298K) δ, ppm: 7.75 (t, J=7.6 Hz, 1H), 7.72 (d, J=7.6 Hz, 4H), 7.65 (d, J=7.6 Hz, 2H), 7.43 (d, J=7.4 Hz, 2H), 7.34 (d, J=7.4 Hz, 4H), 7.27 (d, J=7.4 Hz, 2H), 4.29 (bs, 4H), 3.32 (t, J = 7.4 Hz, 4H), 2.75 (bs, 4H), 2.45 (s, 6H), 2.41 (s, 3H); ^{13}C-NMR ($CDCl_3$, 300MHz, 298K) δ, ppm: 155.3, 143.8, 143.5, 139.0, 135.9, 135.2, 130.0, 129.8, 127.2, 127.1, 124.2, 55.0, 50.4, 47.4, 21.5; HR-MS (ESI-TOF) m/z calc for [**$PyNTs_3$** + Na]$^+$ 691.1689 found 691.1681.

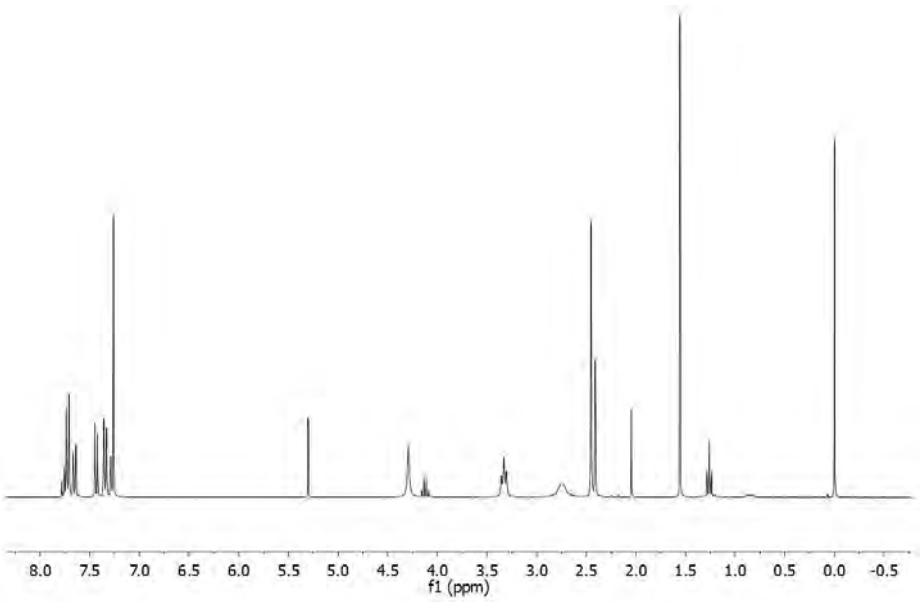

Figure S1. ^{1}H-NMR spectrum of **PyNTs$_3$** in $CDCl_3$ at 298 K.

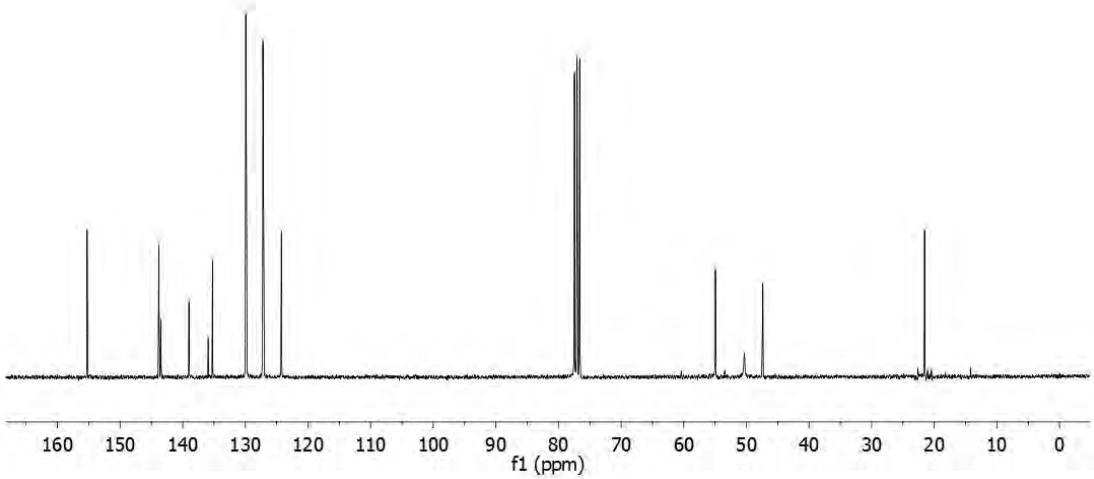

Figure S2. ^{13}C-NMR spectrum of **PyNTs$_3$** in $CDCl_3$ at 298 K.

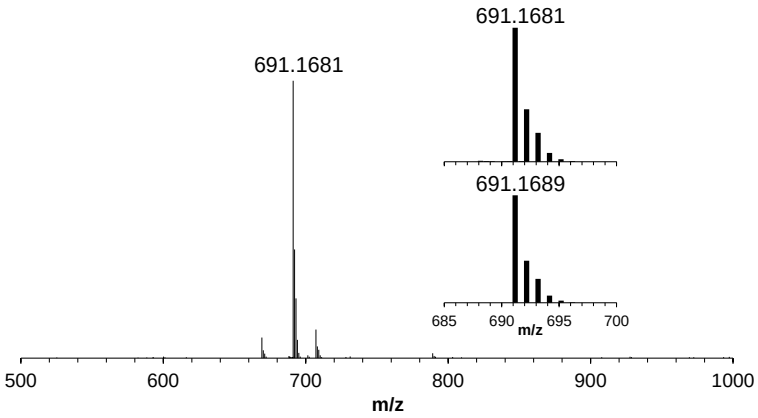

Figure S3. HR-MS of PyNTs$_3$.

Synthesis of $PyNH_3$: $PyNTs_3$ (3.80 g, 5.68 mmol) was introduced in a 50 mL round-bottom flask and concentrated H_2SO_4 (25 mL) was added. The mixture was heated for 30 minutes at 160 ºC. After cooling down to room temperature, water (40 mL) was carefully added. The mixture was extracted with CH_2Cl_2 (3x30 mL) and the combined organic phases were discarded. The aqueous phase was then brought to pH>14 by adding the necessary amount of a 30% NaOH aqueous solution and the extracted with CH_2Cl_2 (3x50 mL). The combined organic phases were dried with $MgSO_4$, filtered and the solvent was removed under reduced pressure, obtaining a white crystalline solid that was used in the next step without further purification. The yield of the reaction ranged from 55% to 80%. ^{1}H-NMR ($CDCl_3$, 300 MHz, 298 K) δ, ppm: 7.52 (t, J = 7.5 Hz, 1H), 7.00 (d, J = 7.5 Hz, 2H), 3.96 (s, 4H), 2.71-2-68 (m, 8H), 2.27-2.24 (m, 3H). ^{13}C-NMR ($CDCl_3$, 300 MHz, 298 K) δ, ppm: 159.7, 136.4, 119.8, 53.8, 49.2. HR-MS (ESI-TOF) *m/z*: calc for [**$PyNH_3$**+H]$^+$ 207.1604 found 207.1606; calc for [**$PyNH_3$**+Na]$^+$ 229.1424 found 229.1418.

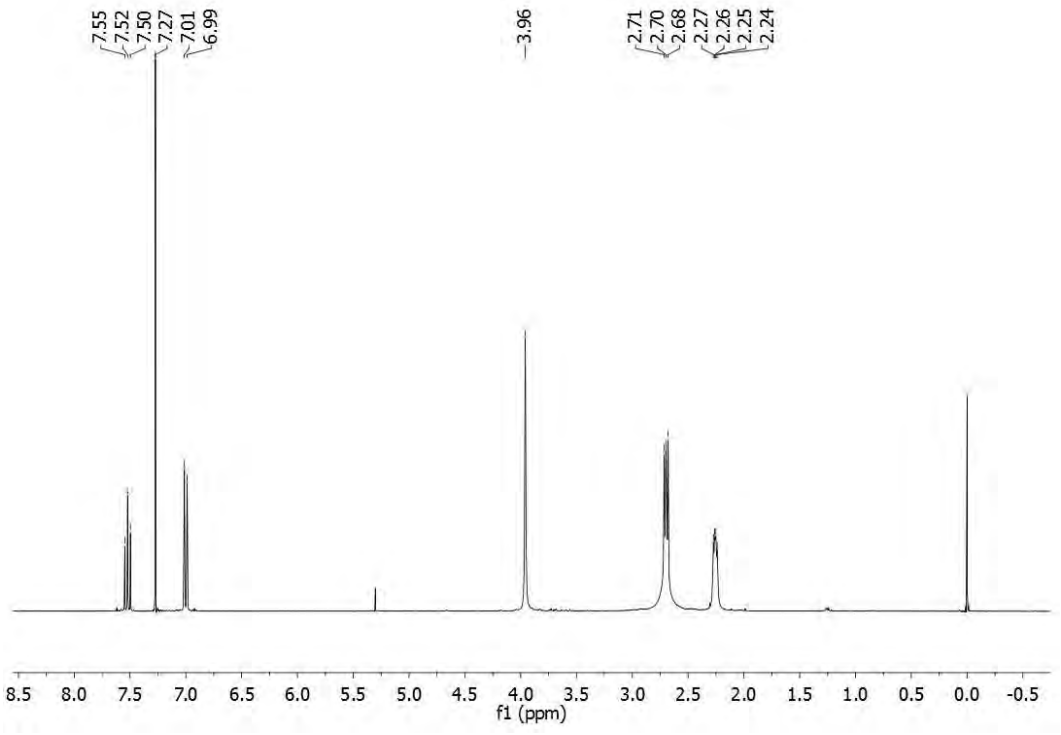

Figure S4. ^{1}H-NMR spectrum of **$PyNH_3$** in $CDCl_3$ at 298 K.

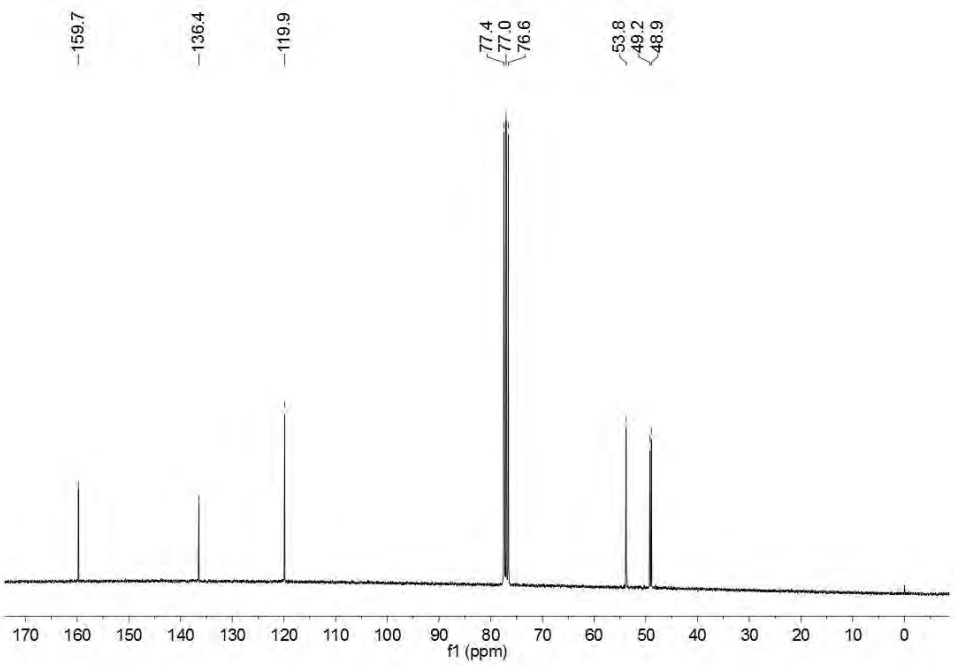

Figure S5. ^{13}C-NMR spectrum of **$PyNH_3$** in $CDCl_3$ at 298 K.

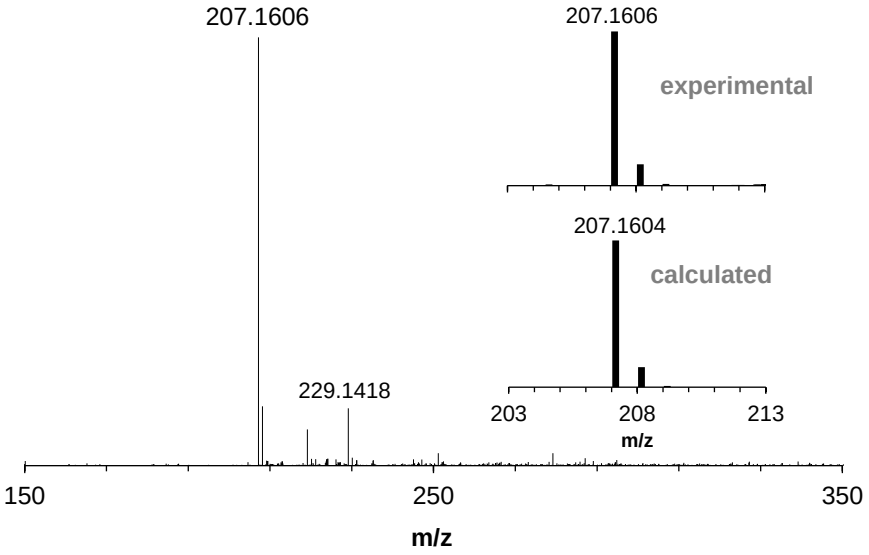

Figure S6. HR-MS of $PyNH_3$.

Synthesis of $PyNMe_3$: The final **$PyNMe_3$** ligand was prepared by methylation of $PyNH_3$ following the procedure previously described by us.[1]

III. Reaction of 2 towards alkenes: kinetic analysis by UV/Vis stopped-flow

Generation of 2. In a typical experiment, a 1 mM solution of **1** in dry acetonitrle was prepared inside the glovebox. 2 mL of this solution were placed in a UV-Vis cuvette (2 μmol of **1**). The quartz cell was capped with a septum and taken out of the box, placed in the Unisoku cryostat of the UV-Vis spectrophotometer and cooled down to 238 K. After reaching thermal equilibrium an UV-Vis spectrum of the starting complex was recorded. Then, 50 μL of a solution containing 66 μL of 32% peracetic acid in 2 mL of dry MeCN were added (8 μmol). The formation of a band at λ_{max} = 490 nm and a shoulder at λ_{max} = 660 nm was observed. Compound **2** was fully formed after 70 seconds.

Compound **2** could be also generated at -60 ºC in a similar way by adding peracetic acid (20 μmol) to 2 mL of a 1 mM pre-cooled solution of **1** (2 μmol) in a MeCN:acetone 1:3 mixture. Maximum formation of **2** (Abs ~ 1.8 at λ_{max} = 490 nm) was achieved within 300 seconds.

Kinetic analysis of reactions of 2 towards alkenes. Kinetics of the reaction of **2** and selected olefins were measured in sequential stopped-flow experiments in which a pseudo-first order excess of substrate was added after **2** reached its maximum concentration. Experiments were carried out by mixing thermostated MeCN:acetone 1:3 solutions of **1** and peracetic acid (1:4 ratio) in a delay line at -60 ºC. The resulting solution was aged for the time required to achieve the maximum concentration of **2** and then it was mixed with a solution containing the desired amount of substrate. The concentration of the substrate in the observation cell was changed by using different ratios of the volumes in the second mixing. In any case, the substrate concentration was always in pseudo-first order excess with respect to **2**. Data acquired after the second mixing were analyzed using the standard software of the stopped-flow instrument. In all cases a satisfactory fit was obtained for the disappearance of **2** using a single exponential.

Table S1. Observed rate constants (k_{obs}) measured at -60 ºC for the reaction of **2** with different substrates in MeCN:acetone (1:3). The concentration of iron was (1-3)×10^{-4} M, and pseudo-first order conditions were kept in all cases using at least a 10:1 substrate:Fe molar ratio.

	k_{obs}, s^{-1}						
[substate], M	1-octene	trans-2-octene	cis-2-octene	2-methyl-2-hexene	styrene	*cis*-cyclooctene	2,3-dimethyl-2-butene
0.002	-	0.030(1)	0.152(1)	0.272(2)	0.308(6)	1.06(3)	1.96(3)
0.003	-	-	-	-	-	1.42(4)	3.47(5)
0.004	-	0.044(2)	0.335(2)	0.527(4)	0.66(1)	1.54(6)	4.17(7)
0.005	-	0.052(2)	0.413(4)	0.663(5)	0.86(2)	1.79(8)	4.86(8)
0.006	-	-	-	-	-	-	5.29(9)
0.007	-	0.072(1)	0.545(2)	0.953(7)	1.06(2)	2.3(1)	6.4(1)
0.008	-	0.087(2)	0.670(3)	1.13(1)	1.20(2)	3.0(1)	-
0.009	-	-	-	-	1.34(3)	-	-
0.010	-	0.093(2)	0.833(3)	1.43(1)	1.47(3)	-	-
0.012	-	0.115(2)	0.990(6)	1.74(1)	1.72(4)	-	-
0.013	-	0.130(3)	1.114(4)	1.99(1)	-	-	-
0.015	-	0.147(3)	1.235(5)	2.18(2)	-	-	-
0.017	-	0.179(3)	1.37(2)	2.39(2)	-	-	-
0.018	-	0.180(4)	1.47(2)	-	-	-	-
0.02	0.119(5)	-	-	-	-	-	-
0.04	0.32(1)	-	-	-	-	-	-
0.05	0.40(1)	-	-	-	-	-	-
0.07	0.56(1)	-	-	-	-	-	-
0.08	0.65(2)	-	-	-	-	-	-
0.10	0.87(2)	-	-	-	-	-	-
0.12	0.96(2)	-	-	-	-	-	-
0.13	1.09(3)	-	-	-	-	-	-
0.15	1.29(3)	-	-	-	-	-	-
0.17	1.57(3)	-	-	-	-	-	-
0.18	1.68(4)	-	-	-	-	-	-

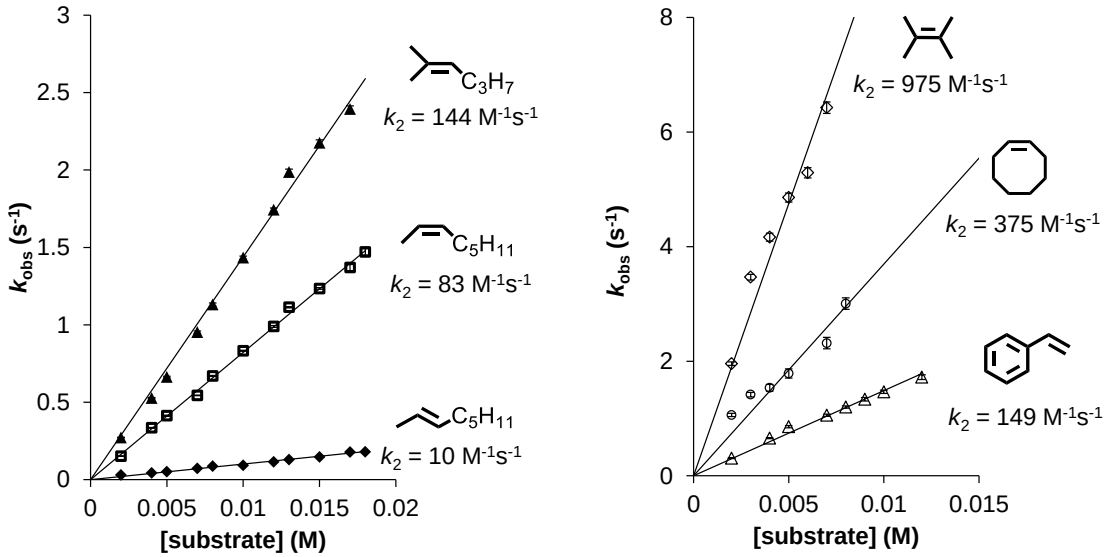

Figure S7. Plots of k_{obs} against substrate concentration for the reaction of **2** with different olefins in a MeCN:acetone 1:3 mixture at -60 ºC (full diamonds: trans-2-octene, empty squares: *cis*-2-octene, full triangles: 2-methyl-2-hexene, empty triangles: styrene, empty circles: cyclooctene, empty diamonds: 2,3-dimethyl-2-butene).

Table S2. Second order rate constants (k_2) for the reaction of **2** with different olefins at -60 ºC in MeCN:acetone 1:3.

substrate	**k_2 , $M^{-1}\cdot s^{-1}$**
1-octene	8.8 ± 0.2
trans-2-octene	10.1 ± 0.2
cis-2-octene	82.6 ± 0.3
2-methyl-2-hexene	144 ± 1
styrene	149 ± 3
cis-cyclooctene	375 ± 15
2,3-dimethyl-2-butene	975 ± 16

Table S3. Second order rate constants (k_2) for the reaction of **2** with 1-octene in MeCN:acetone 1:3 at different temperatures.

T, ºC	**k_2, $M^{-1}s^{-1}$**
-60	8.8 ± 0.2
-55	14.2 ± 0.3
-50	21.8 ± 0.2
-45	33.4 ± 0.5
-40	45.6 ± 0.4
-35	61.9 ± 0.6
-30	82.0 ± 0.6
-25	116 ± 2
-20	145 ± 2

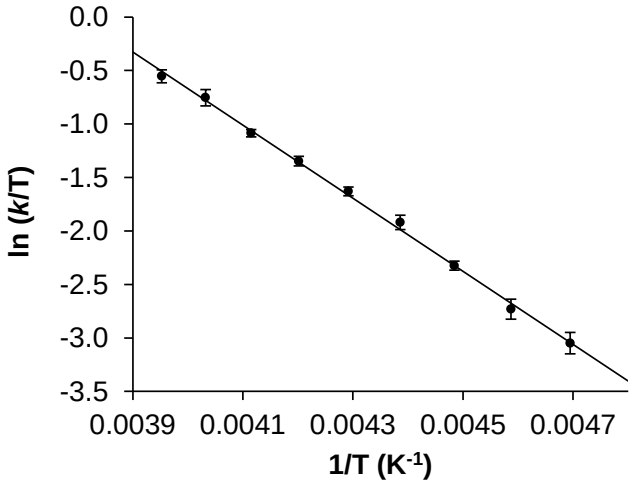

Figure S8. Eyring plot for the reaction of **2** with 1-octene in MeCN:acetone 1:3.

Table S4. Second order rate constants (k_2) for the reaction of **2** with different para-substituted styrenes in MeCN:acetone 1:3 at -60 ºC.

substrate	**k_2, $M^{-1}\cdot s^{-1}$**
4-nitrostyrene	20.3 ± 0.3
4-trifuloromethylstyrene	23.6 ± 0.3
4-chlorostyrene	117 ± 2
styrene	149 ± 3
4-methylstyrene	392 ± 9

Comparison with heme systems

A comparison can be also stablished between **2** and synthetic iron(IV)-oxo porphyrin radical species, which reproduce the electronic structure of Cpd I of cytochrome P450 and related enzymes. The second order rate constant of 375 M^{-1} s^{-1} at -60 ºC for the reaction of **2** with *cis*-cyclooctene is 3 orders of magnitude faster than the 0.29 M^{-1} s^{-1} determined for the Cpd I model $[Fe^{IV}(O)(TMP\bullet)(F)]^0$ (TMP = 5,10,15,20-tetramesitylporphyrin) at the same temperature.[3] Furthermore, second order rate constants for reactions of CpdI models with cyclohexene (-15 ºC, k_2 = 48 $M^{-1}s^{-1}$)[4] and *cis*-stilbene (-35 ºC, k_2 = 7.0 $M^{-1}s^{-1}$)[5] further illustrate the superior reactivity of **2**.

IV. Reaction of 2 towards alkenes: product analyses

Analysis of the oxidation products. Once **2** was fully formed, 100 μL of a solution containing a known amount of the desired substrate were added in the UV-vis cuvette. Right after the complete decay of the band at λ = 490 nm, 50 μL of a $NaHSO_3$ solution 40% in water were added in order to quench the excess peracetic acid. At this point biphenyl was added as an internal standard and the solution was then filtered through Celite® to remove the formed precipitate. Acetic anhydride (1 mL) and 1-methylimidazole (0.1 mL) were then added and the mixture was stirred for 15 minutes at room temperature to esterify the alcohol products. Afterwards, ~3 mL of ice were added and stirred for 10 minutes. The organic products were extracted with $CHCl_3$ (2 mL). The organic layer was washed with H_2SO_4 (2 mL, 1M), saturated aqueous $NaHCO_3$ (2 mL) and water (2 mL). The resulting organic layer was dried over $MgSO_4$, filtered through a short path of Celite® and subjected to GC analysis.

Catalytic experiments at -60 ºC with 1/AcOOH in MeCN:acetone 1:3

In a typical experiment, 2 mL of a 1 mM solution of **1** in MeCN were placed in a 20 mL vial together with the appropriate amount of the desired substrate. Then, 204 μL of a 98.5 mM solution (20 μmol) of peracetic acid in acetone was added over 30 minutes at -60 ºC. The solution was stirred for 15 min and then 100 μL of a $NaHSO_3$ solution 40% in water were added to quench unreacted peracetic acid. At this point biphenyl was added as an internal standard and the solution was then filtered through Celite® to remove the formed precipitate. The iron complex was removed by passing the solution through a short path of silica followed by elution with ethyl acetate (2 mL). Finally, the solution was dried with $MgSO_4$, filtered through a short path of Celite® and subjected to GC analysis.

V. Reaction of 2 towards sulfides

Compound **2** can also perform the oxygen-atom transfer towards sulfides such as thioanisole, a substrate commonly employed to interrogate relative reactivities of iron(IV)-oxo complexes. Reactions between **2** and sulfides were so fast that proper kinetic data could not be obtained with our stopped-flow equipment even at -60 ºC. However, the k_2 value for the reaction of **2** with thioanisole could be estimated to be larger than 10^3 M^{-1} s^{-1} at -60 ºC. For comparison, values of the order of 10^3 M^{-1} s^{-1} at -60 ºC have been reported for the reaction of thioanisole with high spin Fe^{III}-iodosylarene intermediates,[6] while a Cpd I model performs the oxidation of dimethylsulfide with a k_2 value in the order of 10^4 $M^{-1}s^{-1}$ at -15 ºC.[4] Instead, well-defined iron(IV)-oxo species typically show second order rate constants several orders of magnitude slower.[7,8]

VI. References

(1) Serrano-Plana, J.; Oloo, W. N.; Acosta-Rueda, L.; Meier, K. K.; Verdejo, B.; García-España, E.; Basallote, M. G.; Münck, E.; Que, L.; Company, A.; Costas, M. *J. Am. Chem. Soc.* **2015**, *137*, 15833.

(2) Searle, G. H.; Geue, R. J. *Aust. J. Chem.* **1984**, *37*, 959.

(3) Takahashi, A.; Yamaki, D.; Ikemura, K.; Kurahashi, T.; Ogura, T.; Hada, M.; Fujii, H. *Inorg. Chem.* **2012**, *51*, 7296.

(4) Ji, L.; Franke, A.; Brindell, M.; Oszajca, M.; Zahl, A.; van Eldik, R. *Chem. Eur. J.* **2014**, *20*, 14437.

(5) Hessenauer-Ilicheva, N.; Franke, A.; Meyer, D.; Woggon, W.-D.; van Eldik, R. *J. Am. Chem. Soc.* **2007**, *129*, 12473.

(6) Hong, S.; Wang, B.; Seo, M. S.; Lee, Y.-M.; Kim, M. J.; Kim, H. R.; Ogura, T.; Garcia-Serres, R.; Clémancey, M.; Latour, J.-M.; Nam, W. *Angew. Chem. Int. Ed.* **2014**, *53*, 6388.

(7) Park, M. J.; Lee, J.; Suh, Y.; Kim, J.; Nam, W. *J. Am. Chem. Soc.* **2006**, *128*, 2630.

(8) Company, A.; Prat, I.; Frisch, J. R.; Mas-Ballesté, D. R.; Güell, M.; Juhász, G.; Ribas, X.; Münck, D. E.; Luis, J. M.; Que, L.; Costas, M. *Chem. Eur. J.* **2011**, *17*, 1622.

Supporting Information Chapter VII

Evidence for acid-triggered heterolytic O-O cleavage in a nonheme Fe^{III}-OOH species

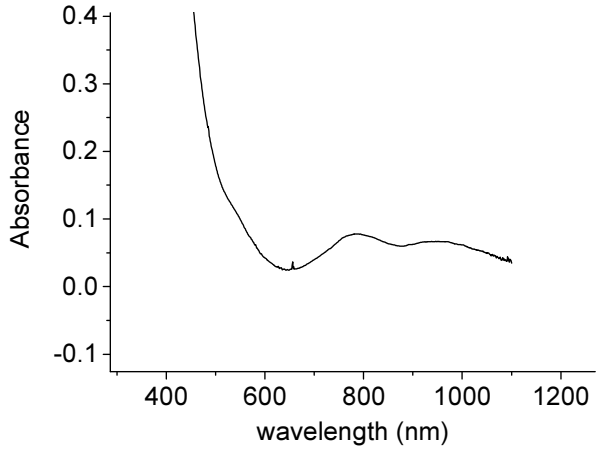

Figure S1. UV-vis spectrum of $[Fe^{IV}(O)(PyNMe_3)]^{2+}$ generated after the addition of $Bu_4N(IO_4)$ (1.1 equiv) to **1** (1 mM) in acetonitrile at -40ºC.

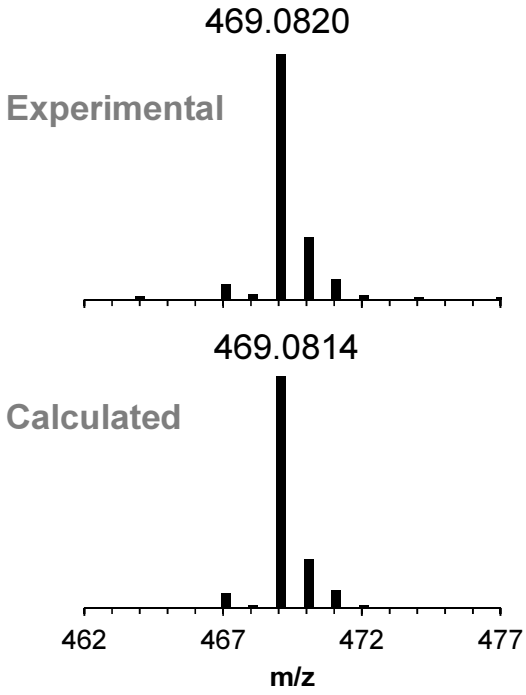

Figure S2. CSI-MS at -40ºC of $[Fe^{IV}(O)(PyNMe_3)]^{2+}$ generated by addition of $Bu_4N(IO_4)$ (1.1 equiv) to **1** in acetonitrile at -40ºC (top) along with the isotopic pattern calculated for $\{[Fe^{IV}(O)(PyNMe_3)](CF_3SO_3)\}^+$

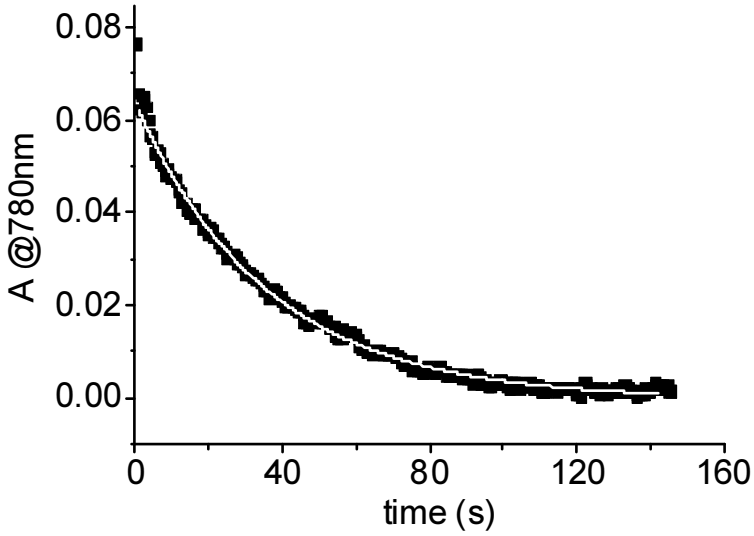

Figure S3. Decay of the spectroscopic features at λ_{max} = 780 nm of $[Fe^{IV}(O)(PyNMe3)]^{2+}$ after addition of excess 4-methylthioanisole fitted to a single exponential function (white line)